Public release; distribution is unlimited.

Data Report: Acoustic Mid-Ocean Dynamics Experiment (AMODE)

by Brian D. Dushaw, Peter F. Worcester*, Bruce D. Cornuelle*, Anne R. Marshall*, Bruce M. Howe, Shaun Leach, James A. Mercer, and Robert C. Spindel

Technical Memorandum
APL-UW TM2-96
March 1996

Applied Physics Laboratory University of Washington
1013 NE 40th Street Seattle, Washington 98105-6698

Contract # NSF OCE-9415650
ONR N00014-87-K-0760
ONR N00014-91-J-4055

Scripps Institution of Oceanography, University of California, San Diego, 92093-0225

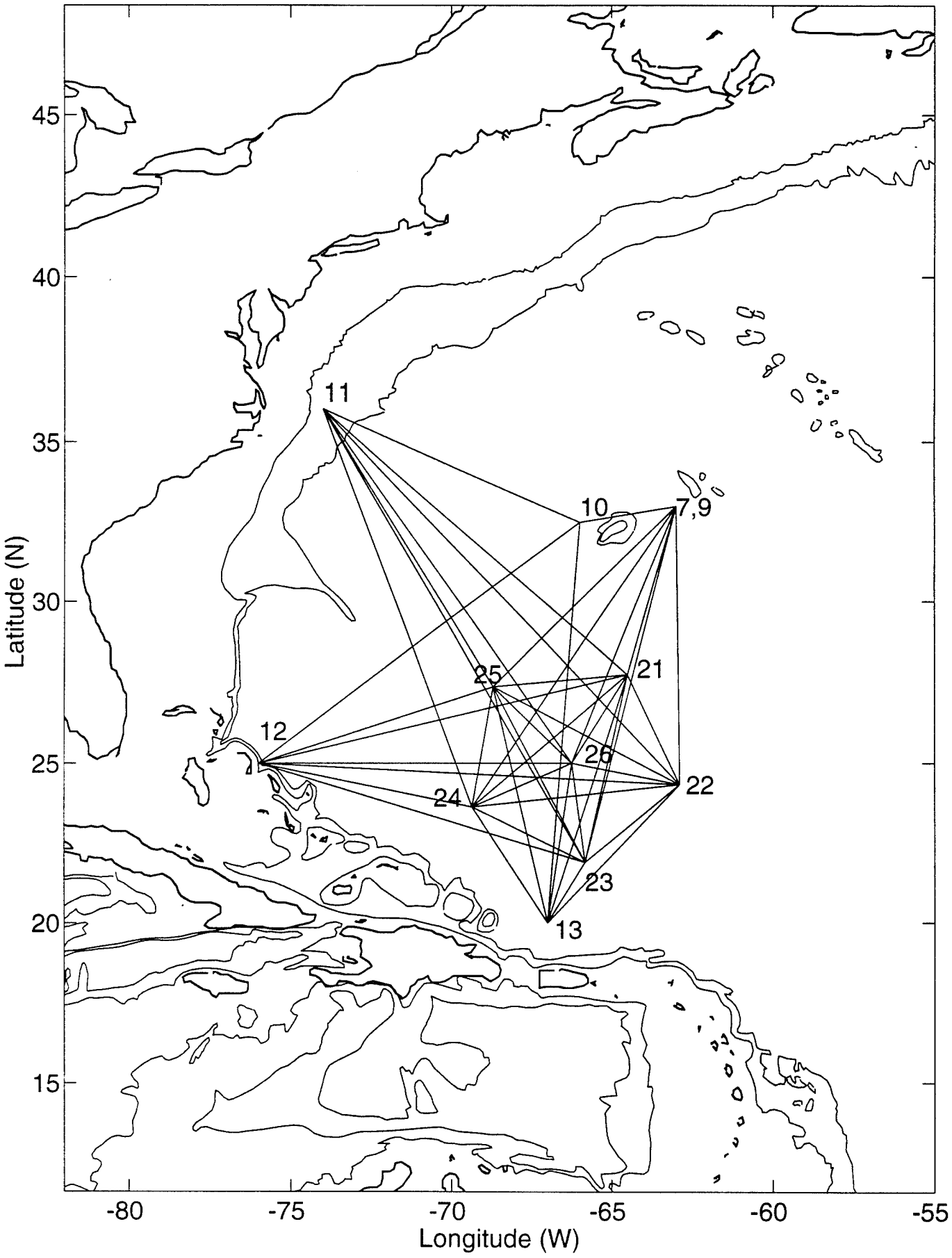
45
40
35
30
25
20
15
Latitude (N)
-80
-75
-70
-65
-60
-55
Longitude (W)
11
10
7,9
25
21
12
26
22
24
23
13

Data Report: Acoustic Mid-Ocean Dynamics Experiment (AMODE)

by Brian D. Dushaw, Peter F. Worcester*, Bruce D. Cornuelle*, Anne R. Marshall*, Bruce M. Howe, Shaun Leach, James A. Mercer, and Robert C. Spindel

Technical Memorandum
APL-UW TM2-96
March 1996

Applied Physics Laboratory University of Washington
1013 NE 40th Street Seattle, Washington 98105-6698

Contract # NSF OCE-9415650
ONR N00014-87-K-0760
ONR N00014-91-J-4055

**Scripps Institution of Oceanography, University of California, San Diego, 92093-0225*

ACKNOWLEDGMENTS

Numerous people have contributed to the collection and analysis of the data described in this report. The principal investigators for AMODE/MST were K. Metzger and T. Birdsall at the University of Michigan; B. Cornuelle, R. Davis, R. Knox, W. Munk and P. Worcester at the Scripps Institution of Oceanography; and B. Howe, J. Mercer, and R. Spindel at the Applied Physics Laboratory, University of Washington. Peter Worcester and his group at S.I.O. successfully deployed and recovered the tomography moorings and their sophisticated transceivers. Bruce Howe from the Applied Physics Laboratory of the University of Washington has made numerous contributions to AMODE; he calculated the mooring motion and clock correction time series essential to the acoustic data, for example. He also was the leading investigator for the Moving Ship Tomography (MST) component of the experiment. Anne Marshall and Bruce Cornuelle tracked the resolved ray arrival time series from the acoustic dot plots (a procedure which can best be described as a laborious black art). K. Bader, A. Ganse, D. Horwitt, S. Leach and B. Ma assisted in the first critical stage of the data analysis. Credit for the success of the AMODE experiment belongs largely to the dedicated engineers and technicians participating in this project from the Scripps Institution of Oceanography (S. Abbott, K. Hardy, B. Norwich, D. Horwitt, B. Ma, D. Peckham, P. Russo, R. Truesdale) and the Applied Physics Laboratory of the University of Washington (K. Bader, L. Nielson, R. Odom, B. Paisley). Success of the deployment field work relied on the assistance of Capt. P. Howland and the crew of the *R/V Oceanus*. Success of the recovery field work relied on the assistance of Capt. T. Tyler and the crew of the *R/V Endeavor*. This research is supported by the Office of Naval Research, the Office of Naval Technology, and the National Science Foundation.

CONTENTS

A. INTRODUCTION . . . . . A1—A3

B. OVERVIEW . . . . . B1—B8

C. MOORING MOTION AND CLOCK CORRECTIONS . . . . . C1—C5

D. ABSOLUTE MOORING POSITIONS . . . . . D1—D2

E. ABSOLUTE TRAVEL TIMES E1

F. FINAL CUTOFF TRAVEL TIMES: Paths 1→3 and 3→1 . . . . . F1—F11

G. ACOUSTIC DATA PROCESSING: Paths 1→2 and 2→1 . . . . . G1—G12

H. ACOUSTIC DATA: Paths 1→3 and 3→1 . . . . . H1—H11

I. ACOUSTIC DATA: Paths 1→4 and 4→1 . . . . . I1—I11

J. ACOUSTIC DATA: Paths 1→5a and 5a→1 . . . . . J1—J9

K. ACOUSTIC DATA: Paths 1→5b and 5b→1 . . . . . K1—K8

L. ACOUSTIC DATA: Paths 1→6 and 6→1 . . . . . L1—L10

M. ACOUSTIC DATA: Paths 2→3 and 3→2 . . . . . M1—M10

N. ACOUSTIC DATA: Paths 2→4 and 4→2 . . . . . N1—N10

O. ACOUSTIC DATA: Paths 2→5a and 5a→2 . . . . . O1—O9

P. ACOUSTIC DATA: Paths 2→5b and 5b→2 . . . . . P1—P9

Q. ACOUSTIC DATA: Paths 2→6 and 6→2 . . . . . Q1—Q10

R. ACOUSTIC DATA: Paths 3→4 and 4→3 . . . . . R1—R10

S. ACOUSTIC DATA: Paths 3→5a and 5a→3 . . . . . S1—S9

T. ACOUSTIC DATA: Paths 3→5b and 5b→3 . . . . . T1—T9

U. ACOUSTIC DATA: Paths 3→6 and 6→3 . . . . . U1—U10

V. ACOUSTIC DATA: Paths 4→5a and 5a→4 . . . . . V1—V8

W. ACOUSTIC DATA: Paths 4→5b and 5b→4 . . . . . W1—W8

X. ACOUSTIC DATA: Paths 4→6 and 6→4 . . . . . X1—X10

Y. ACOUSTIC DATA: Paths 5a→6 and 6→5a . . . . . Y1—Y8

Z. ACOUSTIC DATA: Paths 5b→6 and 6→5b . . . . . Z1—Z8

AA. DATA IN NODC FORMAT . . . . . AA1—AA5

AB. SOSUS ARRAY RECEPTIONS: Dot Plots . . . . . AB1—AB42

REFERENCES

LIST OF TABLES

TABLE B-1. AMODE Reciprocal Travel Time Time Series. B2

TABLE C-1. Offsets for Mooring 2 (Receiver) Travel-Time Time Series. C2

TABLE D-1. AMODE Positions and Their Uncertainties. D1

TABLE D-2. Range Between AMODE Moorings in Kilometers D2

TABLE G-1. Travel Time Statistics 1←→2. . . . . G4

TABLE G-2. Tidal Current Harmonic Constants 1←→2. . . . . G5

TABLE G-3. Tidal Sound Speed Harmonic Constants 1←→2. . . . . G5

TABLE H-1. Travel Time Statistics 1←→3. . . . . H1

TABLE H-2. Tidal Current Harmonic Constants 1←→3. . . . . H2

TABLE H-3. Tidal Sound Speed Harmonic Constants 1←→3. . . . . H2

TABLE I-1. Travel Time Statistics 1←→4. . . . . I2

TABLE I-2. Tidal Current Harmonic Constants 1←→4. . . . . I3

TABLE I-3. Tidal Sound Speed Harmonic Constants 1←→4. . . . . I3

TABLE J-1. Travel Time Statistics 1←→5a. J2

TABLE J-2. Tidal Current Harmonic Constants 1←→5a. J3

TABLE J-3. Tidal Sound Speed Harmonic Constants 1←→5a. J3

TABLE K-1. Travel Time Statistics 1←→5b. K2

TABLE K-2. Tidal Current Harmonic Constants 1←→5b. K3

TABLE K-3. Tidal Sound Speed Harmonic Constants 1←→5b. K3

TABLE L-1. Travel Time Statistics 1←→6. . . . . L2

TABLE L-2. Tidal Current Harmonic Constants 1←→6. . . . . L3

TABLE L-3. Tidal Sound Speed Harmonic Constants 1←→6. . . . . L3

TABLE M-1. Travel Time Statistics 2←→3. . . . . M2

TABLE M-2. Tidal Current Harmonic Constants 2←→3. . . . . M3

TABLE M-3. Tidal Sound Speed Harmonic Constants 2←→3. . . . . M3

TABLE N-1. Travel Time Statistics 2←→4. . . . . N2

TABLE N-2. Tidal Current Harmonic Constants 2←→4. . . . . N3

TABLE N-3. Tidal Sound Speed Harmonic Constants 2←→4. . . . . N3
TABLE O-1. Travel Time Statistics 2←→5a. O2
TABLE O-2. Tidal Current Harmonic Constants 2←→5a. O3
TABLE O-3. Tidal Sound Speed Harmonic Constants 2←→5a. O3
TABLE P-1. Travel Time Statistics 2←→5b. P2
TABLE P-2. Tidal Current Harmonic Constants 2←→5b. P3
TABLE P-3. Tidal Sound Speed Harmonic Constants 2←→5b. P3
TABLE Q-1. Travel Time Statistics 2←→6. . . . . Q2
TABLE Q-2. Tidal Current Harmonic Constants 2←→6. . . . . Q3
TABLE Q-3. Tidal Sound Speed Harmonic Constants 2←→6. . . . . Q3
TABLE R-1. Travel Time Statistics 3←→4. . . . . R2
TABLE R-2. Tidal Current Harmonic Constants 3←→4. . . . . R3
TABLE R-3. Tidal Sound Speed Harmonic Constants 3←→4. . . . . R3
TABLE S-1. Travel Time Statistics 3←→5a. S2
TABLE S-2. Tidal Current Harmonic Constants 3←→5a. S3
TABLE S-3. Tidal Sound Speed Harmonic Constants 3←→5a. S3
TABLE T-1. Travel Time Statistics 3←→5b. T2
TABLE T-2. Tidal Current Harmonic Constants 3←→5b. T3
TABLE T-3. Tidal Sound Speed Harmonic Constants 3←→5b. T3
TABLE U-1. Travel Time Statistics 3←→6. . . . . U2
TABLE U-2. Tidal Current Harmonic Constants 3←→6. . . . . U3
TABLE U-3. Tidal Sound Speed Harmonic Constants 3←→6. . . . . U3
TABLE V-1. Travel Time Statistics 4←→5a. V2
TABLE V-2. Tidal Current Harmonic Constants 4←→5a. V3
TABLE V-3. Tidal Sound Speed Harmonic Constants 4←→5a. V3
TABLE W-1. Travel Time Statistics 4←→5b. W2
TABLE W-2. Tidal Current Harmonic Constants 4←→5b. W3
TABLE W-3. Tidal Sound Speed Harmonic Constants 4←→5b. W3
TABLE X-1. Travel Time Statistics 4←→6. . . . . X2
TABLE X-2. Tidal Current Harmonic Constants 4←→6. . . . . X3
TABLE X-3. Tidal Sound Speed Harmonic Constants 4←→6. . . . . X3

TABLE Y-1. Travel Time Statistics 5a←→6. . . . . Y2
TABLE Y-2. Tidal Current Harmonic Constants 5a←→6. . . . . Y3
TABLE Y-3. Tidal Sound Speed Harmonic Constants 5a←→6. . . . . Y3
TABLE Z-1. Travel Time Statistics 5b←→6. . . . . Z2
TABLE Z-2. Tidal Current Harmonic Constants 5b←→6. . . . . Z3
TABLE Z-3. Tidal Sound Speed Harmonic Constants 5b←→6. . . . . Z3

A. *INTRODUCTION*

The Acoustic Mid-Ocean Dynamics Experiment/Moving Ship Tomography Experiment (AMODE/MST) was conducted in 1991–2 (Howe et al., 1991; AMODE Group, 1994; Howe and Worcester, 1994; Howe et al., 1994; Boyd et al., 1994) (FIGURE A-1). The AMODE/MST experiment encompassed an area of ocean about 1000-km across mid-way between Bermuda and Puerto Rico.

The MST-proper data set, which is NOT described in this report, consists of travel time data from the six AMODE moored transceivers to an acoustic array lowered from a circumnavigating ship.

This report is a second generation description of the reciprocal acoustic travel times between the moored transceivers. Peter Worcester remains the primary contact regarding this data set. Previous reports (Worcester and Howe, 1991; Dushaw, 1992; Worcester and Dushaw, 1993; Ganse and Howe, 1993a,b) have described the raw acoustic, hydrographic, and bathymetric data from AMODE. This report describes the resolved, tracked ray travel times, the mooring motion and clock corrections to those travel times, and the editing and filtering procedures used to obtain a clean data set appropriate for use in oceanographic studies. This discussion applies to the travel time data derived from the four-element hydrophone arrays that were on each mooring. Additional, deeper, single hydrophones were also deployed on moorings 3, 5a, and 6, but these data are not discussed here.

The AMODE transceiver moorings are numbered from 1 to 6. Mooring 1 is located at the northeastern vertex of the AMODE pentagon, and mooring numbers increase clockwise around the array. Mooring 6 is at the center of the array. There is a mooring number 7, which is the acoustic source which was deployed near to and on the south side of Bermuda.

The acoustic travel times from the AMODE transceivers to Navy SOSUS arrays located around the Western North Atlantic basin were also recorded. This report contains the "dot plots" from these receptions; these data are only briefly discussed.

The AMODE data set is currently being used by several workers. Bruce Cornuelle et al. (1995a, 1995b, 1996) is working on assimilating the tomographic data into a quasigeostrophic model, and testing predictability, with promising success. Bruce is using a slightly different data product than that described in this report; he has devised his own data filtering and editing procedures and he uses the travel time data in its original "one-way" form rather than the sum or difference of reciprocal travel times as described in this report. David Chester et al. (1994, 1995a, 1995b) has examined the mean current field (general circulation) determined from the AMODE data, as well as the eddy variability apparent in both the sum (temperature) and difference (current and vorticity) travel times. John Colosi has recently begun to examine the internal wave effects on the travel times. Brian Dushaw has examined the high-frequency (> 1 cpd) travel time variances (Dushaw et al., 1994a) as a means of checking the quality of the data (the high-frequency variances are also of interest in their own right) and the barotropic and baroclinic tidal signals apparent in both sum and difference travel times (Dushaw et al., 1994b; Dushaw et al., 1995a; Dushaw et al., 1995b; Dushaw et al., 1996).

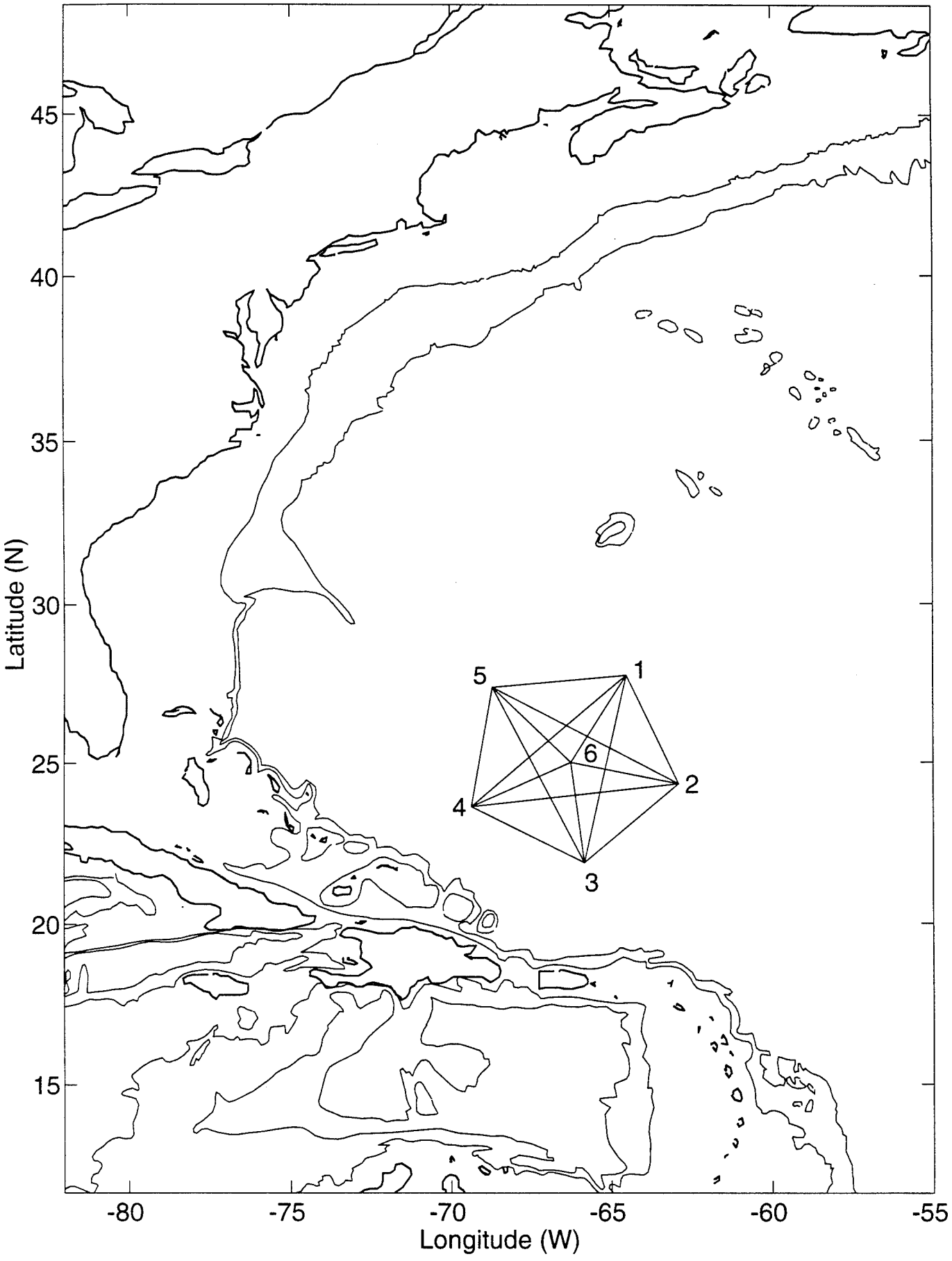
45
40
35
30
25
20
15
Latitude (N)
-80
-75
-70
-65
-60
-55
Longitude (W)
1
2
3
4
5
6

FIGURE A-1

Even with this work, the AMODE data set, together with the MST data and the AMODE-SOSUS data (FIGURES A-1, AB-2) (and data from the cotemporal Multi-Dimensional Array (MDA) experiment (Boyd et al., 1992)), remains underutilized for its ability to describe deep-ocean processes.

B. OVERVIEW

In section C, the corrections to the ray travel times for the motion of the moorings and clock drift are described. The positioning of the AMODE moorings is discussed in section D. In section E, a description of how to calculate the absolute travel times from the travel times recorded by the AVATARS, and after the mooring motion and clock corrections have been made, is given.

In Section F, the determination of "final cutoff" travel times, derived from the transmissons between transceivers 1 and 3 only, is described. To date, the "final cutoff" travel times have been determined for the 1←→3 path only; the task of determining these travel times for the other 38 paths and developing a proper theoretical interpretation of these data remains.

Section G is a description of the ray travel time data for the path between transceivers 1 and 2. In this section, the various figures and calculations are derived and discussed in detail. In subsequent sections (H–Z), the description of data from the other paths is limited to notes particular to each path, since the basic procedure for data reduction for these paths is nearly identical to that for the 1←→2 path.

In section AA, the NODC data format for the tomographic data is described.

We conclude with a brief description of the SOSUS array receptions in section AB. The section includes the "dot plots" for these receptions. The array geometries (location, depth, etc.) are classified, hence only travel times with an offset can be shown.

The TABLE B-1 on the next page summarizes the time series of reciprocal travel times from each path of AMODE. FIGURE B-1 (a–e) shows the measured barotropic current and relative vorticity determined from each of the five equilateral triangles of AMODE. FIGURE B-2 summarizes the high-frequency variances and correlation of the travel times as a function of upper or lower turning depth. These data have been determined from high-pass filtered, detided travel times as described in subsequent sections. The short, intermediate, and long ranges refered to in FIGURE B-2 refer to the three nominal ranges of paths in AMODE, namely 350, 410, and 660 km (TABLE D-2 gives the exact ranges). These high-frequency variances scale linearly with range, though this would not be expected for longer range transmissions (J. Colosi, personal communication).

TABLE B-1. AMODE Reciprocal Travel Time Time Series.

Path	Start Day (yearday)	End Day (yearday)	Record Length* (yeardays)	Resolved Ray† Arrivals
1←→2	80	275	195	10
1←→3	80	275	195	13
1←→4	80	275	195	16
1←→5a	80	140	60	14
1←→5b	165	275	110	12
1←→6	80	275	195	9
2←→3	80	350	270	8
2←→4	86	250	164	10
2←→5a	80	140	60	14
2←→5b	165	350	185	15
2←→6	80	350	270	9
3←→4	80	290	210	8
3←→5a	80	140	60	13
3←→5b	165	290	125	10
3←→6	77	350	273	8
4←→5a	79	140	61	11
4←→5b	166	300	134	10
4←→6	77	300	223	9
5a←→6	77	166	89	10
5b←→6	167	430	263	10

*This is the Record Length of good data; the AMODE instruments continued to receive until long after the acoustic sources faded for lack of energy. For some paths, the time series of one-way travel times (i.e. without demanding a reciprocal time series) is significantly longer than the times indicated here.
†Not all Resolved Ray Arrivals are present for the entire time series.

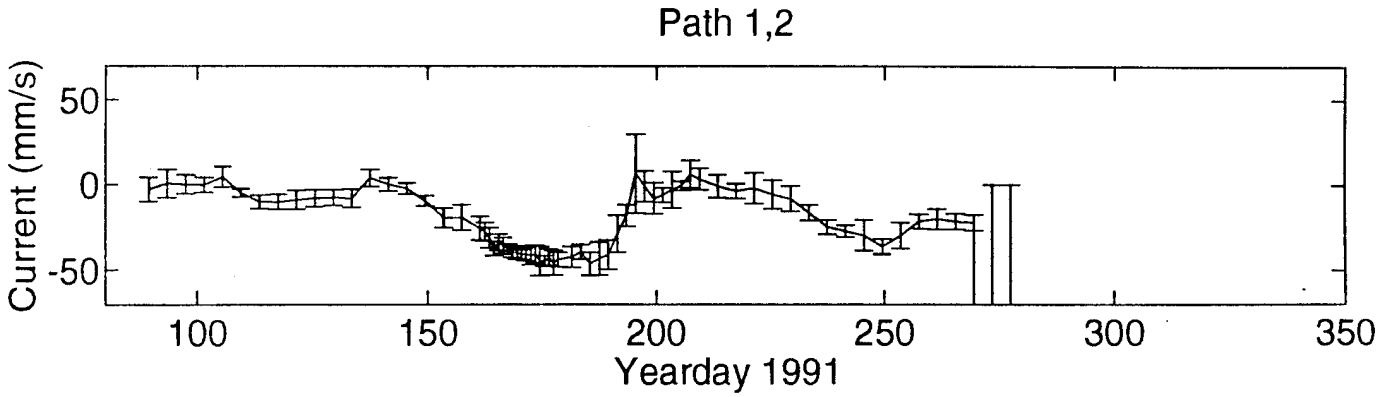
Path 1,2
Current (mm/s)
50
0
-50
100
150
200
250
300
350
Yearday 1991

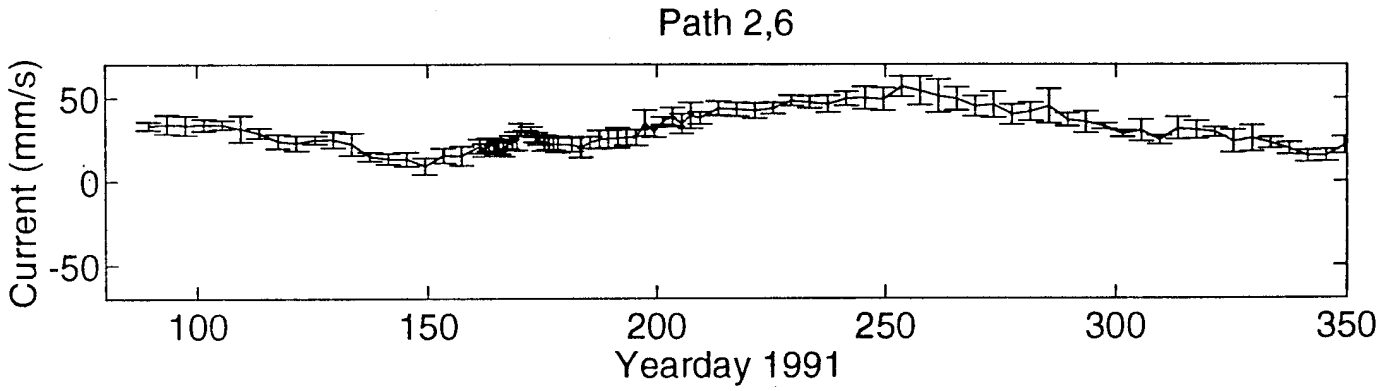
Path 2,6
Current (mm/s)
50
0
-50
100
150
200
250
300
350
Yearday 1991

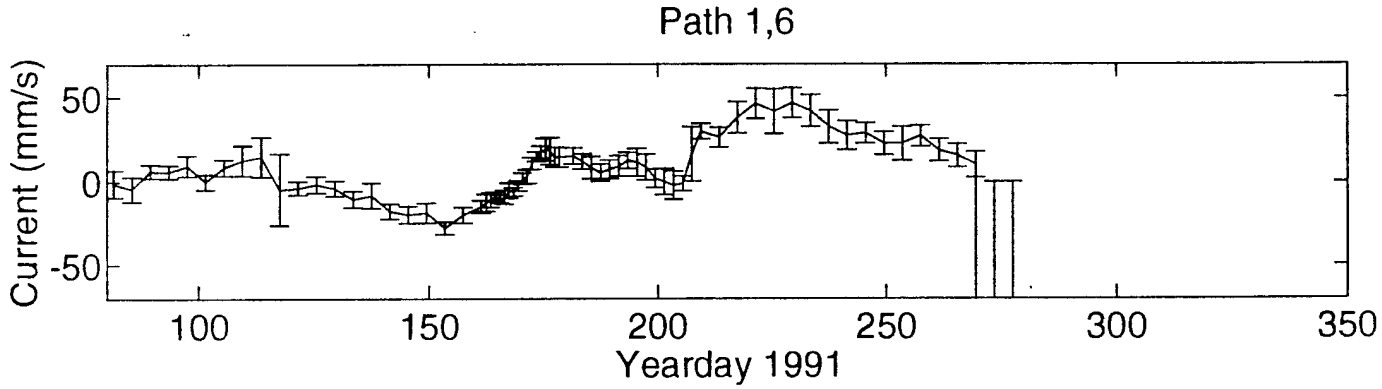
Path 1,6
Current (mm/s)
50
0
-50
100
150
200
250
300
350
Yearday 1991

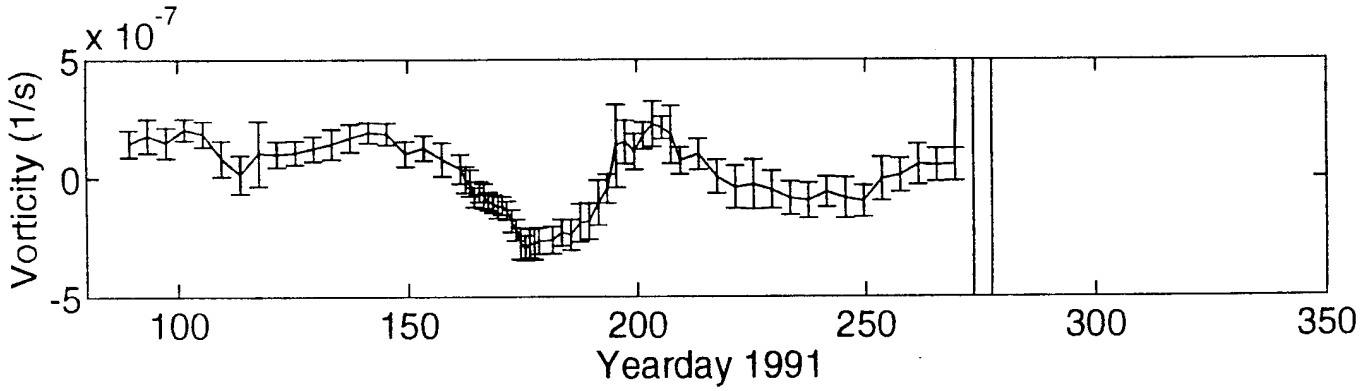
x 10^-7
Vorticity (1/s)
5
0
-5
100
150
200
250
300
350
Yearday 1991

FIGURE B-1a

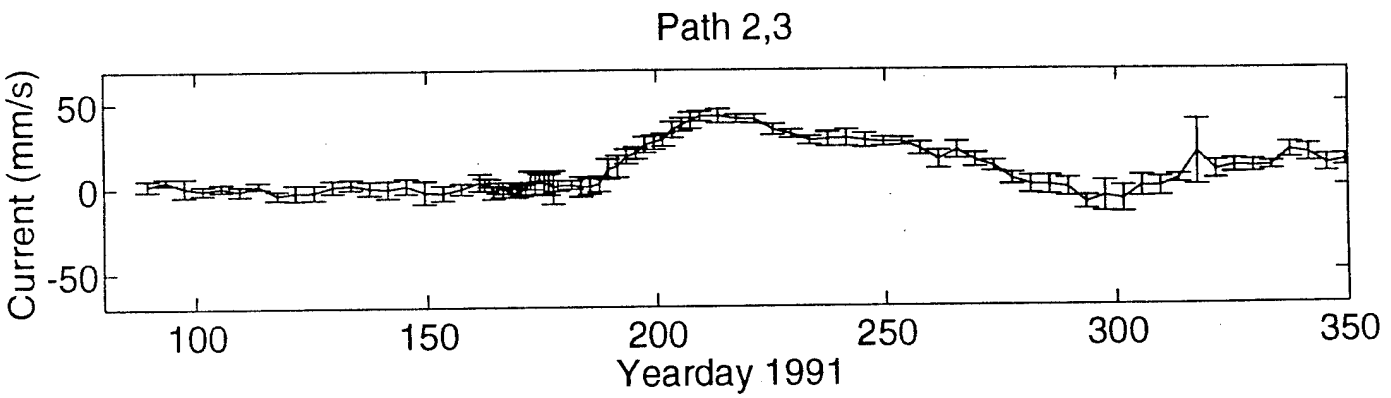
Path 2,3
Current (mm/s)
50
0
-50
100
150
200
250
300
350
Yearday 1991

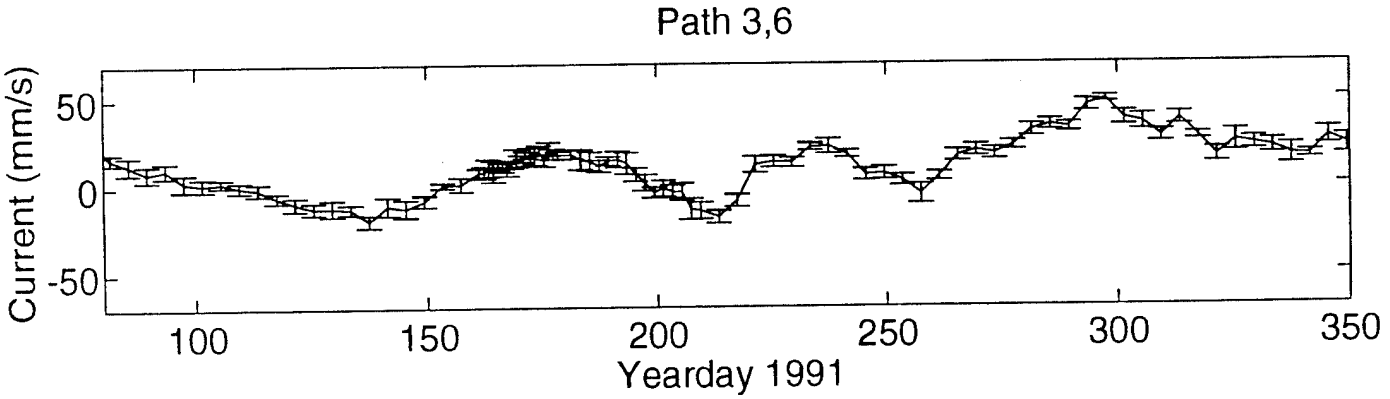
Path 3,6
Current (mm/s)
50
0
-50
100
150
200
250
300
350
Yearday 1991

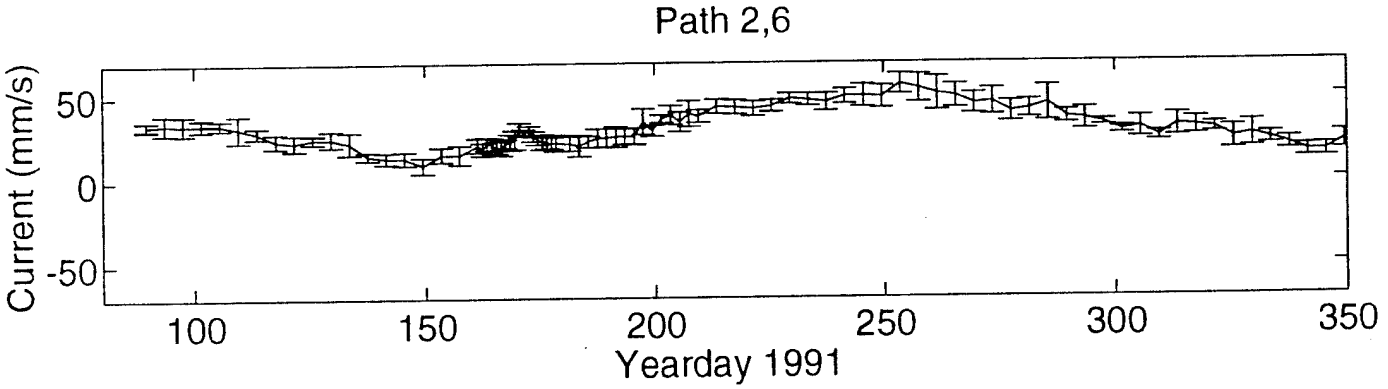
Path 2,6
Current (mm/s)
50
0
-50
100
150
200
250
300
350
Yearday 1991

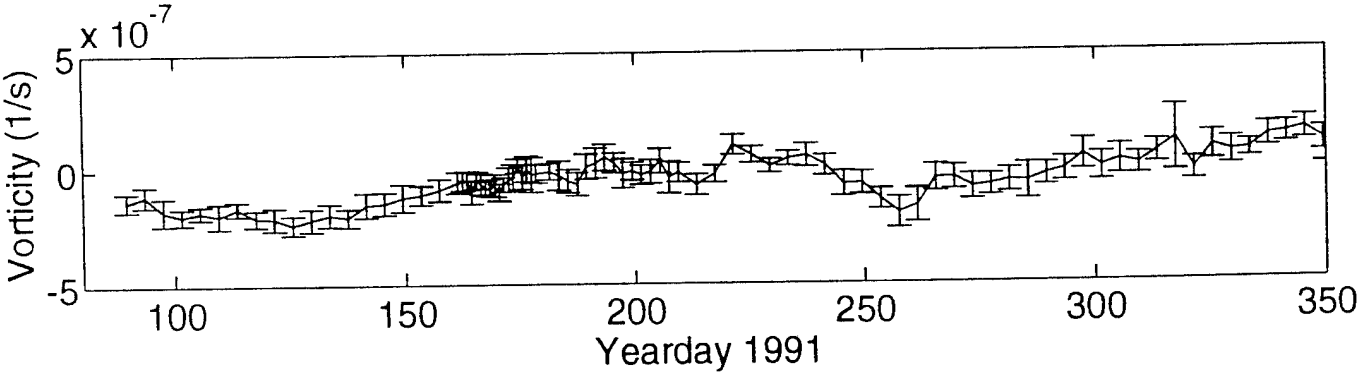
x 10^-7
Vorticity (1/s)
5
0
-5
100
150
200
250
300
350
Yearday 1991

FIGURE B-1b

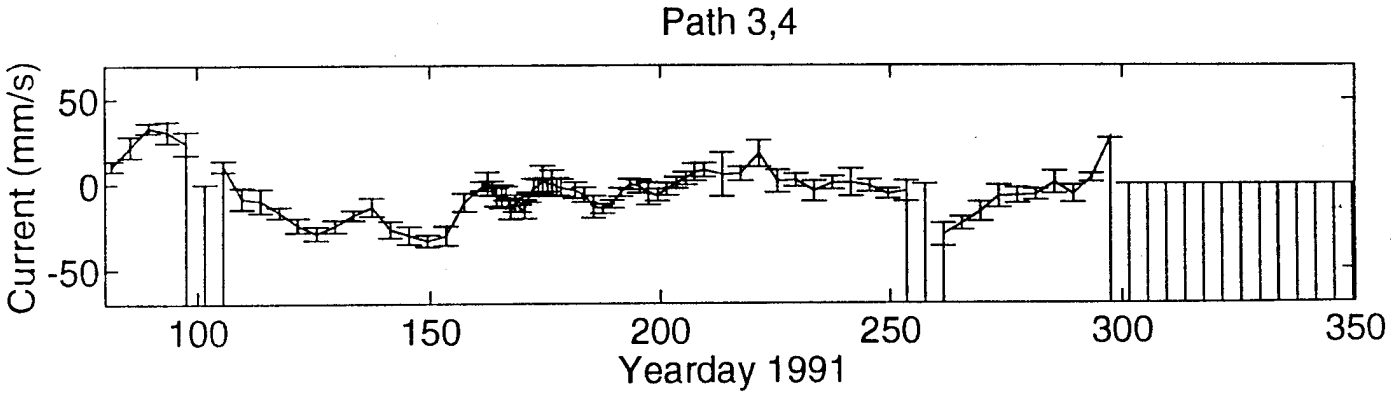
Path 3,4
Current (mm/s)
50
0
-50
100
150
200
250
300
350
Yearday 1991

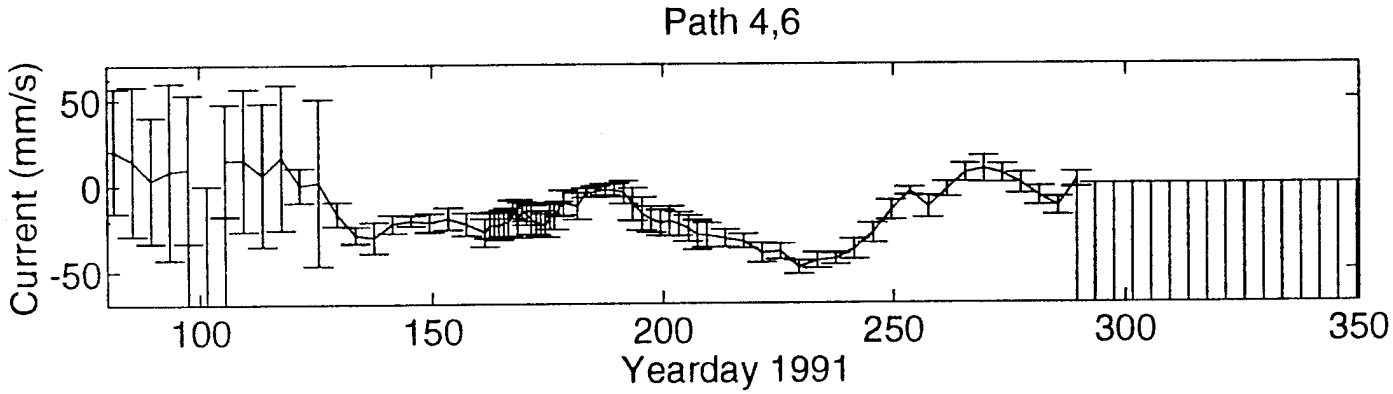
Path 4,6
Current (mm/s)
50
0
-50
100
150
200
250
300
350
Yearday 1991

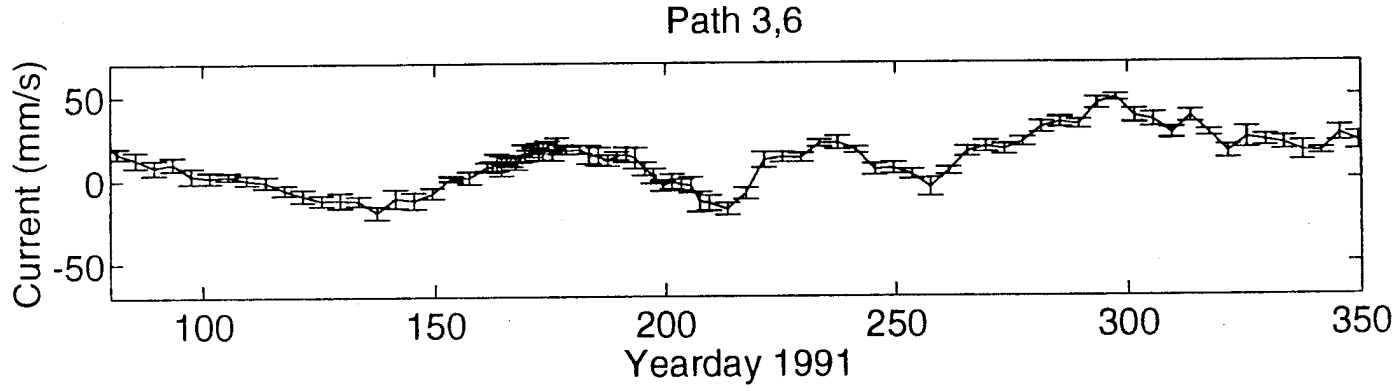
Path 3,6
Current (mm/s)
50
0
-50
100
150
200
250
300
350
Yearday 1991

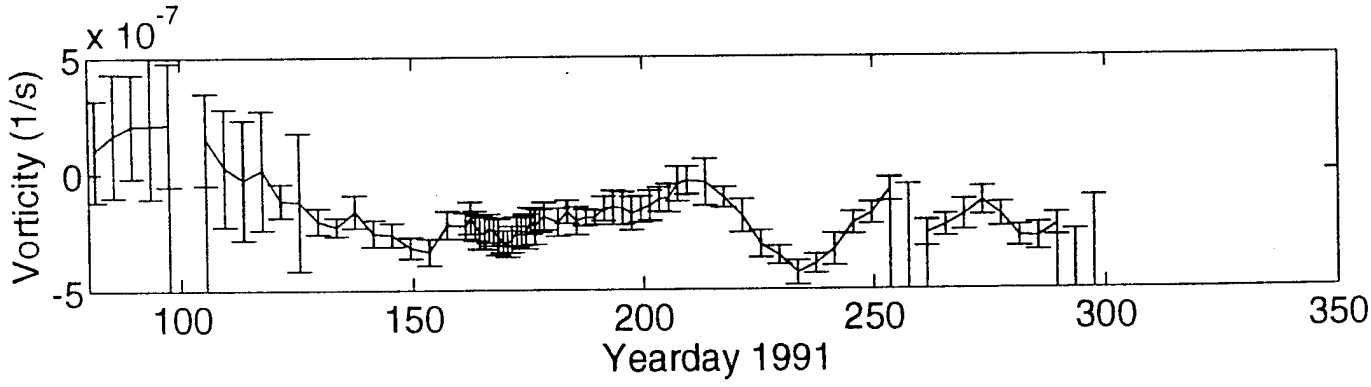
x 10^-7
Vorticity (1/s)
5
0
-5
100
150
200
250
300
350
Yearday 1991

FIGURE B-1c

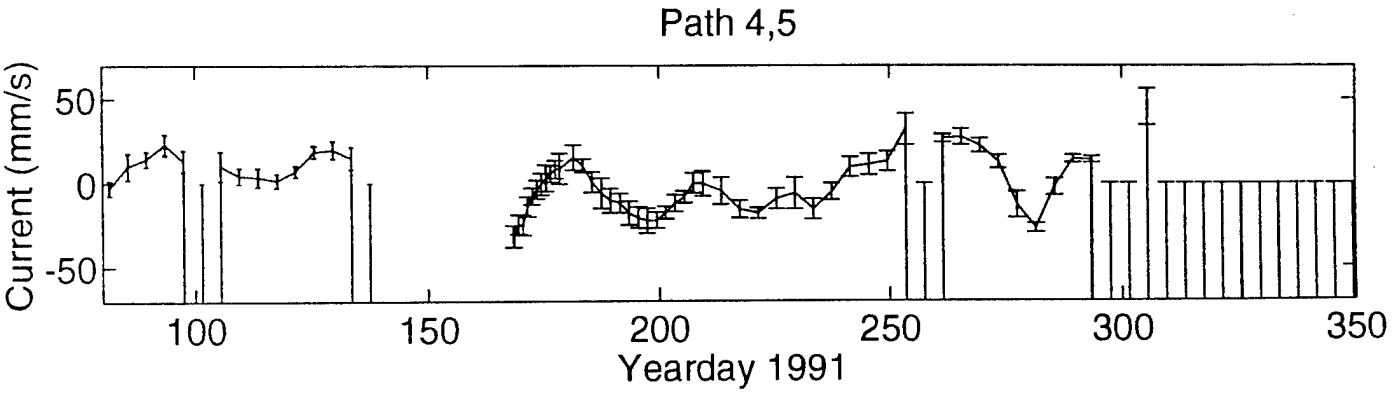
Path 4,5
Current (mm/s)
50
0
-50
100
150
200
250
300
350
Yearday 1991

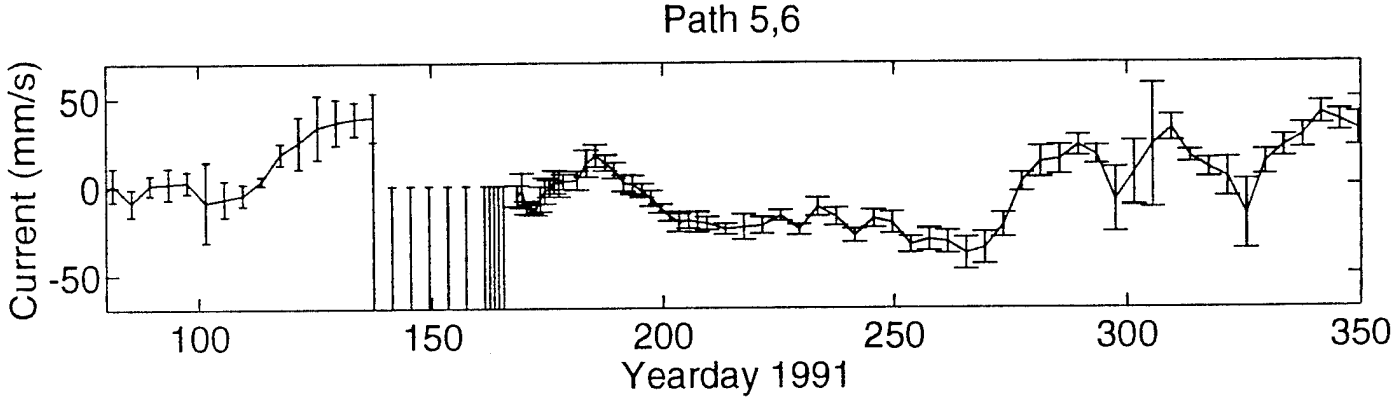
Path 5,6
Current (mm/s)
50
0
-50
100
150
200
250
300
350
Yearday 1991

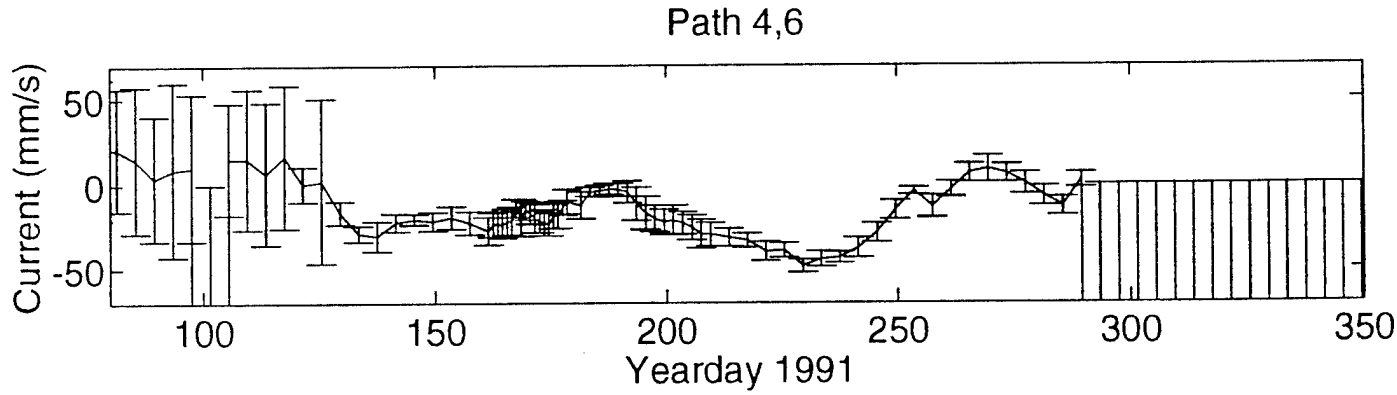
Path 4,6
Current (mm/s)
50
0
-50
100
150
200
250
300
350
Yearday 1991

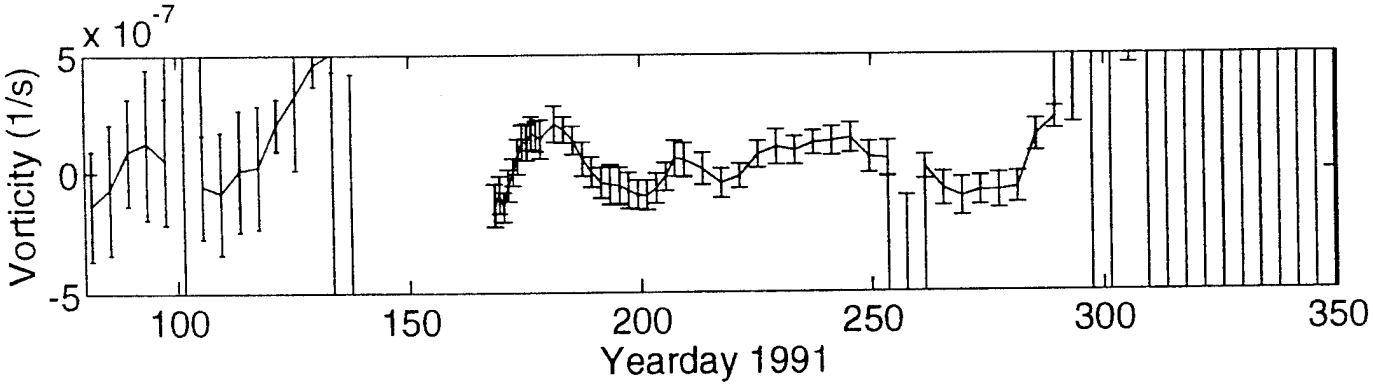
x 10^-7
Vorticity (1/s)
5
0
-5
100
150
200
250
300
350
Yearday 1991

FIGURE B-1d

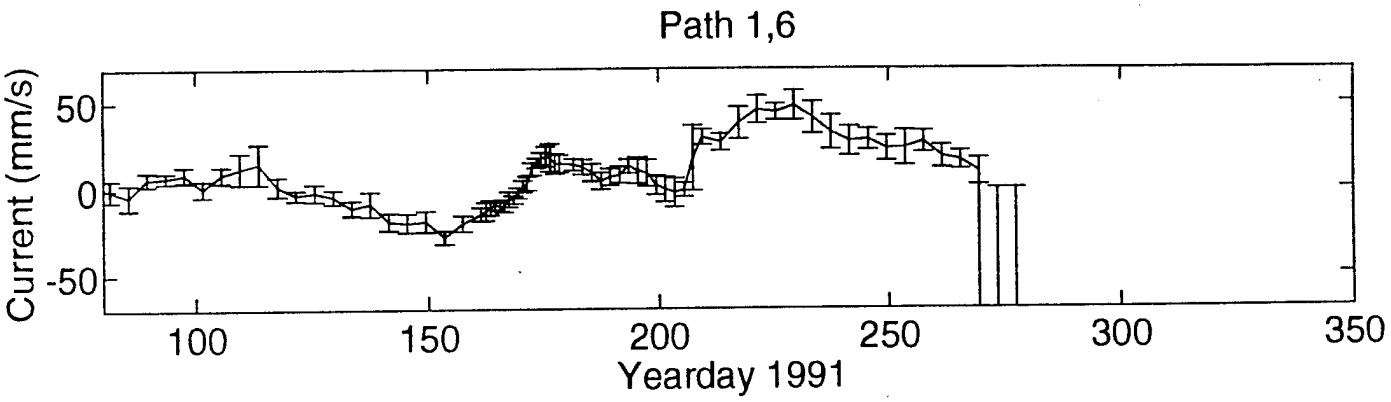
Path 1,6
Current (mm/s)
50
0
-50
100
150
200
250
300
350
Yearday 1991

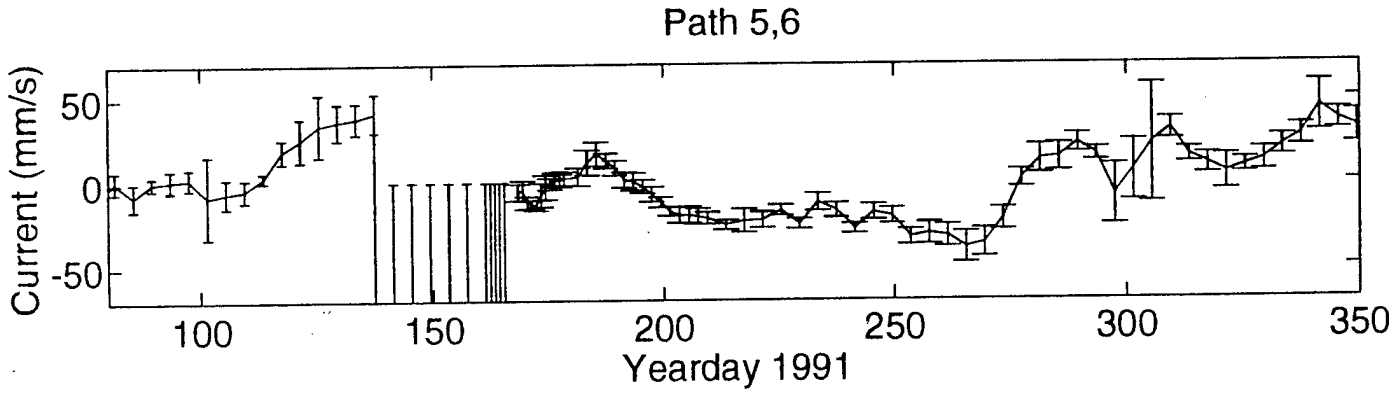
Path 5,6
Current (mm/s)
50
0
-50
100
150
200
250
300
350
Yearday 1991

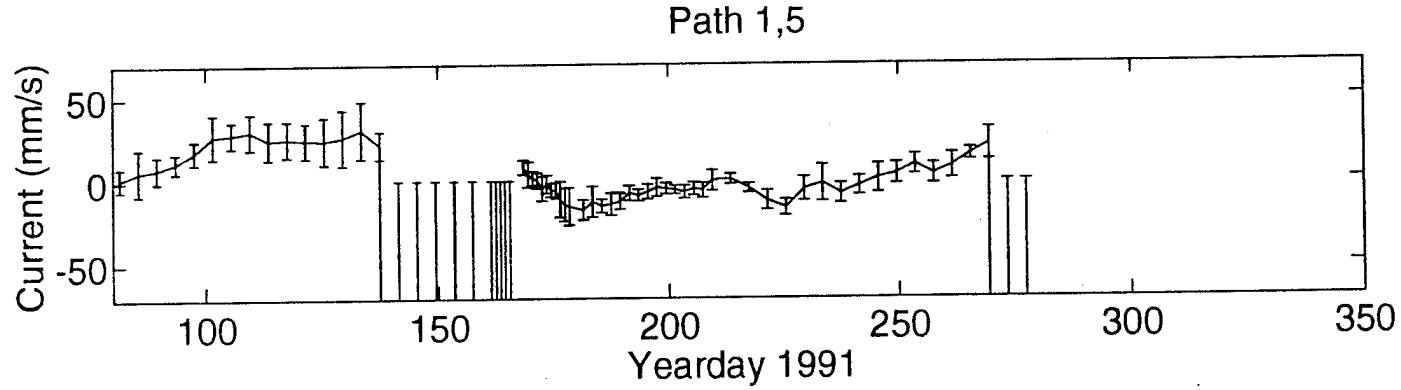
Path 1,5
Current (mm/s)
50
0
-50
100
150
200
250
300
350
Yearday 1991

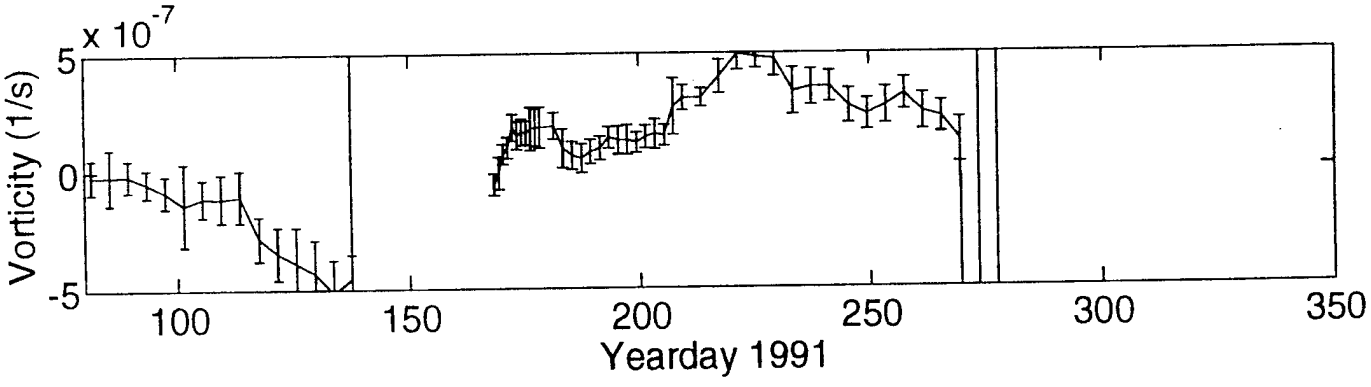
x 10^-7
Vorticity (1/s)
5
0
-5
100
150
200
250
300
350
Yearday 1991

FIGURE B-1e

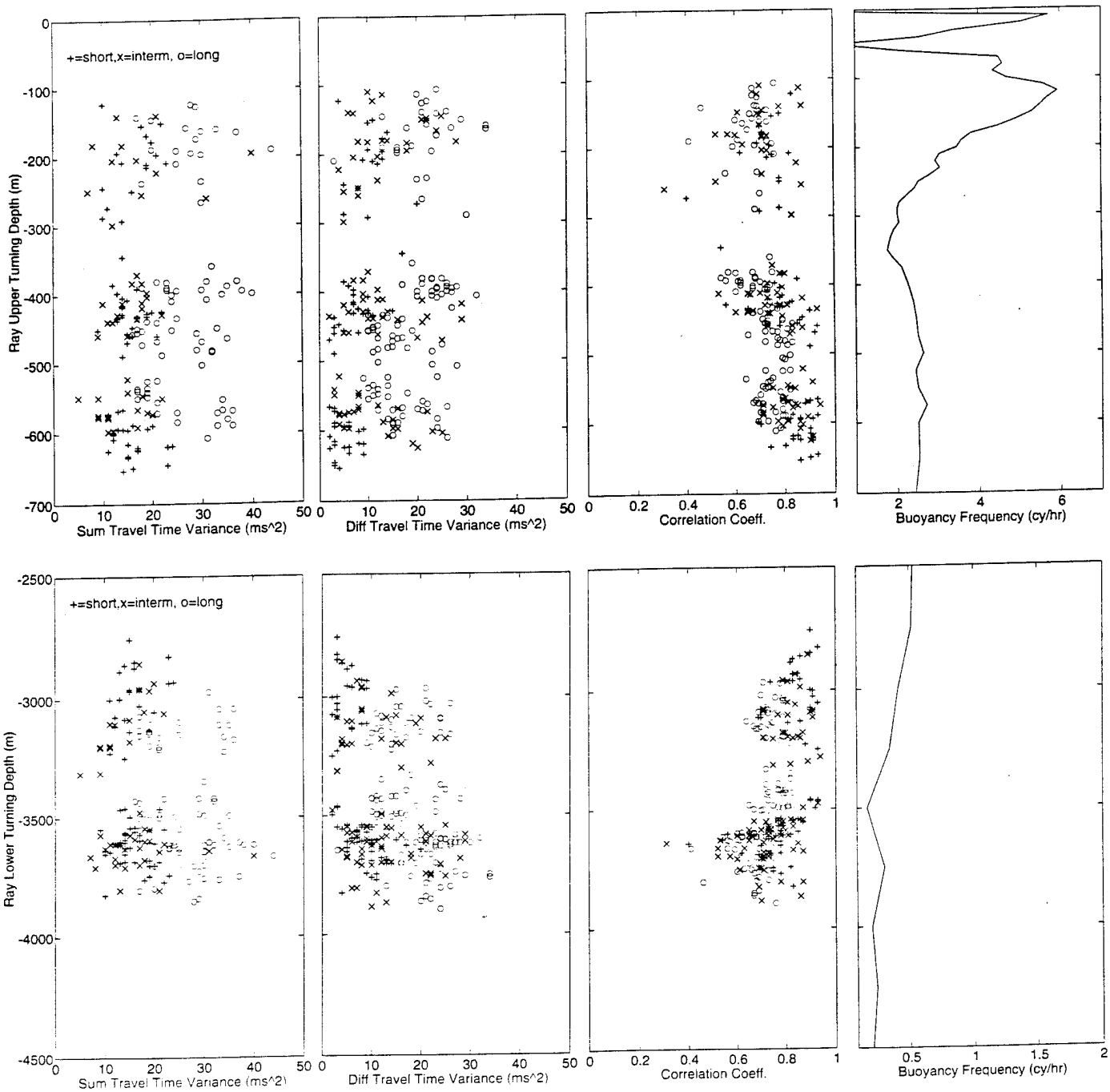
+=short,x=interm, o=long
Ray Upper Turning Depth (m)
Sum Travel Time Variance (ms^2)
Diff Travel Time Variance (ms^2)
Correlation Coeff.
Buoyancy Frequency (cy/hr)
+=short,x=interm, o=long
Ray Lower Turning Depth (m)
Sum Travel Time Variance (ms^2)
Diff Travel Time Variance (ms^2)
Correlation Coeff.
Buoyancy Frequency (cy/hr)

FIGURE B-2

C. MOORING MOTION AND CLOCK CORRECTIONS

Bruce Howe generated the time series of mooring motion, clock drift, and mooring tilt which are used to correct the travel times. The procedure by which these time series are used to make the corrections is given in Bruce Cornuelle's dissertation (1983). The motion of the moorings is determined through a tracking system which employs four acoustic transponders deployed on the sea floor around each mooring. The clock drift is determined using an highly accurate rubidium frequency standard which is used regularly to monitor the frequency changes in the AVATAR crystal oscillators (a rubidium clock draws too much power for continual use). Timing is checked by pinging the moorings at deployment and recovery, while they are in the water; the ping time recorded by the AVATARS is checked against GPS timing (see Worcester and Dushaw, 1993).

For deriving travel times of reciprocal transmissions, the travel times to the receiving hydrophones must be corrected to the depth of the acoustic source on the receiving mooring. For this reason, and to properly apply the corrections for mooring tilt, the corrections are dependent on the ray arrival angle. Failure to take this into account leads to biases of 4–9 ms (which are unacceptable) in the difference of reciprocal ray travel times.

FIGURE C-1 shows time series of clock corrections, mooring motion corrections, uncorrected travel times, and corrected travel times for the path from mooring 1 to mooring 2. The corrections and travel times are for the seventh resolved ray arrival (clock corrections identical for all rays). The top two panels of this figure show the corrections for each mooring separately (X's refer to one mooring, O's to the other). FIGURE C-2 shows a small section of the time series in FIGURE C-1.

FIGURE C-3 shows time series of clock corrections, mooring motion corrections, uncorrected travel times, and corrected travel times for path from mooring 1 to mooring 4. The corrections and travel times are for the seventh resolved ray arrival (clock corrections identical for all rays). The top two panels of this figure show the corrections for each mooring separately (X's refer to one mooring, O's to the other). Mooring 4 had particularly energetic motion during the experiment.

The travel time net uncertainties are a combination of timing uncertainty, mooring positioning uncertainty, absolute position uncertainty, and the uncertainty inherent to deriving a travel time from an acoustic pulse of finite width. The uncertainties in the positioning are dominant, but these are only one millisecond.

The travel time uncertainty associated with the signal processing only is:

$$\sigma = (2\pi \times \mathrm{SNR} \times (\text{RMS bandwidth}))^{-1}$$

The rms bandwidth for the AMODE transmissions is 27 Hz. The signal-to-noise ratios are generally greater than 10, which gives uncertainties less than 0.5 ms.

As explained by Worcester and Dushaw (1993), receptions from all moorings at mooring 2 were occasionally shifted by an exact integer number of seconds due to a failing chip in the mooring 2 electronics. This is not a problem for the time series once

the shifts have been taken into account. TABLE C-1 shows the offsets that were added to the time series of travel times at mooring 2.

TABLE C-1. Offsets for Mooring 2 (Receiver) Travel-Time Time Series.

Source #	Timeframe (yearday 1991)	Offset (s)
1 & 3	0–197.87	0
	199.0–199.125	1
	199.25–221.37	2
	221.5–221.625	3
	221.87–end	4
4 & 5	0–197.87	0
	199.0–199.25	1
	199.37–221.37	2
	221.5–end	4
6	0–197.87	0
	199.0–217.87	2
	221.0–end	4

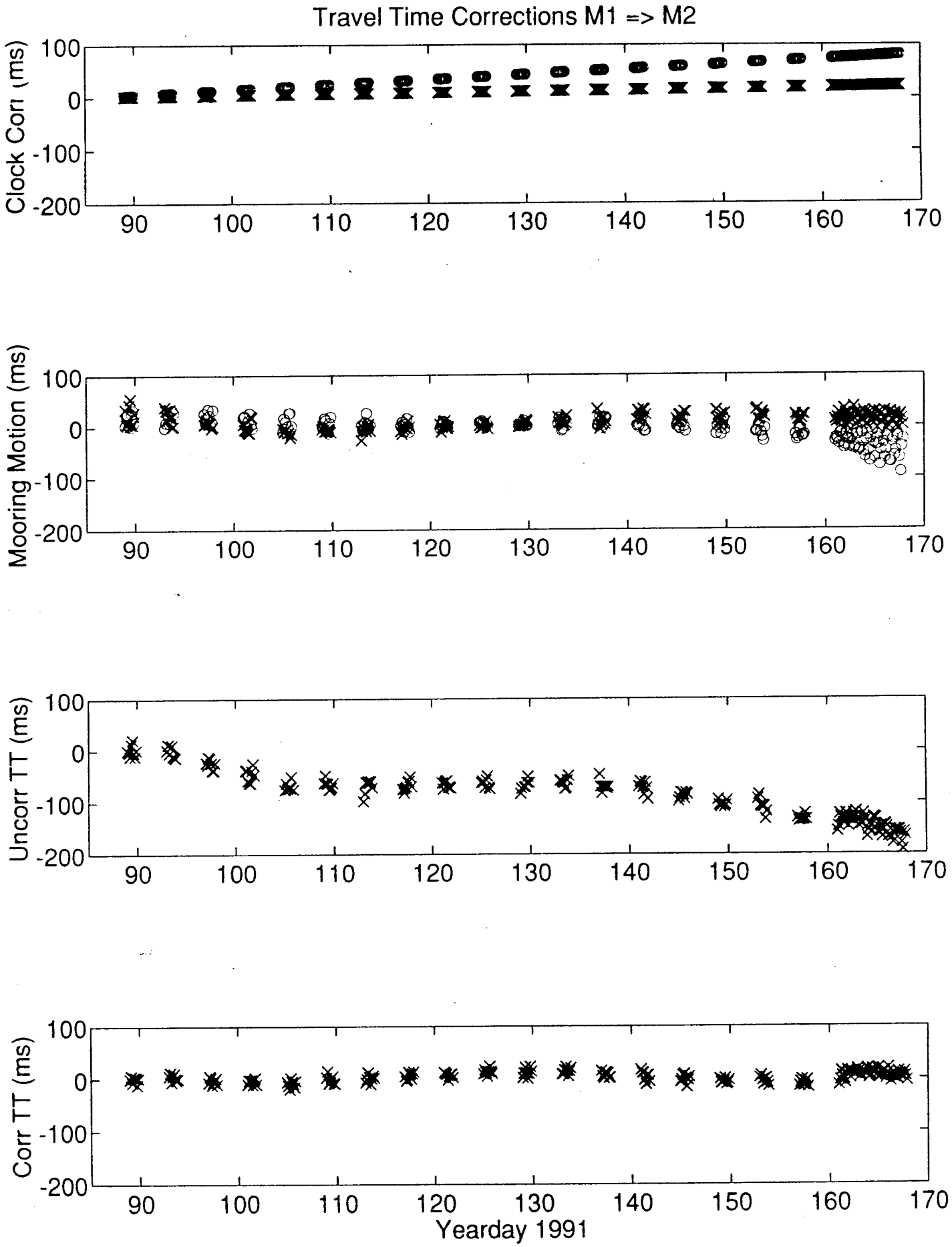
Travel Time Corrections M1 => M2
Clock Corr (ms)
Mooring Motion (ms)
Uncorr TT (ms)
Corr TT (ms)
100
0
-100
-200
90
100
110
120
130
140
150
160
170
Yearday 1991

FIGURE C-1

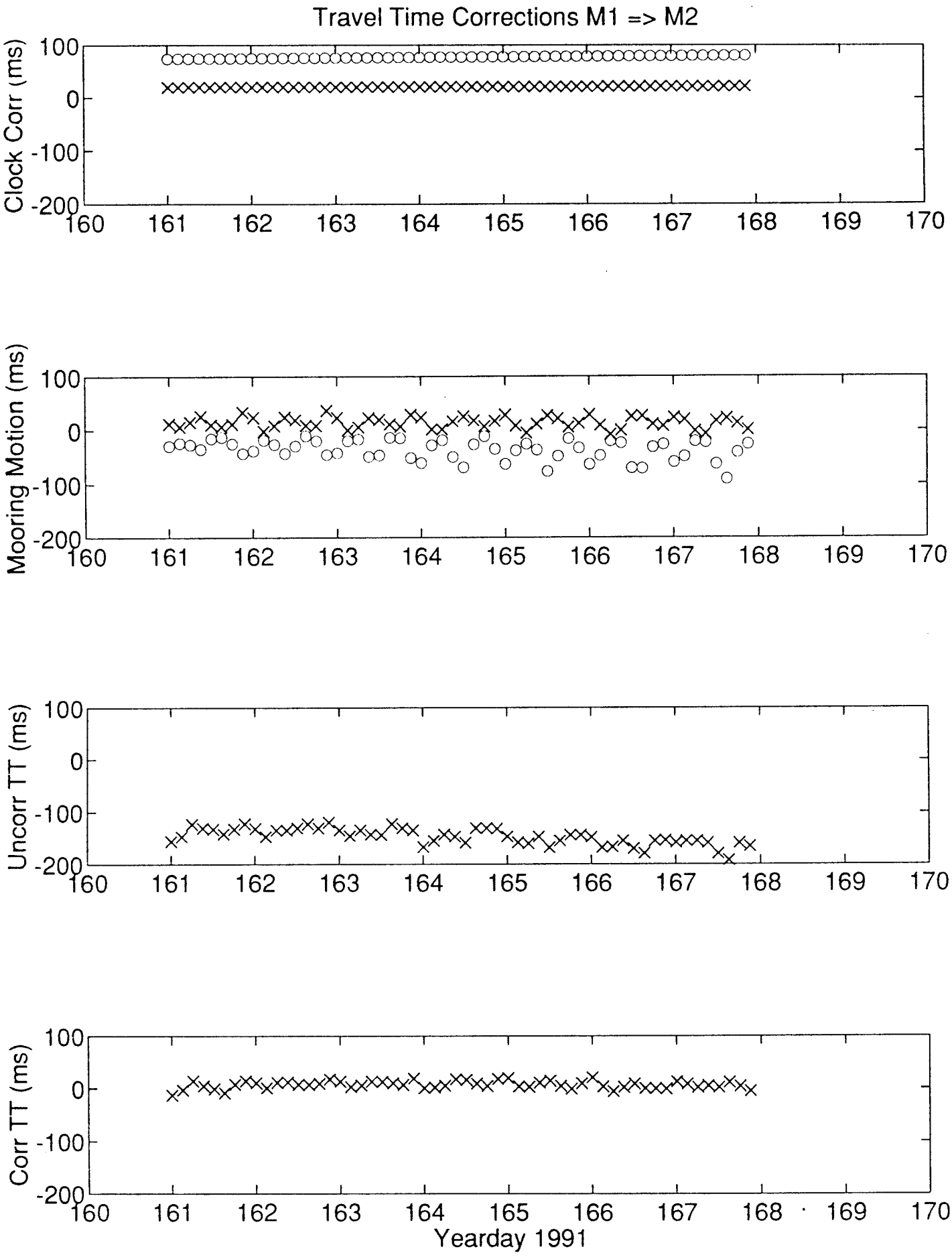
Travel Time Corrections M1 => M2
Clock Corr (ms)
Mooring Motion (ms)
Uncorr TT (ms)
Corr TT (ms)
100
0
-100
-200
160
161
162
163
164
165
166
167
168
169
170
Yearday 1991

FIGURE C-2

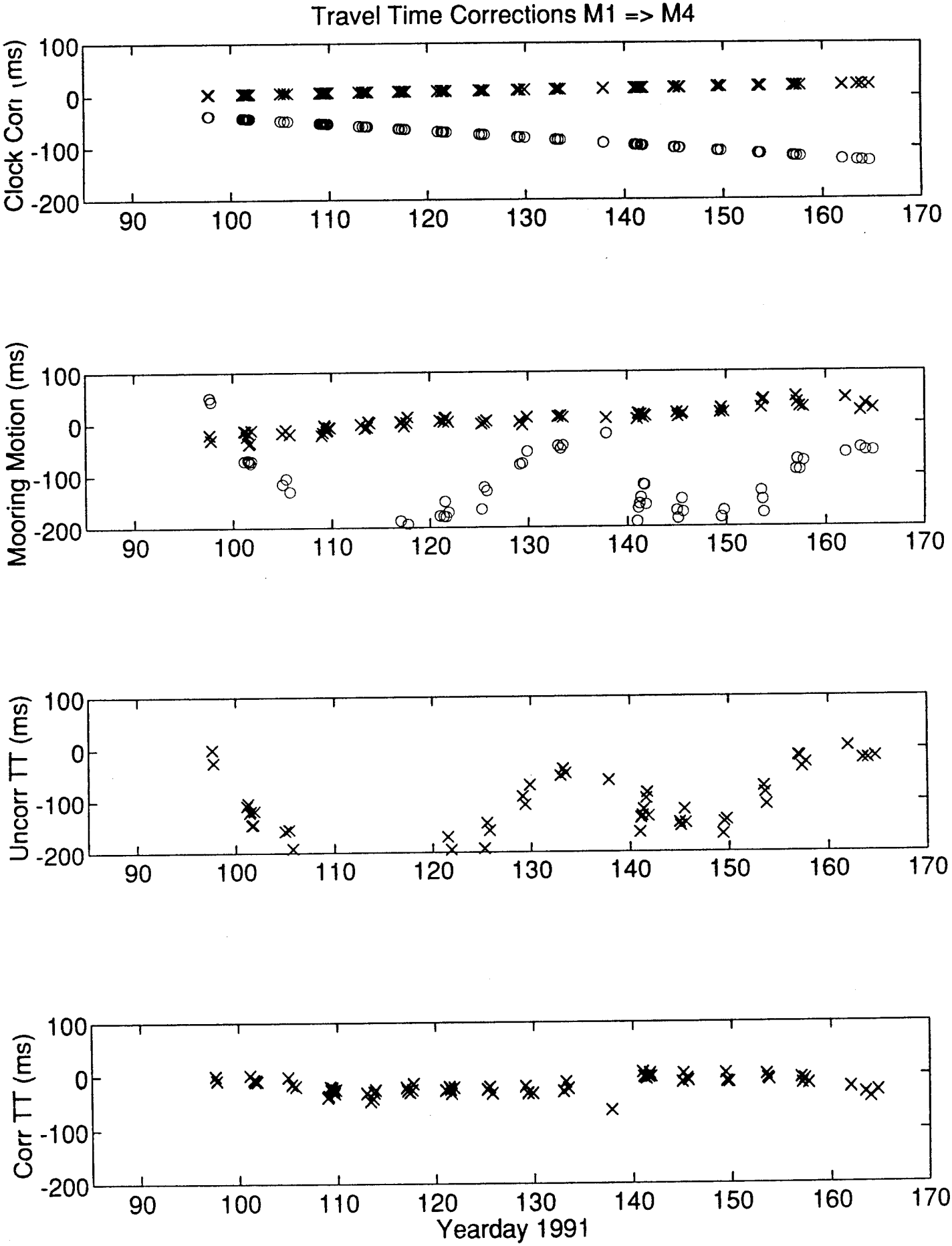
Travel Time Corrections M1 => M4
Clock Corr (ms)
Mooring Motion (ms)
Uncorr TT (ms)
Corr TT (ms)
100
0
-100
-200
90
100
110
120
130
140
150
160
170
Yearday 1991

FIGURE C-3

D. ABSOLUTE MOORING POSITIONS

Since the most recent data report on the AMODE data set (Worcester and Dushaw 1993), Bruce Howe has revised the positions of transceiver moorings slightly. The change was to set the reference position used for the mooring motion time series equal to the locations of the mooring anchors. The idea was that using this reference would reduce the chance (unlikely in any case) that the derivation of mooring positioning would be affected by the nonlinear inverse procedures used on the acoustic transponder data used to track the mooring motion.

The corrections for mooring motion correct the locations of the moorings to these fixed positions. TABLE D-1 shows the AMODE mooring positions and their uncertainties. TABLE D-2 shows the ranges between the AMODE moorings (calculated from the positions of TABLE D-1).

TABLE D-1. AMODE Positions and Their Uncertainties.

Mooring	Latitude (north)	Uncert. (m)	Longitude (west)	Uncert. (m)	Source Depth (m)	No. of Array Elements
1	27°43.2329' 27.720549°	0.6	64°31.1107' 64.518511°	0.9	985	4
2	24°20.0499' 24.334164°	0.5	62°53.3477' 62.889129°	0.8	996	4
3	21°53.9489' 21.899142°	0.5	65°49.8894' 65.831490°	0.8	1003	6
4	23°38.2722' 23.637869°	0.5	69°21.5593' 69.359321°	0.8	1008	4
5a	27°20.9623' 27.349372°	0.6	68°42.3019' 68.705032°	0.9	1014	6
5b	27°21.1214' 27.352024°	0.6	68°43.5229' 68.725381°	0.9	979	4
6	25°00.0178' 25.000296°	0.5	66°15.0826' 66.251377°	0.8	992	6
7 (Bermuda)	31°54.924' 31.915400°	-	64°10.306' 64.171767°	-	956	0

TABLE D-2. Ranges Between AMODE Moorings in Kilometers

mooring #	1	2	3	4	5a	5b	6
1	-	409.072	658.345	663.725	415.568	417.534	347.474
2	-	-	404.398	662.862	671.823	673.732	348.223
3	-	-	-	410.258	670.087	671.246	346.123
4	-	-	-	-	416.389	416.361	349.675
5a	-	-	-	-	-	-	357.609
5b	-	-	-	-	-	-	359.218

E. ABSOLUTE TRAVEL TIMES

The AMODE receivers record travel time as "T relative," to which the known offset and various instrumental delays and corrections must be added to obtain the absolute ray travel time from acoustic source to receiver. The mooring motion and clock corrections that are applied to the data account for some of these delays. In this section, the factors to be added to the post-mooring/clock corrected travel times to make them absolute travel times are described.

From a memorandum by Peter Worcester dated November 1993 the absolute travel times are given as (with a sign change for "delta t clock" to reflect current convention)

TTabs = { (T start rec.) + 0.001 s + (TT rel.) -
(delta t clock) - (delta t rec. delay)}

- { (T start trans.) + 0.001 s -
(delta t clock) - (delta t src delay) }

- (T sequence)

The mooring motion and clock corrections include the clock corrections and the source/receiver delays (which are, according to a memoradum from B. Howe dated Oct. 12, 1989, 13 ms and 7.4 ms, respectively), so that

TTabs = (T APL) + (T start rec.) - (T start trans.) - (T sequence)

= (T APL) + (344 (247 for src 6), 385, 556 s) - 97 (0 for src 6) s - 24.564 s

= (T APL) + (222.436, 263.436, 434.436 s)

n<->6	n<->m	n<->m
	n≠m+2	n=m+2
	n≠m+3	n=m+3

where "T APL" are the travel times corrected for mooring motion, clock corrections, and source/receiver delays; (n,m) refer to transceiver numbers; and "n<->m" means "for transmissions between transceivers n and m."

The uncertainty of the absolute travel times, including the contributions of mooring motion and clock correction uncertainties, is 1 ms. This value is much less than the internal wave variability, however – the travel time uncertainties are dominated by physical processes over which we have no control. The measurement uncertainties are included in the data files in NODC format to be described in section AA.

F. FINAL CUTOFF TRAVEL TIMES: Paths 1→3 and 3→1

The "final cutoff" travel time has proved to be an important datum for resolving sound speed variability near the sound channel axis. This was true for the 1987 Reciprocal Tomography Experiment data, and for the 1988–1989 Greenland Sea Tomography Experiment data. This travel time is defined as the time of the latest arriving acoustic energy. The final portion (final few seconds) of the acoustic arrival pattern is quite complicated with unstable amplitudes, perhaps caused by a complicated, chaotic interaction of the acoustic modes with the internal wave field. The "final cutoff" time may perhaps be best associated with the travel time of the gravest acoustic mode; this travel time is usually much more stable than the travel time for the final, largest peak. (But this was not the case for the Greenland Sea data when individual mode arrivals were resolved.) For the purposes of inversions, the "final cutoff" travel time is associated with the latest arriving ray predicted by raytracing; this is NOT generally the ray with the smallest angle at the source or receiver.

There are, however, many unresolved issues associated with this travel time. The ray or mode sampling that should be associated with this travel time in an inversion is unknown. The physical interpretation of this travel time is ill defined, at best. Further, the internal wave effects on this travel time, both temporal variation and possible biases, can be significant. In particular, the 1989 SLICE experiment showed that for a receiver located off of the sound channel axis this travel time can be significantly biased because of the diffusion of acoustic energy away from the sound channel axis by the internal wave field.

The receiving hydrophones of AMODE were located at about 1000 m depth, while the sound channel axis was located at about 1200 m depth. Thus, it is likely that for this experiment the final cutoff travel times would be affected (biased) by the internal wave field. For some applications, such as examination of tidal variability or eddy variability, the internal wave effects, such as a time independent bias, may be inconsequential. However, the principle applied to these data should be *caveat emptor*, since the full nature of these travel times and their response to oceanic phenomena is poorly understood. Typically these data are assigned large uncertainty to account for our lack of understanding of them. Even with large uncertainty, these data still are an important (if not the only) constraint in determining the sound speed variability near the sound channel axis.

The procedure for deriving the final cutoff travel times is not routine as yet, since the definition of the "final cutoff" requires significant "hands on" interpretation (and quite a lot of disk space since the complete, continuous receptions are required). Only a preliminary determination of the final cutoff travel times for the path between moorings 1 and 3 has been made to date, because the derivation of the time series is rather laborious and time consuming. The importance of these data to resolution in the inversion argues for the completion of this task, however.

For an acoustic reception at a single hydrophone, the final cutoff is determined by the time at which the acoustic amplitude begins to increase (relative to a background rms level) as travel time decreases. The latter part of receptions on yeardays 161 and 162 are shown in FIGURE F-1 for transmissions from mooring 1 to mooring 3. Note that the

absolute travel times are found by adding 434.436 s, as described in section E. Each transmission has four receptions, one for each of the four hydrophones. The final cutoff travel time for each hydrophone is indicated by a vertical line, with the hydrophone number indicated by the height of an asterisk on that line (lowest asterisk is hydrophone 1). FIGURE F-2 shows the complete reception; it is identical to FIGURE F-1 otherwise. The arrival pattern reciprocal to that of FIGURE F-1, viz. receptions at mooring 1 from mooring 3, is shown in FIGURE F-3.

FIGURES F-4 (Path 1→3) and F-5 (Path 3→1) show nine-day time series of final cutoff travel times of the four hydrophones. The four travel times independently derived from the four hydrophones are generally consistent, and tidal variability is evident.

The final cutoff travel time used for the inversions is given as the average of the travel times from the four hydrophones (this procedure assumes zero arrival angle). The astute reader will notice that the final cutoff travel times for the four hydrophones are not always identical; oftentimes the time for one hydrophone is much different than that of the others. Travel times from single hydrophones that are inconsistent with the other three hydrophones are removed as outliers when the average is calculated. The complete time series of final cutoff travel times for the paths 1→3 and 3→1 are shown in FIGURE F-6. Outliers in this time series are evident. The high-frequency variability in the time series, evident by the rapid variation of travel time for the receptions on a particular day, is due to tidal or internal wave variability together with noise inherently introduced by the procedure to derive the time series. These time series should be compared with the ray travel times of section H.

With the two time series of reciprocal travel times, the sum (sound speed) and difference (current) travel times may be formed. The results from the RTE87 experiment have shown that it is possible to use the difference travel times calculated from these data as a measure of current. The sum and difference travel times are separated into low-frequency and high-frequency components by the average of travel times on each day. FIGURE F-7 shows the low-pass filtered difference and sum travel times. Both of these time series are similar to the results from the ray arrivals (section H); differences between the final cutoff time series and those from the ray travel times are likely caused by the depth dependence of the variability. FIGURES F-8 and F-9 show the high-pass filtered sum and difference travel times. Tidal variability is evident; the detided time series are shown in the second panel of these figures.

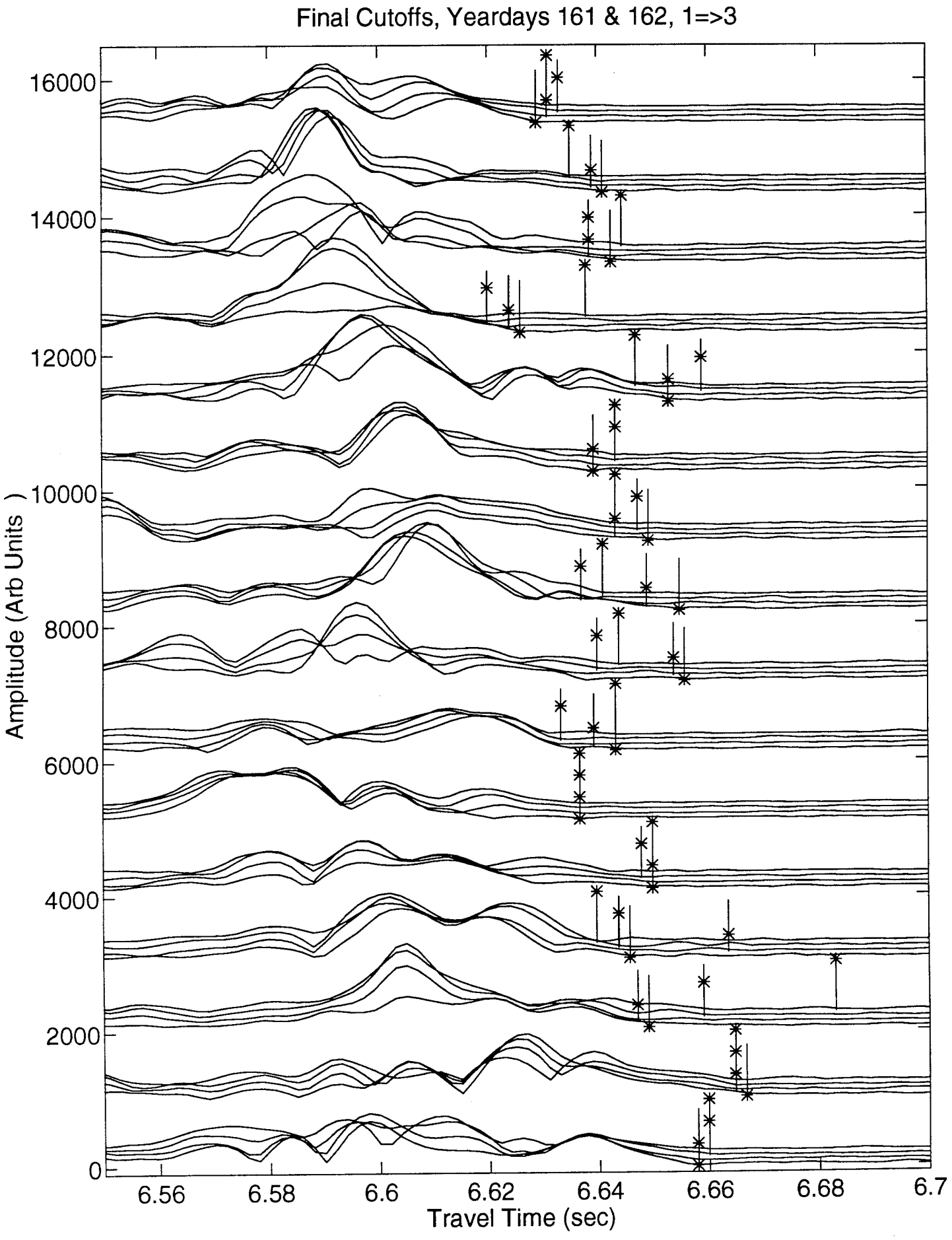
Final Cutoffs, Yeardays 161 & 162, 1=>3
16000
14000
12000
10000
8000
6000
4000
2000
0
Amplitude (Arb Units)
6.56
6.58
6.6
6.62
6.64
6.66
6.68
6.7
Travel Time (sec)

FIGURE F-1

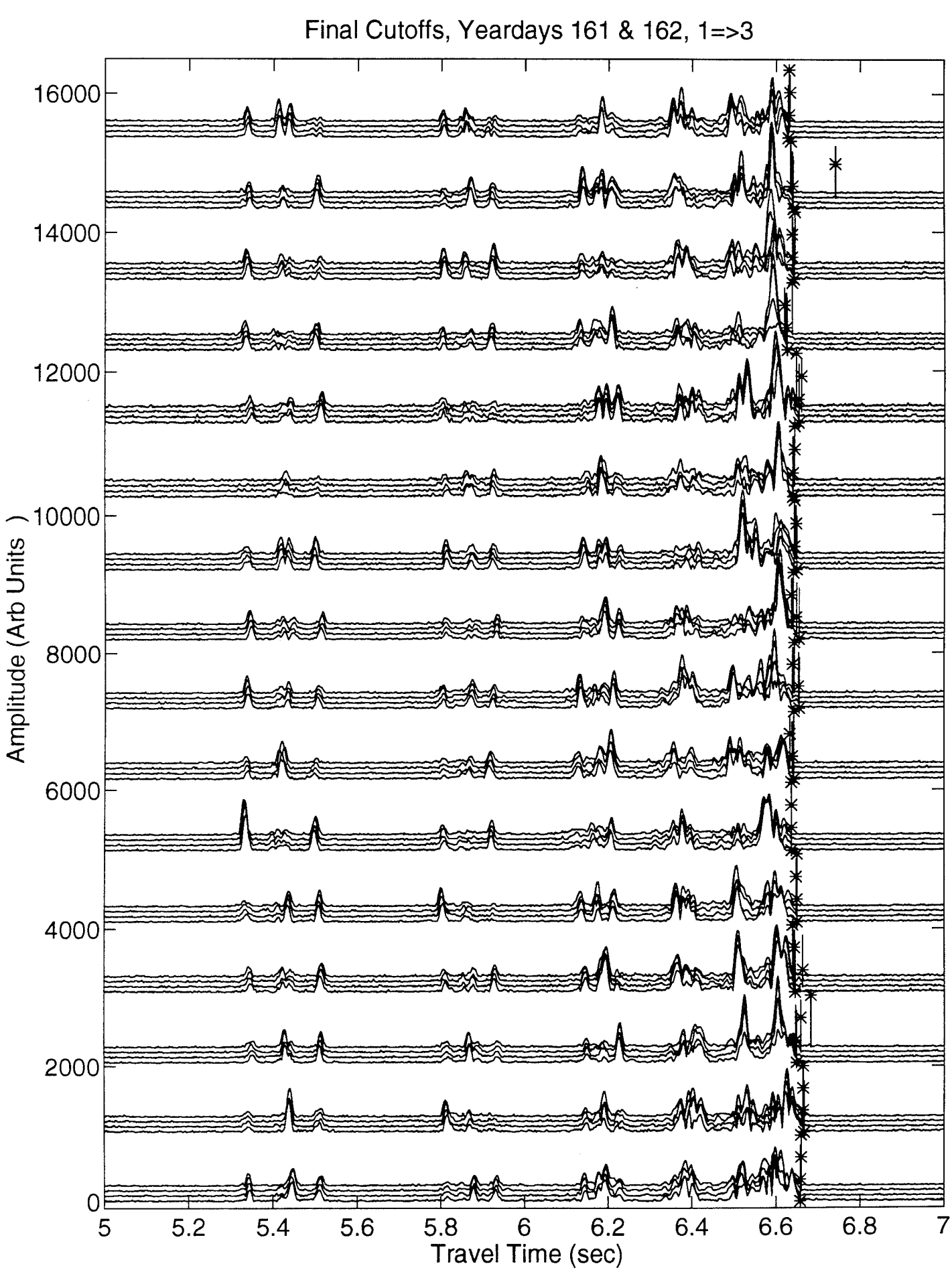
Final Cutoffs, Yeardays 161 & 162, 1=>3
Amplitude (Arb Units)
16000
14000
12000
10000
8000
6000
4000
2000
0
5
5.2
5.4
5.6
5.8
6
6.2
6.4
6.6
6.8
7
Travel Time (sec)

FIGURE F-2

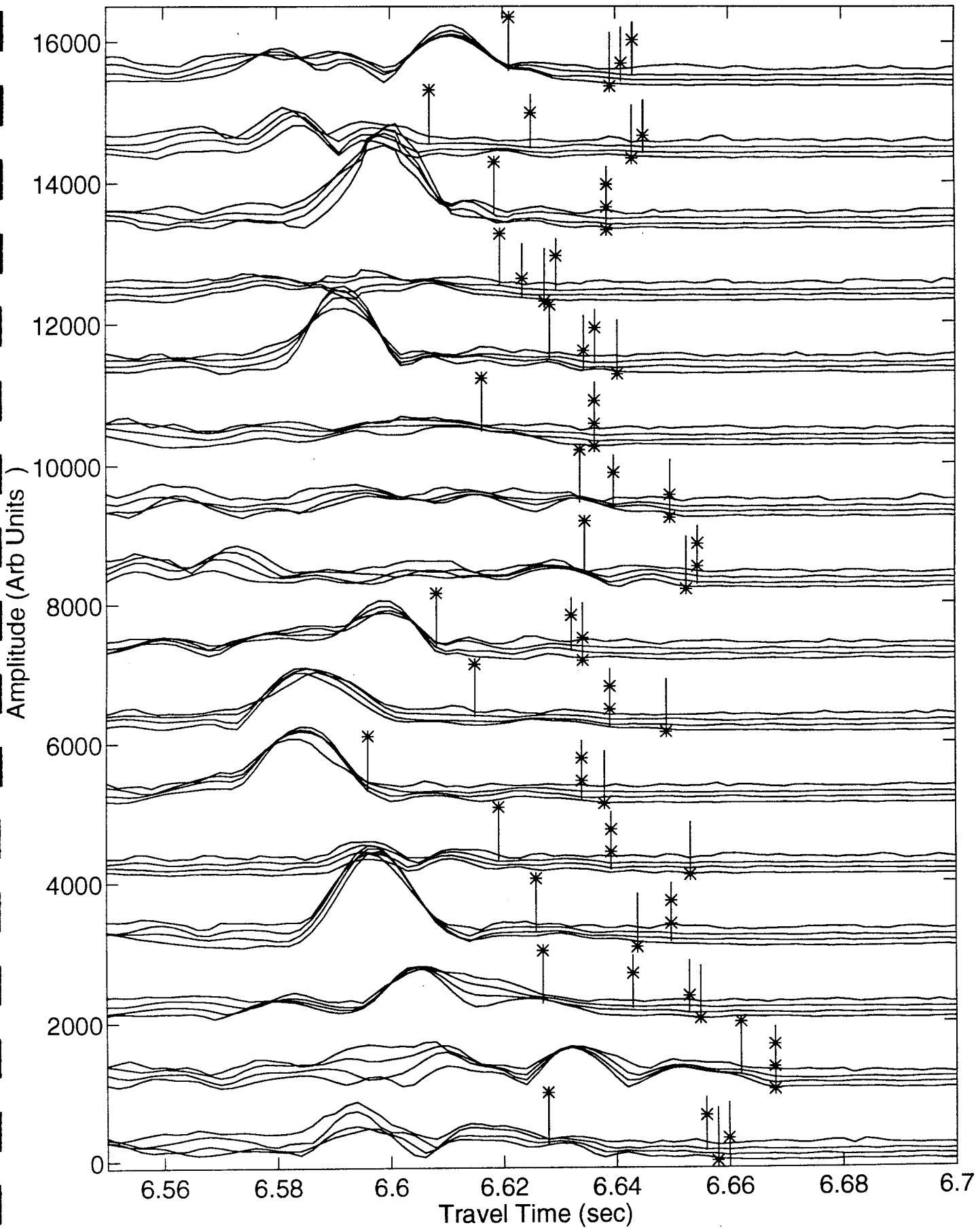
Final Cutoffs, Yeardays 161 & 162, 3=>1
16000
14000
12000
10000
8000
6000
4000
2000
0
Amplitude (Arb Units)
6.56
6.58
6.6
6.62
6.64
6.66
6.68
6.7
Travel Time (sec)

FIGURE F-3

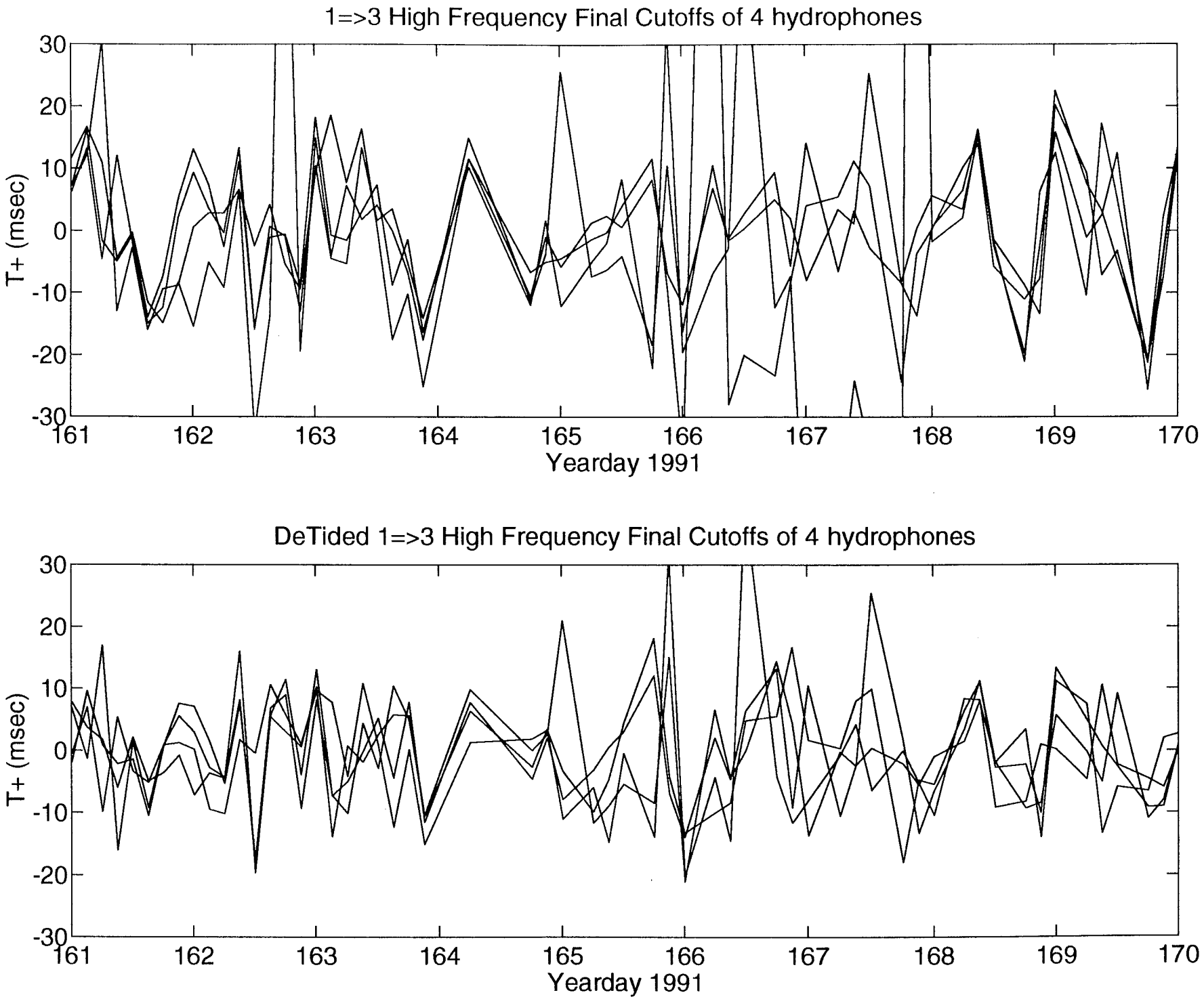
1=>3 High Frequency Final Cutoffs of 4 hydrophones
T+ (msec)
30
20
10
0
-10
-20
-30
161
162
163
164
165
166
167
168
169
170
Yearday 1991
DeTided 1=>3 High Frequency Final Cutoffs of 4 hydrophones
T+ (msec)
30
20
10
0
-10
-20
-30
161
162
163
164
165
166
167
168
169
170
Yearday 1991

FIGURE F-4

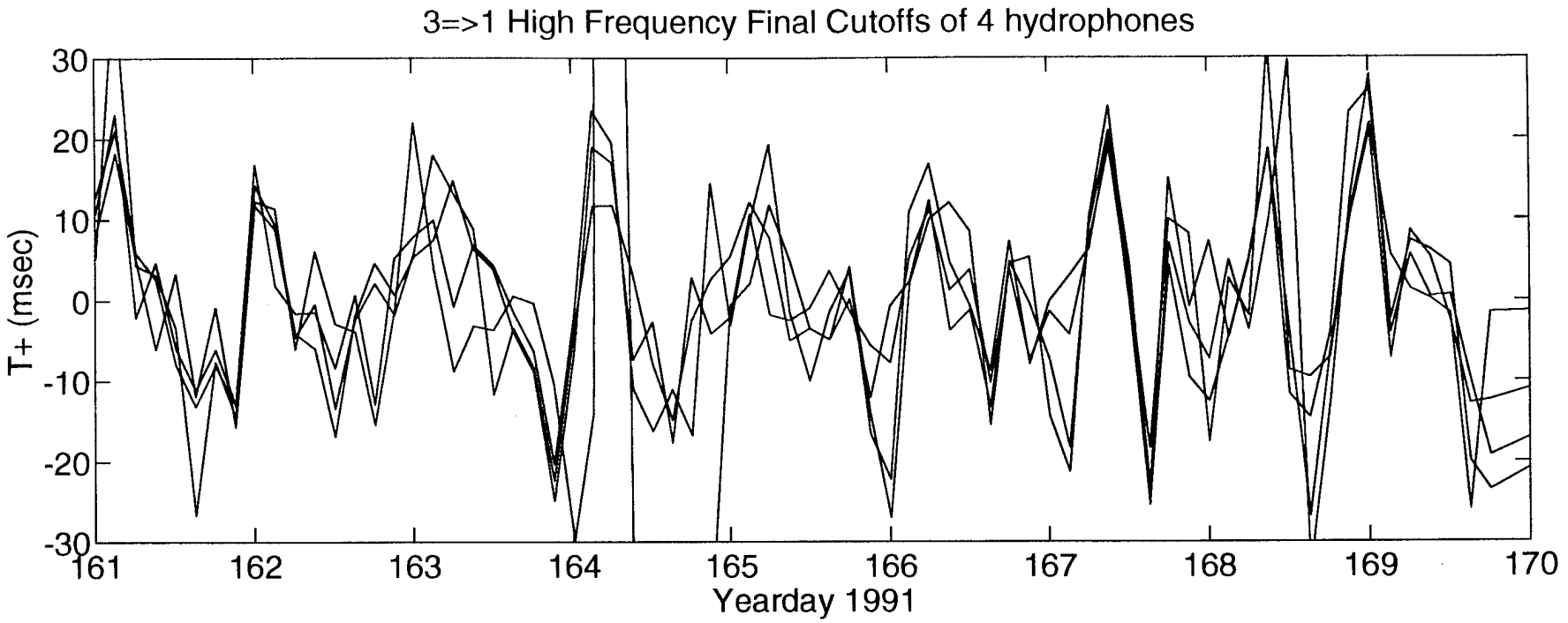
3=>1 High Frequency Final Cutoffs of 4 hydrophones
T+ (msec)
30
20
10
0
-10
-20
-30
161
162
163
164
165
166
167
168
169
170
Yearday 1991

FIGURE F-5

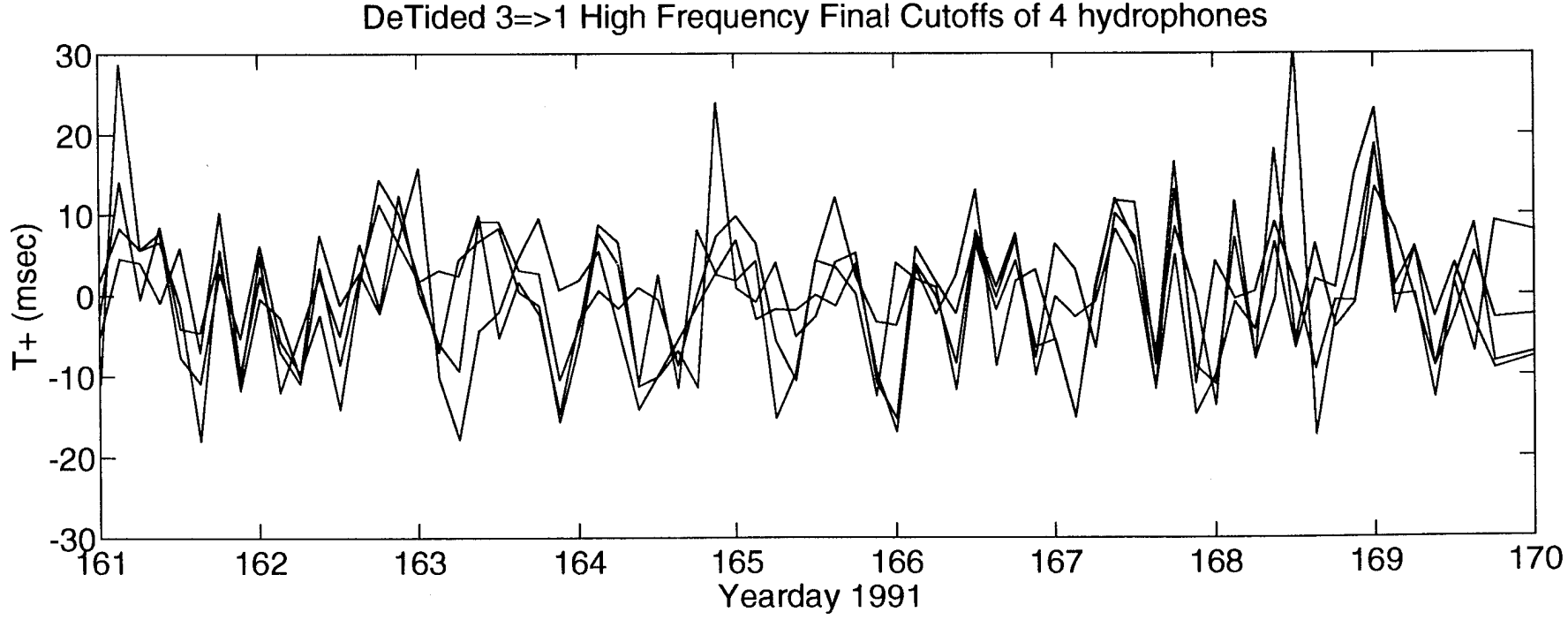
DeTided 3=>1 High Frequency Final Cutoffs of 4 hydrophones
T+ (msec)
30
20
10
0
-10
-20
-30
161
162
163
164
165
166
167
168
169
170
Yearday 1991

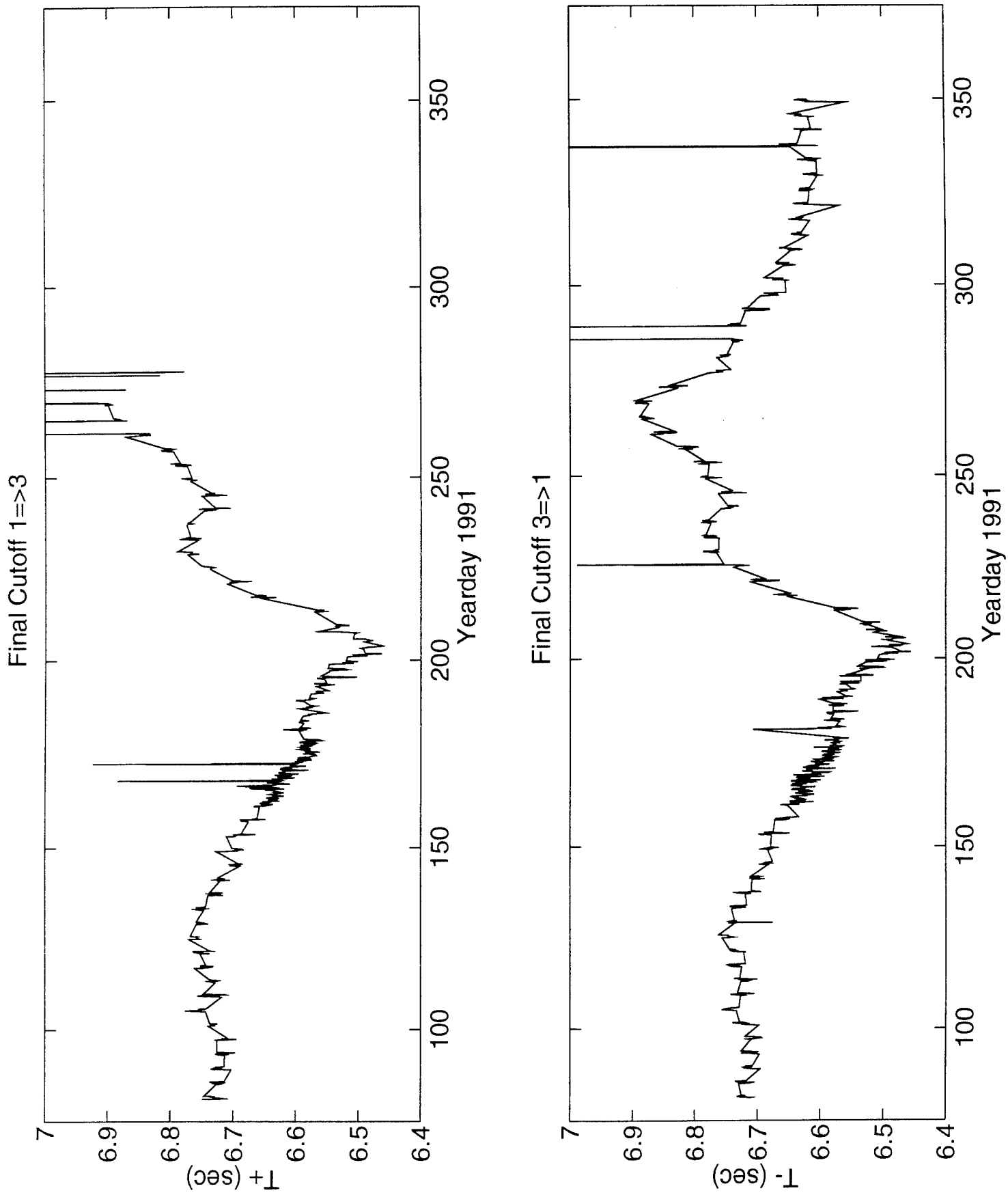
Final Cutoff 1=>3
T+ (sec)
Yearday 1991
Final Cutoff 3=>1
T- (sec)
Yearday 1991

FIGURE F-6

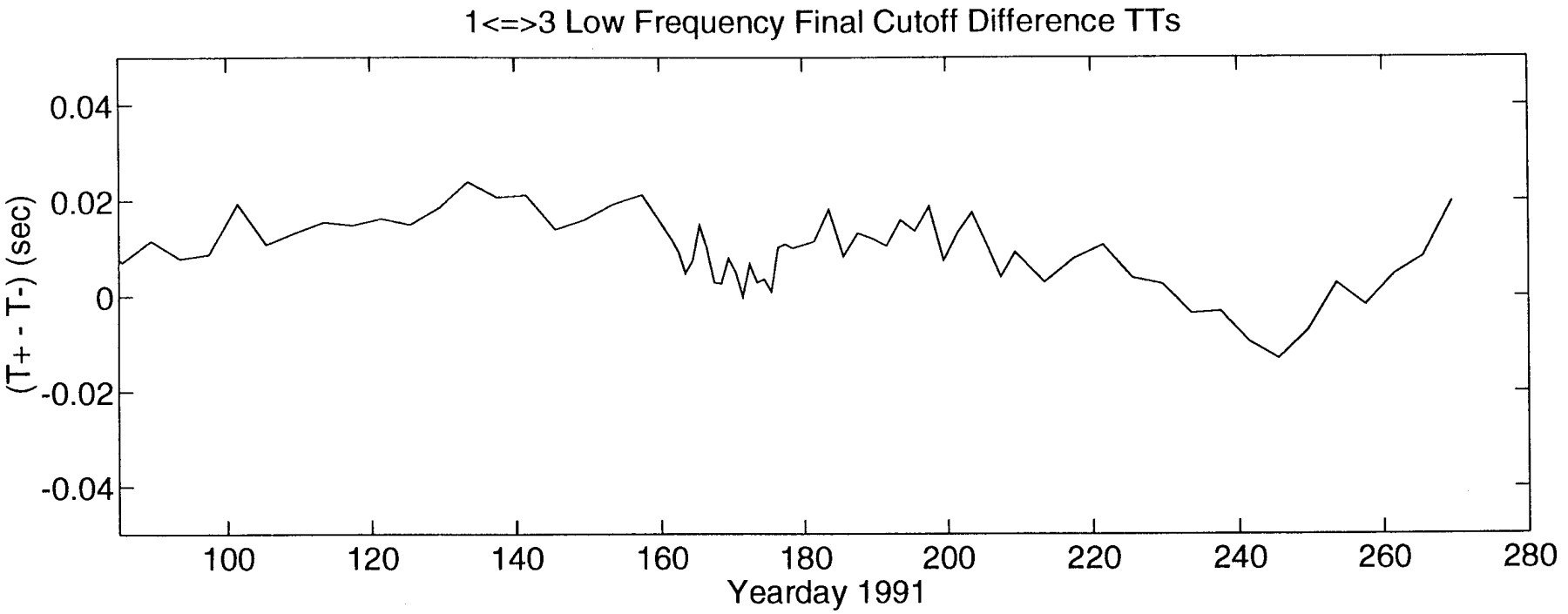
1<=>3 Low Frequency Final Cutoff Difference TTs
0.04
0.02
0
-0.02
-0.04
(T+ - T-) (sec)
100
120
140
160
180
200
220
240
260
280
Yearday 1991

FIGURE F-7

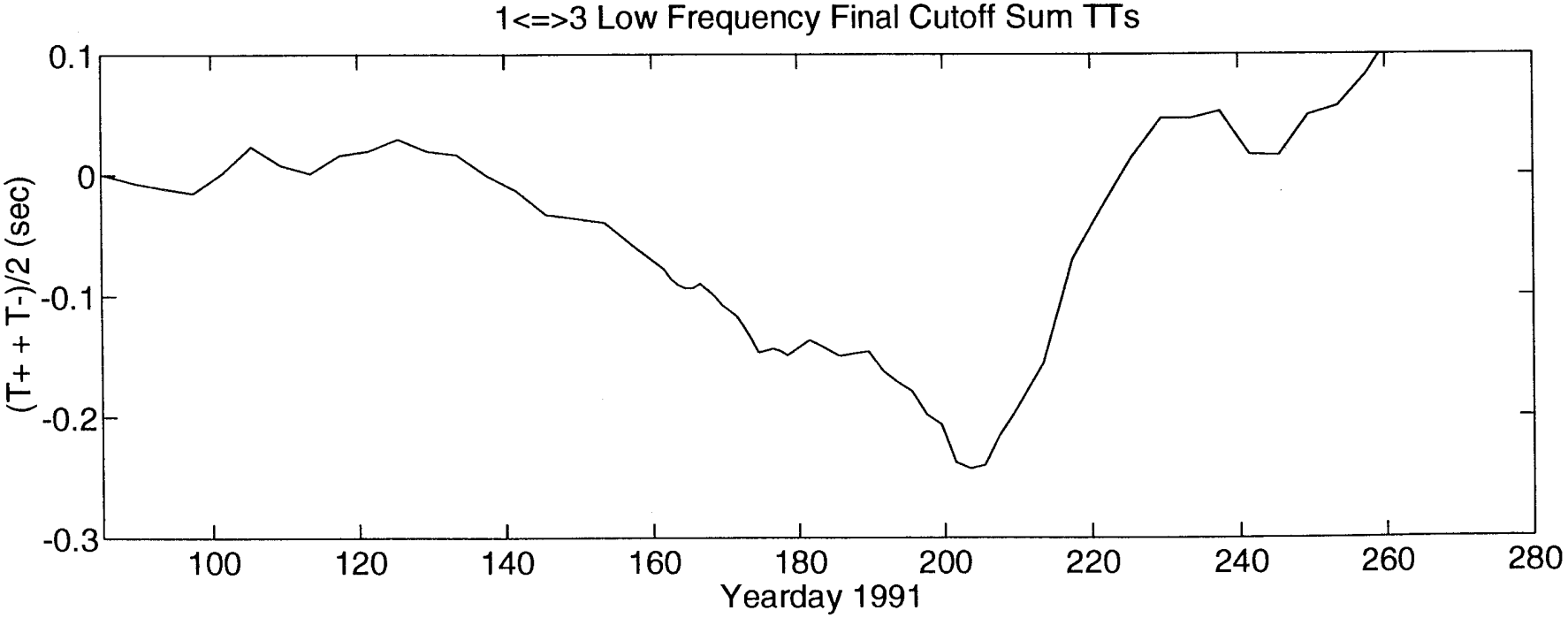
1<=>3 Low Frequency Final Cutoff Sum TTs
0.1
0
-0.1
-0.2
-0.3
(T+ + T-)/2 (sec)
100
120
140
160
180
200
220
240
260
280
Yearday 1991

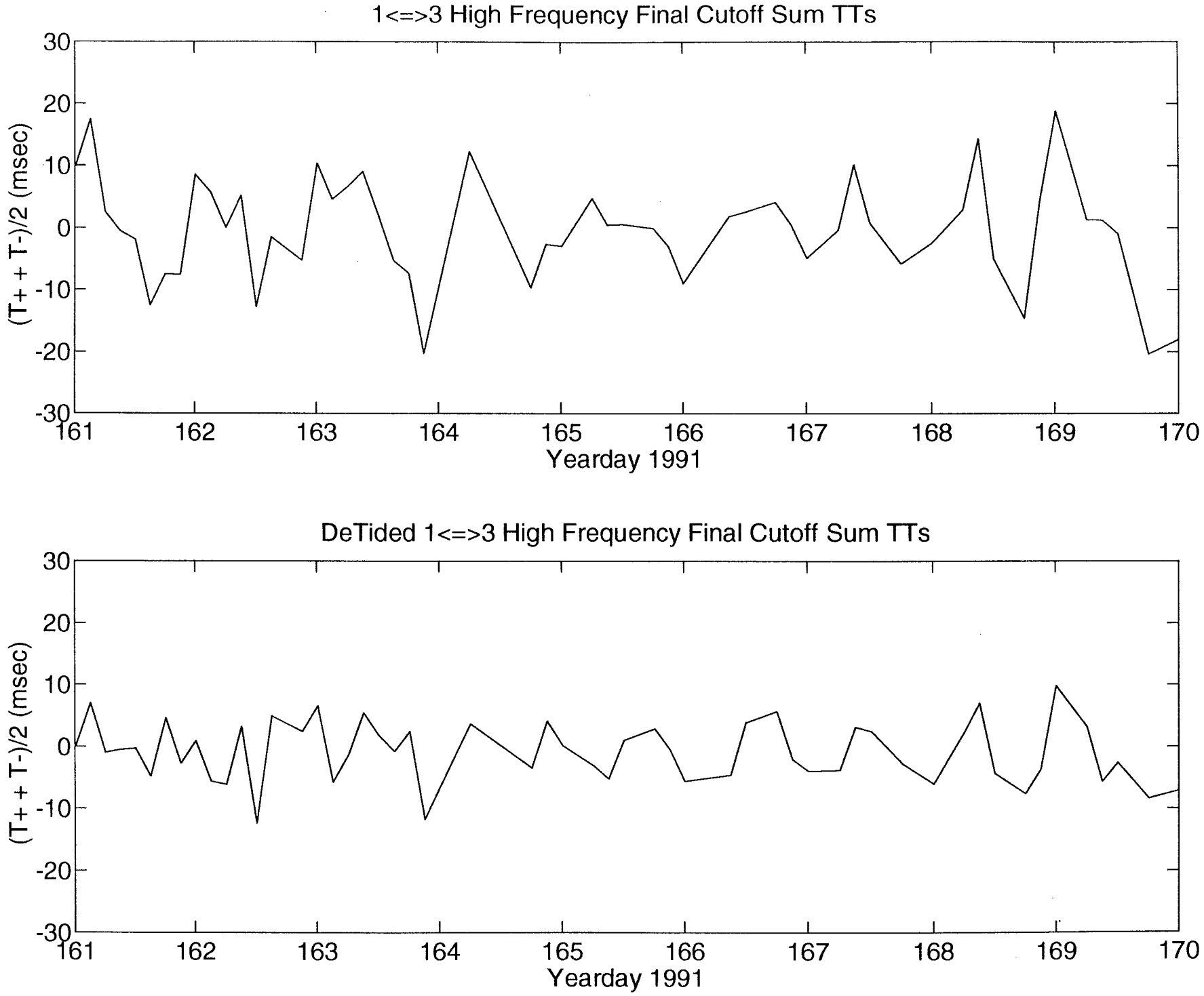
1<=>3 High Frequency Final Cutoff Sum TTs
(T+ + T-)/2 (msec)
30
20
10
0
-10
-20
-30
161
162
163
164
165
166
167
168
169
170
Yearday 1991
DeTided 1<=>3 High Frequency Final Cutoff Sum TTs
(T+ + T-)/2 (msec)
30
20
10
0
-10
-20
-30
161
162
163
164
165
166
167
168
169
170
Yearday 1991

FIGURE F-8

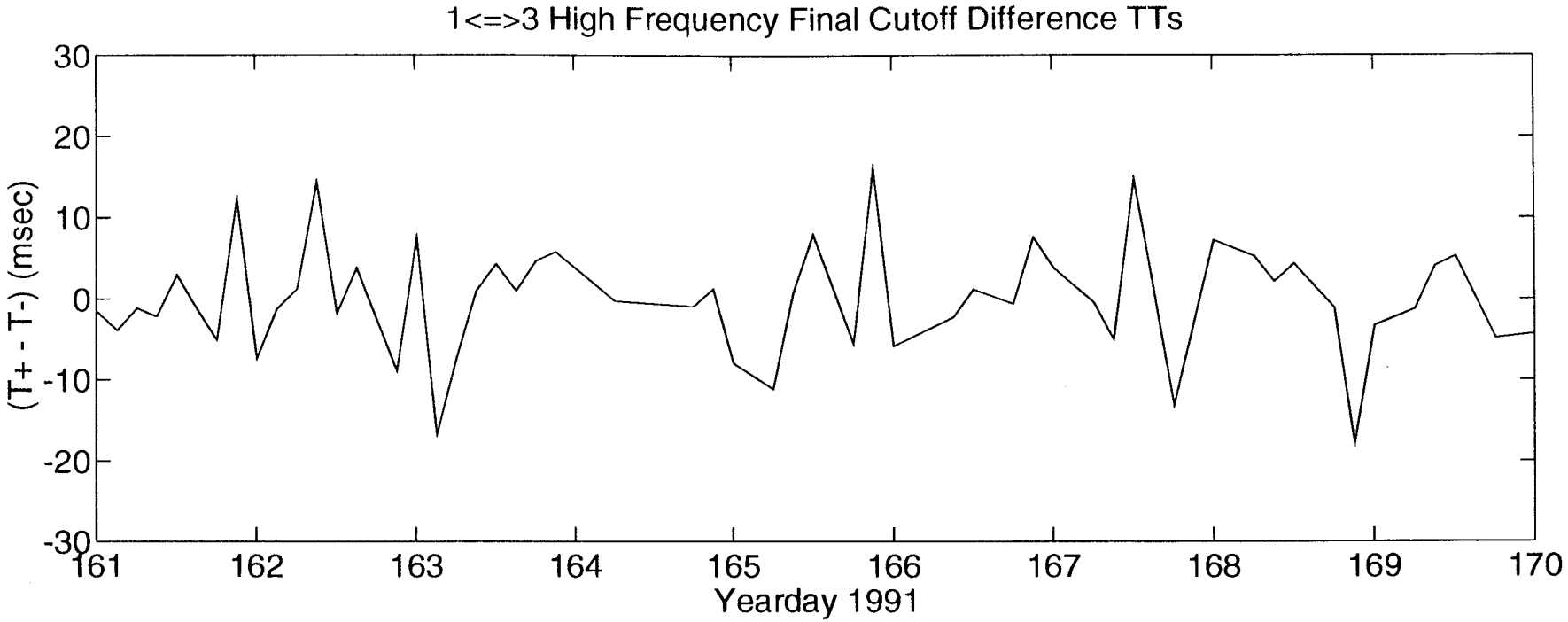
1<=>3 High Frequency Final Cutoff Difference TTs
(T+ - T-) (msec)
30
20
10
0
-10
-20
-30
161
162
163
164
165
166
167
168
169
170
Yearday 1991

FIGURE F-9

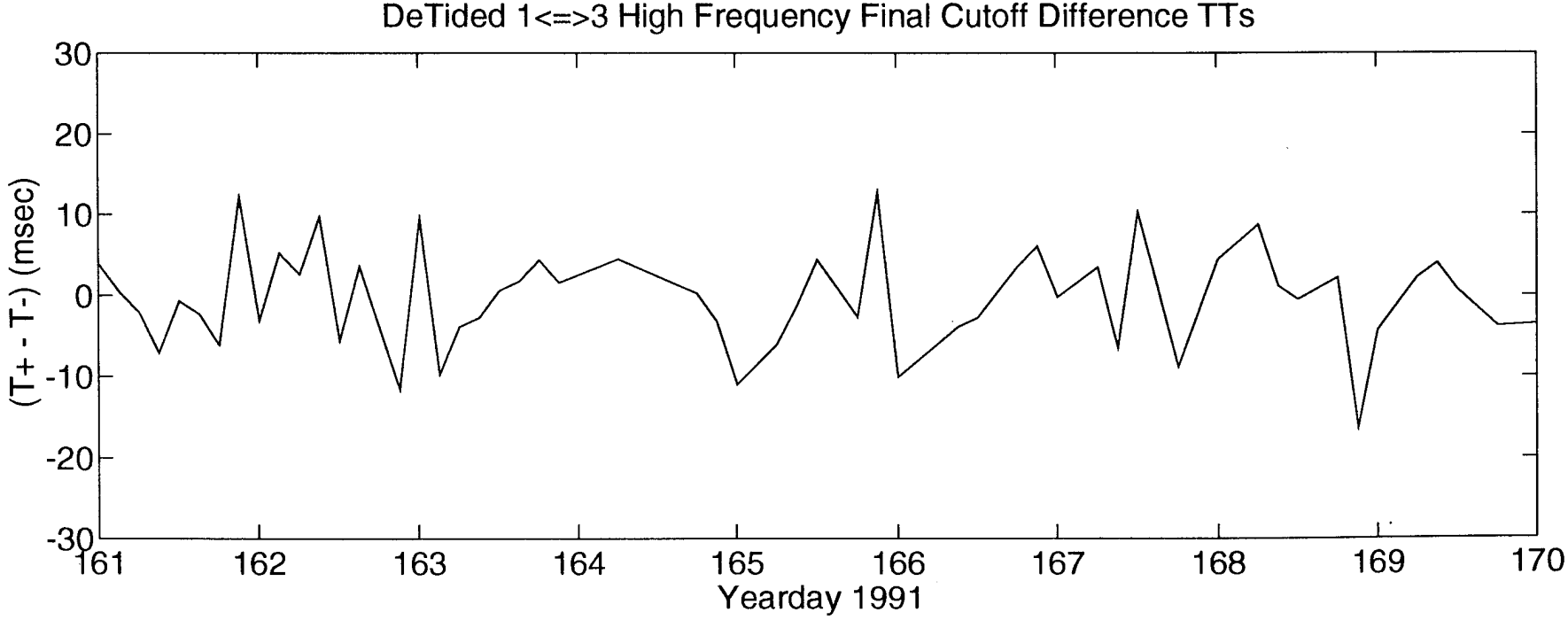
DeTided 1<=>3 High Frequency Final Cutoff Difference TTs
(T+ - T-) (msec)
30
20
10
0
-10
-20
-30
161
162
163
164
165
166
167
168
169
170
Yearday 1991

G. *ACOUSTIC DATA PROCESSING: Paths 1→2 and 2→1*

The acoustic ray, travel time data in this report begins with the tracked ray arrival time series (B. Cornuelle and A. Marshall tracked the ray travel times; the "dot plots" from which the tracked data are derived can be found in Worcester and Dushaw, 1993). There are 40 such time series, since mooring 5a was replaced with mooring 5b mid-way through the experiment and since the transmissions were reciprocal (2×15 paths + 2×5 paths for mooring 5b). [Travel time data recorded by the two additional, deeper, single hydrophones on moorings 3, 5a, and 6 are not discussed in this report.] These travel times (typically 10–20 arrivals were resolved on each path) are identified with specific predicted raypaths, which associates raypath sampling, angle of departure/incidence at the acoustic source/receiver, number of ray turning points, etc., with the resolved travel times. The travel time data are then corrected for mooring motion and clock drift. The correction for mooring motion is raypath dependent, since it depends on the ray angles at the transceivers. Both the travel time data and the predicted ray properties are used to identify reciprocal ray arrivals with each other. "Data" that are determined not to have a reciprocal counterpart are discarded; the tracking procedure oftentimes has to contend with considerable noise. The corrected data are used to form sum and difference travel times.

To remove outliers, which do horrible things when they are put into an inversion, the high-frequency components of the sum and difference travel-time time series are examined. Because the transmissions occurred quadrihourly on every fourth day, except during the few weeks during MST (yeardays 161–178 daily, 181–209 every other day), the high-pass-filtered time series is derived by removing the average travel time of each transmission day. The high-pass-filtered sum and difference travel times are dominated by tidal signals – baroclinic displacement and barotropic current, respectively. To identify outliers, the tides must be removed from each ray travel-time time series separately; the procedure is iterative since the estimated tidal signal may be distorted by the outliers. Based upon histograms of the detided, high-frequency time series, outliers are defined to be travel times greater than ±15 ms for the sum travel times and ±10–12 ms (the larger value is used for the longer paths) for the differential travel times. The variability of the detided, high-frequency time series is mainly due to internal waves; they affect the travel times themselves and decorrelate reciprocal raypaths. Outliers probably result from an occasional inherent inability to discern the desired ray arrival from noise (or secondary ray arrivals) in the tracking procedure. Once the outliers are flagged, all time series are derived again, but without the effect of the outliers.

With the general description above, the time series specific to Paths 1→2 and 2→1 are now described. The first panel of FIGURE G-1 shows the average sound speed profile from AMODE CTD data (this sound speed profile is approximated well by the Levitus sound speed), and the second panel shows the first two baroclinic (or internal tide) modes. FIGURE G-2 shows the raypaths, roughly corresponding to FIGURE G-1, for which travel times were resolved. The raypaths were actually determined using range-dependent Levitus sound speed, interpolated onto the acoustic path. This figure gives a sense of the vertical resolution that may be obtained in an inversion of the travel time data; resolution of variability is at depths for which the rays have turning points. Note that the "final cutoff" travel times may be available at some time in the future, these

data correspond to a ray confined near the sound channel axis.

FIGURE G-3 shows the low-pass filtered difference (top panel) and sum (bottom panel) travel times corresponding to the rays of FIGURE G-2.

FIGURE G-4 shows the high-pass filtered difference travel times for a small portion of the time series obtained during the time of more frequent transmissions during the MST experiment. The bottom panel shows the time series after the phase-locked tidal signals have been removed. FIGURE G-5 shows the same time series, but during a time of the normal transmission schedule.

FIGURE G-6 shows the high-pass filtered sum travel times for a small portion of the time series obtained during the time of more frequent transmissions during the MST experiment. The bottom panel shows the time series after the phase-locked tidal signals have been removed. This tidal variability is caused by the internal tide. FIGURE G-7 shows the same time series, but during a time of the normal transmission schedule.

After the travel time time series have been edited for outliers, high-pass filtered, and detided, the high-frequency variances are calculated (TABLE G-1). Note that this table sometimes contains statistics for more rays than are indicated in TABLE B-1; some of the ray arrivals in TABLE G-1 have not been identified with predicted arrivals. Also, sometimes there is initial ambiguity about the pairing of reciprocal arrivals, in which case sum and difference travel times are calculated for all reasonable cases; later it becomes obvious which arrivals have been improperly paired. The correlation $<T^+ T^->$ and variance $<T^2>$ are calculated from the sum and difference travel time variances in this table. The variance of the travel times is mainly due to internal wave variability, and this value determines the uncertainties assigned to the travel times in an inversion. The correlation coefficient is a measure of the reciprocity of reciprocal raypaths. This measure is conservative, because correlation is not a necessary condition for the determination of current from the difference of reciprocal travel times. Values of correlation that are 0.5 or greater assure that the reciprocal raypaths are indeed effectively identical, since good correlation implies that the reciprocal raypaths have not separated by more than an internal wave correlation length. Histograms of the detided, high-frequency travel times are shown in FIGURES G-8 and G-9; the variances from TABLE G-1 are measures of the width of these histograms.

TABLES G-2 and G-3 show the results of tidal analysis of the time series of difference (current) and sum (sound speed) travel times. For these tables, the tidal analysis is performed on each travel time time series separately, and then the average and rms of the harmonic constants are calculated. Current or sound speed amplitude is determined from travel time by a simple scaling factor; the harmonic constants are more accurately determined by inverting the data for current or sound speed (this is not done here).

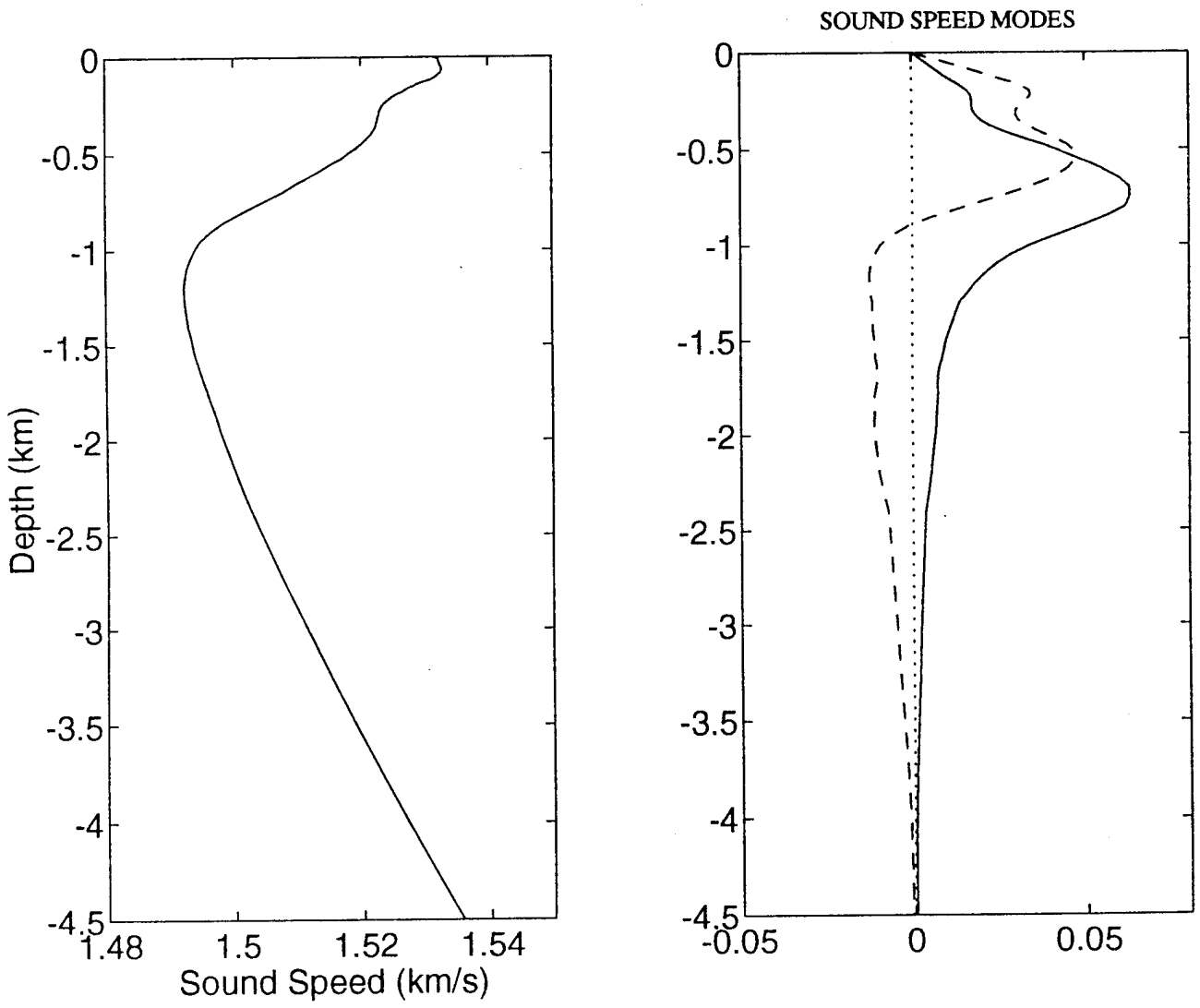
SOUND SPEED MODES
Depth (km)
0
-0.5
-1
-1.5
-2
-2.5
-3
-3.5
-4
-4.5
1.48
1.5
1.52
1.54
Sound Speed (km/s)
-0.05
0
0.05

FIGURE G-1

TABLE G-1. Travel Time Statistics 1←→2.

Ray #	Number of data	$<(T^+ + T^-)^2>$ (ms^2)	$<(T^+ - T^-)^2>$ (ms^2)	$<T^+ T^->$ (ms^2)	$<T^2>$ (ms^2)	$\frac{<T^+ T^->}{<T^2>}$
1	232	12	8	10	14	0.71
2	415	24	17	20	29	0.70
3	162	14	16	10	18	0.57
4	174	13	17	9	17	0.52
5	465	11	8	9	13	0.69
6	456	13	9	11	15	0.70
7	459	13	10	10	15	0.67
8	466	14	9	12	16	0.72
9	504	12	3	11	13	0.87
10	494	12	5	10	13	0.80
11	458	13	9	11	15	0.71
12	458	15	10	13	18	0.71
13	468	14	4	13	15	0.86

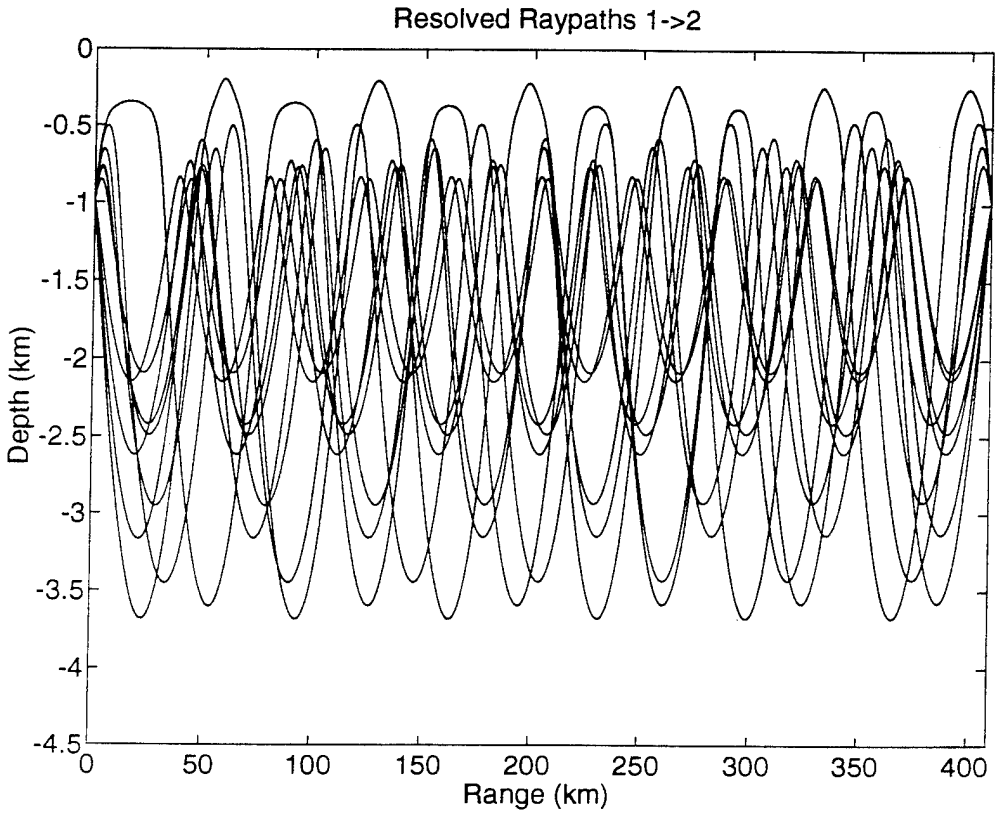

FIGURE G-2

TABLE G-2. Tidal Current Harmonic Constants 1←→2.

Constituent	Amplitude (mm/s)	Uncertainty (mm/s)	Phase (°G)	Uncertainty (°)
M_2	12.25	1.29	109.7	3.0
S_2	3.31	0.81	131.6	26.9
N_2	3.32	0.94	91.5	15.3
K_2	1.78	0.72	125.4	37.1
O_1	1.18	0.74	232.5	91.9
K_1	1.44	0.66	206.5	36.3
P_1	1.02	0.77	254.2	39.3
Q_1	1.23	0.84	182.2	64.3

Values and their uncertainty are determined by the average and rms of harmonic constants from tidal analyses of the separate raypath travel time series. The amplitudes do not include the lunar node factors. 60 ± 12 % of the high-frequency variance is accounted for by the tides.

TABLE G-3. Tidal Sound Speed Harmonic Constants 1←→2.

Constituent	Amplitude (mm/s)	Uncertainty (mm/s)	Phase (°G)	Uncertainty (°)
M_2	10.06	1.69	119.2	6.6
S_2	1.91	0.87	324.0	29.5
N_2	2.01	0.64	64.5	25.0
K_2	2.16	0.70	25.9	43.8
O_1	1.77	0.56	247.1	36.2
K_1	3.29	0.75	80.1	14.2
P_1	2.03	0.66	49.8	67.4
Q_1	1.68	0.41	181.4	30.5

Values and their uncertainty are determined by the average and rms of harmonic constants from tidal analyses of the separate raypath travel time series. The amplitudes do not include the lunar node factors. 41 ± 8 % of the high-frequency variance is accounted for by the tides. Because sum travel times are used to derive these numbers, the amplitudes have been divided by a factor of two compared to the amplitudes for current.

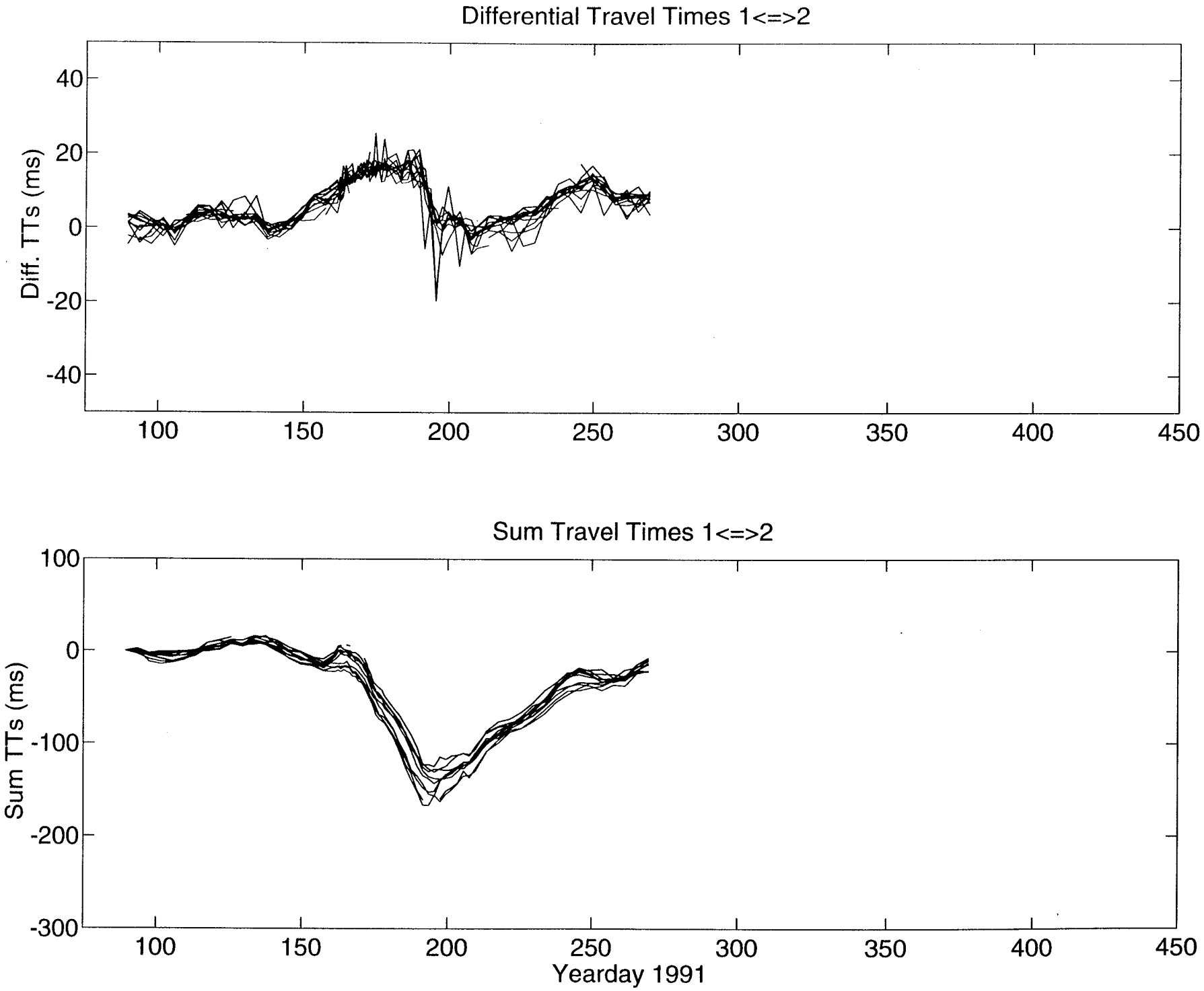
Differential Travel Times 1<=>2
Diff. TTs (ms)
40
20
0
-20
-40
100
150
200
250
300
350
400
450
Sum Travel Times 1<=>2
Sum TTs (ms)
100
0
-100
-200
-300
100
150
200
250
300
350
400
450
Yearday 1991

FIGURE G-3

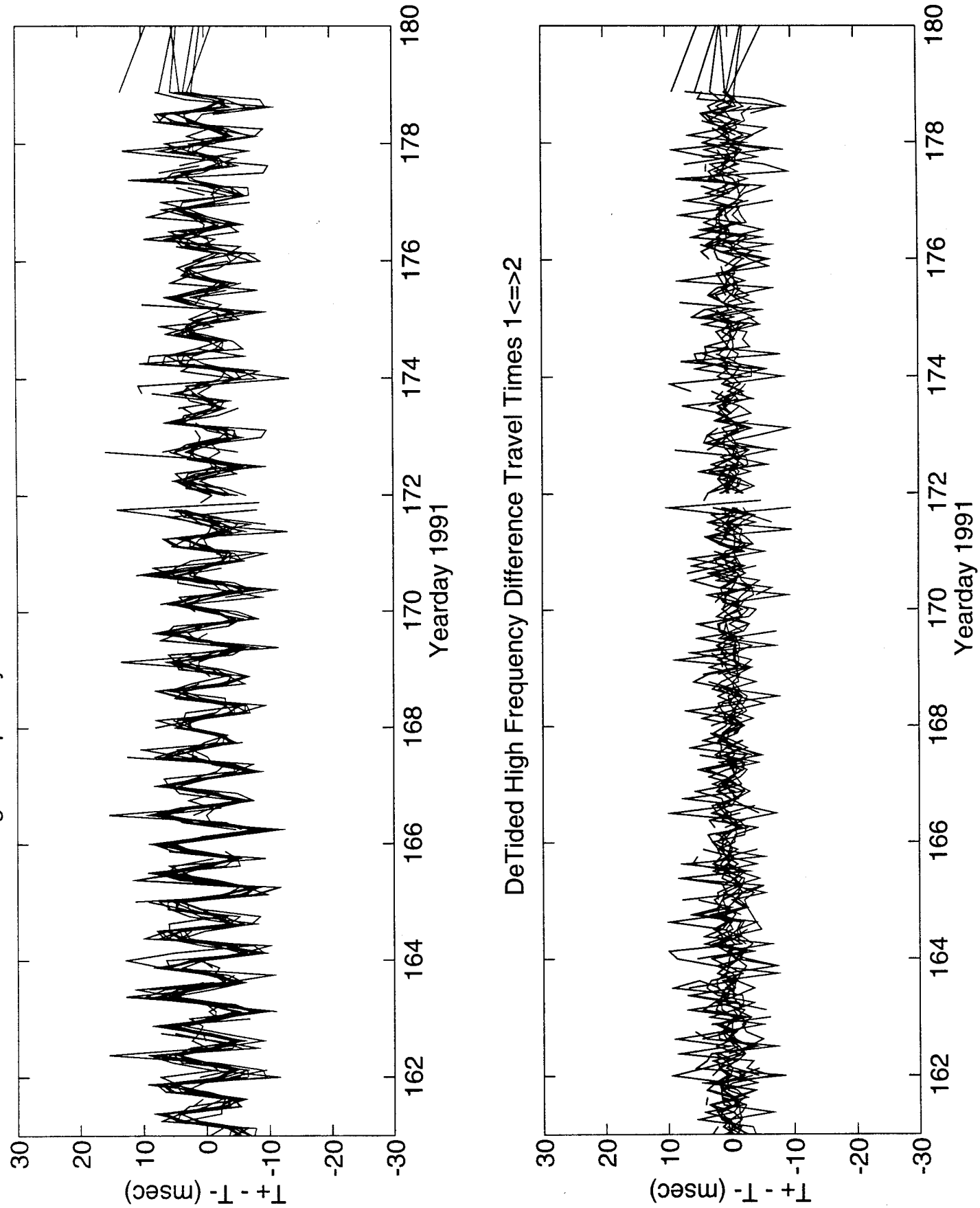
High Frequency Difference Travel Times 1<=>2
T+ - T- (msec)
30
20
10
0
-10
-20
-30
162
164
166
168
170
172
174
176
178
180
Yearday 1991
DeTided High Frequency Difference Travel Times 1<=>2
T+ - T- (msec)
30
20
10
0
-10
-20
-30
162
164
166
168
170
172
174
176
178
180
Yearday 1991

FIGURE G-4

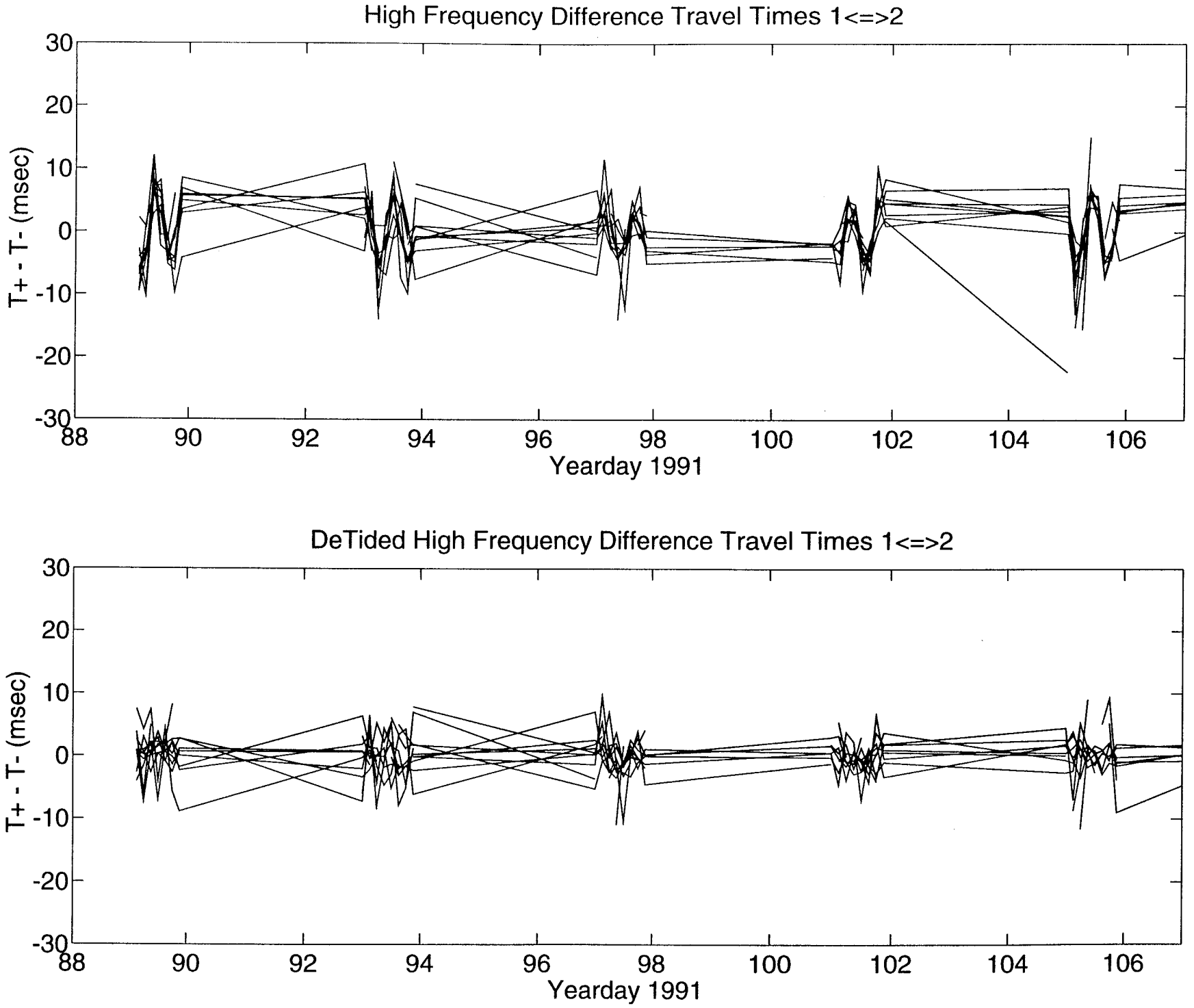
High Frequency Difference Travel Times 1<=>2
T+ - T- (msec)
Yearday 1991
DeTided High Frequency Difference Travel Times 1<=>2
T+ - T- (msec)
Yearday 1991

FIGURE G-5

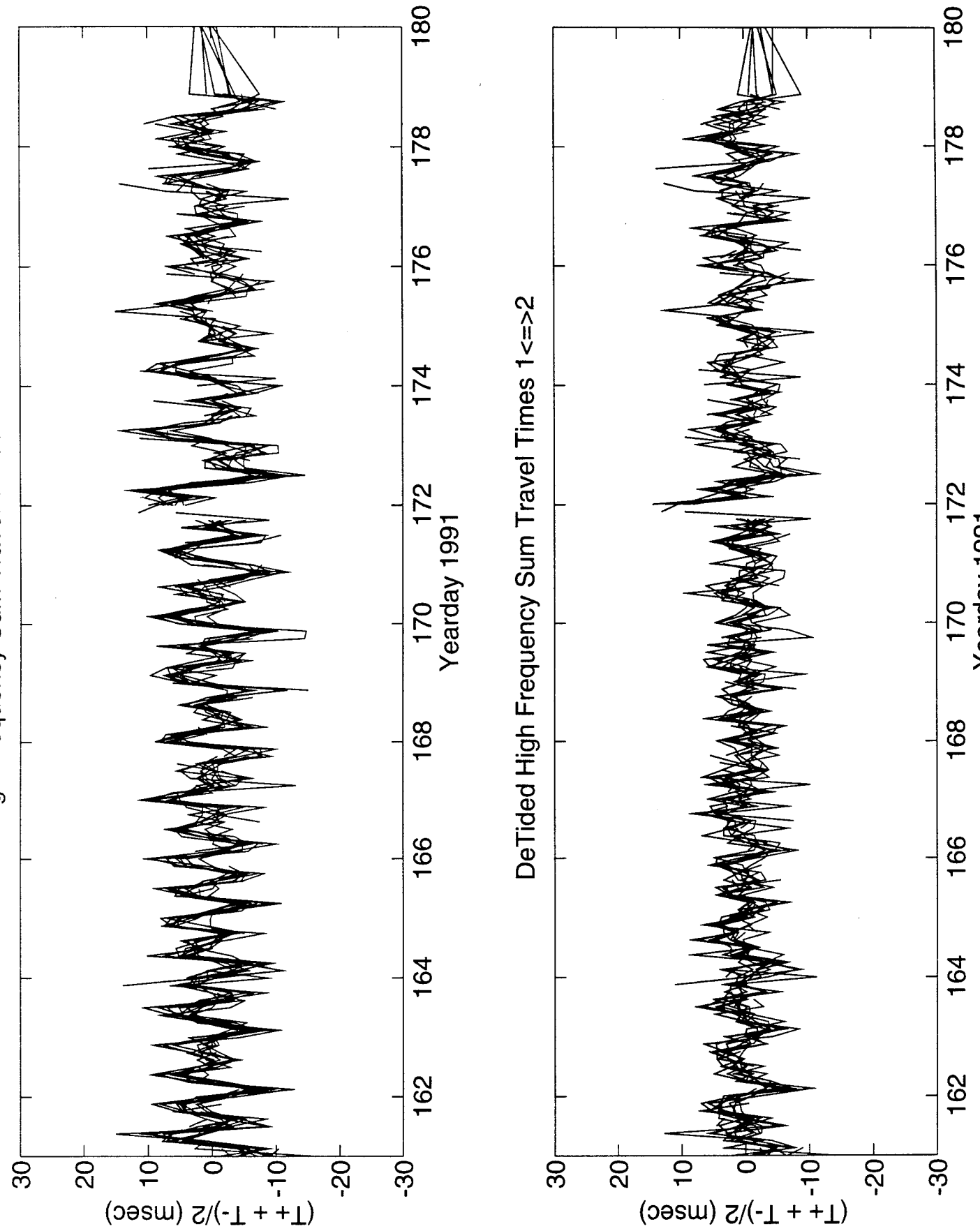
High Frequency Sum Travel Times 1<=>2
DeTided High Frequency Sum Travel Times 1<=>2
(T+ + T-)/2 (msec)
Yearday 1991
30
20
10
0
-10
-20
-30
162
164
166
168
170
172
174
176
178
180

FIGURE G-6

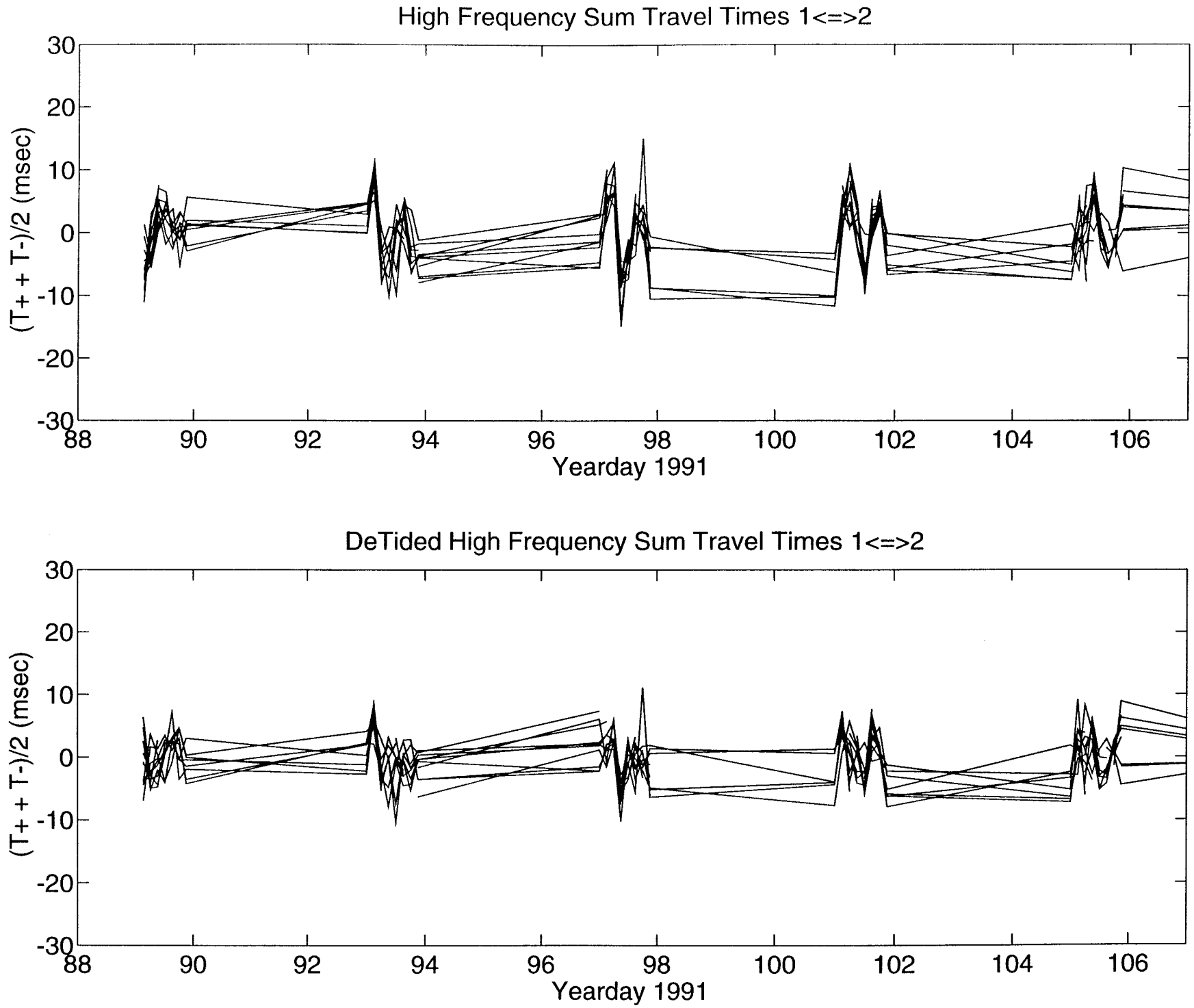
High Frequency Sum Travel Times 1<=>2
(T+ + T-)/2 (msec)
Yearday 1991
DeTided High Frequency Sum Travel Times 1<=>2
(T+ + T-)/2 (msec)
Yearday 1991

FIGURE G-7

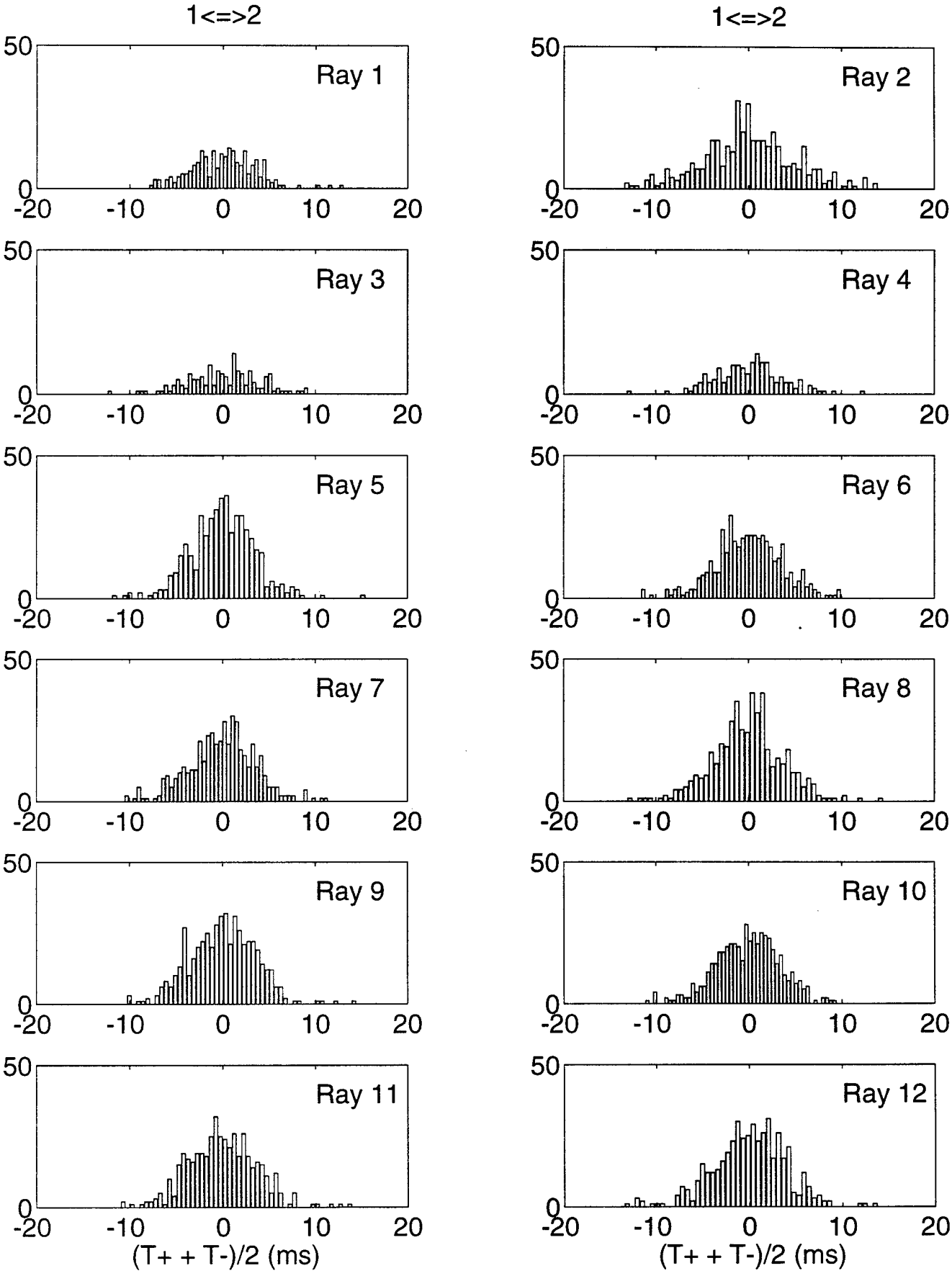
1<=>2
1<=>2
Ray 1
Ray 2
Ray 3
Ray 4
Ray 5
Ray 6
Ray 7
Ray 8
Ray 9
Ray 10
Ray 11
Ray 12
50
0
-20
-10
0
10
20
(T+ + T-)/2 (ms)
(T+ + T-)/2 (ms)

FIGURE G-8

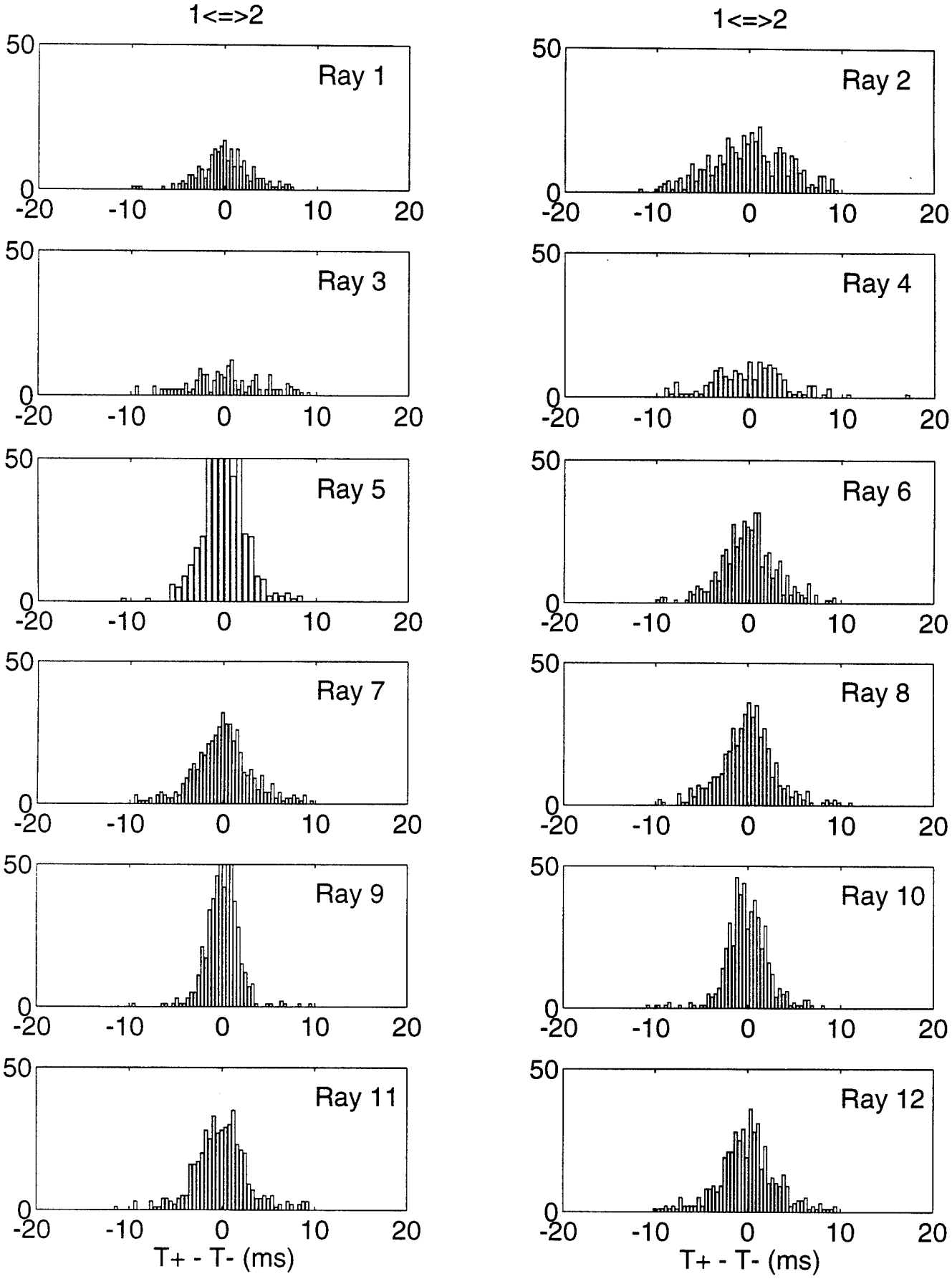
1<=>2
Ray 1
Ray 2
Ray 3
Ray 4
Ray 5
Ray 6
Ray 7
Ray 8
Ray 9
Ray 10
Ray 11
Ray 12
50
0
-20
-10
0
10
20
T+ - T- (ms)

FIGURE G-9

H. ACOUSTIC DATA: Paths 1→3 and 3→1

FIGURE H-1 shows the raypaths, corresponding roughly to FIGURE G-1, for which travel times were resolved. The raypaths were actually determined using range-dependent Levitus sound speed, interpolated onto the acoustic path. Note that the "final cutoff" travel times have been derived for this acoustic path only, and these data correspond to a ray confined near the sound channel axis.

FIGURE H-2 shows the low-pass filtered difference (top panel) and sum (bottom panel) travel times corresponding to the rays of FIGURE H-1.

FIGURE H-3 shows the high-pass filtered difference travel times for a small portion of the time series obtained during the time of more frequent transmissions during the MST experiment. The bottom panel shows the time series after the phase-locked tidal signals have been removed. FIGURE H-4 shows the same time series, but during a time of the normal transmission schedule.

FIGURE H-5 shows the high-pass filtered sum travel times for a small portion of the time series obtained during the time of more frequent transmissions during the MST experiment. The bottom panel shows the time series after the phase-locked tidal signals have been removed. This tidal variability is caused by the internal tide. FIGURE H-6 shows the same time series, but during a time of the normal transmission schedule.

After the travel time time series have been edited for outliers, high-pass filtered, and detided, the high-frequency variances are calculated (TABLE H-1). Note that this table sometimes contains statistics for more rays than are indicated in TABLE B-1; some of the ray arrivals in TABLE H-1 have not been identified with predicted arrivals. Also, sometimes there is initial ambiguity about the pairing of reciprocal arrivals, in which case sum and difference travel times are calculated for all reasonable cases; later it becomes obvious which arrivals have been improperly paired. The correlation $<T^+ T^->$ and variance $<T^2>$ are calculated from the sum and difference travel time variances in this table. The variance of the travel times is mainly due to internal wave variability, and this value determines the uncertainties assigned to the travel times in an inversion. The correlation coefficient is a measure of the reciprocity of reciprocal raypaths. This measure is conservative, because correlation is not a necessary condition for the determination of current from the difference of reciprocal travel times. Values of correlation that are 0.5 or greater assure that the reciprocal raypaths are indeed effectively identical, since good correlation implies that the reciprocal raypaths have not separated by more than an internal wave correlation length. Histograms of the detided, high-frequency travel times are shown in FIGURES H-7 and H-8; the variances from TABLE H-1 are measures of the width of these histograms.

TABLES H-2 and H-3 show the results of tidal analysis of the time series of difference (current) and sum (sound speed) travel times. For these tables, the tidal analysis is performed on each travel time time series separately and then the average and rms of the harmonic constants are calculated. Current or sound speed amplitude is determined from travel time by a simple scaling factor; the harmonic constants are more accurately determined by inverting the data for current or sound speed (this is not done here).

TABLE H-1. Travel Time Statistics 1←→3.

Ray #	Number of data	$<(T^+ + T^-)^2>$ (ms^2)	$<(T^+ - T^-)^2>$ (ms^2)	$<T^+ T^->$ (ms^2)	$<T^2>$ (ms^2)	$\frac{<T^+ T^->}{<T^2>}$
1	281	16	17	12	20	0.59
2	346	29	23	23	35	0.66
3	349	27	19	22	32	0.70
4	384	20	16	16	24	0.67
5	352	27	21	22	32	0.67
6	326	24	22	19	30	0.62
7	364	23	15	19	27	0.72
8	427	19	12	16	22	0.73
9	408	25	13	21	28	0.77
10	416	17	11	14	20	0.72
11	425	18	12	15	21	0.72
12	417	18	13	15	21	0.71
13	399	22	11	20	25	0.79
14	402	21	14	17	24	0.70
15	411	21	15	18	25	0.71

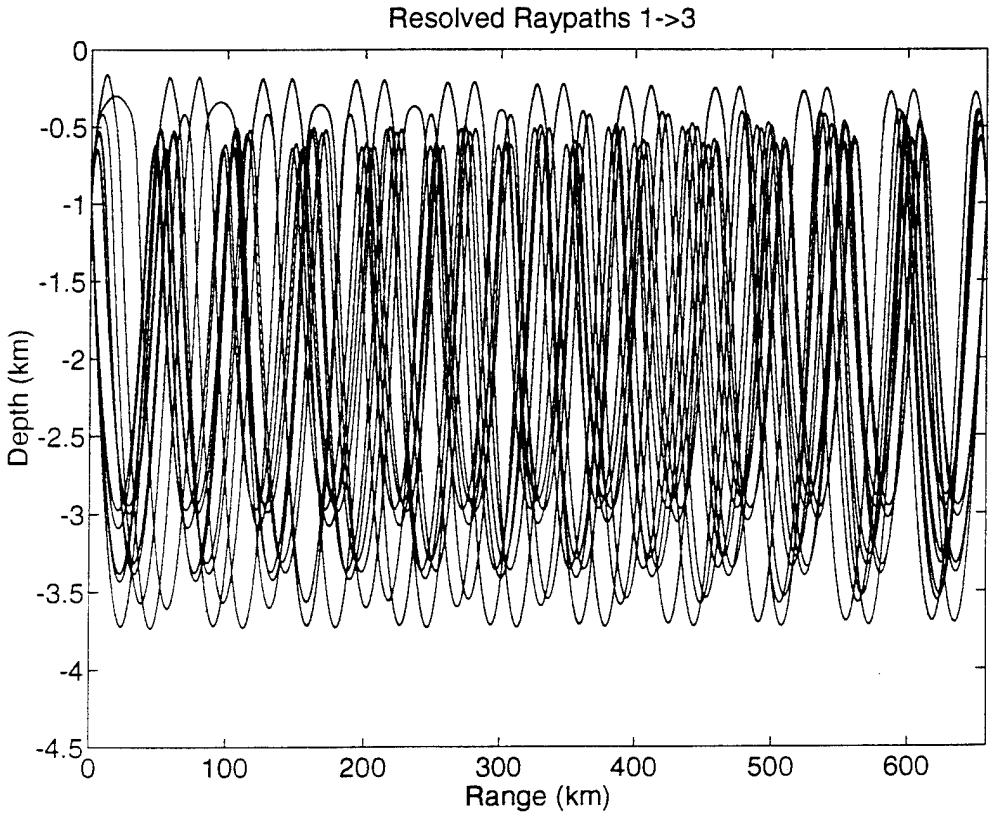

FIGURE H-1

TABLE H-2. Tidal Current Harmonic Constants 1←→3.

Constituent	Amplitude (mm/s)	Uncertainty (mm/s)	Phase (°G)	Uncertainty (°)
M_2	5.65	0.72	115.9	5.4
S_2	1.95	0.56	156.6	19.5
N_2	1.54	0.35	100.1	52.0
K_2	0.98	0.51	176.0	62.3
O_1	1.16	0.68	253.5	37.2
K_1	1.16	0.49	218.1	56.9
P_1	0.96	0.54	174.2	85.3
Q_1	0.96	0.50	166.9	98.5

Values and their uncertainty are determined by the average and rms of harmonic constants from tidal analyses of the separate raypath travel time series. The amplitudes do not include the lunar node factors. 35 ± 7 % of the high-frequency variance is accounted for by the tides.

TABLE H-3. Tidal Sound Speed Harmonic Constants 1←→3.

Constituent	Amplitude (mm/s)	Uncertainty (mm/s)	Phase (°G)	Uncertainty (°)
M_2	6.00	1.34	336.4	13.8
S_2	1.40	0.48	176.4	54.7
N_2	3.02	0.59	274.8	14.4
K_2	0.85	0.40	79.8	47.9
O_1	1.62	0.53	213.8	33.9
K_1	5.70	0.71	71.0	8.1
P_1	2.35	0.58	53.0	13.9
Q_1	0.93	0.42	108.8	79.1

Values and their uncertainty are determined by the average and rms of harmonic constants from tidal analyses of the separate raypath travel time series. The amplitudes do not include the lunar node factors. 42 ± 8 % of the high-frequency variance is accounted for by the tides. Because sum travel times are used to derive these numbers, the amplitudes have been divided by a factor of two compared to the amplitudes for current.

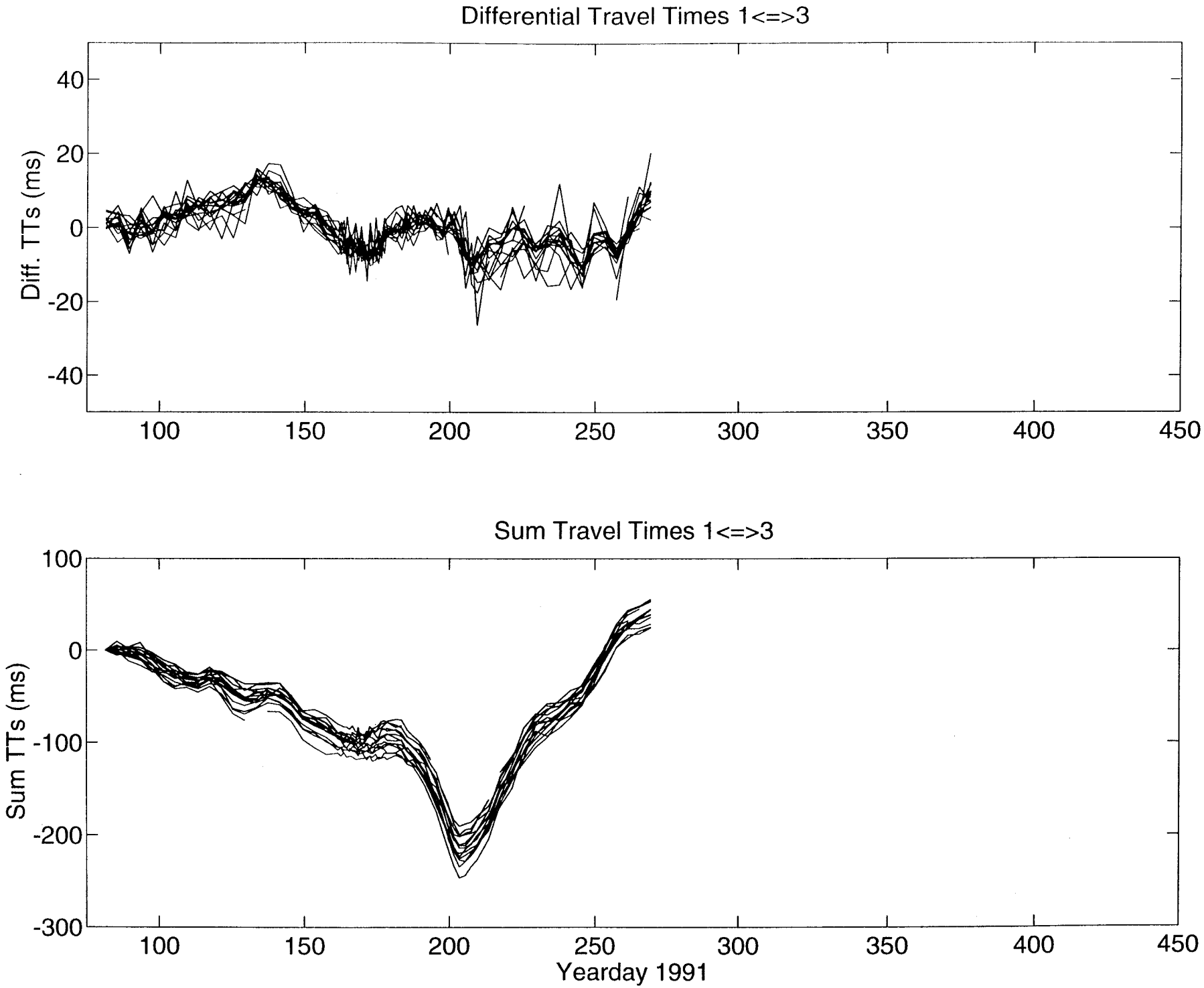
Differential Travel Times 1<=>3
Diff. TTs (ms)
40
20
0
-20
-40
100
150
200
250
300
350
400
450
Sum Travel Times 1<=>3
Sum TTs (ms)
100
0
-100
-200
-300
100
150
200
250
300
350
400
450
Yearday 1991

FIGURE H-2

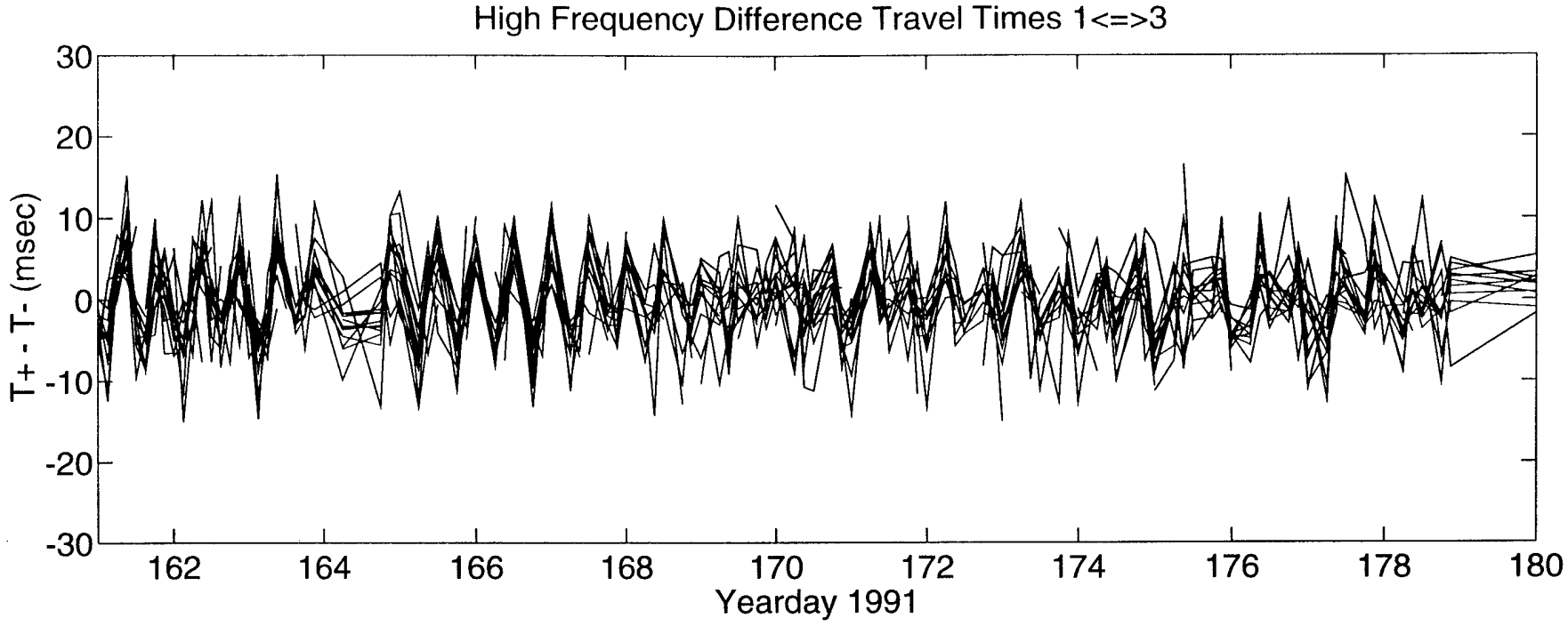
High Frequency Difference Travel Times 1<=>3
T+ - T- (msec)
30
20
10
0
-10
-20
-30
162
164
166
168
170
172
174
176
178
180
Yearday 1991

FIGURE H-3

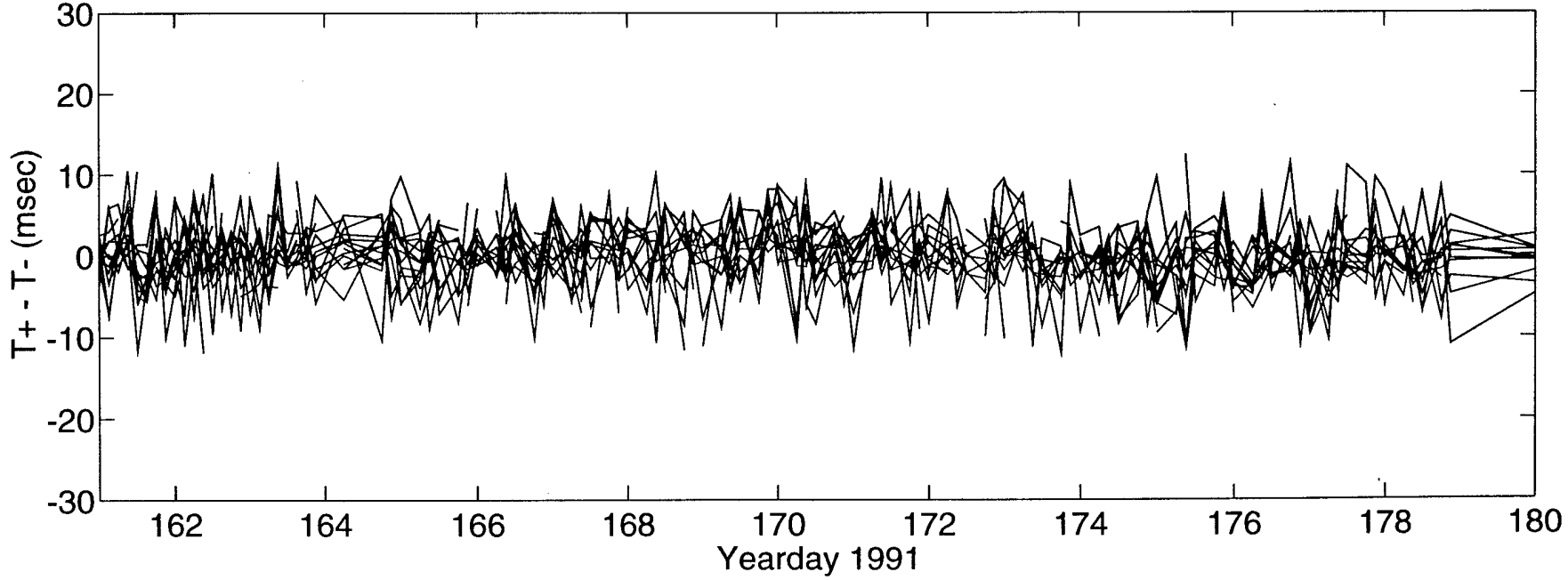
DeTided High Frequency Difference Travel Times 1<=>3
T+ - T- (msec)
30
20
10
0
-10
-20
-30
162
164
166
168
170
172
174
176
178
180
Yearday 1991

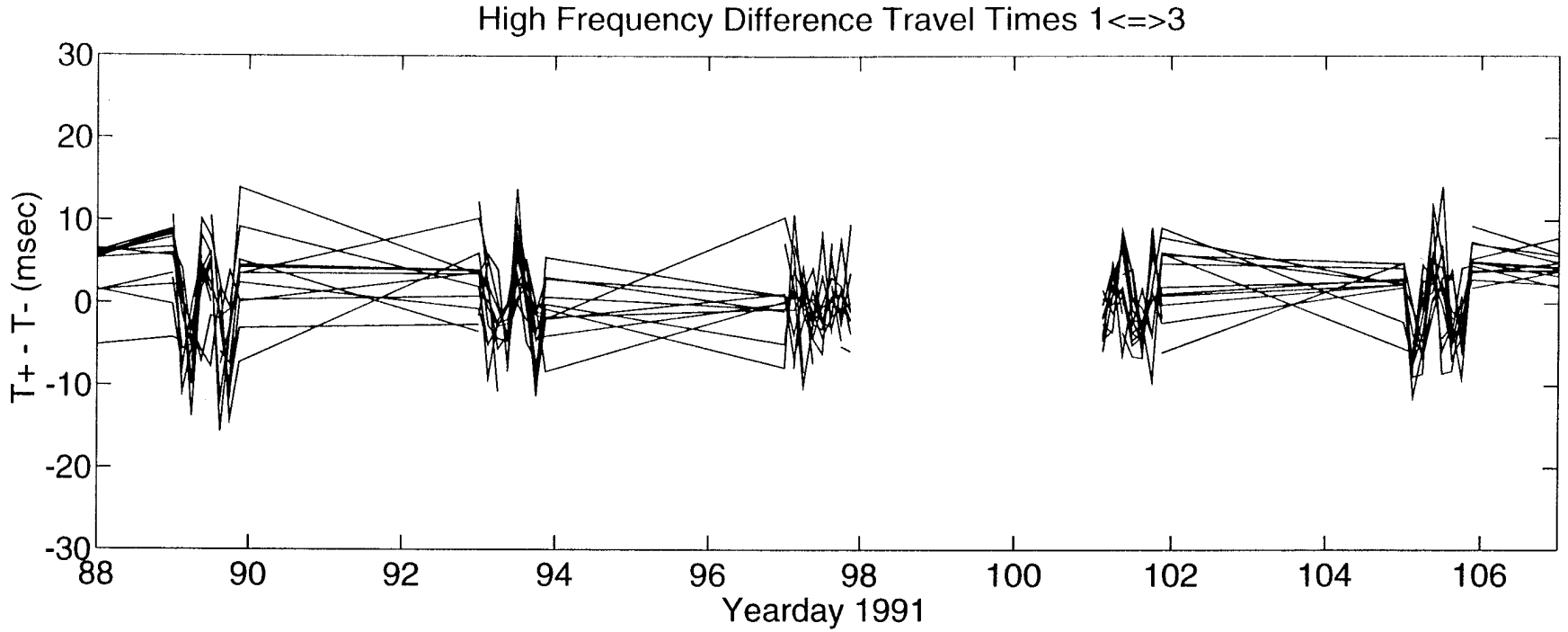
High Frequency Difference Travel Times 1<=>3
T+ - T- (msec)
30
20
10
0
-10
-20
-30
88
90
92
94
96
98
100
102
104
106
Yearday 1991

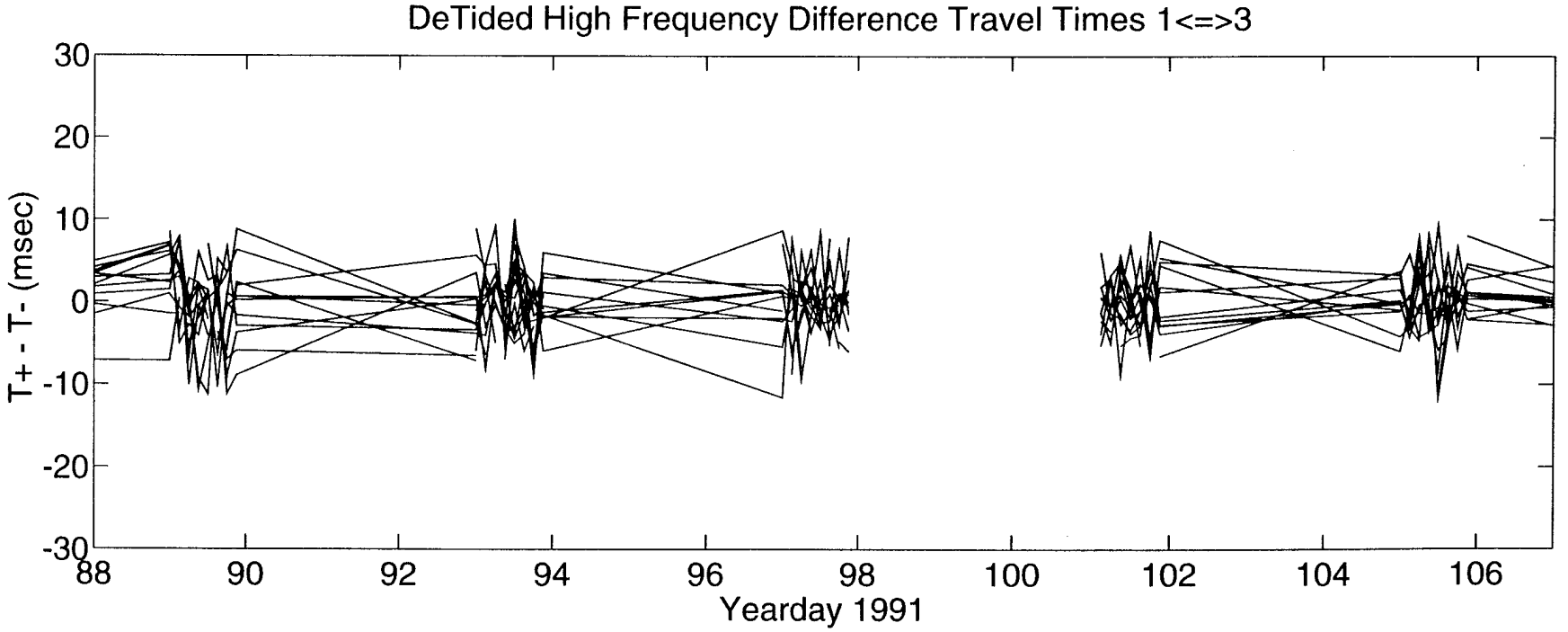
DeTided High Frequency Difference Travel Times 1<=>3
T+ - T- (msec)
30
20
10
0
-10
-20
-30
88
90
92
94
96
98
100
102
104
106
Yearday 1991

FIGURE H-4

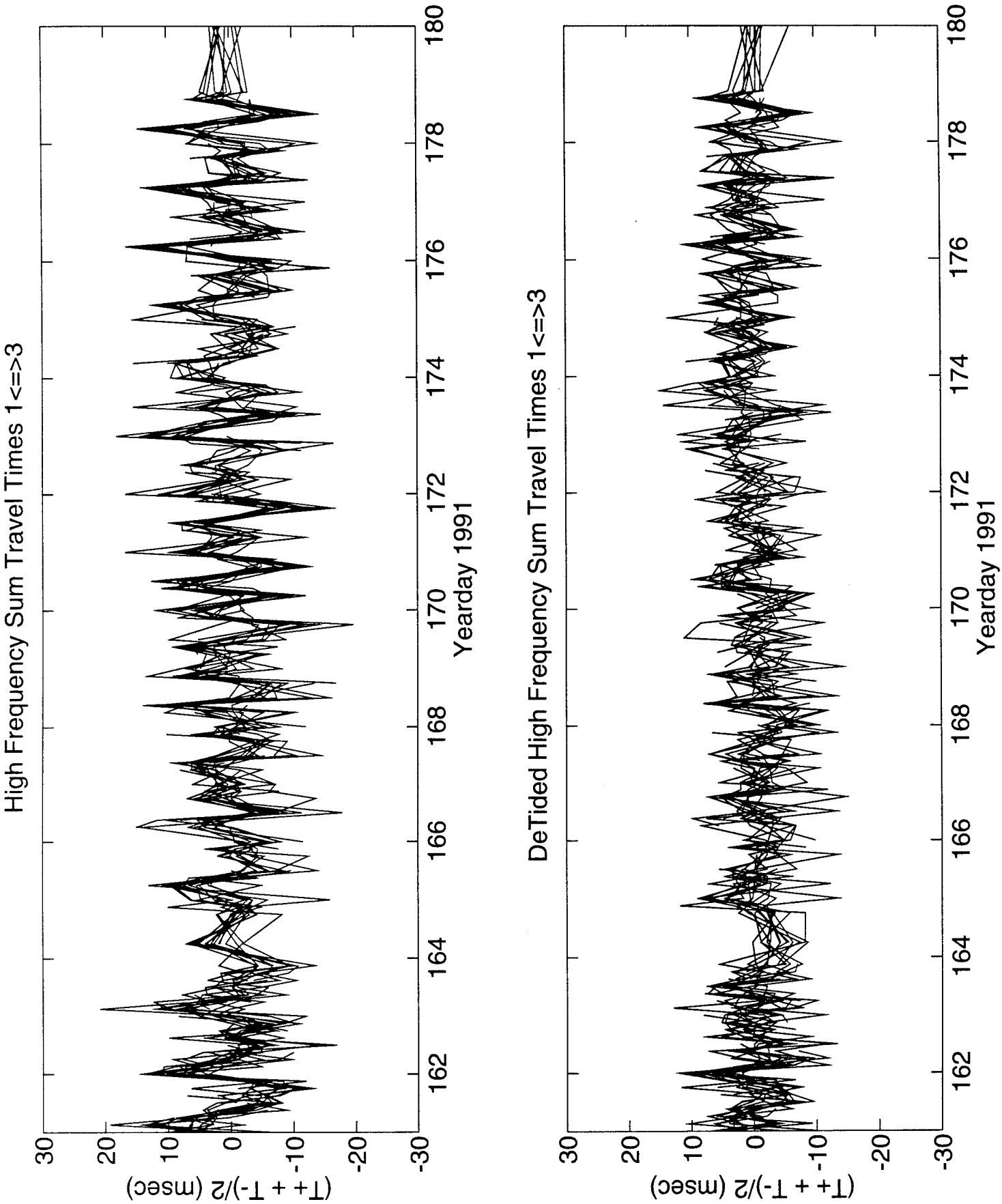
High Frequency Sum Travel Times 1<=>3
(T+ + T-)/2 (msec)
30
20
10
0
-10
-20
-30
162
164
166
168
170
172
174
176
178
180
Yearday 1991
DeTided High Frequency Sum Travel Times 1<=>3
(T+ + T-)/2 (msec)
30
20
10
0
-10
-20
-30
162
164
166
168
170
172
174
176
178
180
Yearday 1991

FIGURE H-5

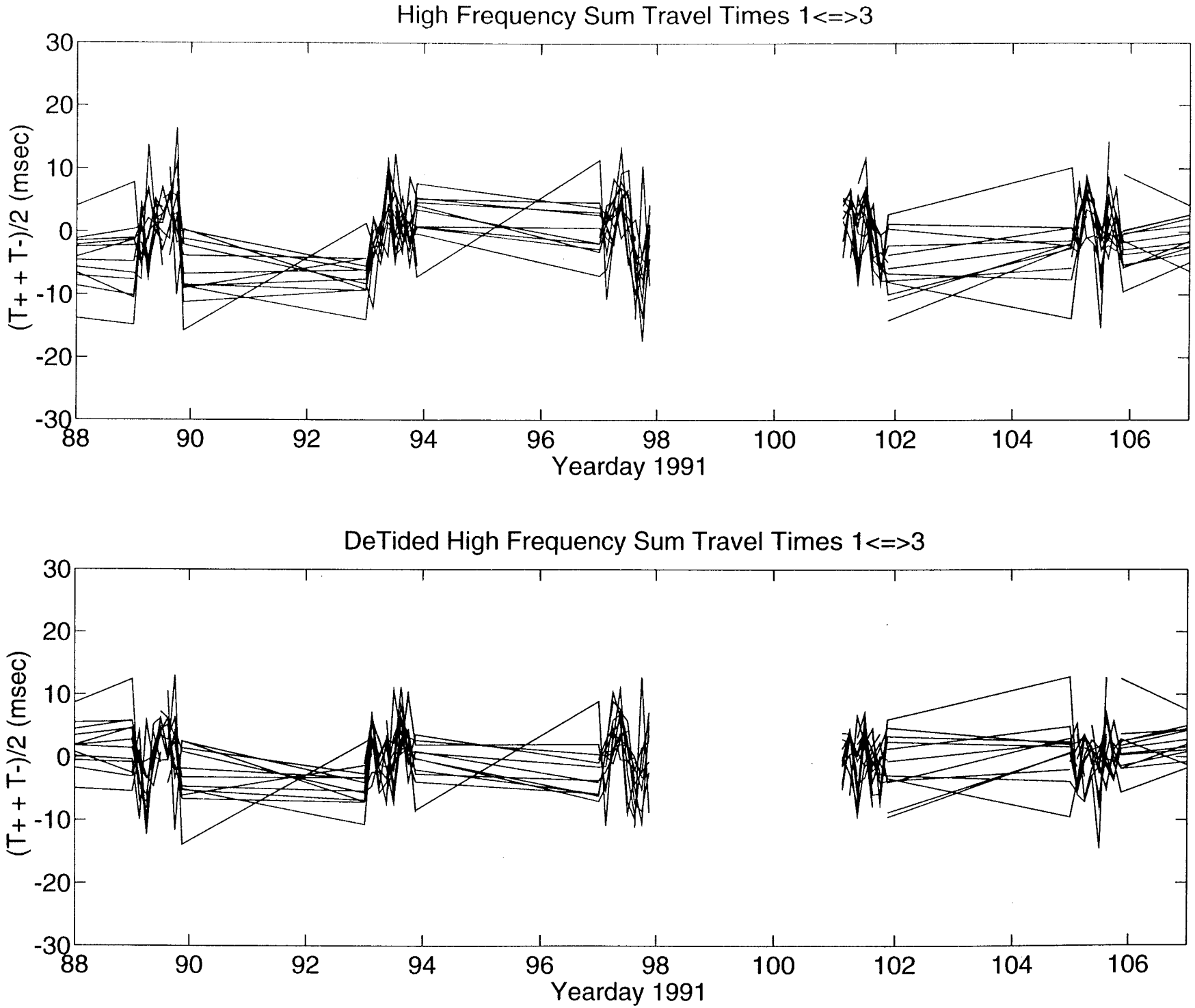
High Frequency Sum Travel Times 1<=>3
(T+ + T-)/2 (msec)
30
20
10
0
-10
-20
-30
88
90
92
94
96
98
100
102
104
106
Yearday 1991
DeTided High Frequency Sum Travel Times 1<=>3
(T+ + T-)/2 (msec)
30
20
10
0
-10
-20
-30
88
90
92
94
96
98
100
102
104
106
Yearday 1991

FIGURE H-6

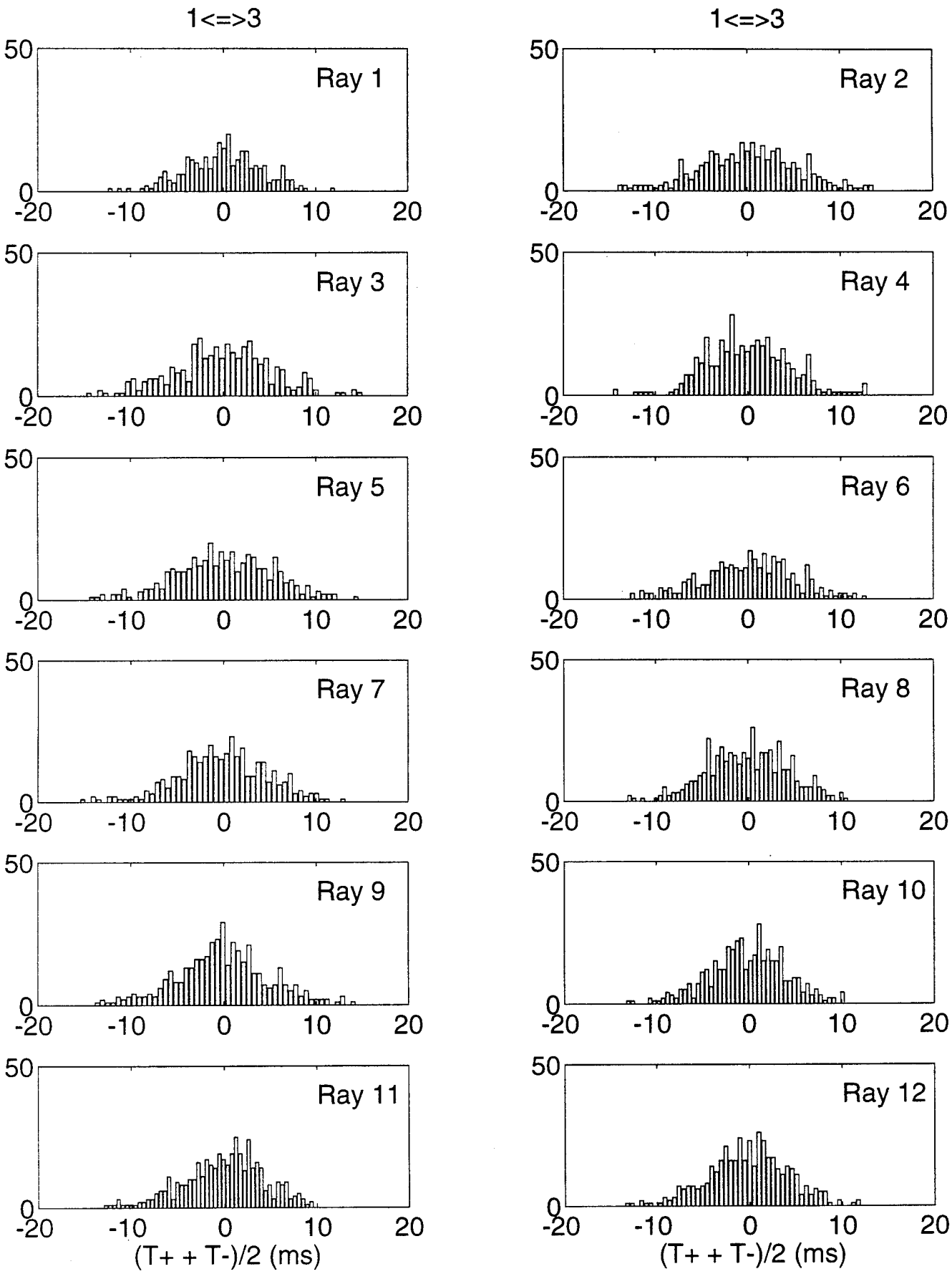
1<=>3
1<=>3
Ray 1
Ray 2
Ray 3
Ray 4
Ray 5
Ray 6
Ray 7
Ray 8
Ray 9
Ray 10
Ray 11
Ray 12
50
0
-20
-10
0
10
20
(T+ + T-)/2 (ms)
(T+ + T-)/2 (ms)

FIGURE H-7

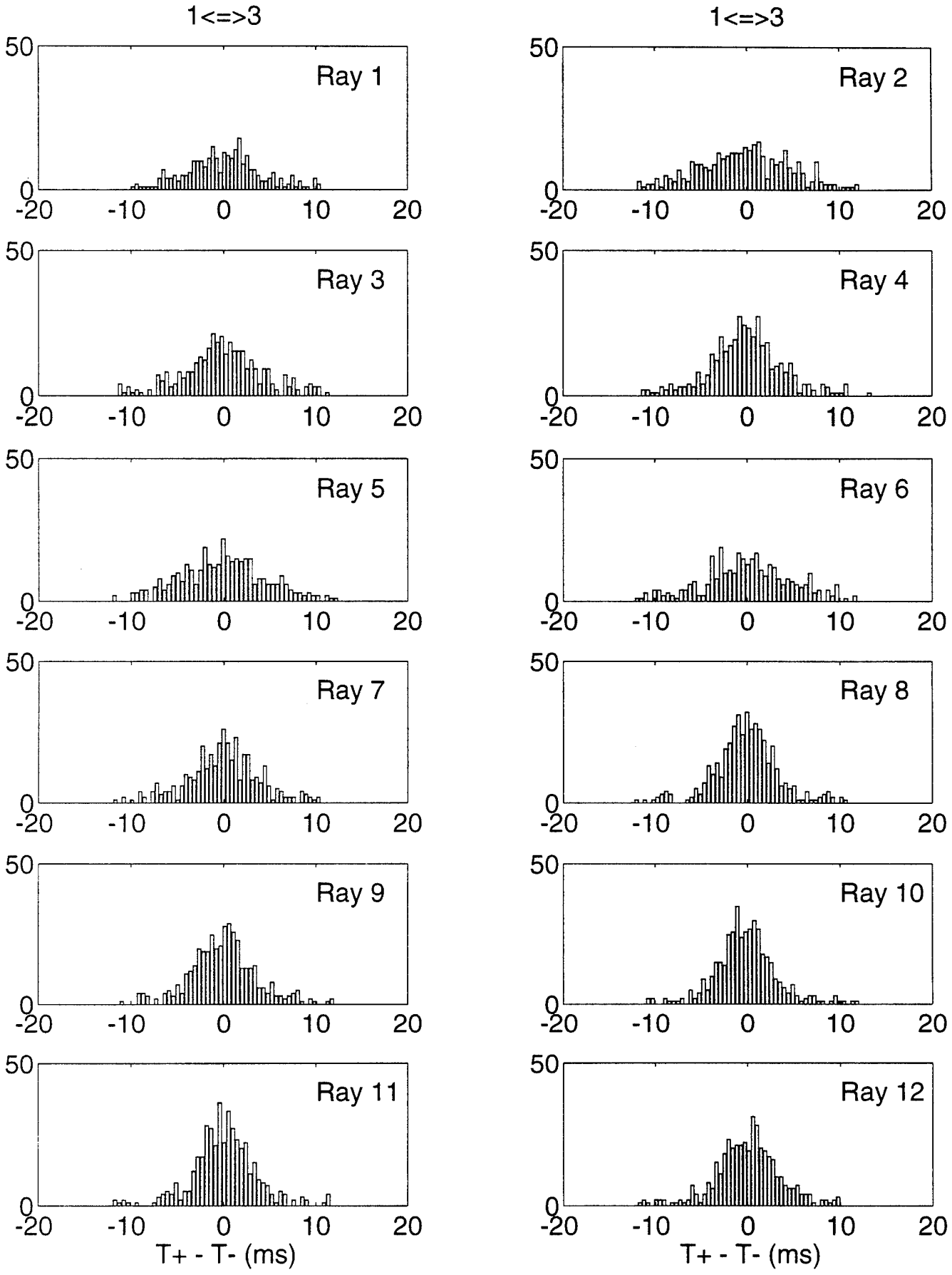
1<=>3
Ray 1
Ray 2
Ray 3
Ray 4
Ray 5
Ray 6
Ray 7
Ray 8
Ray 9
Ray 10
Ray 11
Ray 12
50
0
-20
-10
0
10
20
T+ - T- (ms)

FIGURE H-8

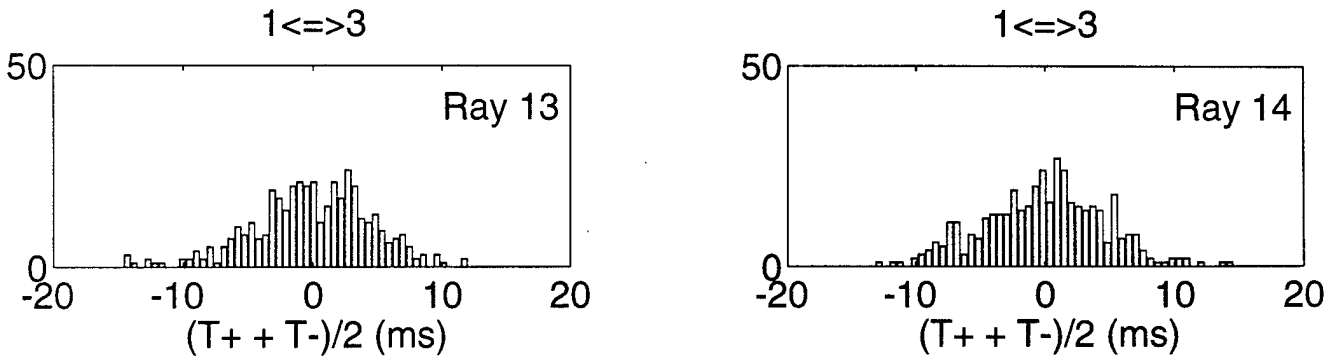

FIGURE H-7 (cont.)

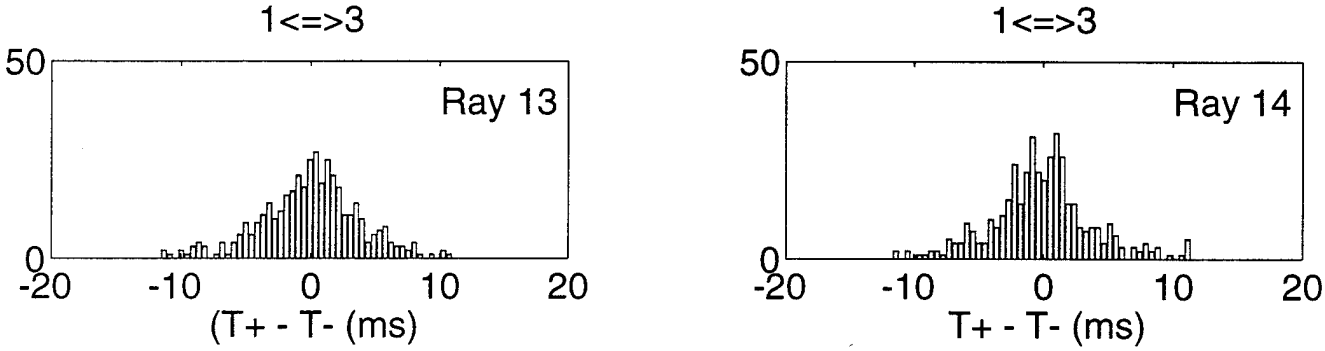

FIGURE H-8 (cont.)

I. ACOUSTIC DATA: Paths 1→4 and 4→1

FIGURE I-1 shows the raypaths, corresponding roughly to FIGURE G-1, for which travel times were resolved. The raypaths were actually determined using range-dependent Levitus sound speed, interpolated onto the acoustic path. Note that the "final cutoff" travel times may be available at some time in the future, these data correspond to a ray confined near the sound channel axis.

FIGURE I-2 shows the low-pass filtered difference (top panel) and sum (bottom panel) travel times corresponding to the rays of FIGURE I-1.

FIGURE I-3 shows the high-pass filtered difference travel times for a small portion of the time series obtained during the time of more frequent transmissions during the MST experiment. The bottom panel shows the time series after the phase-locked tidal signals have been removed. FIGURE I-4 shows the same time series, but during a time of the normal transmission schedule.

FIGURE I-5 shows the high-pass filtered sum travel times for a small portion of the time series obtained during the time of more frequent transmissions during the MST experiment. The bottom panel shows the time series after the phase-locked tidal signals have been removed. This tidal variability is caused by the internal tide. FIGURE I-6 shows the same time series, but during a time of the normal transmission schedule.

After the travel time time series have been edited for outliers, high-pass filtered, and detided, the high-frequency variances are calculated (TABLE I-1). Note that this table sometimes contains statistics for more rays than are indicated in TABLE B-1; some of the ray arrivals in TABLE I-1 have not been identified with predicted arrivals. Also, sometimes there is initial ambiguity about the pairing of reciprocal arrivals, in which case sum and difference travel times are calculated for all reasonable cases; later it becomes obvious which arrivals have been improperly paired. The correlation $<T^+ T^->$ and variance $<T^2>$ are calculated from the sum and difference travel time variances in this table. The variance of the travel times is mainly due to internal wave variability, and this value determines the uncertainties assigned to the travel times in an inversion. The correlation coefficient is a measure of the reciprocity of reciprocal raypaths. This measure is conservative, because correlation is not a necessary condition for the determination of current from the difference of reciprocal travel times. Values of correlation that are 0.5 or greater assure that the reciprocal raypaths are indeed effectively identical, since good correlation implies that the reciprocal raypaths have not separated by more than an internal wave correlation length. Histograms of the detided, high-frequency travel times are shown in FIGURES I-7 and I-8; the variances from TABLE I-1 are measures of the width of these histograms.

TABLES I-2 and I-3 show the results of tidal analysis of the time series of difference (current) and sum (sound speed) travel times. For these tables, the tidal analysis is performed on each travel time time series separately and then the average and rms of the harmonic constants are calculated. Current or sound speed amplitude is determined from travel time by a simple scaling factor; the harmonic constants are more accurately determined by inverting the data for current or sound speed (this is not done here).

TABLE I-1. Travel Time Statistics 1←→4.

Ray #	Number of data	$<(T^+ + T^-)^2>$ (ms^2)	$<(T^+ - T^-)^2>$ (ms^2)	$<T^+ T^->$ (ms^2)	$<T^2>$ (ms^2)	$\frac{<T^+ T^->}{<T^2>}$
1	25	3	2	3	4	0.76
2	44	13	23	8	19	0.41
3	301	30	23	24	35	0.68
4	352	26	20	21	31	0.68
5	360	21	15	17	24	0.69
6	419	24	13	20	27	0.76
7	268	32	20	27	36	0.73
8	321	25	19	20	30	0.67
9	332	27	16	23	31	0.74
10	448	23	10	21	26	0.81
11	421	28	13	25	32	0.80
12	434	23	11	20	26	0.79
13	456	24	9	22	26	0.82
14	398	24	17	20	29	0.70
15	411	24	15	20	27	0.73
16	341	24	17	19	28	0.69
17	446	26	14	22	29	0.76

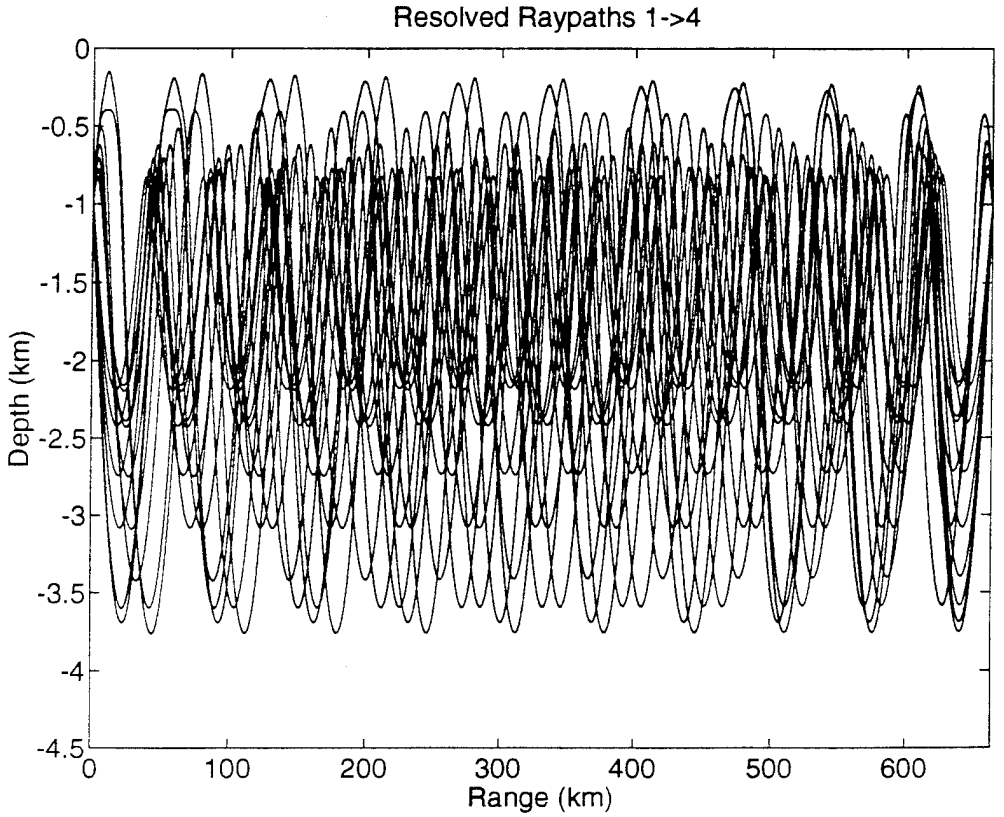

FIGURE I-1

TABLE I-2. Tidal Current Harmonic Constants 1←→4.

Constituent	Amplitude (mm/s)	Uncertainty (mm/s)	Phase (°G)	Uncertainty (°)
M_2	2.47	0.64	248.9	15.2
S_2	1.43	0.76	228.2	52.7
N_2	1.22	0.80	251.4	46.8
K_2	0.93	0.70	217.1	88.9
O_1	1.25	0.92	169.2	97.3
K_1	1.08	1.03	184.1	44.3
P_1	0.82	0.66	203.8	93.0
Q_1	0.69	0.49	201.5	87.3

Values and their uncertainty are determined by the average and rms of harmonic constants from tidal analyses of the separate raypath travel time series. The amplitudes do not include the lunar node factors. 15 ± 4 % of the high-frequency variance is accounted for by the tides.

TABLE I-3. Tidal Sound Speed Harmonic Constants 1←→4.

Constituent	Amplitude (mm/s)	Uncertainty (mm/s)	Phase (°G)	Uncertainty (°)
M_2	3.52	0.58	311.4	17.8
S_2	1.42	0.66	100.3	44.9
N_2	1.27	0.51	291.4	64.6
K_2	1.33	0.57	171.1	64.7
O_1	2.35	0.63	135.7	17.6
K_1	2.54	0.77	17.9	15.7
P_1	1.25	0.64	62.4	56.0
Q_1	1.22	0.55	55.7	41.7

Values and their uncertainty are determined by the average and rms of harmonic constants from tidal analyses of the separate raypath travel time series. The amplitudes do not include the lunar node factors. 20 ± 4 % of the high-frequency variance is accounted for by the tides. Because sum travel times are used to derive these numbers, the amplitudes have been divided by a factor of two compared to the amplitudes for current.

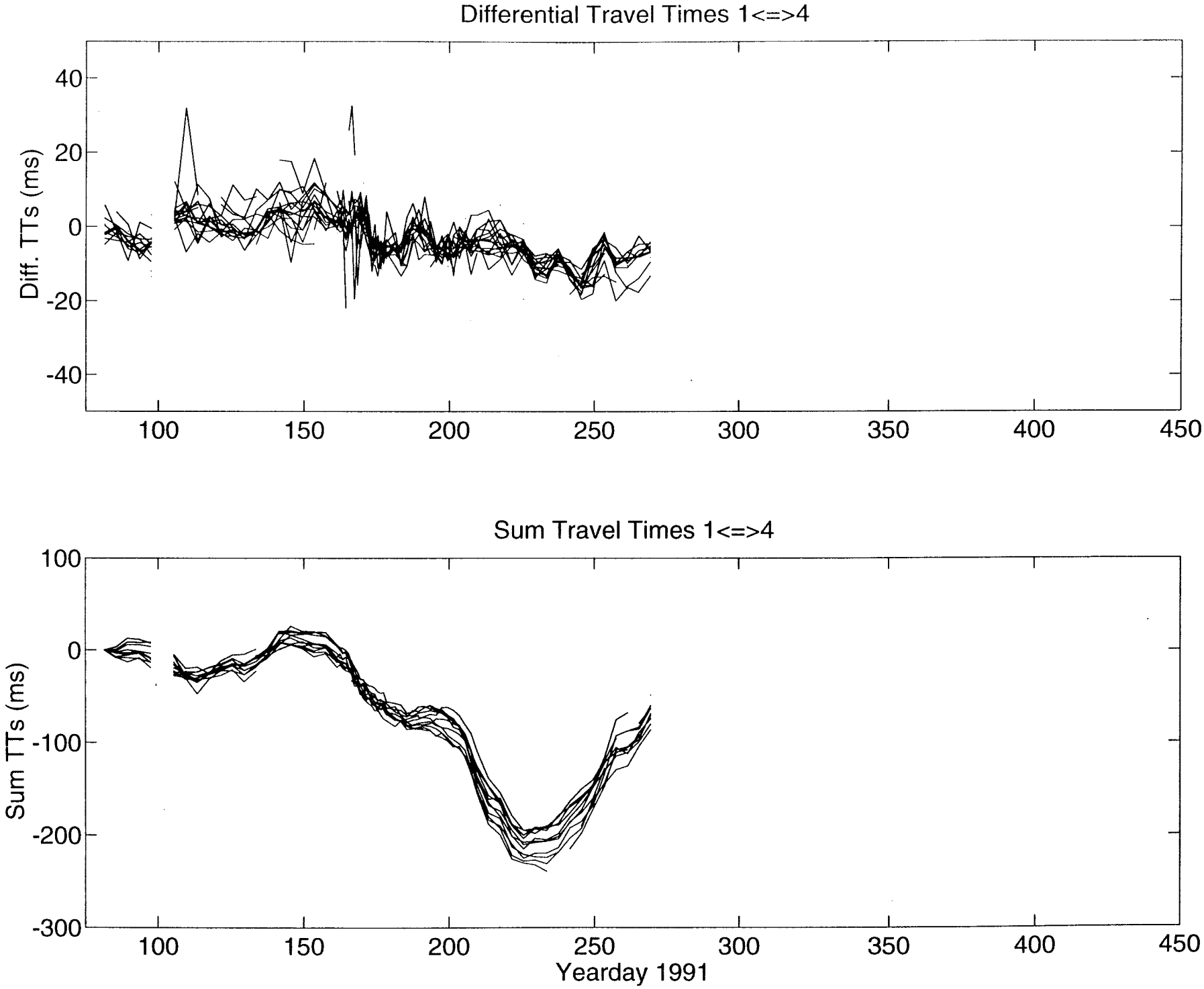
Differential Travel Times 1<=>4
Diff. TTs (ms)
40
20
0
-20
-40
100
150
200
250
300
350
400
450
Sum Travel Times 1<=>4
Sum TTs (ms)
100
0
-100
-200
-300
100
150
200
250
300
350
400
450
Yearday 1991

FIGURE I-2

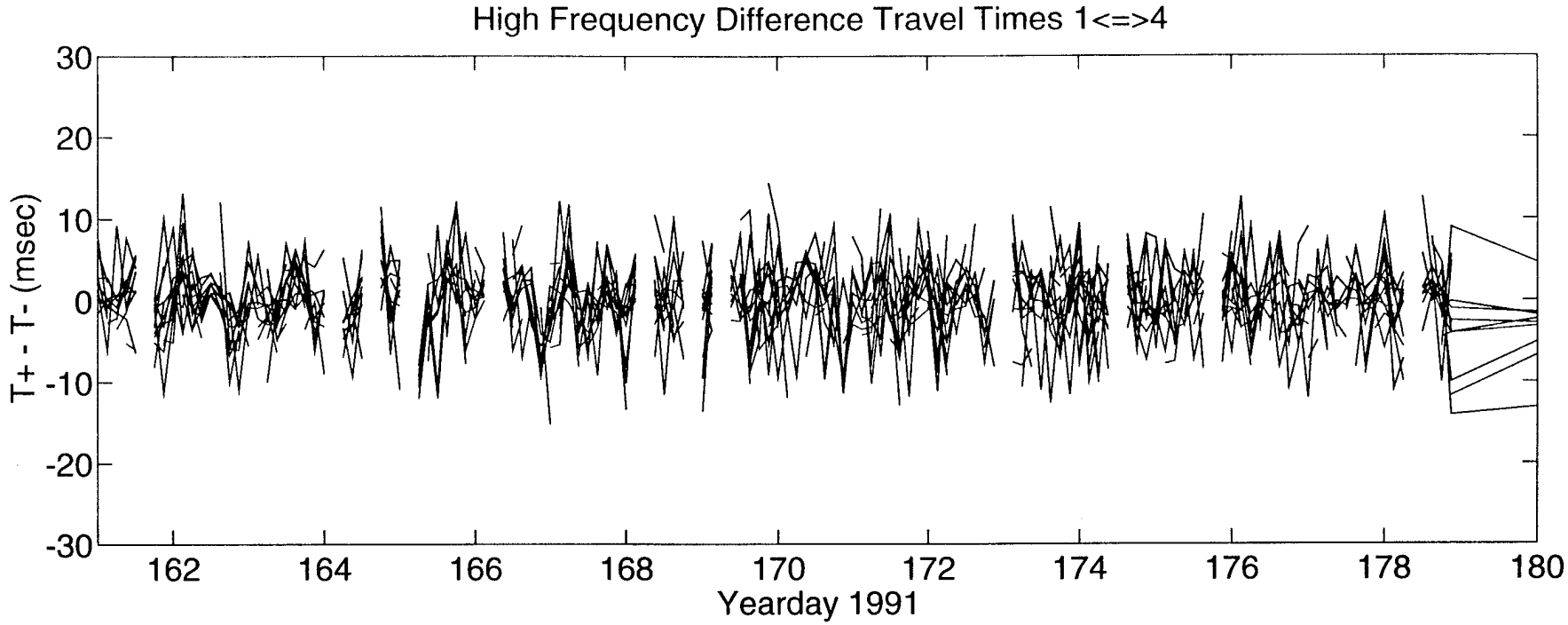
High Frequency Difference Travel Times 1<=>4
T+ - T- (msec)
30
20
10
0
-10
-20
-30
162
164
166
168
170
172
174
176
178
180
Yearday 1991

FIGURE I-3

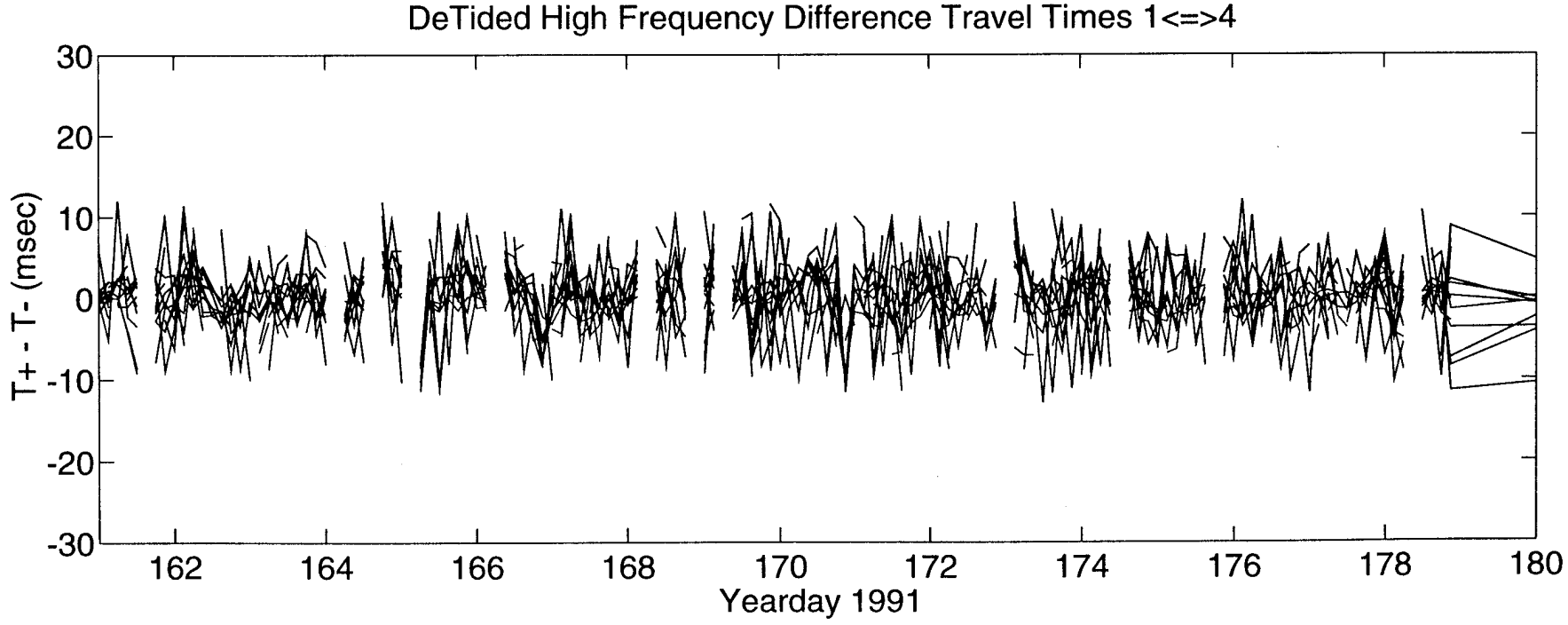
DeTided High Frequency Difference Travel Times 1<=>4
T+ - T- (msec)
30
20
10
0
-10
-20
-30
162
164
166
168
170
172
174
176
178
180
Yearday 1991

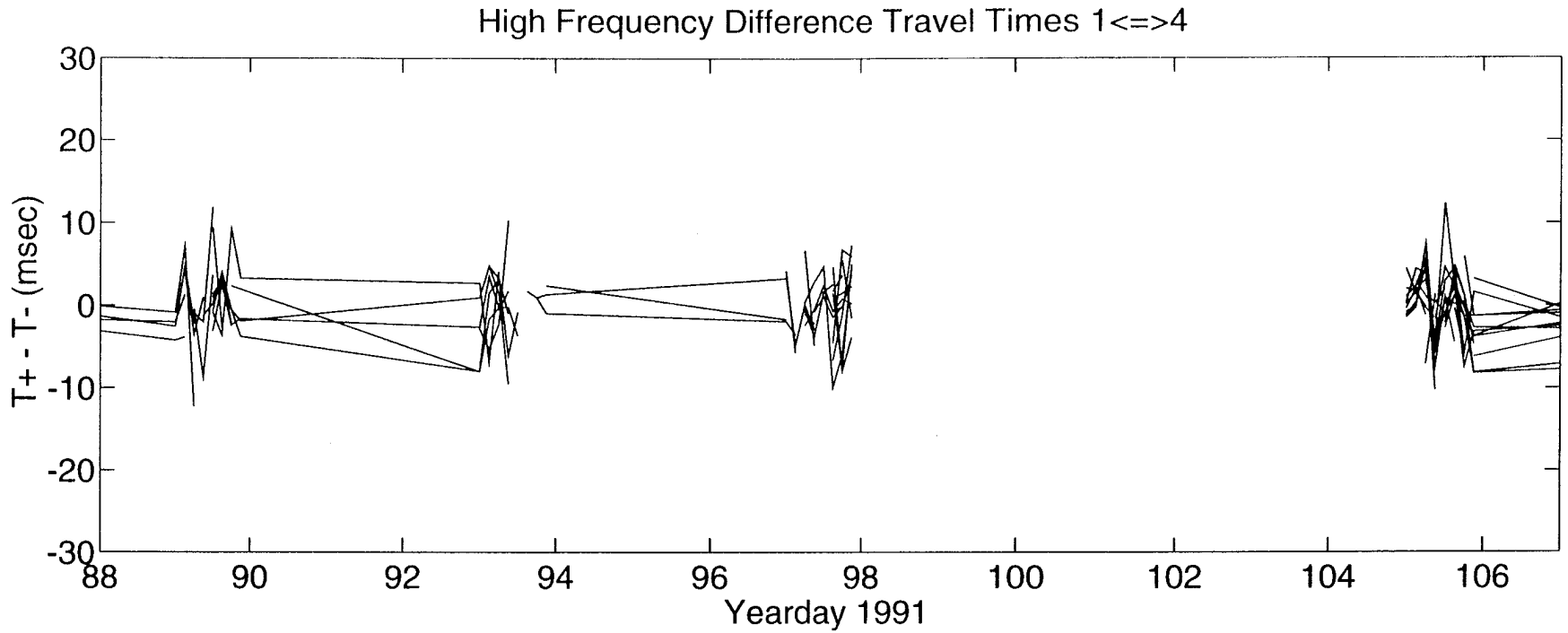
High Frequency Difference Travel Times 1<=>4
T+ - T- (msec)
30
20
10
0
-10
-20
-30
88
90
92
94
96
98
100
102
104
106
Yearday 1991

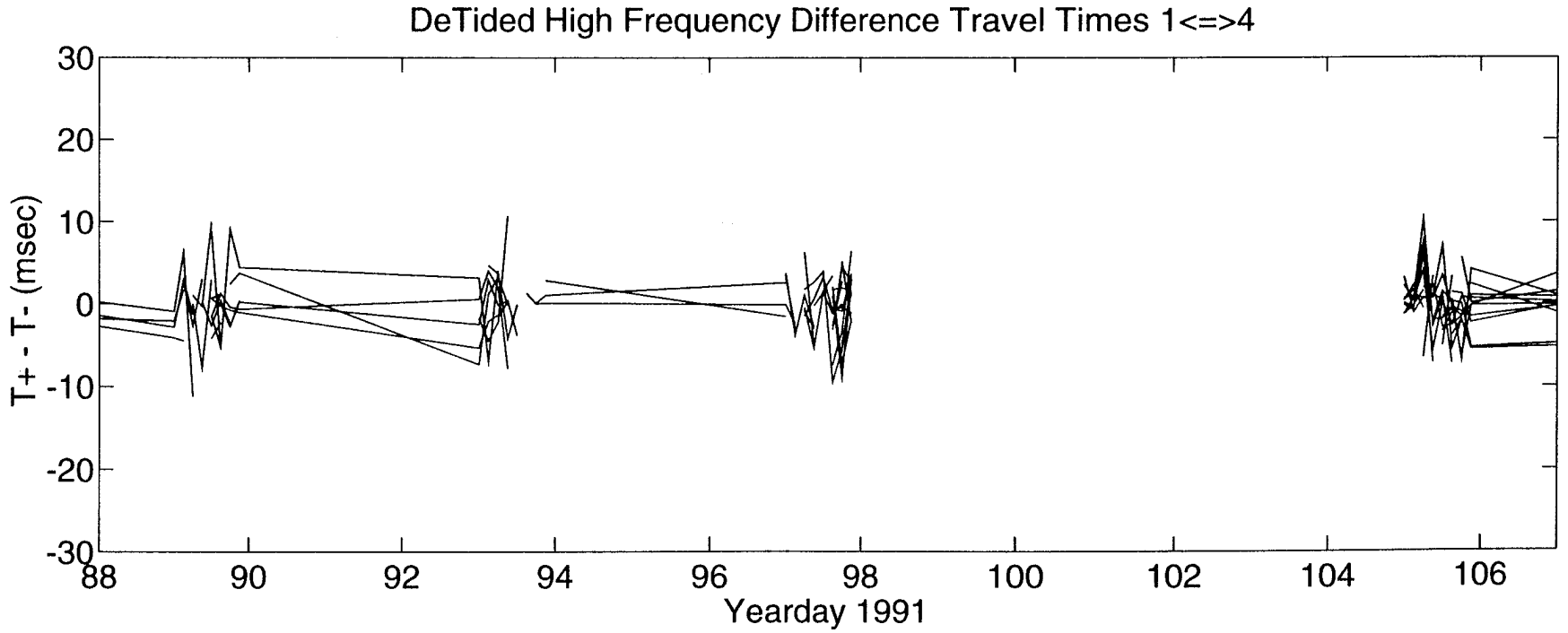
DeTided High Frequency Difference Travel Times 1<=>4
T+ - T- (msec)
30
20
10
0
-10
-20
-30
88
90
92
94
96
98
100
102
104
106
Yearday 1991

FIGURE I-4

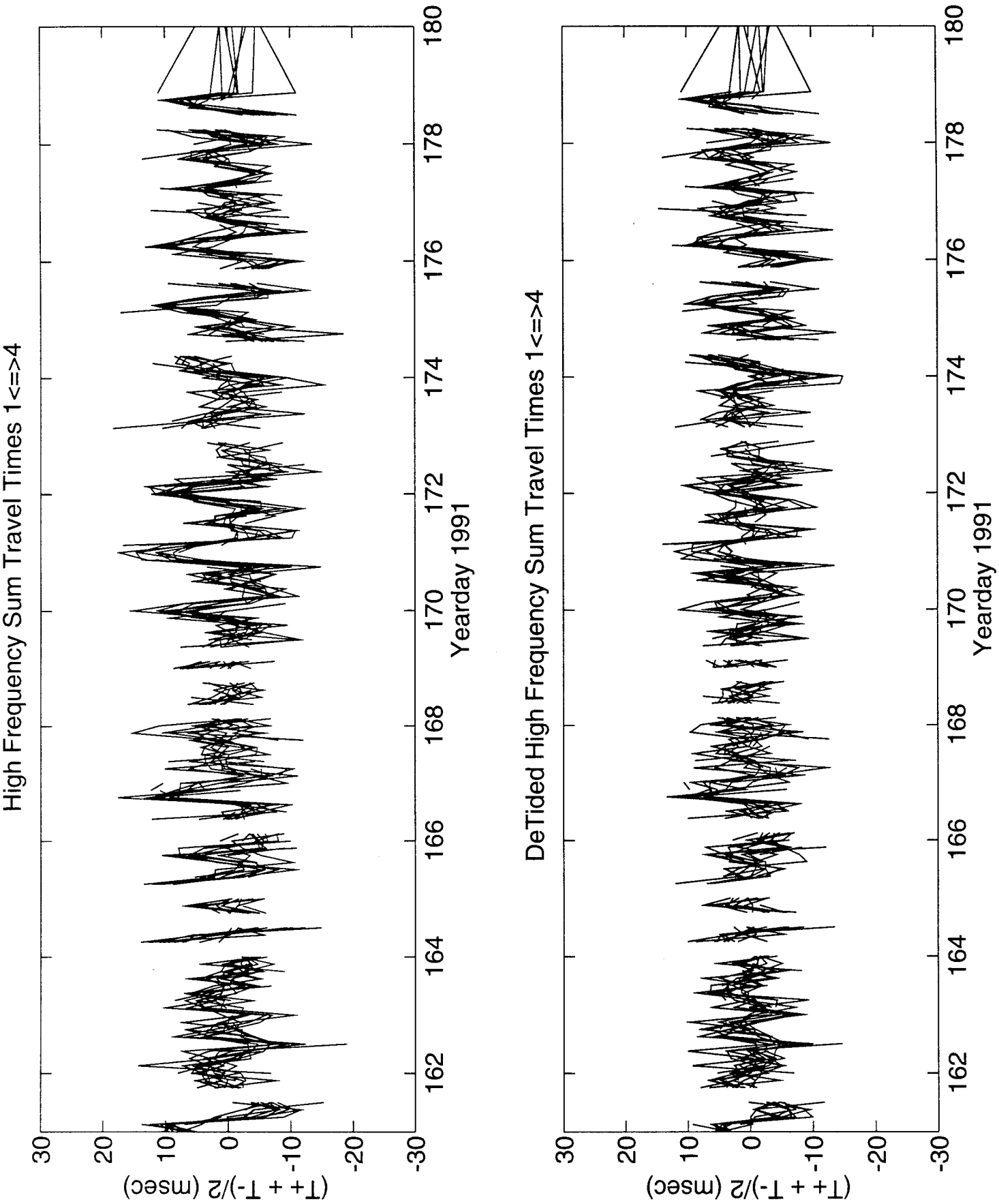
High Frequency Sum Travel Times 1<=>4
(T+ + T-)/2 (msec)
30
20
10
0
-10
-20
-30
162
164
166
168
170
172
174
176
178
180
Yearday 1991
DeTided High Frequency Sum Travel Times 1<=>4
(T+ + T-)/2 (msec)
30
20
10
0
-10
-20
-30
162
164
166
168
170
172
174
176
178
180
Yearday 1991

FIGURE I-5

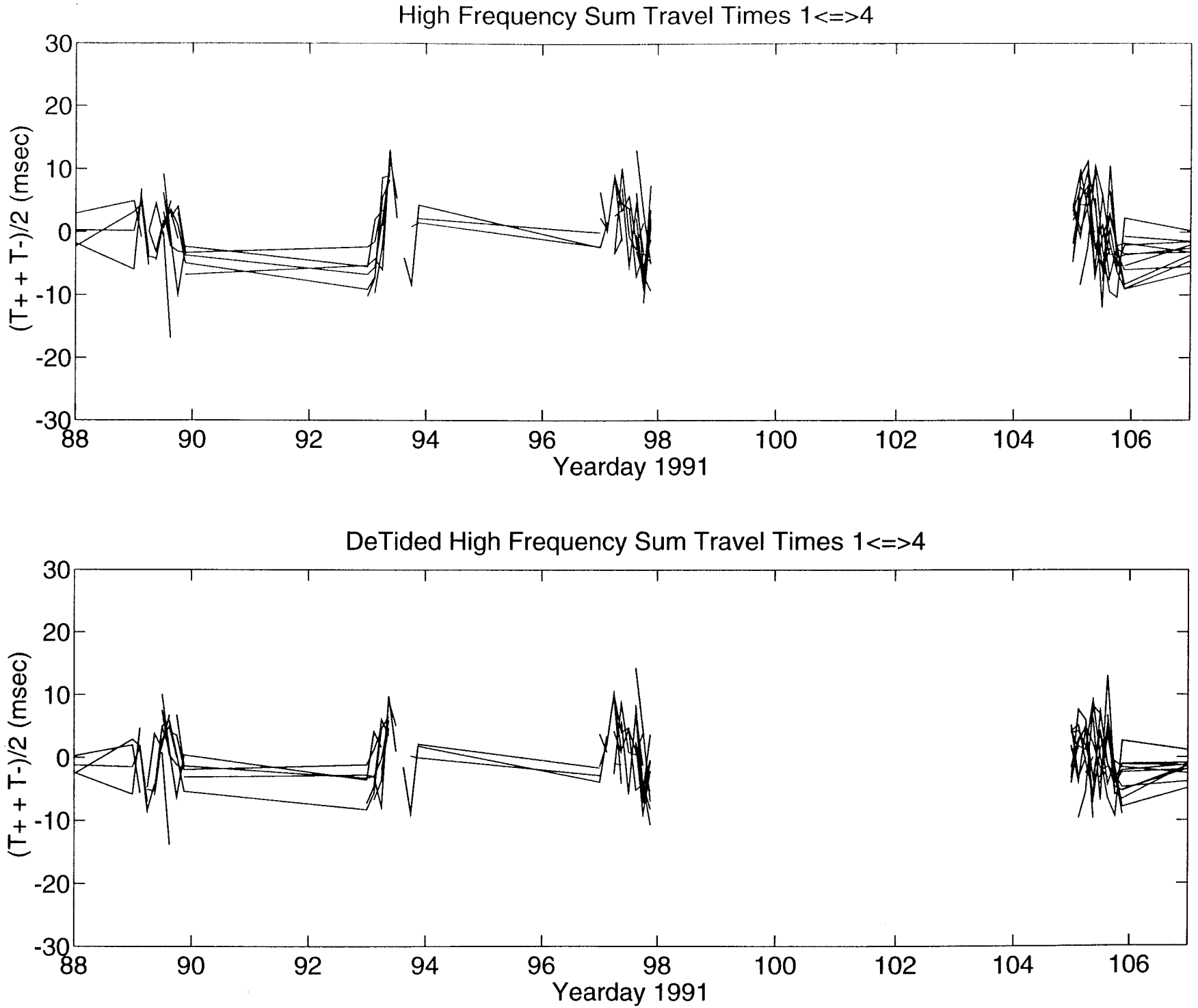
High Frequency Sum Travel Times 1<=>4
(T+ + T-)/2 (msec)
30
20
10
0
-10
-20
-30
88
90
92
94
96
98
100
102
104
106
Yearday 1991
DeTided High Frequency Sum Travel Times 1<=>4
(T+ + T-)/2 (msec)
30
20
10
0
-10
-20
-30
88
90
92
94
96
98
100
102
104
106
Yearday 1991

FIGURE 1-6

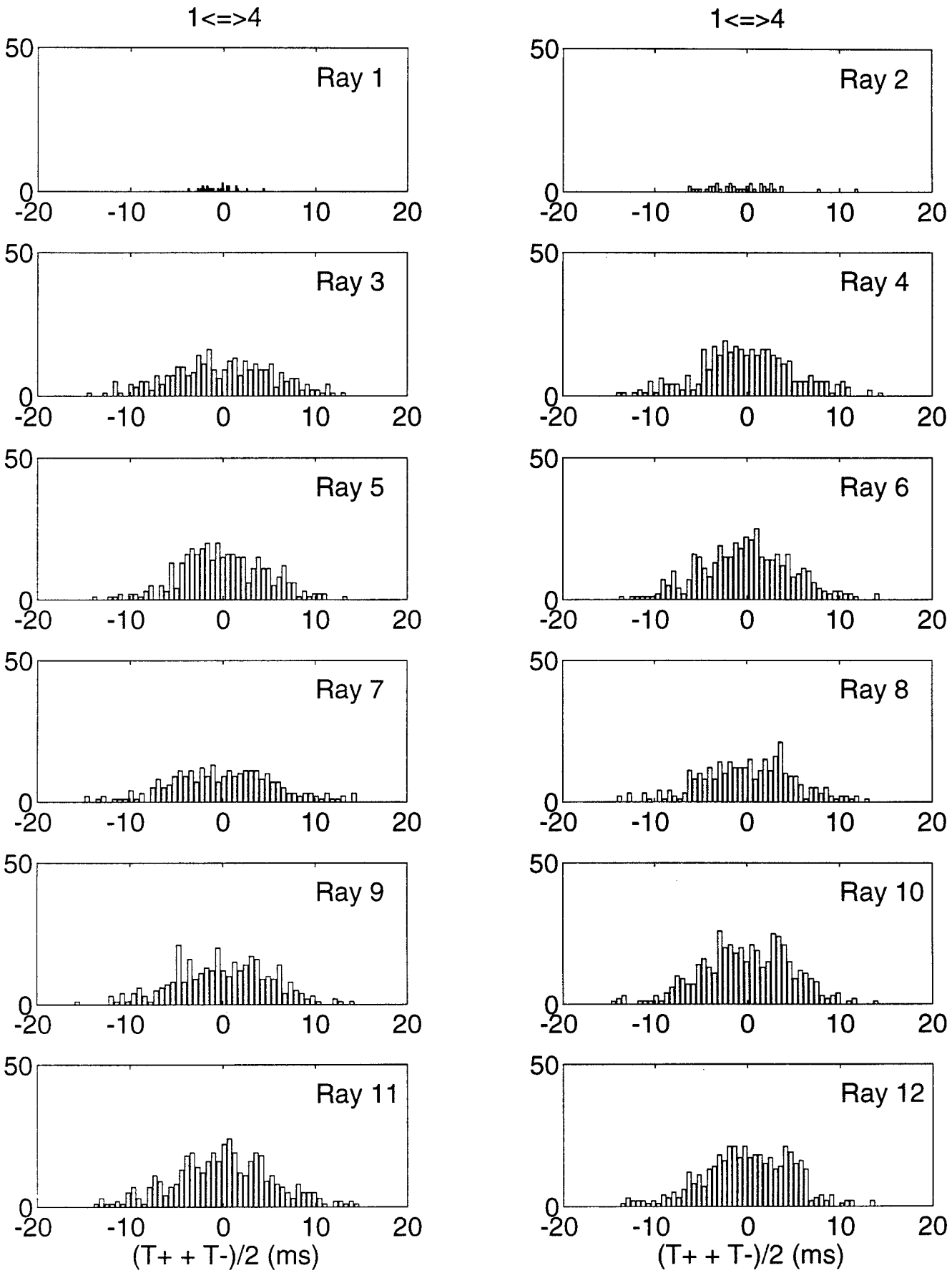
1<=>4
1<=>4
Ray 1
Ray 2
Ray 3
Ray 4
Ray 5
Ray 6
Ray 7
Ray 8
Ray 9
Ray 10
Ray 11
Ray 12
50
0
-20
-10
0
10
20
(T+ + T-)/2 (ms)

FIGURE I-7

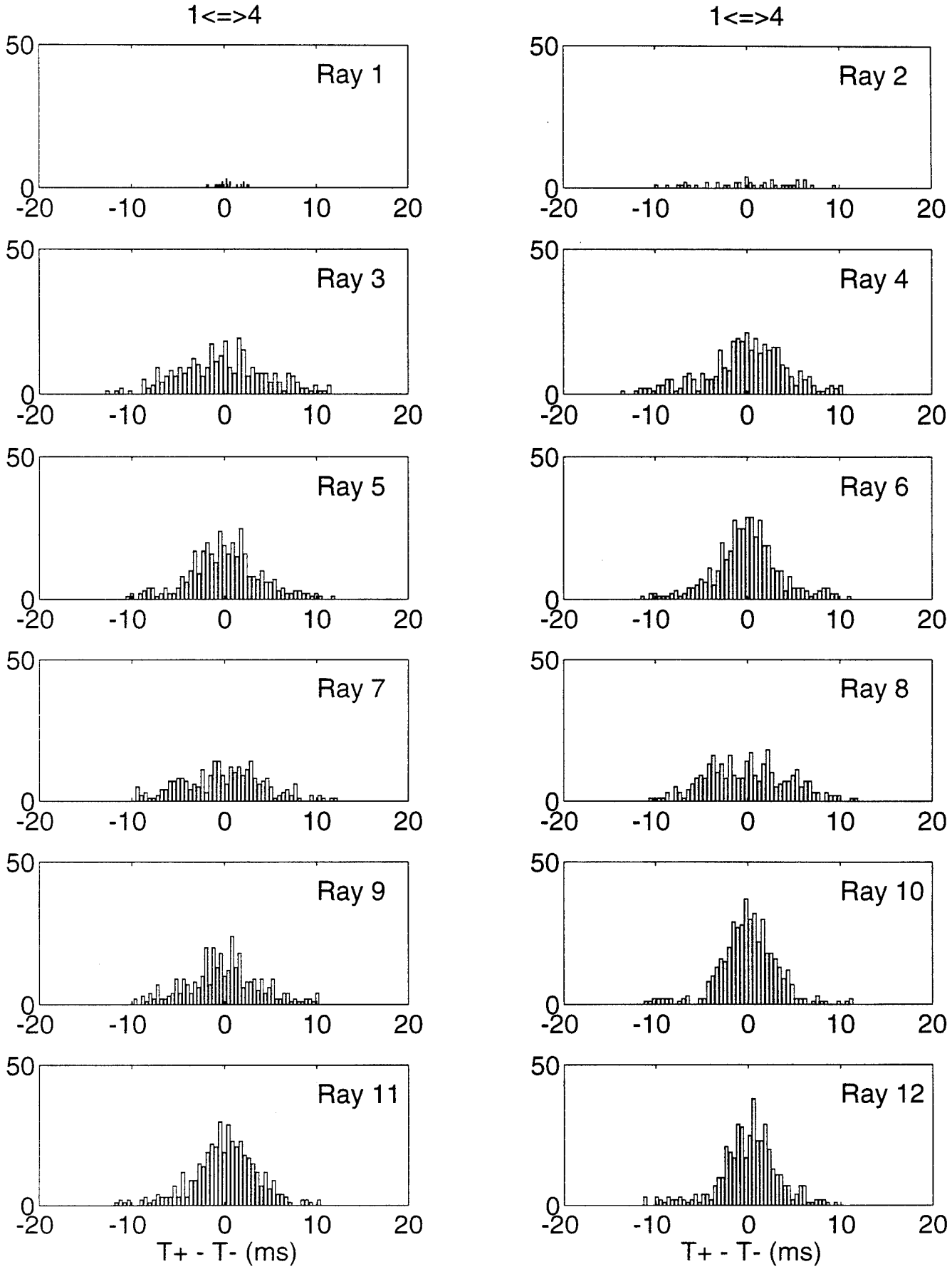
1<=>4
Ray 1
1<=>4
Ray 2
Ray 3
Ray 4
Ray 5
Ray 6
Ray 7
Ray 8
Ray 9
Ray 10
Ray 11
Ray 12
50
0
-20
-10
0
10
20
T+ - T- (ms)

FIGURE I-8

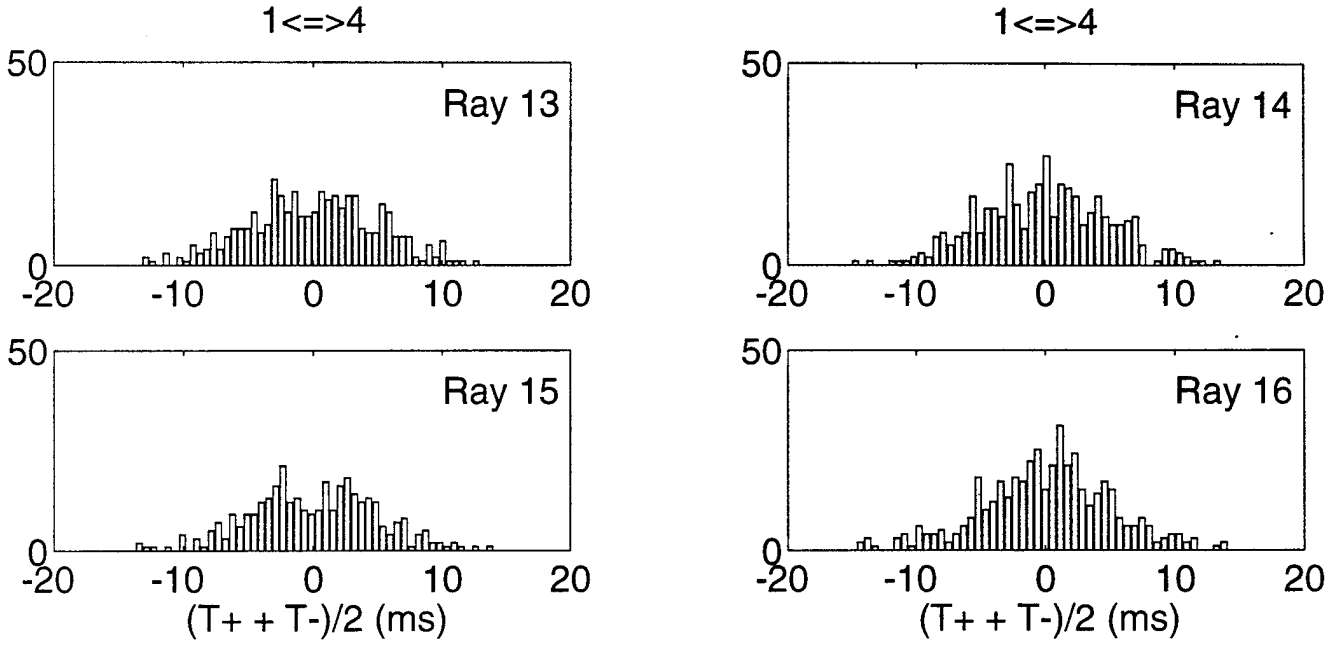

FIGURE I-7 (cont.)

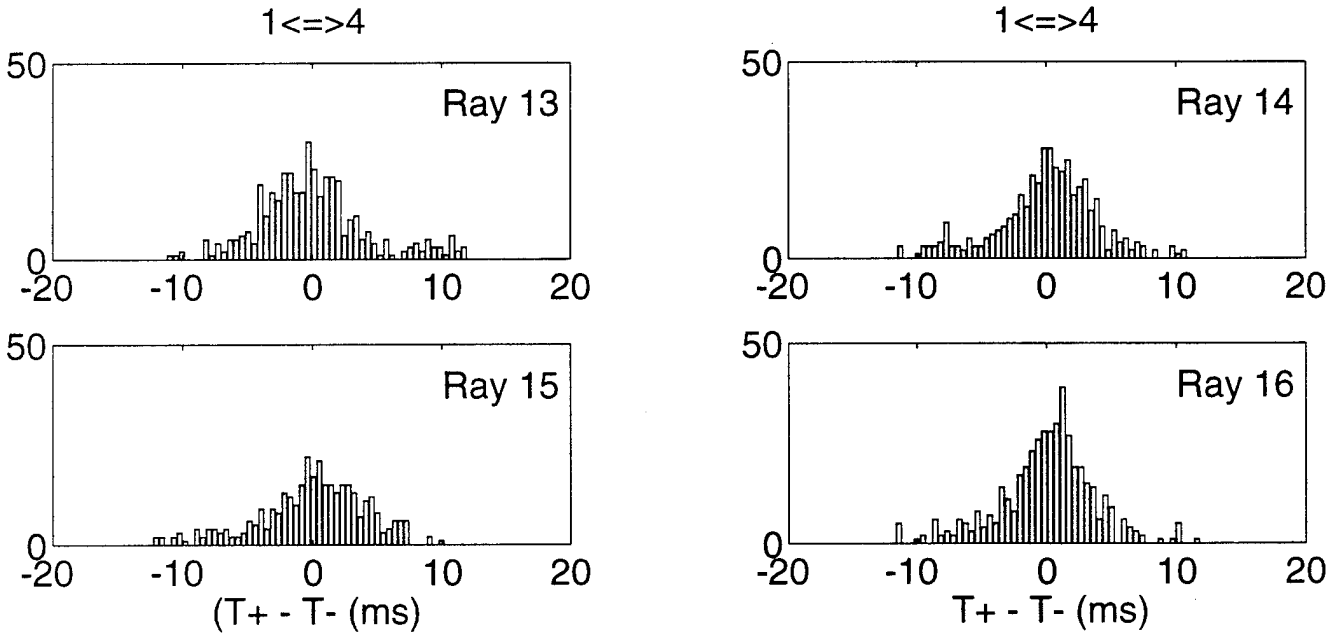

FIGURE I-8 (cont.)

J. ACOUSTIC DATA: Paths 1→5a and 5a→1

FIGURE J-1 shows the raypaths, corresponding roughly to FIGURE G-1, for which travel times were resolved. The raypaths were actually determined using range-dependent Levitus sound speed, interpolated onto the acoustic path. Note that the "final cutoff" travel times may be available at some time in the future, these data correspond to a ray confined near the sound channel axis.

FIGURE J-2 shows the low-pass filtered difference (top panel) and sum (bottom panel) travel times corresponding to the rays of FIGURE J-1. Note that mooring 5a had failed by yearday 140, to be replaced later by mooring 5b.

FIGURE J-3 shows the high-pass filtered difference travel times for a small portion of the time series. The bottom panel shows the time series after the phase-locked tidal signals have been removed.

FIGURE J-4 shows the high-pass filtered sum travel times for a small portion of the time series. The bottom panel shows the time series after the phase-locked tidal signals have been removed. This tidal variability is caused by the internal tide.

After the travel time time series have been edited for outliers, high-pass filtered, and detided, the high-frequency variances are calculated (TABLE J-1). Note that this table sometimes contains statistics for more rays than are indicated in TABLE B-1; some of the ray arrivals in TABLE J-1 have not been identified with predicted arrivals. Also, sometimes there is initial ambiguity about the pairing of reciprocal arrivals, in which case sum and difference travel times are calculated for all reasonable cases; later it becomes obvious which arrivals have been improperly paired. The correlation $<T^+ T^->$ and variance $<T^2>$ are calculated from the sum and difference travel time variances in this table. The variance of the travel times is mainly due to internal wave variability, and this value determines the uncertainties assigned to the travel times in an inversion. The correlation coefficient is a measure of the reciprocity of reciprocal raypaths. This measure is conservative, because correlation is not a necessary condition for the determination of current from the difference of reciprocal travel times. Values of correlation that are 0.5 or greater assure that the reciprocal raypaths are indeed effectively identical, since good correlation implies that the reciprocal raypaths have not separated by more than an internal wave correlation length. Histograms of the detided, high-frequency travel times are shown in FIGURES J-5 and J-6; the variances from TABLE J-1 are measures of the width of these histograms.

TABLES J-2 and J-3 show the results of tidal analysis of the time series of difference (current) and sum (sound speed) travel times. For these tables, the tidal analysis is performed on each travel time time series separately and then the average and rms of the harmonic constants are calculated. Current or sound speed amplitude is determined from travel time by a simple scaling factor; the harmonic constants are more accurately determined by inverting the data for current or sound speed (this is not done here).

TABLE J-1. Travel Time Statistics 1←→5a.

Ray #	Number of data	$<(T^+ + T^-)^2>$ (ms^2)	$<(T^+ - T^-)^2>$ (ms^2)	$<T^+ T^->$ (ms^2)	$<T^2>$ (ms^2)	$\frac{<T^+ T^->}{<T^2>}$
1	31	8	16	4	12	0.31
2	21	4	1	4	4	0.85
3	40	18	17	14	23	0.63
4	92	28	18	23	32	0.73
5	95	22	21	16	27	0.61
6	89	25	17	21	30	0.71
7	106	10	7	8	12	0.70
8	97	29	18	25	34	0.73
9	93	29	18	25	34	0.73
10	103	21	10	19	24	0.79
11	108	25	10	22	27	0.82
12	112	22	3	21	22	0.94
13	105	23	7	22	25	0.87
14	105	25	11	22	27	0.79
15	111	20	4	19	21	0.90

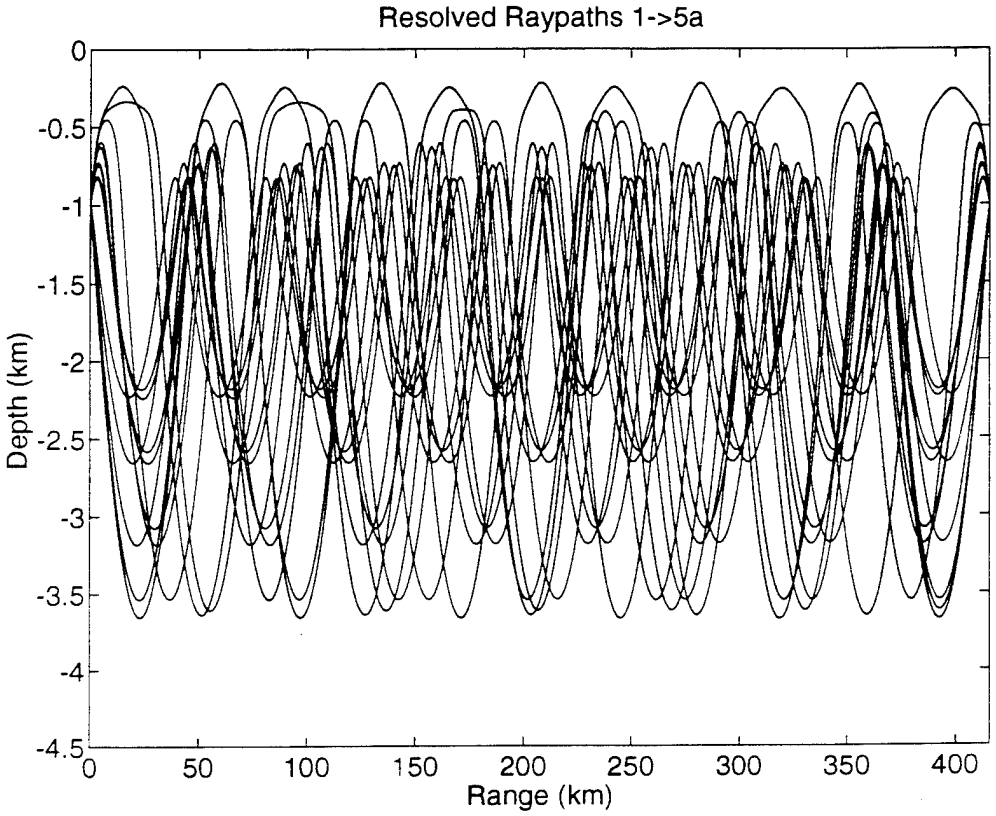

FIGURE J-1

TABLE J-2. Tidal Current Harmonic Constants 1←→5a.

Constituent	Amplitude (mm/s)	Uncertainty (mm/s)	Phase (°G)	Uncertainty (°)
M_2	10.36	2.38	273.8	18.4
S_2	6.28	3.99	260.5	89.3
N_2	3.66	2.47	246.4	60.6
K_2	5.30	3.92	189.2	112.3
O_1	2.07	1.13	150.8	86.6
K_1	3.97	2.02	153.9	87.8
P_1	4.04	1.71	262.6	97.0
Q_1	2.32	1.63	221.1	90.2

Values and their uncertainty are determined by the average and rms of harmonic constants from tidal analyses of the separate raypath travel time series. The amplitudes do not include the lunar node factors. 53 ± 10 % of the high-frequency variance is accounted for by the tides.

TABLE J-3. Tidal Sound Speed Harmonic Constants 1←→5a.

Constituent	Amplitude (mm/s)	Uncertainty (mm/s)	Phase (°G)	Uncertainty (°)
M_2	8.29	2.10	180.5	16.7
S_2	4.13	1.83	142.5	77.4
N_2	6.56	2.10	110.8	17.4
K_2	4.91	2.54	343.1	60.1
O_1	2.47	2.06	284.5	83.4
K_1	4.91	2.85	62.8	74.6
P_1	4.02	1.60	310.4	61.4
Q_1	5.16	1.46	245.5	18.5

Values and their uncertainty are determined by the average and rms of harmonic constants from tidal analyses of the separate raypath travel time series. The amplitudes do not include the lunar node factors. 39 ± 9 % of the high-frequency variance is accounted for by the tides. Because sum travel times are used to derive these numbers, the amplitudes have been divided by a factor of two compared to the amplitudes for current.

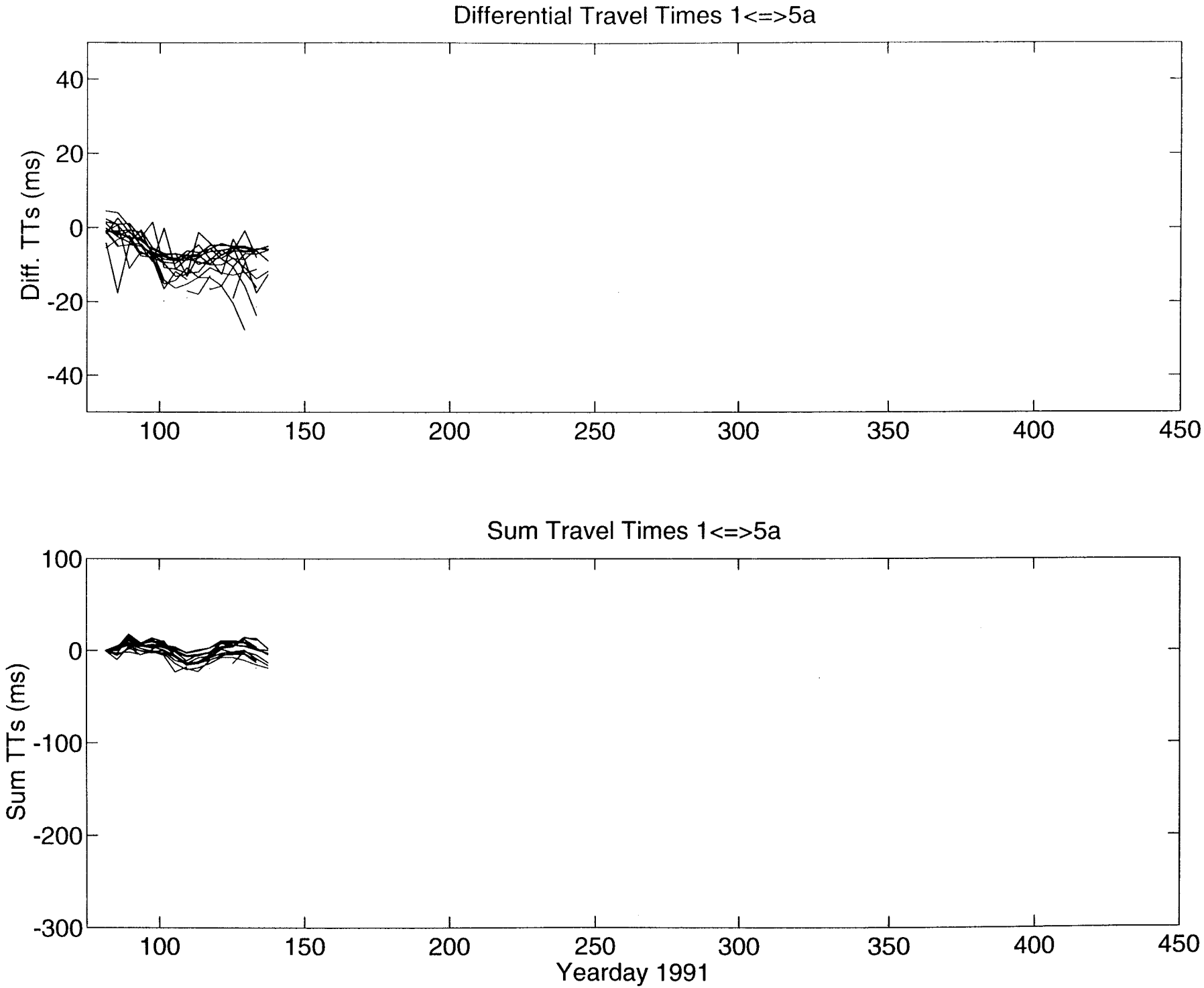
Differential Travel Times 1<=>5a
Diff. TTs (ms)
40
20
0
-20
-40
100
150
200
250
300
350
400
450
Sum Travel Times 1<=>5a
Sum TTs (ms)
100
0
-100
-200
-300
100
150
200
250
300
350
400
450
Yearday 1991

FIGURE J-2

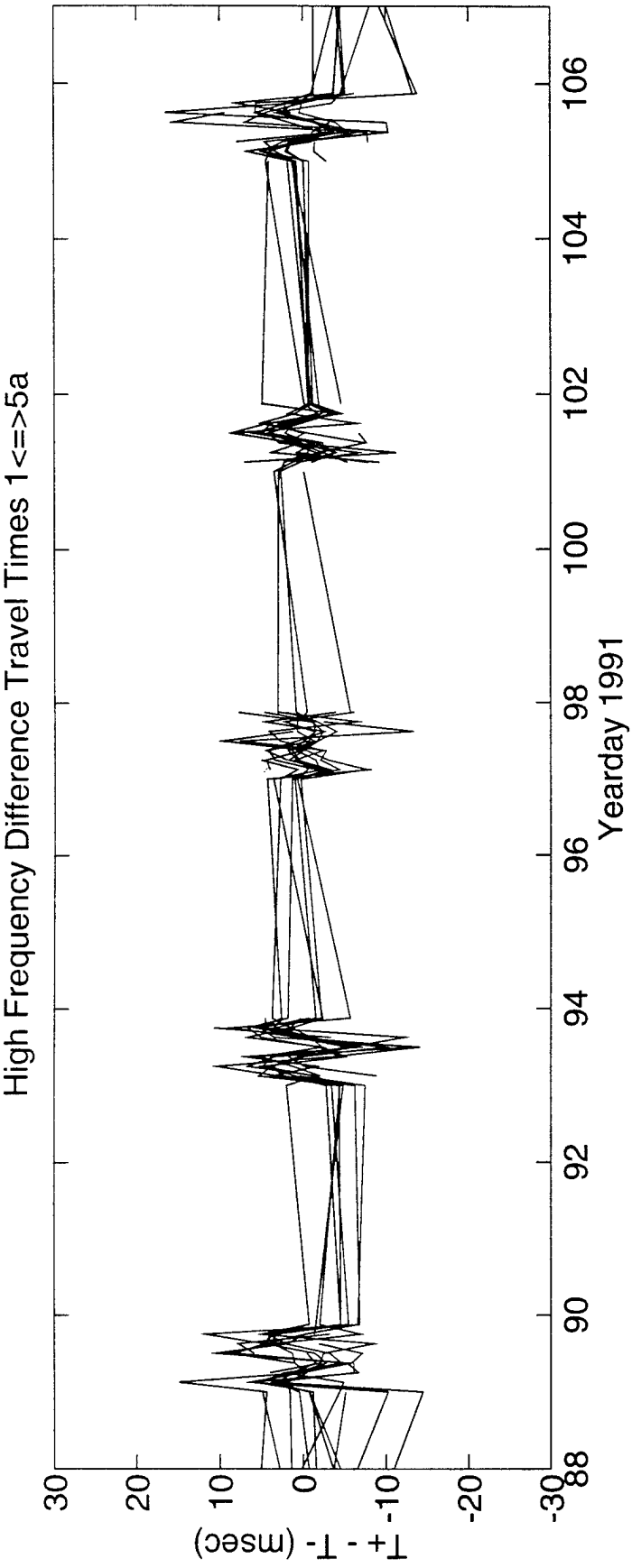
High Frequency Difference Travel Times 1<=>5a
T+ - T- (msec)
30
20
10
0
-10
-20
-30
88
90
92
94
96
98
100
102
104
106
Yearday 1991

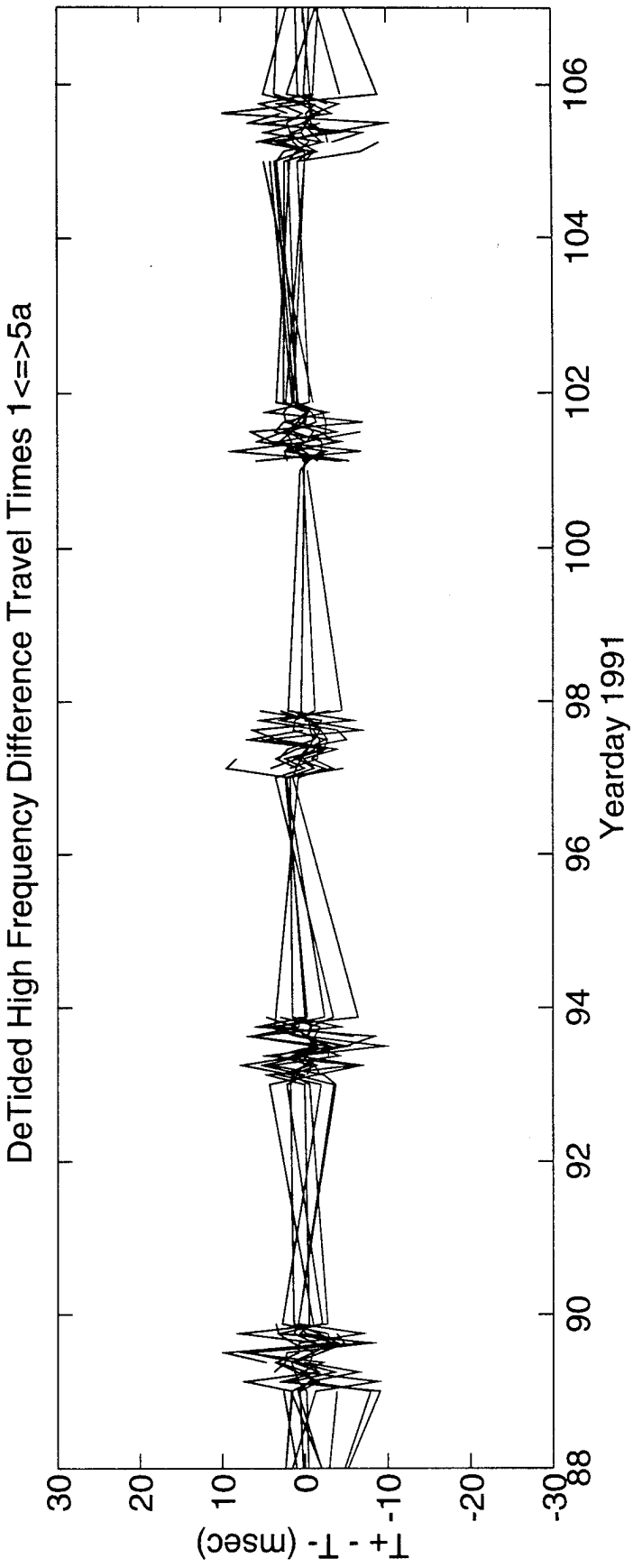
DeTided High Frequency Difference Travel Times 1<=>5a
T+ - T- (msec)
30
20
10
0
-10
-20
-30
88
90
92
94
96
98
100
102
104
106
Yearday 1991

FIGURE J-3

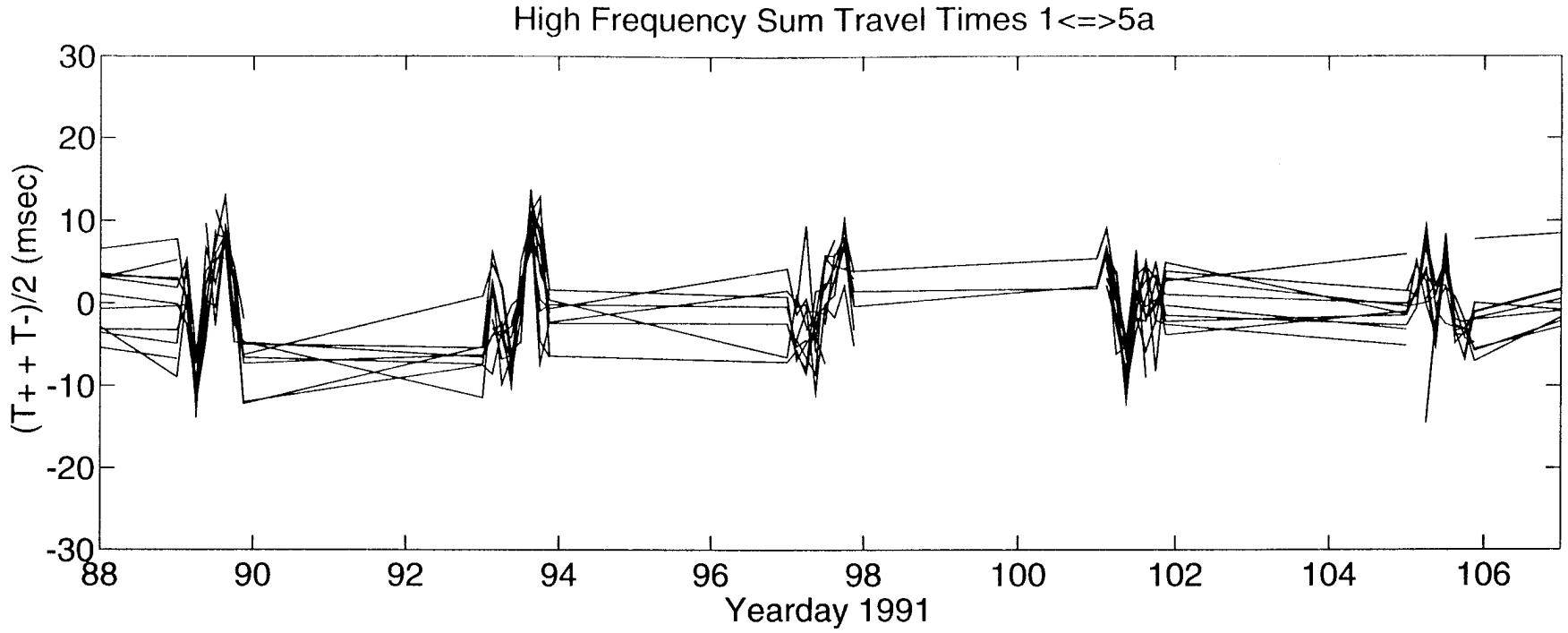
High Frequency Sum Travel Times 1<=>5a
(T+ + T-)/2 (msec)
30
20
10
0
-10
-20
-30
88
90
92
94
96
98
100
102
104
106
Yearday 1991

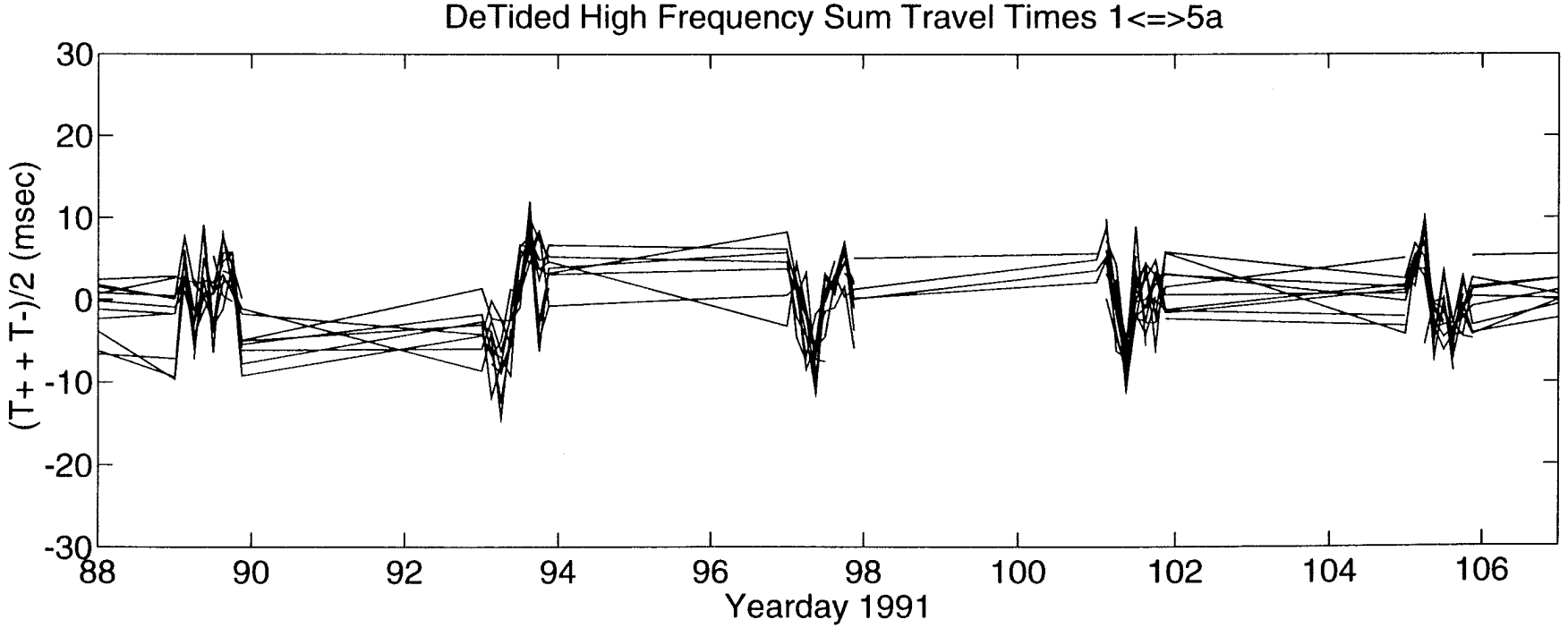
DeTided High Frequency Sum Travel Times 1<=>5a
(T+ + T-)/2 (msec)
30
20
10
0
-10
-20
-30
88
90
92
94
96
98
100
102
104
106
Yearday 1991

FIGURE J-4

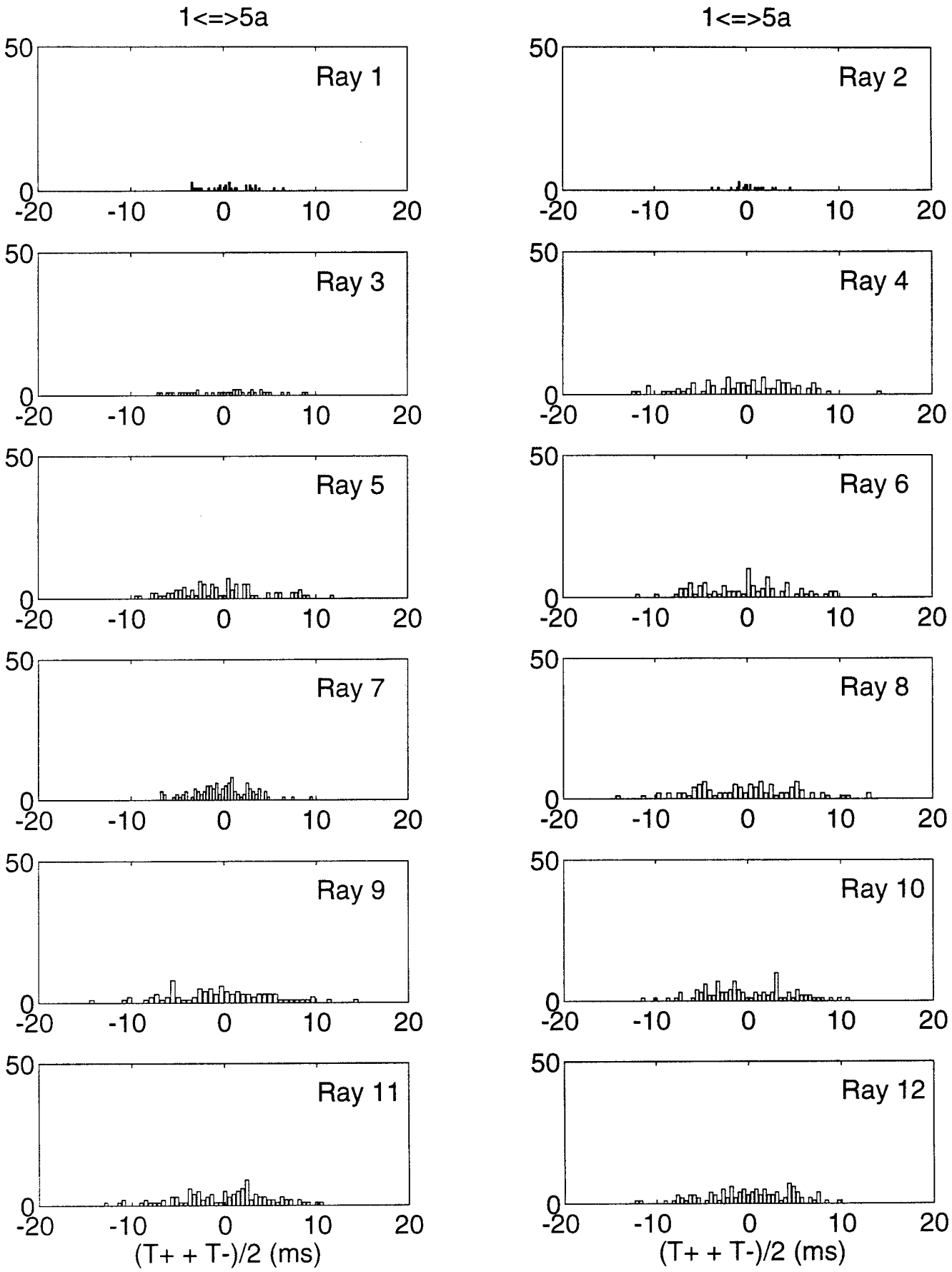
1<=>5a
1<=>5a
Ray 1
Ray 2
Ray 3
Ray 4
Ray 5
Ray 6
Ray 7
Ray 8
Ray 9
Ray 10
Ray 11
Ray 12
50
0
-20
-10
0
10
20
(T+ + T-)/2 (ms)

FIGURE J-5

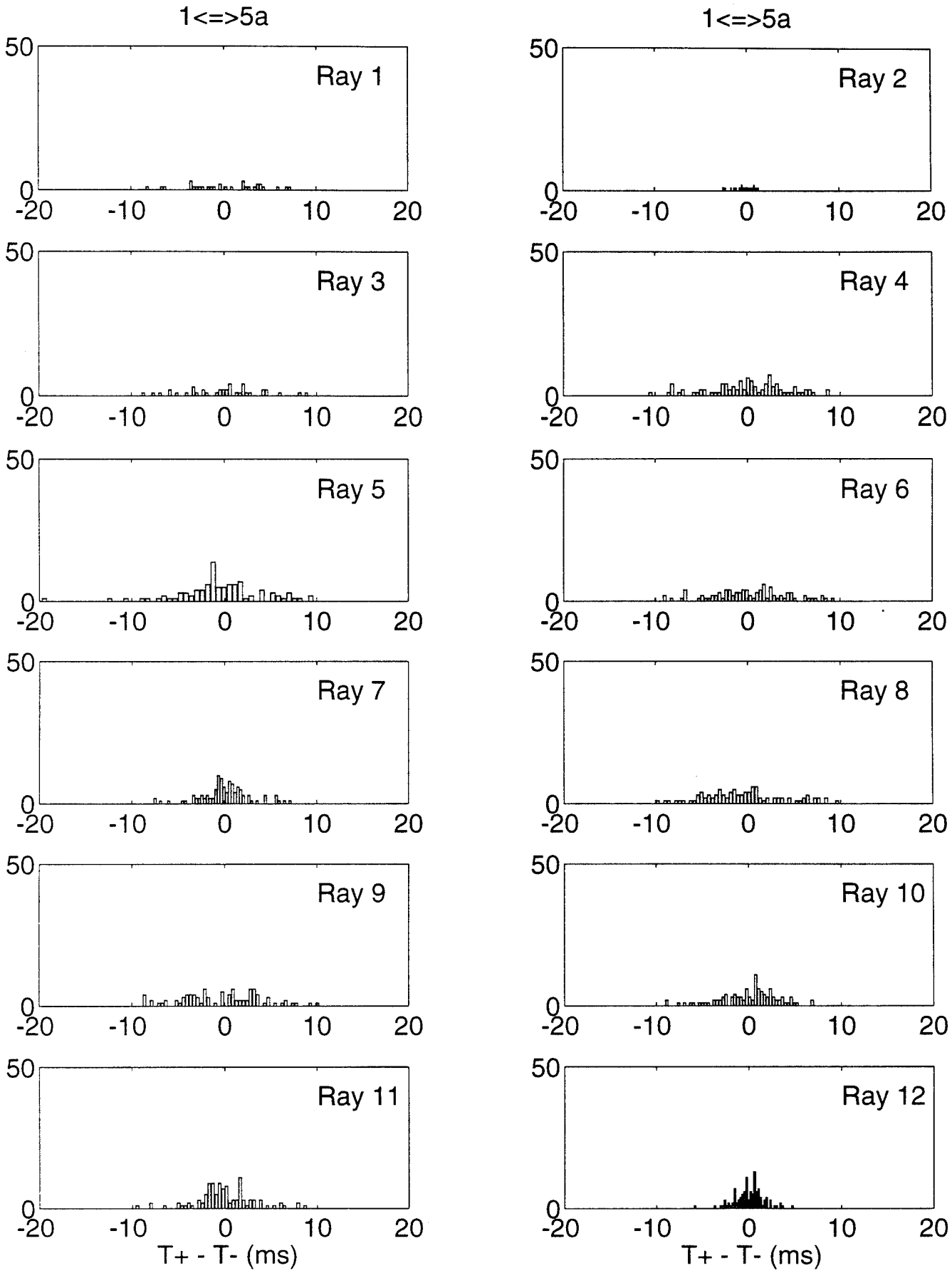
1<=>5a
1<=>5a
Ray 1
Ray 2
Ray 3
Ray 4
Ray 5
Ray 6
Ray 7
Ray 8
Ray 9
Ray 10
Ray 11
Ray 12
50
0
-20
-10
0
10
20
T+ - T- (ms)

FIGURE J-6

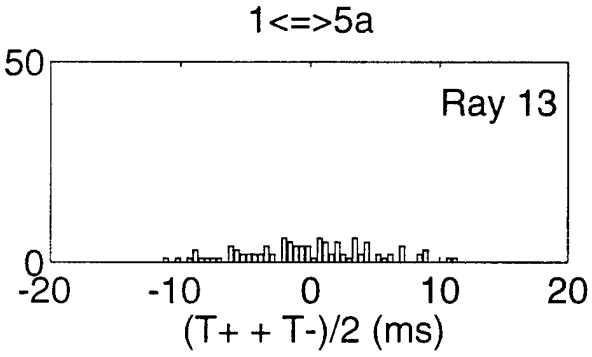

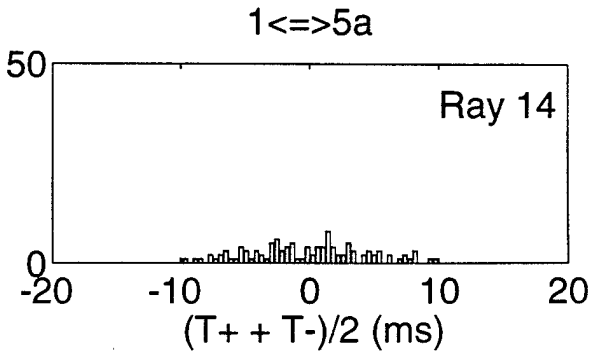

FIGURE J-5 (cont.)

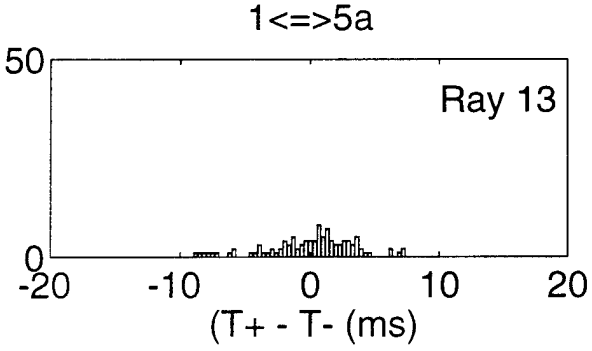

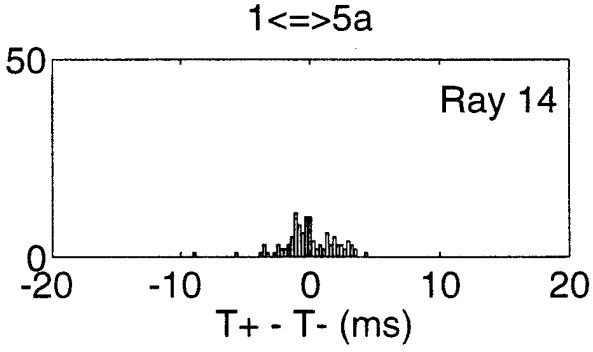

FIGURE J-6 (cont.)

K. ACOUSTIC DATA: Paths 1→5b and 5b→1

FIGURE K-1 shows the raypaths, corresponding roughly to FIGURE G-1, for which travel times were resolved. The raypaths were actually determined using range-dependent Levitus sound speed, interpolated onto the acoustic path. Note that the "final cutoff" travel times may be available at some time in the future, these data correspond to a ray confined near the sound channel axis.

FIGURE K-2 shows the low-pass filtered difference (top panel) and sum (bottom panel) travel times corresponding to the rays of FIGURE K-1.

FIGURE K-3 shows the high-pass filtered difference travel times for a small portion of the time series obtained during the time of more frequent transmissions during the MST experiment. The bottom panel shows the time series after the phase-locked tidal signals have been removed.

FIGURE K-4 shows the high-pass filtered sum travel times for a small portion of the time series obtained during the time of more frequent transmissions during the MST experiment. The bottom panel shows the time series after the phase-locked tidal signals have been removed. This tidal variability is caused by the internal tide.

After the travel time time series have been edited for outliers, high-pass filtered, and detided, the high-frequency variances are calculated (TABLE K-1). Note that this table sometimes contains statistics for more rays than are indicated in TABLE B-1; some of the ray arrivals in TABLE K-1 have not been identified with predicted arrivals. Also, sometimes there is initial ambiguity about the pairing of reciprocal arrivals, in which case sum and difference travel times are calculated for all reasonable cases; later it becomes obvious which arrivals have been improperly paired. The correlation $<T^+ T^->$ and variance $<T^2>$ are calculated from the sum and difference travel time variances in this table. The variance of the travel times is mainly due to internal wave variability, and this value determines the uncertainties assigned to the travel times in an inversion. The correlation coefficient is a measure of the reciprocity of reciprocal raypaths. This measure is conservative, because correlation is not a necessary condition for the determination of current from the difference of reciprocal travel times. Values of correlation that are 0.5 or greater assure that the reciprocal raypaths are indeed effectively identical, since good correlation implies that the reciprocal raypaths have not separated by more than an internal wave correlation length. Histograms of the detided, high-frequency travel times are shown in FIGURES K-5 and K-6; the variances from TABLE K-1 are measures of the width of these histograms.

TABLES K-2 and K-3 show the results of tidal analysis of the time series of difference (current) and sum (sound speed) travel times. For these tables, the tidal analysis is performed on each travel time time series separately and then the average and rms of the harmonic constants are calculated. Current or sound speed amplitude is determined from travel time by a simple scaling factor; the harmonic constants are more accurately determined by inverting the data for current or sound speed (this is not done here).

TABLE K-1. Travel Time Statistics 1←→5b.

Ray #	Number of data	$<(T^+ + T^-)^2>$ (ms^2)	$<(T^+ - T^-)^2>$ (ms^2)	$<T^+ T^->$ (ms^2)	$<T^2>$ (ms^2)	$\frac{<T^+ T^->}{<T^2>}$
1	292	18	12	15	21	0.71
2	239	21	15	17	24	0.69
3	266	22	15	18	26	0.70
4	317	13	4	12	14	0.86
5	257	21	17	17	26	0.66
6	288	16	9	13	18	0.74
7	250	22	18	17	26	0.65
8	303	20	7	18	22	0.83
9	318	16	4	15	17	0.89
10	289	16	5	14	17	0.86
11	293	15	6	13	17	0.81
12	320	19	3	18	20	0.91

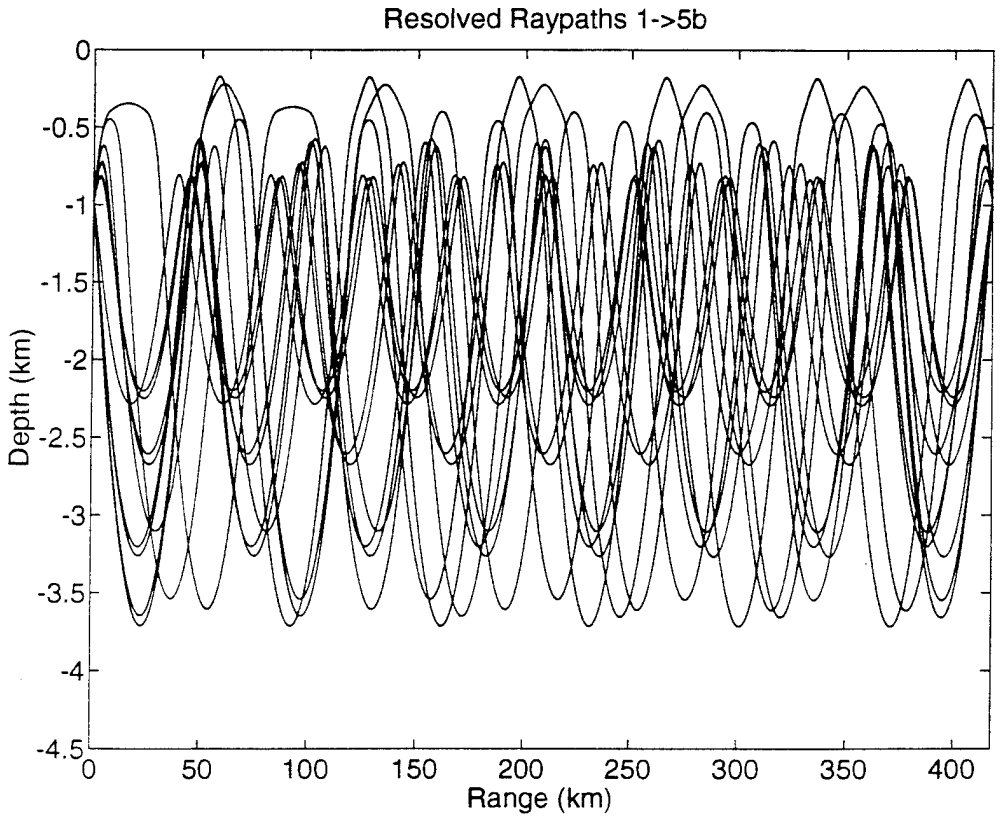

FIGURE K-1

TABLE K-2. Tidal Current Harmonic Constants 1←→5b.

Constituent	Amplitude (mm/s)	Uncertainty (mm/s)	Phase (°G)	Uncertainty (°)
M_2	9.00	1.05	275.6	6.5
S_2	2.53	0.87	305.5	54.1
N_2	2.90	1.21	257.5	25.0
K_2	1.58	0.90	331.8	62.4
O_1	1.65	0.99	197.9	75.7
K_1	1.81	0.98	152.3	71.9
P_1	1.50	1.15	183.0	82.5
Q_1	1.38	0.94	173.8	74.2

Values and their uncertainty are determined by the average and rms of harmonic constants from tidal analyses of the separate raypath travel time series. The amplitudes do not include the lunar node factors. 47 ± 15 % of the high-frequency variance is accounted for by the tides.

TABLE K-3. Tidal Sound Speed Harmonic Constants 1←→5b.

Constituent	Amplitude (mm/s)	Uncertainty (mm/s)	Phase (°G)	Uncertainty (°)
M_2	15.78	2.46	112.5	5.3
S_2	1.68	0.75	177.9	138.5
N_2	4.03	0.53	105.1	21.6
K_2	1.48	0.91	304.2	59.4
O_1	1.21	0.52	240.5	51.3
K_1	4.31	1.43	98.5	23.7
P_1	2.80	0.96	48.8	32.2
Q_1	1.40	0.48	174.5	45.6

Values and their uncertainty are determined by the average and rms of harmonic constants from tidal analyses of the separate raypath travel time series. The amplitudes do not include the lunar node factors. 54 ± 8 % of the high-frequency variance is accounted for by the tides. Because sum travel times are used to derive these numbers, the amplitudes have been divided by a factor of two compared to the amplitudes for current.

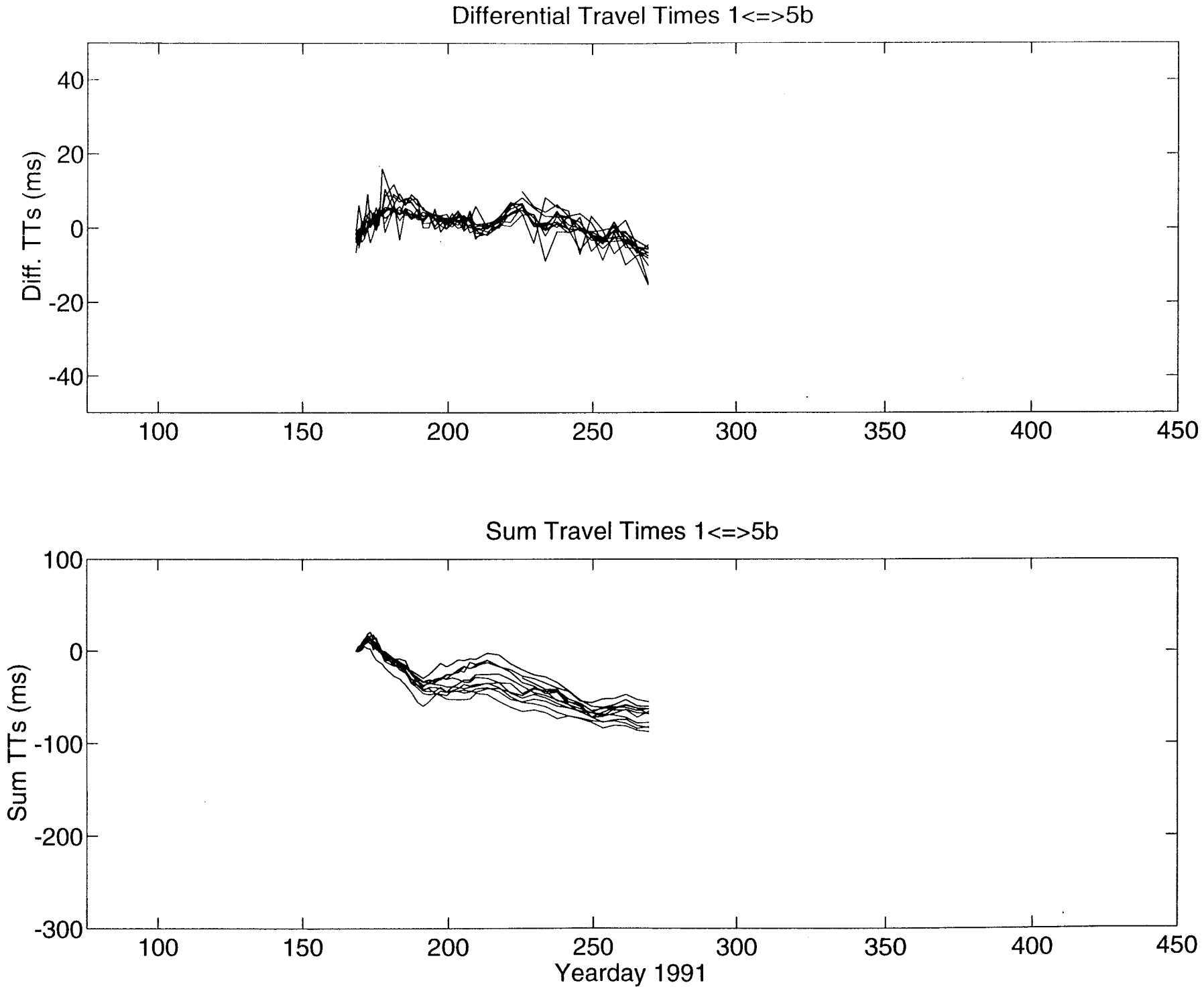
Differential Travel Times 1<=>5b
Diff. TTs (ms)
40
20
0
-20
-40
100
150
200
250
300
350
400
450
Sum Travel Times 1<=>5b
Sum TTs (ms)
100
0
-100
-200
-300
100
150
200
250
300
350
400
450
Yearday 1991

FIGURE K-2

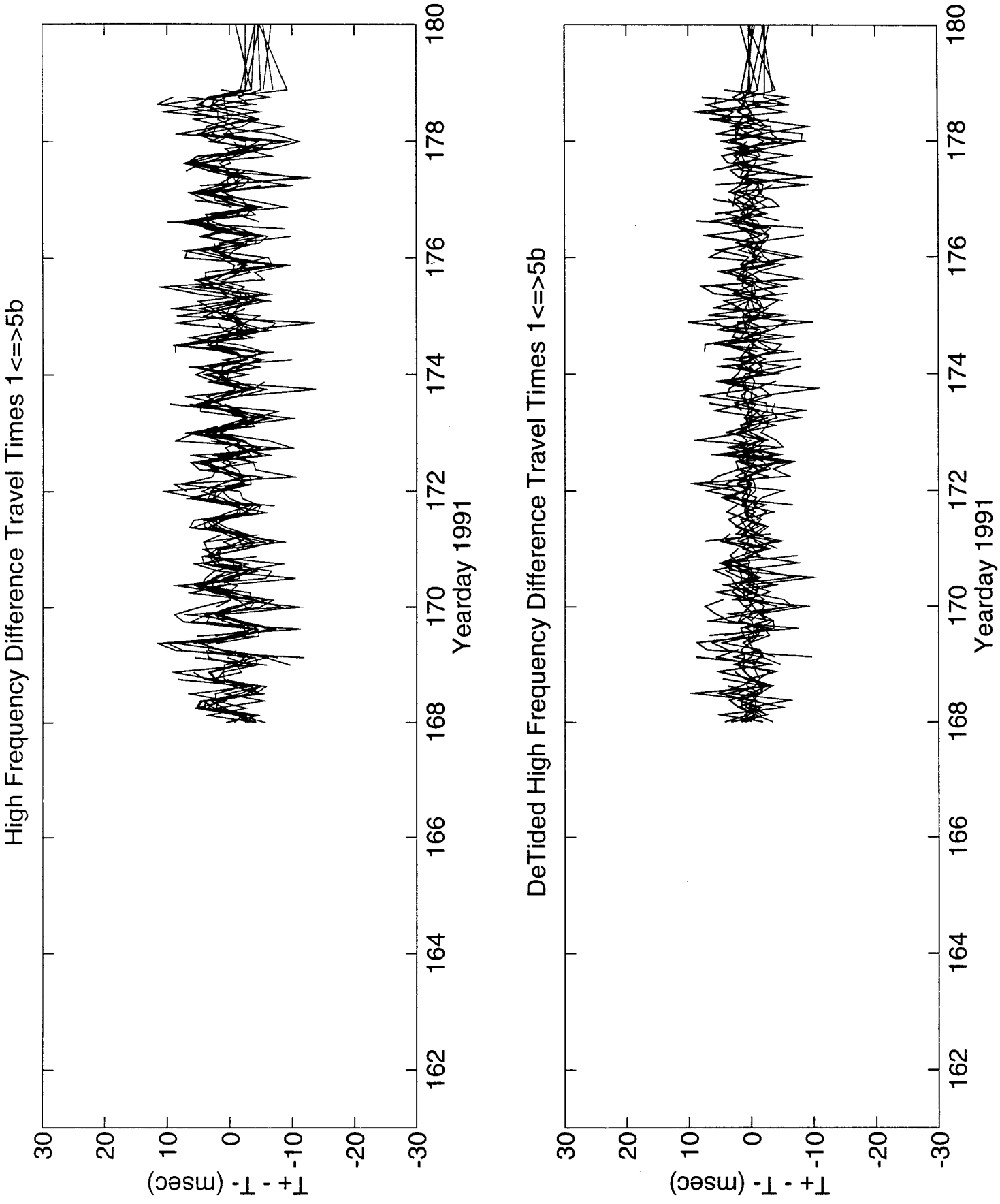
High Frequency Difference Travel Times 1<=>5b
T+ - T- (msec)
30
20
10
0
-10
-20
-30
162
164
166
168
170
172
174
176
178
180
Yearday 1991
DeTided High Frequency Difference Travel Times 1<=>5b
T+ - T- (msec)
30
20
10
0
-10
-20
-30
162
164
166
168
170
172
174
176
178
180
Yearday 1991

FIGURE K-3

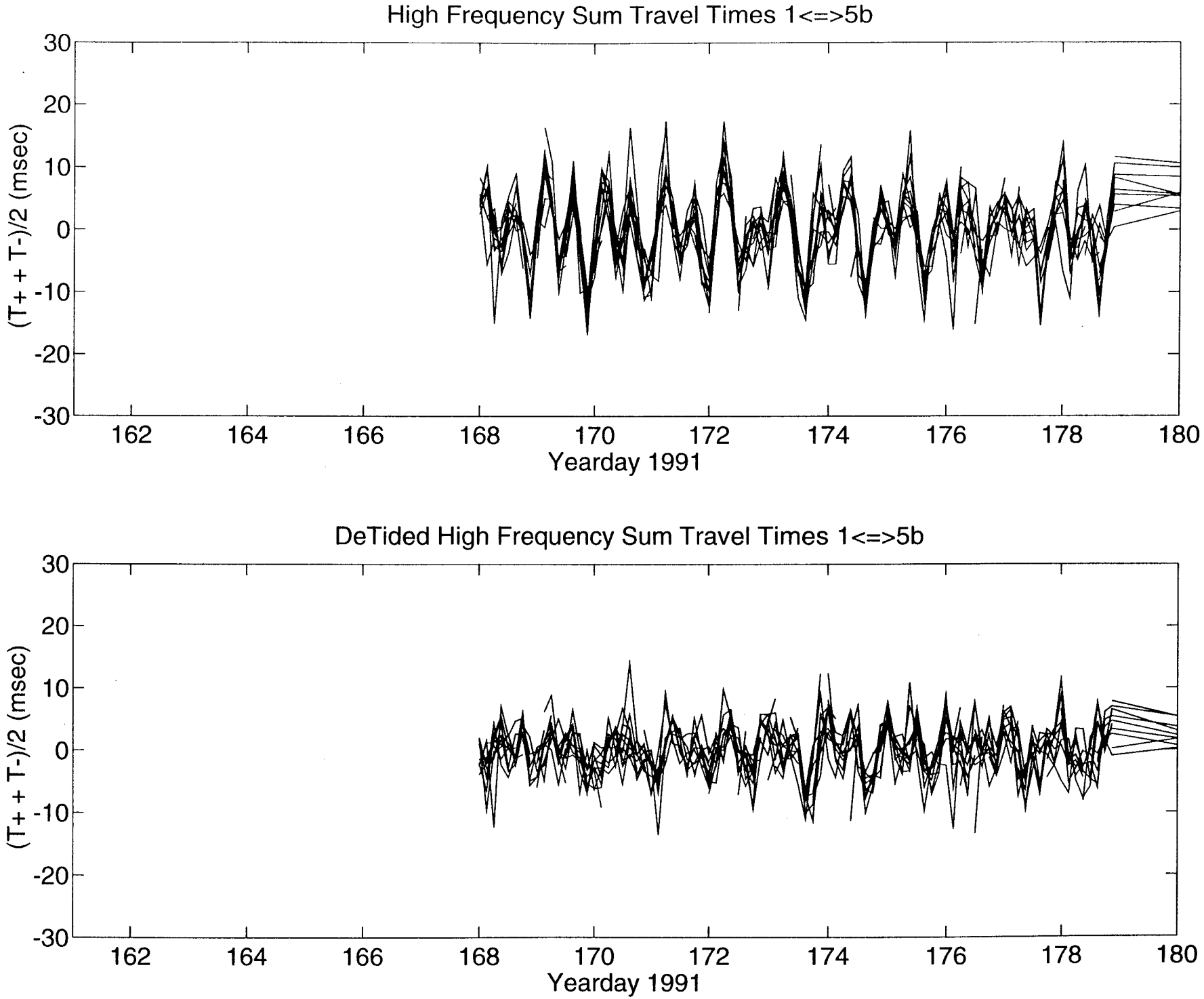
High Frequency Sum Travel Times 1<=>5b
(T+ + T-)/2 (msec)
30
20
10
0
-10
-20
-30
162
164
166
168
170
172
174
176
178
180
Yearday 1991
DeTided High Frequency Sum Travel Times 1<=>5b
(T+ + T-)/2 (msec)
30
20
10
0
-10
-20
-30
162
164
166
168
170
172
174
176
178
180
Yearday 1991

FIGURE K-4

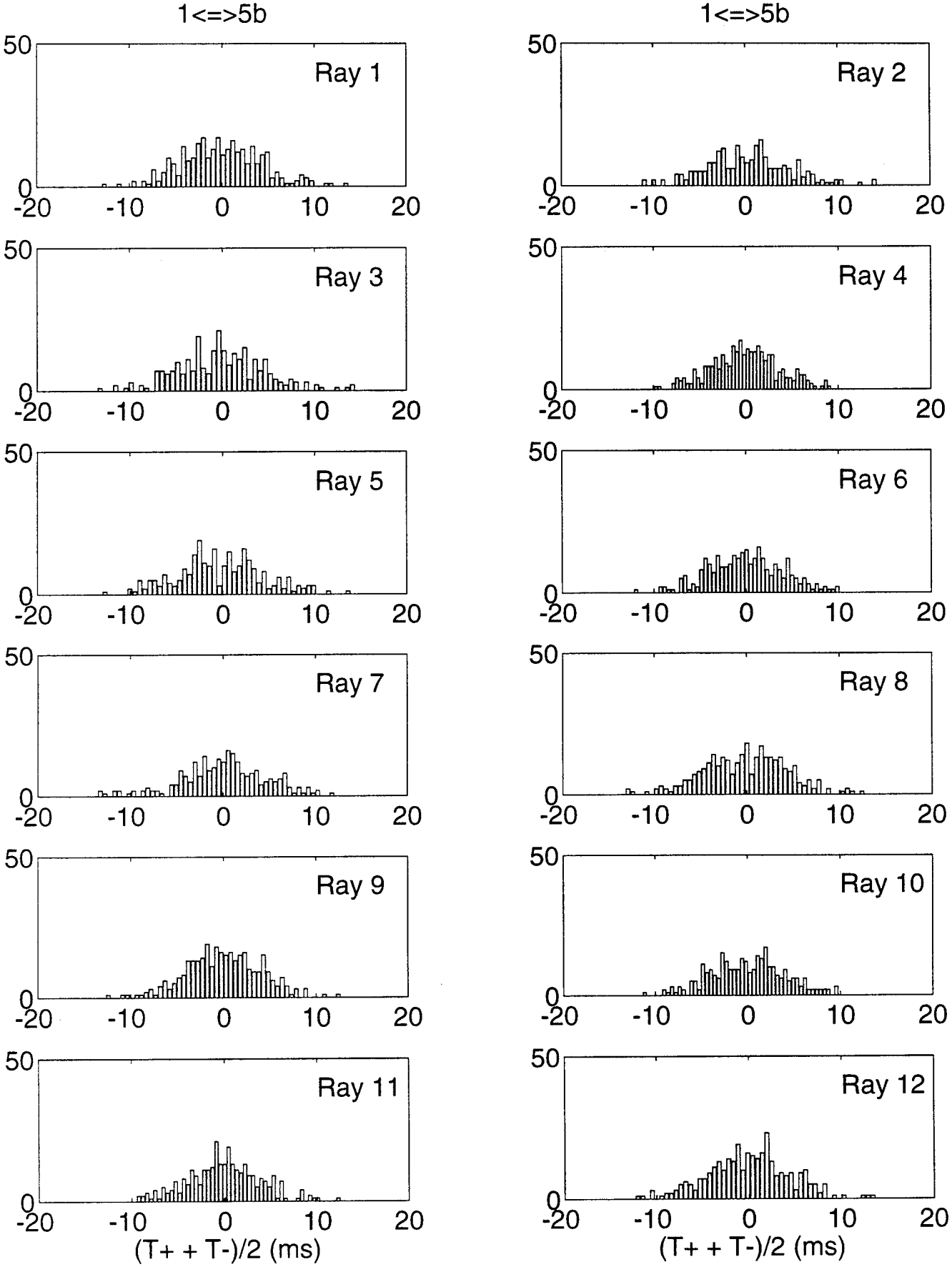
1<=>5b
1<=>5b
Ray 1
Ray 2
Ray 3
Ray 4
Ray 5
Ray 6
Ray 7
Ray 8
Ray 9
Ray 10
Ray 11
Ray 12
50
0
-20
-10
0
10
20
(T+ + T-)/2 (ms)

FIGURE K-5

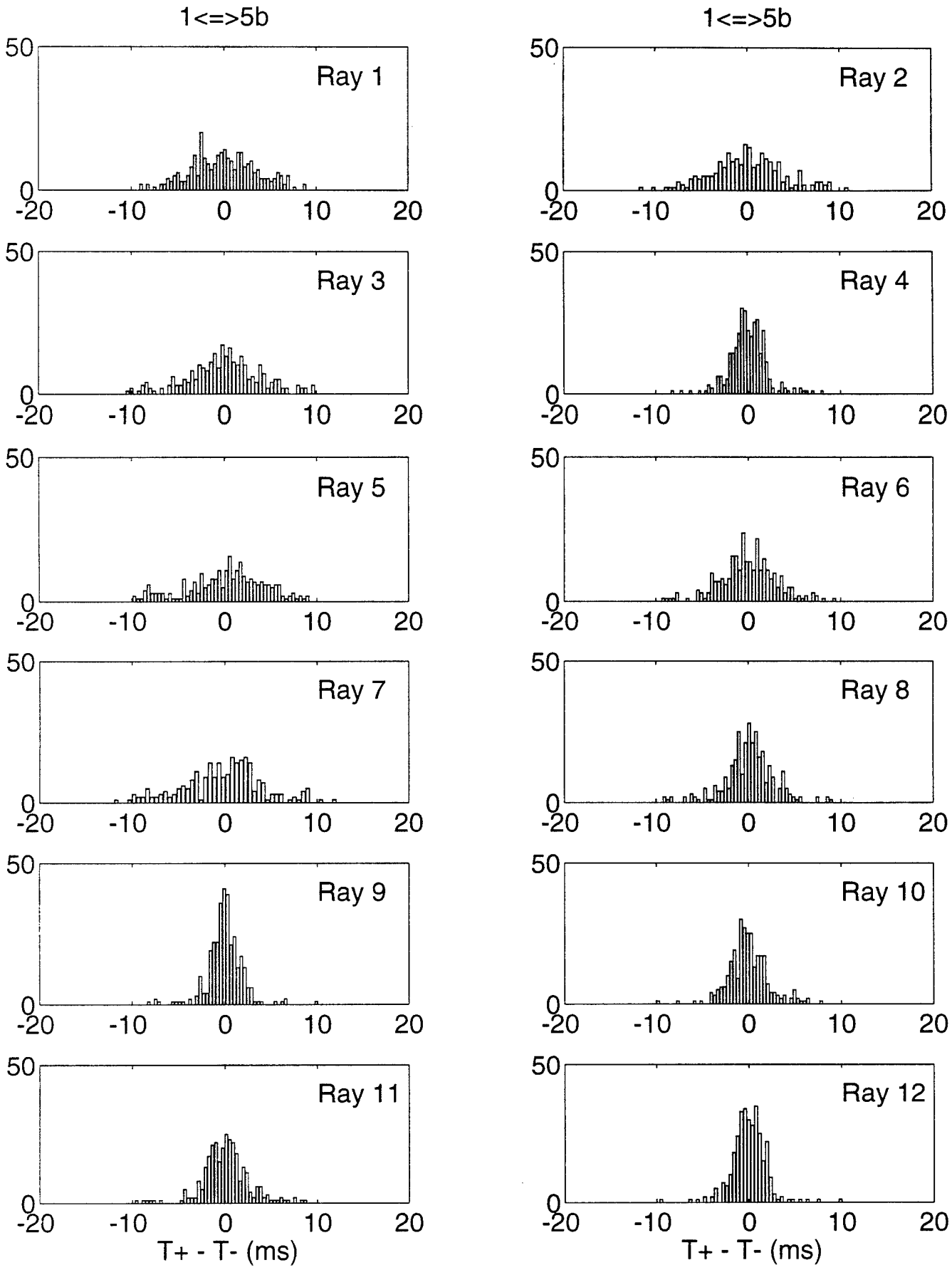
1<=>5b
1<=>5b
Ray 1
Ray 2
Ray 3
Ray 4
Ray 5
Ray 6
Ray 7
Ray 8
Ray 9
Ray 10
Ray 11
Ray 12
50
0
-20
-10
0
10
20
T+ - T- (ms)

FIGURE K-6

L. ACOUSTIC DATA: Paths 1→6 and 6→1

FIGURE L-1 shows the raypaths, roughly corresponding to FIGURE G-1, for which travel times were resolved. The raypaths were actually determined using range-dependent Levitus sound speed, interpolated onto the acoustic path. Note that the "final cutoff" travel times may be available at some time in the future, these data correspond to a ray confined near the sound channel axis.

FIGURE L-2 shows the low-pass filtered difference (top panel) and sum (bottom panel) travel times corresponding to the rays of FIGURE L-1.

FIGURE L-3 shows the high-pass filtered difference travel times for a small portion of the time series obtained during the time of more frequent transmissions during the MST experiment. The bottom panel shows the time series after the phase-locked tidal signals have been removed. FIGURE L-4 shows the same time series, but during a time of the normal transmission schedule.

FIGURE L-5 shows the high-pass filtered sum travel times for a small portion of the time series obtained during the time of more frequent transmissions during the MST experiment. The bottom panel shows the time series after the phase-locked tidal signals have been removed. This tidal variability is caused by the internal tide. FIGURE L-6 shows the same time series, but during a time of the normal transmission schedule.

After the travel time time series have been edited for outliers, high-pass filtered, and detided, the high-frequency variances are calculated (TABLE L-1). Note that this table sometimes contains statistics for more rays than are indicated in TABLE B-1; some of the ray arrivals in TABLE L-1 have not been identified with predicted arrivals. Also, sometimes there is initial ambiguity about the pairing of reciprocal arrivals, in which case sum and difference travel times are calculated for all reasonable cases; later it becomes obvious which arrivals have been improperly paired. The correlation $<T^+ T^->$ and variance $<T^2>$ are calculated from the sum and difference travel time variances in this table. The variance of the travel times is mainly due to internal wave variability, and this value determines the uncertainties assigned to the travel times in an inversion. The correlation coefficient is a measure of the reciprocity of reciprocal raypaths. This measure is conservative, because correlation is not a necessary condition for the determination of current from the difference of reciprocal travel times. Values of correlation that are 0.5 or greater assure that the reciprocal raypaths are indeed effectively identical, since good correlation implies that the reciprocal raypaths have not separated by more than an internal wave correlation length. Histograms of the detided, high-frequency travel times are shown in FIGURES L-7 and L-8; the variances from TABLE L-1 are measures of the width of these histograms.

TABLES L-2 and L-3 show the results of tidal analysis of the time series of difference (current) and sum (sound speed) travel times. For these tables, the tidal analysis is performed on each travel time time series separately and then the average and rms of the harmonic constants are calculated. Current or sound speed amplitude is determined from travel time by a simple scaling factor; the harmonic constants are more accurately determined by inverting the data for current or sound speed (this is not done here).

TABLE L-1. Travel Time Statistics 1←→6.

Ray #	Number of data	$<(T^+ + T^-)^2>$ (ms^2)	$<(T^+ - T^-)^2>$ (ms^2)	$<T^+ T^->$ (ms^2)	$<T^2>$ (ms^2)	$\frac{<T^+ T^->}{<T^2>}$
1	139	10	5	9	11	0.78
2	472	19	14	16	23	0.70
3	461	20	13	16	23	0.71
4	515	10	4	9	11	0.83
5	495	14	7	12	16	0.78
6	499	16	8	14	18	0.78
7	492	15	5	14	16	0.85
8	530	14	3	13	15	0.90
9	512	12	2	11	13	0.90
10	449	15	9	12	17	0.74
11	460	15	6	13	16	0.80
12	487	14	4	13	15	0.86

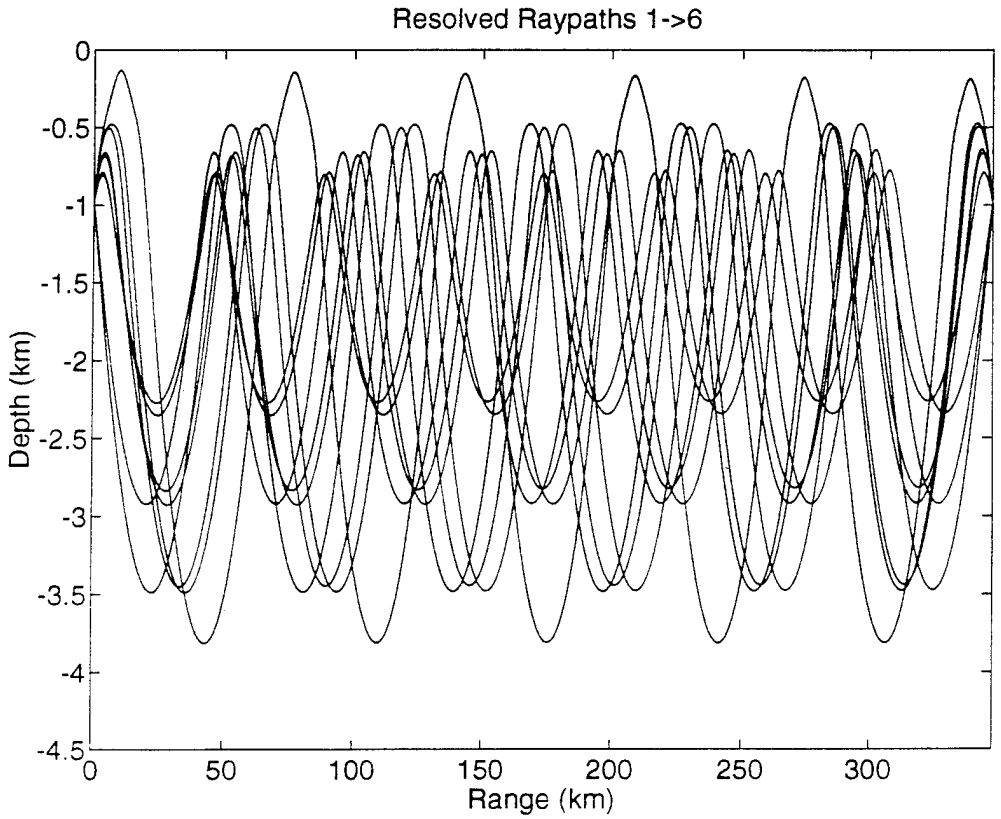

FIGURE L-1

TABLE L-2. Tidal Current Harmonic Constants 1←→6.

Constituent	Amplitude (mm/s)	Uncertainty (mm/s)	Phase (°G)	Uncertainty (°)
M_2	2.50	0.56	145.5	11.6
S_2	1.47	0.72	162.3	43.9
N_2	0.74	0.47	145.7	76.6
K_2	1.02	0.47	179.4	71.6
O_1	0.92	0.54	201.9	65.7
K_1	1.47	0.51	181.0	62.3
P_1	0.85	0.74	123.0	90.9
Q_1	0.74	0.44	156.1	64.3

Values and their uncertainty are determined by the average and rms of harmonic constants from tidal analyses of the separate raypath travel time series. The amplitudes do not include the lunar node factors. 13 ± 5 % of the high-frequency variance is accounted for by the tides.

TABLE L-3. Tidal Sound Speed Harmonic Constants 1←→6.

Constituent	Amplitude (mm/s)	Uncertainty (mm/s)	Phase (°G)	Uncertainty (°)
M_2	10.09	1.60	135.4	9.6
S_2	2.14	0.40	311.5	33.9
N_2	1.48	0.42	35.9	48.8
K_2	2.10	0.95	36.1	33.8
O_1	2.28	0.91	200.5	22.8
K_1	6.89	1.32	45.5	5.2
P_1	2.16	0.79	20.7	16.9
Q_1	1.19	0.43	126.6	23.8

Values and their uncertainty are determined by the average and rms of harmonic constants from tidal analyses of the separate raypath travel time series. The amplitudes do not include the lunar node factors. 38 ± 8 % of the high-frequency variance is accounted for by the tides. Because sum travel times are used to derive these numbers, the amplitudes have been divided by a factor of two compared to the amplitudes for current.

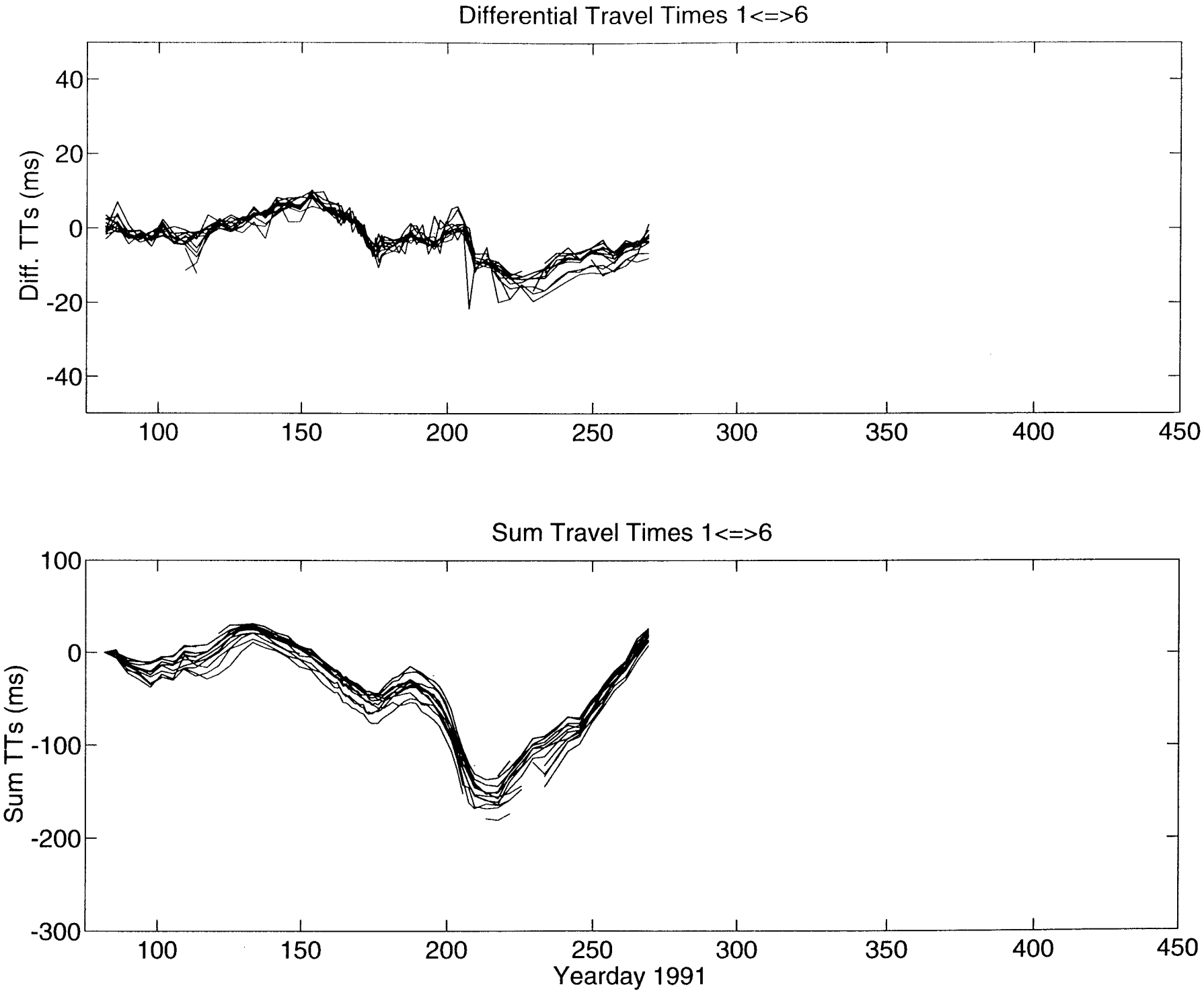
Differential Travel Times 1<=>6
Diff. TTs (ms)
40
20
0
-20
-40
100
150
200
250
300
350
400
450
Sum Travel Times 1<=>6
Sum TTs (ms)
100
0
-100
-200
-300
100
150
200
250
300
350
400
450
Yearday 1991

FIGURE L-2

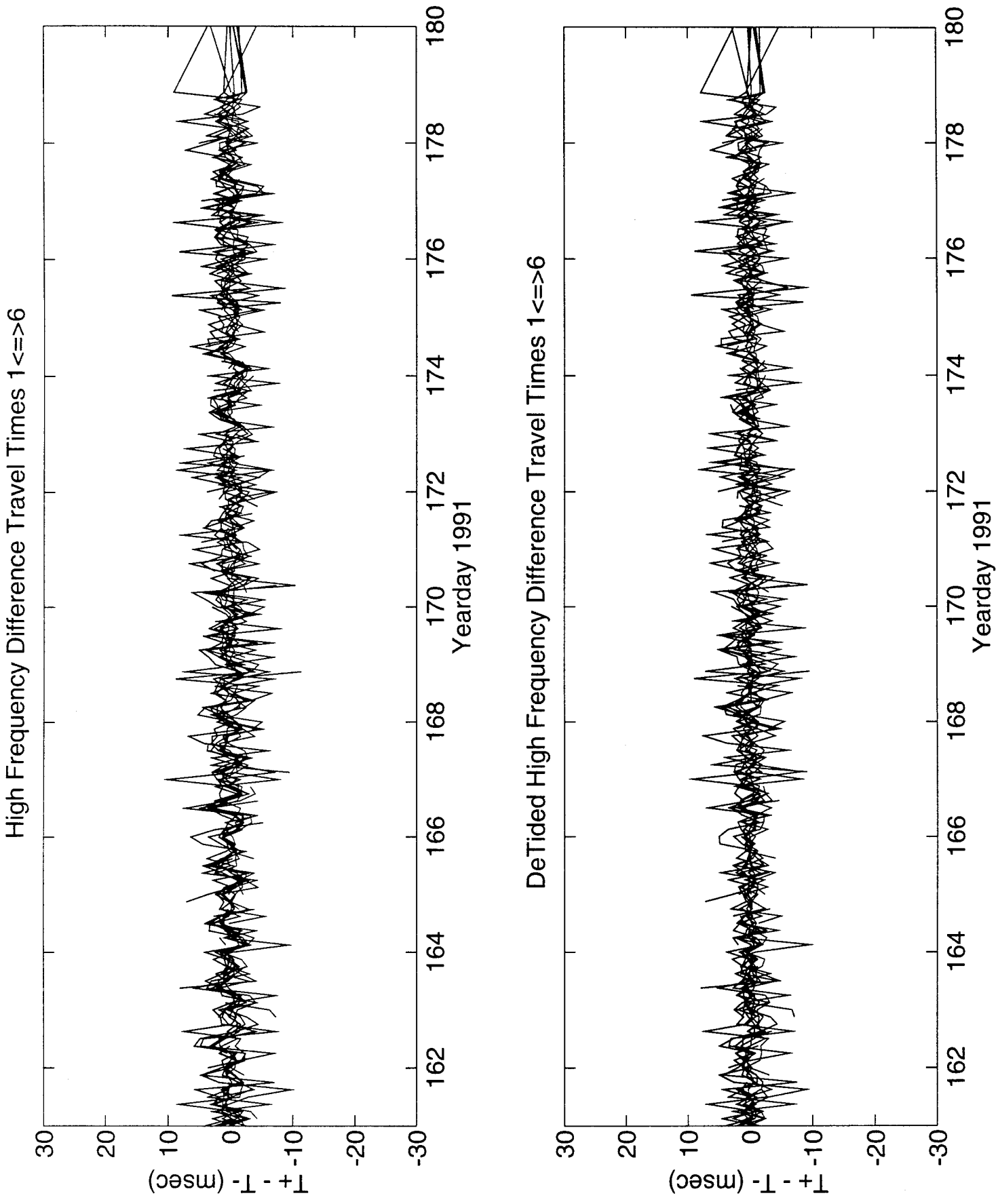
High Frequency Difference Travel Times 1<=>6
T+ - T- (msec)
30
20
10
0
-10
-20
-30
162
164
166
168
170
172
174
176
178
180
Yearday 1991
DeTided High Frequency Difference Travel Times 1<=>6
T+ - T- (msec)
30
20
10
0
-10
-20
-30
162
164
166
168
170
172
174
176
178
180
Yearday 1991

FIGURE L-3

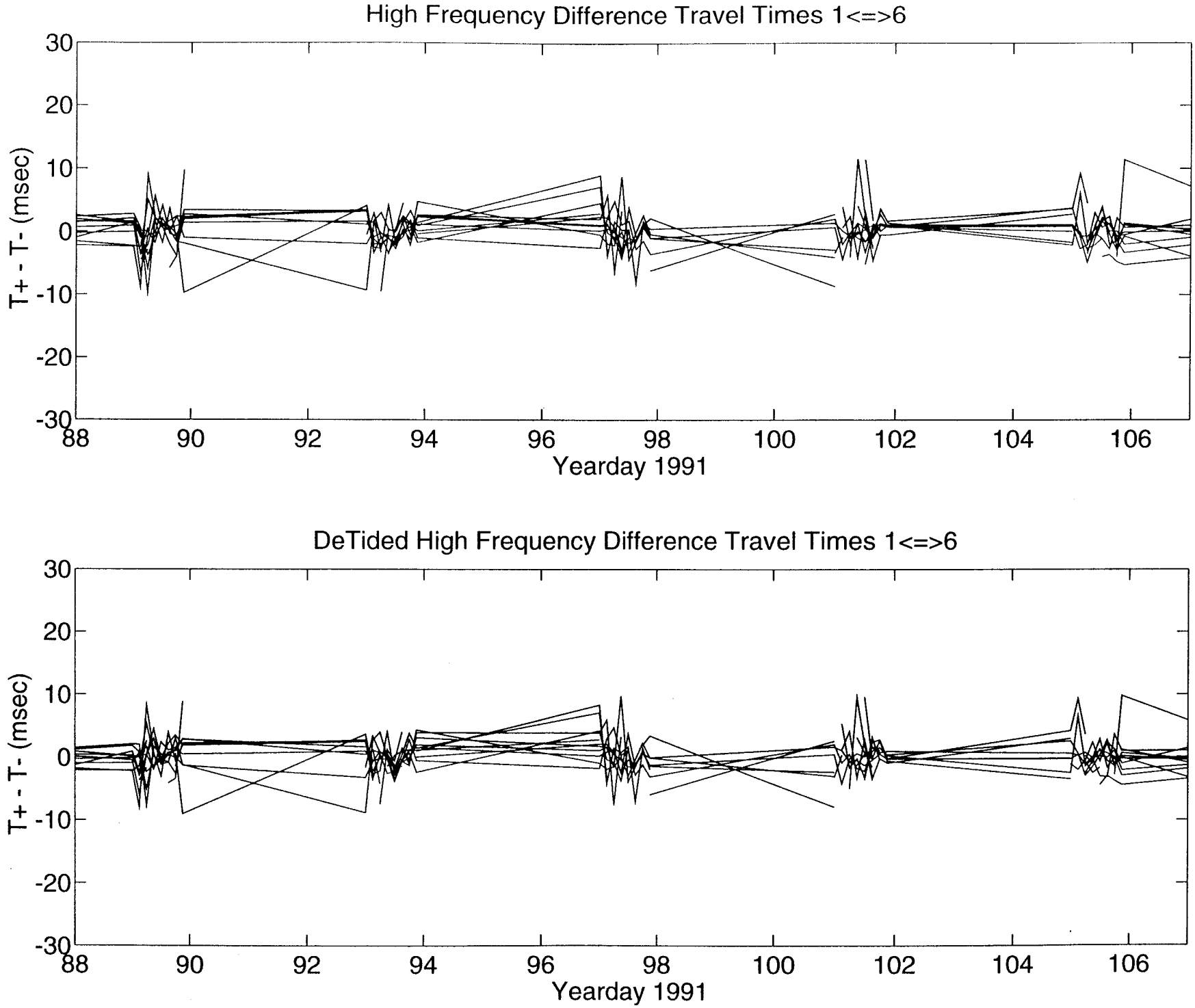
High Frequency Difference Travel Times 1<=>6
T+ - T- (msec)
Yearday 1991
DeTided High Frequency Difference Travel Times 1<=>6
T+ - T- (msec)
Yearday 1991

FIGURE L-4

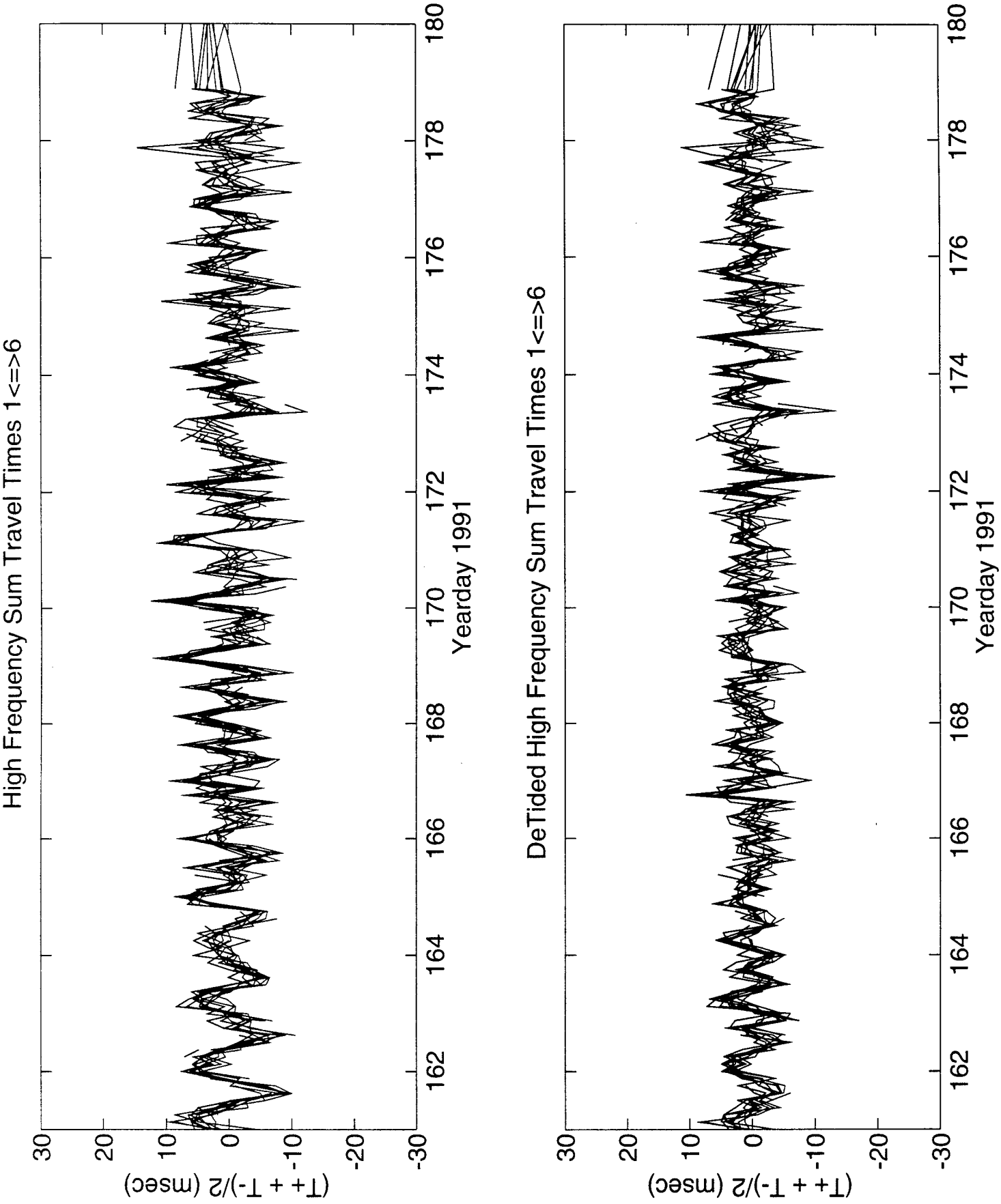
High Frequency Sum Travel Times 1<=>6
DeTided High Frequency Sum Travel Times 1<=>6
(T+ + T-)/2 (msec)
Yearday 1991
30
20
10
0
-10
-20
-30
162
164
166
168
170
172
174
176
178
180

FIGURE L-5

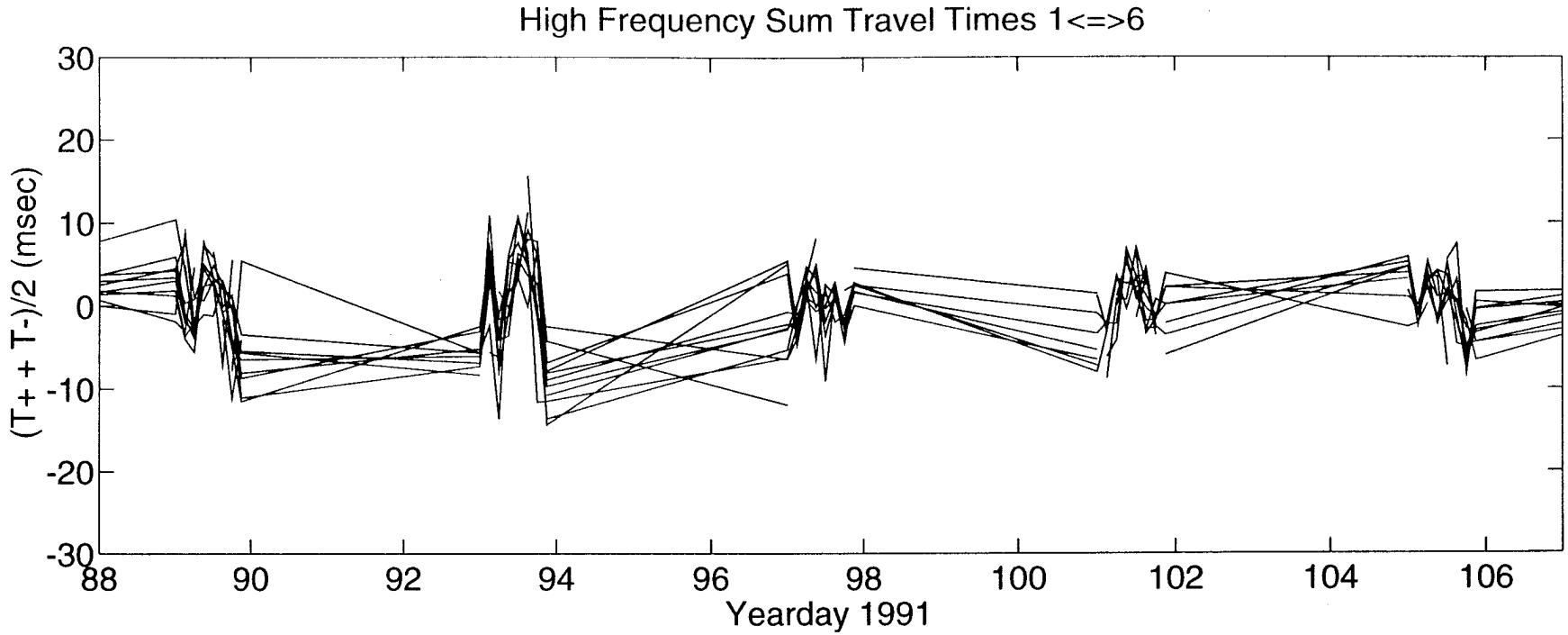
High Frequency Sum Travel Times 1<=>6
(T+ + T-)/2 (msec)
30
20
10
0
-10
-20
-30
88
90
92
94
96
98
100
102
104
106
Yearday 1991

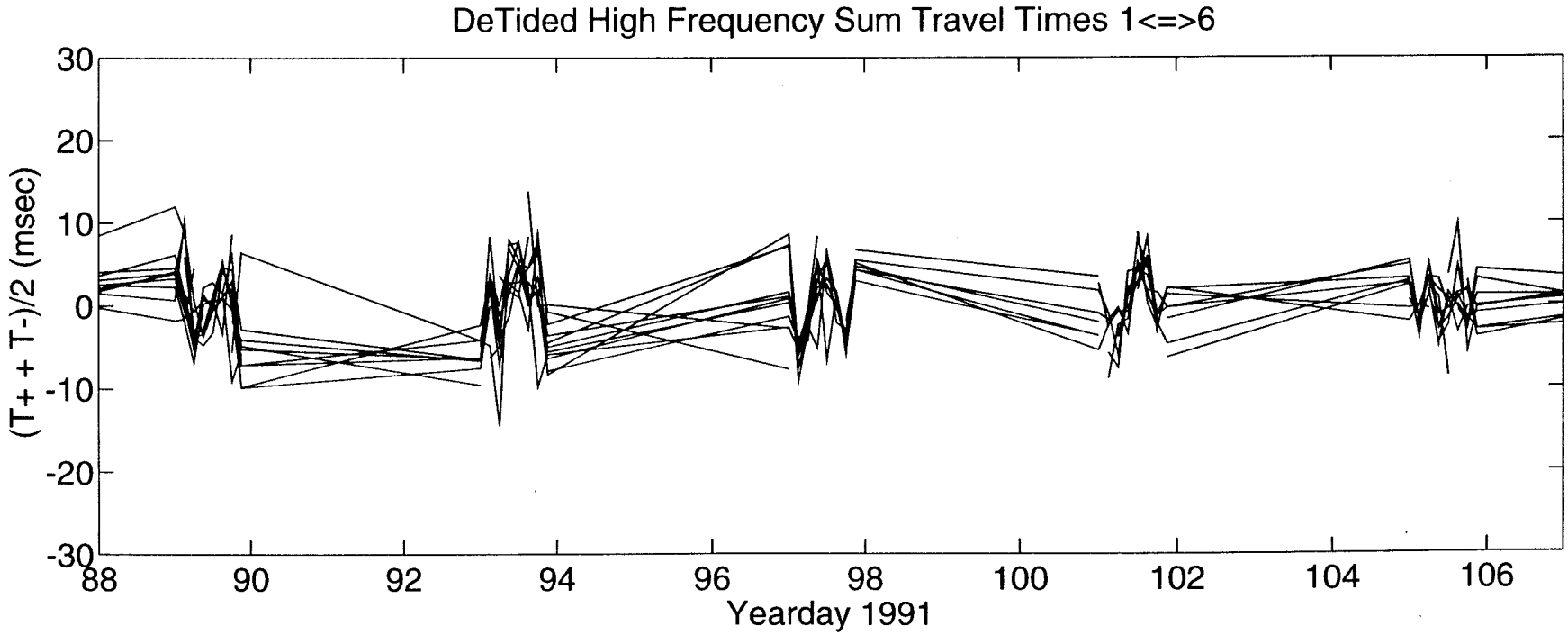
DeTided High Frequency Sum Travel Times 1<=>6
(T+ + T-)/2 (msec)
30
20
10
0
-10
-20
-30
88
90
92
94
96
98
100
102
104
106
Yearday 1991

FIGURE L-6

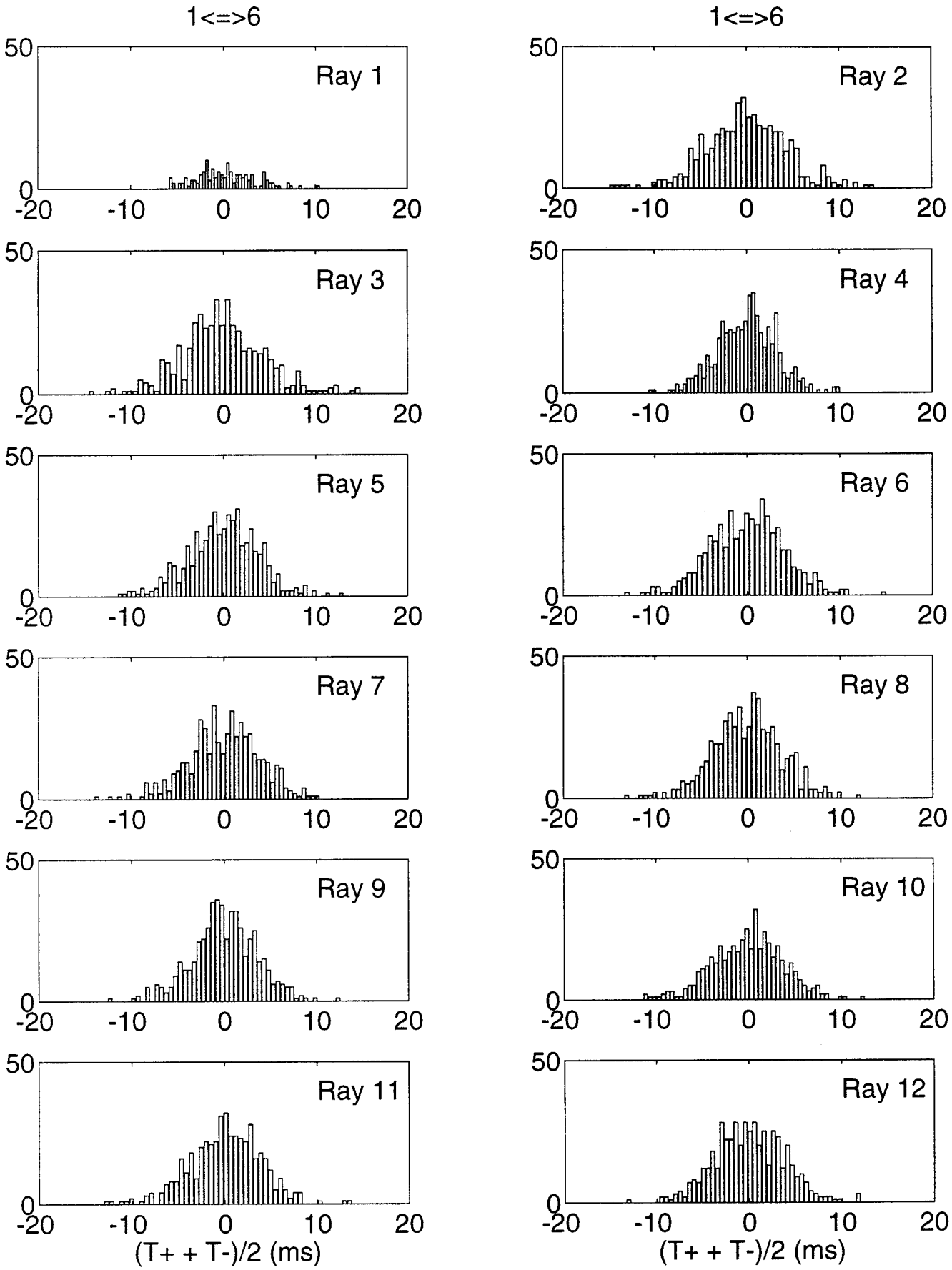
1<=>6
1<=>6
Ray 1
Ray 2
Ray 3
Ray 4
Ray 5
Ray 6
Ray 7
Ray 8
Ray 9
Ray 10
Ray 11
Ray 12
50
0
-20
-10
0
10
20
(T+ + T-)/2 (ms)

FIGURE L-7

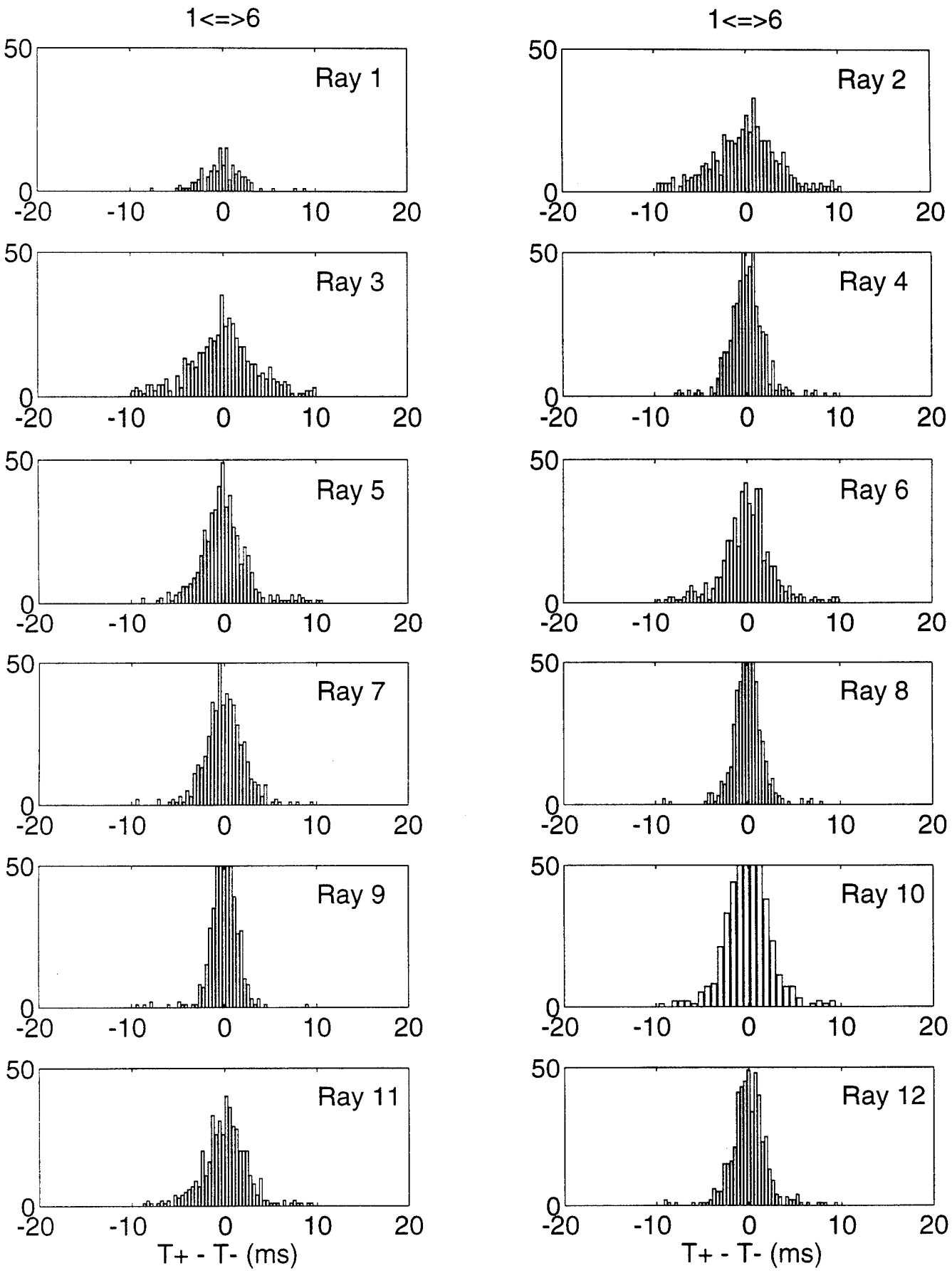
1<=>6
1<=>6
Ray 1
Ray 2
Ray 3
Ray 4
Ray 5
Ray 6
Ray 7
Ray 8
Ray 9
Ray 10
Ray 11
Ray 12
50
0
-20
-10
0
10
20
T+ - T- (ms)

FIGURE L-8

M. ACOUSTIC DATA: Paths 2→3 and 3→2

FIGURE M-1 shows the raypaths, roughly corresponding to FIGURE G-1, for which travel times were resolved. The raypaths were actually determined using range-dependent Levitus sound speed, interpolated onto the acoustic path. Note that the "final cutoff" travel times may be available at some time in the future, these data correspond to a ray confined near the sound channel axis.

FIGURE M-2 shows the low-pass filtered difference (top panel) and sum (bottom panel) travel times corresponding to the rays of FIGURE M-1.

FIGURE M-3 shows the high-pass filtered difference travel times for a small portion of the time series obtained during the time of more frequent transmissions during the MST experiment. The bottom panel shows the time series after the phase-locked tidal signals have been removed. FIGURE M-4 shows the same time series, but during a time of the normal transmission schedule.

FIGURE M-5 shows the high-pass filtered sum travel times for a small portion of the time series obtained during the time of more frequent transmissions during the MST experiment. The bottom panel shows the time series after the phase-locked tidal signals have been removed. This tidal variability is caused by the internal tide. FIGURE M-6 shows the same time series, but during a time of the normal transmission schedule.

After the travel time time series have been edited for outliers, high-pass filtered, and detided, the high-frequency variances are calculated (TABLE M-1). Note that this table sometimes contains statistics for more rays than are indicated in TABLE B-1; some of the ray arrivals in TABLE M-1 have not been identified with predicted arrivals. Also, sometimes there is initial ambiguity about the pairing of reciprocal arrivals, in which case sum and difference travel times are calculated for all reasonable cases; later it becomes obvious which arrivals have been improperly paired. The correlation $<T^+ T^->$ and variance $<T^2>$ are calculated from the sum and difference travel time variances in this table. The variance of the travel times is mainly due to internal wave variability, and this value determines the uncertainties assigned to the travel times in an inversion. The correlation coefficient is a measure of the reciprocity of reciprocal raypaths. This measure is conservative, because correlation is not a necessary condition for the determination of current from the difference of reciprocal travel times. Values of correlation that are 0.5 or greater assure that the reciprocal raypaths are indeed effectively identical, since good correlation implies that the reciprocal raypaths have not separated by more than an internal wave correlation length. Histograms of the detided, high-frequency travel times are shown in FIGURES M-7 and M-8; the variances from TABLE M-1 are measures of the width of these histograms.

TABLES M-2 and M-3 show the results of tidal analysis of the time series of difference (current) and sum (sound speed) travel times. For these tables, the tidal analysis is performed on each travel time time series separately and then the average and rms of the harmonic constants are calculated. Current or sound speed amplitude is determined from travel time by a simple scaling factor; the harmonic constants are more accurately determined by inverting the data for current or sound speed (this is not done here).

TABLE M-1. Travel Time Statistics 2←→3.

Ray #	Number of data	$\langle (T^+ + T^-)^2 \rangle$ (ms^2)	$\langle (T^+ - T^-)^2 \rangle$ (ms^2)	$\langle T^+ T^- \rangle$ (ms^2)	$\langle T^2 \rangle$ (ms^2)	$\frac{\langle T^+ T^- \rangle}{\langle T^2 \rangle}$
1	470	18	5	17	20	0.87
2	465	16	7	15	18	0.80
3	504	18	9	16	20	0.77
4	496	19	9	17	21	0.79
5	550	17	2	16	17	0.93
6	564	15	3	15	16	0.91
7	521	19	8	17	21	0.81
8	542	17	8	15	19	0.79
9	543	17	4	16	18	0.89

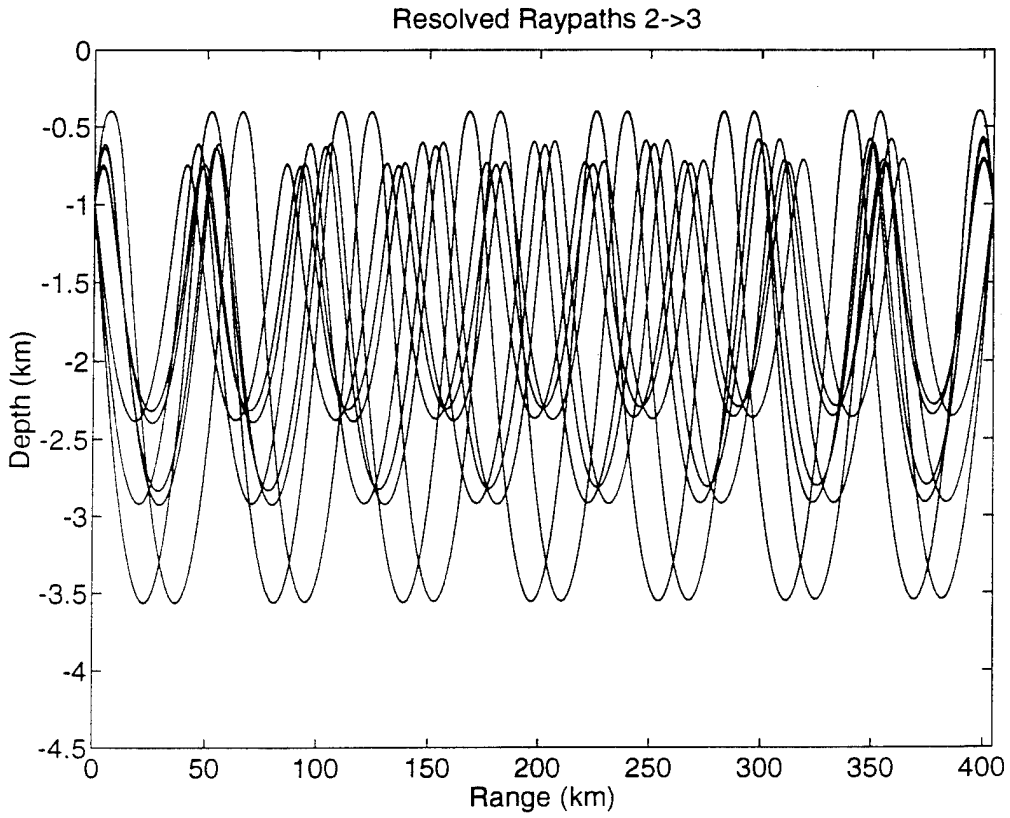

FIGURE M-1

TABLE M-2. Tidal Current Harmonic Constants 2←→3.

Constituent	Amplitude (mm/s)	Uncertainty (mm/s)	Phase (°G)	Uncertainty (°)
M_2	2.92	0.64	264.5	3.1
S_2	0.77	0.40	281.1	78.5
N_2	0.79	0.51	264.3	65.5
K_2	0.48	0.25	207.9	87.7
O_1	0.81	0.57	174.3	71.3
K_1	1.02	0.45	193.6	67.0
P_1	0.72	0.30	257.7	88.6
Q_1	0.51	0.21	181.6	102.4

Values and their uncertainty are determined by the average and rms of harmonic constants from tidal analyses of the separate raypath travel time series. The amplitudes do not include the lunar node factors. 15 ± 6 % of the high-frequency variance is accounted for by the tides.

TABLE M-3. Tidal Sound Speed Harmonic Constants 2←→3.

Constituent	Amplitude (mm/s)	Uncertainty (mm/s)	Phase (°G)	Uncertainty (°)
M_2	5.26	0.75	118.7	21.4
S_2	1.64	0.71	359.0	21.7
N_2	1.02	0.55	61.5	80.1
K_2	2.77	0.58	296.6	9.8
O_1	3.32	0.50	27.7	11.5
K_1	4.18	0.59	140.9	10.3
P_1	2.00	0.67	109.3	21.7
Q_1	2.398	0.60	338.8	10.3

Values and their uncertainty are determined by the average and rms of harmonic constants from tidal analyses of the separate raypath travel time series. The amplitudes do not include the lunar node factors. 27 ± 4 % of the high-frequency variance is accounted for by the tides. Because sum travel times are used to derive these numbers, the amplitudes have been divided by a factor of two compared to the amplitudes for current.

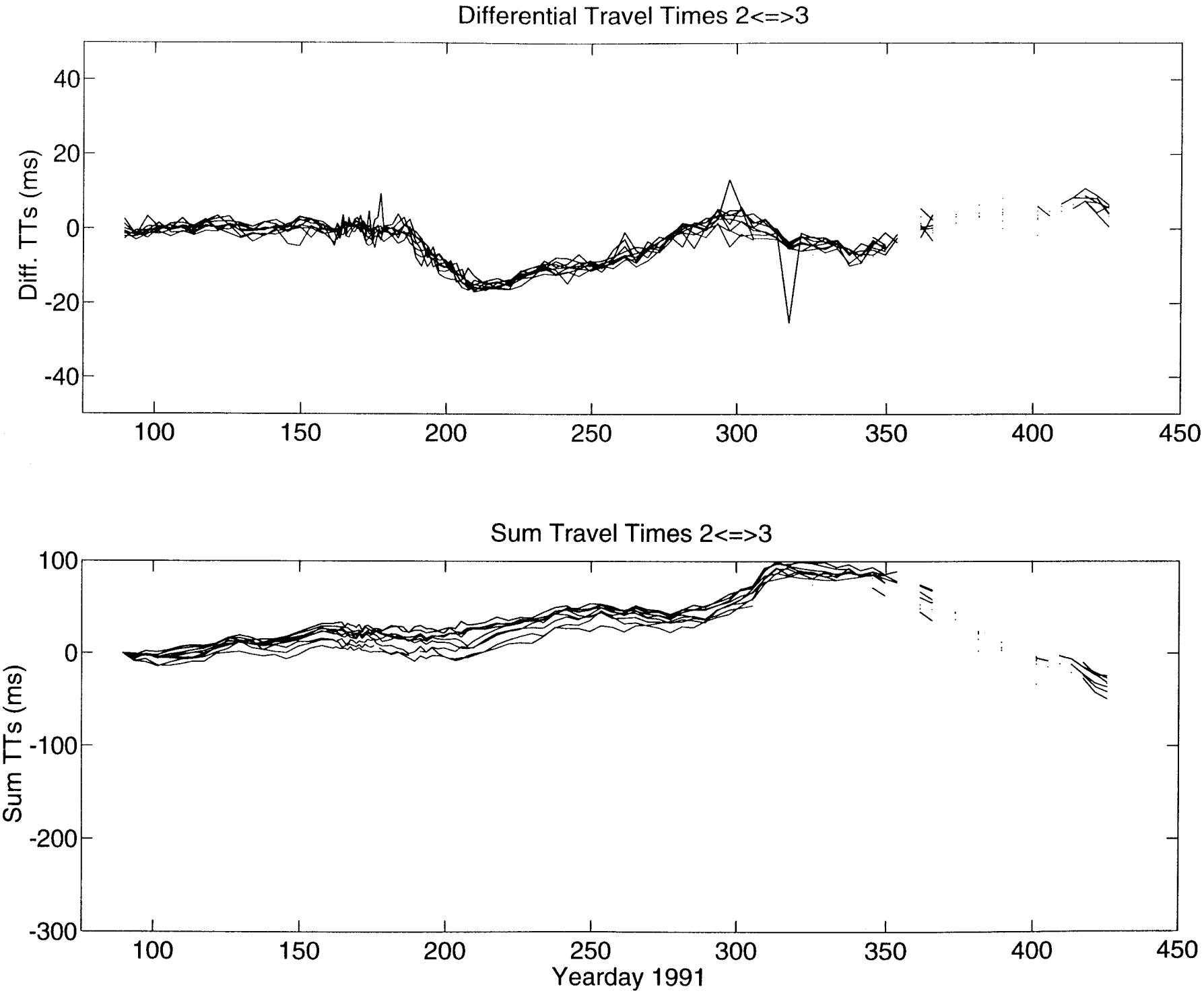
Differential Travel Times 2<=>3
Diff. TTs (ms)
40
20
0
-20
-40
100
150
200
250
300
350
400
450
Sum Travel Times 2<=>3
Sum TTs (ms)
100
0
-100
-200
-300
100
150
200
250
300
350
400
450
Yearday 1991

FIGURE M-2

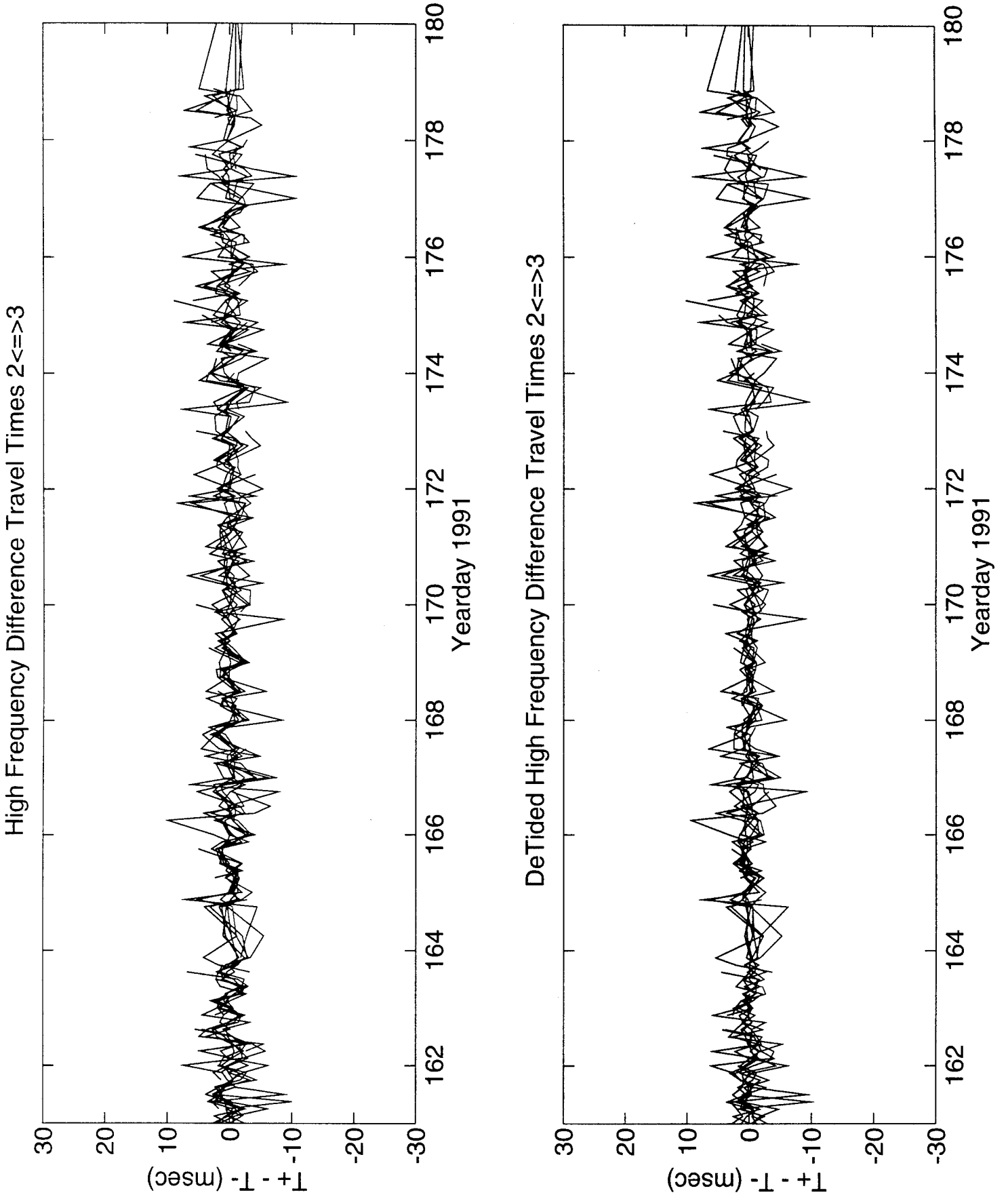
High Frequency Difference Travel Times 2<=>3
T+ - T- (msec)
30
20
10
0
-10
-20
-30
162
164
166
168
170
172
174
176
178
180
Yearday 1991
DeTided High Frequency Difference Travel Times 2<=>3
T+ - T- (msec)
30
20
10
0
-10
-20
-30
162
164
166
168
170
172
174
176
178
180
Yearday 1991

FIGURE M-3

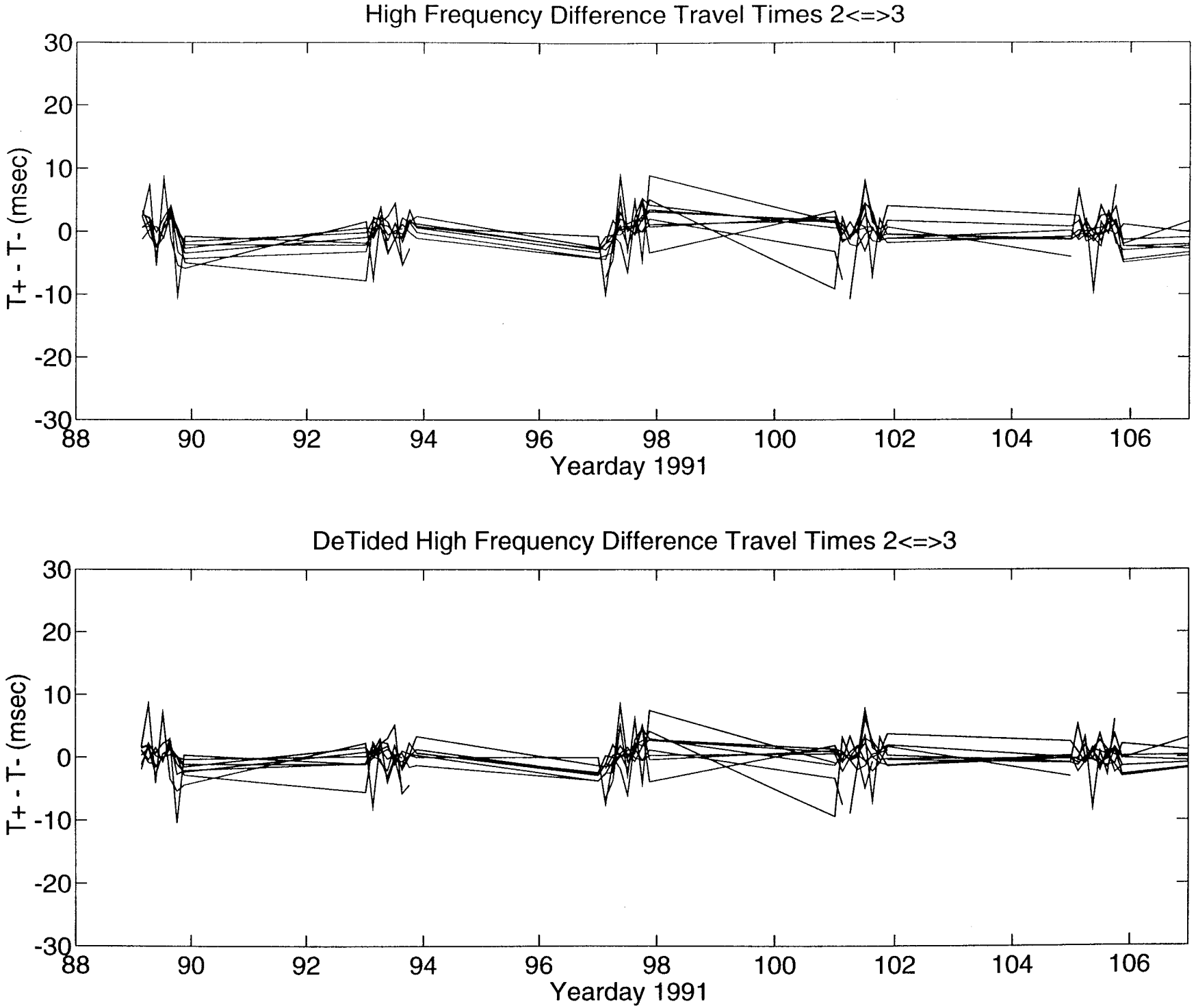
High Frequency Difference Travel Times 2<=>3
T+ - T- (msec)
30
20
10
0
-10
-20
-30
88
90
92
94
96
98
100
102
104
106
Yearday 1991
DeTided High Frequency Difference Travel Times 2<=>3
T+ - T- (msec)
30
20
10
0
-10
-20
-30
88
90
92
94
96
98
100
102
104
106
Yearday 1991

FIGURE M-4

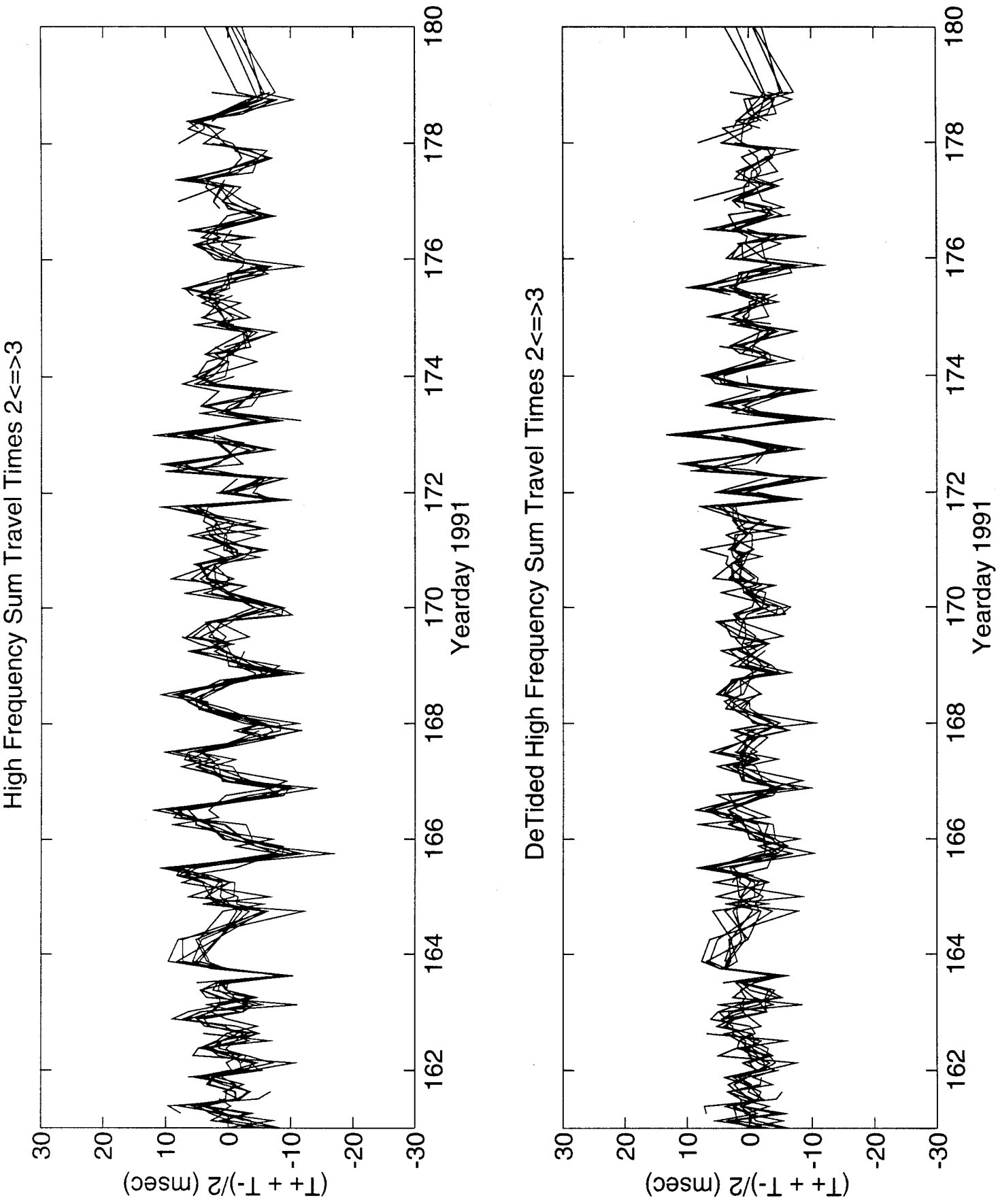
High Frequency Sum Travel Times 2<=>3
(T+ + T-)/2 (msec)
30
20
10
0
-10
-20
-30
162
164
166
168
170
172
174
176
178
180
Yearday 1991
DeTided High Frequency Sum Travel Times 2<=>3
(T+ + T-)/2 (msec)
30
20
10
0
-10
-20
-30
162
164
166
168
170
172
174
176
178
180
Yearday 1991

FIGURE M-5

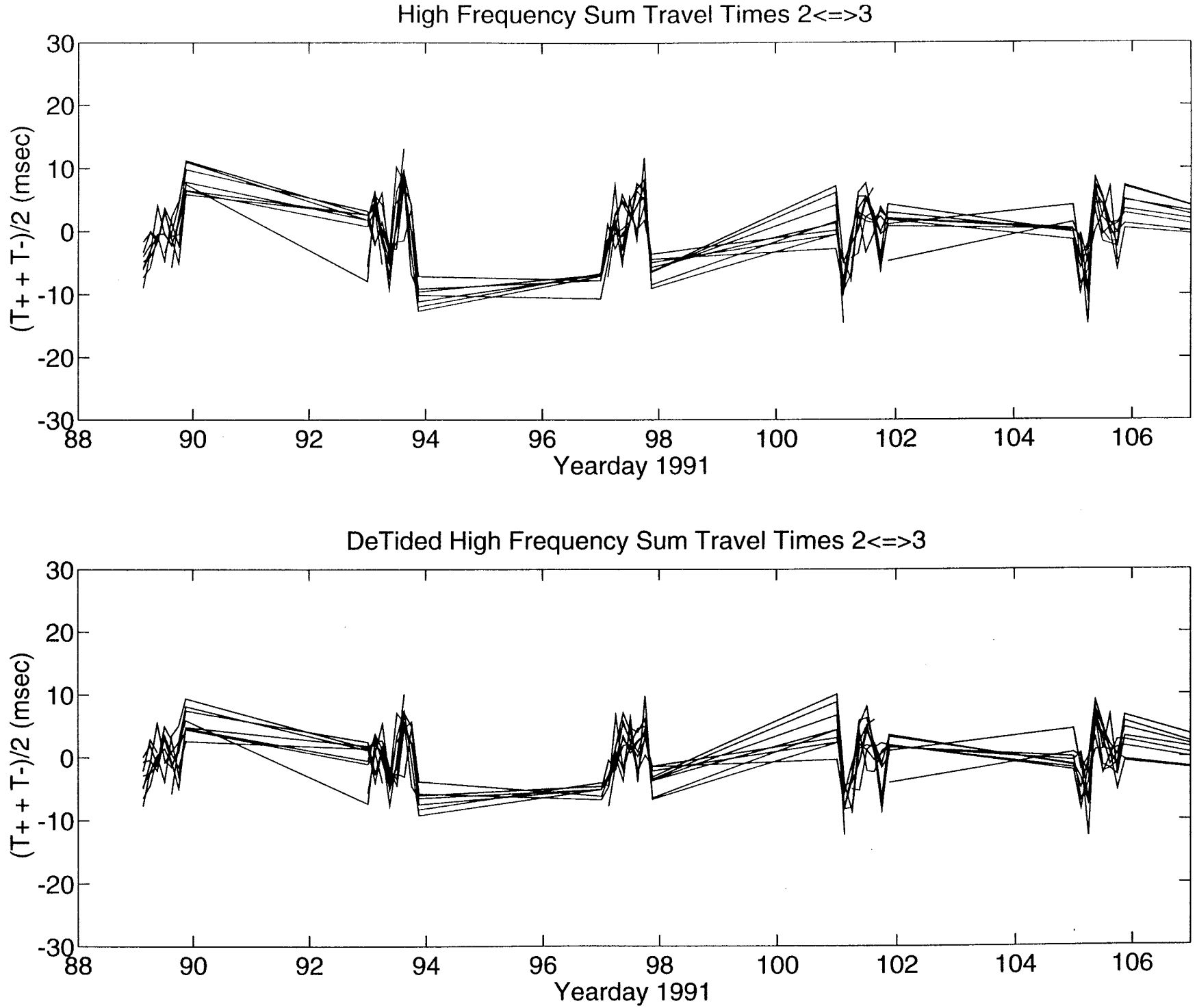
High Frequency Sum Travel Times 2<=>3
(T+ + T-)/2 (msec)
30
20
10
0
-10
-20
-30
88
90
92
94
96
98
100
102
104
106
Yearday 1991
DeTided High Frequency Sum Travel Times 2<=>3
(T+ + T-)/2 (msec)
30
20
10
0
-10
-20
-30
88
90
92
94
96
98
100
102
104
106
Yearday 1991

FIGURE M-6

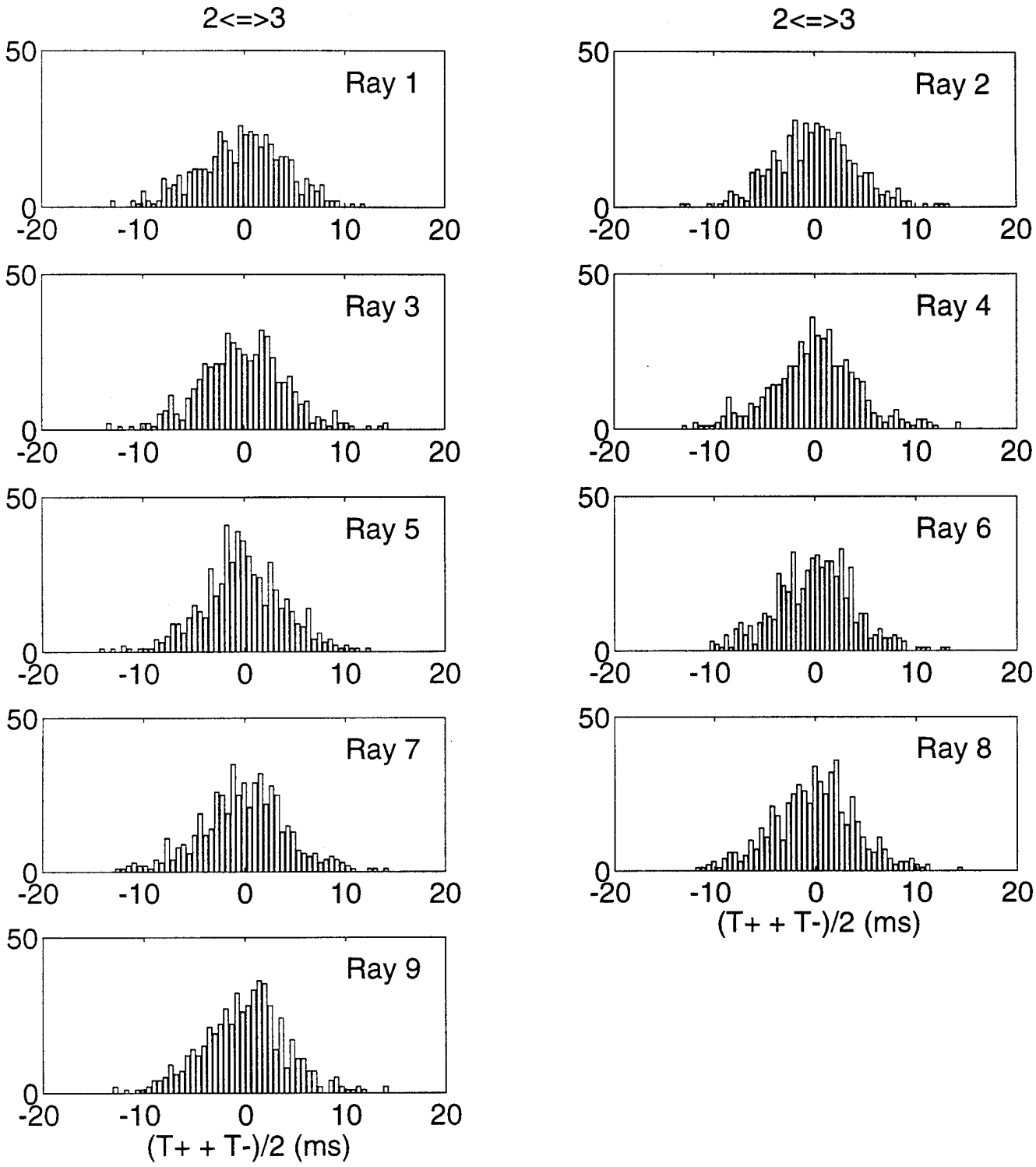
2<=>3
Ray 1
Ray 2
Ray 3
Ray 4
Ray 5
Ray 6
Ray 7
Ray 8
Ray 9
50
0
-20
-10
0
10
20
(T+ + T-)/2 (ms)

FIGURE M-7

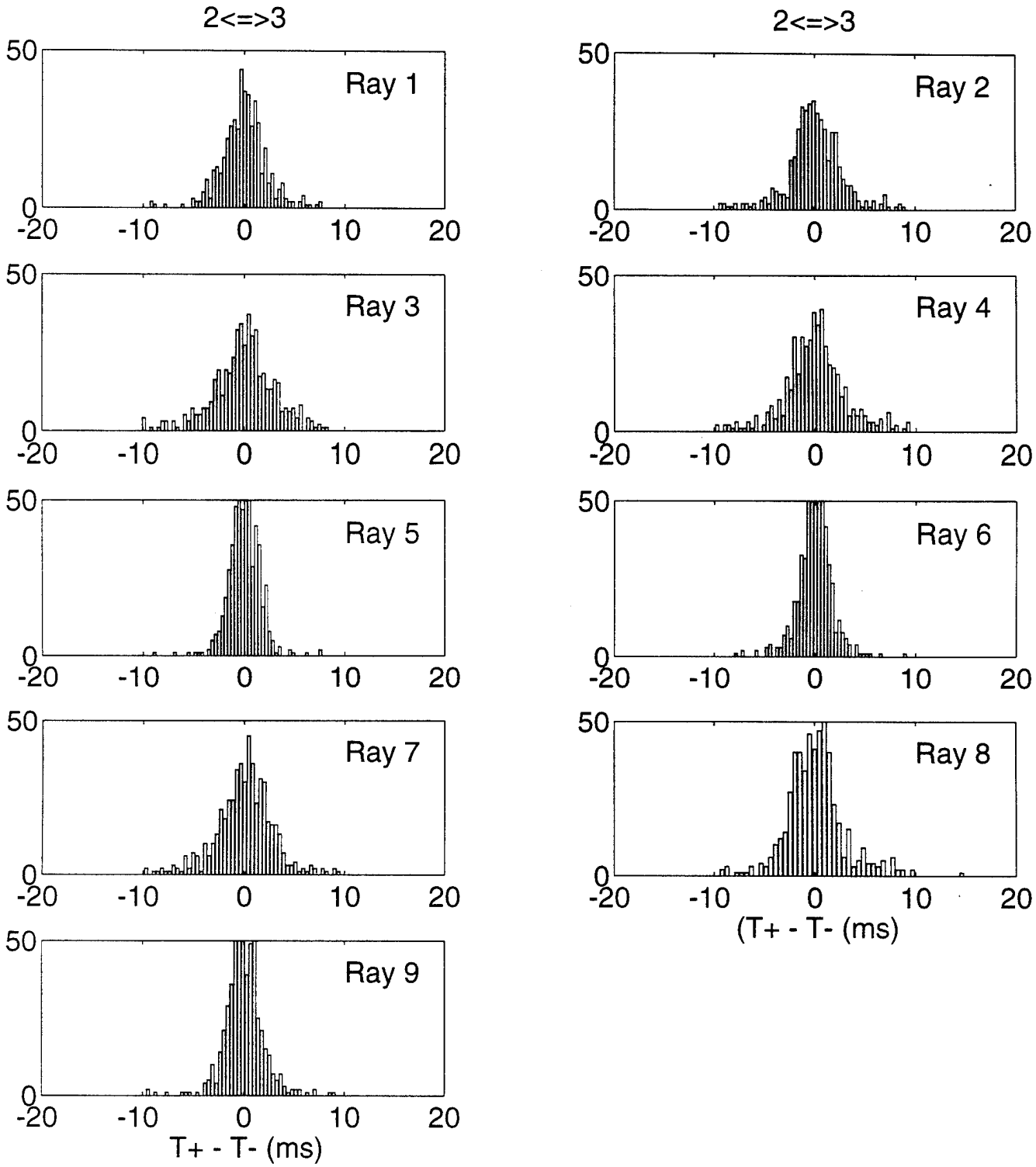
2<=>3
Ray 1
Ray 2
Ray 3
Ray 4
Ray 5
Ray 6
Ray 7
Ray 8
Ray 9
50
0
-20
-10
0
10
20
T+ - T- (ms)
(T+ - T- (ms)

FIGURE M-8

N. ACOUSTIC DATA: Paths 2→4 and 4→2

FIGURE N-1 shows the raypaths, roughly corresponding to FIGURE G-1, for which travel times were resolved. The raypaths were actually determined using range-dependent Levitus sound speed, interpolated onto the acoustic path. Note that the "final cutoff" travel times may be available at some time in the future, these data correspond to a ray confined near the sound channel axis.

FIGURE N-2 shows the low-pass filtered difference (top panel) and sum (bottom panel) travel times corresponding to the rays of FIGURE N-1.

FIGURE N-3 shows the high-pass filtered difference travel times for a small portion of the time series obtained during the time of more frequent transmissions during the MST experiment. The bottom panel shows the time series after the phase-locked tidal signals have been removed. FIGURE N-4 shows the same time series, but during a time of the normal transmission schedule.

FIGURE N-5 shows the high-pass filtered sum travel times for a small portion of the time series obtained during the time of more frequent transmissions during the MST experiment. The bottom panel shows the time series after the phase-locked tidal signals have been removed. This tidal variability is caused by the internal tide. FIGURE N-6 shows the same time series, but during a time of the normal transmission schedule.

After the travel time time series have been edited for outliers, high-pass filtered, and detided, the high-frequency variances are calculated (TABLE N-1). Note that this table sometimes contains statistics for more rays than are indicated in TABLE B-1; some of the ray arrivals in TABLE N-1 have not been identified with predicted arrivals. Also, sometimes there is initial ambiguity about the pairing of reciprocal arrivals, in which case sum and difference travel times are calculated for all reasonable cases; later it becomes obvious which arrivals have been improperly paired. The correlation $<T^+ T^->$ and variance $<T^2>$ are calculated from the sum and difference travel time variances in this table. The variance of the travel times is mainly due to internal wave variability, and this value determines the uncertainties assigned to the travel times in an inversion. The correlation coefficient is a measure of the reciprocity of reciprocal raypaths. This measure is conservative, because correlation is not a necessary condition for the determination of current from the difference of reciprocal travel times. Values of correlation that are 0.5 or greater assure that the reciprocal raypaths are indeed effectively identical, since good correlation implies that the reciprocal raypaths have not separated by more than an internal wave correlation length. Histograms of the detided, high-frequency travel times are shown in FIGURES N-7 and N-8; the variances from TABLE N-1 are measures of the width of these histograms.

TABLES N-2 and N-3 show the results of tidal analysis of the time series of difference (current) and sum (sound speed) travel times. For these tables, the tidal analysis is performed on each travel time time series separately and then the average and rms of the harmonic constants are calculated. Current or sound speed amplitude is determined from travel time by a simple scaling factor; the harmonic constants are more accurately determined by inverting the data for current or sound speed (this is not done here).

TABLE N-1. Travel Time Statistics 2←→4.

Ray #	Number of data	$\langle (T^+ + T^-)^2 \rangle$ (ms^2)	$\langle (T^+ - T^-)^2 \rangle$ (ms^2)	$\langle T^+ T^- \rangle$ (ms^2)	$\langle T^2 \rangle$ (ms^2)	$\frac{\langle T^+ T^- \rangle}{\langle T^2 \rangle}$
1	216	32	19	27	36	0.74
2	246	31	25	25	38	0.67
3	249	37	21	32	42	0.75
4	269	34	20	29	39	0.74
5	381	29	10	26	31	0.83
6	378	29	15	25	33	0.78
7	375	32	14	28	35	0.80
8	399	30	12	27	32	0.82
9	405	33	12	30	36	0.83
10	382	36	16	32	40	0.80
11	388	33	15	29	36	0.79
12	380	31	15	28	35	0.78

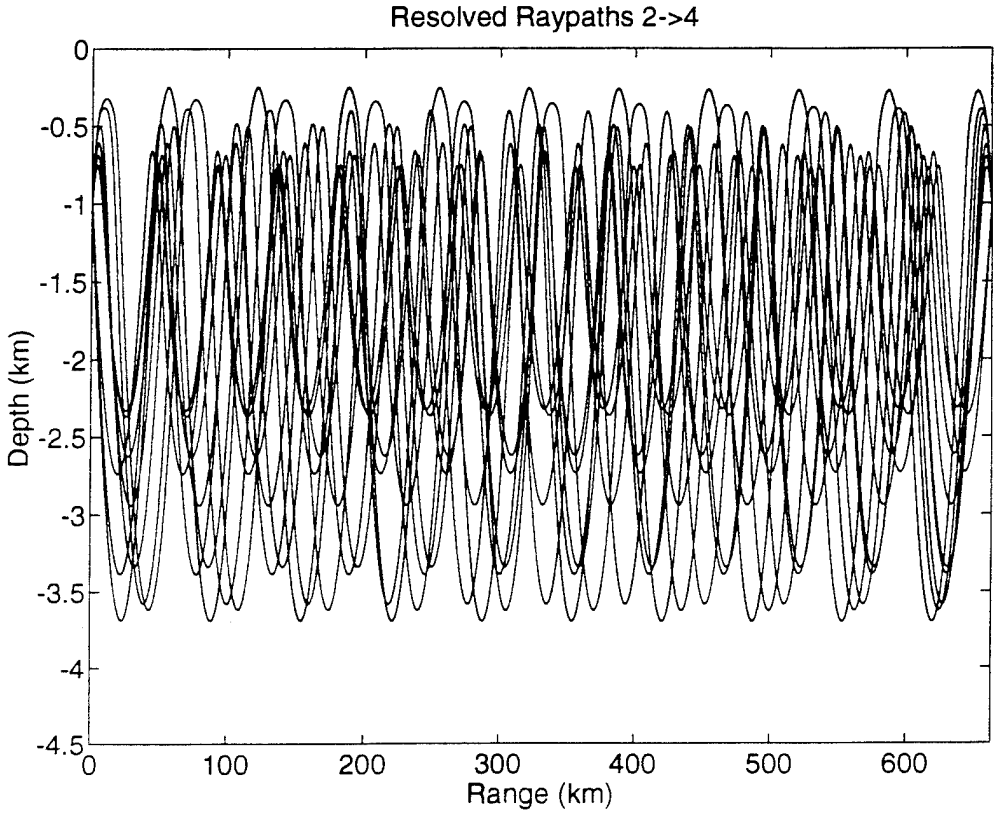

FIGURE N-1

TABLE N-2. Tidal Current Harmonic Constants 2←→4.

Constituent	Amplitude (mm/s)	Uncertainty (mm/s)	Phase (°G)	Uncertainty (°)
M_2	9.28	0.54	282.8	4.4
S_2	1.71	0.57	313.1	37.2
N_2	2.54	0.28	267.7	14.3
K_2	0.92	0.57	184.6	119.1
O_1	0.87	0.58	190.8	74.8
K_1	1.57	0.74	77.0	29.4
P_1	1.09	0.45	170.8	68.7
Q_1	1.07	0.69	181.5	102.9

Values and their uncertainty are determined by the average and rms of harmonic constants from tidal analyses of the separate raypath travel time series. The amplitudes do not include the lunar node factors. 55 ± 7 % of the high-frequency variance is accounted for by the tides.

TABLE N-3. Tidal Sound Speed Harmonic Constants 2←→4.

Constituent	Amplitude (mm/s)	Uncertainty (mm/s)	Phase (°G)	Uncertainty (°)
M_2	12.75	1.97	285.5	2.9
S_2	3.63	0.83	55.6	20.5
N_2	4.44	0.61	239.7	9.2
K_2	1.57	1.23	5.5	67.9
O_1	5.91	0.76	154.7	8.3
K_1	7.84	1.41	252.2	4.4
P_1	2.46	0.80	221.8	16.7
Q_1	2.28	0.37	354.9	24.1

Values and their uncertainty are determined by the average and rms of harmonic constants from tidal analyses of the separate raypath travel time series. The amplitudes do not include the lunar node factors. 64 ± 5 % of the high-frequency variance is accounted for by the tides. Because sum travel times are used to derive these numbers, the amplitudes have been divided by a factor of two compared to the amplitudes for current.

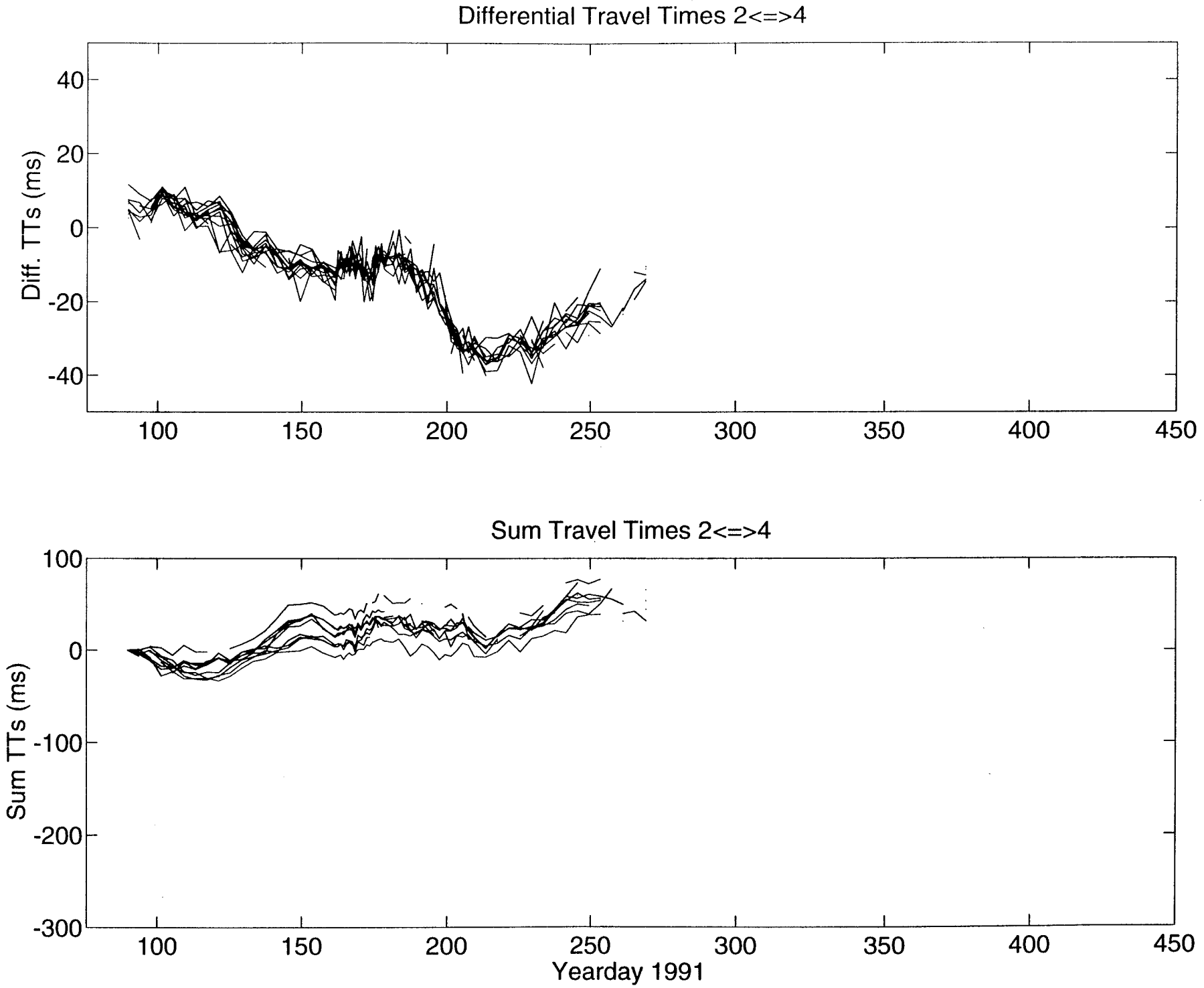
Differential Travel Times 2<=>4
Diff. TTs (ms)
40
20
0
-20
-40
100
150
200
250
300
350
400
450
Sum Travel Times 2<=>4
Sum TTs (ms)
100
0
-100
-200
-300
100
150
200
250
300
350
400
450
Yearday 1991

FIGURE N-2

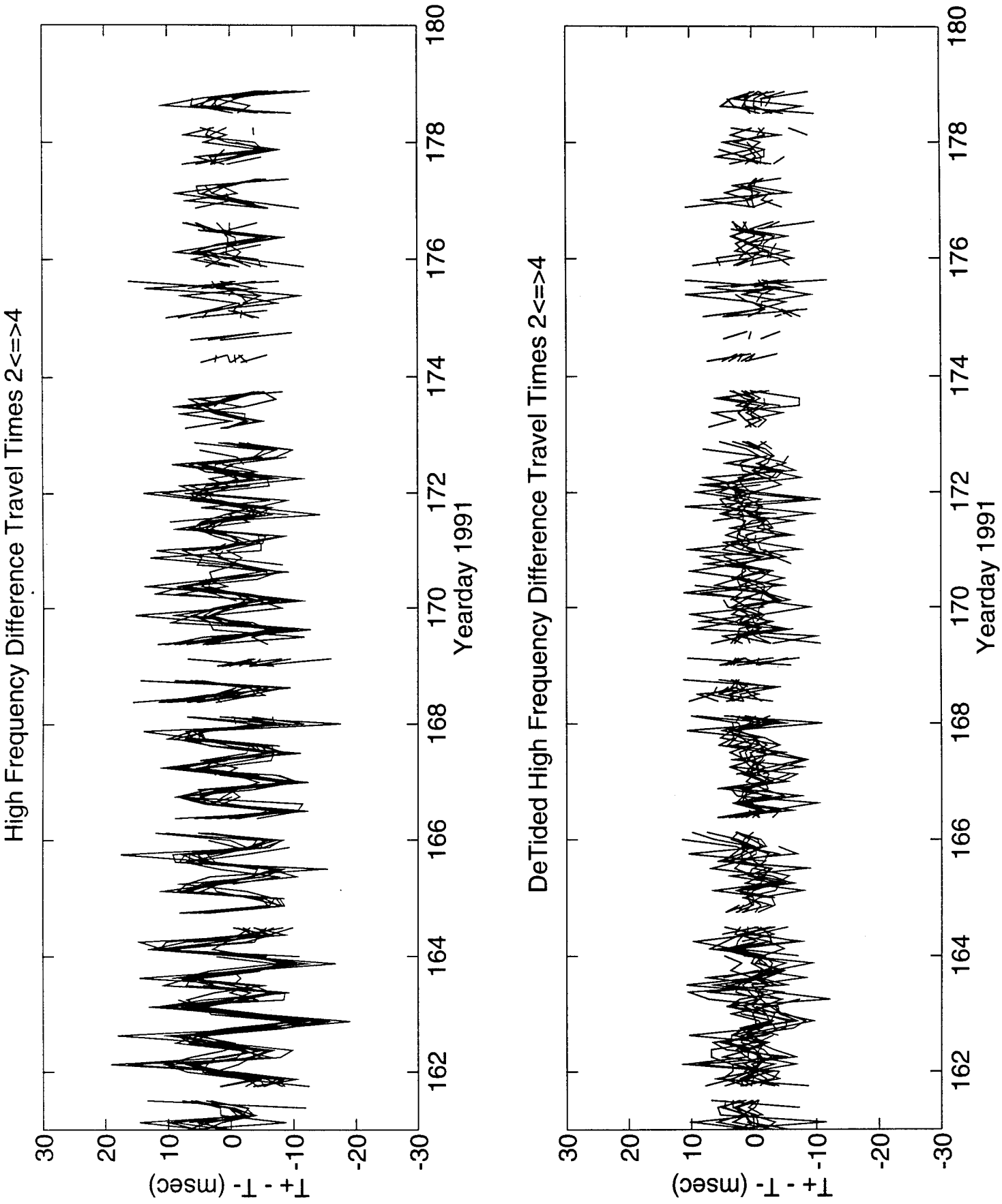
High Frequency Difference Travel Times 2<=>4
T+ - T- (msec)
30
20
10
0
-10
-20
-30
162
164
166
168
170
172
174
176
178
180
Yearday 1991
DeTided High Frequency Difference Travel Times 2<=>4
T+ - T- (msec)
30
20
10
0
-10
-20
-30
162
164
166
168
170
172
174
176
178
180
Yearday 1991

FIGURE N-3

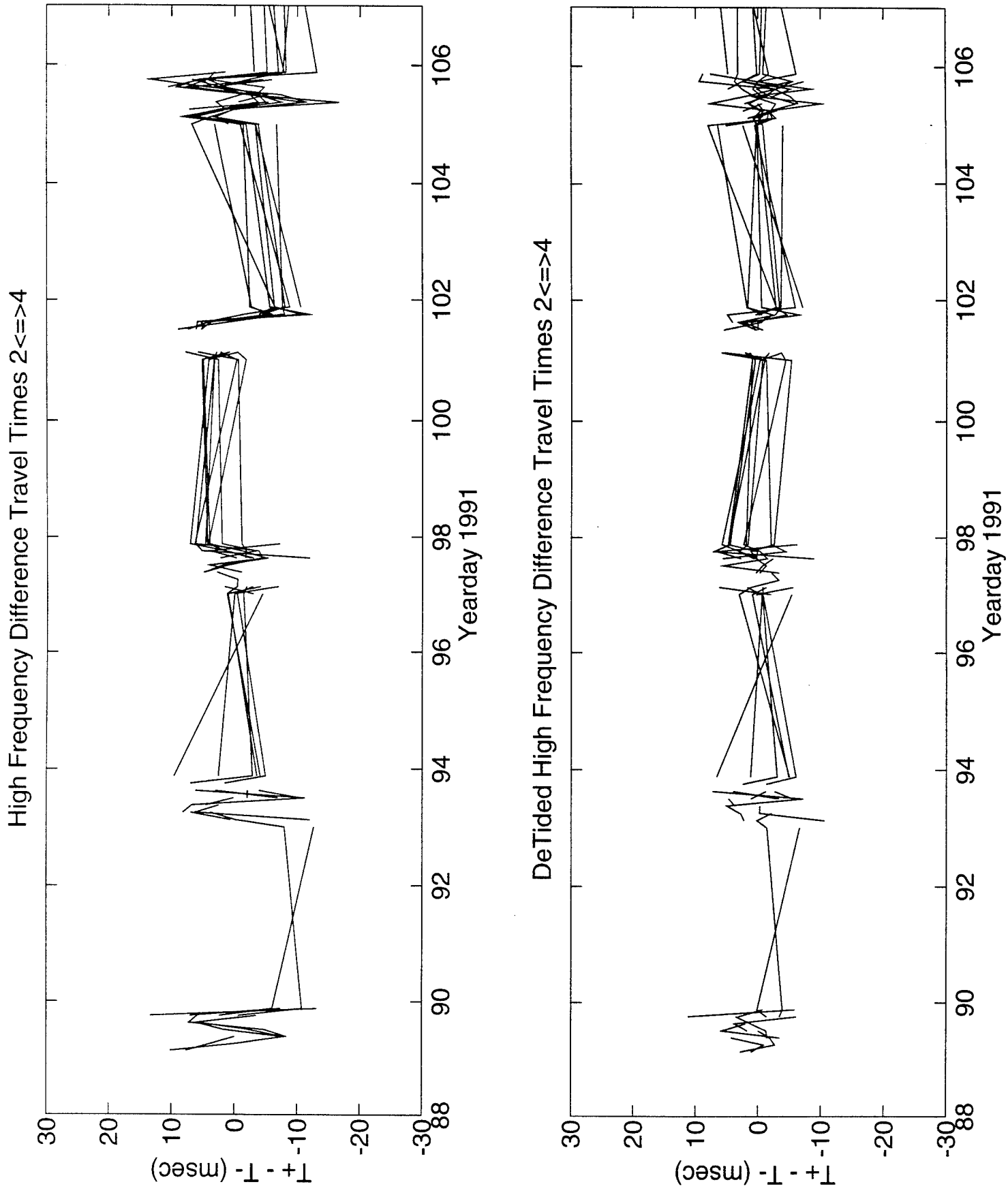
High Frequency Difference Travel Times 2<=>4
DeTided High Frequency Difference Travel Times 2<=>4
T+ - T- (msec)
Yearday 1991
30
20
10
0
-10
-20
-30
88
90
92
94
96
98
100
102
104
106

FIGURE N-4

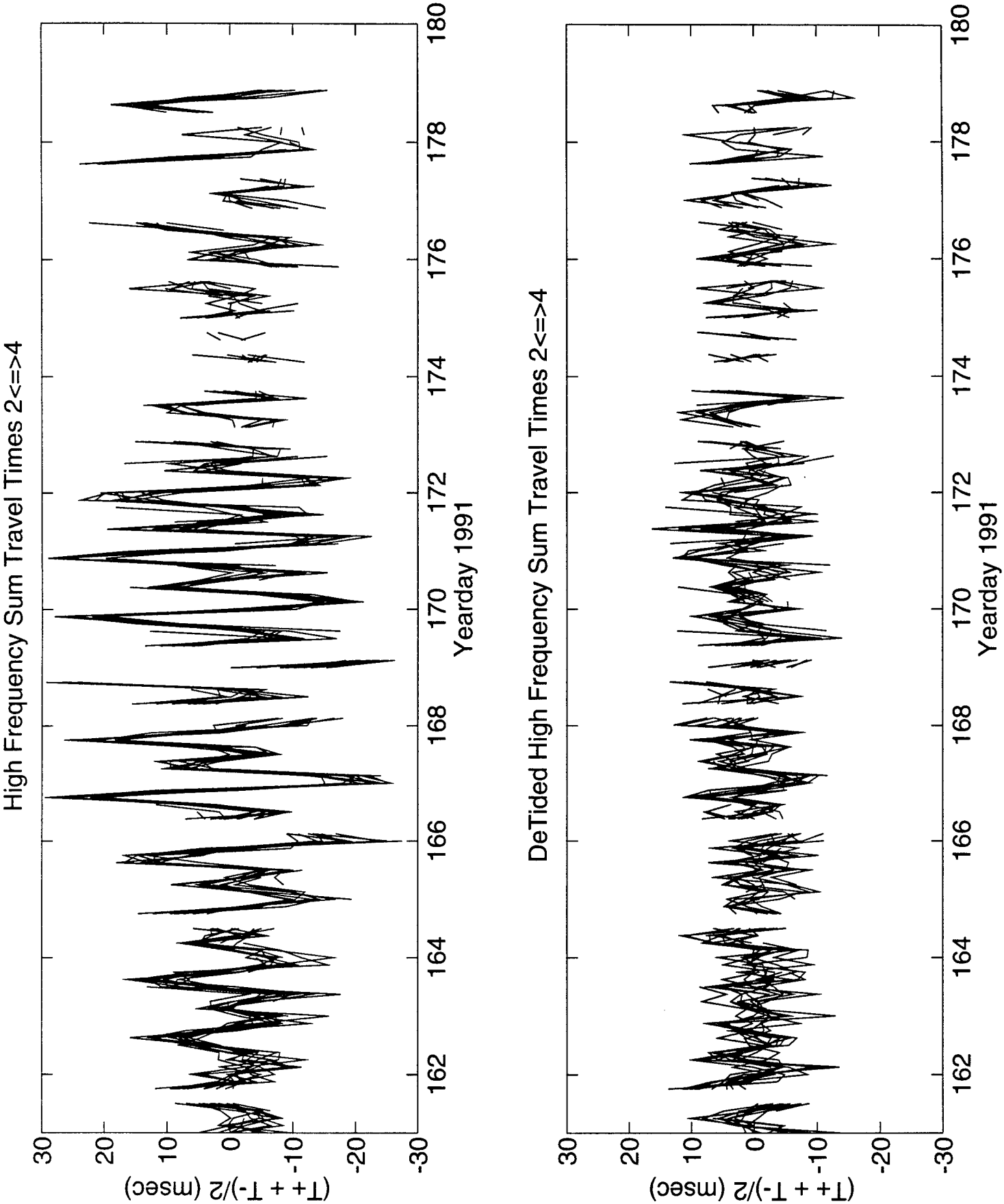
High Frequency Sum Travel Times 2<=>4
(T+ + T-)/2 (msec)
30
20
10
0
-10
-20
-30
162
164
166
168
170
172
174
176
178
180
Yearday 1991
DeTided High Frequency Sum Travel Times 2<=>4
(T+ + T-)/2 (msec)
30
20
10
0
-10
-20
-30
162
164
166
168
170
172
174
176
178
180
Yearday 1991

FIGURE N-5

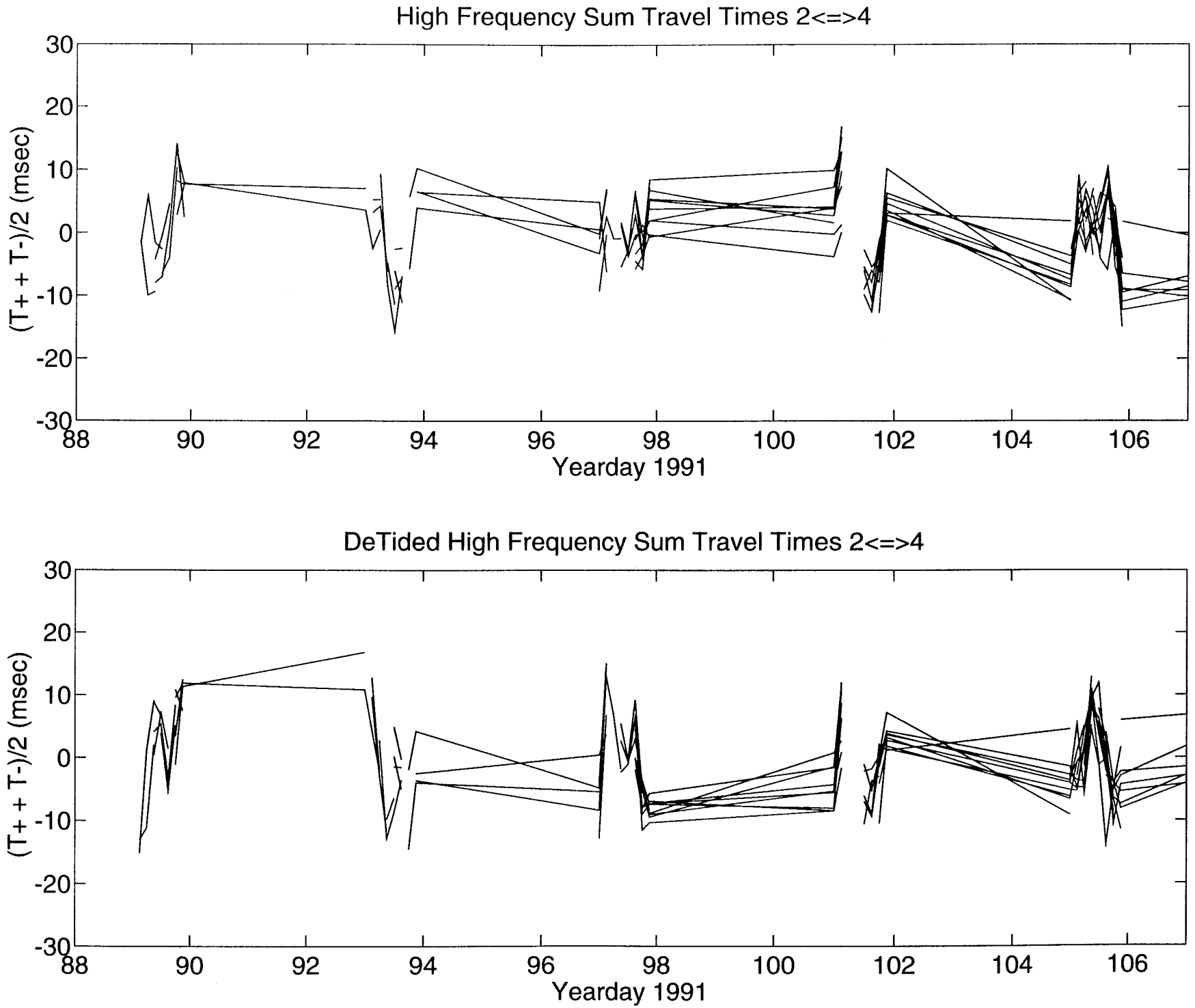
High Frequency Sum Travel Times 2<=>4
(T+ + T-)/2 (msec)
Yearday 1991
DeTided High Frequency Sum Travel Times 2<=>4
(T+ + T-)/2 (msec)
Yearday 1991

FIGURE N-6

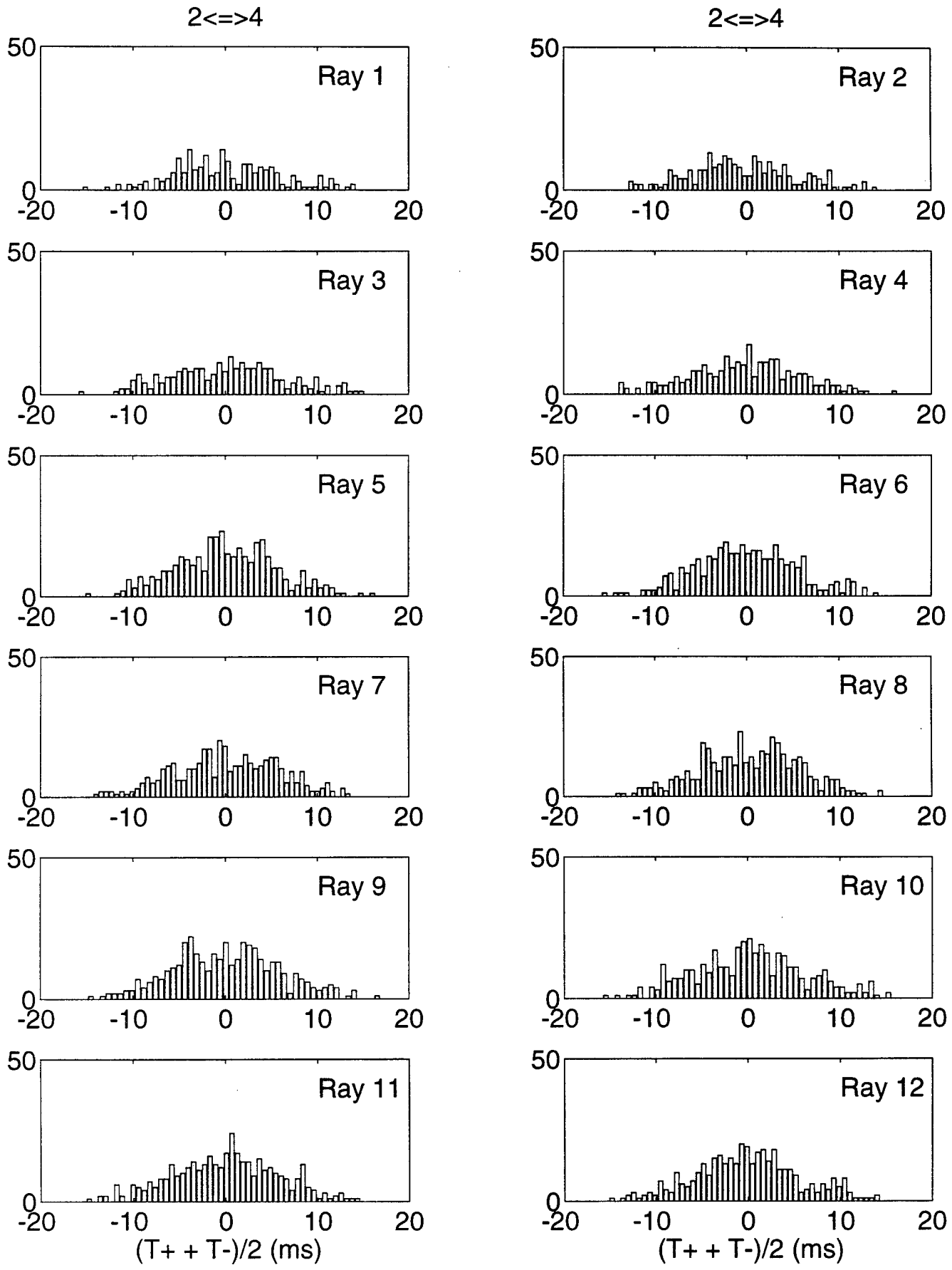
2<=>4
2<=>4
Ray 1
Ray 2
Ray 3
Ray 4
Ray 5
Ray 6
Ray 7
Ray 8
Ray 9
Ray 10
Ray 11
Ray 12
50
0
-20
-10
0
10
20
(T+ + T-)/2 (ms)

FIGURE N-7

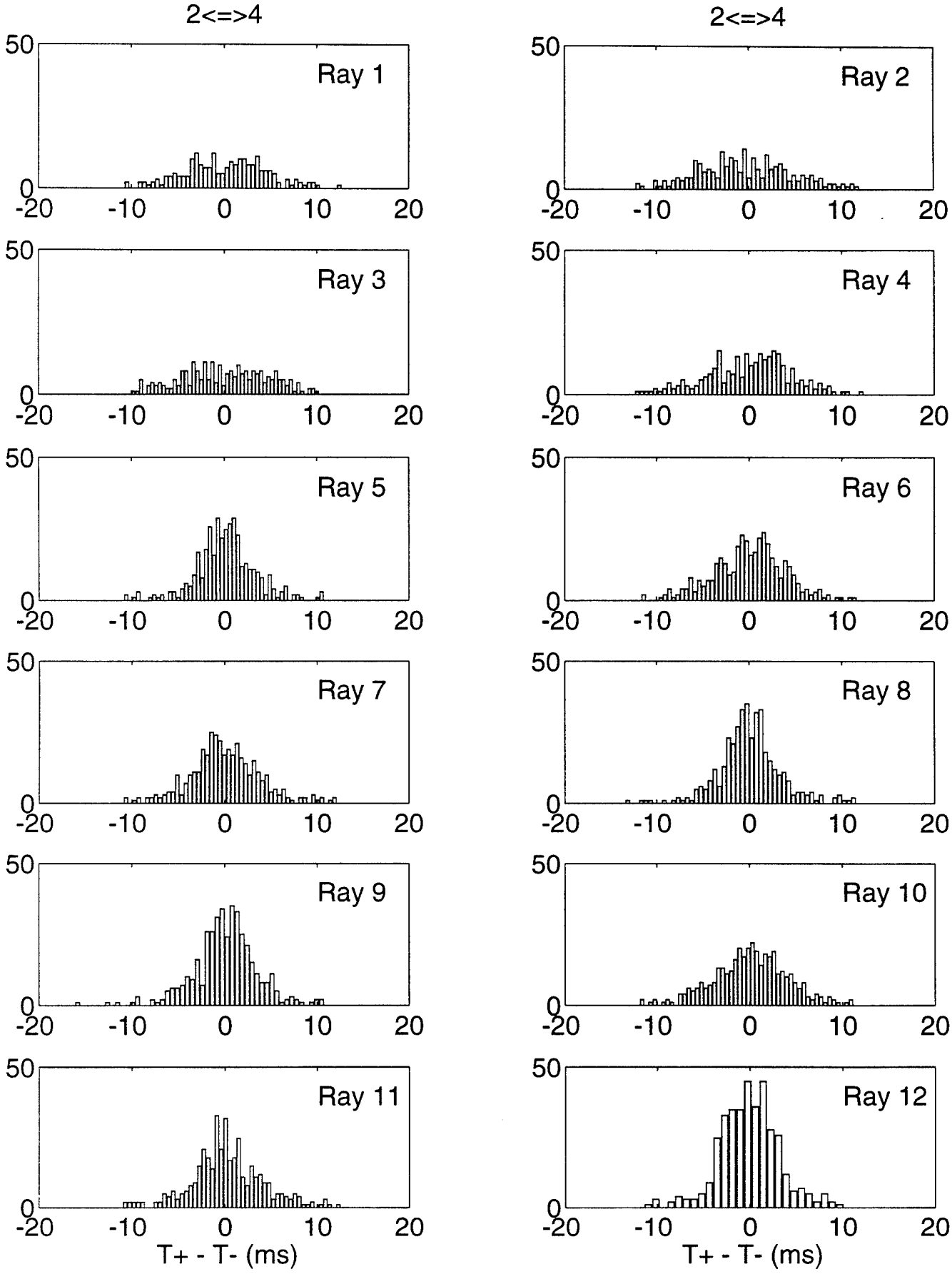
2<=>4
2<=>4
Ray 1
Ray 2
Ray 3
Ray 4
Ray 5
Ray 6
Ray 7
Ray 8
Ray 9
Ray 10
Ray 11
Ray 12
50
0
-20
-10
0
10
20
T+ - T- (ms)

FIGURE N-8

O. ACOUSTIC DATA: Paths 2→5a and 5a→2

FIGURE O-1 shows the raypaths, roughly corresponding to FIGURE G-1, for which travel times were resolved. The raypaths were actually determined using range-dependent Levitus sound speed, interpolated onto the acoustic path. Note that the "final cutoff" travel times may be available at some time in the future, these data correspond to a ray confined near the sound channel axis.

FIGURE O-2 shows the low-pass filtered difference (top panel) and sum (bottom panel) travel times corresponding to the rays of FIGURE O-1. Note that mooring 5a had failed by yearday 140, to be replaced later by mooring 5b.

FIGURE O-3 shows the high-pass filtered difference travel times for a small portion of the time series obtained during the time of more frequent transmissions during the MST experiment. The bottom panel shows the time series after the phase-locked tidal signals have been removed.

FIGURE O-4 shows the high-pass filtered sum travel times for a small portion of the time series obtained during the time of more frequent transmissions during the MST experiment. The bottom panel shows the time series after the phase-locked tidal signals have been removed. This tidal variability is caused by the internal tide.

After the travel time time series have been edited for outliers, high-pass filtered, and detided, the high-frequency variances are calculated (TABLE O-1). Note that this table sometimes contains statistics for more rays than are indicated in TABLE B-1; some of the ray arrivals in TABLE O-1 have not been identified with predicted arrivals. Also, sometimes there is initial ambiguity about the pairing of reciprocal arrivals, in which case sum and difference travel times are calculated for all reasonable cases; later it becomes obvious which arrivals have been improperly paired. The correlation $<T^+ T^->$ and variance $<T^2>$ are calculated from the sum and difference travel time variances in this table. The variance of the travel times is mainly due to internal wave variability, and this value determines the uncertainties assigned to the travel times in an inversion. The correlation coefficient is a measure of the reciprocity of reciprocal raypaths. This measure is conservative, because correlation is not a necessary condition for the determination of current from the difference of reciprocal travel times. Values of correlation that are 0.5 or greater assure that the reciprocal raypaths are indeed effectively identical, since good correlation implies that the reciprocal raypaths have not separated by more than an internal wave correlation length. Histograms of the detided, high-frequency travel times are shown in FIGURES O-5 and O-6; the variances from TABLE O-1 are measures of the width of these histograms.

TABLES O-2 and O-3 show the results of tidal analysis of the time series of difference (current) and sum (sound speed) travel times. For these tables, the tidal analysis is performed on each travel time time series separately and then the average and rms of the harmonic constants are calculated. Current or sound speed amplitude is determined from travel time by a simple scaling factor; the harmonic constants are more accurately determined by inverting the data for current or sound speed (this is not done here).

TABLE O-1. Travel Time Statistics 2←→5a.

Ray #	Number of data	$<(T^+ + T^-)^2>$ (ms^2)	$<(T^+ - T^-)^2>$ (ms^2)	$<T^+ T^->$ (ms^2)	$<T^2>$ (ms^2)	$\frac{<T^+ T^->}{<T^2>}$
1	81	20	19	15	25	0.61
2	85	30	18	25	34	0.73
3	67	27	22	22	33	0.67
4	83	28	22	22	33	0.67
5	72	24	23	18	30	0.62
6	82	38	27	32	45	0.70
7	74	24	24	18	30	0.60
8	93	18	11	15	21	0.73
9	84	18	15	15	22	0.65
10	87	21	12	18	24	0.75
11	92	22	11	19	25	0.77
12	92	21	10	18	23	0.78
13	91	21	15	17	25	0.69
14	83	25	20	20	30	0.67
15	90	25	14	22	29	0.76

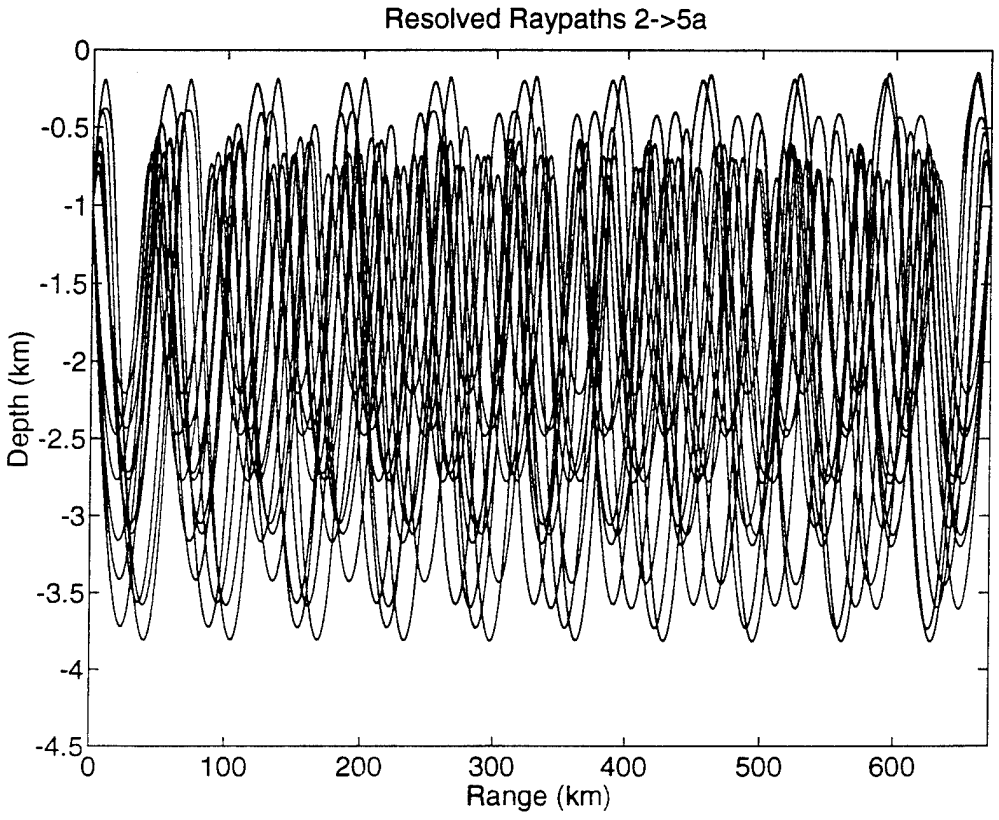

FIGURE O-1

TABLE O-2. Tidal Current Harmonic Constants 2←→5a.

Constituent	Amplitude (mm/s)	Uncertainty (mm/s)	Phase (°G)	Uncertainty (°)
M_2	12.58	1.77	284.1	8.1
S_2	5.46	2.38	280.8	92.6
N_2	3.24	1.33	277.1	35.6
K_2	3.46	2.14	253.8	100.2
O_1	2.35	1.53	188.3	101.3
K_1	4.62	2.56	43.5	57.3
P_1	3.46	1.67	298.9	88.1
Q_1	2.05	0.84	194.6	106.7

Values and their uncertainty are determined by the average and rms of harmonic constants from tidal analyses of the separate raypath travel time series. The amplitudes do not include the lunar node factors. 70 ± 9 % of the high-frequency variance is accounted for by the tides.

TABLE O-3. Tidal Sound Speed Harmonic Constants 2←→5a.

Constituent	Amplitude (mm/s)	Uncertainty (mm/s)	Phase (°G)	Uncertainty (°)
M_2	13.83	1.50	88.4	6.7
S_2	3.27	1.91	158.7	106.8
N_2	2.37	1.04	255.5	73.0
K_2	3.02	1.76	181.3	105.3
O_1	1.85	0.93	199.4	56.3
K_1	7.04	2.33	35.2	39.3
P_1	6.93	2.04	334.4	38.0
Q_1	2.44	1.38	328.1	72.9

Values and their uncertainty are determined by the average and rms of harmonic constants from tidal analyses of the separate raypath travel time series. The amplitudes do not include the lunar node factors. 63 ± 5 % of the high-frequency variance is accounted for by the tides. Because sum travel times are used to derive these numbers, the amplitudes have been divided by a factor of two compared to the amplitudes for current.

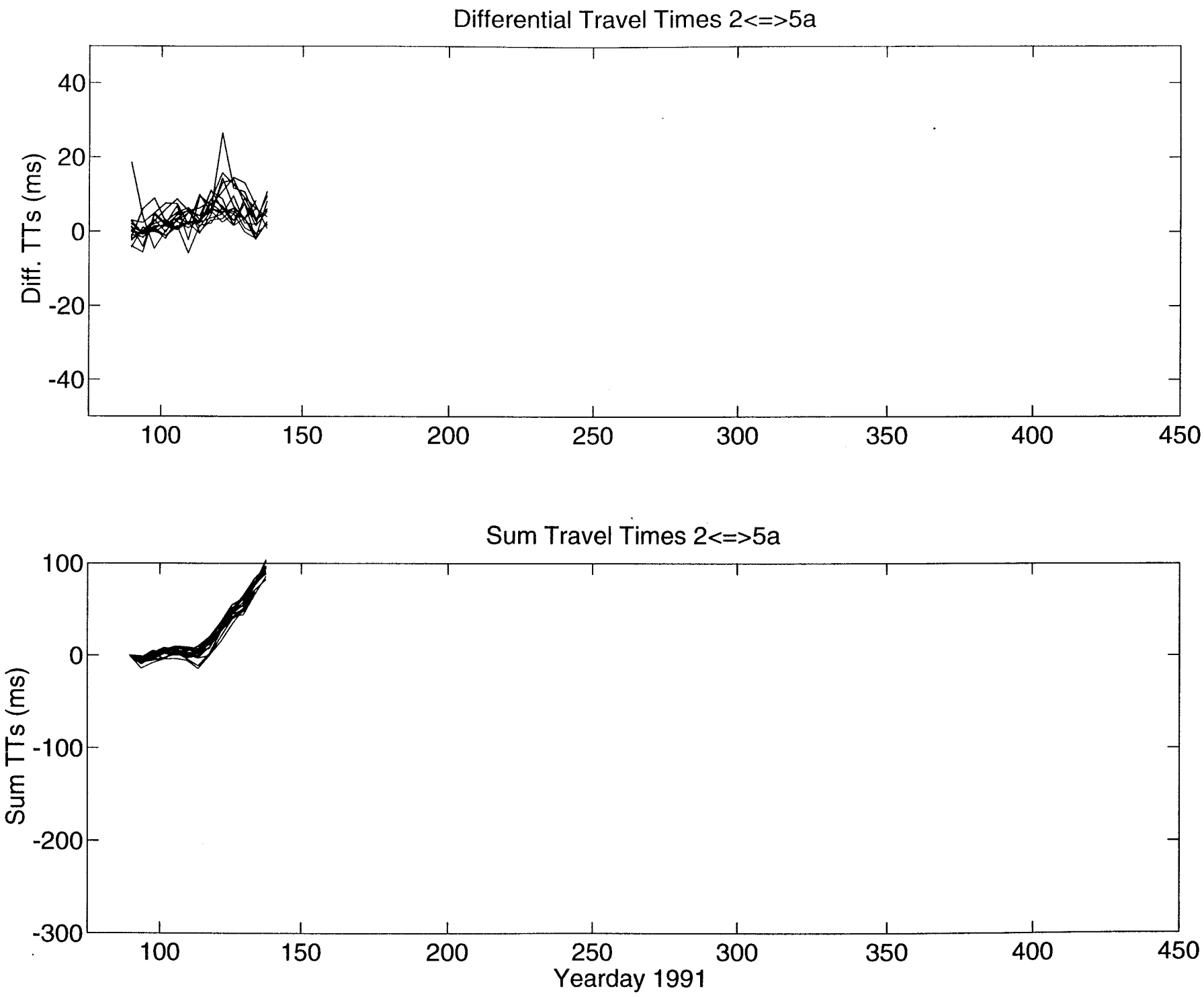
Differential Travel Times 2<=>5a
Diff. TTs (ms)
40
20
0
-20
-40
100
150
200
250
300
350
400
450
Sum Travel Times 2<=>5a
Sum TTs (ms)
100
0
-100
-200
-300
100
150
200
250
300
350
400
450
Yearday 1991

FIGURE O-2

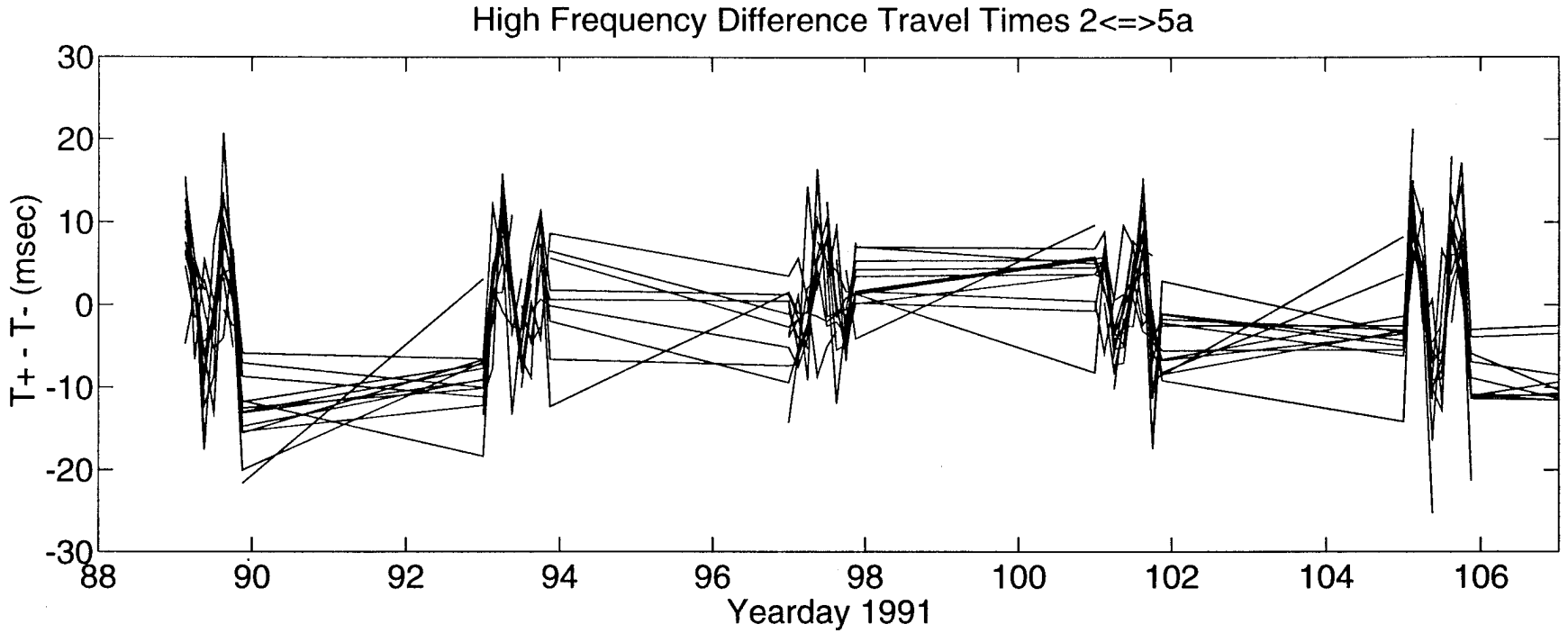
High Frequency Difference Travel Times 2<=>5a
T+ - T- (msec)
30
20
10
0
-10
-20
-30
88
90
92
94
96
98
100
102
104
106
Yearday 1991

FIGURE O-3

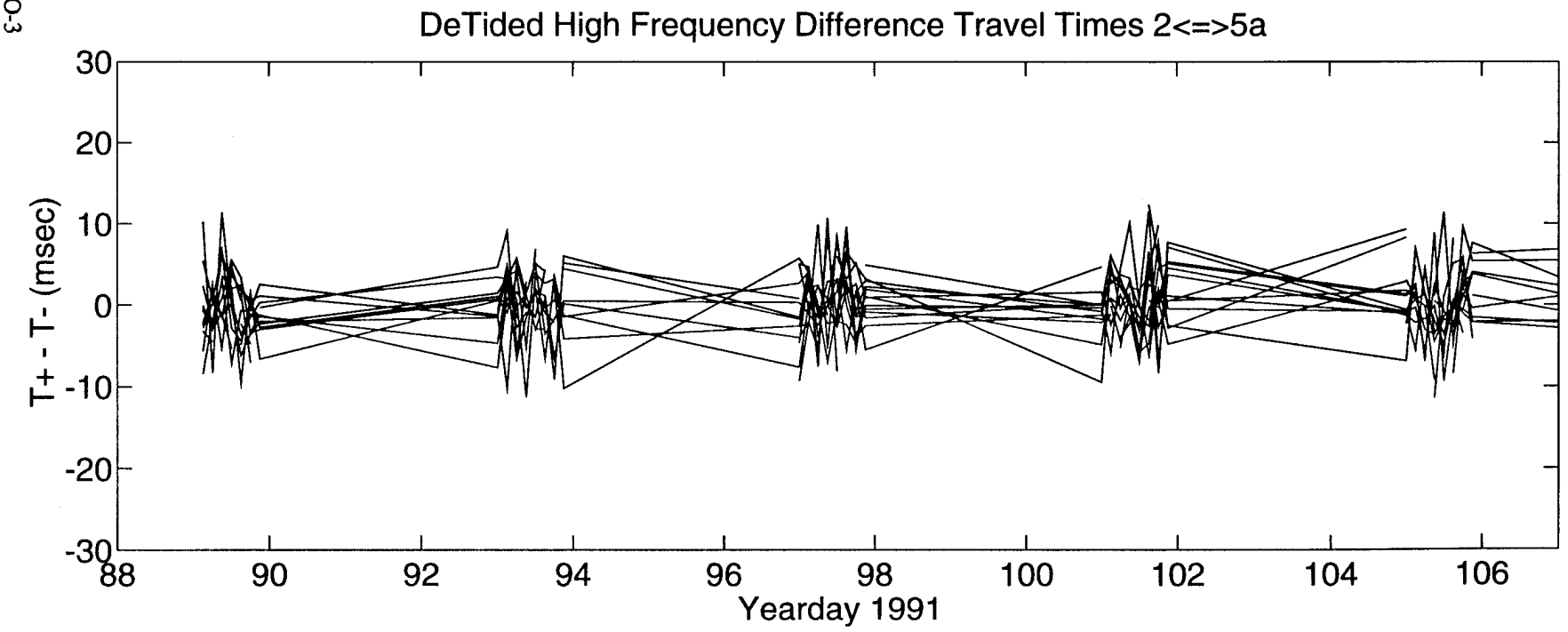
DeTided High Frequency Difference Travel Times 2<=>5a
T+ - T- (msec)
30
20
10
0
-10
-20
-30
88
90
92
94
96
98
100
102
104
106
Yearday 1991

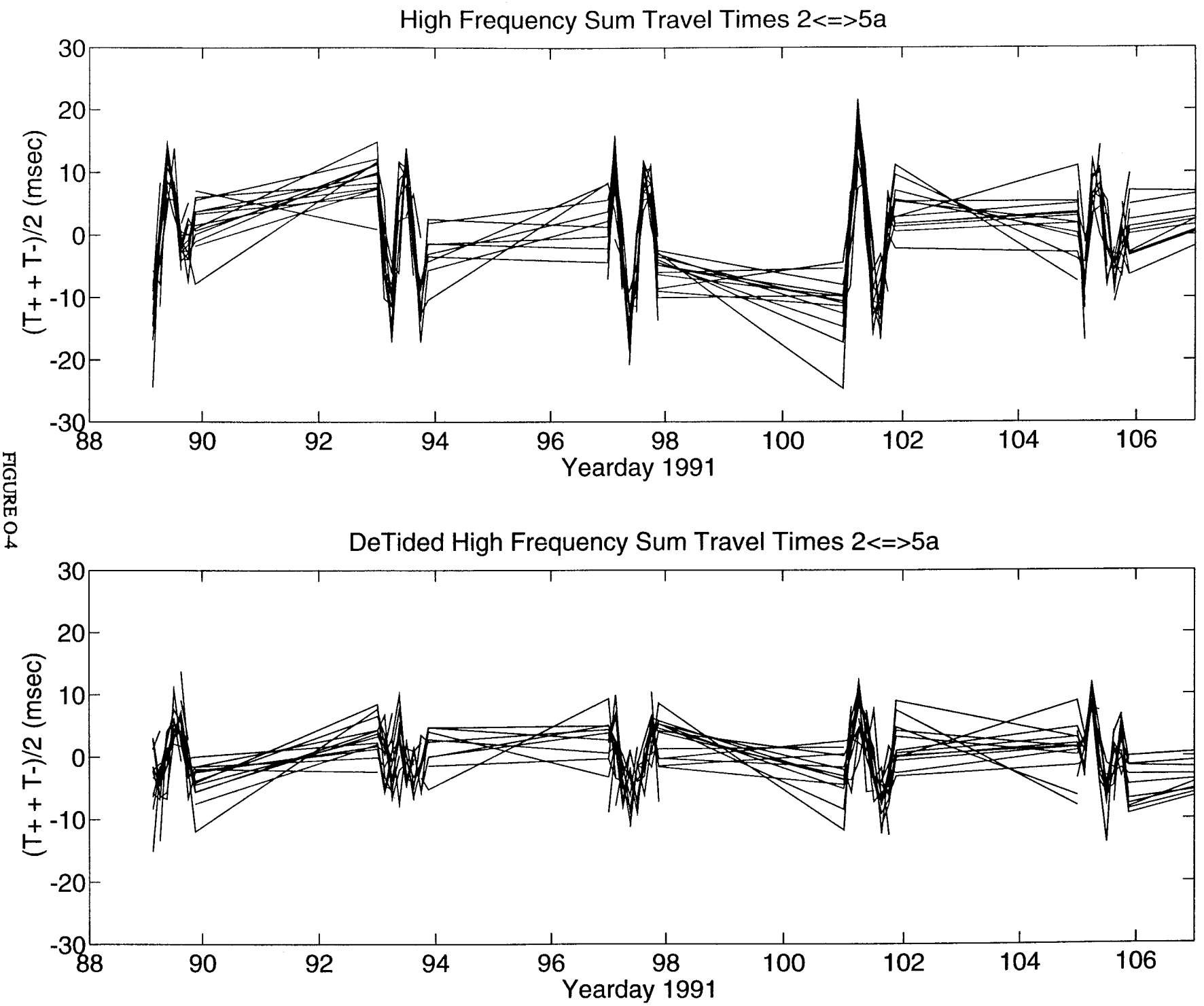
High Frequency Sum Travel Times 2<=>5a
(T+ + T-)/2 (msec)
Yearday 1991
DeTided High Frequency Sum Travel Times 2<=>5a
(T+ + T-)/2 (msec)
Yearday 1991

FIGURE O-4

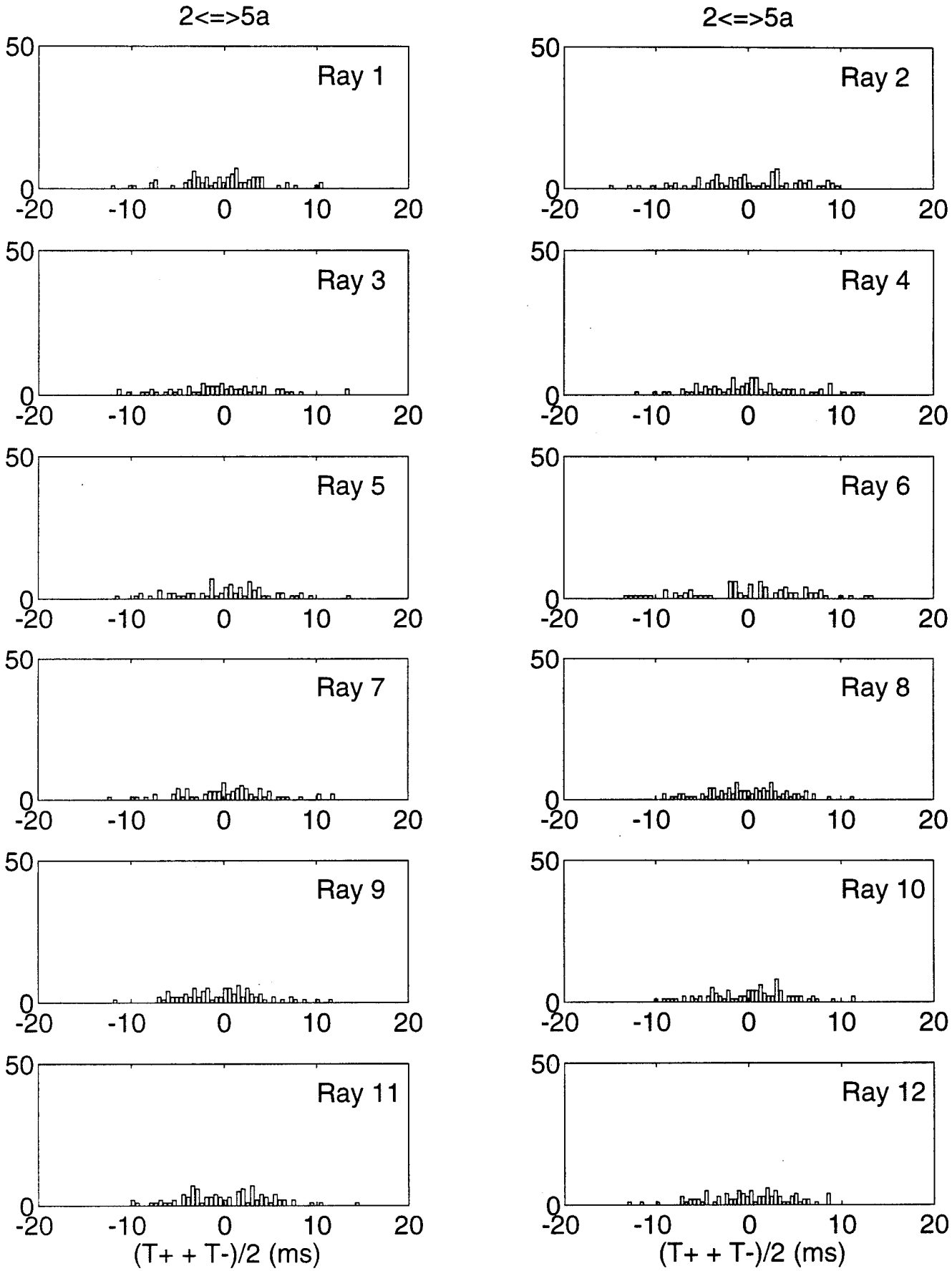
2<=>5a
2<=>5a
Ray 1
Ray 2
Ray 3
Ray 4
Ray 5
Ray 6
Ray 7
Ray 8
Ray 9
Ray 10
Ray 11
Ray 12
50
0
-20
-10
0
10
20
(T+ + T-)/2 (ms)

FIGURE O-5

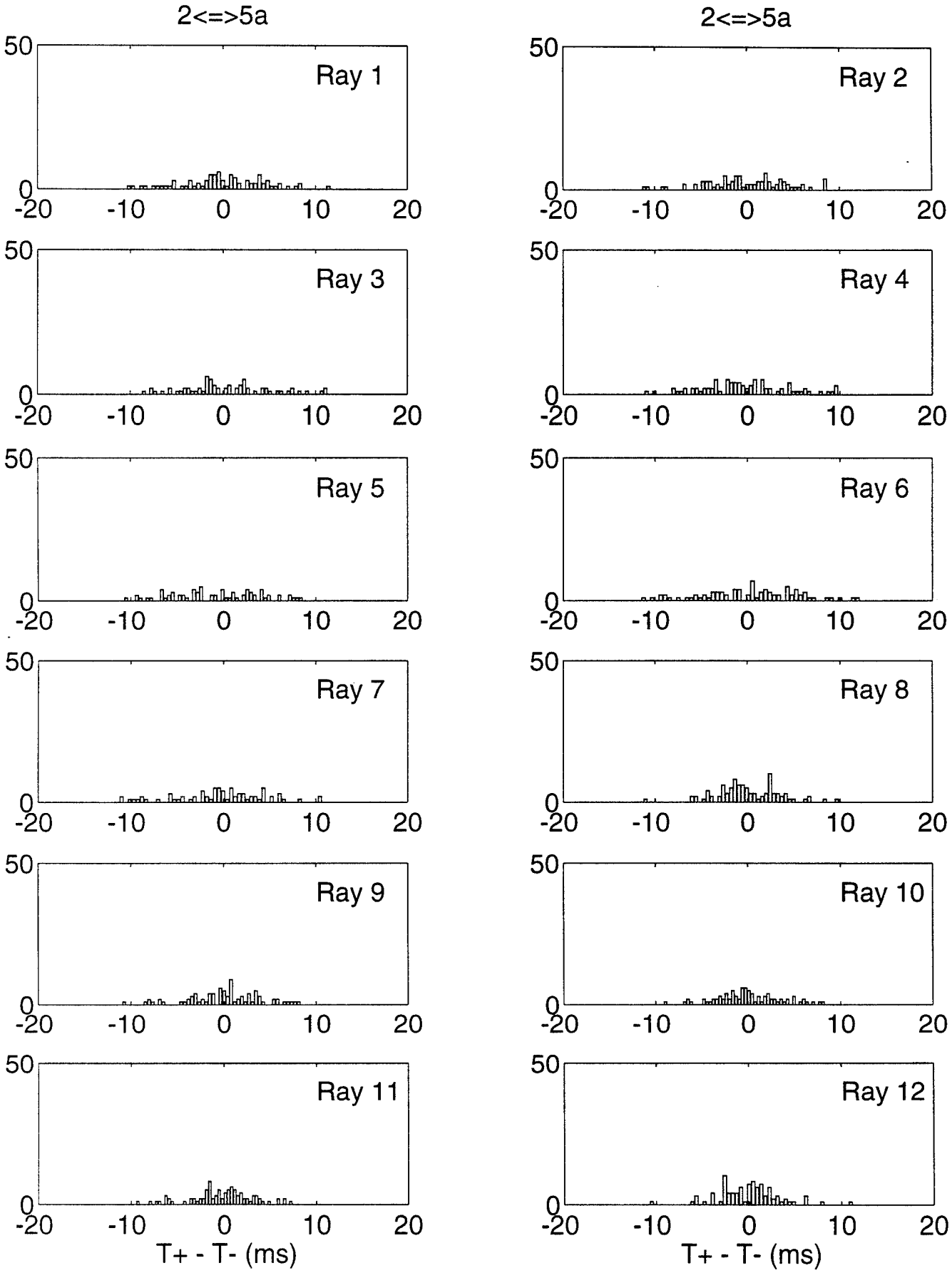
2<=>5a
2<=>5a
Ray 1
Ray 2
Ray 3
Ray 4
Ray 5
Ray 6
Ray 7
Ray 8
Ray 9
Ray 10
Ray 11
Ray 12
50
0
-20
-10
0
10
20
T+ - T- (ms)

FIGURE O-6

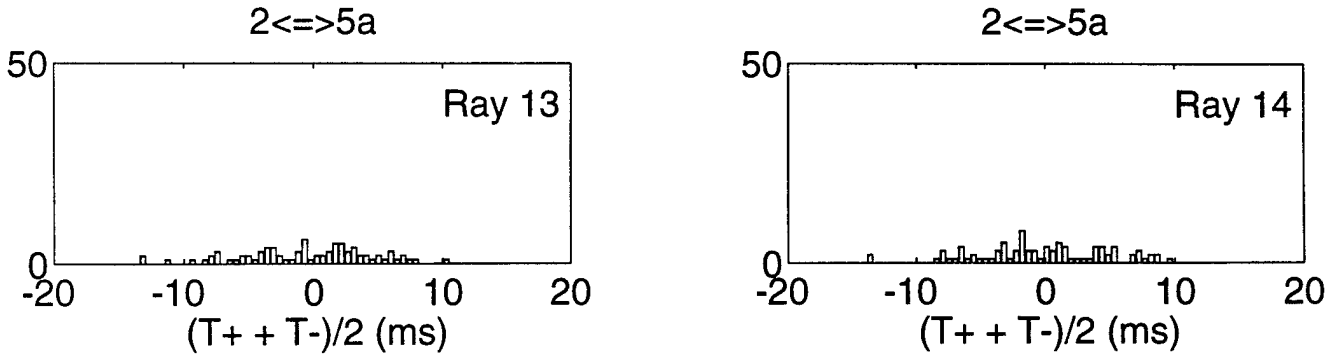

FIGURE O-5 (cont.)

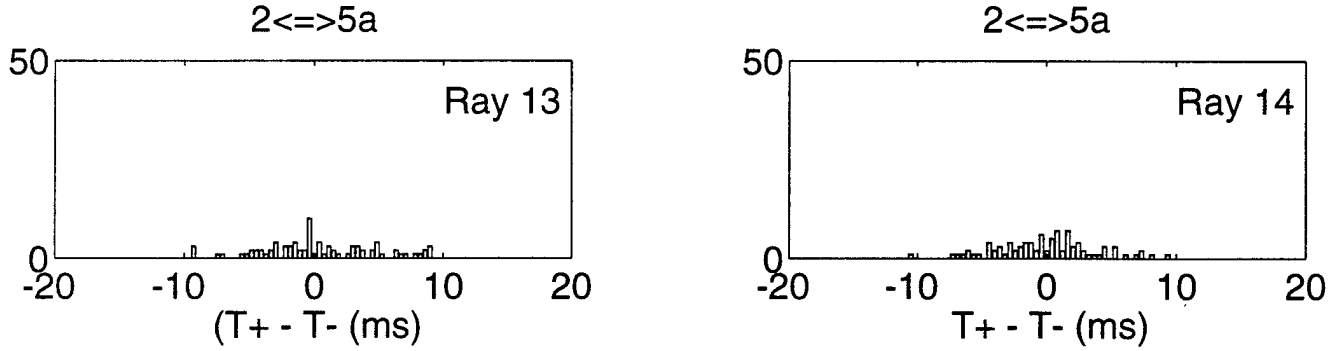

FIGURE O-6 (cont.)

P. ACOUSTIC DATA: Paths 2→5b and 5b→2

FIGURE P-1 shows the raypaths, corresponding roughly to FIGURE G-1, for which travel times were resolved. The raypaths were actually determined using range-dependent Levitus sound speed, interpolated onto the acoustic path. Note that the "final cutoff" travel times may be available at some time in the future, these data correspond to a ray confined near the sound channel axis.

FIGURE P-2 shows the low-pass filtered difference (top panel) and sum (bottom panel) travel times corresponding to the rays of FIGURE P-1.

FIGURE P-3 shows the high-pass filtered difference travel times for a small portion of the time series obtained during the time of more frequent transmissions during the MST experiment. The bottom panel shows the time series after the phase-locked tidal signals have been removed.

FIGURE P-4 shows the high-pass filtered sum travel times for a small portion of the time series obtained during the time of more frequent transmissions during the MST experiment. The bottom panel shows the time series after the phase-locked tidal signals have been removed. This tidal variability is caused by the internal tide.

After the travel time time series have been edited for outliers, high-pass filtered, and detided, the high-frequency variances are calculated (TABLE P-1). Note that this table sometimes contains statistics for more rays than are indicated in TABLE B-1; some of the ray arrivals in TABLE P-1 have not been identified with predicted arrivals. Also, sometimes there is initial ambiguity about the pairing of reciprocal arrivals, in which case sum and difference travel times are calculated for all reasonable cases; later it becomes obvious which arrivals have been improperly paired. The correlation $<T^+ T^->$ and variance $<T^2>$ are calculated from the sum and difference travel time variances in this table. The variance of the travel times is mainly due to internal wave variability, and this value determines the uncertainties assigned to the travel times in an inversion. The correlation coefficient is a measure of the reciprocity of reciprocal raypaths. This measure is conservative, because correlation is not a necessary condition for the determination of current from the difference of reciprocal travel times. Values of correlation that are 0.5 or greater assure that the reciprocal raypaths are indeed effectively identical, since good correlation implies that the reciprocal raypaths have not separated by more than an internal wave correlation length. Histograms of the detided, high-frequency travel times are shown in FIGURES P-5 and P-6; the variances from TABLE P-1 are measures of the width of these histograms.

TABLES P-2 and P-3 show the results of tidal analysis of the time series of difference (current) and sum (sound speed) travel times. For these tables, the tidal analysis is performed on each travel time time series separately and then the average and rms of the harmonic constants are calculated. Current or sound speed amplitude is determined from travel time by a simple scaling factor; the harmonic constants are more accurately determined by inverting the data for current or sound speed (this is not done here).

TABLE P-1. Travel Time Statistics 2←→5b.

Ray #	Number of data	$<(T^+ + T^-)^2>$ (ms^2)	$<(T^+ - T^-)^2>$ (ms^2)	$<T^+ T^->$ (ms^2)	$<T^2>$ (ms^2)	$\frac{<T^+ T^->}{<T^2>}$
1	133	25	16	21	30	0.73
2	245	37	34	29	46	0.63
3	222	33	34	25	42	0.60
4	243	29	21	23	34	0.69
5	228	35	26	28	41	0.68
6	228	40	26	34	47	0.72
7	234	30	28	23	37	0.62
8	261	31	20	26	36	0.73
9	387	33	16	29	37	0.79
10	411	30	16	26	34	0.77
11	387	35	15	32	39	0.81
12	446	32	12	29	35	0.83
13	447	34	14	31	38	0.82
14	404	36	17	32	40	0.79
15	367	34	26	27	40	0.68
16	448	35	17	31	40	0.79

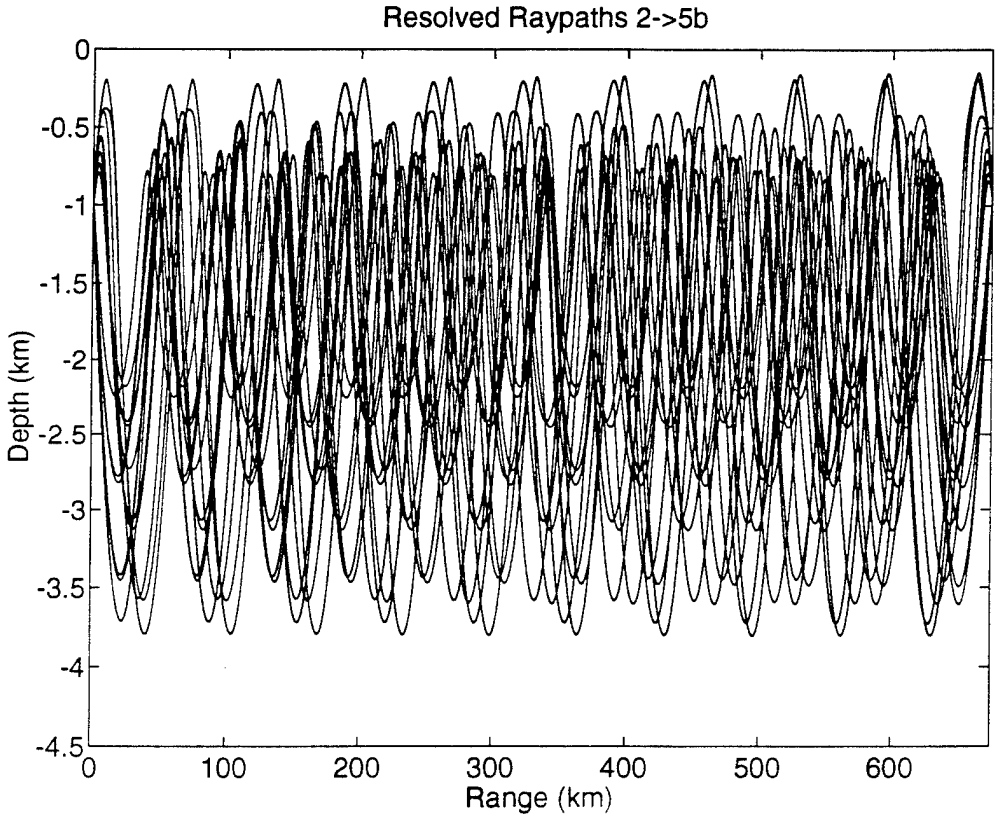

FIGURE P-1

TABLE P-2. Tidal Current Harmonic Constants 2←→5b.

Constituent	Amplitude (mm/s)	Uncertainty (mm/s)	Phase (°G)	Uncertainty (°)
M_2	11.84	1.22	284.1	7.6
S_2	3.19	1.10	308.7	18.6
N_2	3.25	0.85	262.8	25.8
K_2	1.94	0.84	297.9	65.4
O_1	1.12	0.58	48.8	78.7
K_1	1.55	0.75	66.9	56.4
P_1	1.11	0.61	91.4	65.0
Q_1	1.23	0.90	217.6	107.7

Values and their uncertainty are determined by the average and rms of harmonic constants from tidal analyses of the separate raypath travel time series. The amplitudes do not include the lunar node factors. 62 ± 9 % of the high-frequency variance is accounted for by the tides.

TABLE P-3. Tidal Sound Speed Harmonic Constants 2←→5b.

Constituent	Amplitude (mm/s)	Uncertainty (mm/s)	Phase (°G)	Uncertainty (°)
M_2	6.81	1.30	65.9	11.1
S_2	3.16	1.53	223.6	20.5
N_2	3.53	0.89	334.8	16.1
K_2	1.45	0.55	125.3	77.6
O_1	1.99	0.73	161.0	50.6
K_1	1.26	0.92	37.8	78.5
P_1	2.05	1.10	179.5	151.6
Q_1	1.25	0.51	151.1	65.6

Values and their uncertainty are determined by the average and rms of harmonic constants from tidal analyses of the separate raypath travel time series. The amplitudes do not include the lunar node factors. 36 ± 7 % of the high-frequency variance is accounted for by the tides. Because sum travel times are used to derive these numbers, the amplitudes have been divided by a factor of two compared to the amplitudes for current.

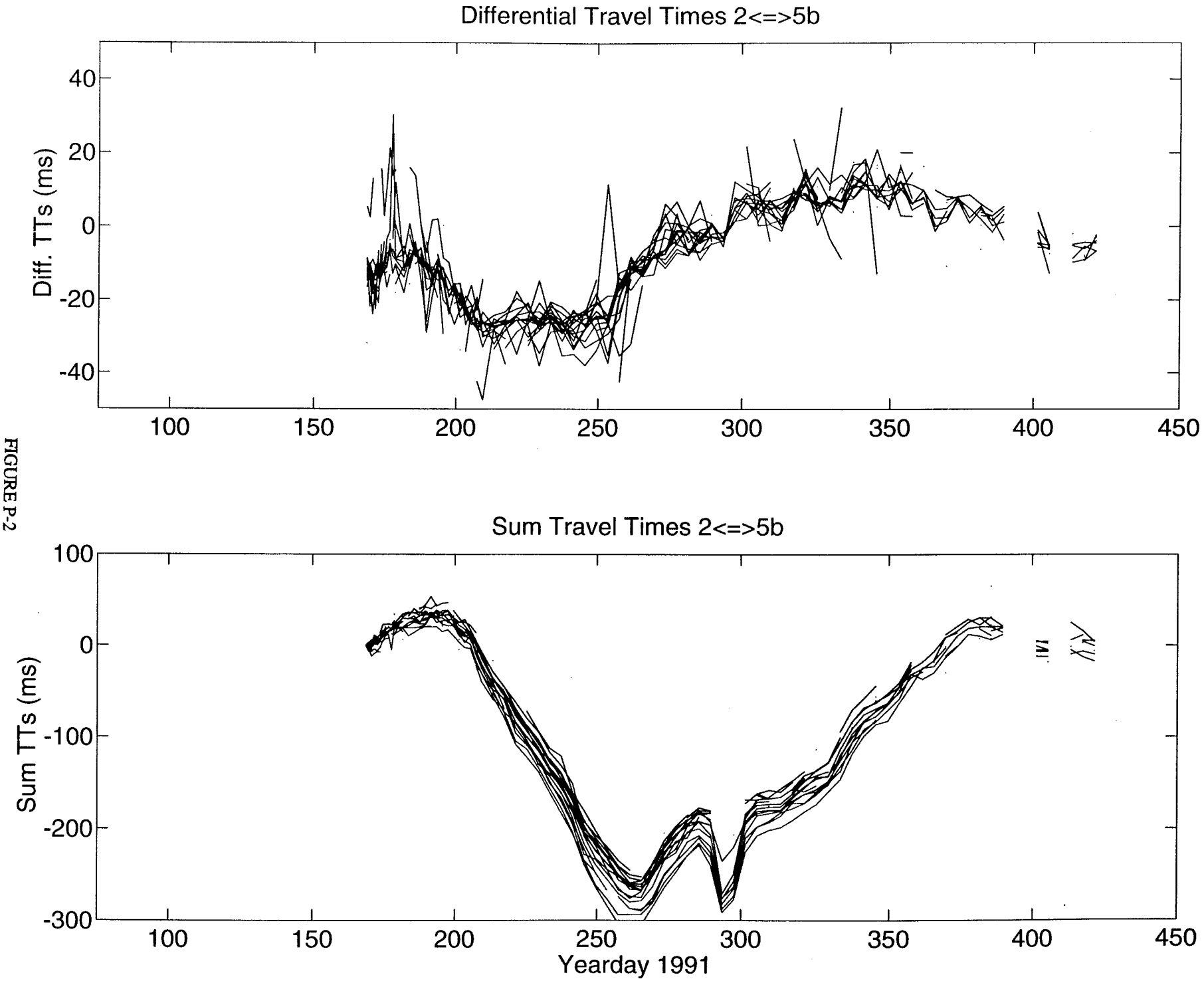
Differential Travel Times 2<=>5b
Diff. TTs (ms)
40
20
0
-20
-40
100
150
200
250
300
350
400
450
Sum Travel Times 2<=>5b
Sum TTs (ms)
100
0
-100
-200
-300
100
150
200
250
300
350
400
450
Yearday 1991

FIGURE P-2

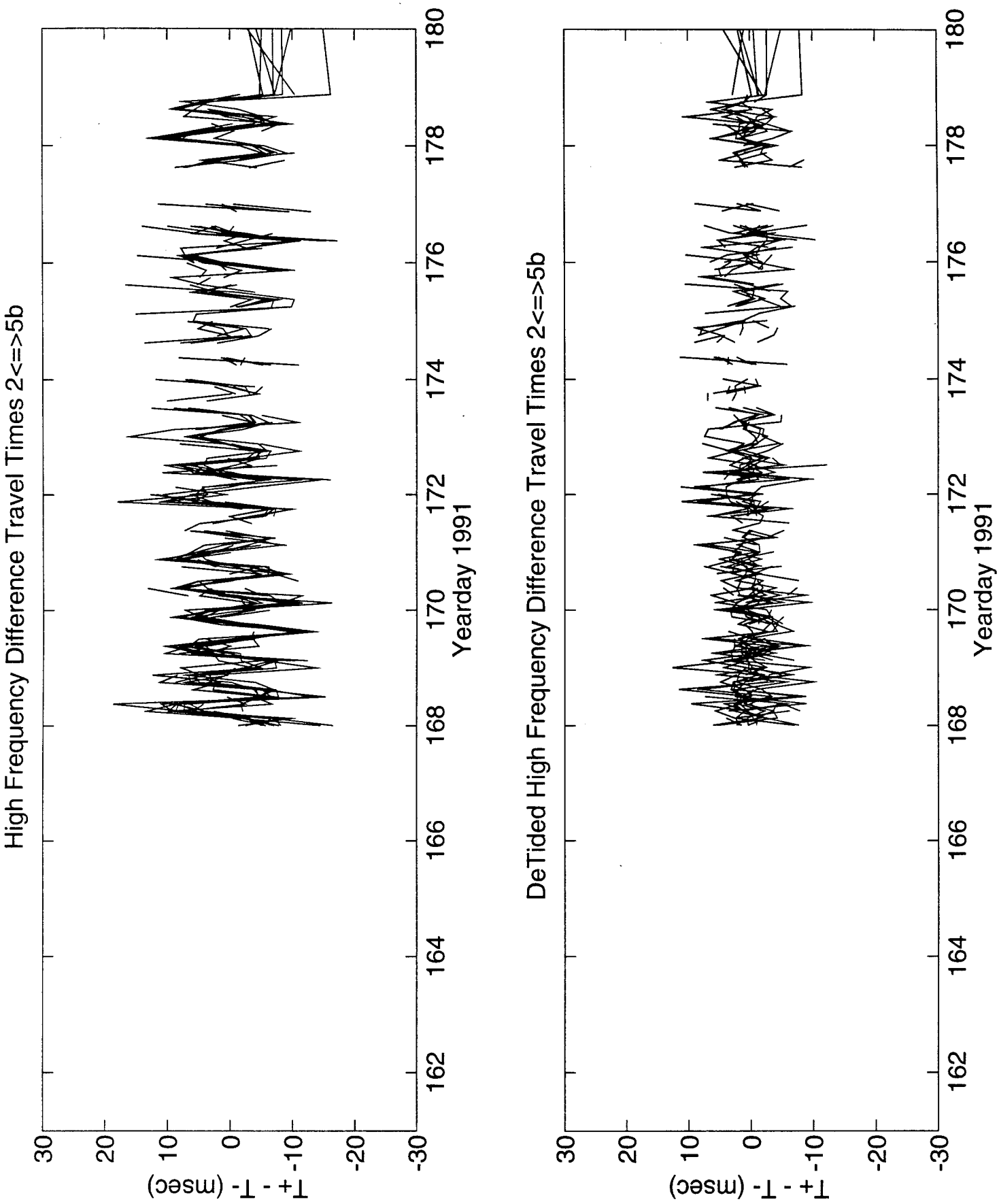
High Frequency Difference Travel Times 2<=>5b
T+ - T- (msec)
30
20
10
0
-10
-20
-30
162
164
166
168
170
172
174
176
178
180
Yearday 1991
DeTided High Frequency Difference Travel Times 2<=>5b
T+ - T- (msec)
30
20
10
0
-10
-20
-30
162
164
166
168
170
172
174
176
178
180
Yearday 1991

FIGURE P-3

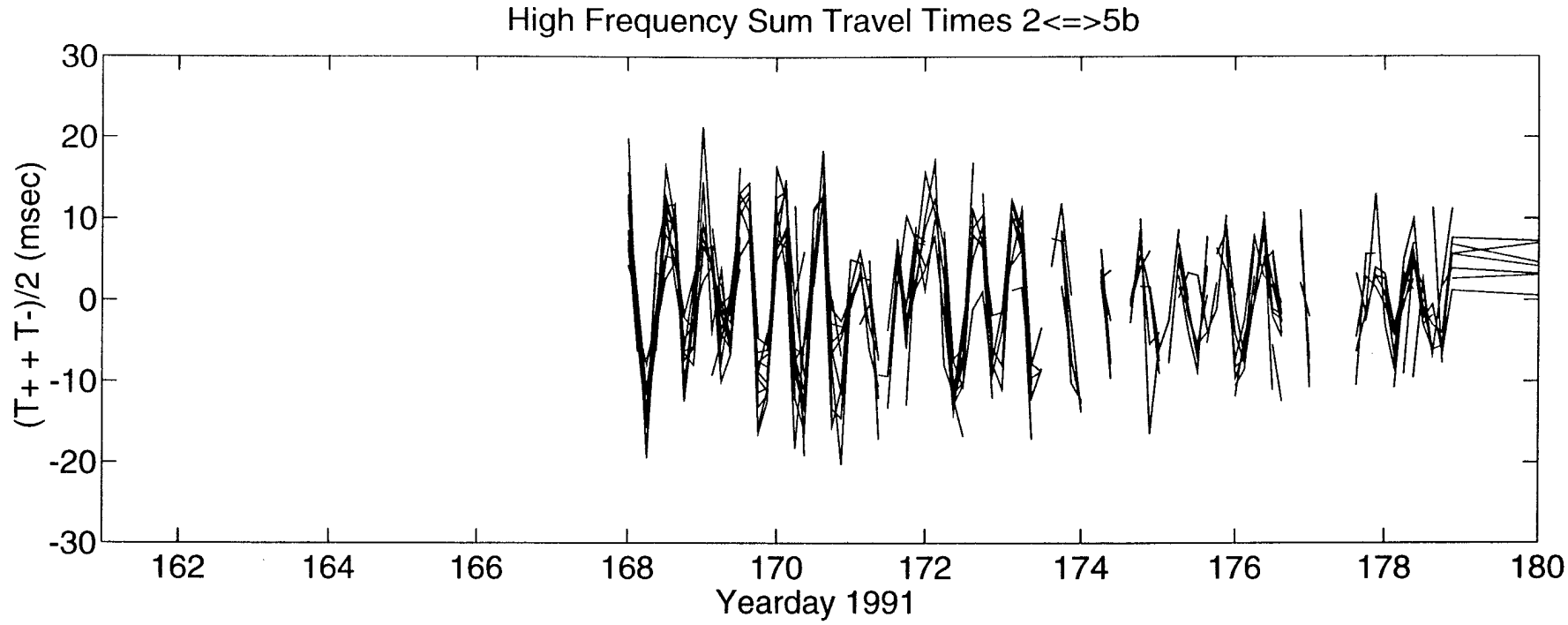
High Frequency Sum Travel Times 2<=>5b
(T+ + T-)/2 (msec)
30
20
10
0
-10
-20
-30
162
164
166
168
170
172
174
176
178
180
Yearday 1991

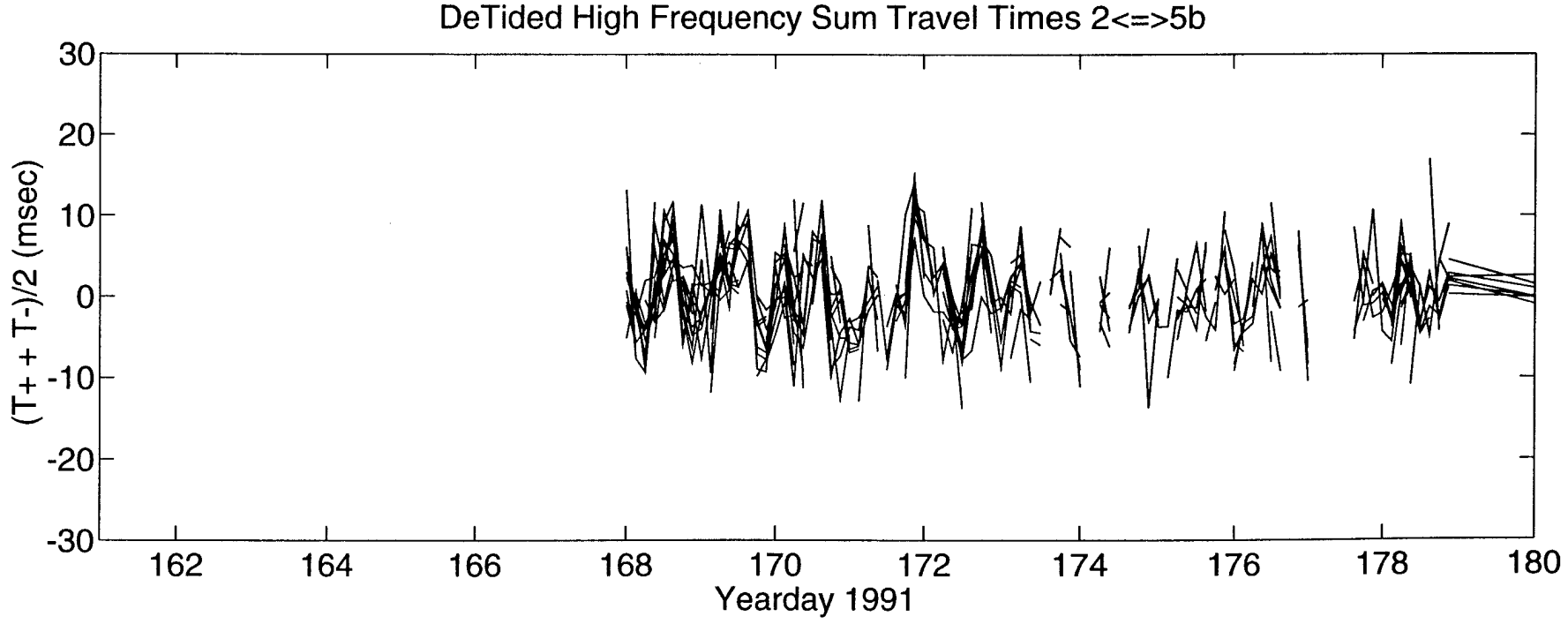
DeTided High Frequency Sum Travel Times 2<=>5b
(T+ + T-)/2 (msec)
30
20
10
0
-10
-20
-30
162
164
166
168
170
172
174
176
178
180
Yearday 1991

FIGURE P-4

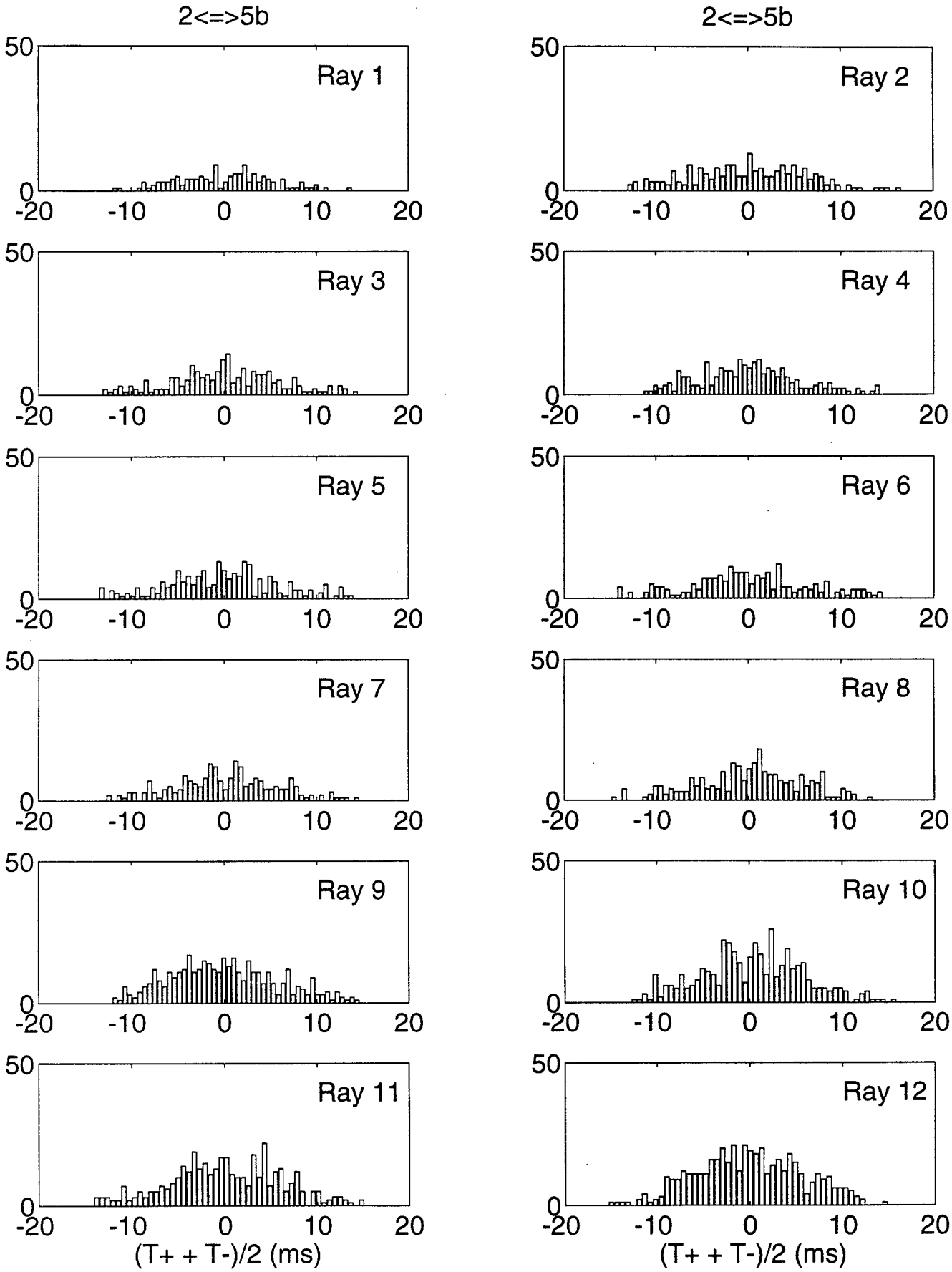
2<=>5b
2<=>5b
Ray 1
Ray 2
Ray 3
Ray 4
Ray 5
Ray 6
Ray 7
Ray 8
Ray 9
Ray 10
Ray 11
Ray 12
50
0
-20
-10
0
10
20
(T+ + T-)/2 (ms)

FIGURE P-5

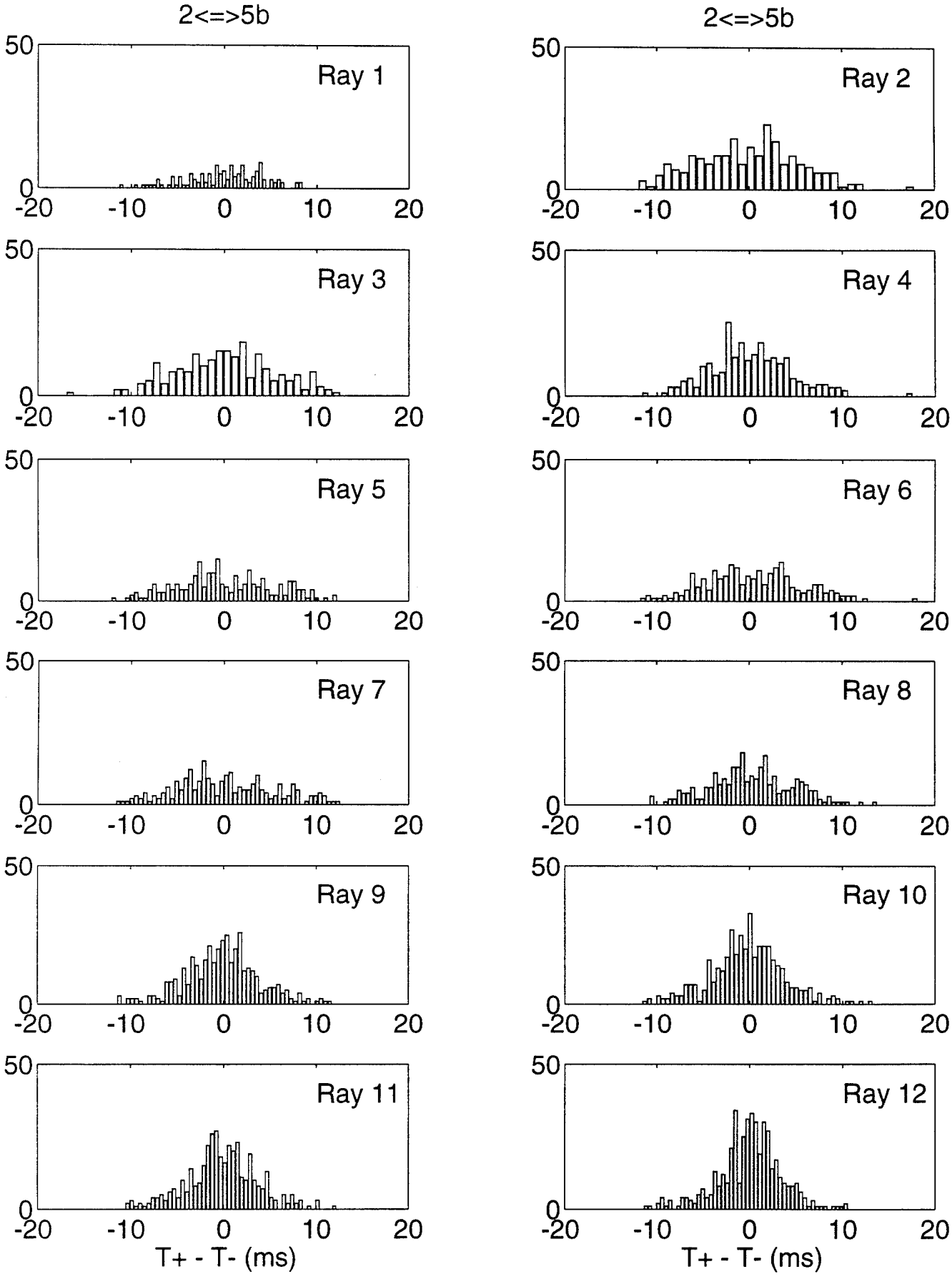
2<=>5b
Ray 1
Ray 2
Ray 3
Ray 4
Ray 5
Ray 6
Ray 7
Ray 8
Ray 9
Ray 10
Ray 11
Ray 12
50
0
-20
-10
0
10
20
T+ - T- (ms)

FIGURE P-6

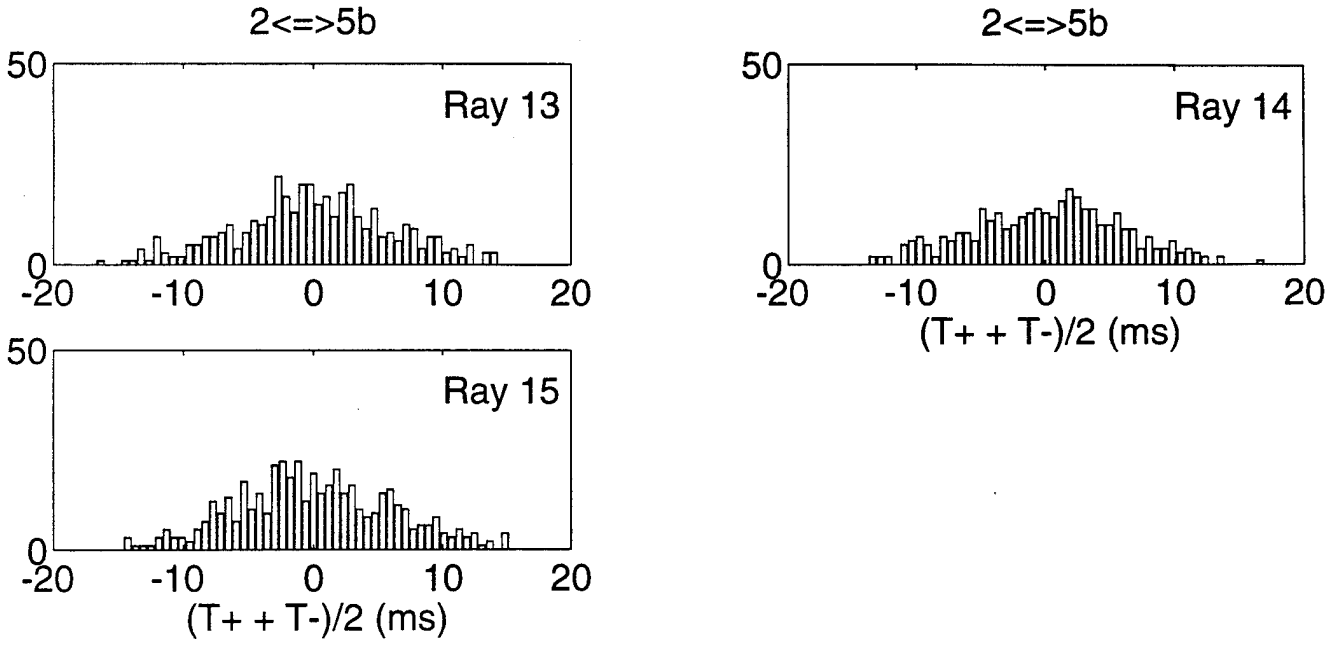

FIGURE P-5 (cont.)

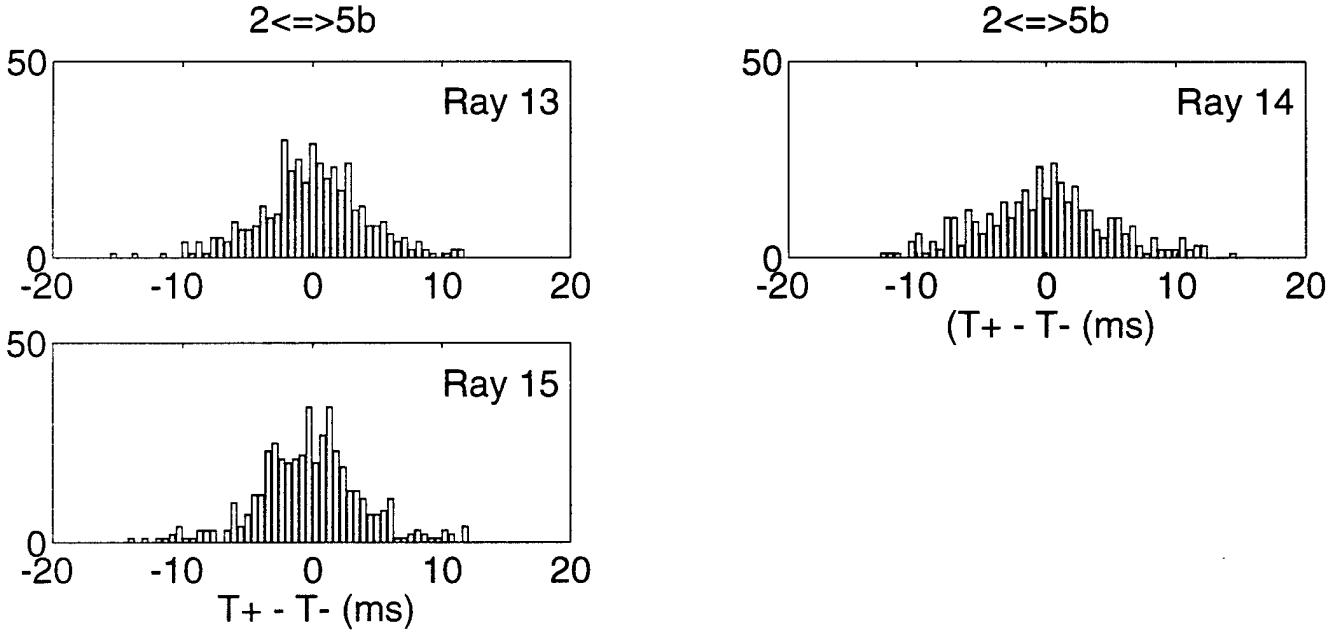

FIGURE P-6 (cont.)

Q. ACOUSTIC DATA: Paths 2→6 and 6→2

FIGURE Q-1 shows the raypaths, roughly corresponding to FIGURE G-1, for which travel times were resolved. The raypaths were actually determined using range-dependent Levitus sound speed, interpolated onto the acoustic path. Note that the "final cutoff" travel times may be available at some time in the future, these data correspond to a ray confined near the sound channel axis.

FIGURE Q-2 shows the low-pass filtered difference (top panel) and sum (bottom panel) travel times corresponding to the rays of FIGURE Q-1.

FIGURE Q-3 shows the high-pass filtered difference travel times for a small portion of the time series obtained during the time of more frequent transmissions during the MST experiment. The bottom panel shows the time series after the phase-locked tidal signals have been removed. FIGURE Q-4 shows the same time series, but during a time of the normal transmission schedule.

FIGURE Q-5 shows the high-pass filtered sum travel times for a small portion of the time series obtained during the time of more frequent transmissions during the MST experiment. The bottom panel shows the time series after the phase-locked tidal signals have been removed. This tidal variability is caused by the internal tide. FIGURE Q-6 shows the same time series, but during a time of the normal transmission schedule.

After the travel time time series have been edited for outliers, high-pass filtered, and detided, the high-frequency variances are calculated (TABLE Q-1). Note that this table sometimes contains statistics for more rays than are indicated in TABLE B-1; some of the ray arrivals in TABLE Q-1 have not been identified with predicted arrivals. Also, sometimes there is initial ambiguity about the pairing of reciprocal arrivals, in which case sum and difference travel times are calculated for all reasonable cases; later it becomes obvious which arrivals have been improperly paired. The correlation $<T^+ T^->$ and variance $<T^2>$ are calculated from the sum and difference travel time variances in this table. The variance of the travel times is mainly due to internal wave variability, and this value determines the uncertainties assigned to the travel times in an inversion. The correlation coefficient is a measure of the reciprocity of reciprocal raypaths. This measure is conservative, because correlation is not a necessary condition for the determination of current from the difference of reciprocal travel times. Values of correlation that are 0.5 or greater assure that the reciprocal raypaths are indeed effectively identical, since good correlation implies that the reciprocal raypaths have not separated by more than an internal wave correlation length. Histograms of the detided, high-frequency travel times are shown in FIGURES Q-7 and Q-8; the variances from TABLE Q-1 are measures of the width of these histograms.

TABLES Q-2 and Q-3 show the results of tidal analysis of the time series of difference (current) and sum (sound speed) travel times. For these tables, the tidal analysis is performed on each travel time time series separately and then the average and rms of the harmonic constants are calculated. Current or sound speed amplitude is determined from travel time by a simple scaling factor; the harmonic constants are more accurately determined by inverting the data for current or sound speed (this is not done here).

TABLE Q-1. Travel Time Statistics 2←→6.

Ray #	Number of data	$\langle (T^+ + T^-)^2 \rangle$ (ms^2)	$\langle (T^+ - T^-)^2 \rangle$ (ms^2)	$\langle T^+ T^- \rangle$ (ms^2)	$\langle T^2 \rangle$ (ms^2)	$\frac{\langle T^+ T^- \rangle}{\langle T^2 \rangle}$
1	629	23	9	21	26	0.82
2	655	17	6	16	18	0.85
3	705	19	10	17	22	0.77
4	727	22	8	20	24	0.83
5	795	21	3	20	21	0.93
6	803	20	3	20	21	0.93
7	734	23	9	21	25	0.83
8	727	24	8	22	26	0.85
9	784	23	3	22	24	0.93

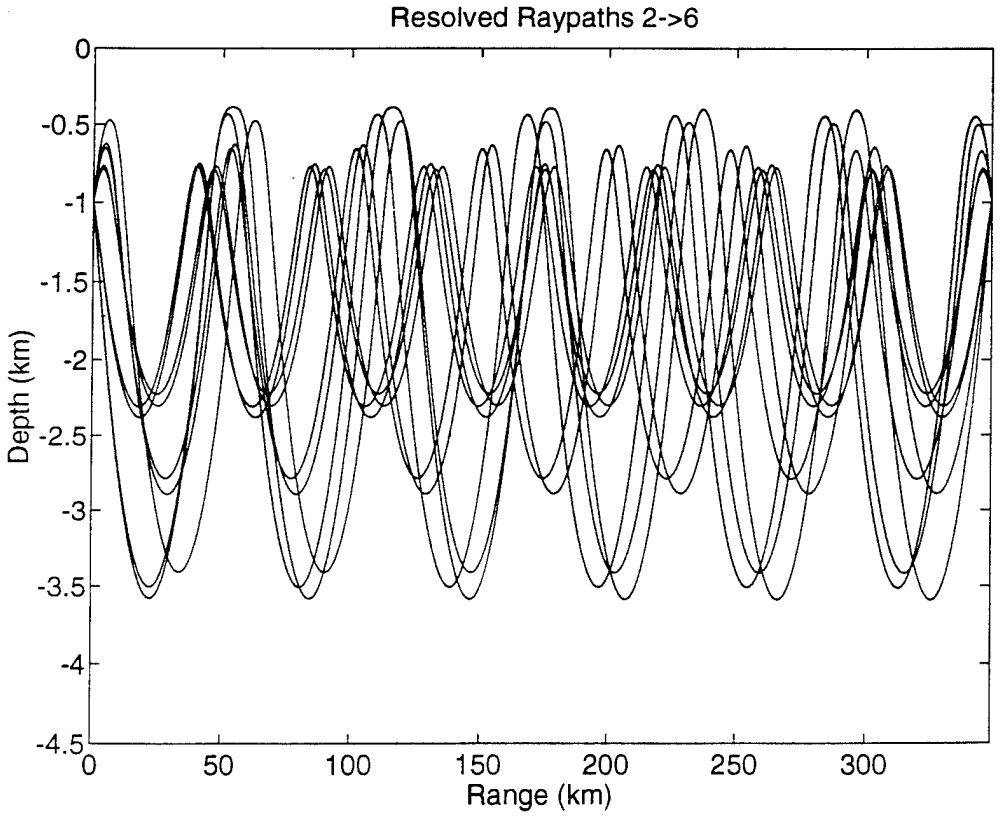

FIGURE Q-1

TABLE Q-2. Tidal Current Harmonic Constants 2←→6.

Constituent	Amplitude (mm/s)	Uncertainty (mm/s)	Phase (°G)	Uncertainty (°)
M_2	12.72	0.53	283.6	4.0
S_2	2.78	0.31	297.1	8.6
N_2	2.99	0.51	266.7	11.9
K_2	0.86	0.55	318.4	72.4
O_1	0.78	0.40	46.0	35.4
K_1	0.99	0.47	131.1	35.5
P_1	1.02	0.49	108.6	52.7
Q_1	0.62	0.19	173.4	136.8

Values and their uncertainty are determined by the average and rms of harmonic constants from tidal analyses of the separate raypath travel time series. The amplitudes do not include the lunar node factors. 62 ± 12 % of the high-frequency variance is accounted for by the tides.

TABLE Q-3. Tidal Sound Speed Harmonic Constants 2←→6.

Constituent	Amplitude (mm/s)	Uncertainty (mm/s)	Phase (°G)	Uncertainty (°)
M_2	7.29	0.91	275.2	19.1
S_2	2.52	0.50	20.0	20.4
N_2	3.17	0.70	206.4	18.4
K_2	1.17	0.63	350.5	36.0
O_1	4.50	1.24	150.3	9.3
K_1	9.56	0.79	265.3	5.1
P_1	2.62	0.51	259.8	13.
Q_1	1.18	0.71	221.9	58.1

Values and their uncertainty are determined by the average and rms of harmonic constants from tidal analyses of the separate raypath travel time series. The amplitudes do not include the lunar node factors. 34 ± 3 % of the high-frequency variance is accounted for by the tides. Because sum travel times are used to derive these numbers, the amplitudes have been divided by a factor of two compared to the amplitudes for current.

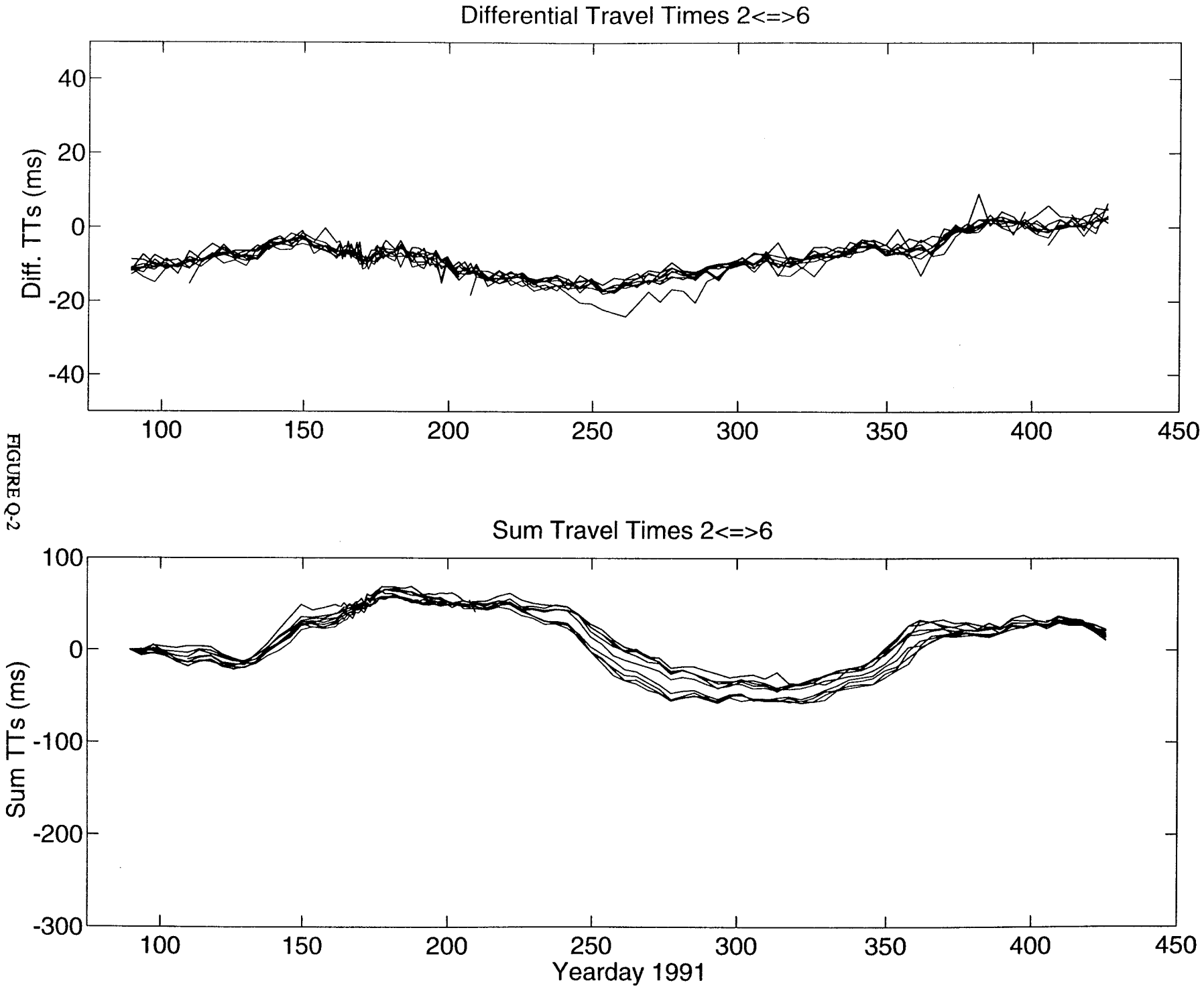
Differential Travel Times 2<=>6
Diff. TTs (ms)
40
20
0
-20
-40
100
150
200
250
300
350
400
450
Sum Travel Times 2<=>6
Sum TTs (ms)
100
0
-100
-200
-300
100
150
200
250
300
350
400
450
Yearday 1991

FIGURE Q-2

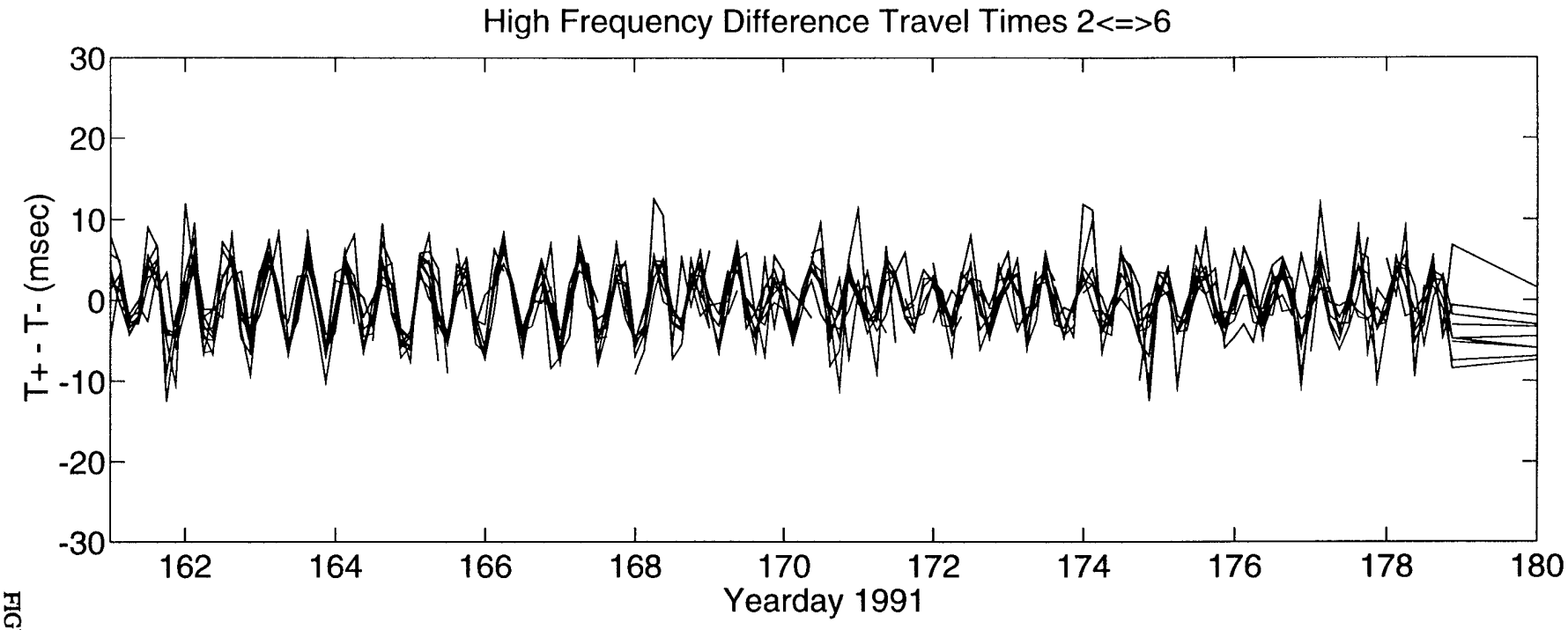
High Frequency Difference Travel Times 2<=>6
T+ - T- (msec)
30
20
10
0
-10
-20
-30
162
164
166
168
170
172
174
176
178
180
Yearday 1991

FIGURE Q-3

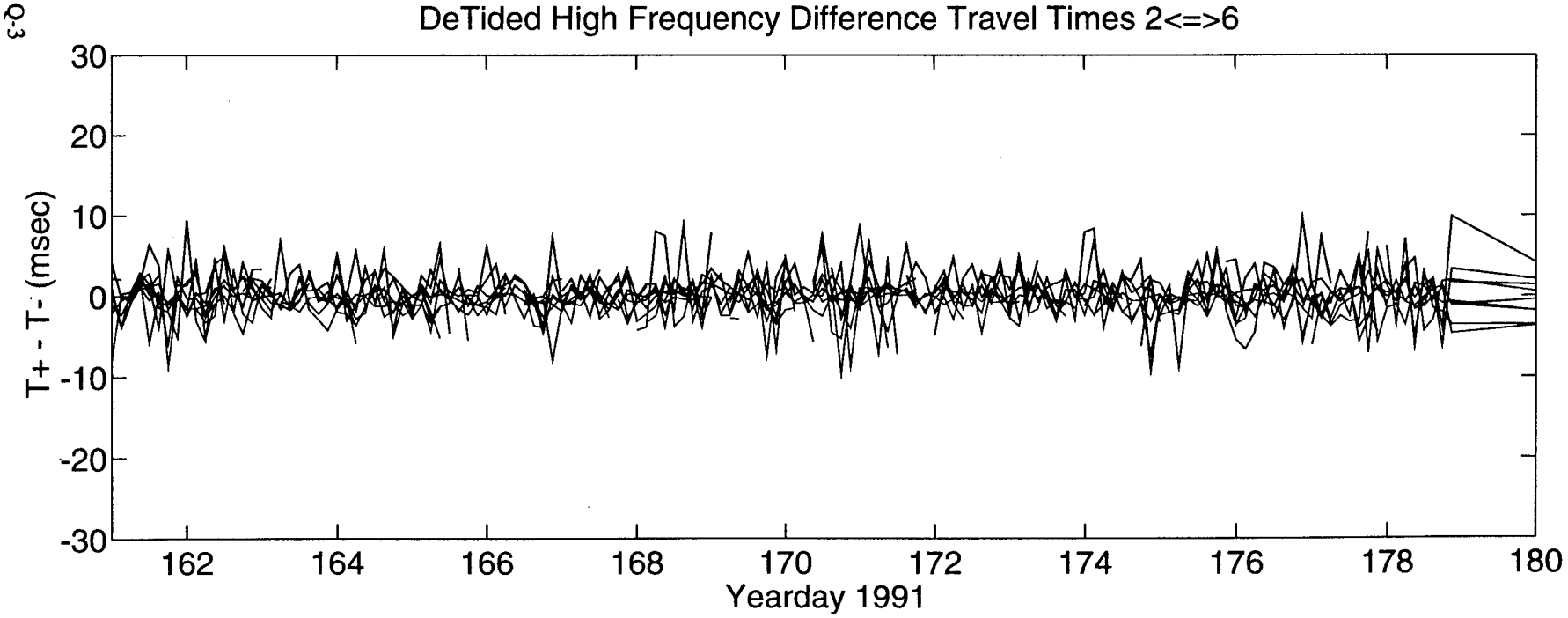
DeTided High Frequency Difference Travel Times 2<=>6
T+ - T- (msec)
30
20
10
0
-10
-20
-30
162
164
166
168
170
172
174
176
178
180
Yearday 1991

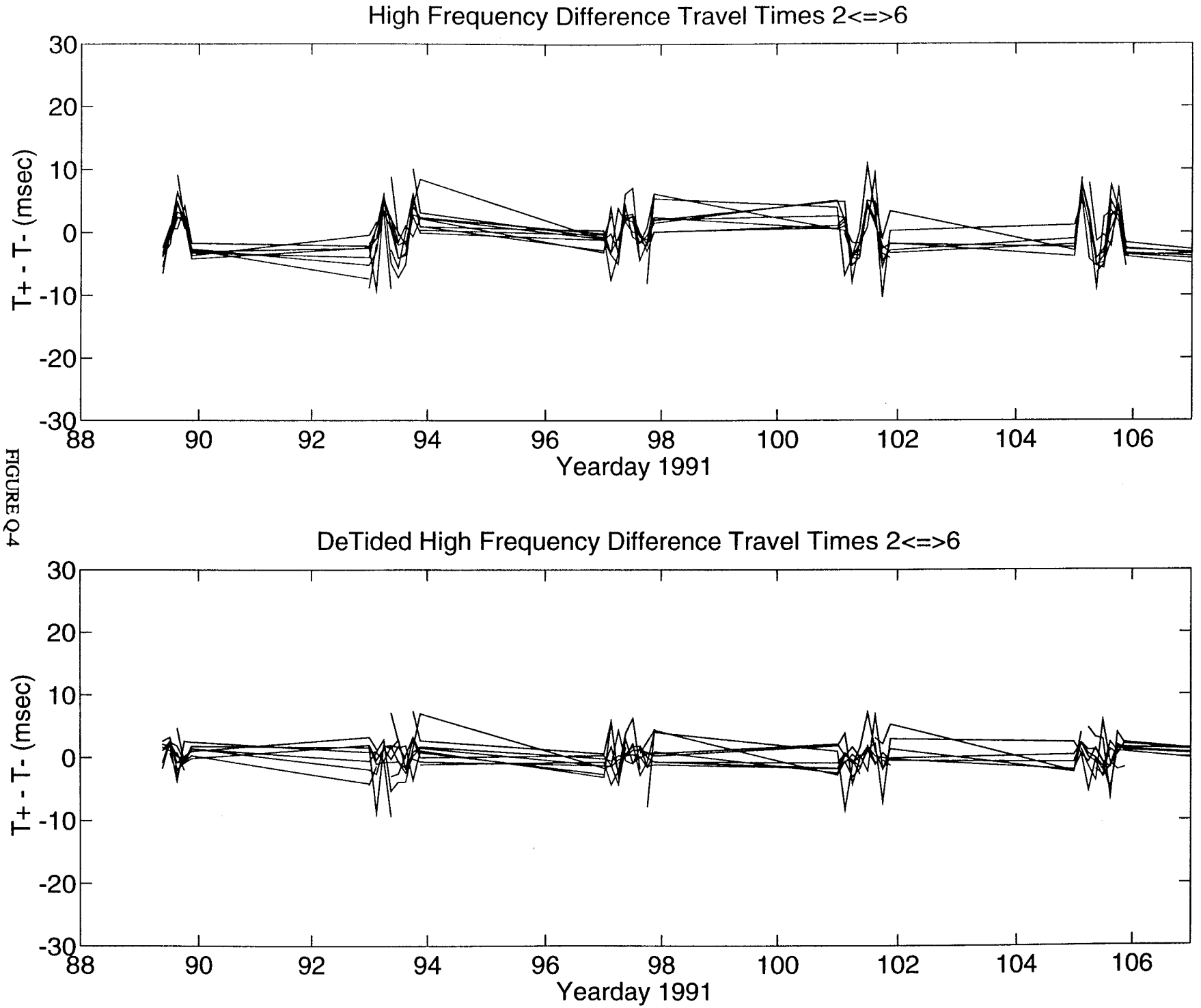
High Frequency Difference Travel Times 2<=>6
T+ - T- (msec)
30
20
10
0
-10
-20
-30
88
90
92
94
96
98
100
102
104
106
Yearday 1991
DeTided High Frequency Difference Travel Times 2<=>6
T+ - T- (msec)
30
20
10
0
-10
-20
-30
88
90
92
94
96
98
100
102
104
106
Yearday 1991

FIGURE Q-4

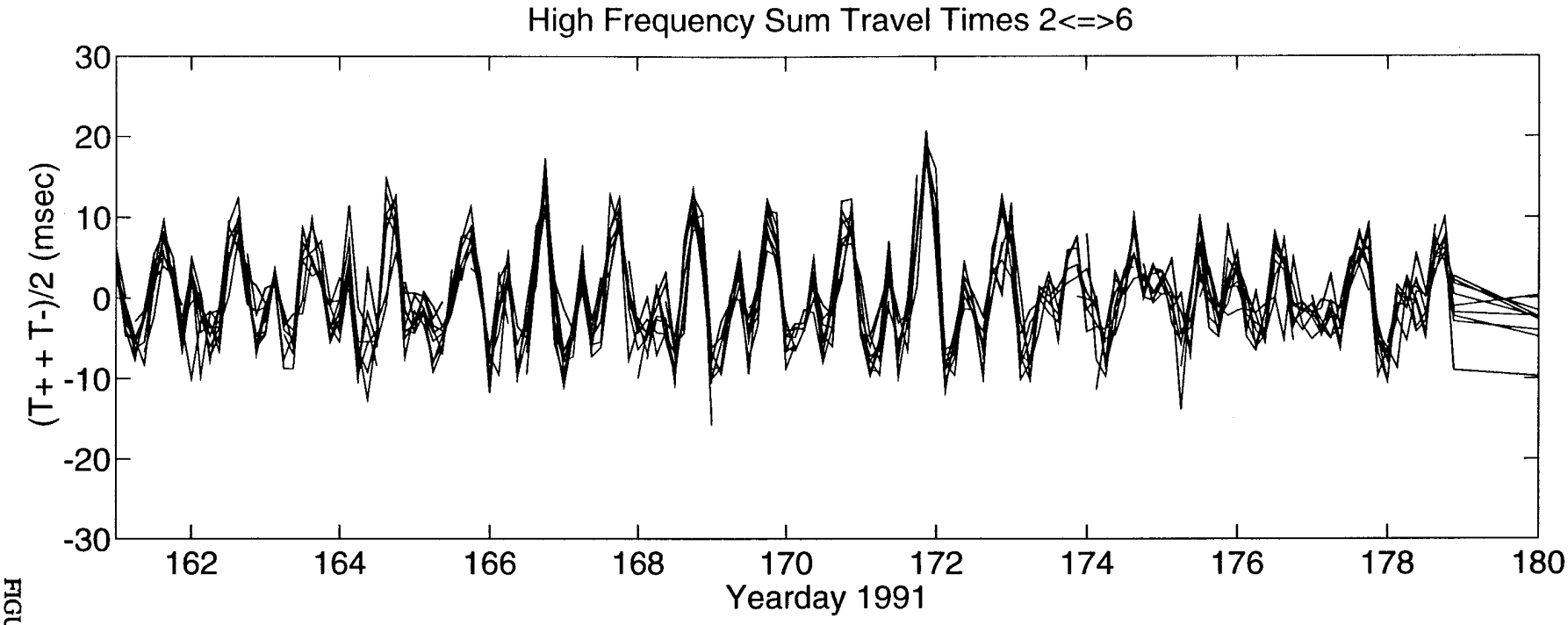
High Frequency Sum Travel Times 2<=>6
(T+ + T-)/2 (msec)
30
20
10
0
-10
-20
-30
162
164
166
168
170
172
174
176
178
180
Yearday 1991

FIGURE Q-5

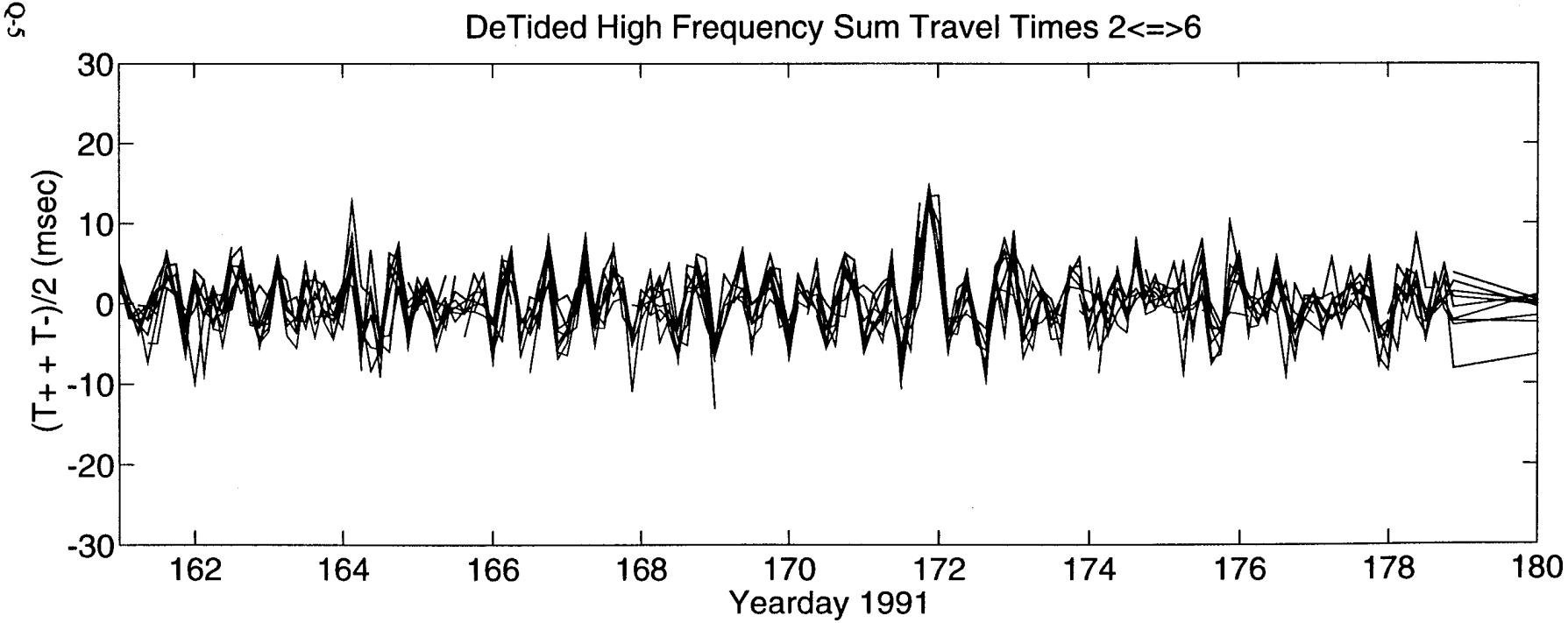
DeTided High Frequency Sum Travel Times 2<=>6
(T+ + T-)/2 (msec)
30
20
10
0
-10
-20
-30
162
164
166
168
170
172
174
176
178
180
Yearday 1991

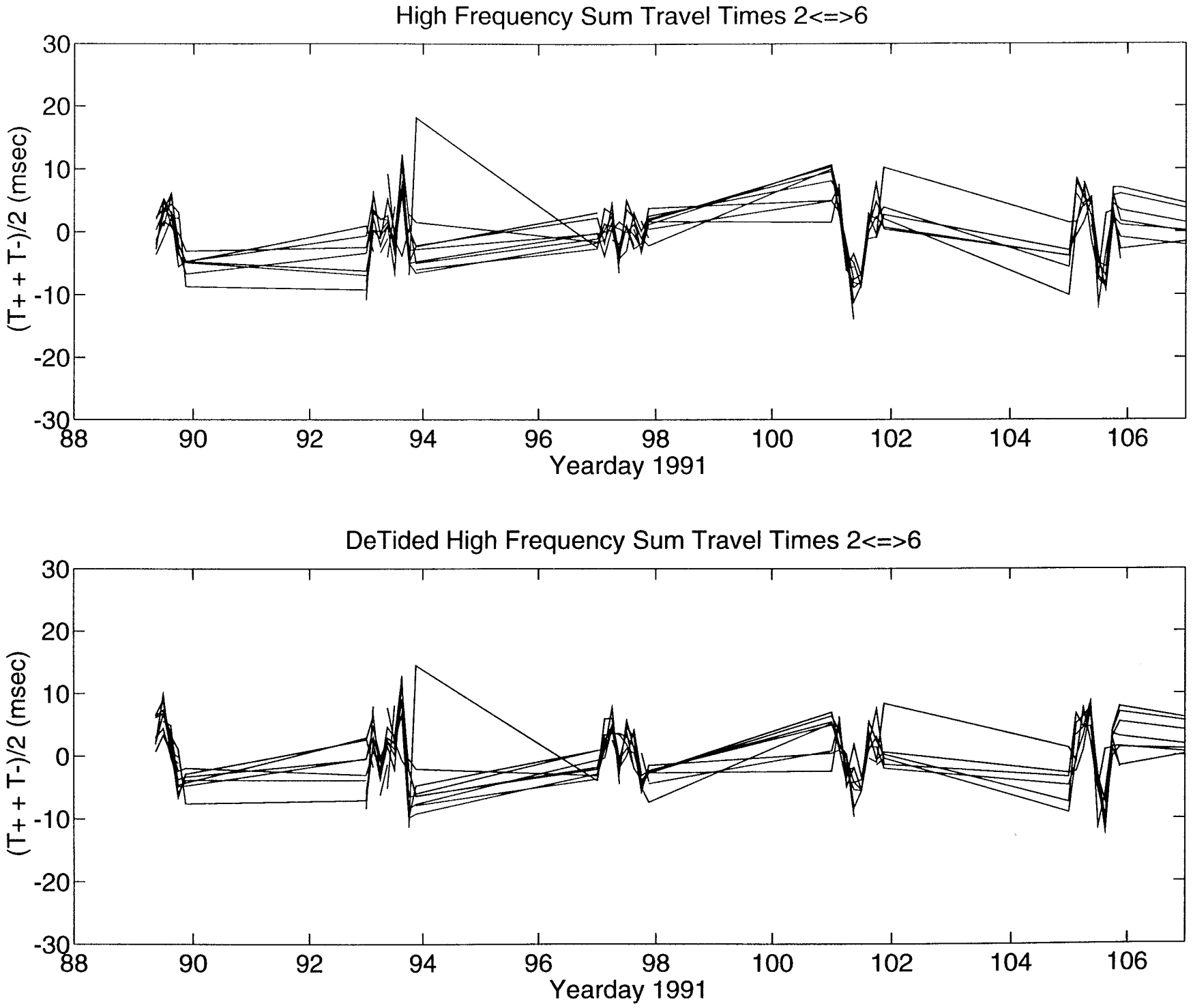
High Frequency Sum Travel Times 2<=>6
(T+ + T-)/2 (msec)
Yearday 1991
DeTided High Frequency Sum Travel Times 2<=>6
(T+ + T-)/2 (msec)
Yearday 1991

FIGURE Q-6

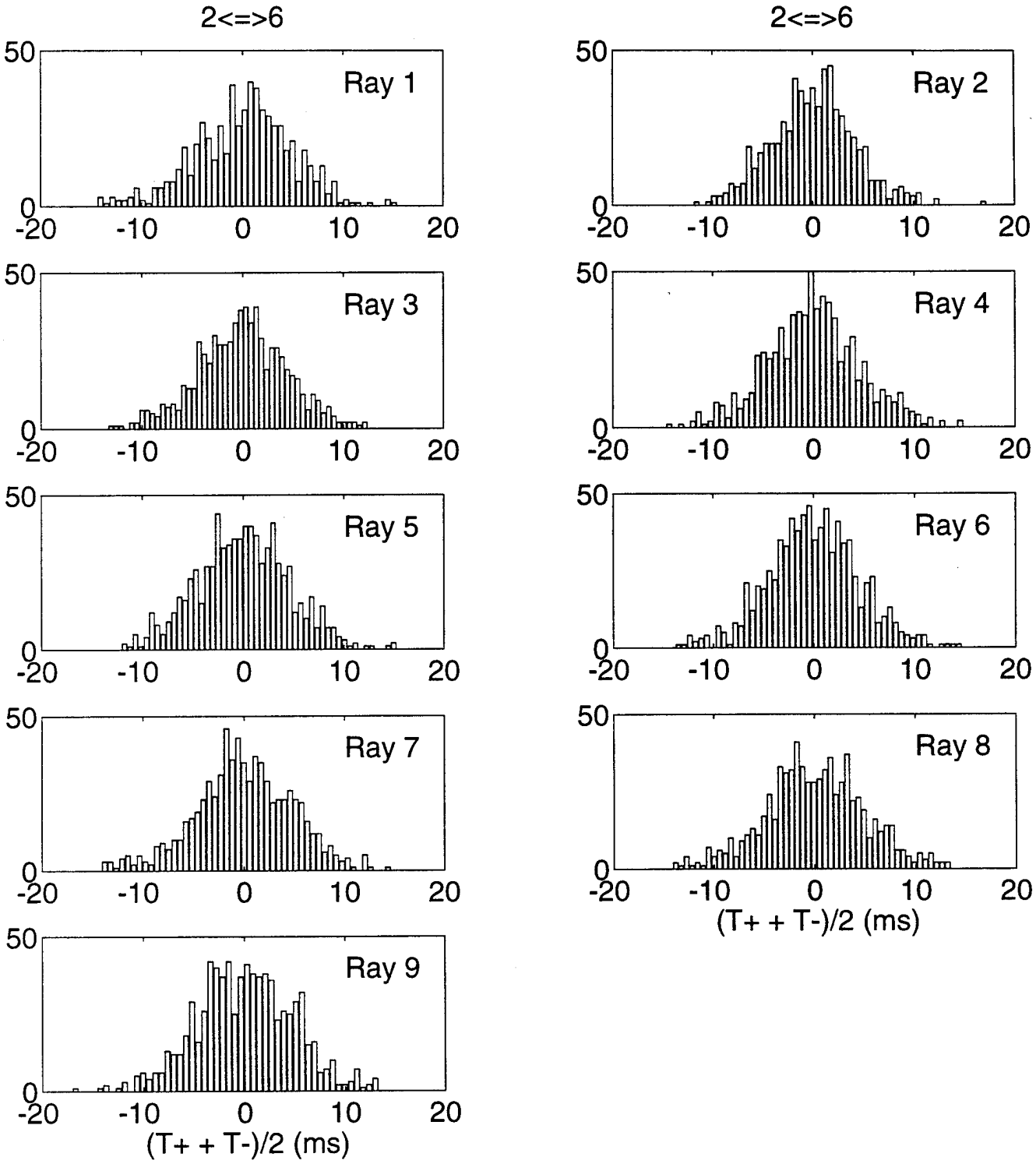
2<=>6
Ray 1
Ray 2
Ray 3
Ray 4
Ray 5
Ray 6
Ray 7
Ray 8
Ray 9
50
0
-20
-10
0
10
20
(T+ + T-)/2 (ms)

FIGURE Q-7

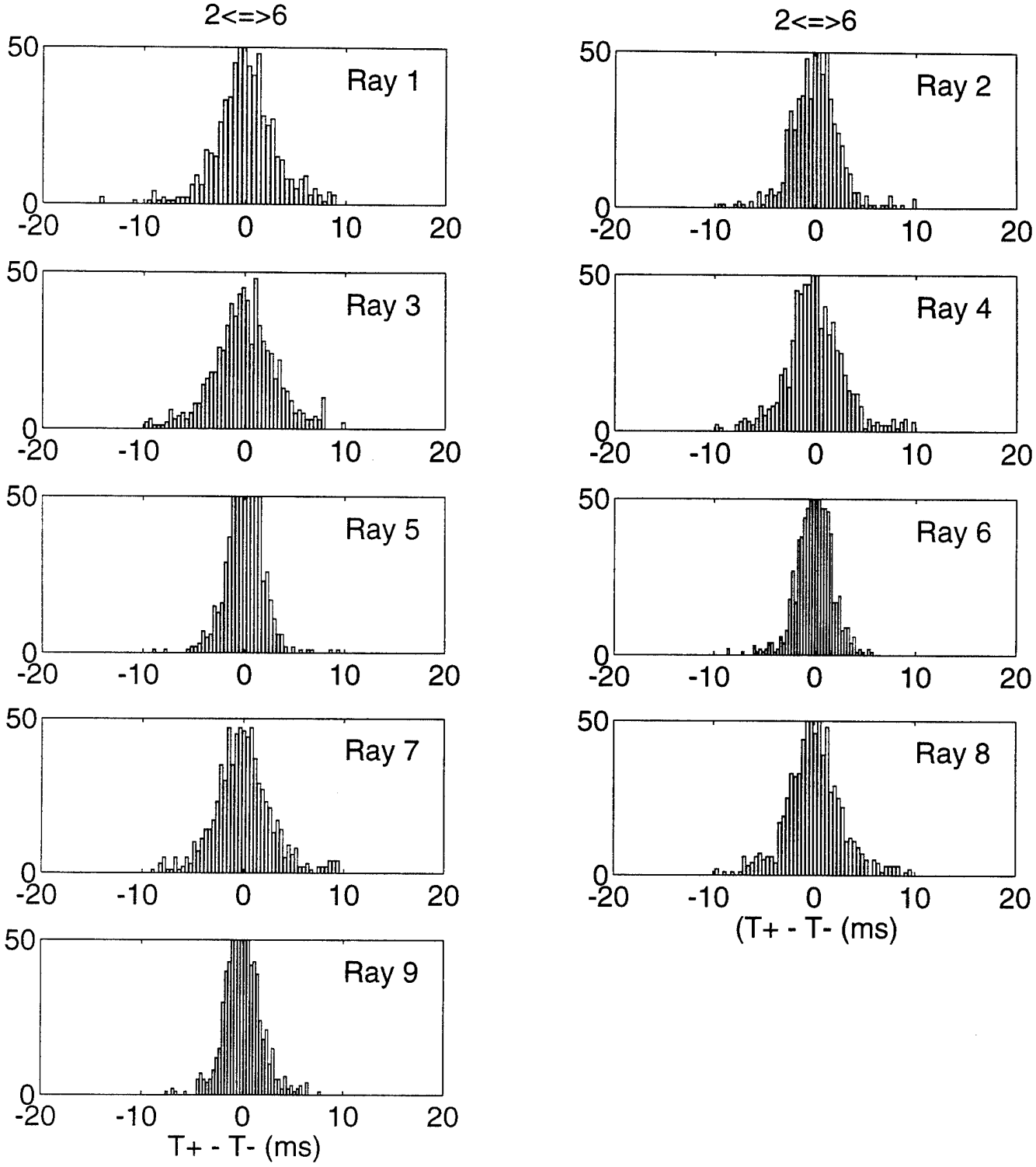
2<=>6
Ray 1
Ray 2
Ray 3
Ray 4
Ray 5
Ray 6
Ray 7
Ray 8
Ray 9
50
0
-20
-10
0
10
20
T+ - T- (ms)
(T+ - T- (ms)

FIGURE Q-8

R. *ACOUSTIC DATA: Paths 3→4 and 4→3*

FIGURE R-1 shows the raypaths, roughly corresponding to FIGURE G-1, for which travel times were resolved. The raypaths were actually determined using range-dependent Levitus sound speed, interpolated onto the acoustic path. Note that the "final cutoff" travel times may be available at some time in the future, these data correspond to a ray confined near the sound channel axis.

FIGURE R-2 shows the low-pass filtered difference (top panel) and sum (bottom panel) travel times corresponding to the rays of FIGURE R-1.

FIGURE R-3 shows the high-pass filtered difference travel times for a small portion of the time series obtained during the time of more frequent transmissions during the MST experiment. The bottom panel shows the time series after the phase-locked tidal signals have been removed. FIGURE R-4 shows the same time series, but during a time of the normal transmission schedule.

FIGURE R-5 shows the high-pass filtered sum travel times for a small portion of the time series obtained during the time of more frequent transmissions during the MST experiment. The bottom panel shows the time series after the phase-locked tidal signals have been removed. This tidal variability is caused by the internal tide. FIGURE R-6 shows the same time series, but during a time of the normal transmission schedule.

After the travel time time series have been edited for outliers, high-pass filtered, and detided, the high-frequency variances are calculated (TABLE R-1). Note that this table sometimes contains statistics for more rays than are indicated in TABLE B-1; some of the ray arrivals in TABLE R-1 have not been identified with predicted arrivals. Also, sometimes there is initial ambiguity about the pairing of reciprocal arrivals, in which case sum and difference travel times are calculated for all reasonable cases; later it becomes obvious which arrivals have been improperly paired. The correlation $<T^+ T^->$ and variance $<T^2>$ are calculated from the sum and difference travel time variances in this table. The variance of the travel times is mainly due to internal wave variability, and this value determines the uncertainties assigned to the travel times in an inversion. The correlation coefficient is a measure of the reciprocity of reciprocal raypaths. This measure is conservative, because correlation is not a necessary condition for the determination of current from the difference of reciprocal travel times. Values of correlation that are 0.5 or greater assure that the reciprocal raypaths are indeed effectively identical, since good correlation implies that the reciprocal raypaths have not separated by more than an internal wave correlation length. Histograms of the detided, high-frequency travel times are shown in FIGURES R-7 and R-8; the variances from TABLE R-1 are measures of the width of these histograms.

TABLES R-2 and R-3 show the results of tidal analysis of the time series of difference (current) and sum (sound speed) travel times. For these tables, the tidal analysis is performed on each travel time time series separately and then the average and rms of the harmonic constants are calculated. Current or sound speed amplitude is determined from travel time by a simple scaling factor; the harmonic constants are more accurately determined by inverting the data for current or sound speed (this is not done here).

TABLE R-1. Travel Time Statistics 3←→4.

Ray #	Number of data	$\langle (T^+ + T^-)^2 \rangle$ (ms^2)	$\langle (T^+ - T^-)^2 \rangle$ (ms^2)	$\langle T^+ T^- \rangle$ (ms^2)	$\langle T^2 \rangle$ (ms^2)	$\frac{\langle T^+ T^- \rangle}{\langle T^2 \rangle}$
1	325	12	5	11	13	0.83
2	346	17	10	15	20	0.75
3	362	19	12	16	22	0.73
4	383	18	9	16	20	0.78
5	405	18	5	17	19	0.87
6	423	15	4	14	16	0.87
7	399	22	8	20	24	0.84
8	407	18	8	16	20	0.81
9	407	20	7	18	21	0.84

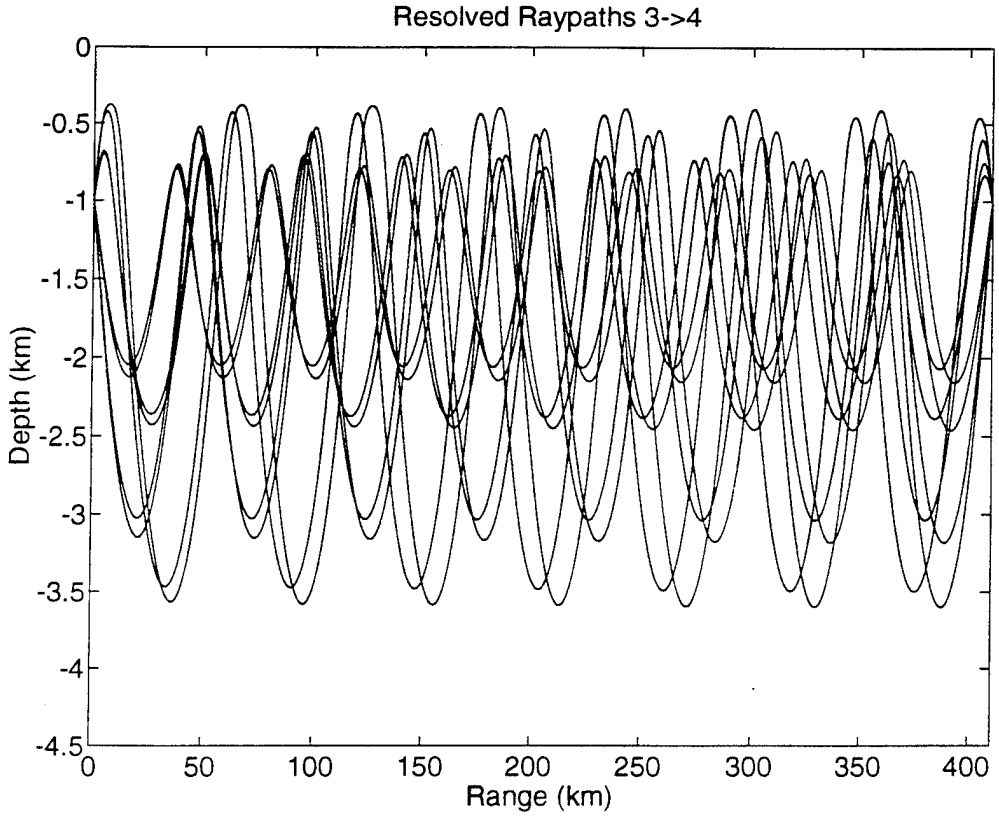

FIGURE R-1

TABLE R-2. Tidal Current Harmonic Constants 3←→4.

Constituent	Amplitude (mm/s)	Uncertainty (mm/s)	Phase (°G)	Uncertainty (°)
M_2	12.18	0.54	284.4	2.4
S_2	2.42	0.84	322.9	18.1
N_2	3.04	0.53	270.2	10.9
K_2	1.16	0.43	326.0	35.5
O_1	1.19	0.59	56.1	67.9
K_1	1.42	0.56	95.0	34.2
P_1	1.06	0.53	93.6	90.5
Q_1	0.94	0.46	267.1	90.3

Values and their uncertainty are determined by the average and rms of harmonic constants from tidal analyses of the separate raypath travel time series. The amplitudes do not include the lunar node factors. 63 ± 10 % of the high-frequency variance is accounted for by the tides.

TABLE R-3. Tidal Sound Speed Harmonic Constants 3←→4.

Constituent	Amplitude (mm/s)	Uncertainty (mm/s)	Phase (°G)	Uncertainty (°)
M_2	10.21	1.64	235.4	6.5
S_2	2.34	0.62	339.6	20.9
N_2	2.26	0.77	176.2	28.3
K_2	1.43	0.75	272.4	44.9
O_1	2.00	0.89	338.9	33.8
K_1	4.69	0.85	107.3	10.7
P_1	1.32	0.68	83.4	52.8
Q_1	3.09	0.66	19.2	15.2

Values and their uncertainty are determined by the average and rms of harmonic constants from tidal analyses of the separate raypath travel time series. The amplitudes do not include the lunar node factors. 38 ± 7 % of the high-frequency variance is accounted for by the tides. Because sum travel times are used to derive these numbers, the amplitudes have been divided by a factor of two compared to the amplitudes for current.

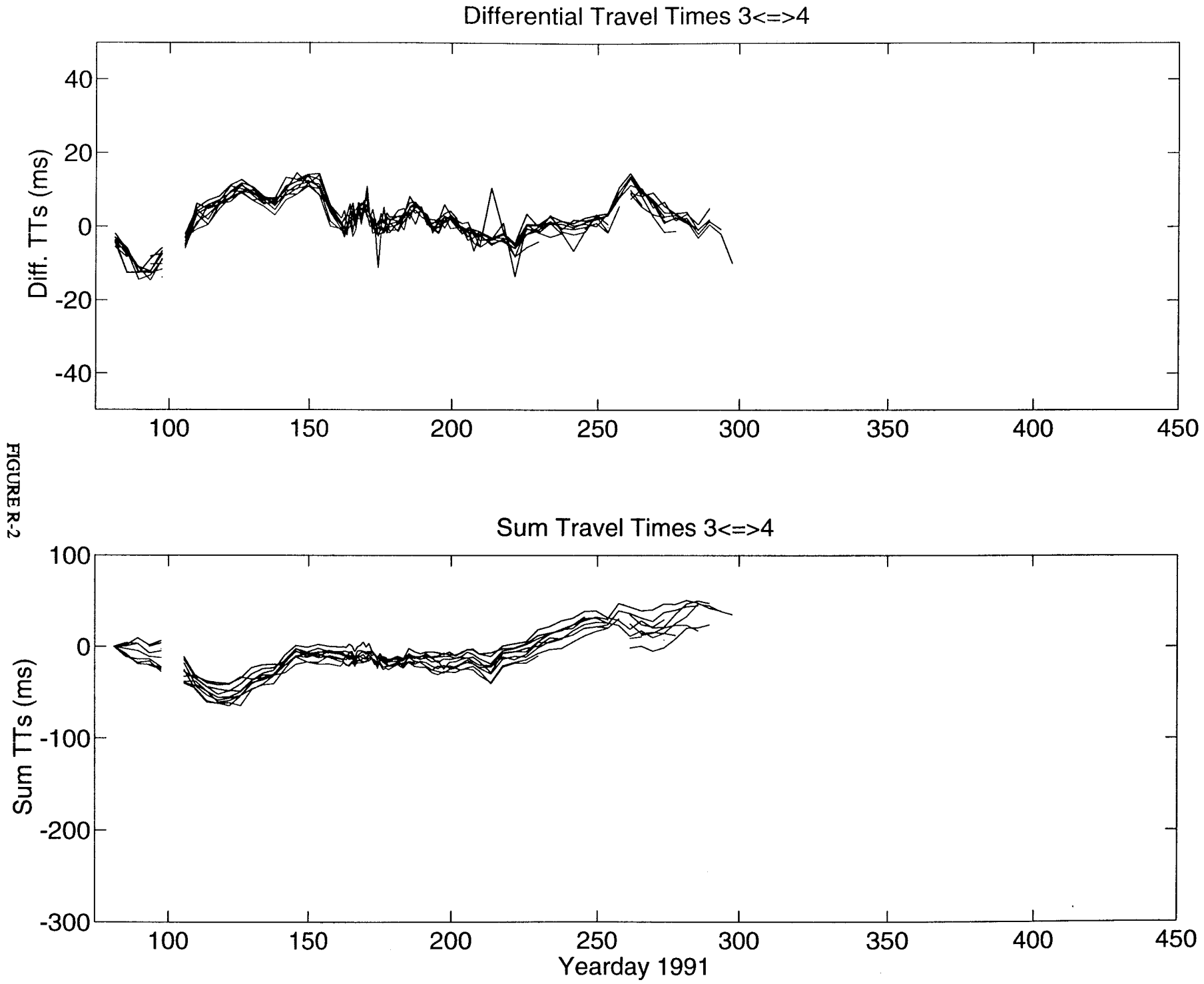
Differential Travel Times 3<=>4
Diff. TTs (ms)
40
20
0
-20
-40
100
150
200
250
300
350
400
450
Sum Travel Times 3<=>4
Sum TTs (ms)
100
0
-100
-200
-300
100
150
200
250
300
350
400
450
Yearday 1991

FIGURE R-2

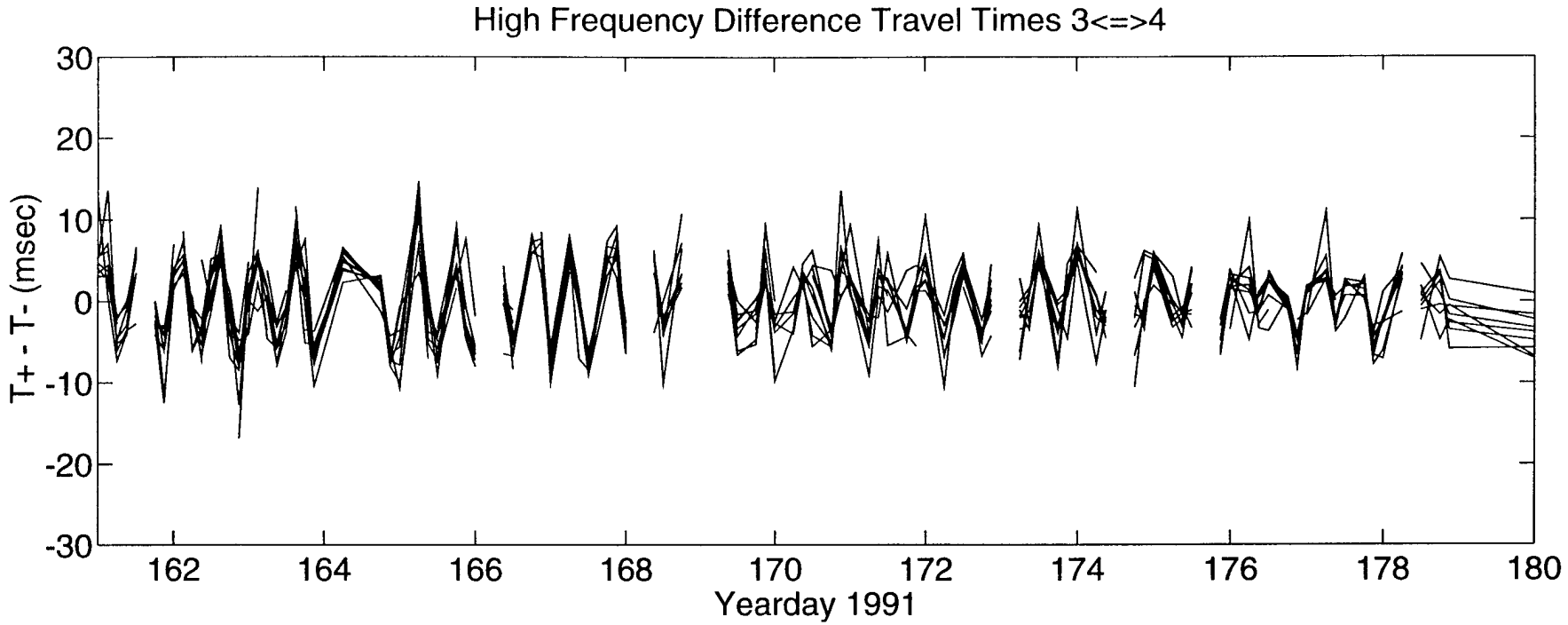
High Frequency Difference Travel Times 3<=>4
T+ - T- (msec)
30
20
10
0
-10
-20
-30
162
164
166
168
170
172
174
176
178
180
Yearday 1991

FIGURE R-3

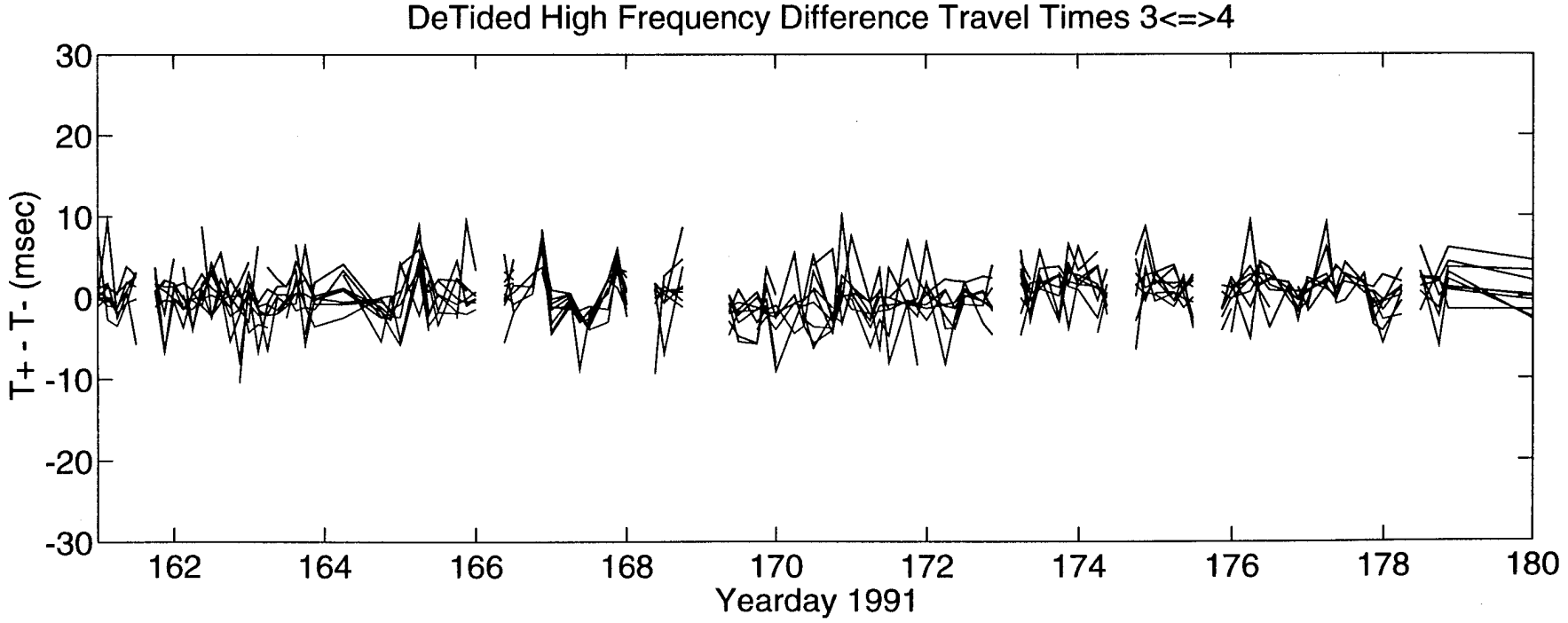
DeTided High Frequency Difference Travel Times 3<=>4
T+ - T- (msec)
30
20
10
0
-10
-20
-30
162
164
166
168
170
172
174
176
178
180
Yearday 1991

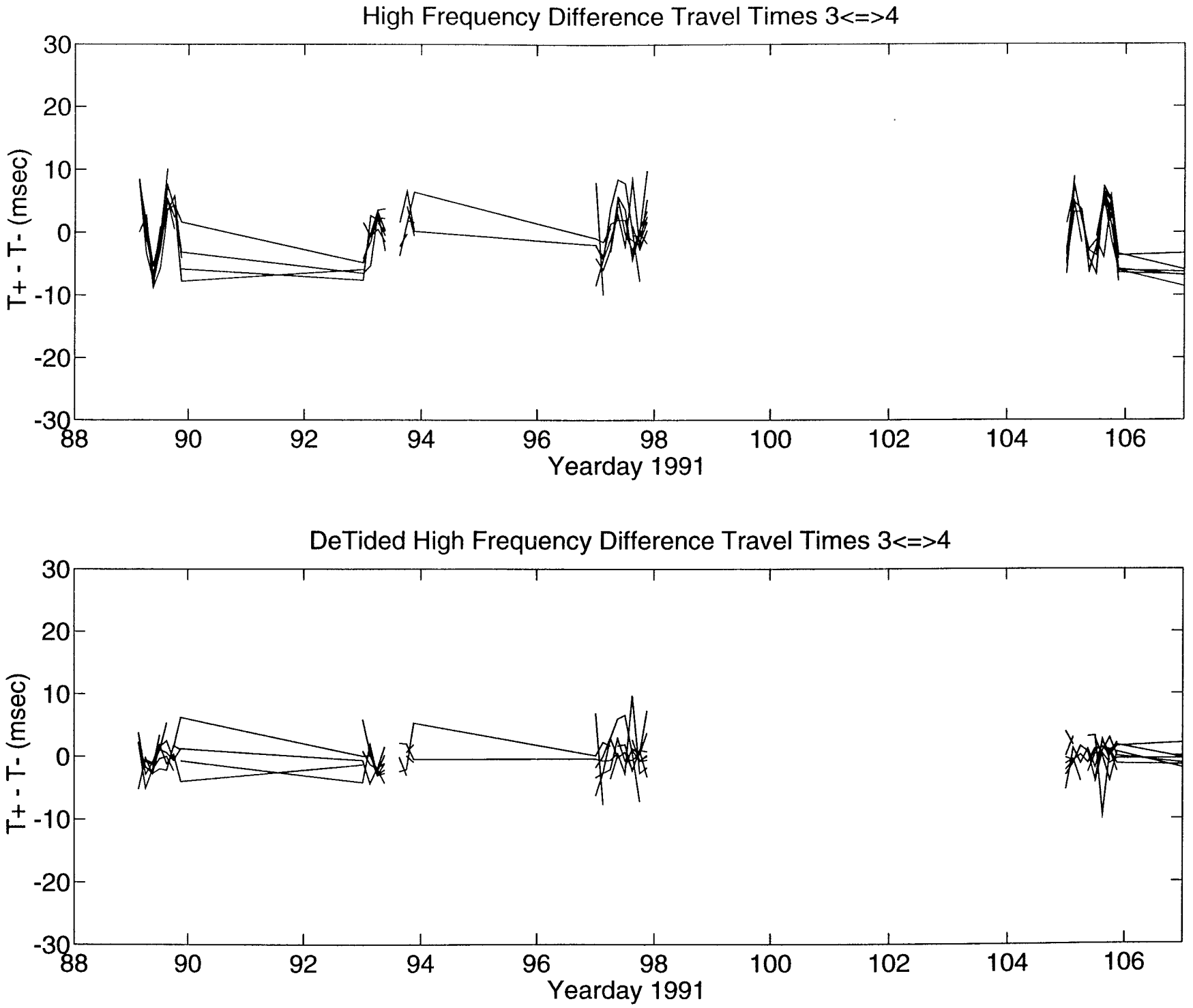
High Frequency Difference Travel Times 3<=>4
T+ - T- (msec)
Yearday 1991
DeTided High Frequency Difference Travel Times 3<=>4
T+ - T- (msec)
Yearday 1991

FIGURE R-4

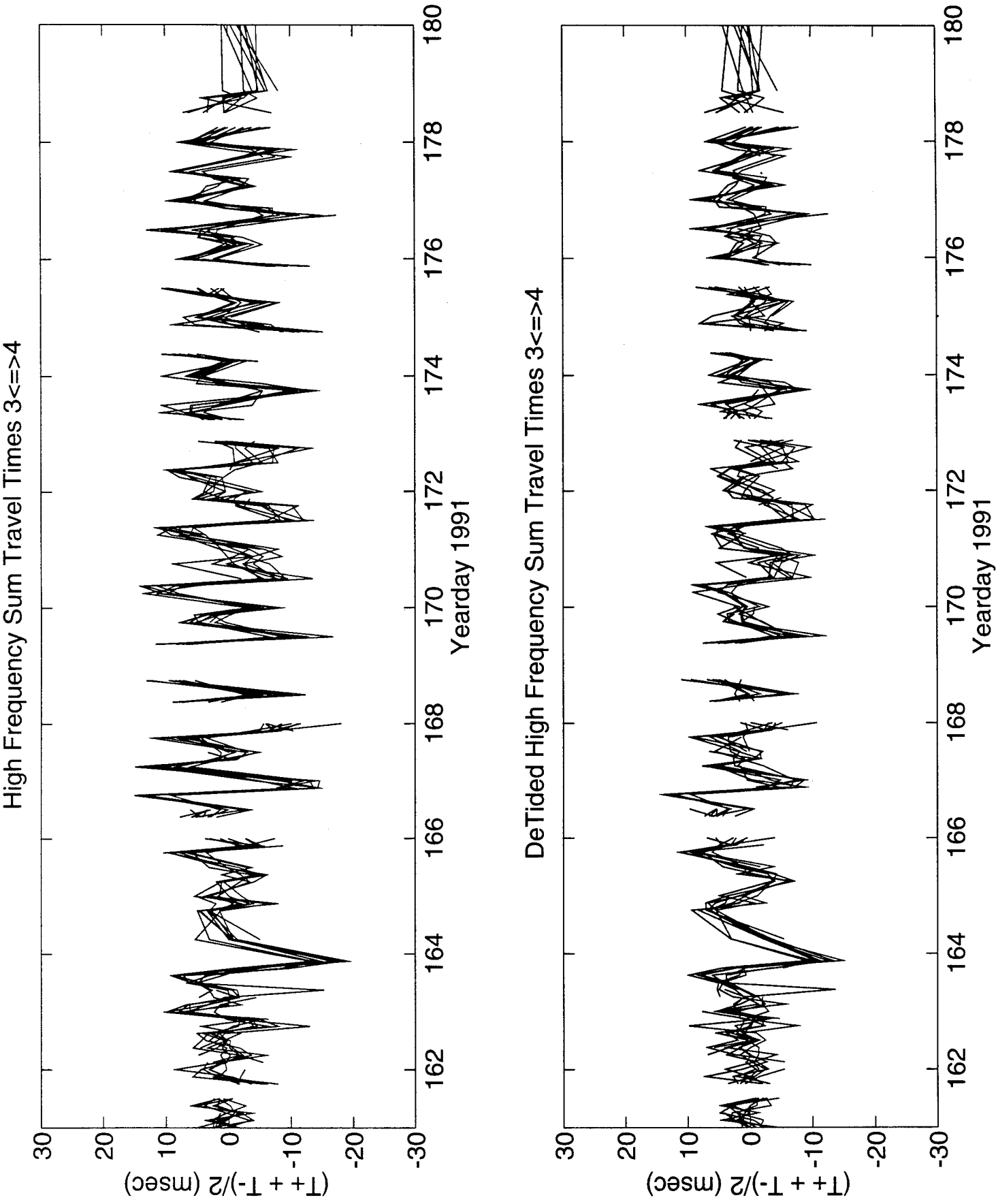
High Frequency Sum Travel Times 3<=>4
DeTided High Frequency Sum Travel Times 3<=>4
(T+ + T-)/2 (msec)
Yearday 1991
30
20
10
0
-10
-20
-30
162
164
166
168
170
172
174
176
178
180

FIGURE R-5

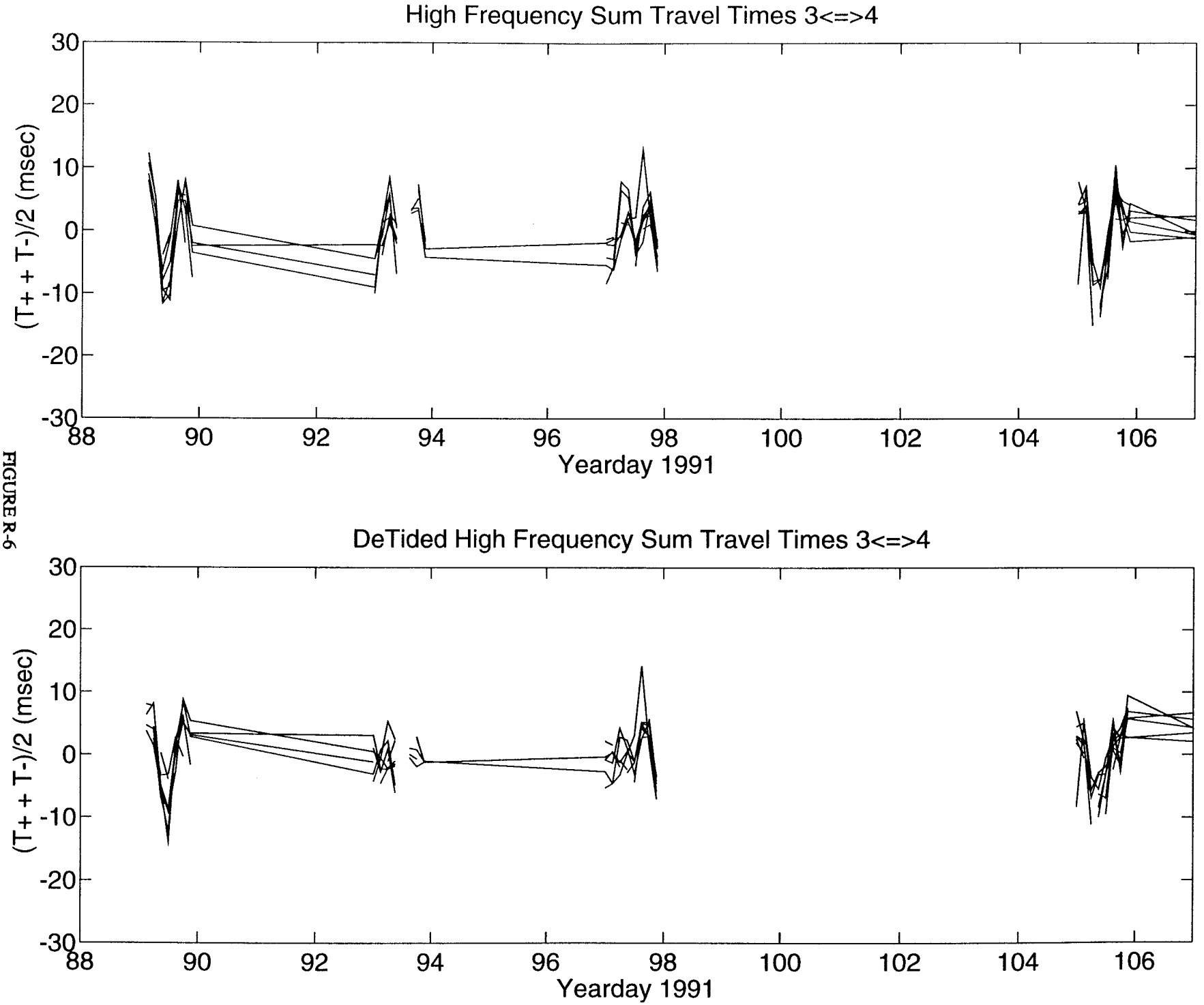
High Frequency Sum Travel Times 3<=>4
(T+ + T-)/2 (msec)
30
20
10
0
-10
-20
-30
88
90
92
94
96
98
100
102
104
106
Yearday 1991
DeTided High Frequency Sum Travel Times 3<=>4
(T+ + T-)/2 (msec)
30
20
10
0
-10
-20
-30
88
90
92
94
96
98
100
102
104
106
Yearday 1991

FIGURE R-6

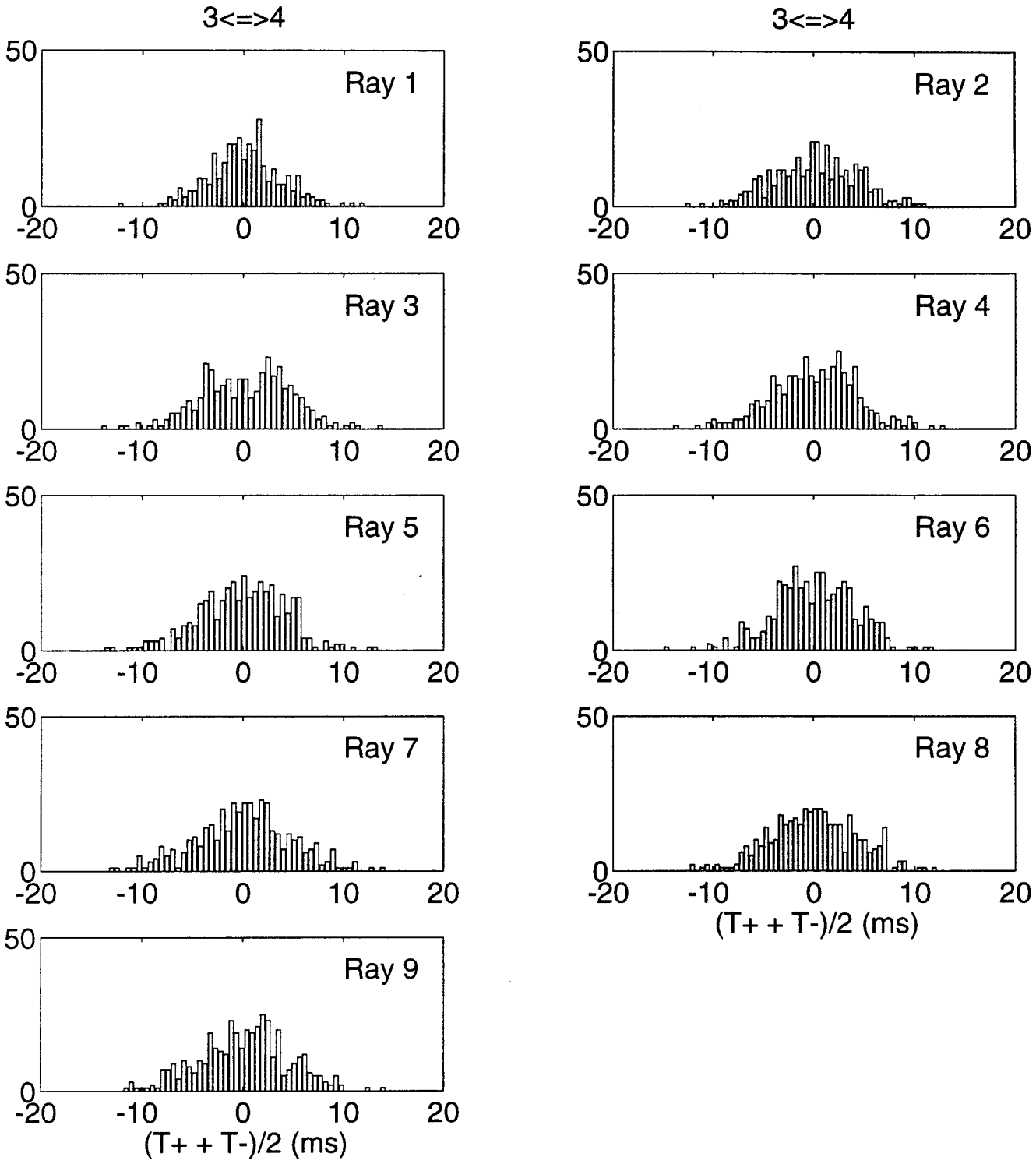
3<=>4
Ray 1
Ray 2
Ray 3
Ray 4
Ray 5
Ray 6
Ray 7
Ray 8
Ray 9
50
0
-20
-10
0
10
20
(T+ + T-)/2 (ms)

FIGURE R-7

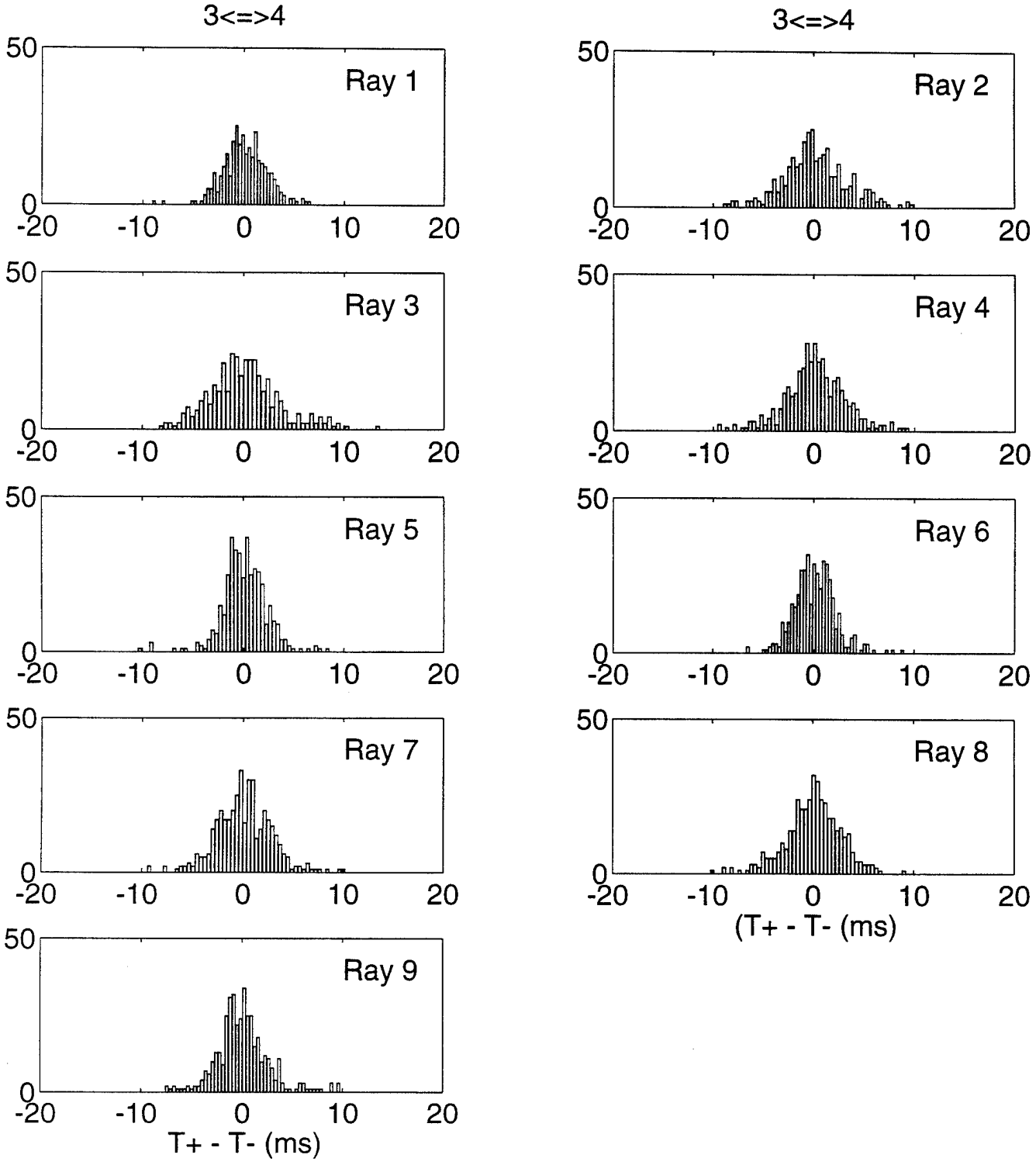
3<=>4
Ray 1
Ray 2
Ray 3
Ray 4
Ray 5
Ray 6
Ray 7
Ray 8
Ray 9
50
0
-20
-10
0
10
20
T+ - T- (ms)

FIGURE R-8

S. *ACOUSTIC DATA: Paths 3→5a and 5a→3*

FIGURE S-1 shows the raypaths, roughly corresponding to FIGURE G-1, for which travel times were resolved. The raypaths were actually determined using range-dependent Levitus sound speed, interpolated onto the acoustic path. Note that the "final cutoff" travel times may be available at some time in the future, these data correspond to a ray confined near the sound channel axis.

FIGURE S-2 shows the low-pass filtered difference (top panel) and sum (bottom panel) travel times corresponding to the rays of FIGURE S-1. Note that mooring 5a had failed by yearday 140, to be replaced later by mooring 5b.

FIGURE S-3 shows the high-pass filtered difference travel times for a small portion of the time series obtained during the time of more frequent transmissions during the MST experiment. The bottom panel shows the time series after the phase-locked tidal signals have been removed.

FIGURE S-4 shows the high-pass filtered sum travel times for a small portion of the time series obtained during the time of more frequent transmissions during the MST experiment. The bottom panel shows the time series after the phase-locked tidal signals have been removed. This tidal variability is caused by the internal tide.

After the travel time time series have been edited for outliers, high-pass filtered, and detided, the high-frequency variances are calculated (TABLE S-1). Note that this table sometimes contains statistics for more rays than are indicated in TABLE B-1; some of the ray arrivals in TABLE S-1 have not been identified with predicted arrivals. Also, sometimes there is initial ambiguity about the pairing of reciprocal arrivals, in which case sum and difference travel times are calculated for all reasonable cases; later it becomes obvious which arrivals have been improperly paired. The correlation $<T^+ T^->$ and variance $<T^2>$ are calculated from the sum and difference travel time variances in this table. The variance of the travel times is mainly due to internal wave variability, and this value determines the uncertainties assigned to the travel times in an inversion. The correlation coefficient is a measure of the reciprocity of reciprocal raypaths. This measure is conservative, because correlation is not a necessary condition for the determination of current from the difference of reciprocal travel times. Values of correlation that are 0.5 or greater assure that the reciprocal raypaths are indeed effectively identical, since good correlation implies that the reciprocal raypaths have not separated by more than an internal wave correlation length. Histograms of the detided, high-frequency travel times are shown in FIGURES S-5 and S-6; the variances from TABLE S-1 are measures of the width of these histograms.

TABLES S-2 and S-3 show the results of tidal analysis of the time series of difference (current) and sum (sound speed) travel times. For these tables, the tidal analysis is performed on each travel time time series separately and then the average and rms of the harmonic constants are calculated. Current or sound speed amplitude is determined from travel time by a simple scaling factor; the harmonic constants are more accurately determined by inverting the data for current or sound speed (this is not done here).

TABLE S-1. Travel Time Statistics 3←→5a.

Ray #	Number of data	$\langle (T^+ + T^-)^2 \rangle$ (ms^2)	$\langle (T^+ - T^-)^2 \rangle$ (ms^2)	$\langle T^+ T^- \rangle$ (ms^2)	$\langle T^2 \rangle$ (ms^2)	$\frac{\langle T^+ T^- \rangle}{\langle T^2 \rangle}$
1	86	30	22	24	35	0.69
2	101	30	21	24	35	0.70
3	107	28	16	24	32	0.75
4	92	17	24	10	23	0.46
5	103	21	23	15	27	0.57
6	99	25	24	19	31	0.61
7	85	23	23	17	28	0.60
8	105	23	17	19	27	0.68
9	121	25	13	22	28	0.77
10	114	24	11	21	27	0.79
11	110	21	17	17	25	0.67
12	124	16	10	14	19	0.73
13	121	19	9	17	22	0.79
14	111	19	12	16	22	0.73
15	116	17	14	13	20	0.64
16	121	17	11	14	20	0.72

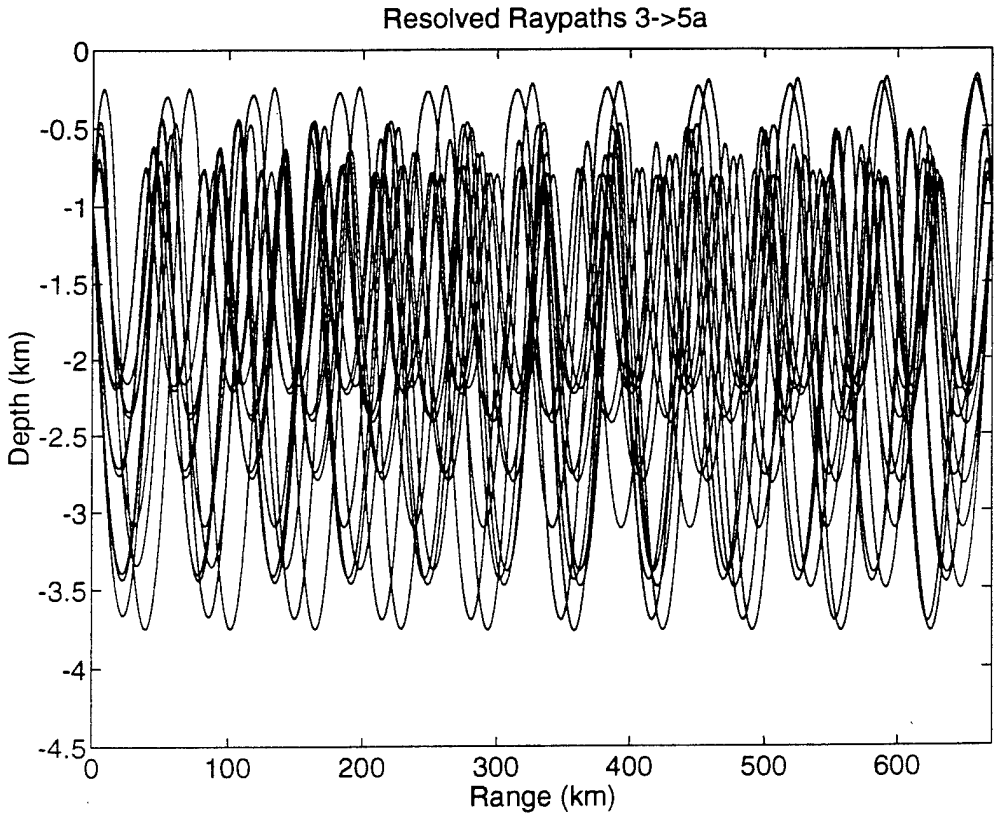

FIGURE S-1

TABLE S-2. Tidal Current Harmonic Constants 3←→5a.

Constituent	Amplitude (mm/s)	Uncertainty (mm/s)	Phase (°G)	Uncertainty (°)
M_2	10.66	2.32	284.9	7.5
S_2	4.04	2.70	227.2	108.4
N_2	2.03	1.29	304.4	62.2
K_2	3.99	3.44	57.7	76.5
O_1	1.95	0.92	17.2	68.0
K_1	3.11	1.90	154.6	112.5
P_1	2.98	1.75	204.4	64.9
Q_1	1.78	1.20	252.0	87.2

Values and their uncertainty are determined by the average and rms of harmonic constants from tidal analyses of the separate raypath travel time series. The amplitudes do not include the lunar node factors. 63 ± 10 % of the high-frequency variance is accounted for by the tides.

TABLE S-3. Tidal Sound Speed Harmonic Constants 3←→5a.

Constituent	Amplitude (mm/s)	Uncertainty (mm/s)	Phase (°G)	Uncertainty (°)
M_2	6.05	3.01	288.3	25.4
S_2	3.91	2.09	190.6	66.5
N_2	2.40	1.16	194.6	114.5
K_2	3.30	1.88	202.3	93.8
O_1	2.53	1.82	120.7	40.9
K_1	2.63	1.91	119.4	73.2
P_1	2.60	1.77	137.9	77.0
Q_1	2.69	1.09	35.1	29.4

Values and their uncertainty are determined by the average and rms of harmonic constants from tidal analyses of the separate raypath travel time series. The amplitudes do not include the lunar node factors. 43 ± 12 % of the high-frequency variance is accounted for by the tides. Because sum travel times are used to derive these numbers, the amplitudes have been divided by a factor of two compared to the amplitudes for current.

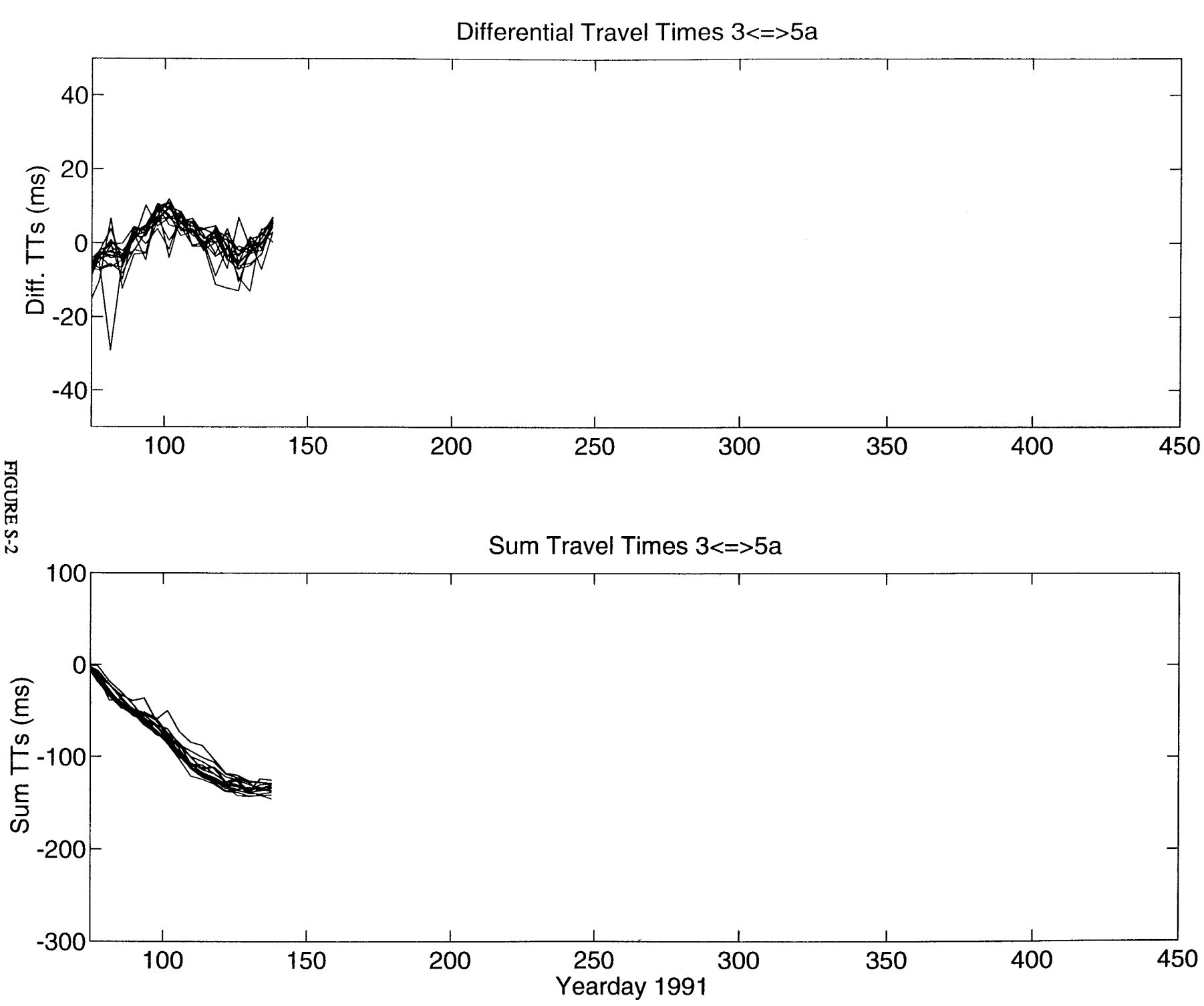
Differential Travel Times 3<=>5a
Diff. TTs (ms)
40
20
0
-20
-40
100
150
200
250
300
350
400
450
Sum Travel Times 3<=>5a
Sum TTs (ms)
100
0
-100
-200
-300
100
150
200
250
300
350
400
450
Yearday 1991

FIGURE S-2

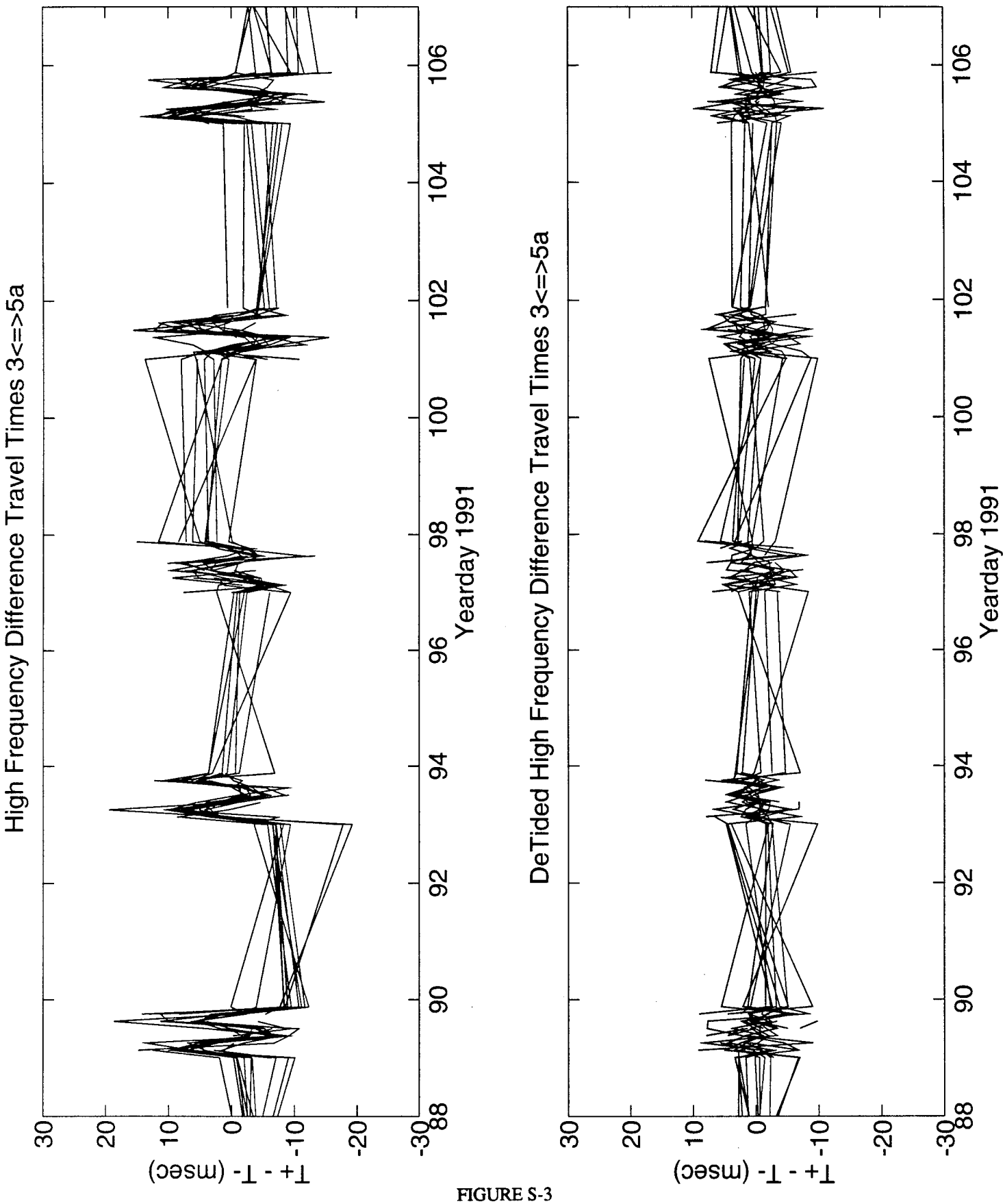
High Frequency Difference Travel Times 3<=>5a
T+ - T- (msec)
30
20
10
0
-10
-20
-30
88
90
92
94
96
98
100
102
104
106
Yearday 1991
DeTided High Frequency Difference Travel Times 3<=>5a
T+ - T- (msec)
30
20
10
0
-10
-20
-30
88
90
92
94
96
98
100
102
104
106
Yearday 1991

FIGURE S-3

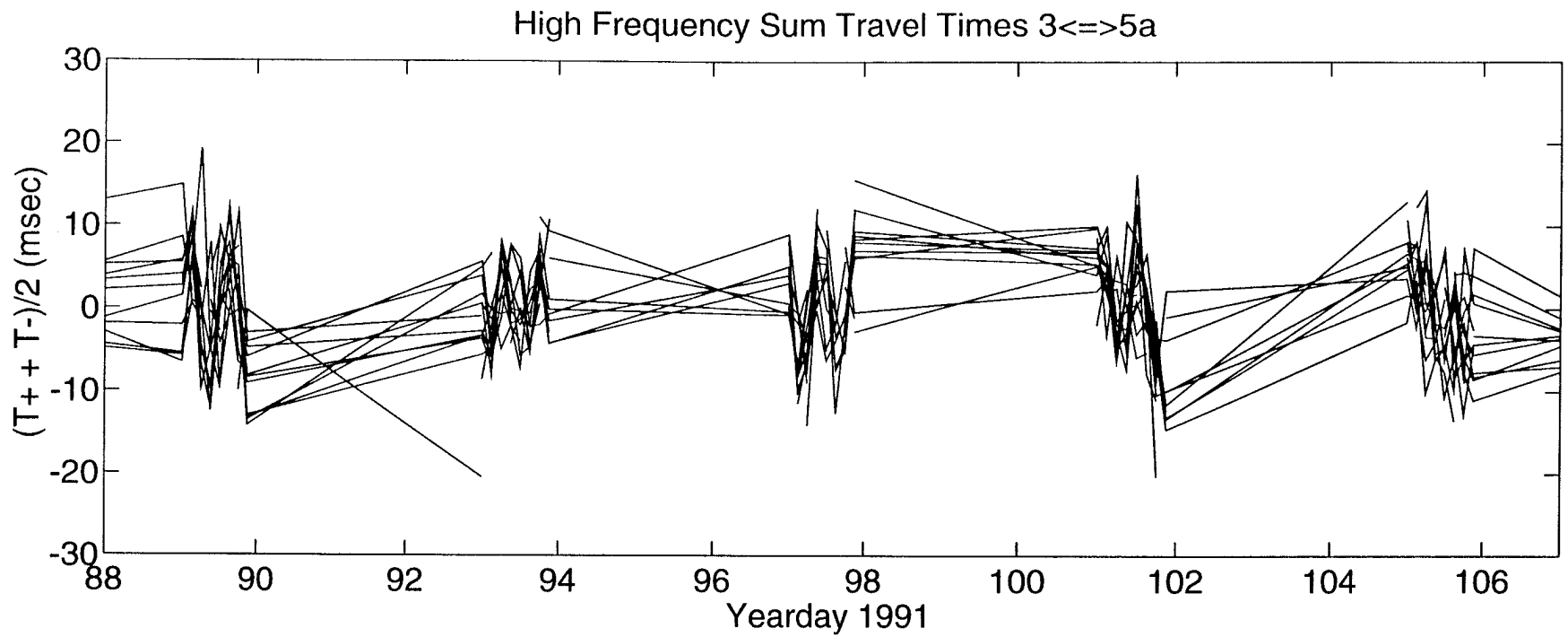
High Frequency Sum Travel Times 3<=>5a
(T+ + T-)/2 (msec)
30
20
10
0
-10
-20
-30
88
90
92
94
96
98
100
102
104
106
Yearday 1991

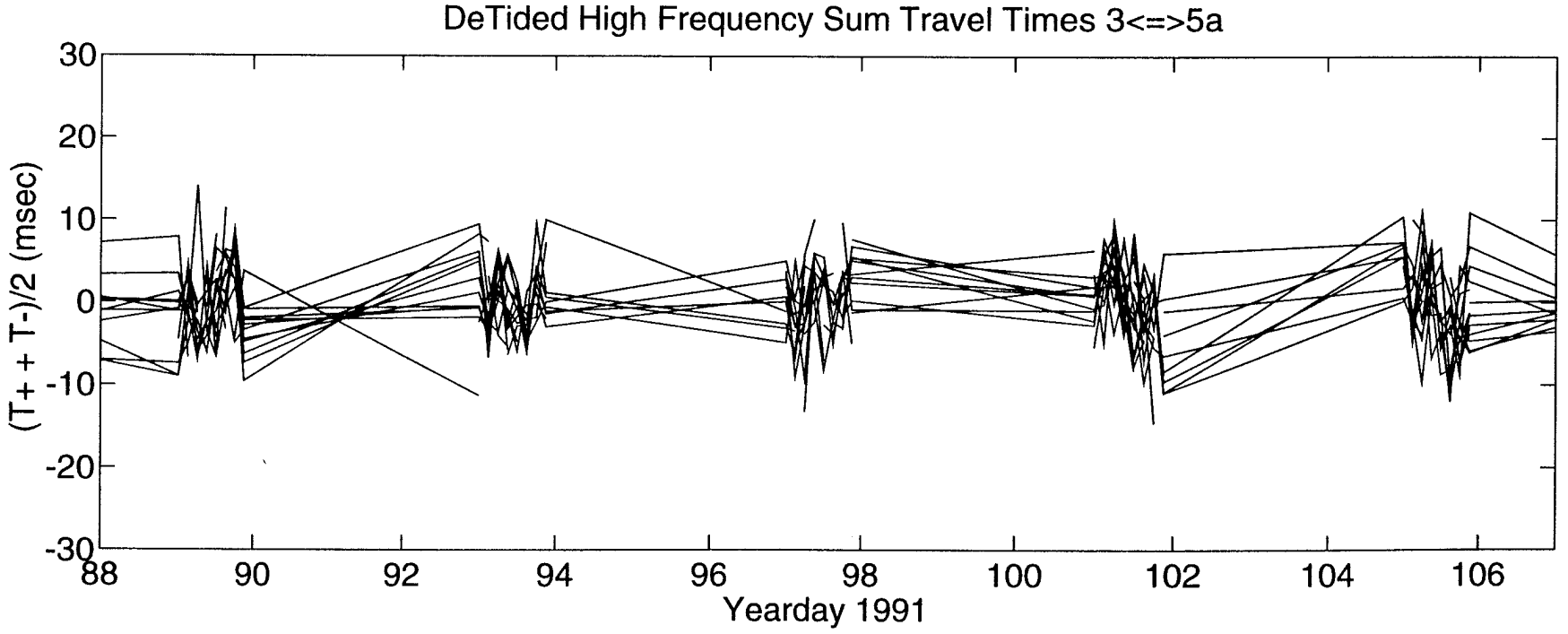
DeTided High Frequency Sum Travel Times 3<=>5a
(T+ + T-)/2 (msec)
30
20
10
0
-10
-20
-30
88
90
92
94
96
98
100
102
104
106
Yearday 1991

FIGURE S-4

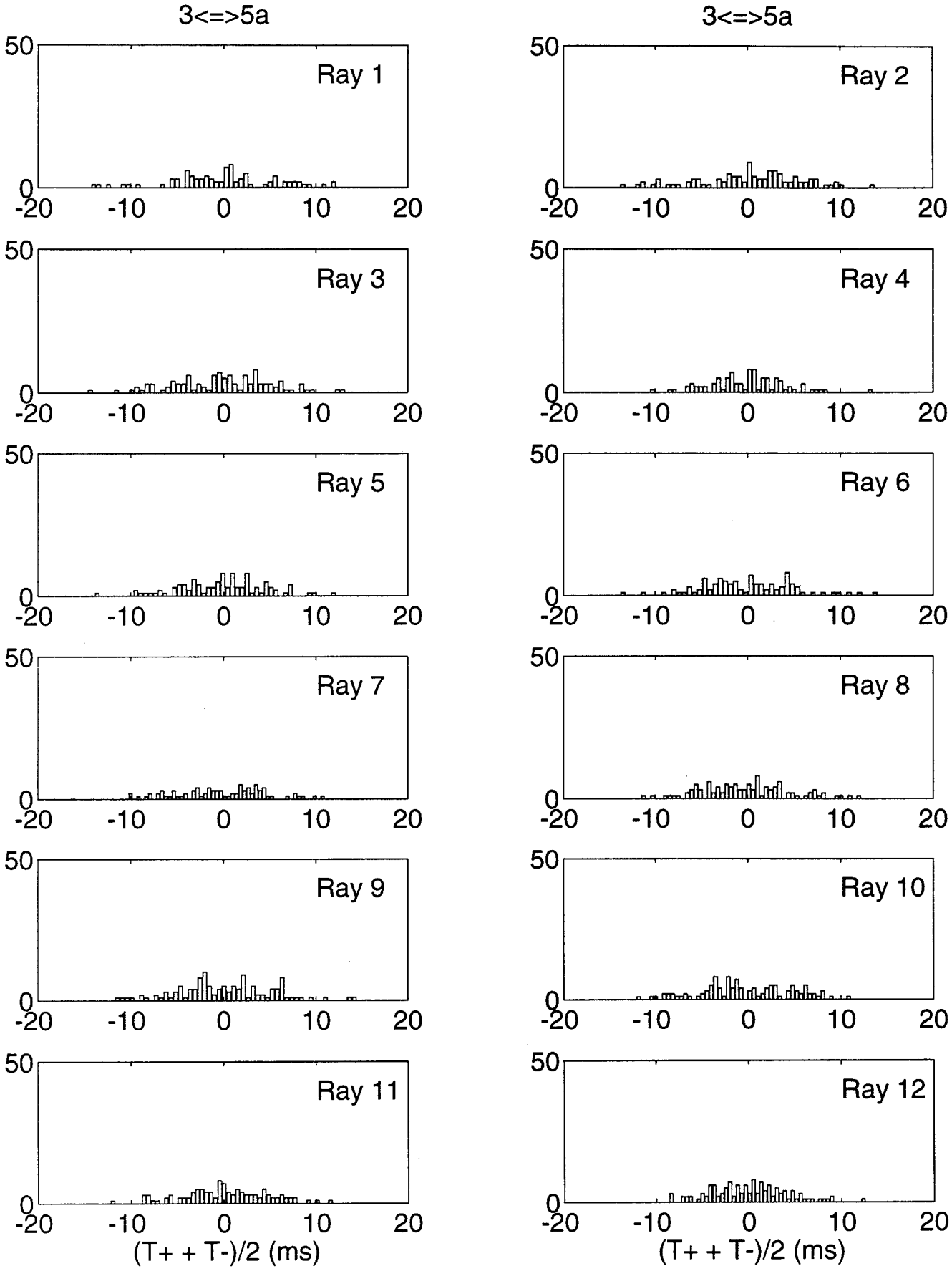
3<=>5a
3<=>5a
Ray 1
Ray 2
Ray 3
Ray 4
Ray 5
Ray 6
Ray 7
Ray 8
Ray 9
Ray 10
Ray 11
Ray 12
50
0
-20
-10
0
10
20
(T+ + T-)/2 (ms)

FIGURE S-5

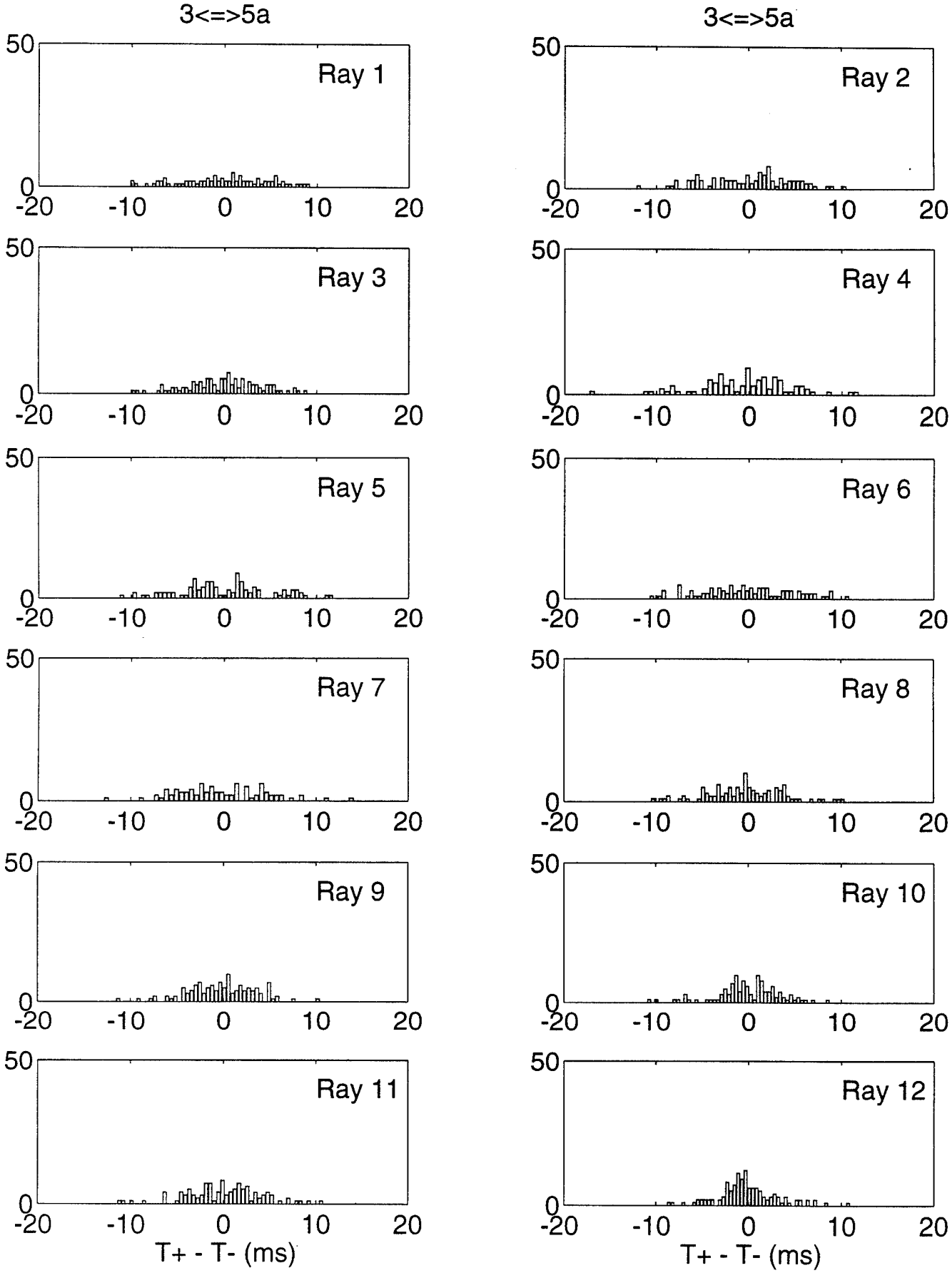
3<=>5a
3<=>5a
Ray 1
Ray 2
Ray 3
Ray 4
Ray 5
Ray 6
Ray 7
Ray 8
Ray 9
Ray 10
Ray 11
Ray 12
50
0
-20
-10
0
10
20
T+ - T- (ms)

FIGURE S-6

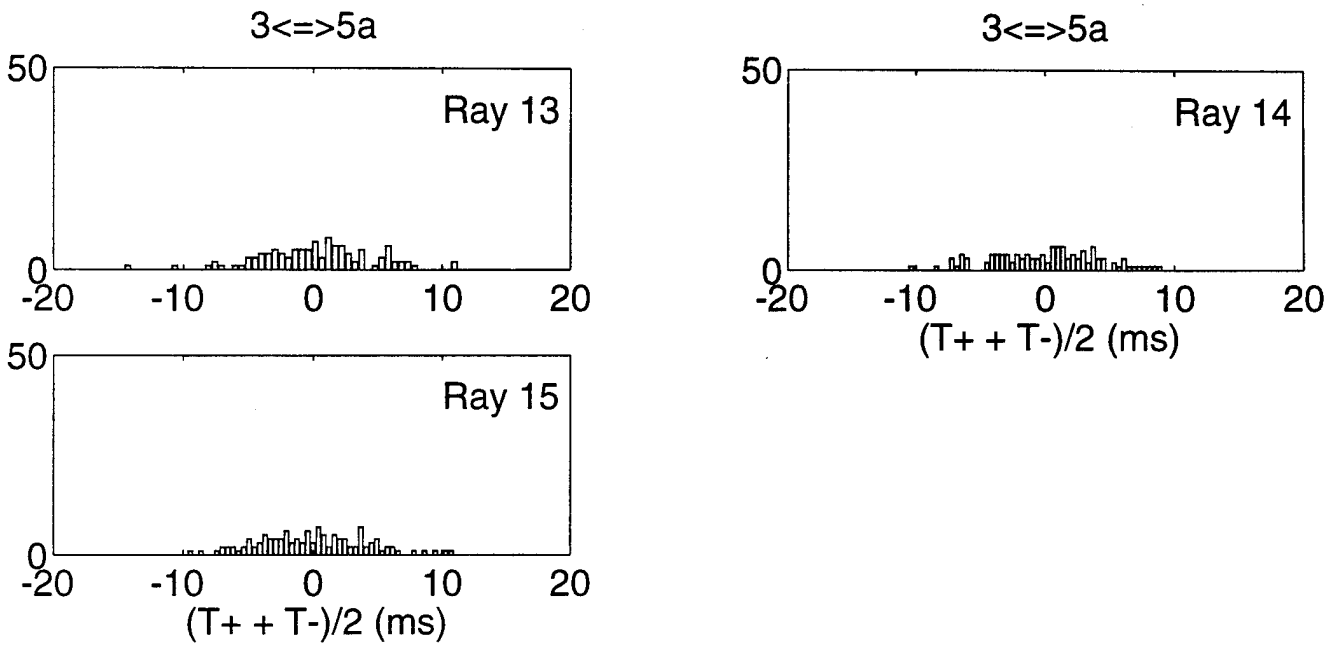

FIGURE S-5 (cont.)

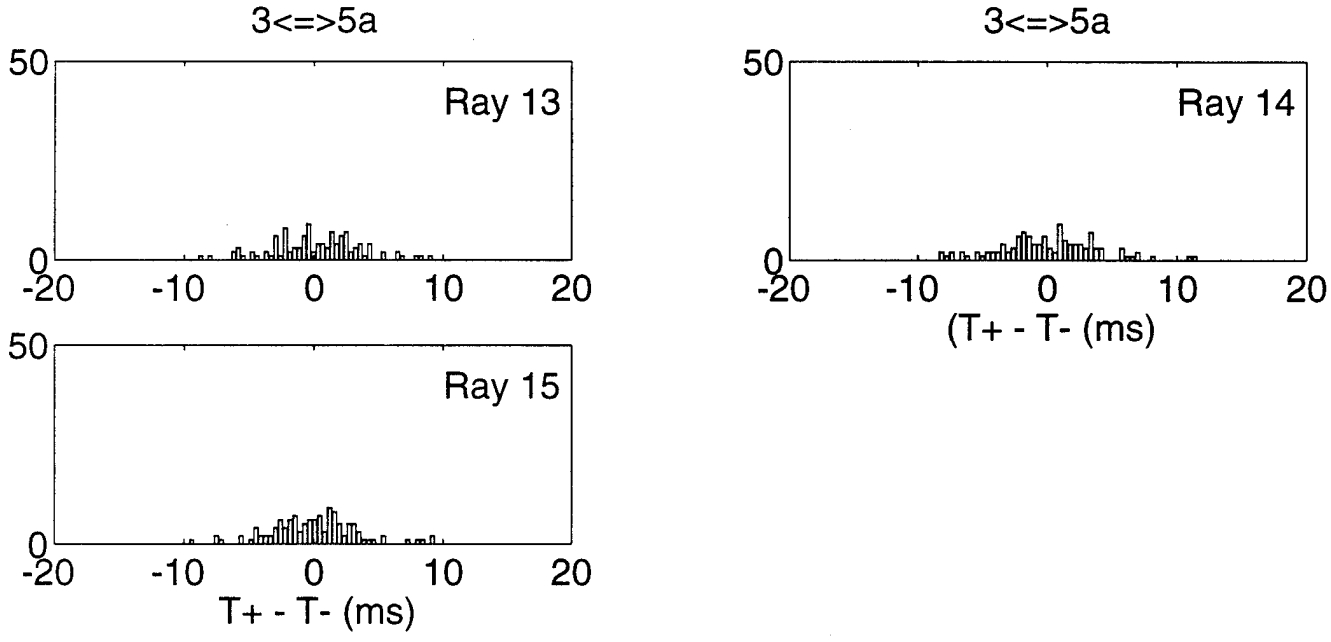

FIGURE S-6 (cont.)

T. ACOUSTIC DATA: Paths 3→5b and 5b→3

FIGURE T-1 shows the raypaths, corresponding roughly to FIGURE G-1, for which travel times were resolved. The raypaths were actually determined using range-dependent Levitus sound speed, interpolated onto the acoustic path. Note that the "final cutoff" travel times may be available at some time in the future, these data correspond to a ray confined near the sound channel axis.

FIGURE T-2 shows the low-pass filtered difference (top panel) and sum (bottom panel) travel times corresponding to the rays of FIGURE T-1.

FIGURE T-3 shows the high-pass filtered difference travel times for a small portion of the time series obtained during the time of more frequent transmissions during the MST experiment. The bottom panel shows the time series after the phase-locked tidal signals have been removed.

FIGURE T-4 shows the high-pass filtered sum travel times for a small portion of the time series obtained during the time of more frequent transmissions during the MST experiment. The bottom panel shows the time series after the phase-locked tidal signals have been removed. This tidal variability is caused by the internal tide.

After the travel time time series have been edited for outliers, high-pass filtered, and detided, the high-frequency variances are calculated (TABLE T-1). Note that this table sometimes contains statistics for more rays than are indicated in TABLE B-1; some of the ray arrivals in TABLE T-1 have not been identified with predicted arrivals. Also, sometimes there is initial ambiguity about the pairing of reciprocal arrivals, in which case sum and difference travel times are calculated for all reasonable cases; later it becomes obvious which arrivals have been improperly paired. The correlation $<T^+ T^->$ and variance $<T^2>$ are calculated from the sum and difference travel time variances in this table. The variance of the travel times is mainly due to internal wave variability, and this value determines the uncertainties assigned to the travel times in an inversion. The correlation coefficient is a measure of the reciprocity of reciprocal raypaths. This measure is conservative, because correlation is not a necessary condition for the determination of current from the difference of reciprocal travel times. Values of correlation that are 0.5 or greater assure that the reciprocal raypaths are indeed effectively identical, since good correlation implies that the reciprocal raypaths have not separated by more than an internal wave correlation length. Histograms of the detided, high-frequency travel times are shown in FIGURES T-5 and T-6; the variances from TABLE T-1 are measures of the width of these histograms.

TABLES T-2 and T-3 show the results of tidal analysis of the time series of difference (current) and sum (sound speed) travel times. For these tables, the tidal analysis is performed on each travel time time series separately and then the average and rms of the harmonic constants are calculated. Current or sound speed amplitude is determined from travel time by a simple scaling factor; the harmonic constants are more accurately determined by inverting the data for current or sound speed (this is not done here).

TABLE T-1. Travel Time Statistics 3←→5b.

Ray #	Number of data	$<(T^+ + T^-)^2>$ (ms^2)	$<(T^+ - T^-)^2>$ (ms^2)	$<T^+ T^->$ (ms^2)	$<T^2>$ (ms^2)	$\frac{<T^+ T^->}{<T^2>}$
1	179	18	20	13	23	0.56
2	166	29	24	23	35	0.65
3	176	30	23	24	36	0.68
4	253	20	13	17	23	0.73
5	205	23	26	16	29	0.56
6	217	18	21	13	23	0.54
7	266	17	10	15	20	0.75
8	279	17	12	14	20	0.71
9	261	19	14	16	23	0.70
10	288	17	11	14	20	0.72
11	276	21	14	18	24	0.72
12	272	17	10	14	19	0.74
13	273	19	11	17	22	0.75
14	273	19	12	16	22	0.73

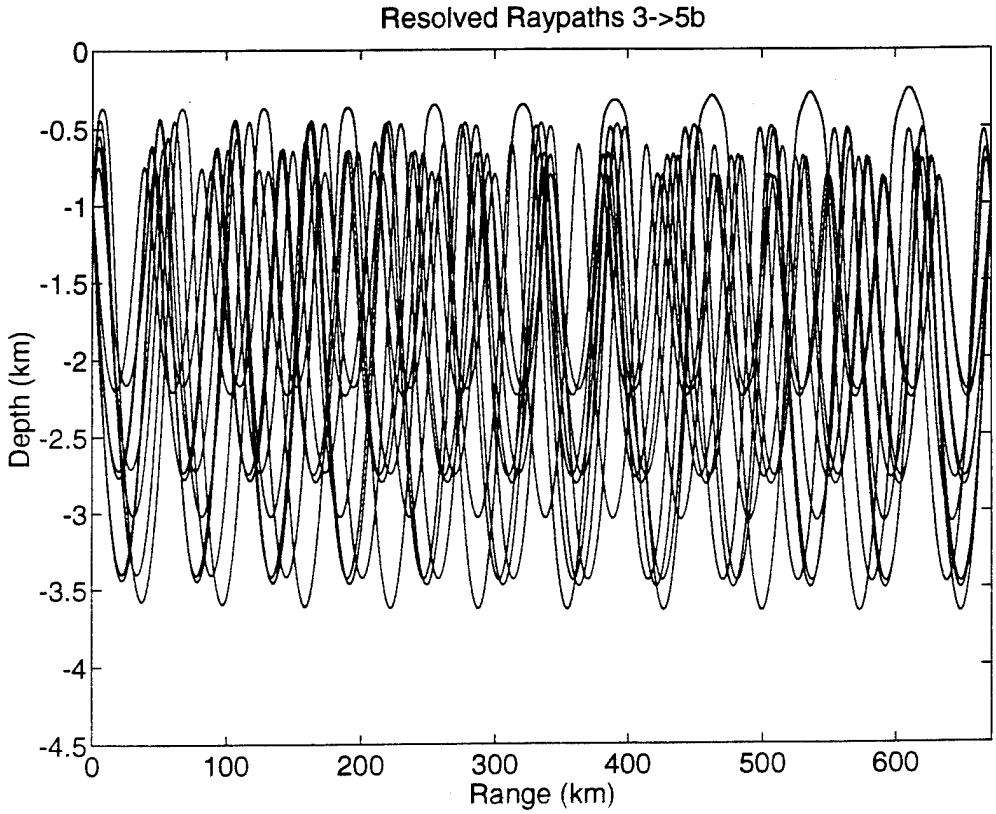

FIGURE T-1

TABLE T-2. Tidal Current Harmonic Constants 3←→5b.

Constituent	Amplitude (mm/s)	Uncertainty (mm/s)	Phase (°G)	Uncertainty (°)
M_2	9.66	1.34	283.4	5.0
S_2	2.48	0.63	324.8	23.7
N_2	2.41	0.83	258.0	28.1
K_2	1.47	0.97	328.1	55.5
O_1	1.18	1.38	48.1	69.8
K_1	1.55	0.67	58.6	66.6
P_1	1.70	0.92	94.7	45.9
Q_1	1.19	0.81	153.6	3

Values and their uncertainty are determined by the average and rms of harmonic constants from tidal analyses of the separate raypath travel time series. The amplitudes do not include the lunar node factors. 57 ± 8 % of the high-frequency variance is accounted for by the tides.

TABLE T-3. Tidal Sound Speed Harmonic Constants 3←→5b.

Constituent	Amplitude (mm/s)	Uncertainty (mm/s)	Phase (°G)	Uncertainty (°)
M_2	5.61	2.41	283.5	23.1
S_2	1.45	0.76	178.1	54.0
N_2	1.91	0.63	258.5	43.4
K_2	1.59	0.71	211.2	60.1
O_1	3.07	0.94	125.1	22.3
K_1	1.22	0.62	343.9	73.2
P_1	1.46	0.90	356.3	65.6
Q_1	1.32	0.52	62.2	69.1

Values and their uncertainty are determined by the average and rms of harmonic constants from tidal analyses of the separate raypath travel time series. The amplitudes do not include the lunar node factors. 33 ± 11 % of the high-frequency variance is accounted for by the tides. Because sum travel times are used to derive these numbers, the amplitudes have been divided by a factor of two compared to the amplitudes for current.

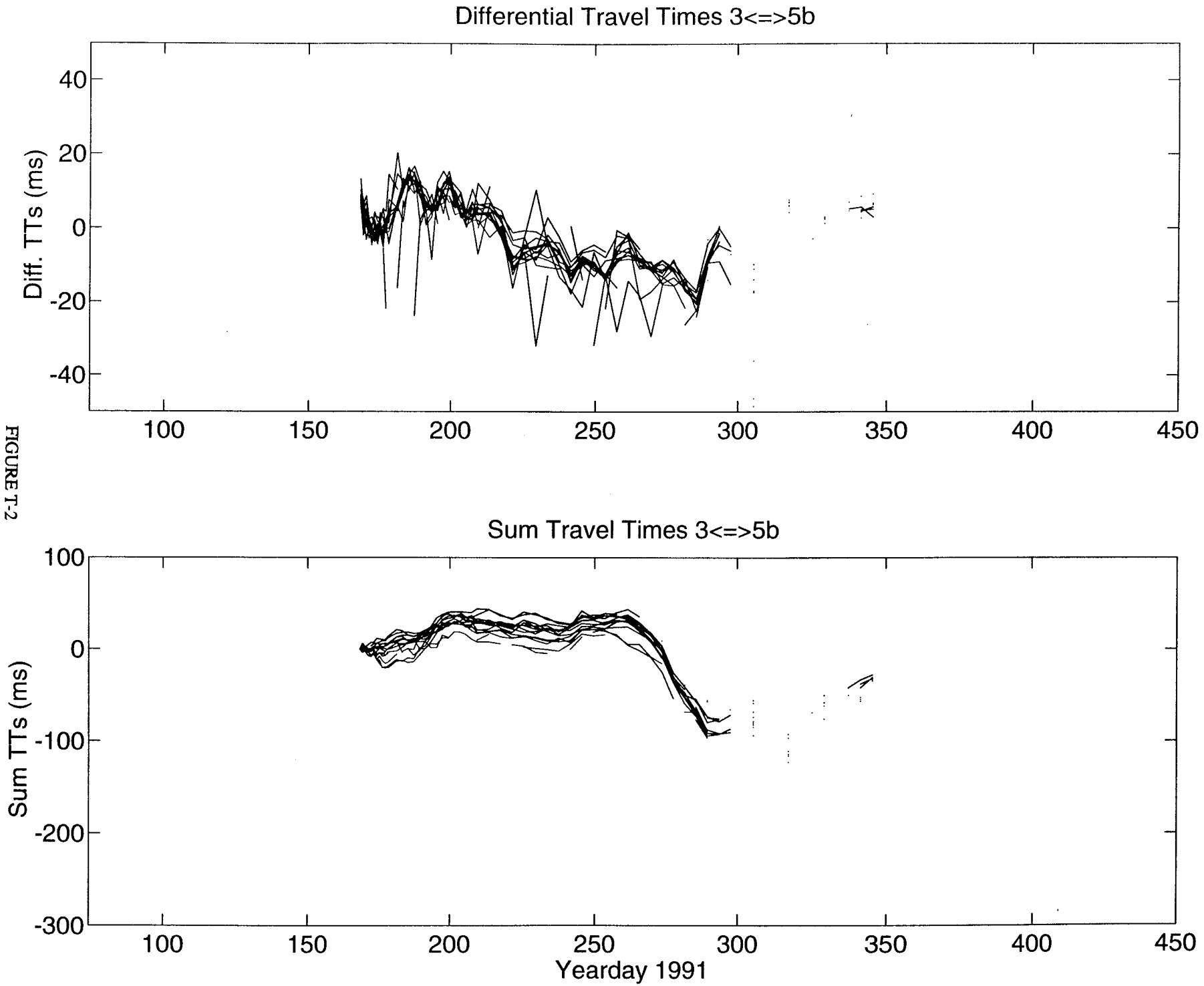
Differential Travel Times 3<=>5b
Diff. TTs (ms)
40
20
0
-20
-40
100
150
200
250
300
350
400
450
Sum Travel Times 3<=>5b
Sum TTs (ms)
100
0
-100
-200
-300
100
150
200
250
300
350
400
450
Yearday 1991

FIGURE T-2

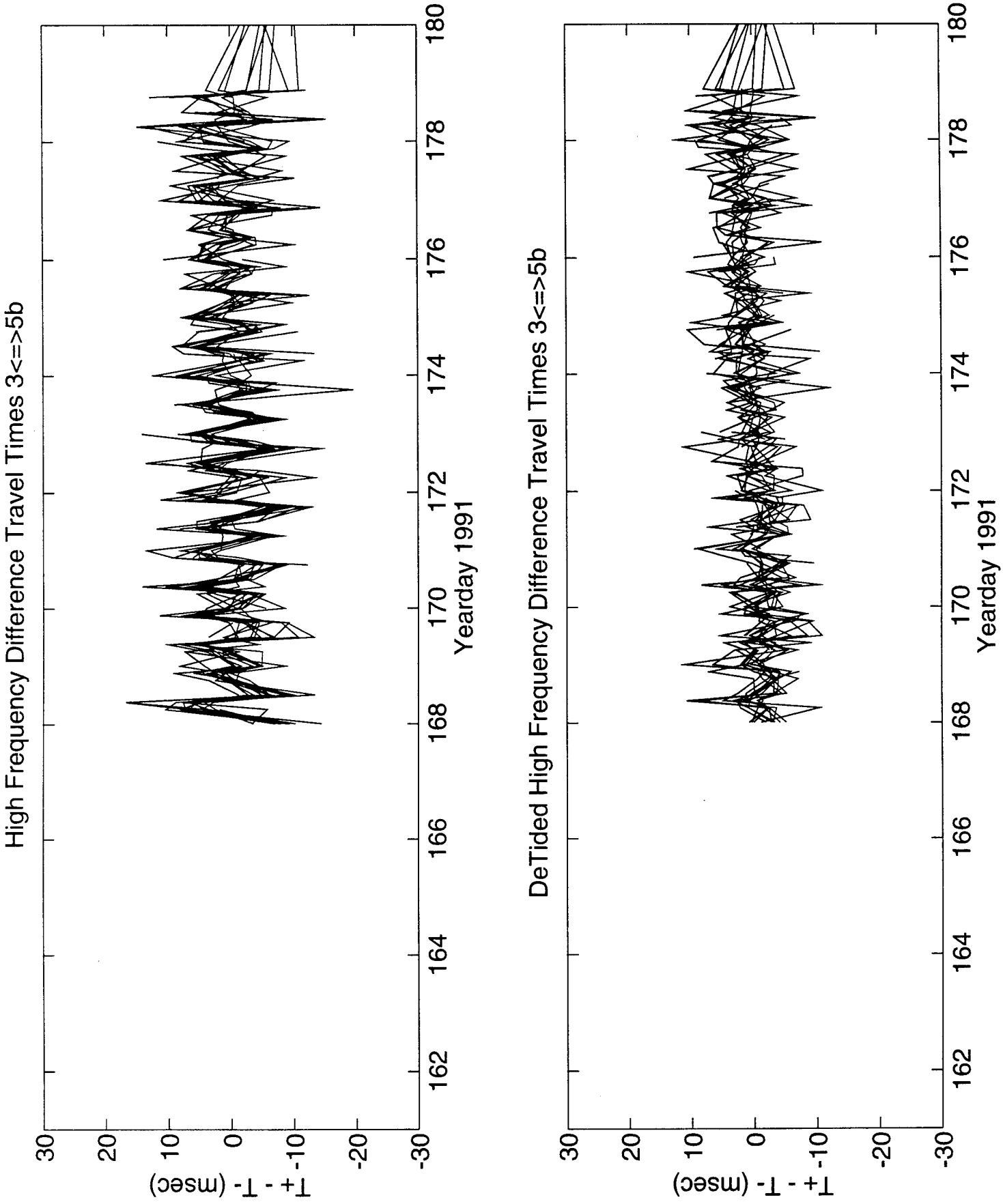
High Frequency Difference Travel Times 3<=>5b
T+ - T- (msec)
30
20
10
0
-10
-20
-30
162
164
166
168
170
172
174
176
178
180
Yearday 1991
DeTided High Frequency Difference Travel Times 3<=>5b
T+ - T- (msec)
30
20
10
0
-10
-20
-30
162
164
166
168
170
172
174
176
178
180
Yearday 1991

FIGURE T-3

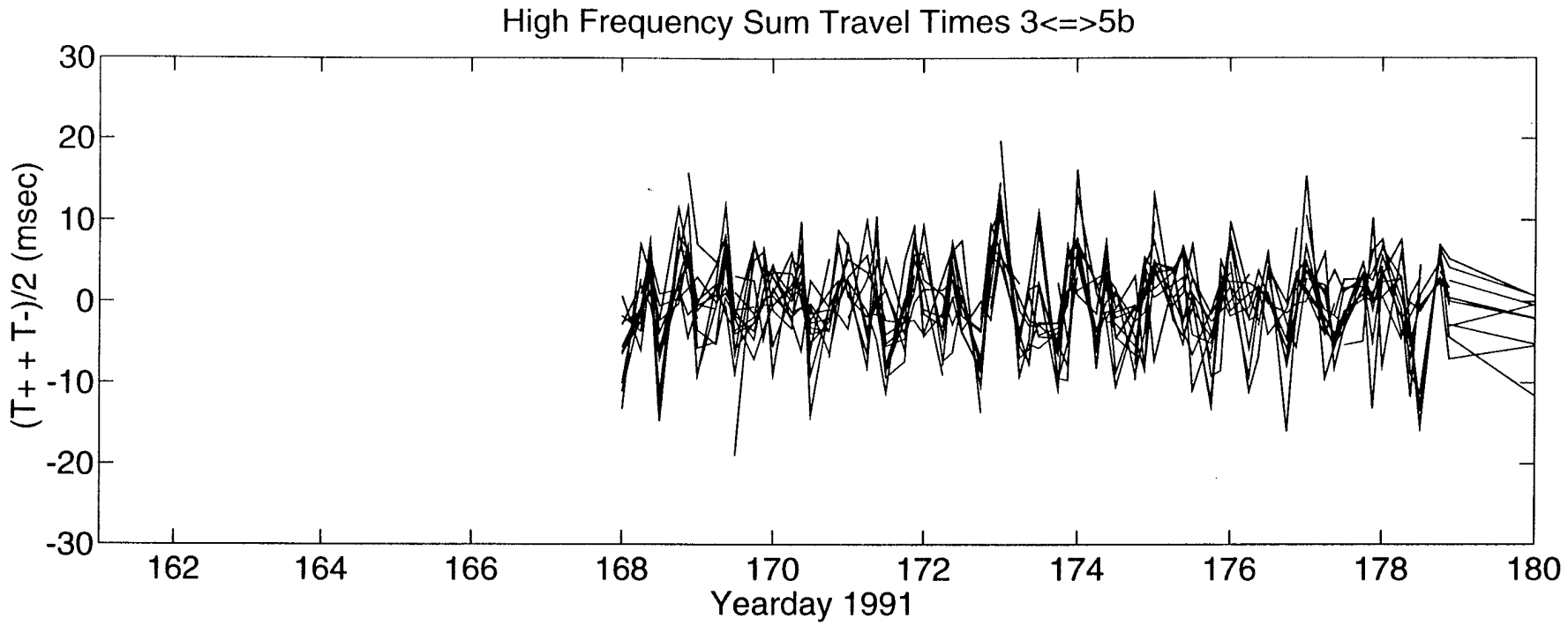
High Frequency Sum Travel Times 3<=>5b
(T+ + T-)/2 (msec)
30
20
10
0
-10
-20
-30
162
164
166
168
170
172
174
176
178
180
Yearday 1991

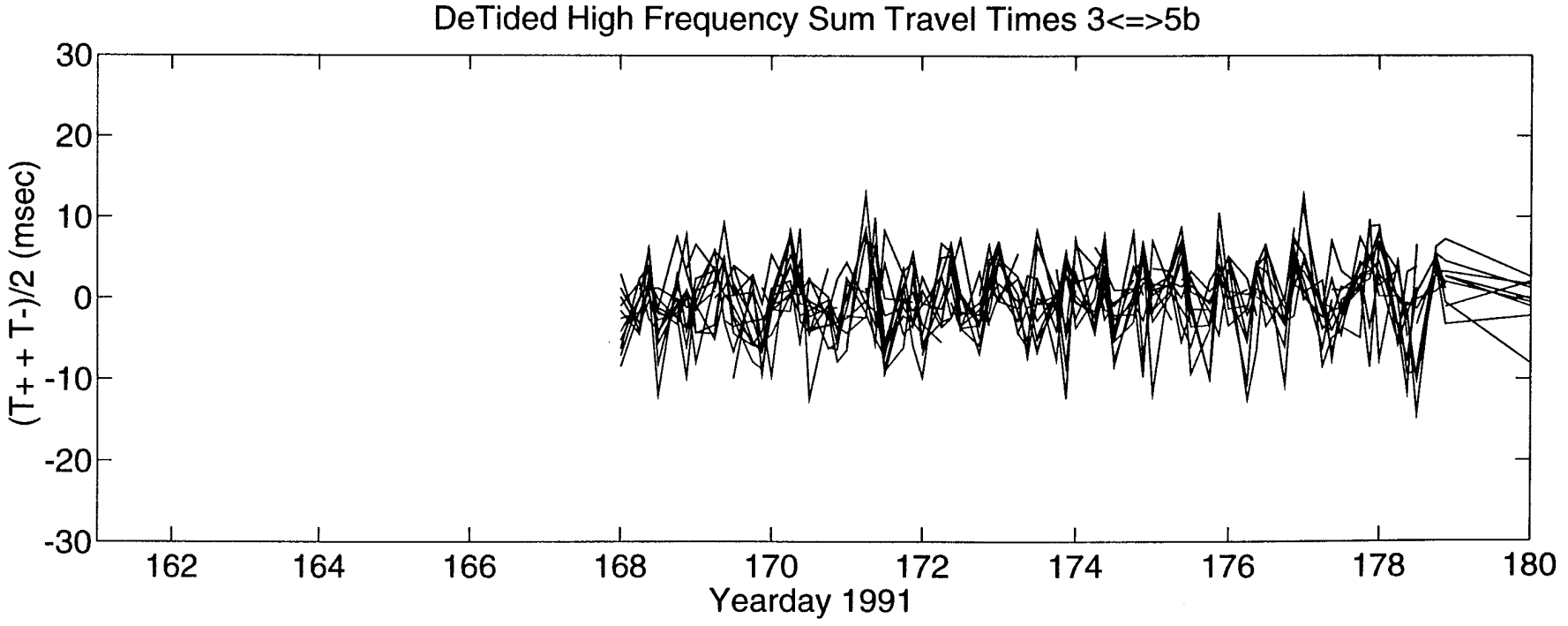
DeTided High Frequency Sum Travel Times 3<=>5b
(T+ + T-)/2 (msec)
30
20
10
0
-10
-20
-30
162
164
166
168
170
172
174
176
178
180
Yearday 1991

FIGURE T-4

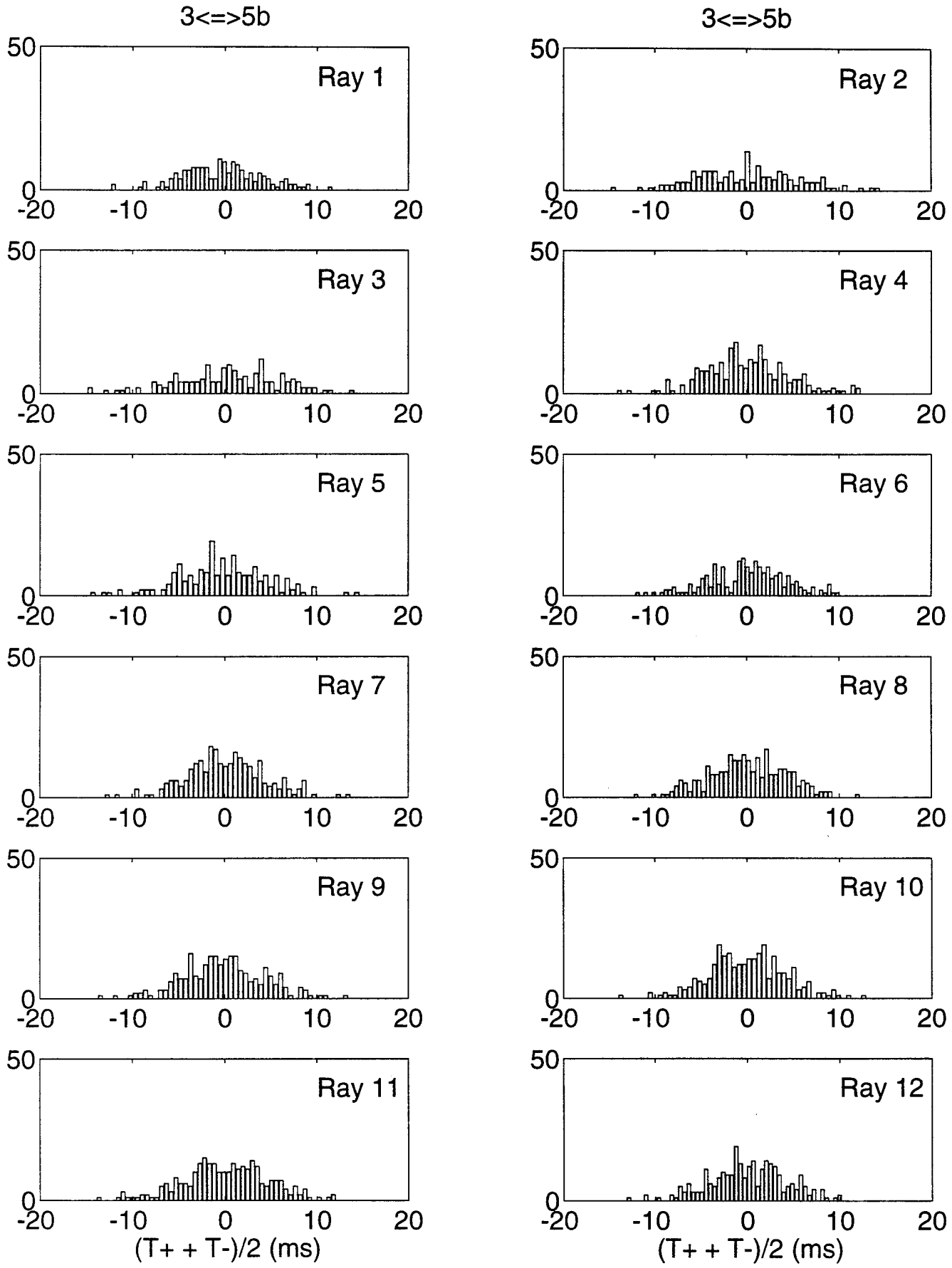
3<=>5b
Ray 1
Ray 2
Ray 3
Ray 4
Ray 5
Ray 6
Ray 7
Ray 8
Ray 9
Ray 10
Ray 11
Ray 12
50
0
-20
-10
0
10
20
(T+ + T-)/2 (ms)

FIGURE T-5

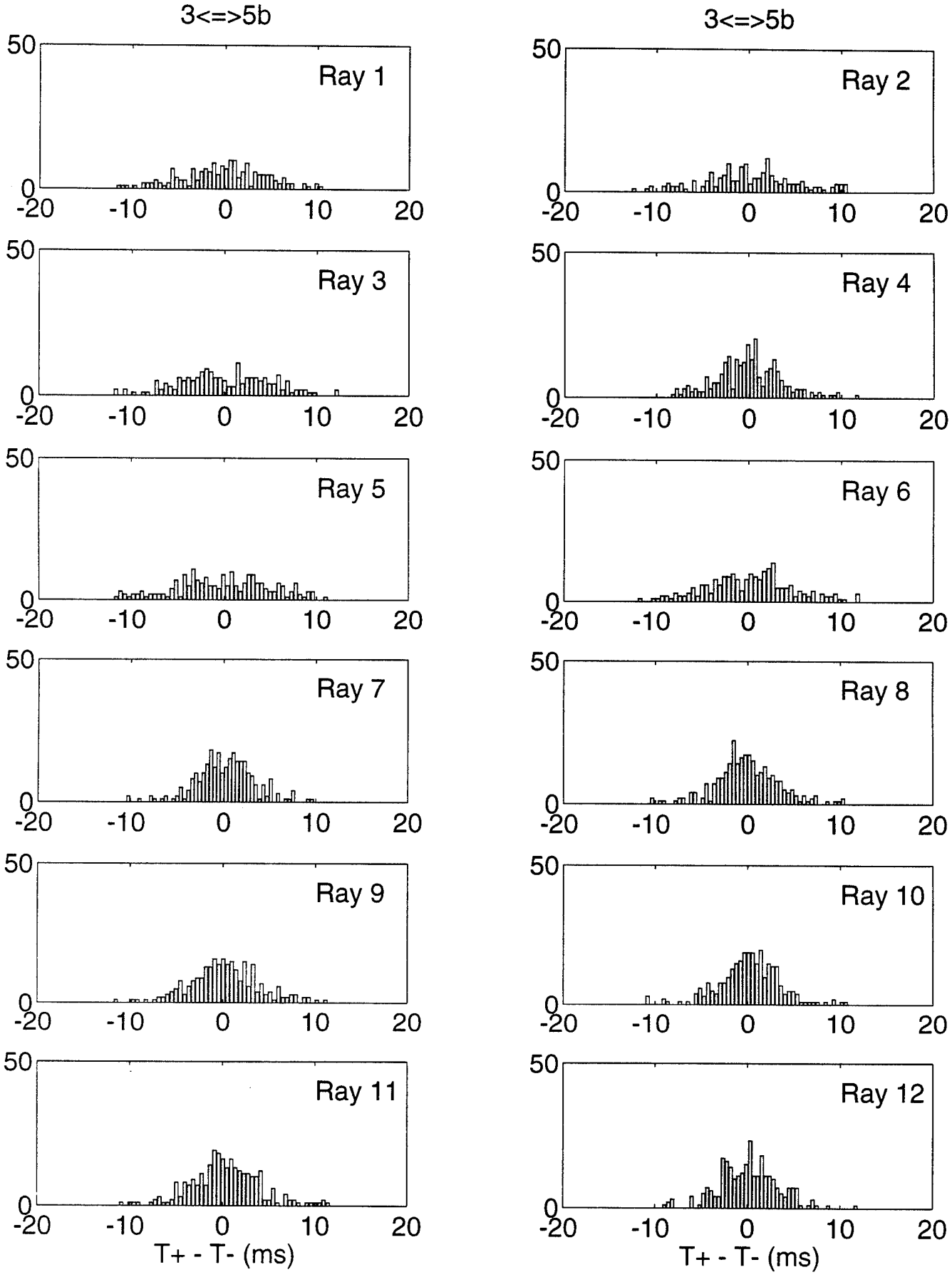
3<=>5b
Ray 1
Ray 2
Ray 3
Ray 4
Ray 5
Ray 6
Ray 7
Ray 8
Ray 9
Ray 10
Ray 11
Ray 12
50
0
-20
-10
0
10
20
T+ - T- (ms)

FIGURE T-6

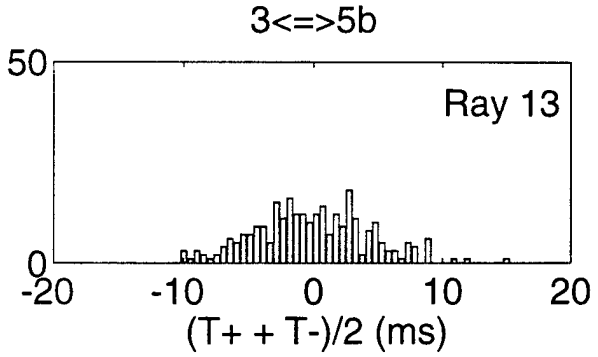

FIGURE T-5 (cont.)

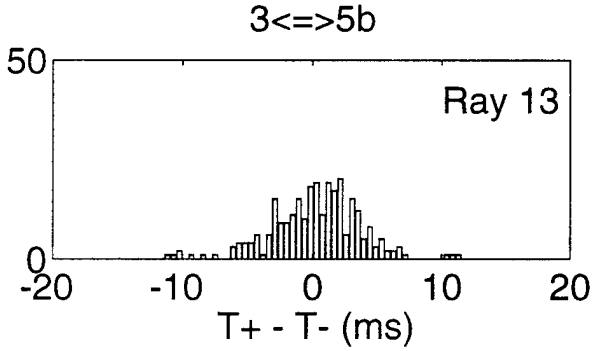

FIGURE T-6 (cont.)

U. ACOUSTIC DATA: Paths 3→6 and 6→3

FIGURE U-1 shows the raypaths, roughly corresponding to FIGURE G-1, for which travel times were resolved. The raypaths were actually determined using range-dependent Levitus sound speed, interpolated onto the acoustic path. Note that the "final cutoff" travel times may be available at some time in the future, these data correspond to a ray confined near the sound channel axis.

FIGURE U-2 shows the low-pass filtered difference (top panel) and sum (bottom panel) travel times corresponding to the rays of FIGURE U-1.

FIGURE U-3 shows the high-pass filtered difference travel times for a small portion of the time series obtained during the time of more frequent transmissions during the MST experiment. The bottom panel shows the time series after the phase-locked tidal signals have been removed. FIGURE U-4 shows the same time series, but during a time of the normal transmission schedule.

FIGURE U-5 shows the high-pass filtered sum travel times for a small portion of the time series obtained during the time of more frequent transmissions during the MST experiment. The bottom panel shows the time series after the phase-locked tidal signals have been removed. This tidal variability is caused by the internal tide. FIGURE U-6 shows the same time series, but during a time of the normal transmission schedule.

After the travel time time series have been edited for outliers, high-pass filtered, and detided, the high-frequency variances are calculated (TABLE U-1). Note that this table sometimes contains statistics for more rays than are indicated in TABLE B-1; some of the ray arrivals in TABLE U-1 have not been identified with predicted arrivals. Also, sometimes there is initial ambiguity about the pairing of reciprocal arrivals, in which case sum and difference travel times are calculated for all reasonable cases; later it becomes obvious which arrivals have been improperly paired. The correlation $<T^+ T^->$ and variance $<T^2>$ are calculated from the sum and difference travel time variances in this table. The variance of the travel times is mainly due to internal wave variability, and this value determines the uncertainties assigned to the travel times in an inversion. The correlation coefficient is a measure of the reciprocity of reciprocal raypaths. This measure is conservative, because correlation is not a necessary condition for the determination of current from the difference of reciprocal travel times. Values of correlation that are 0.5 or greater assure that the reciprocal raypaths are indeed effectively identical, since good correlation implies that the reciprocal raypaths have not separated by more than an internal wave correlation length. Histograms of the detided, high-frequency travel times are shown in FIGURES U-7 and U-8; the variances from TABLE U-1 are measures of the width of these histograms.

TABLES U-2 and U-3 show the results of tidal analysis of the time series of difference (current) and sum (sound speed) travel times. For these tables, the tidal analysis is performed on each travel time time series separately and then the average and rms of the harmonic constants are calculated. Current or sound speed amplitude is determined from travel time by a simple scaling factor; the harmonic constants are more accurately determined by inverting the data for current or sound speed (this is not done here).

TABLE U-1. Travel Time Statistics 3←→6.

Ray #	Number of data	$<(T^+ + T^-)^2>$ (ms^2)	$<(T^+ - T^-)^2>$ (ms^2)	$<T^+ T^->$ (ms^2)	$<T^2>$ (ms^2)	$\frac{<T^+ T^->}{<T^2>}$
1	466	16	8	14	18	0.78
2	540	12	5	10	13	0.79
3	614	14	7	12	16	0.79
4	603	14	7	12	16	0.78
5	650	13	3	12	14	0.90
6	643	13	3	12	13	0.90
7	624	13	5	12	14	0.82
8	622	16	6	14	17	0.83
9	609	15	3	14	16	0.90

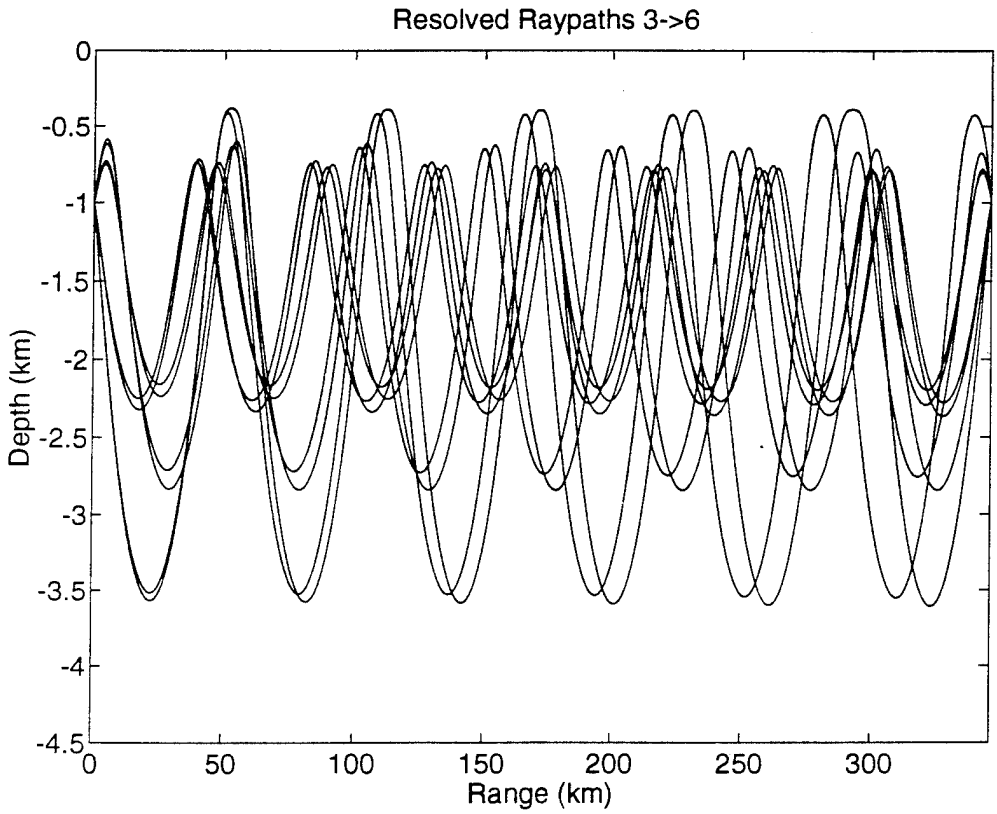

FIGURE U-1

TABLE U-2. Tidal Current Harmonic Constants 3←→6.

Constituent	Amplitude (mm/s)	Uncertainty (mm/s)	Phase (°G)	Uncertainty (°)
M_2	8.40	0.42	290.7	4.5
S_2	2.02	0.44	323.8	15.7
N_2	2.03	0.37	261.7	12.0
K_2	0.81	0.41	19.8	51.3
O_1	1.13	0.41	33.4	23.0
K_1	1.49	0.35	51.2	13.1
P_1	0.97	0.41	123.6	86.3
Q_1	0.68	0.54	247.7	89.8

Values and their uncertainty are determined by the average and rms of harmonic constants from tidal analyses of the separate raypath travel time series. The amplitudes do not include the lunar node factors. 50 ± 12 % of the high-frequency variance is accounted for by the tides.

TABLE U-3. Tidal Sound Speed Harmonic Constants 3←→6.

Constituent	Amplitude (mm/s)	Uncertainty (mm/s)	Phase (°G)	Uncertainty (°)
M_2	6.48	2.49	189.1	15.4
S_2	2.06	0.52	352.2	20.6
N_2	3.21	0.67	157.2	10.0
K_2	2.13	0.52	298.2	20.6
O_1	3.18	0.97	162.5	7.1
K_1	5.47	0.98	58.2	3.4
P_1	1.82	0.46	28.8	34.5
Q_1	1.70	0.43	81.7	19.5

Values and their uncertainty are determined by the average and rms of harmonic constants from tidal analyses of the separate raypath travel time series. The amplitudes do not include the lunar node factors. 30 ± 7 % of the high-frequency variance is accounted for by the tides. Because sum travel times are used to derive these numbers, the amplitudes have been divided by a factor of two compared to the amplitudes for current.

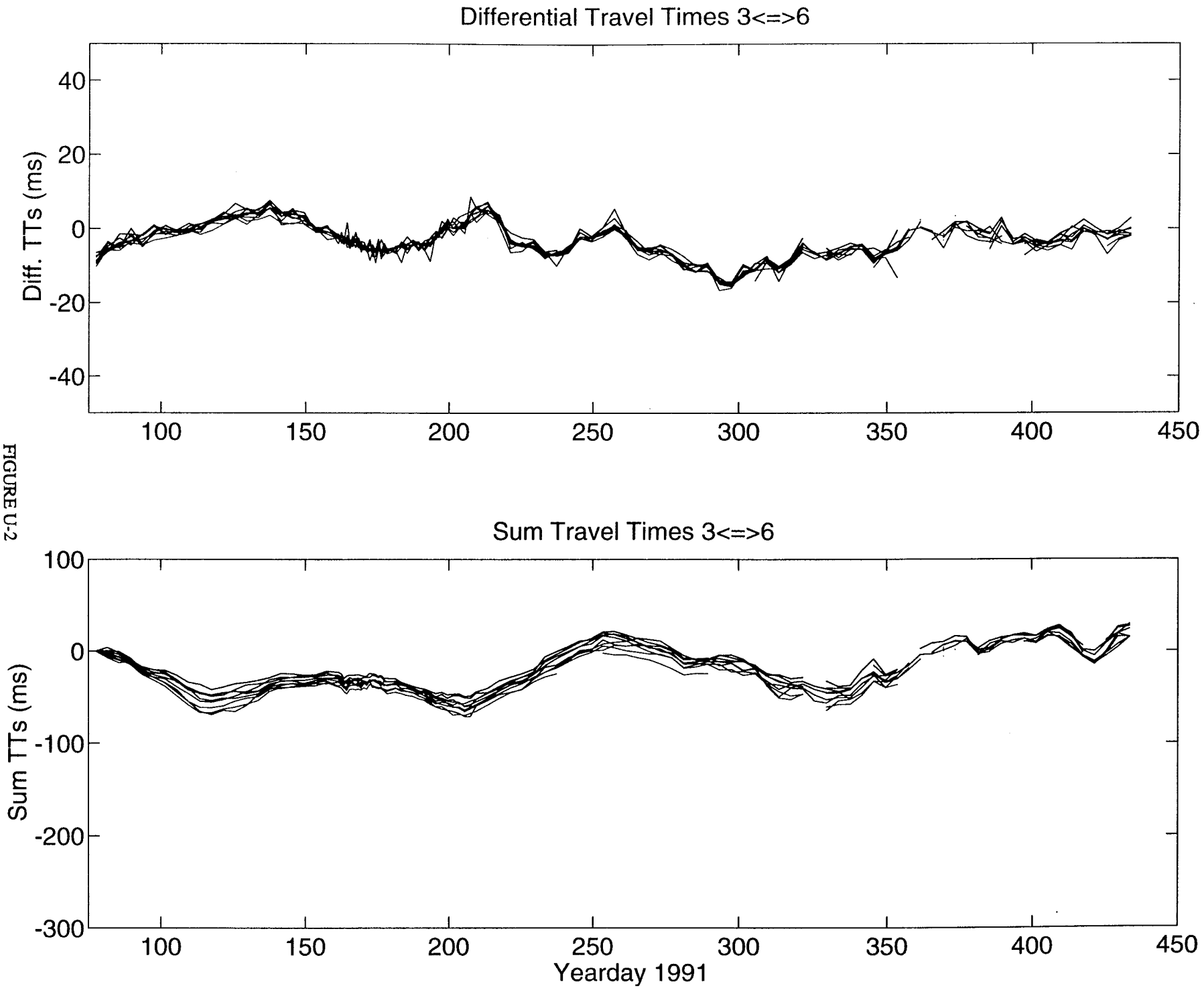
Differential Travel Times 3<=>6
Diff. TTs (ms)
40
20
0
-20
-40
100
150
200
250
300
350
400
450
Sum Travel Times 3<=>6
Sum TTs (ms)
100
0
-100
-200
-300
100
150
200
250
300
350
400
450
Yearday 1991

FIGURE U-2

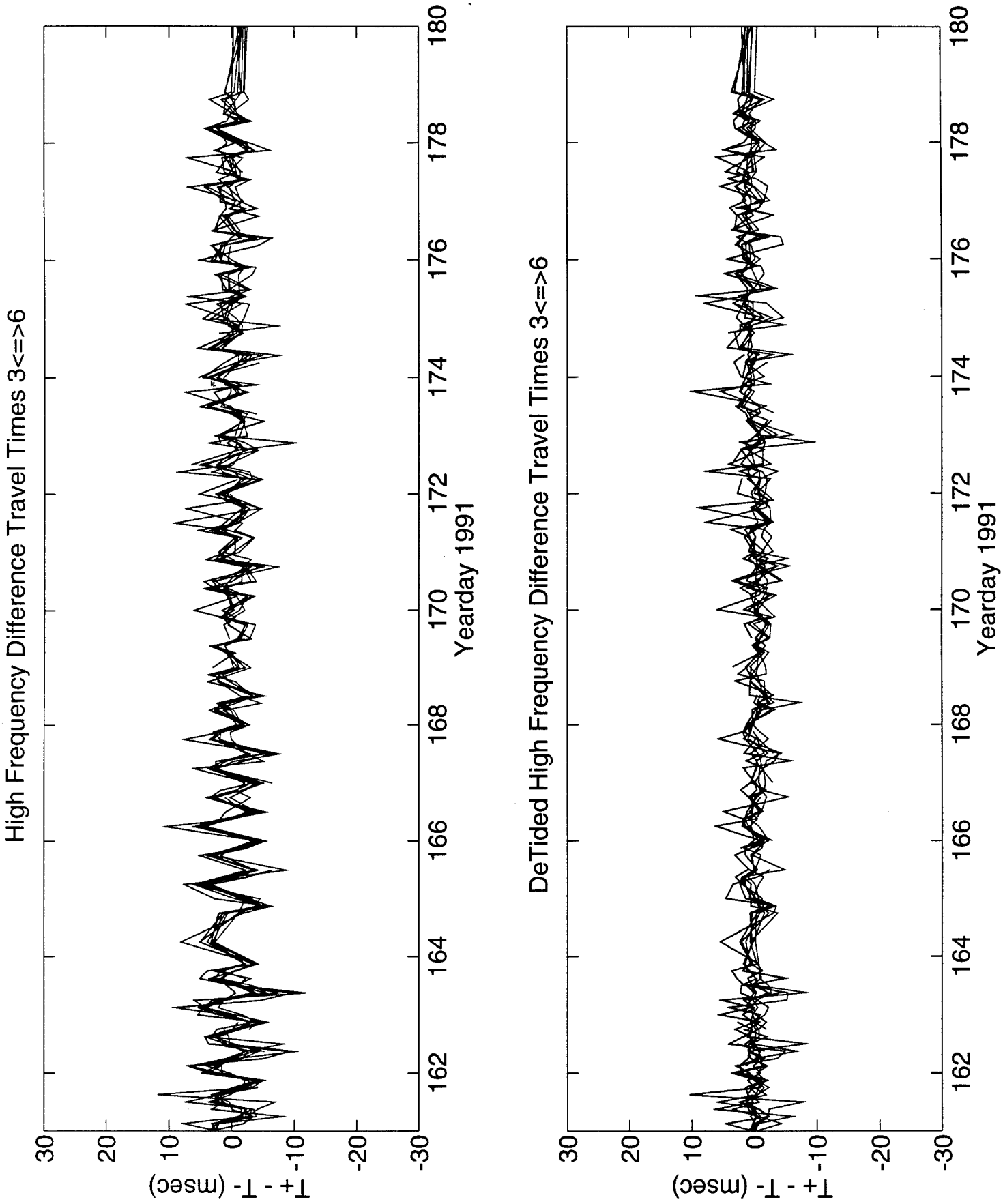
High Frequency Difference Travel Times 3<=>6
T+ - T- (msec)
30
20
10
0
-10
-20
-30
162
164
166
168
170
172
174
176
178
180
Yearday 1991
DeTided High Frequency Difference Travel Times 3<=>6
T+ - T- (msec)
30
20
10
0
-10
-20
-30
162
164
166
168
170
172
174
176
178
180
Yearday 1991

FIGURE U-3

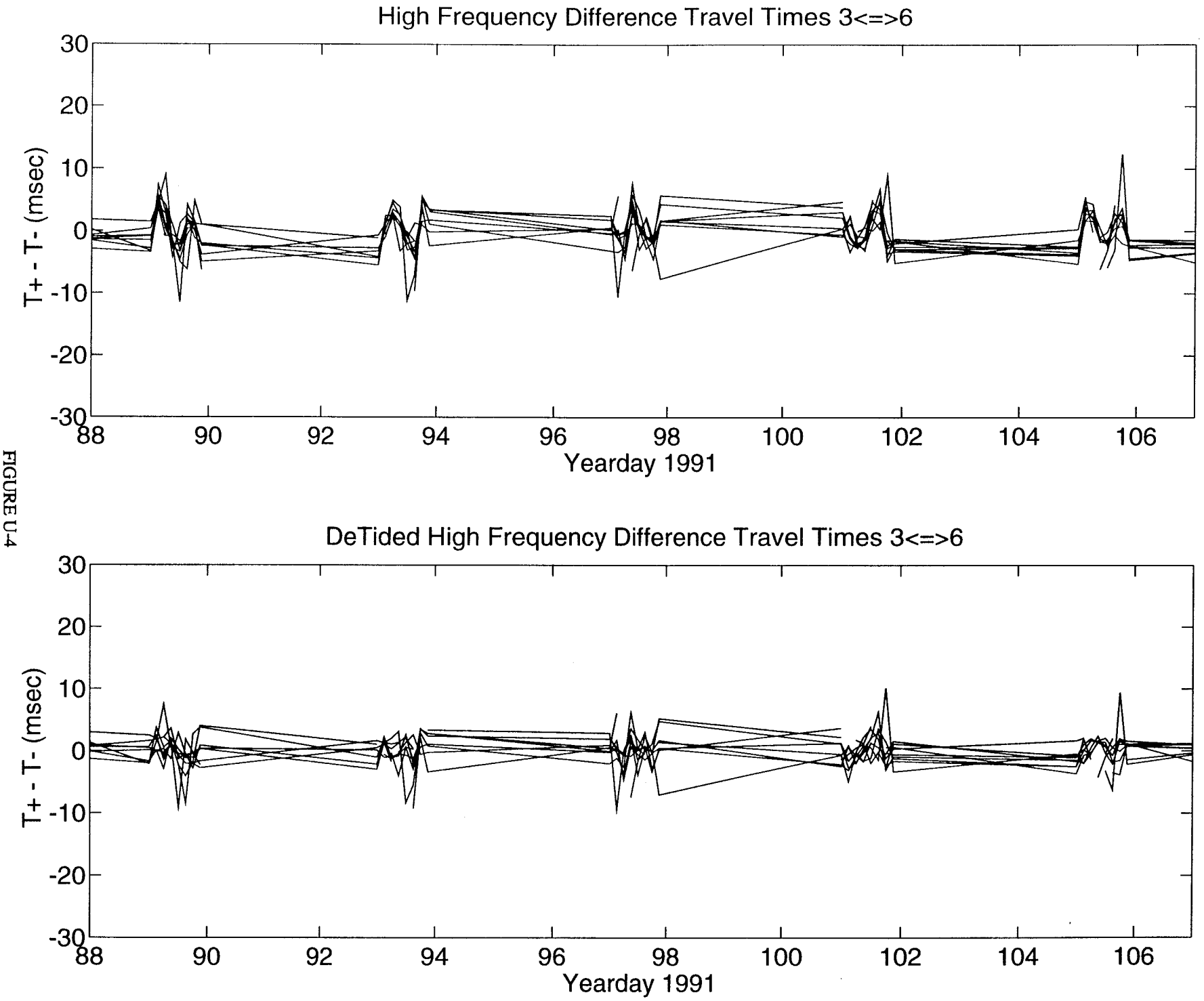
High Frequency Difference Travel Times 3<=>6
T+ - T- (msec)
30
20
10
0
-10
-20
-30
88
90
92
94
96
98
100
102
104
106
Yearday 1991
DeTided High Frequency Difference Travel Times 3<=>6
T+ - T- (msec)
30
20
10
0
-10
-20
-30
88
90
92
94
96
98
100
102
104
106
Yearday 1991

FIGURE U-4

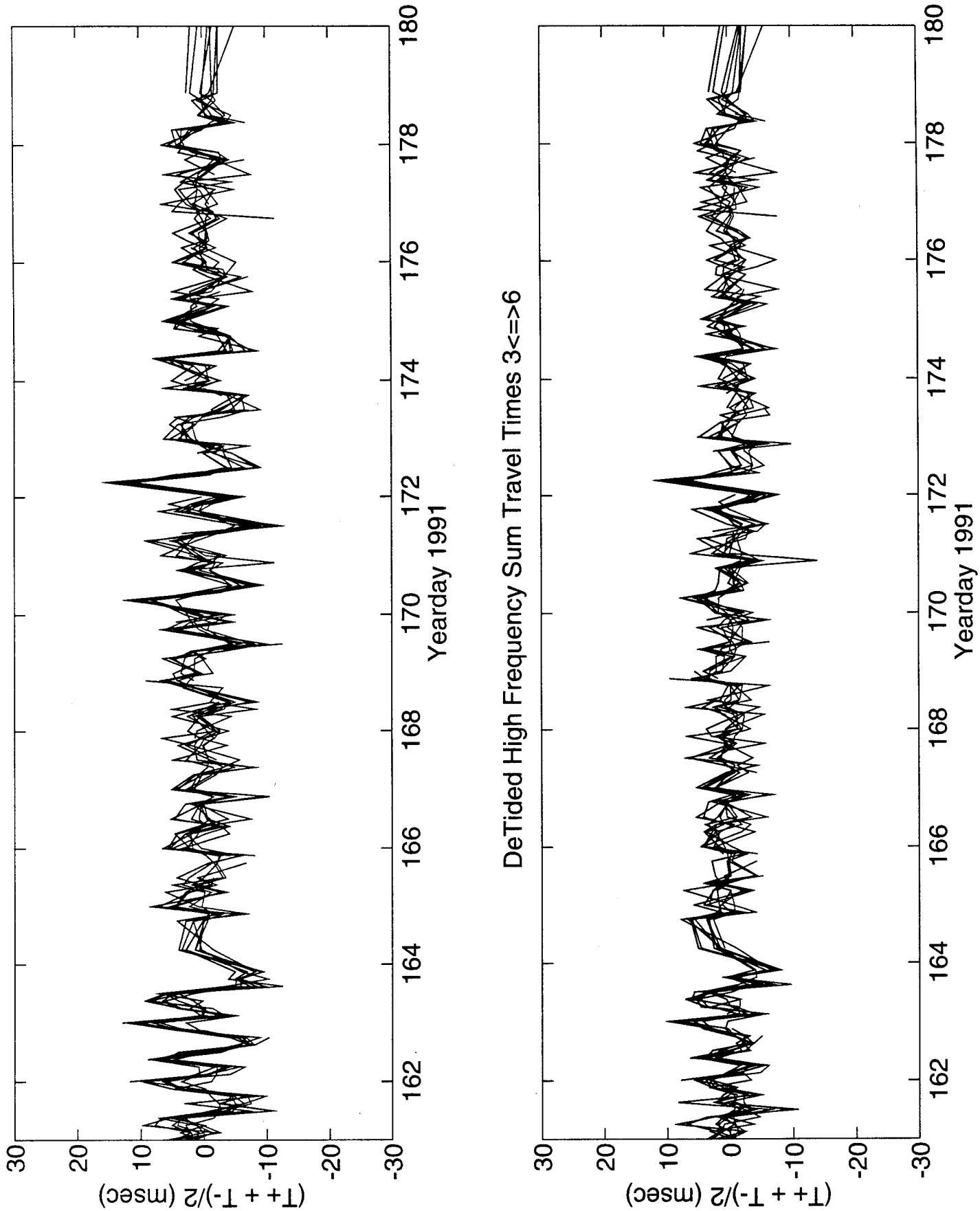
High Frequency Sum Travel Times 3<=>6
DeTided High Frequency Sum Travel Times 3<=>6
(T+ + T-)/2 (msec)
Yearday 1991
30
20
10
0
-10
-20
-30
162
164
166
168
170
172
174
176
178
180

FIGURE U-5

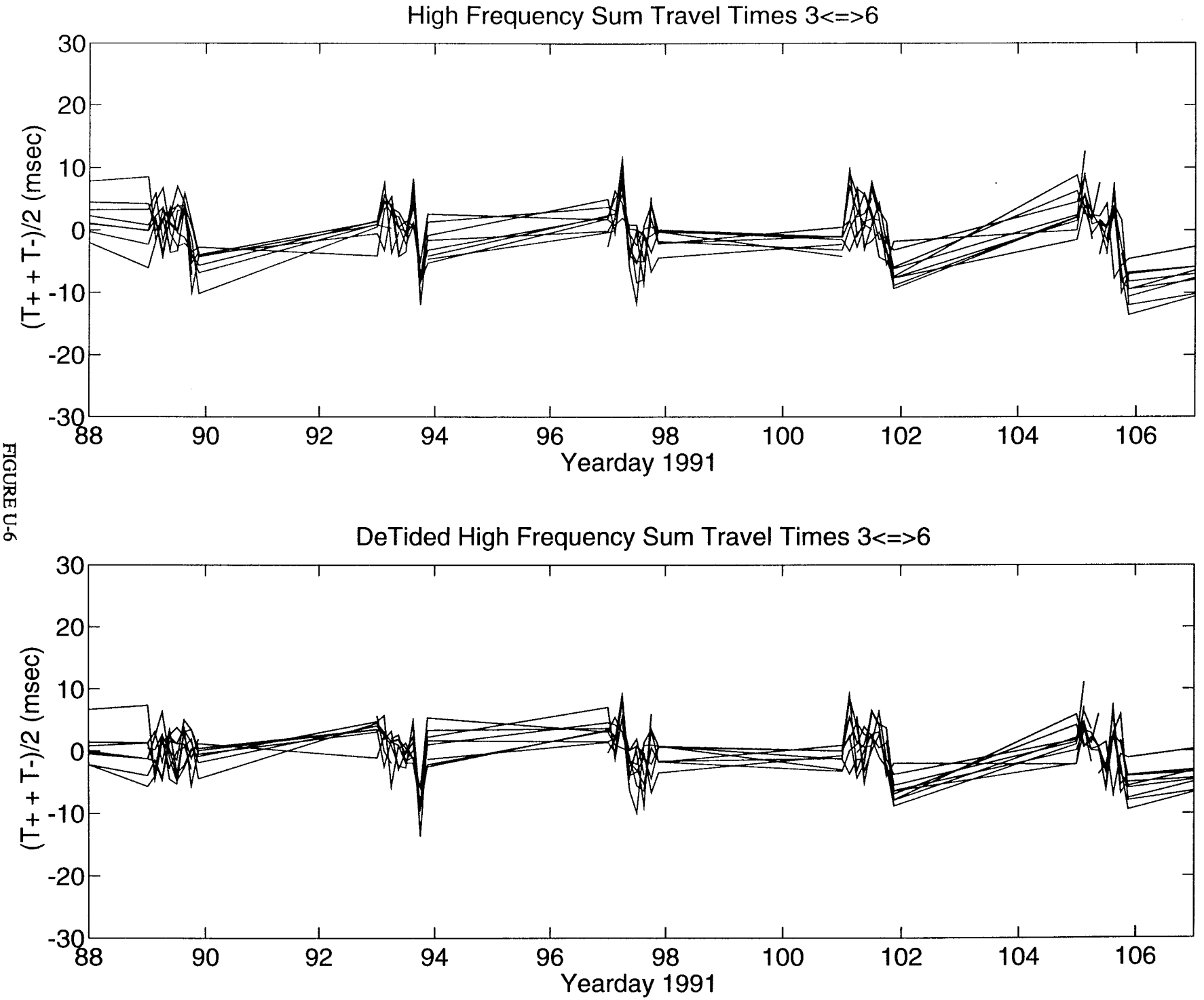
High Frequency Sum Travel Times 3<=>6
(T+ + T-)/2 (msec)
30
20
10
0
-10
-20
-30
88
90
92
94
96
98
100
102
104
106
Yearday 1991
DeTided High Frequency Sum Travel Times 3<=>6
(T+ + T-)/2 (msec)
30
20
10
0
-10
-20
-30
88
90
92
94
96
98
100
102
104
106
Yearday 1991

FIGURE U-6

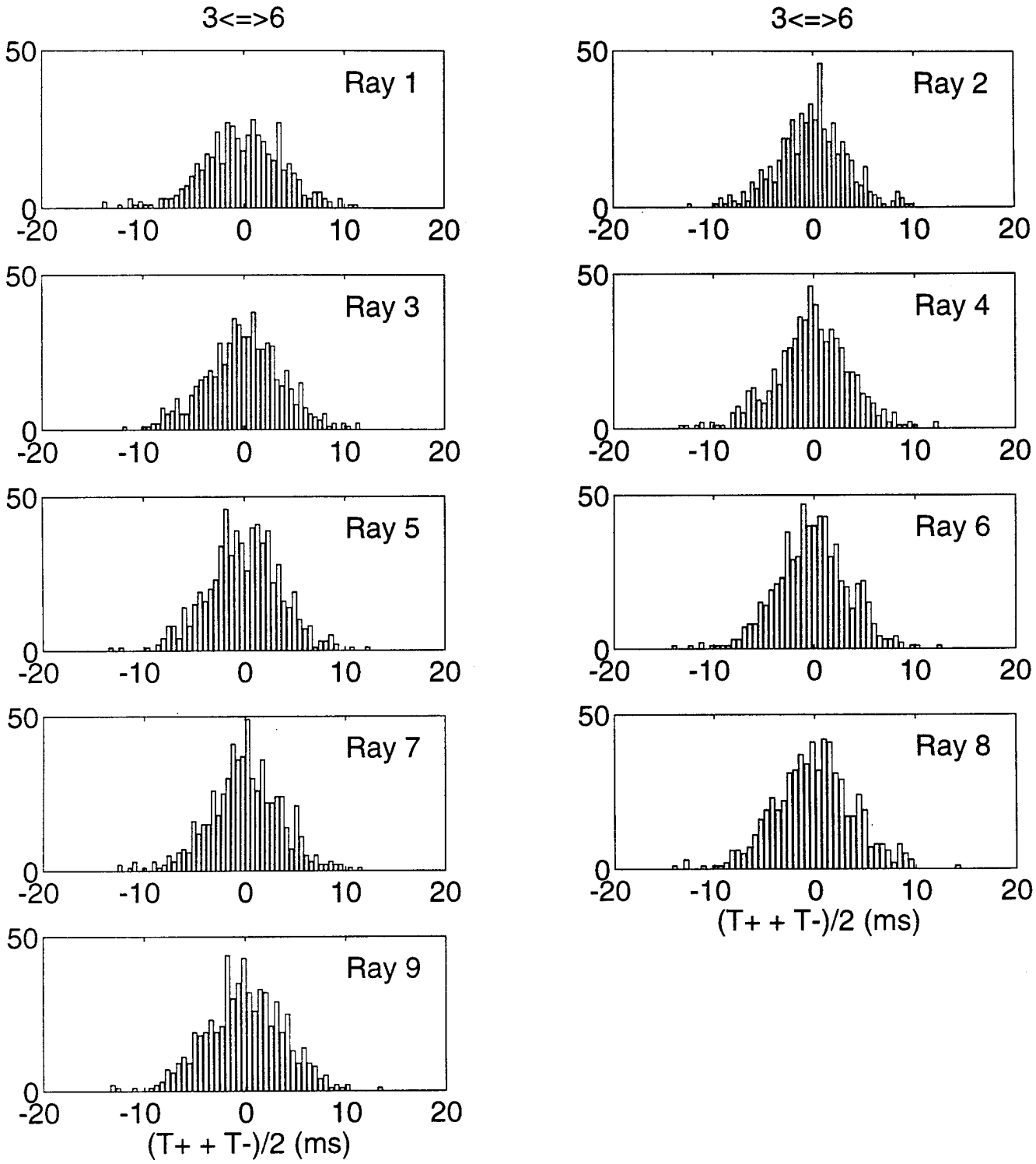
3<=>6
Ray 1
Ray 2
Ray 3
Ray 4
Ray 5
Ray 6
Ray 7
Ray 8
Ray 9
50
0
-20
-10
0
10
20
(T+ + T-)/2 (ms)

FIGURE U-7

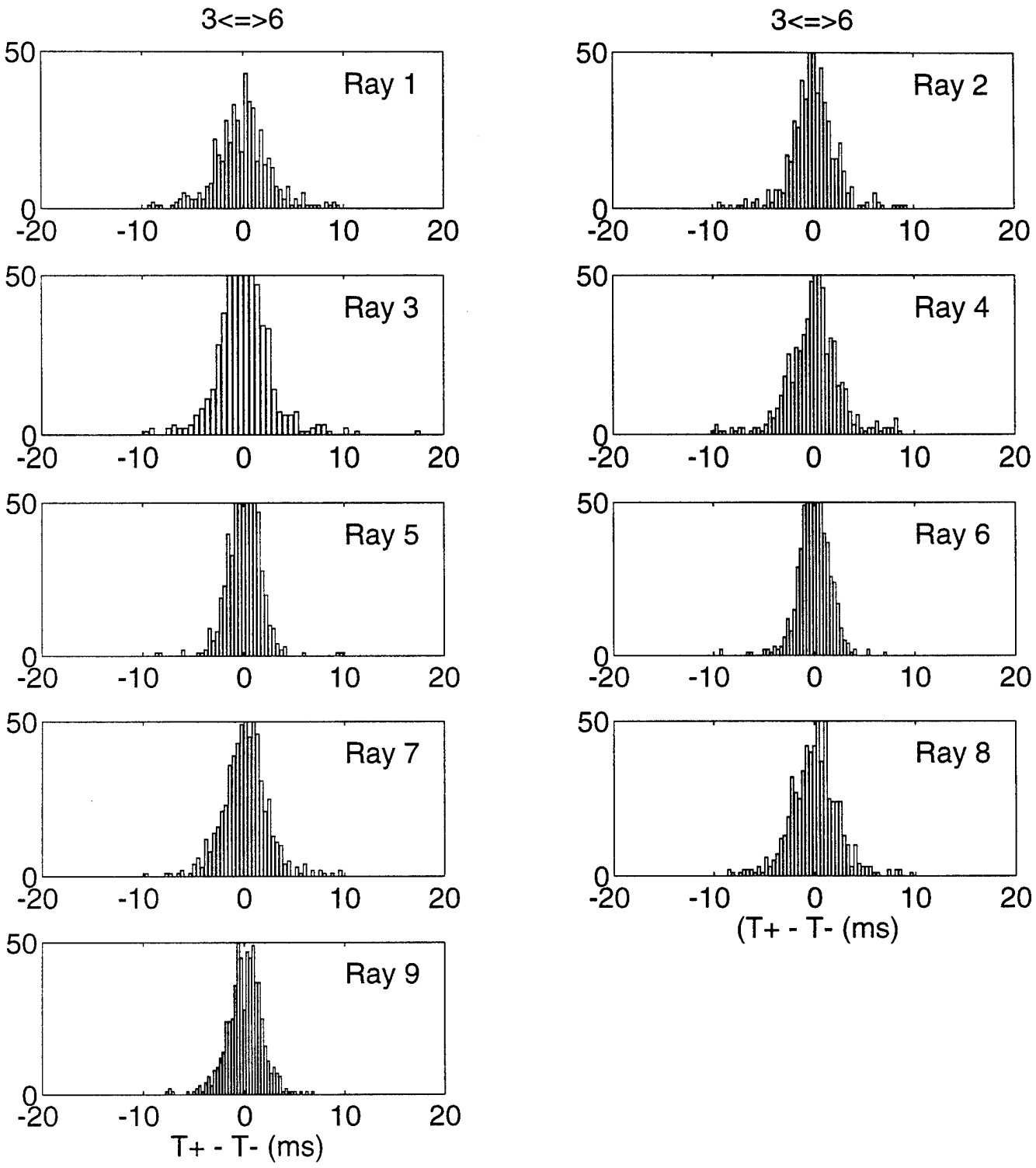
3<=>6
Ray 1
Ray 2
Ray 3
Ray 4
Ray 5
Ray 6
Ray 7
Ray 8
Ray 9
50
0
-20
-10
0
10
20
T+ - T- (ms)
(T+ - T- (ms)

FIGURE U-8

V. ACOUSTIC DATA: Paths 4→5a and 5a→4

FIGURE V-1 shows the raypaths, roughly corresponding to FIGURE G-1, for which travel times were resolved. The raypaths were actually determined using range-dependent Levitus sound speed, interpolated onto the acoustic path. Note that the "final cutoff" travel times may be available at some time in the future, these data correspond to a ray confined near the sound channel axis.

FIGURE V-2 shows the low-pass filtered difference (top panel) and sum (bottom panel) travel times corresponding to the rays of FIGURE V-1. Note that mooring 5a had failed by yearday 140, to be replaced later by mooring 5b.

FIGURE V-3 shows the high-pass filtered difference travel times for a small portion of the time series obtained during the time of more frequent transmissions during the MST experiment. The bottom panel shows the time series after the phase-locked tidal signals have been removed.

FIGURE V-4 shows the high-pass filtered sum travel times for a small portion of the time series obtained during the time of more frequent transmissions during the MST experiment. The bottom panel shows the time series after the phase-locked tidal signals have been removed. This tidal variability is caused by the internal tide.

After the travel time time series have been edited for outliers, high-pass filtered, and detided, the high-frequency variances are calculated (TABLE V-1). Note that this table sometimes contains statistics for more rays than are indicated in TABLE B-1; some of the ray arrivals in TABLE V-1 have not been identified with predicted arrivals. Also, sometimes there is initial ambiguity about the pairing of reciprocal arrivals, in which case sum and difference travel times are calculated for all reasonable cases; later it becomes obvious which arrivals have been improperly paired. The correlation $<T^+ T^->$ and variance $<T^2>$ are calculated from the sum and difference travel time variances in this table. The variance of the travel times is mainly due to internal wave variability, and this value determines the uncertainties assigned to the travel times in an inversion. The correlation coefficient is a measure of the reciprocity of reciprocal raypaths. This measure is conservative, because correlation is not a necessary condition for the determination of current from the difference of reciprocal travel times. Values of correlation that are 0.5 or greater assure that the reciprocal raypaths are indeed effectively identical, since good correlation implies that the reciprocal raypaths have not separated by more than an internal wave correlation length. Histograms of the detided, high-frequency travel times are shown in FIGURES V-5 and V-6; the variances from TABLE V-1 are measures of the width of these histograms.

TABLES V-2 and V-3 show the results of tidal analysis of the time series of difference (current) and sum (sound speed) travel times. For these tables, the tidal analysis is performed on each travel time time series separately and then the average and rms of the harmonic constants are calculated. Current or sound speed amplitude is determined from travel time by a simple scaling factor; the harmonic constants are more accurately determined by inverting the data for current or sound speed (this is not done here).

TABLE V-1. Travel Time Statistics 4←→5a.

Ray #	Number of data	$<(T^+ + T^-)^2>$ (ms^2)	$<(T^+ - T^-)^2>$ (ms^2)	$<T^+ T^->$ (ms^2)	$<T^2>$ (ms^2)	$\frac{<T^+ T^->}{<T^2>}$
1	80	8	8	6	10	0.60
2	72	12	7	10	13	0.73
3	79	21	6	20	23	0.87
4	68	10	12	7	13	0.53
5	74	11	11	8	14	0.60
6	73	13	6	11	14	0.78
7	84	9	6	8	11	0.73
8	89	5	3	5	6	0.75
9	86	11	4	10	13	0.83
10	85	9	6	7	10	0.71
11	92	11	6	10	13	0.77

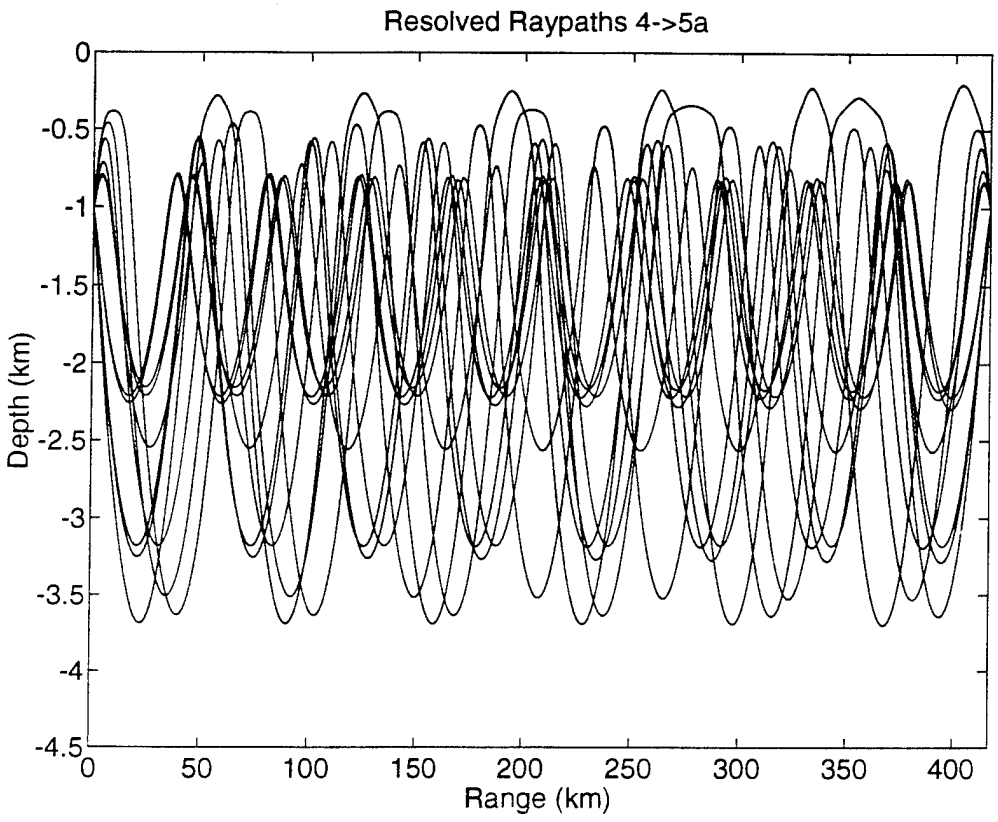

FIGURE V-1

TABLE V-2. Tidal Current Harmonic Constants 4←→5a.

Constituent	Amplitude (mm/s)	Uncertainty (mm/s)	Phase (°G)	Uncertainty (°)
M_2	5.39	1.72	288.8	26.9
S_2	3.54	1.50	184.0	124.1
N_2	1.97	1.25	238.8	75.5
K_2	3.65	1.26	31.6	80.4
O_1	1.65	0.65	84.5	84.5
K_1	3.98	2.53	192.5	127.5
P_1	4.26	2.49	123.0	93.1
Q_1	2.02	1.18	210.5	104.2

Values and their uncertainty are determined by the average and rms of harmonic constants from tidal analyses of the separate raypath travel time series. The amplitudes do not include the lunar node factors. 41 ± 9 % of the high-frequency variance is accounted for by the tides.

TABLE V-3. Tidal Sound Speed Harmonic Constants 4←→5a.

Constituent	Amplitude (mm/s)	Uncertainty (mm/s)	Phase (°G)	Uncertainty (°)
M_2	5.26	1.62	188.1	27.1
S_2	6.00	2.40	318.9	79.2
N_2	2.79	1.49	134.3	41.2
K_2	5.91	2.65	232.9	89.2
O_1	3.13	0.91	44.0	39.0
K_1	3.15	2.06	187.8	89.1
P_1	4.17	3.24	194.8	58.3
Q_1	2.24	1.17	216.9	103.4

Values and their uncertainty are determined by the average and rms of harmonic constants from tidal analyses of the separate raypath travel time series. The amplitudes do not include the lunar node factors. 42 ± 10 % of the high-frequency variance is accounted for by the tides. Because sum travel times are used to derive these numbers, the amplitudes have been divided by a factor of two compared to the amplitudes for current.

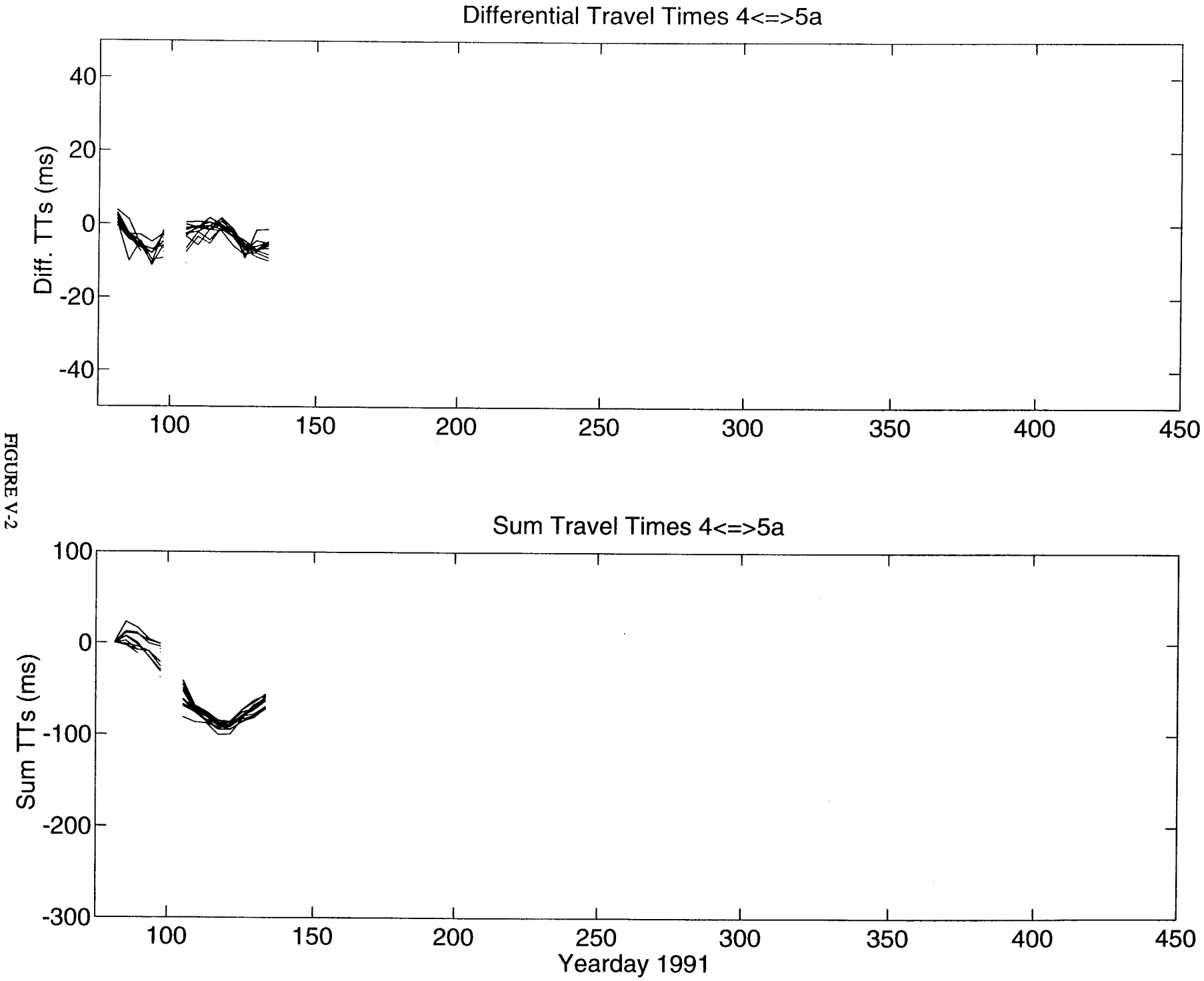
Differential Travel Times 4<=>5a
Diff. TTs (ms)
40
20
0
-20
-40
100
150
200
250
300
350
400
450
Sum Travel Times 4<=>5a
Sum TTs (ms)
100
0
-100
-200
-300
100
150
200
250
300
350
400
450
Yearday 1991

FIGURE V-2

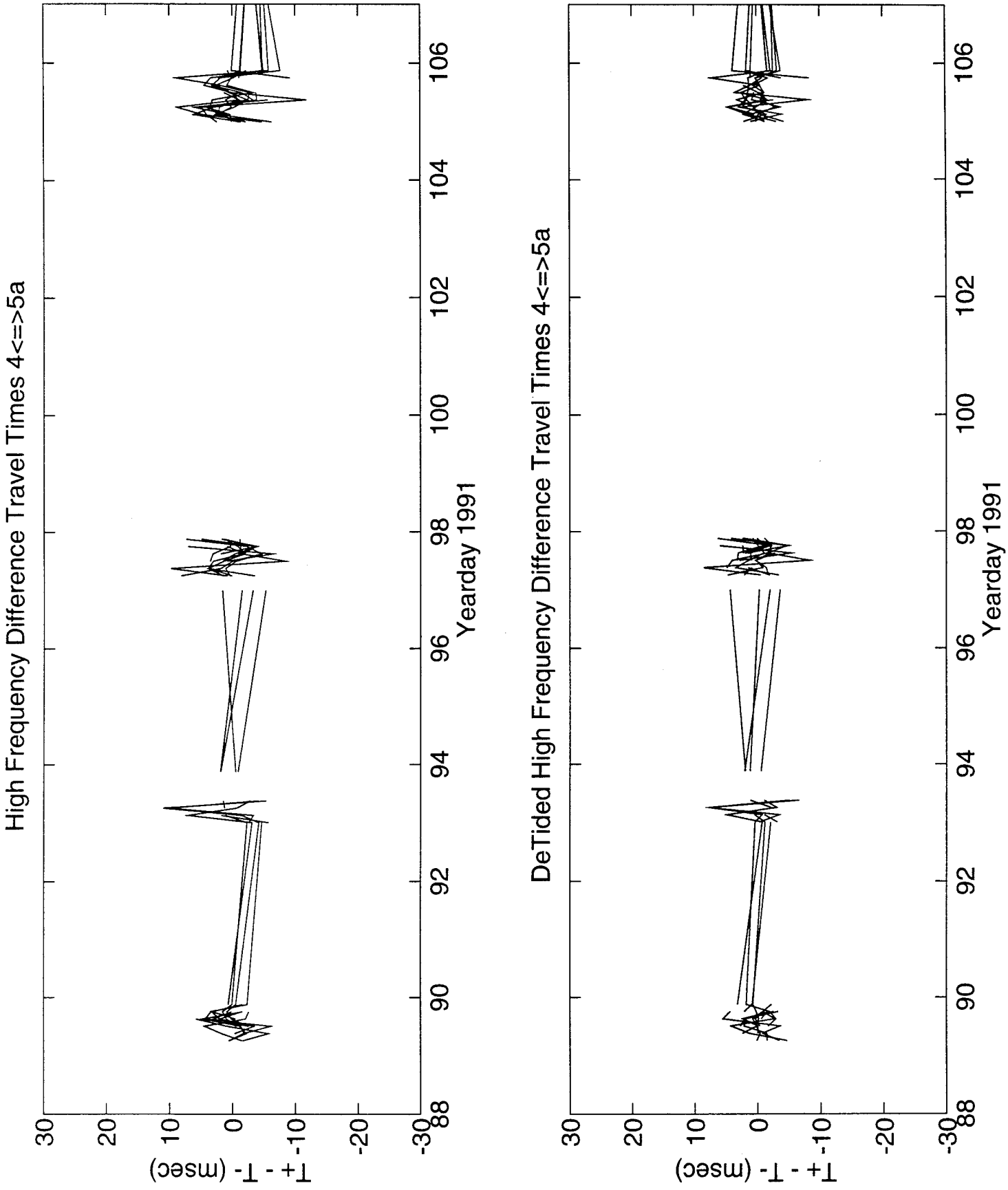
High Frequency Difference Travel Times 4<=>5a
DeTided High Frequency Difference Travel Times 4<=>5a
T+ - T- (msec)
Yearday 1991
30
20
10
0
-10
-20
-30
88
90
92
94
96
98
100
102
104
106

FIGURE V-3

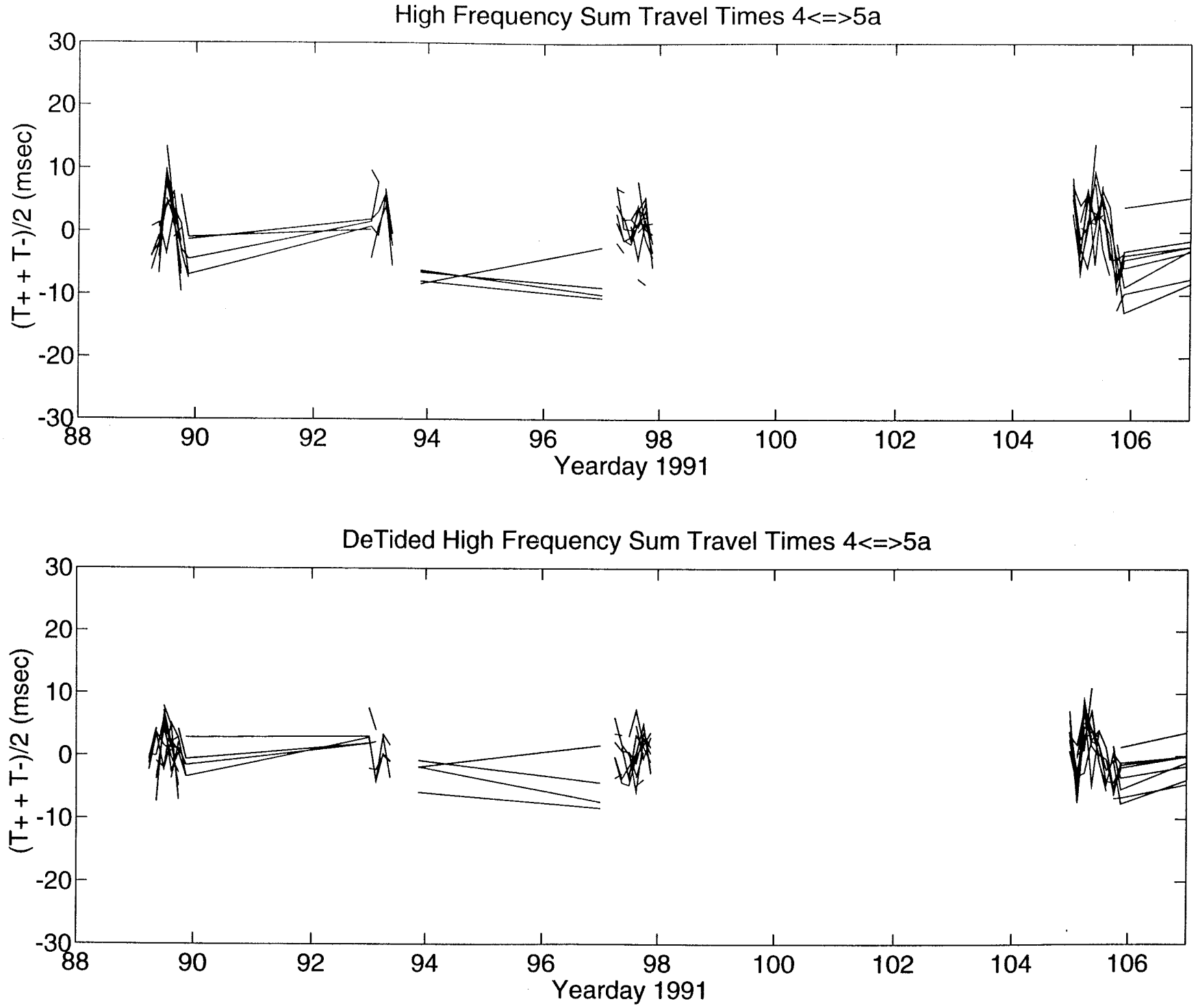
High Frequency Sum Travel Times 4<=>5a
(T+ + T-)/2 (msec)
30
20
10
0
-10
-20
-30
88
90
92
94
96
98
100
102
104
106
Yearday 1991
DeTided High Frequency Sum Travel Times 4<=>5a
(T+ + T-)/2 (msec)
30
20
10
0
-10
-20
-30
88
90
92
94
96
98
100
102
104
106
Yearday 1991

FIGURE V-4

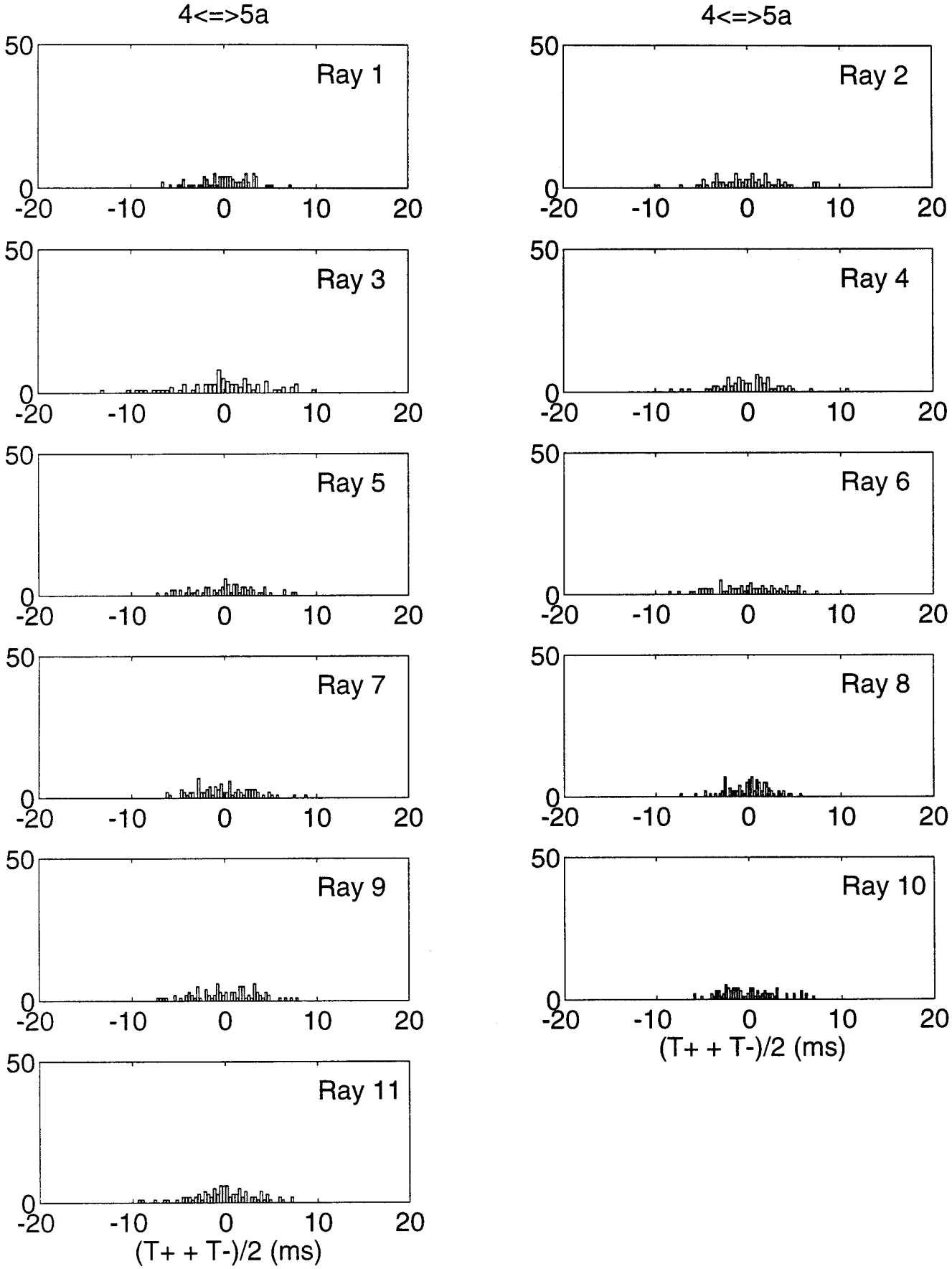
4<=>5a
4<=>5a
Ray 1
Ray 2
Ray 3
Ray 4
Ray 5
Ray 6
Ray 7
Ray 8
Ray 9
Ray 10
Ray 11
50
0
-20
-10
0
10
20
(T+ + T-)/2 (ms)

FIGURE V-5

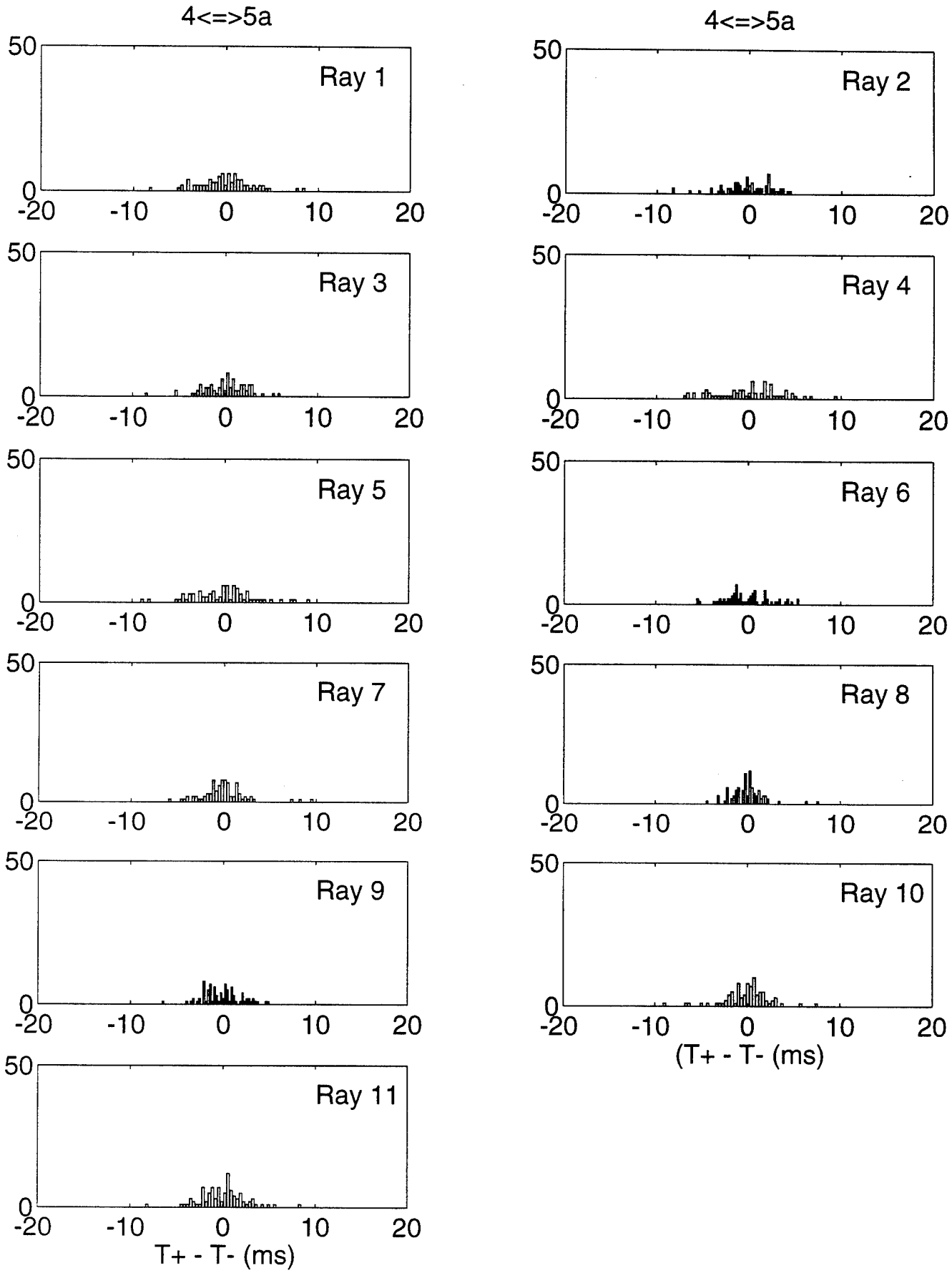
4<=>5a
Ray 1
Ray 2
Ray 3
Ray 4
Ray 5
Ray 6
Ray 7
Ray 8
Ray 9
Ray 10
Ray 11
50
0
-20
-10
0
10
20
T+ - T- (ms)

FIGURE V-6

W. ACOUSTIC DATA: Paths 4→5b and 5b→4

FIGURE W-1 shows the raypaths, corresponding roughly to FIGURE G-1, for which travel times were resolved. The raypaths were actually determined using range-dependent Levitus sound speed, interpolated onto the acoustic path. Note that the "final cutoff" travel times may be available at some time in the future, these data correspond to a ray confined near the sound channel axis.

FIGURE W-2 shows the low-pass filtered difference (top panel) and sum (bottom panel) travel times corresponding to the rays of FIGURE W-1.

FIGURE W-3 shows the high-pass filtered difference travel times for a small portion of the time series obtained during the time of more frequent transmissions during the MST experiment. The bottom panel shows the time series after the phase-locked tidal signals have been removed.

FIGURE W-4 shows the high-pass filtered sum travel times for a small portion of the time series obtained during the time of more frequent transmissions during the MST experiment. The bottom panel shows the time series after the phase-locked tidal signals have been removed. This tidal variability is caused by the internal tide.

After the travel time time series have been edited for outliers, high-pass filtered, and detided, the high-frequency variances are calculated (TABLE W-1). Note that this table sometimes contains statistics for more rays than are indicated in TABLE B-1; some of the ray arrivals in TABLE W-1 have not been identified with predicted arrivals. Also, sometimes there is initial ambiguity about the pairing of reciprocal arrivals, in which case sum and difference travel times are calculated for all reasonable cases; later it becomes obvious which arrivals have been improperly paired. The correlation $<T^+ T^->$ and variance $<T^2>$ are calculated from the sum and difference travel time variances in this table. The variance of the travel times is mainly due to internal wave variability, and this value determines the uncertainties assigned to the travel times in an inversion. The correlation coefficient is a measure of the reciprocity of reciprocal raypaths. This measure is conservative, because correlation is not a necessary condition for the determination of current from the difference of reciprocal travel times. Values of correlation that are 0.5 or greater assure that the reciprocal raypaths are indeed effectively identical, since good correlation implies that the reciprocal raypaths have not separated by more than an internal wave correlation length. Histograms of the detided, high-frequency travel times are shown in FIGURES W-5 and W-6; the variances from TABLE W-1 are measures of the width of these histograms.

TABLES W-2 and W-3 show the results of tidal analysis of the time series of difference (current) and sum (sound speed) travel times. For these tables, the tidal analysis is performed on each travel time time series separately and then the average and rms of the harmonic constants are calculated. Current or sound speed amplitude is determined from travel time by a simple scaling factor; the harmonic constants are more accurately determined by inverting the data for current or sound speed (this is not done here).

TABLE W-1. Travel Time Statistics 4←→5b.

Ray #	Number of data	$\langle (T^+ + T^-)^2 \rangle$ (ms^2)	$\langle (T^+ - T^-)^2 \rangle$ (ms^2)	$\langle T^+ T^- \rangle$ (ms^2)	$\langle T^2 \rangle$ (ms^2)	$\frac{\langle T^+ T^- \rangle}{\langle T^2 \rangle}$
1	133	7	8	5	9	0.52
2	265	14	10	12	16	0.71
3	285	17	12	14	20	0.71
4	278	13	7	12	15	0.78
5	276	14	12	11	17	0.65
6	289	12	10	10	15	0.65
7	279	22	9	20	24	0.81
8	331	15	5	13	16	0.83
9	351	9	3	8	10	0.82
10	330	9	5	8	10	0.75
11	321	11	4	10	12	0.85
12	340	12	5	10	13	0.81

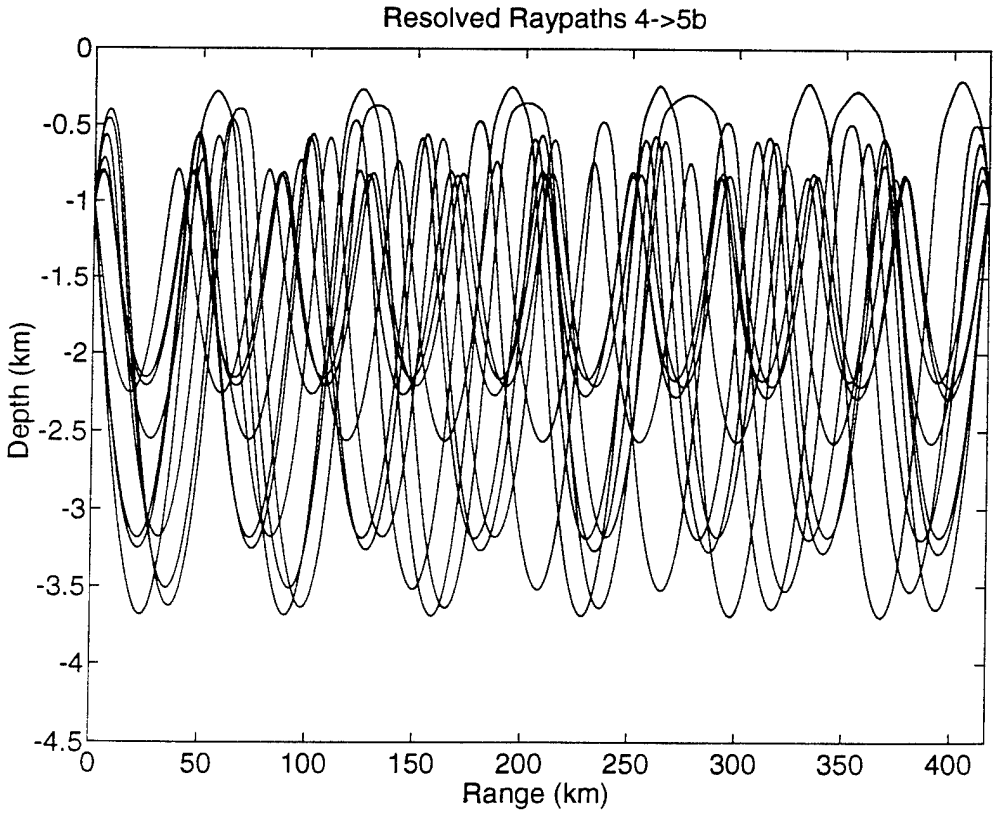

FIGURE W-1

TABLE W-2. Tidal Current Harmonic Constants 4←→5b.

Constituent	Amplitude (mm/s)	Uncertainty (mm/s)	Phase (°G)	Uncertainty (°)
M_2	5.54	0.75	286.1	8.4
S_2	1.52	1.12	316.7	45.6
N_2	1.38	0.52	248.6	31.4
K_2	1.34	0.89	338.3	50.5
O_1	0.92	0.61	205.7	119.7
K_1	1.95	0.78	56.7	36.2
P_1	1.03	0.56	198.8	145.1
Q_1	1.17	0.65	56.3	98.1

Values and their uncertainty are determined by the average and rms of harmonic constants from tidal analyses of the separate raypath travel time series. The amplitudes do not include the lunar node factors. 33 ± 9 % of the high-frequency variance is accounted for by the tides.

TABLE W-3. Tidal Sound Speed Harmonic Constants 4←→5b.

Constituent	Amplitude (mm/s)	Uncertainty (mm/s)	Phase (°G)	Uncertainty (°)
M_2	8.26	1.23	147.0	10.9
S_2	1.35	0.59	300.8	63.9
N_2	3.92	1.00	100.8	17.6
K_2	1.75	0.75	268.4	37.9
O_1	1.36	1.01	47.5	57.1
K_1	2.43	1.02	106.5	35.3
P_1	2.01	1.10	66.5	45.8
Q_1	1.75	0.88	345.2	30.1

Values and their uncertainty are determined by the average and rms of harmonic constants from tidal analyses of the separate raypath travel time series. The amplitudes do not include the lunar node factors. 38 ± 8 % of the high-frequency variance is accounted for by the tides. Because sum travel times are used to derive these numbers, the amplitudes have been divided by a factor of two compared to the amplitudes for current.

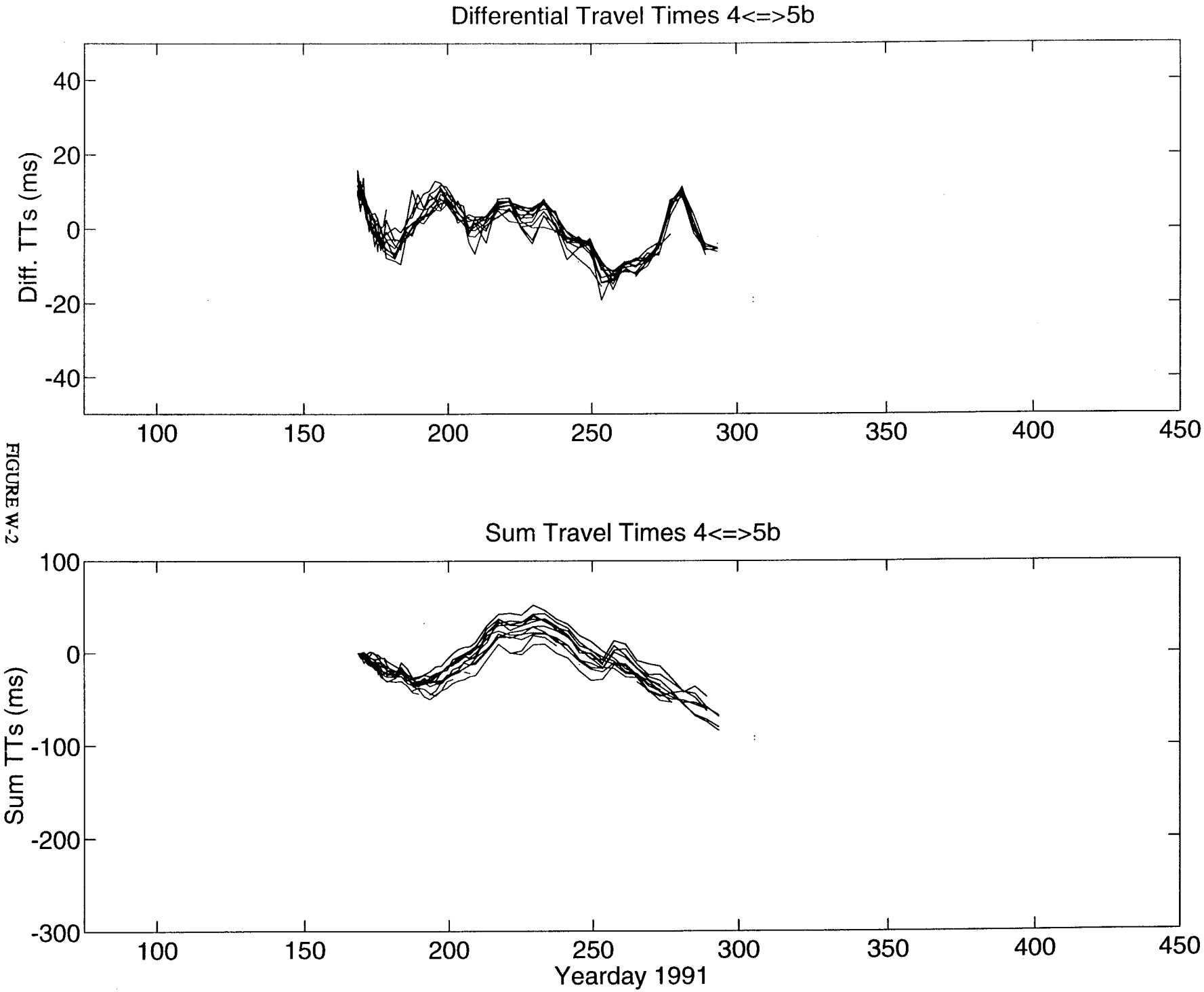
Differential Travel Times 4<=>5b
Diff. TTs (ms)
40
20
0
-20
-40
100
150
200
250
300
350
400
450
Sum Travel Times 4<=>5b
Sum TTs (ms)
100
0
-100
-200
-300
100
150
200
250
300
350
400
450
Yearday 1991

FIGURE W-2

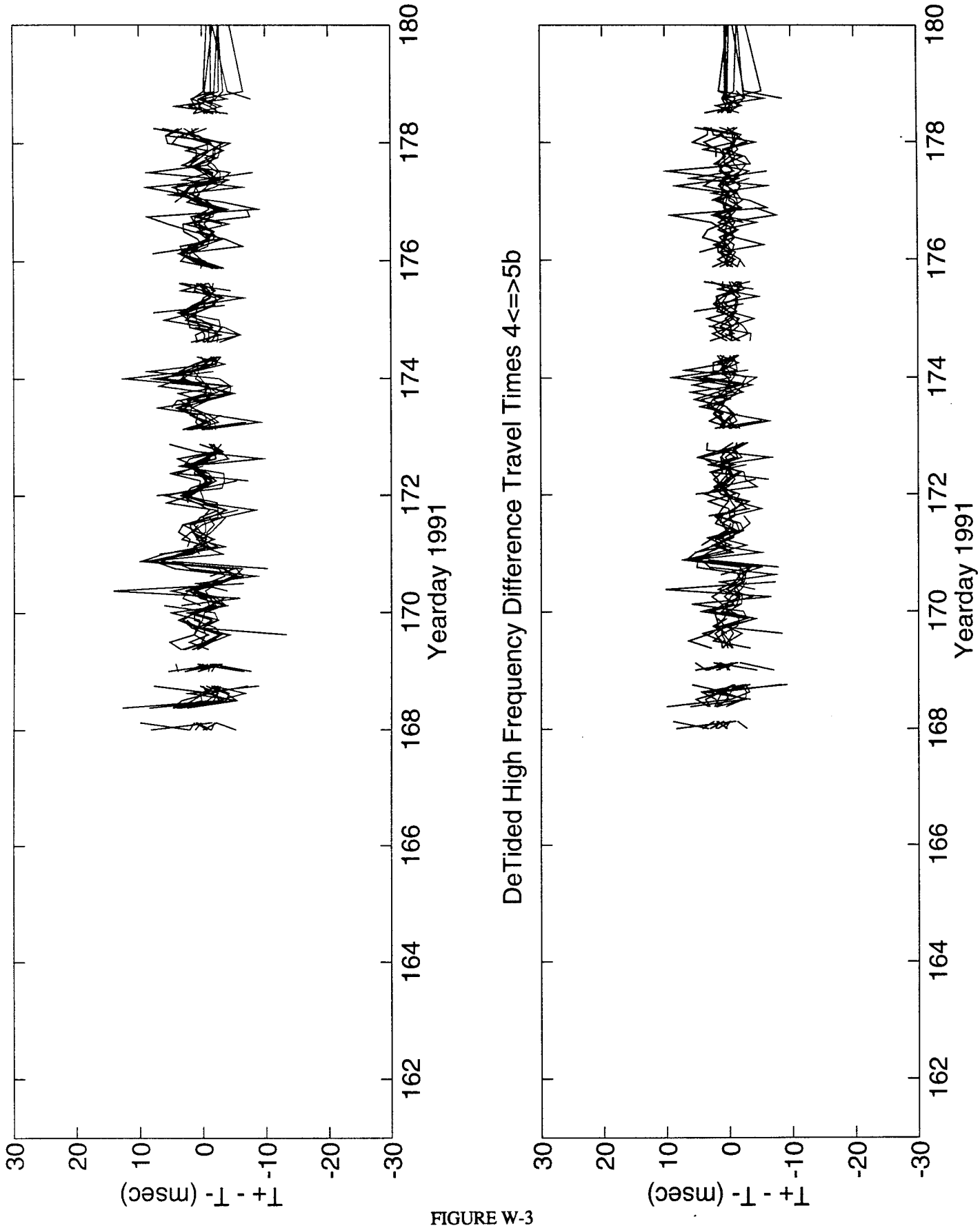
High Frequency Difference Travel Times 4<=>5b
DeTided High Frequency Difference Travel Times 4<=>5b
T+ - T- (msec)
Yearday 1991
30
20
10
0
-10
-20
-30
162
164
166
168
170
172
174
176
178
180

FIGURE W-3

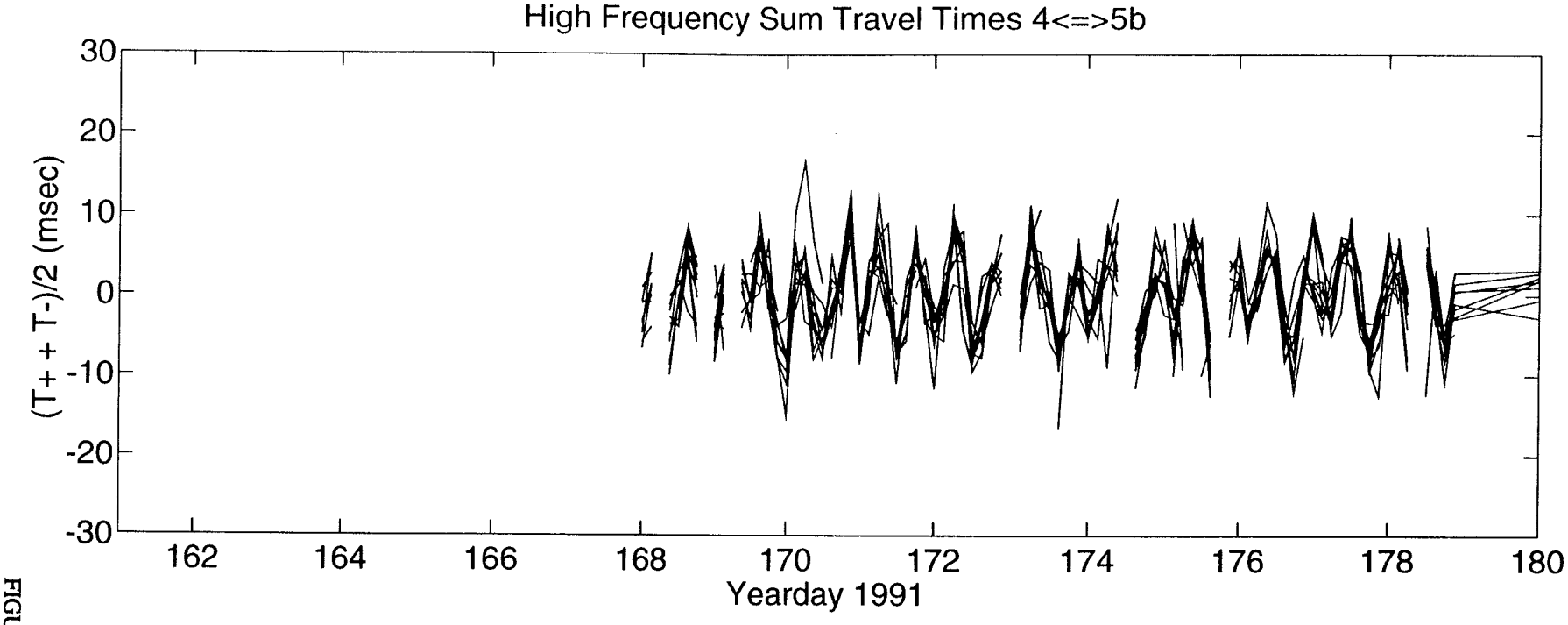
High Frequency Sum Travel Times 4<=>5b
(T+ + T-)/2 (msec)
30
20
10
0
-10
-20
-30
162
164
166
168
170
172
174
176
178
180
Yearday 1991

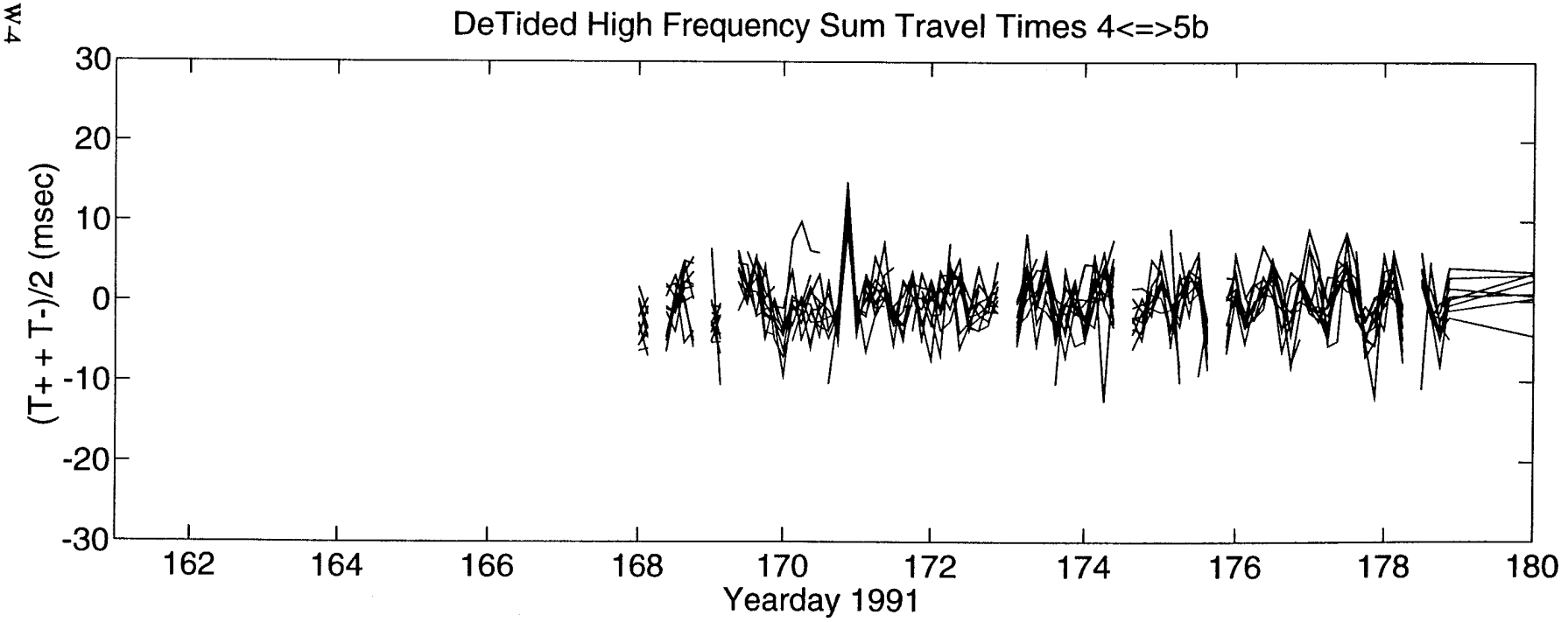
DeTided High Frequency Sum Travel Times 4<=>5b
(T+ + T-)/2 (msec)
30
20
10
0
-10
-20
-30
162
164
166
168
170
172
174
176
178
180
Yearday 1991

FIGURE W-4

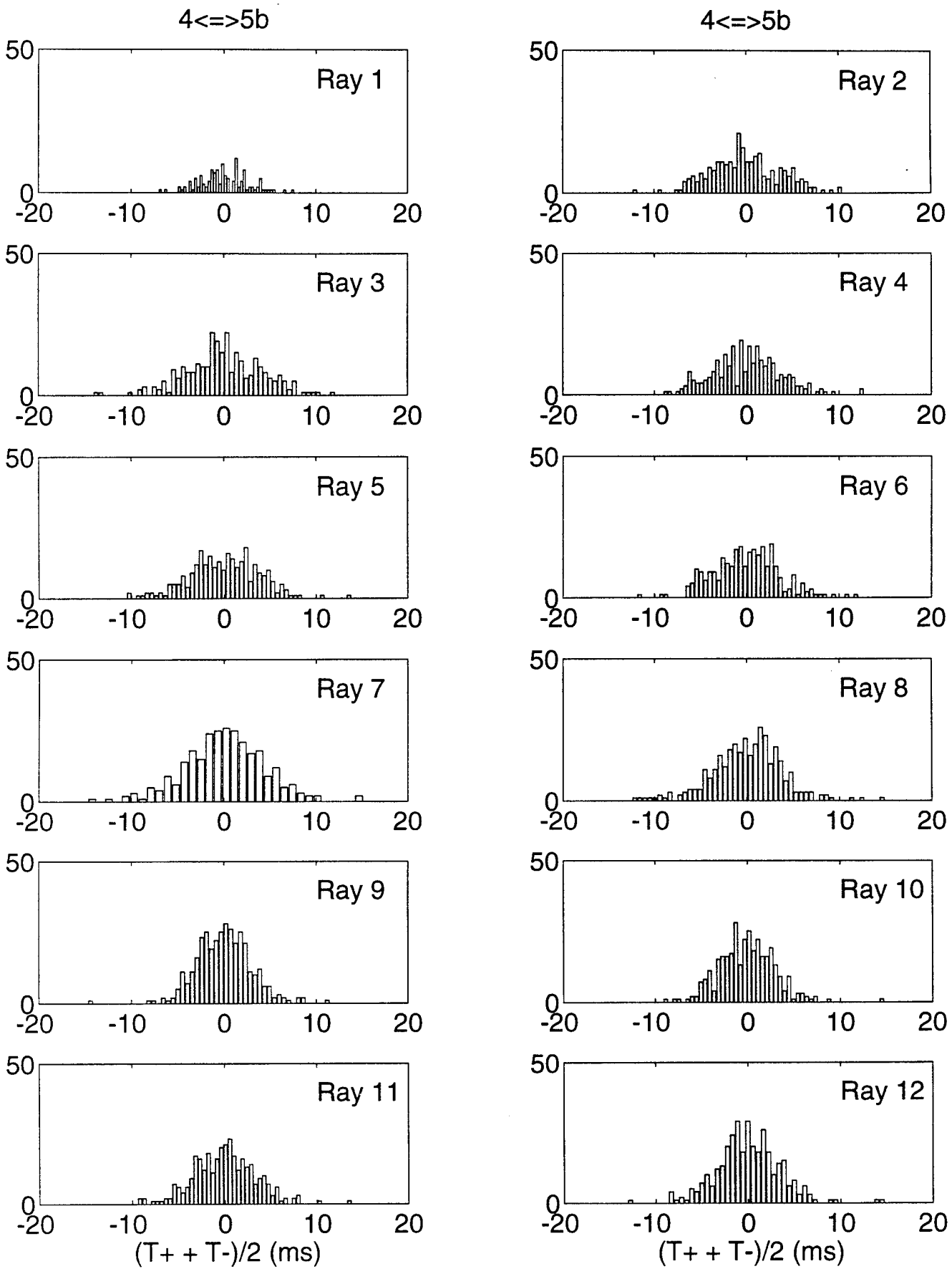
4<=>5b
4<=>5b
Ray 1
Ray 2
Ray 3
Ray 4
Ray 5
Ray 6
Ray 7
Ray 8
Ray 9
Ray 10
Ray 11
Ray 12
50
0
-20
-10
0
10
20
(T+ + T-)/2 (ms)

FIGURE W-5

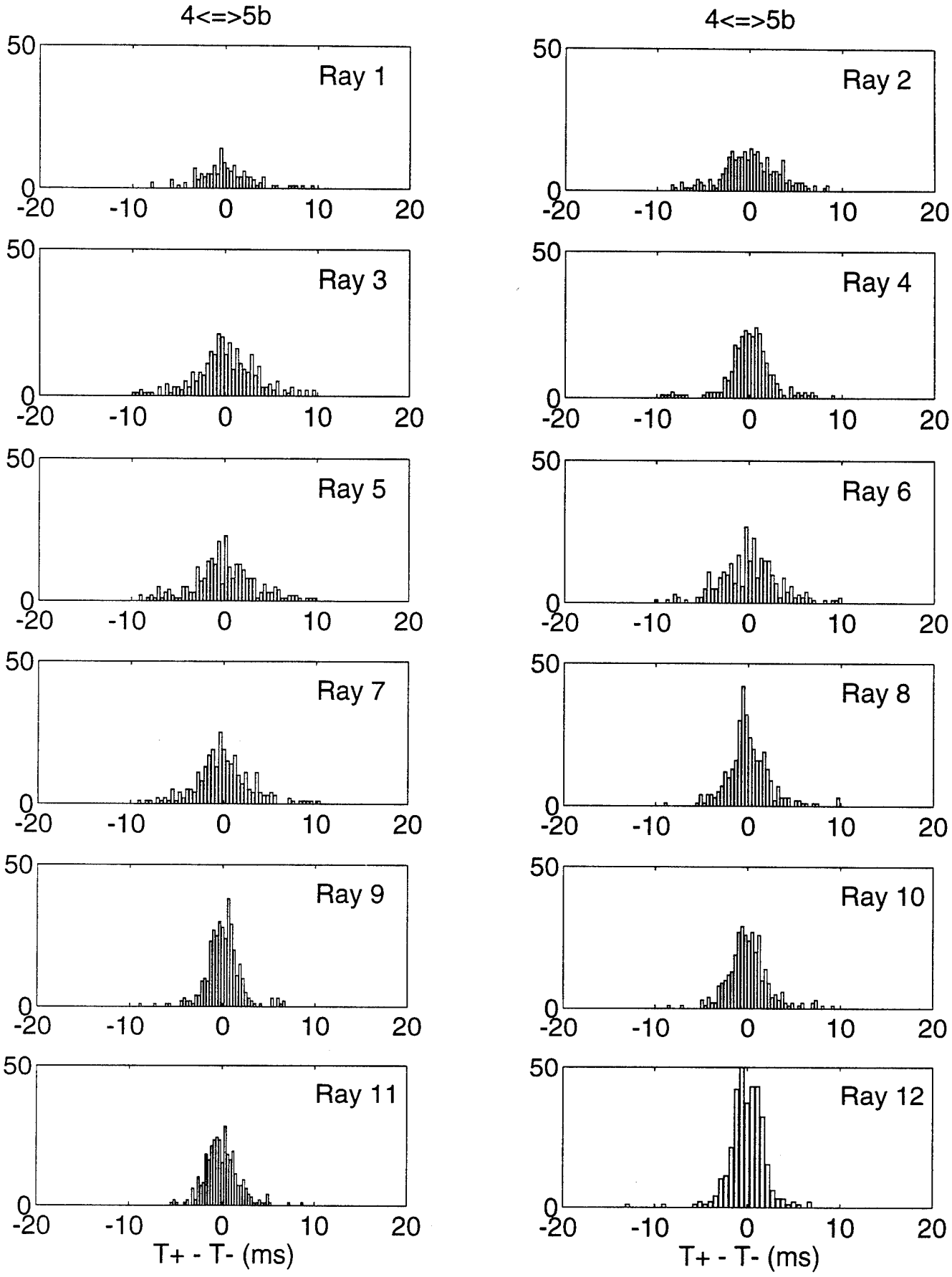
4<=>5b
4<=>5b
Ray 1
Ray 2
Ray 3
Ray 4
Ray 5
Ray 6
Ray 7
Ray 8
Ray 9
Ray 10
Ray 11
Ray 12
50
0
-20
-10
0
10
20
T+ - T- (ms)

FIGURE W-6

X. *ACOUSTIC DATA: Paths 4→6 and 6→4*

FIGURE X-1 shows the raypaths, roughly corresponding to FIGURE G-1, for which travel times were resolved. The raypaths were actually determined using range-dependent Levitus sound speed, interpolated onto the acoustic path. Note that the "final cutoff" travel times may be available at some time in the future, these data correspond to a ray confined near the sound channel axis.

FIGURE X-2 shows the low-pass filtered difference (top panel) and sum (bottom panel) travel times corresponding to the rays of FIGURE X-1.

FIGURE X-3 shows the high-pass filtered difference travel times for a small portion of the time series obtained during the time of more frequent transmissions during the MST experiment. The bottom panel shows the time series after the phase-locked tidal signals have been removed. FIGURE X-4 shows the same time series, but during a time of the normal transmission schedule.

FIGURE X-5 shows the high-pass filtered sum travel times for a small portion of the time series obtained during the time of more frequent transmissions during the MST experiment. The bottom panel shows the time series after the phase-locked tidal signals have been removed. This tidal variability is caused by the internal tide. FIGURE X-6 shows the same time series, but during a time of the normal transmission schedule.

After the travel time time series have been edited for outliers, high-pass filtered, and detided, the high-frequency variances are calculated (TABLE X-1). Note that this table sometimes contains statistics for more rays than are indicated in TABLE B-1; some of the ray arrivals in TABLE X-1 have not been identified with predicted arrivals. Also, sometimes there is initial ambiguity about the pairing of reciprocal arrivals, in which case sum and difference travel times are calculated for all reasonable cases; later it becomes obvious which arrivals have been improperly paired. The correlation $<T^+ T^->$ and variance $<T^2>$ are calculated from the sum and difference travel time variances in this table. The variance of the travel times is mainly due to internal wave variability, and this value determines the uncertainties assigned to the travel times in an inversion. The correlation coefficient is a measure of the reciprocity of reciprocal raypaths. This measure is conservative, because correlation is not a necessary condition for the determination of current from the difference of reciprocal travel times. Values of correlation that are 0.5 or greater assure that the reciprocal raypaths are indeed effectively identical, since good correlation implies that the reciprocal raypaths have not separated by more than an internal wave correlation length. Histograms of the detided, high-frequency travel times are shown in FIGURES X-7 and X-8; the variances from TABLE X-1 are measures of the width of these histograms.

TABLES X-2 and X-3 show the results of tidal analysis of the time series of difference (current) and sum (sound speed) travel times. For these tables, the tidal analysis is performed on each travel time time series separately and then the average and rms of the harmonic constants are calculated. Current or sound speed amplitude is determined from travel time by a simple scaling factor; the harmonic constants are more accurately determined by inverting the data for current or sound speed (this is not done here).

TABLE X-1. Travel Time Statistics 4←→6.

Ray #	Number of data	$\langle (T^+ + T^-)^2 \rangle$ (ms^2)	$\langle (T^+ - T^-)^2 \rangle$ (ms^2)	$\langle T^+ T^- \rangle$ (ms^2)	$\langle T^2 \rangle$ (ms^2)	$\frac{\langle T^+ T^- \rangle}{\langle T^2 \rangle}$
1	325	10	5	9	11	0.78
2	266	14	10	12	17	0.70
3	56	14	17	10	18	0.54
4	435	19	11	16	22	0.75
5	429	13	7	12	15	0.76
6	467	14	7	12	16	0.79
7	480	17	9	15	19	0.77
8	530	15	2	14	16	0.92
9	542	14	3	13	15	0.91
10	519	17	6	16	19	0.83
11	506	17	5	16	19	0.86
12	541	16	3	15	17	0.90

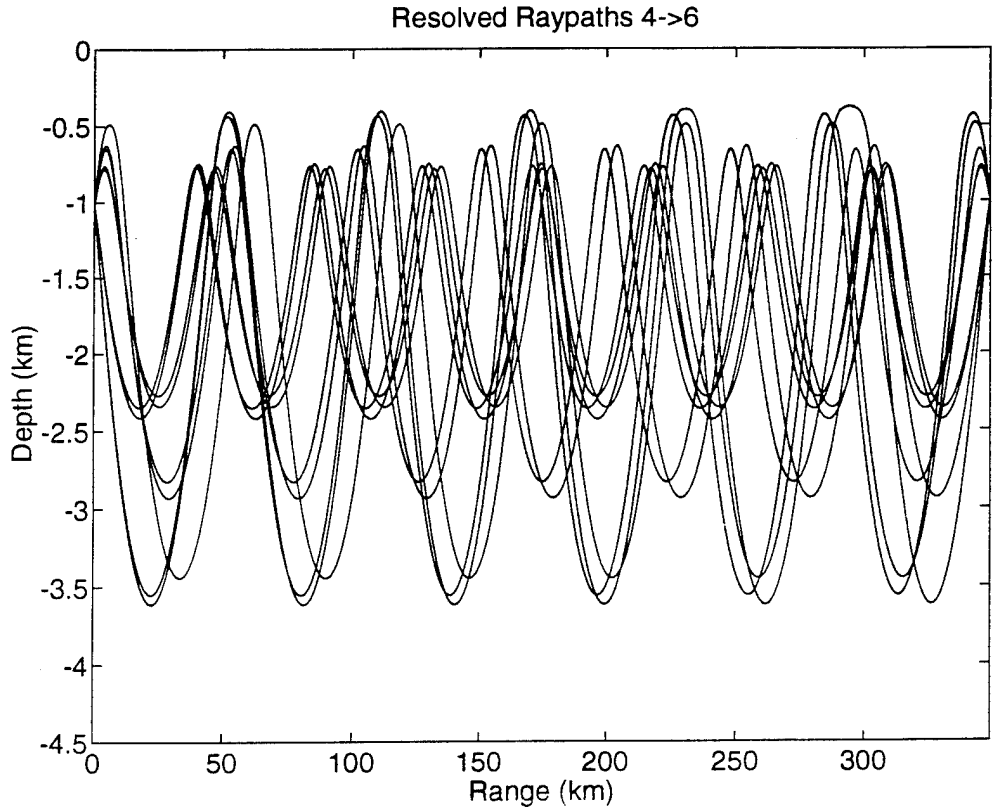

FIGURE X-1

TABLE X-2. Tidal Current Harmonic Constants 4←→6.

Constituent	Amplitude (mm/s)	Uncertainty (mm/s)	Phase (°G)	Uncertainty (°)
M_2	6.60	0.55	96.8	5.0
S_2	1.31	0.55	96.3	34.5
N_2	1.76	0.49	85.7	18.6
K_2	0.96	0.39	97.3	72.6
O_1	0.77	0.30	138.6	83.0
K_1	0.98	0.35	239.8	61.0
P_1	1.10	0.47	371.0	53.4
Q_1	0.81	0.43	245.8	111.4

Values and their uncertainty are determined by the average and rms of harmonic constants from tidal analyses of the separate raypath travel time series. The amplitudes do not include the lunar node factors. 35 ± 11 % of the high-frequency variance is accounted for by the tides.

TABLE X-3. Tidal Sound Speed Harmonic Constants 4←→6.

Constituent	Amplitude (mm/s)	Uncertainty (mm/s)	Phase (°G)	Uncertainty (°)
M_2	2.41	0.77	96.2	72.3
S_2	1.29	0.60	163.4	135.8
N_2	2.32	0.88	124.7	14.8
K_2	1.12	0.41	161.6	70.3
O_1	6.50	0.80	139.5	6.5
K_1	6.28	1.08	279.5	7.3
P_1	2.21	0.71	246.3	22.1
Q_1	2.07	0.56	45.2	17.7

Values and their uncertainty are determined by the average and rms of harmonic constants from tidal analyses of the separate raypath travel time series. The amplitudes do not include the lunar node factors. 27 ± 7 % of the high-frequency variance is accounted for by the tides. Because sum travel times are used to derive these numbers, the amplitudes have been divided by a factor of two compared to the amplitudes for current.

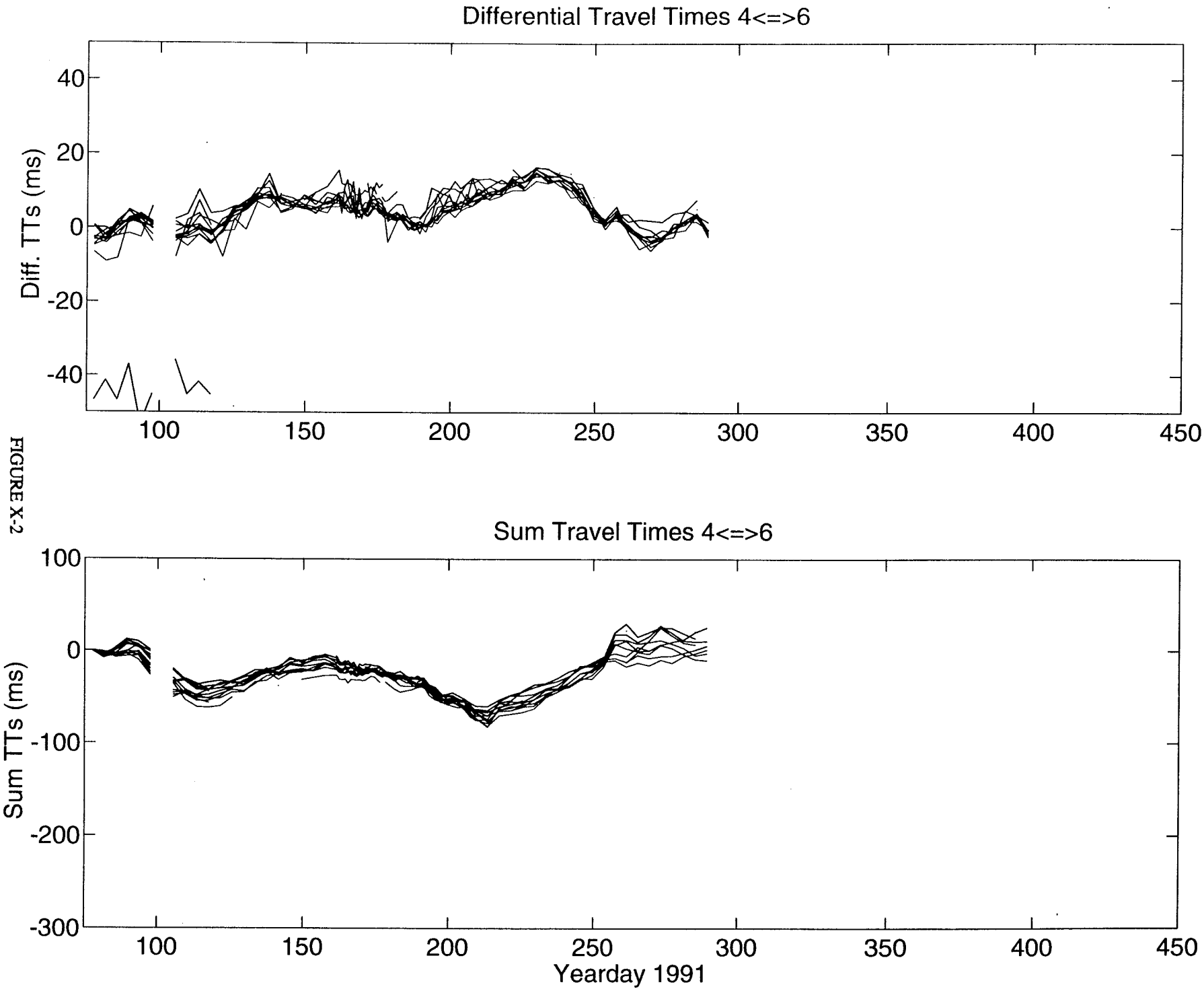
Differential Travel Times 4<=>6
Diff. TTs (ms)
40
20
0
-20
-40
100
150
200
250
300
350
400
450
Sum Travel Times 4<=>6
Sum TTs (ms)
100
0
-100
-200
-300
100
150
200
250
300
350
400
450
Yearday 1991

FIGURE X-2

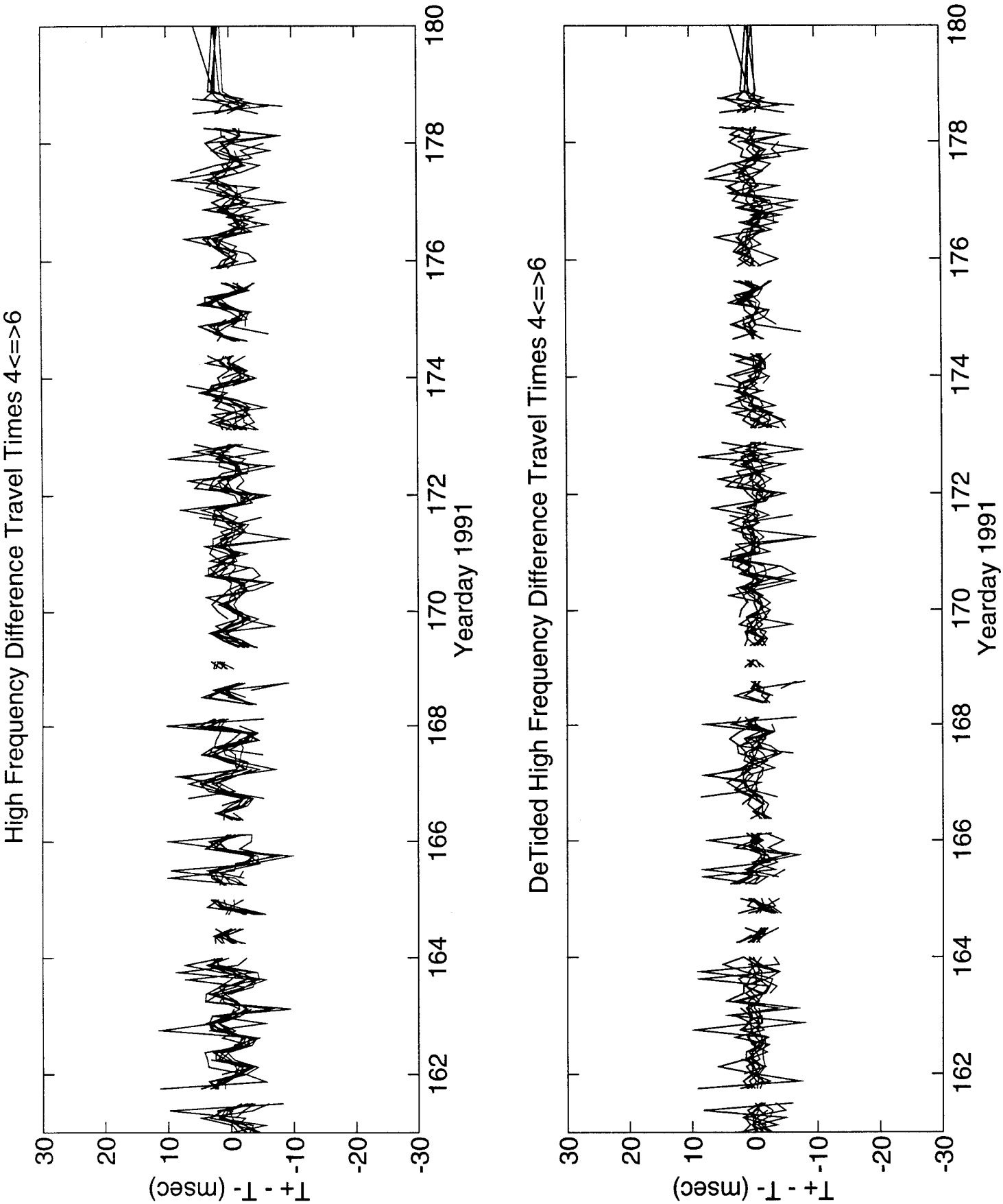
High Frequency Difference Travel Times 4<=>6
T+ - T- (msec)
Yearday 1991
DeTided High Frequency Difference Travel Times 4<=>6
T+ - T- (msec)
Yearday 1991

FIGURE X-3

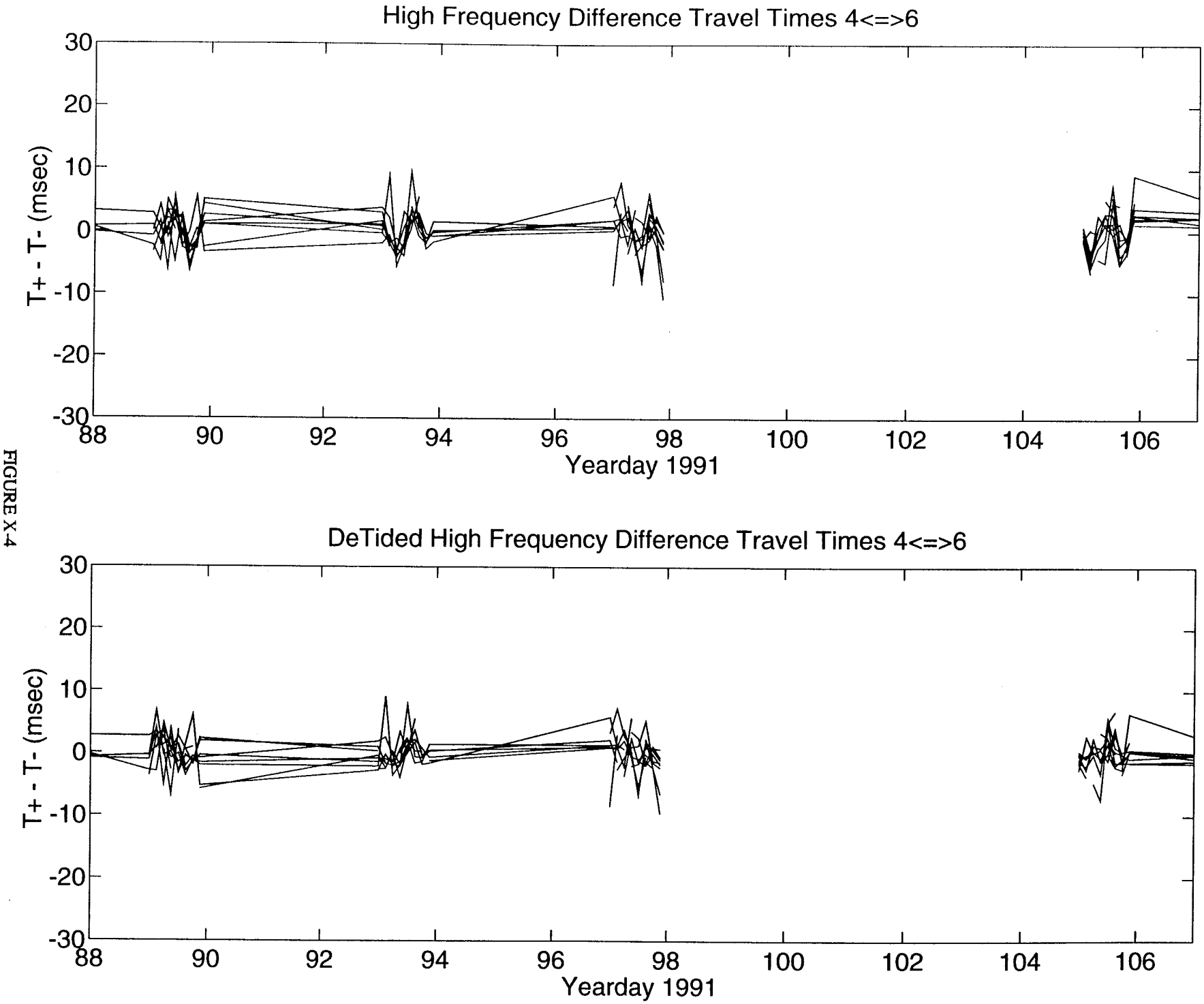
High Frequency Difference Travel Times 4<=>6
T+ - T- (msec)
Yearday 1991
DeTided High Frequency Difference Travel Times 4<=>6
T+ - T- (msec)
Yearday 1991

FIGURE X-4

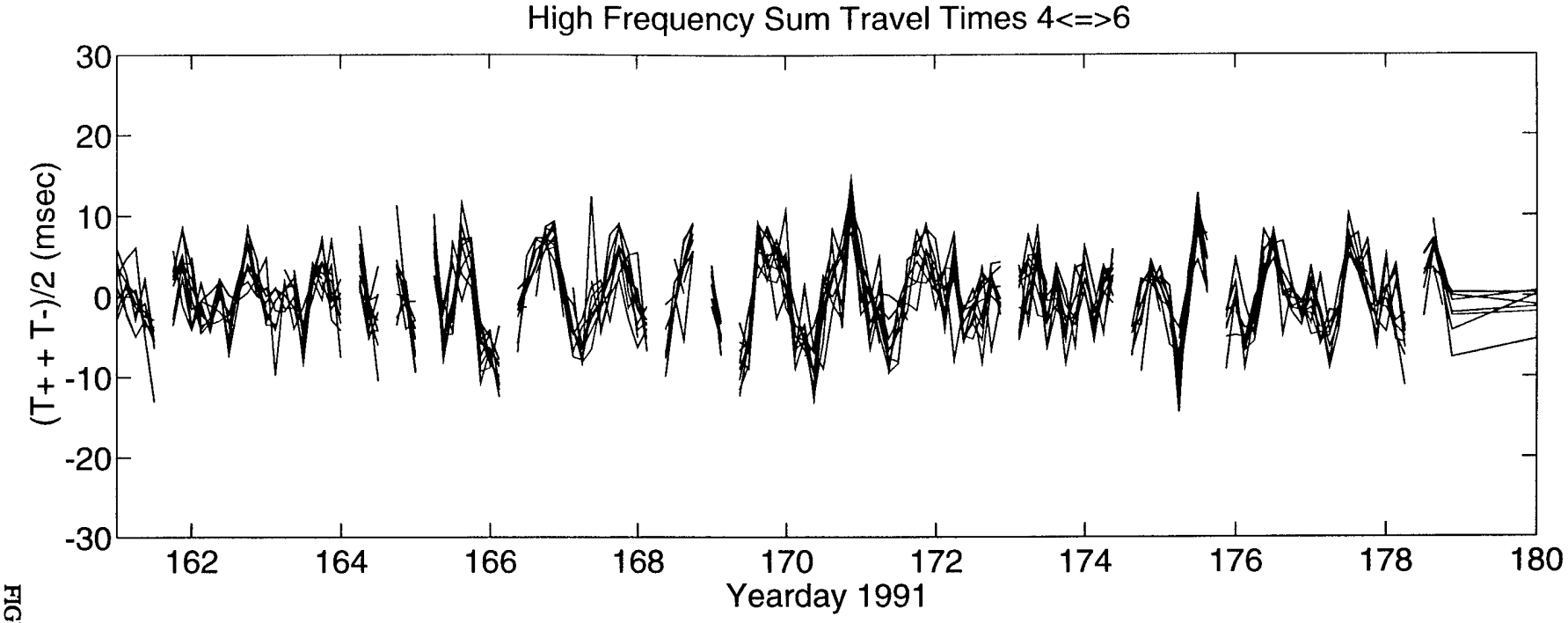
High Frequency Sum Travel Times 4<=>6
(T+ + T-)/2 (msec)
30
20
10
0
-10
-20
-30
162
164
166
168
170
172
174
176
178
180
Yearday 1991

FIGURE X-5

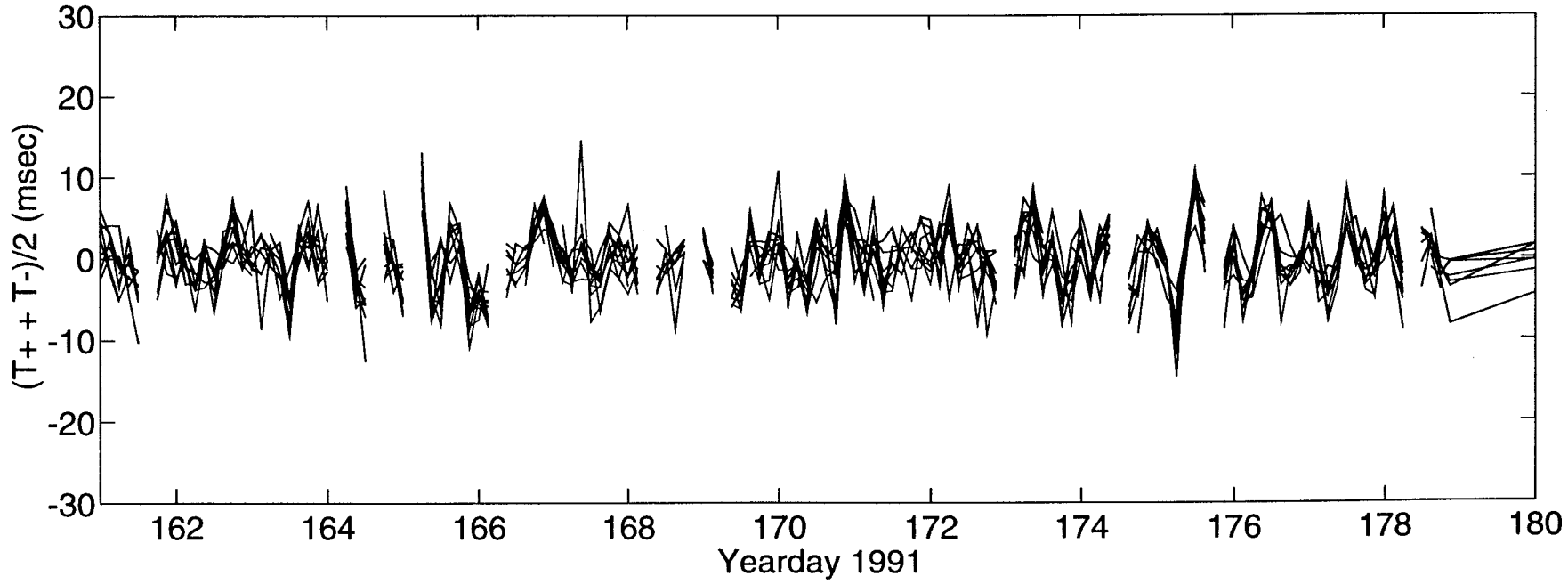
DeTided High Frequency Sum Travel Times 4<=>6
(T+ + T-)/2 (msec)
30
20
10
0
-10
-20
-30
162
164
166
168
170
172
174
176
178
180
Yearday 1991

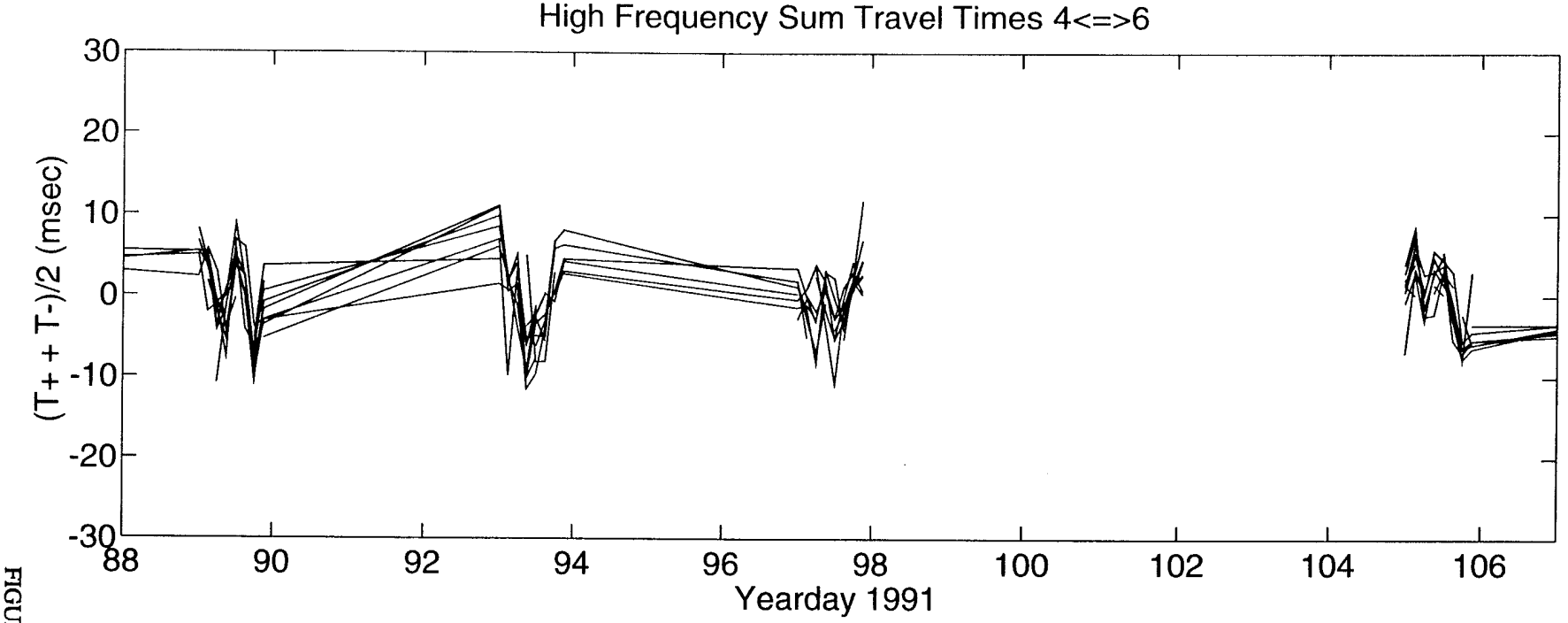
High Frequency Sum Travel Times 4<=>6
(T+ + T-)/2 (msec)
30
20
10
0
-10
-20
-30
88
90
92
94
96
98
100
102
104
106
Yearday 1991

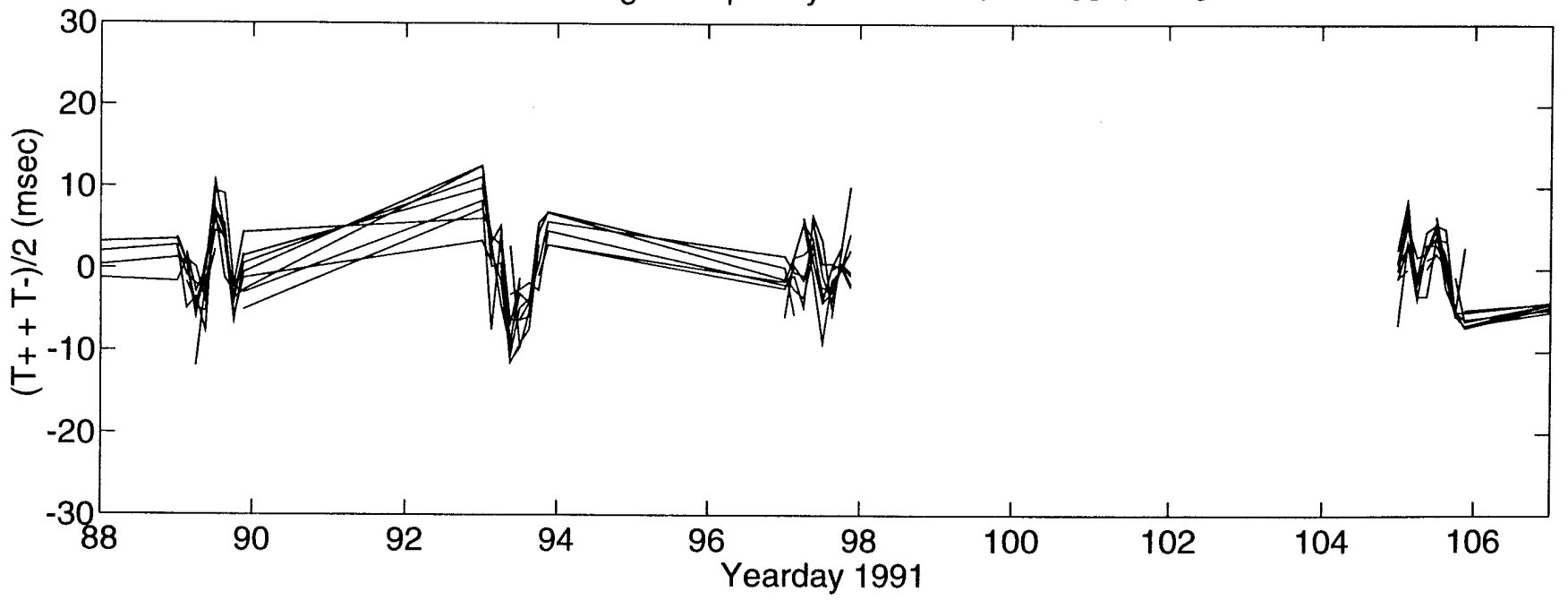
DeTided High Frequency Sum Travel Times 4<=>6
(T+ + T-)/2 (msec)
30
20
10
0
-10
-20
-30
88
90
92
94
96
98
100
102
104
106
Yearday 1991

FIGURE X-6

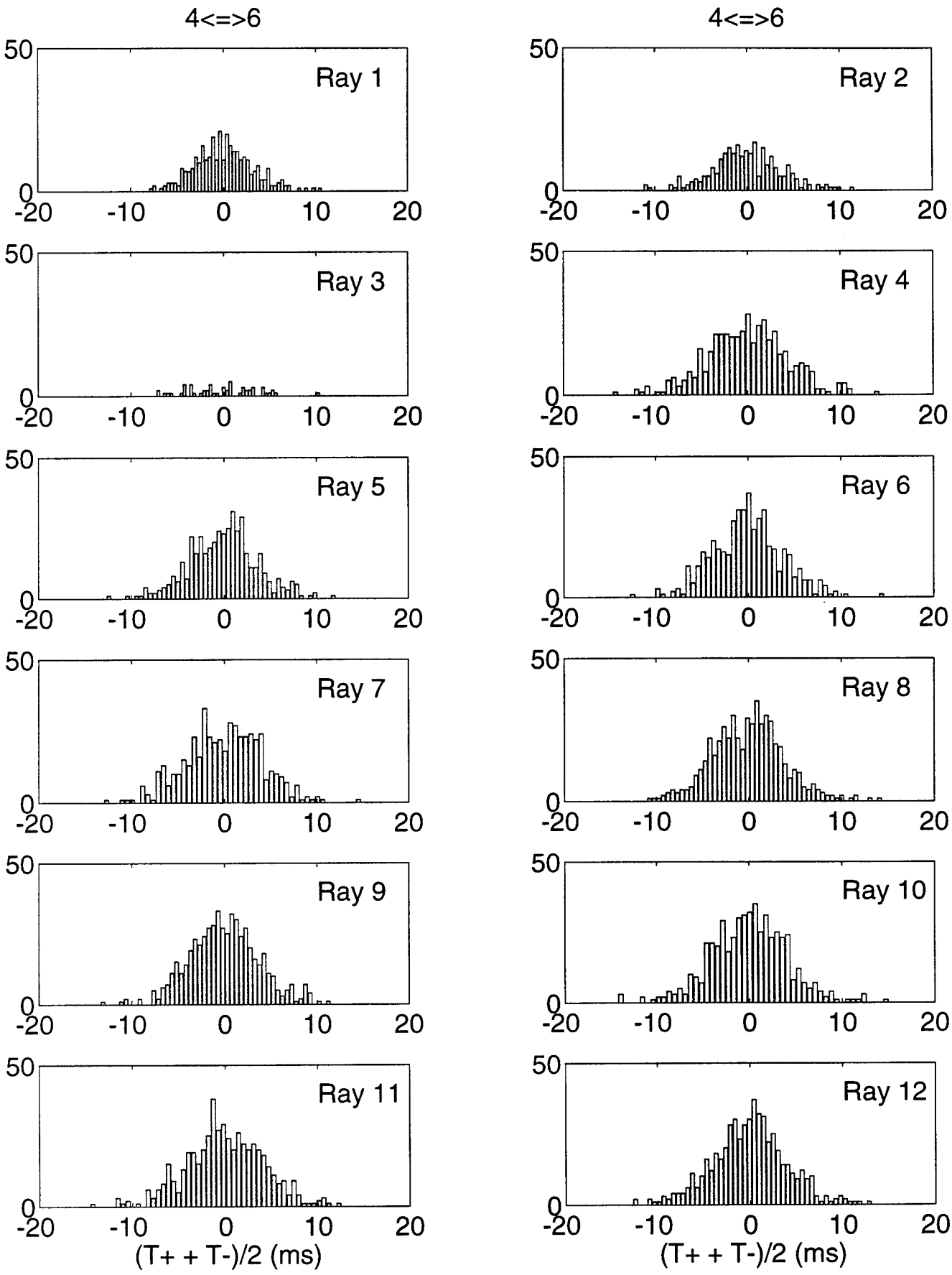
4<=>6
4<=>6
Ray 1
Ray 2
Ray 3
Ray 4
Ray 5
Ray 6
Ray 7
Ray 8
Ray 9
Ray 10
Ray 11
Ray 12
50
0
-20
-10
0
10
20
(T+ + T-)/2 (ms)

FIGURE X-7

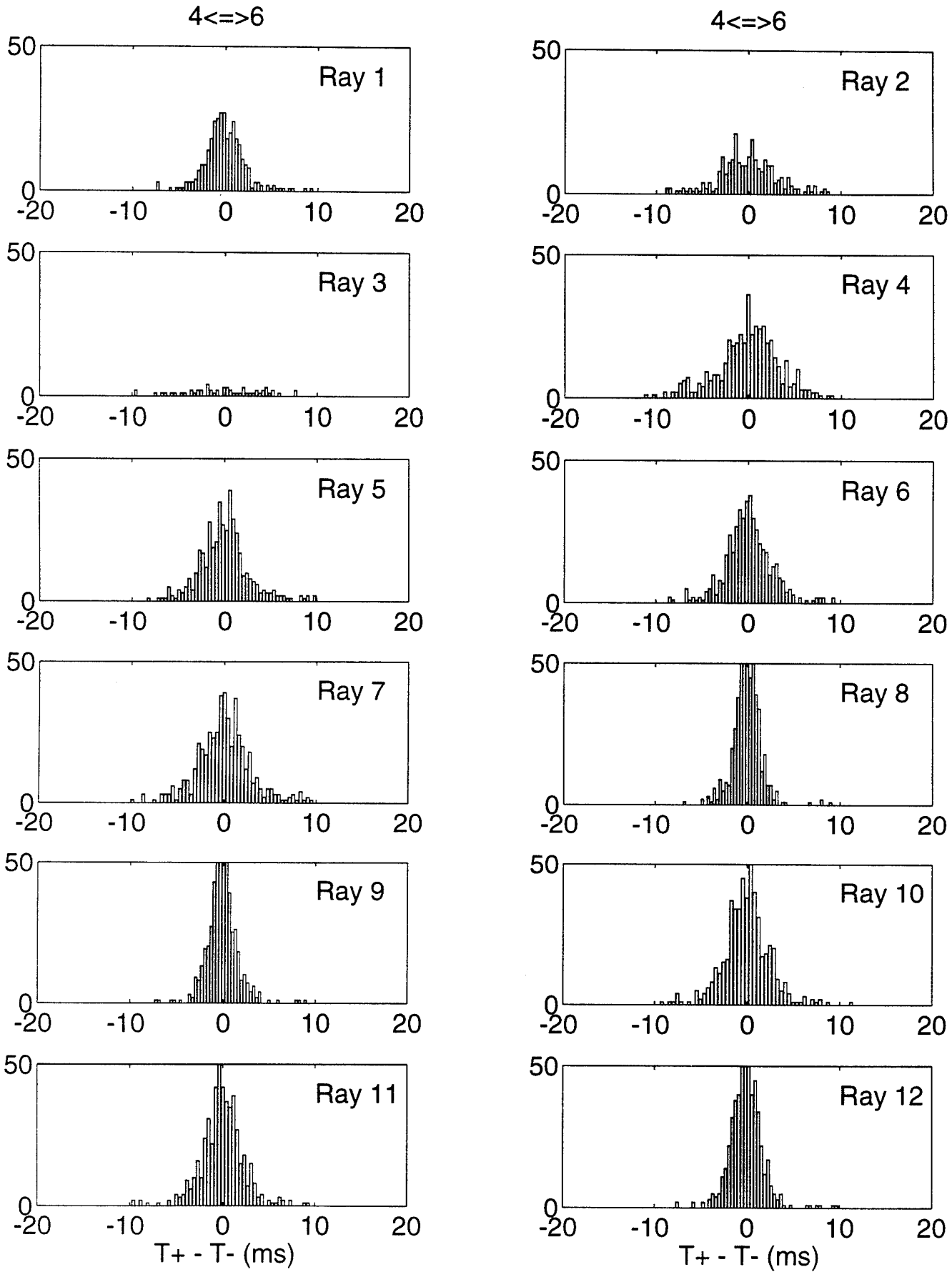
4<=>6
Ray 1
Ray 2
Ray 3
Ray 4
Ray 5
Ray 6
Ray 7
Ray 8
Ray 9
Ray 10
Ray 11
Ray 12
50
0
-20
-10
0
10
20
T+ - T- (ms)

FIGURE X-8

Y. ACOUSTIC DATA: Paths 5a→6 and 6→5a

FIGURE Y-1 shows the raypaths, roughly corresponding to FIGURE G-1, for which travel times were resolved. The raypaths were actually determined using range-dependent Levitus sound speed, interpolated onto the acoustic path. Note that the "final cutoff" travel times may be available at some time in the future, these data correspond to a ray confined near the sound channel axis.

FIGURE Y-2 shows the low-pass filtered difference (top panel) and sum (bottom panel) travel times corresponding to the rays of FIGURE Y-1. Note that mooring 5a had failed by yearday 140, to be replaced later by mooring 5b.

FIGURE Y-3 shows the high-pass filtered difference travel times for a small portion of the time series obtained during the time of more frequent transmissions during the MST experiment. The bottom panel shows the time series after the phase-locked tidal signals have been removed.

FIGURE Y-4 shows the high-pass filtered sum travel times for a small portion of the time series obtained during the time of more frequent transmissions during the MST experiment. The bottom panel shows the time series after the phase-locked tidal signals have been removed. This tidal variability is caused by the internal tide.

After the travel time time series have been edited for outliers, high-pass filtered, and detided, the high-frequency variances are calculated (TABLE Y-1). Note that this table sometimes contains statistics for more rays than are indicated in TABLE B-1; some of the ray arrivals in TABLE Y-1 have not been identified with predicted arrivals. Also, sometimes there is initial ambiguity about the pairing of reciprocal arrivals, in which case sum and difference travel times are calculated for all reasonable cases; later it becomes obvious which arrivals have been improperly paired. The correlation $<T^+ T^->$ and variance $<T^2>$ are calculated from the sum and difference travel time variances in this table. The variance of the travel times is mainly due to internal wave variability, and this value determines the uncertainties assigned to the travel times in an inversion. The correlation coefficient is a measure of the reciprocity of reciprocal raypaths. This measure is conservative, because correlation is not a necessary condition for the determination of current from the difference of reciprocal travel times. Values of correlation that are 0.5 or greater assure that the reciprocal raypaths are indeed effectively identical, since good correlation implies that the reciprocal raypaths have not separated by more than an internal wave correlation length. Histograms of the detided, high-frequency travel times are shown in FIGURES Y-5 and Y-6; the variances from TABLE Y-1 are measures of the width of these histograms.

TABLES Y-2 and Y-3 show the results of tidal analysis of the time series of difference (current) and sum (sound speed) travel times. For these tables, the tidal analysis is performed on each travel time time series separately and then the average and rms of the harmonic constants are calculated. Current or sound speed amplitude is determined from travel time by a simple scaling factor; the harmonic constants are more accurately determined by inverting the data for current or sound speed (this is not done here).

TABLE Y-1. Travel Time Statistics 5a←→6.

Ray #	Number of data	$\langle (T^+ + T^-)^2 \rangle$ (ms^2)	$\langle (T^+ - T^-)^2 \rangle$ (ms^2)	$\langle T^+ T^- \rangle$ (ms^2)	$\langle T^2 \rangle$ (ms^2)	$\frac{\langle T^+ T^- \rangle}{\langle T^2 \rangle}$
1	38	11	20	7	16	0.40
2	95	13	10	11	16	0.69
3	87	14	13	10	17	0.62
4	98	22	11	19	25	0.78
5	102	15	10	13	18	0.73
6	101	13	11	10	16	0.65
7	103	14	15	10	17	0.56
8	113	9	3	8	9	0.86
9	116	11	3	11	12	0.88
10	111	12	8	10	14	0.70
11	110	12	9	10	14	0.69
12	114	11	2	10	11	0.91

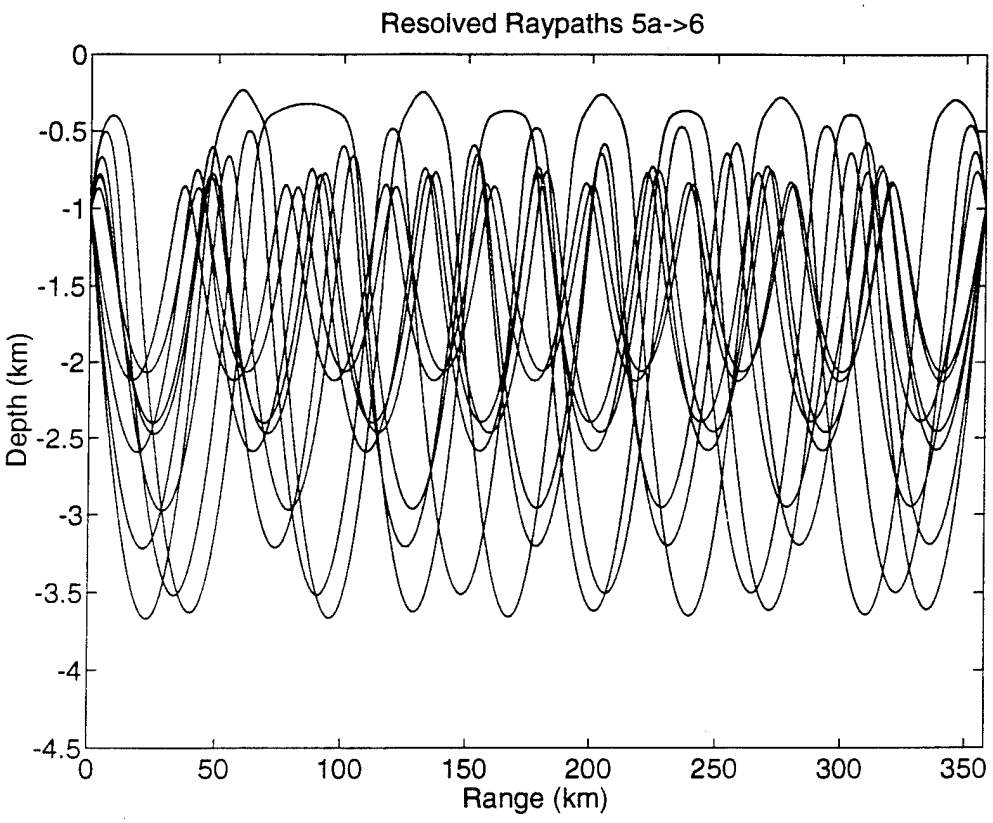

FIGURE Y-1

TABLE Y-2. Tidal Current Harmonic Constants 5a←→6.

Constituent	Amplitude (mm/s)	Uncertainty (mm/s)	Phase (°G)	Uncertainty (°)
M_2	11.22	2.06	107.2	11.2
S_2	5.18	2.14	118.3	44.6
N_2	3.21	1.19	55.1	73.4
K_2	3.49	2.36	173.0	92.3
O_1	2.02	1.37	177.9	93.7
K_1	3.91	2.66	246.7	58.8
P_1	3.31	2.43	103.6	84.8
Q_1	1.69	1.01	192.8	104.9

Values and their uncertainty are determined by the average and rms of harmonic constants from tidal analyses of the separate raypath travel time series. The amplitudes do not include the lunar node factors. 55 ± 17 % of the high-frequency variance is accounted for by the tides.

TABLE Y-3. Tidal Sound Speed Harmonic Constants 5a←→6.

Constituent	Amplitude (mm/s)	Uncertainty (mm/s)	Phase (°G)	Uncertainty (°)
M_2	8.60	0.97	71.5	30.1
S_2	4.22	2.34	27.7	40.3
N_2	3.85	1.48	35.0	34.4
K_2	4.43	2.40	230.8	88.9
O_1	2.32	0.90	132.9	79.1
K_1	6.25	2.55	113.0	35.5
P_1	7.66	1.99	20.1	31.6
Q_1	3.58	1.71	35.3	49.5

Values and their uncertainty are determined by the average and rms of harmonic constants from tidal analyses of the separate raypath travel time series. The amplitudes do not include the lunar node factors. 38 ± 5 % of the high-frequency variance is accounted for by the tides. Because sum travel times are used to derive these numbers, the amplitudes have been divided by a factor of two compared to the amplitudes for current.

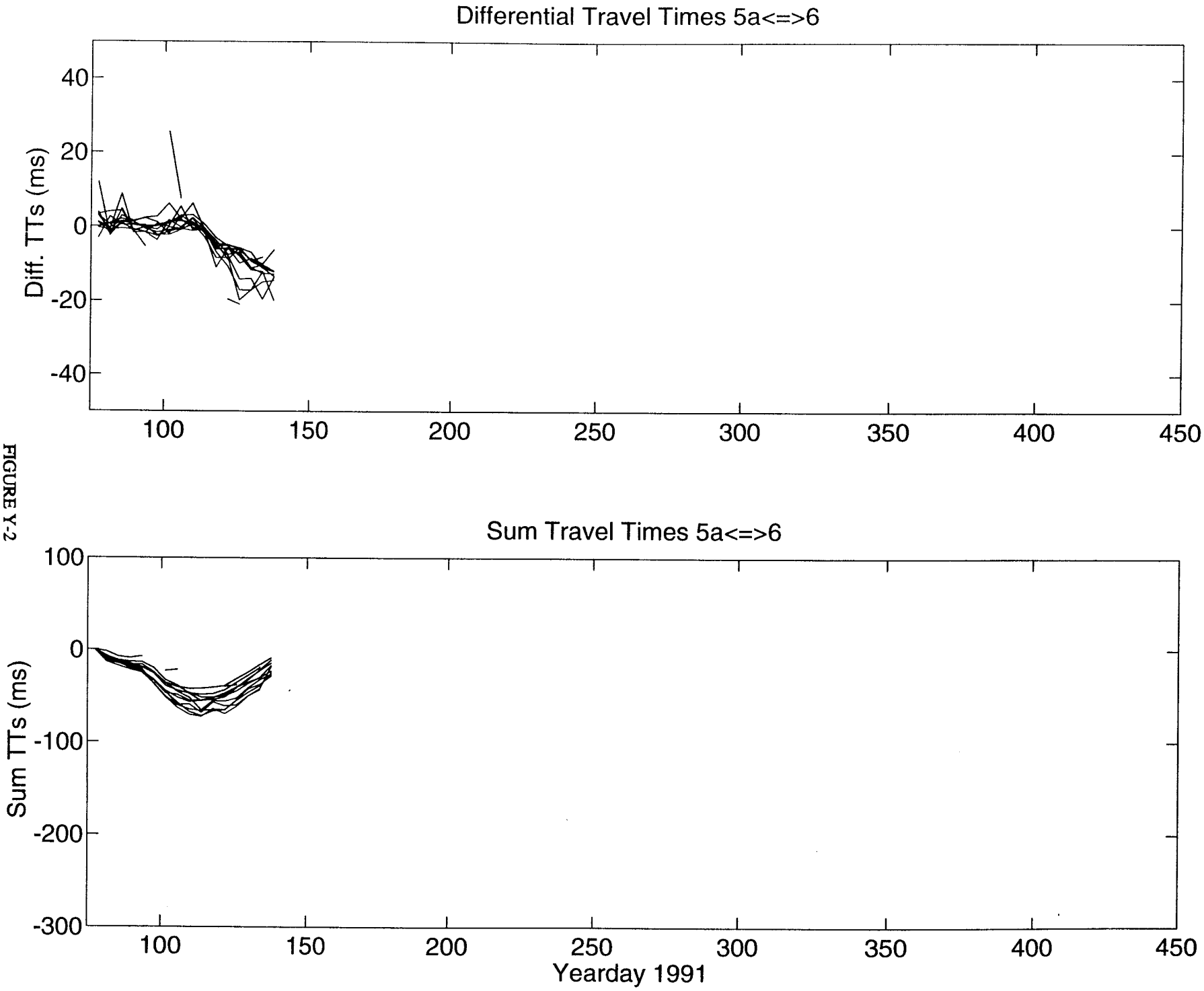
Differential Travel Times 5a<=>6
Diff. TTs (ms)
40
20
0
-20
-40
100
150
200
250
300
350
400
450
Sum Travel Times 5a<=>6
Sum TTs (ms)
100
0
-100
-200
-300
100
150
200
250
300
350
400
450
Yearday 1991

FIGURE Y-2

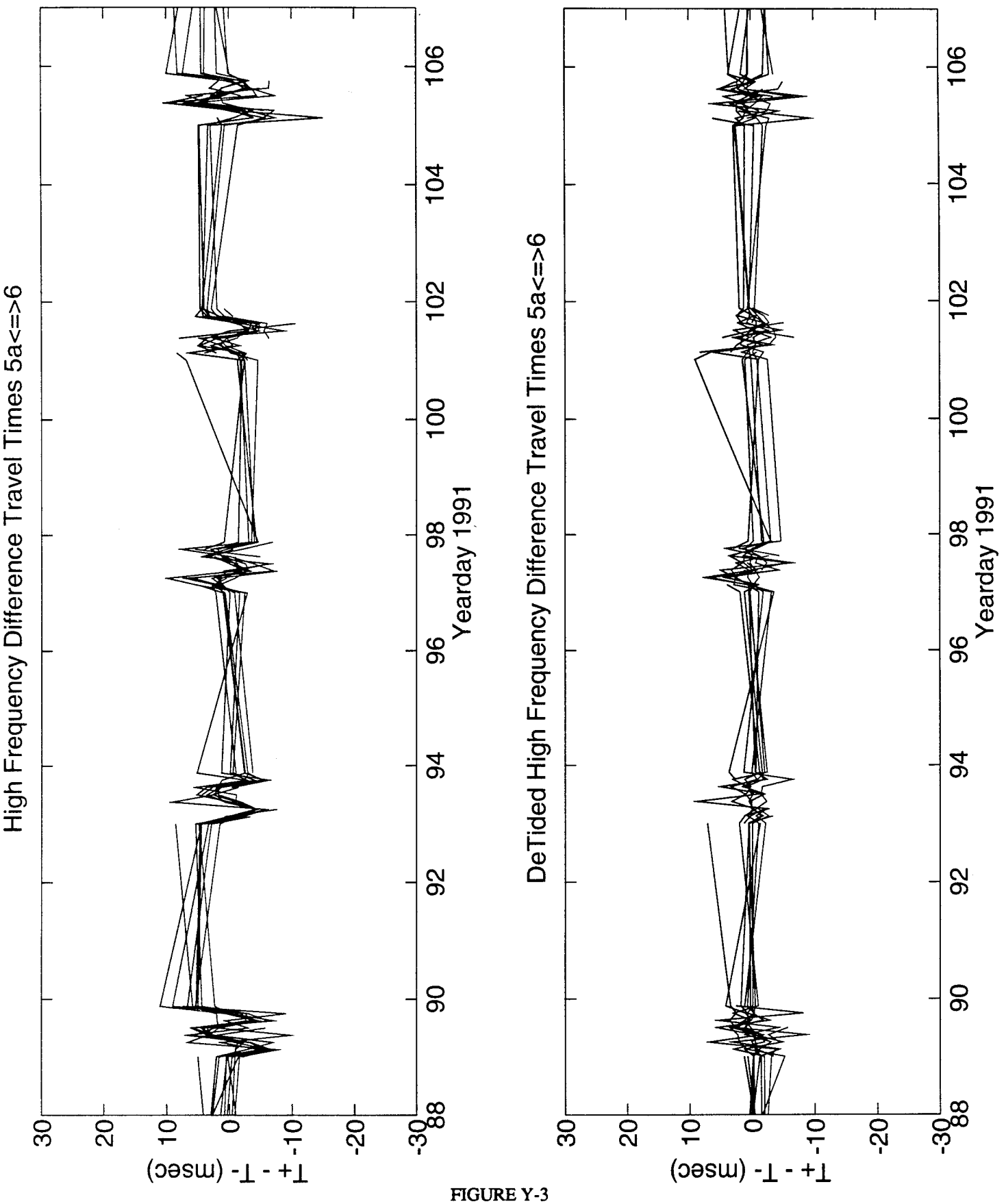
High Frequency Difference Travel Times 5a<=>6
T+ - T- (msec)
Yearday 1991
DeTided High Frequency Difference Travel Times 5a<=>6
T+ - T- (msec)
Yearday 1991

FIGURE Y-3

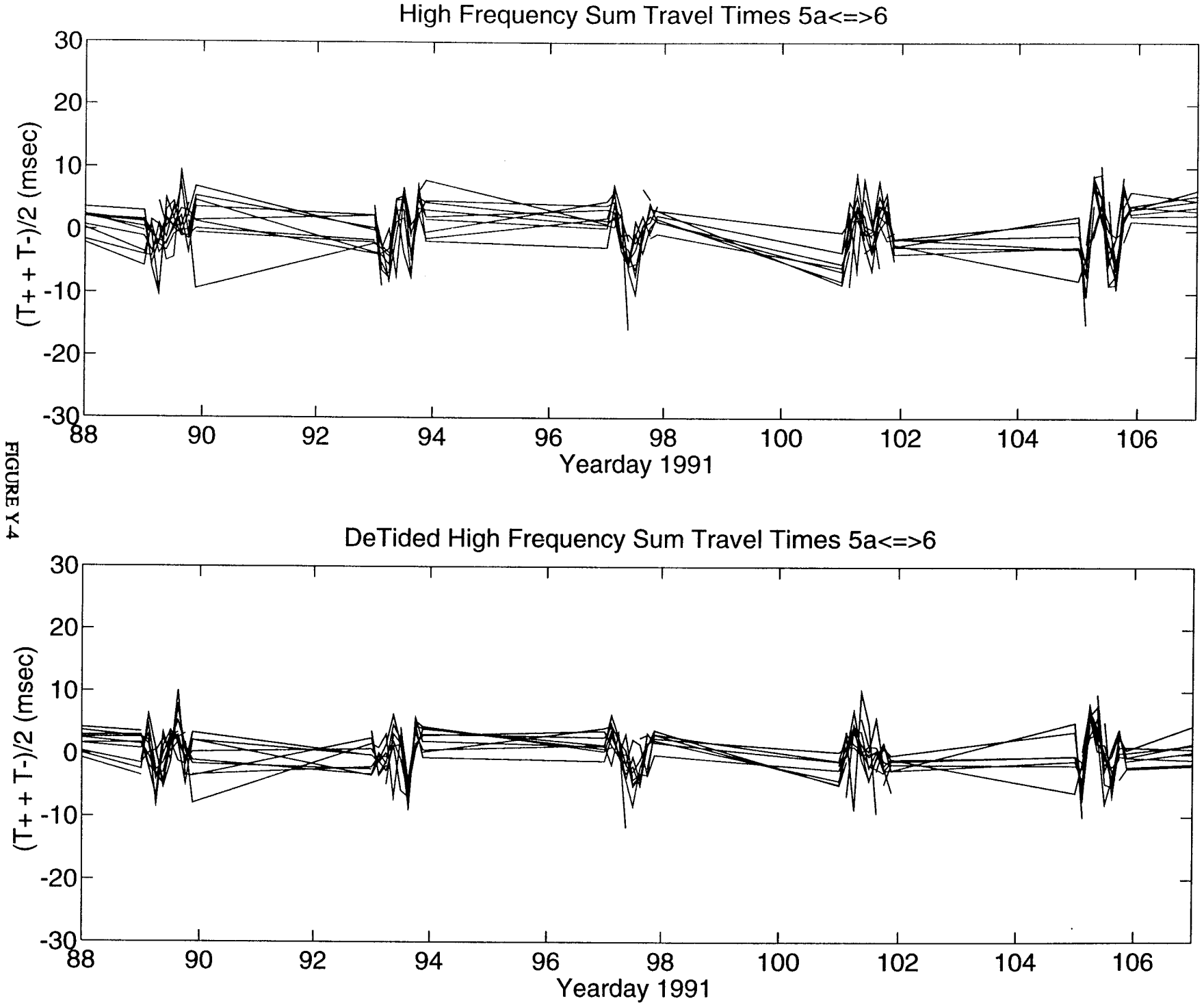
High Frequency Sum Travel Times 5a<=>6
(T+ + T-)/2 (msec)
Yearday 1991
DeTided High Frequency Sum Travel Times 5a<=>6
(T+ + T-)/2 (msec)
Yearday 1991

FIGURE Y-4

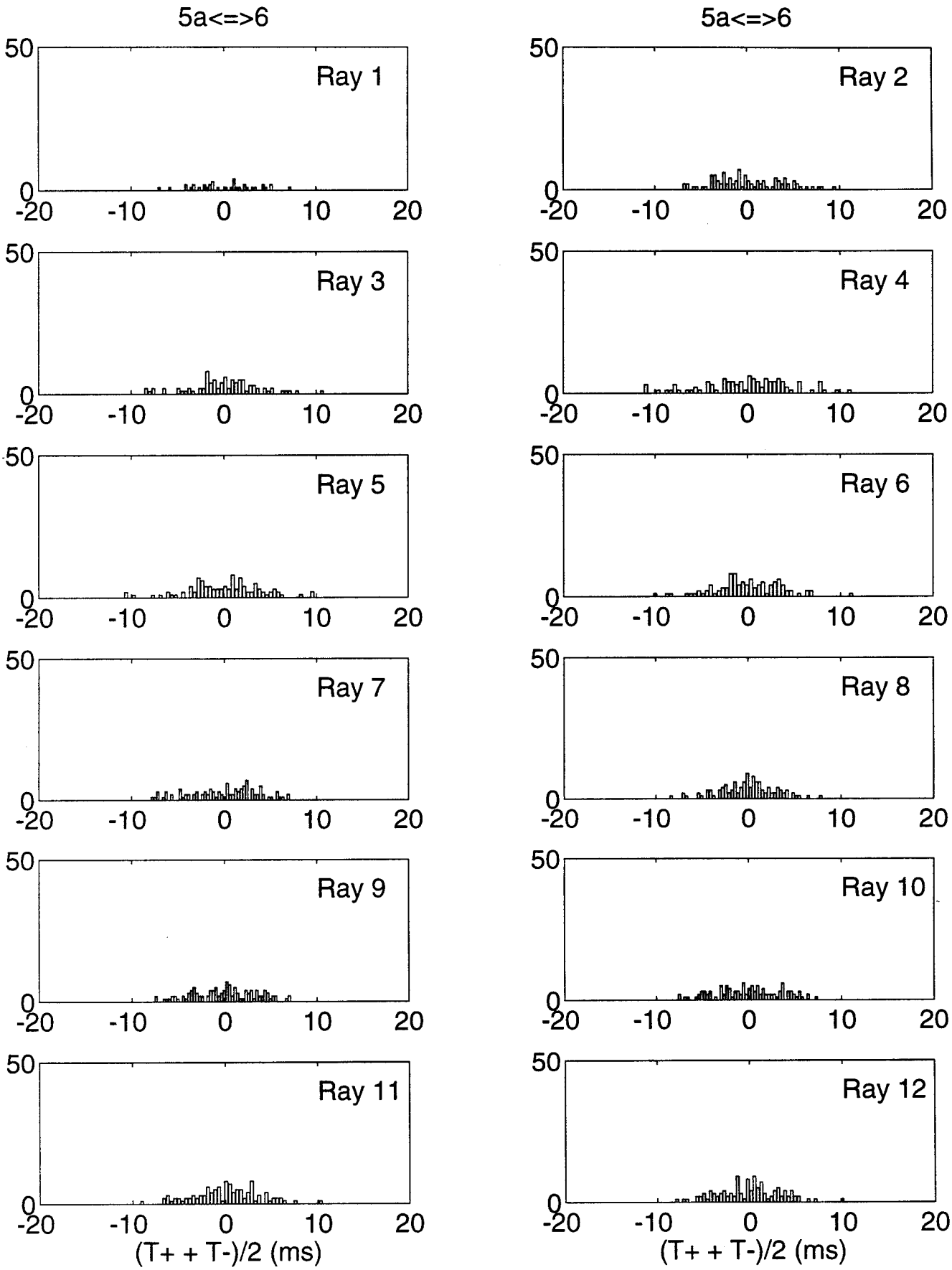
5a<=>6
5a<=>6
Ray 1
Ray 2
Ray 3
Ray 4
Ray 5
Ray 6
Ray 7
Ray 8
Ray 9
Ray 10
Ray 11
Ray 12
50
0
-20
-10
0
10
20
(T+ + T-)/2 (ms)
(T+ + T-)/2 (ms)

FIGURE Y-5

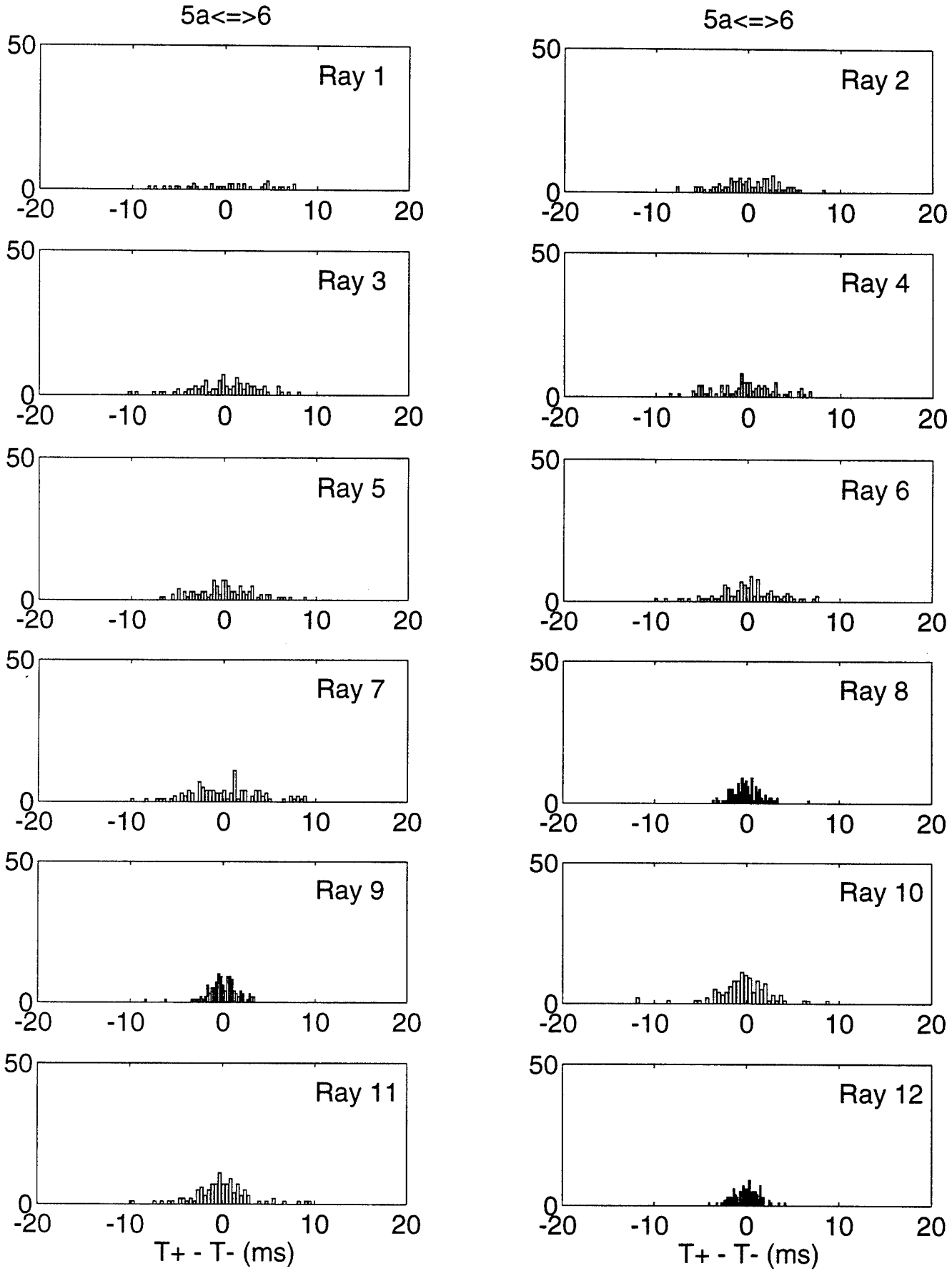
5a<=>6
Ray 1
Ray 2
Ray 3
Ray 4
Ray 5
Ray 6
Ray 7
Ray 8
Ray 9
Ray 10
Ray 11
Ray 12
50
0
-20
-10
0
10
20
T+ - T- (ms)

FIGURE Y-6

Z. ACOUSTIC DATA: Paths 5b→6 and 6→5b

FIGURE Z-1 shows the raypaths, corresponding roughly to FIGURE G-1, for which travel times were resolved. The raypaths were actually determined using range-dependent Levitus sound speed, interpolated onto the acoustic path. Note that the "final cutoff" travel times may be available at some time in the future, these data correspond to a ray confined near the sound channel axis.

FIGURE Z-2 shows the low-pass filtered difference (top panel) and sum (bottom panel) travel times corresponding to the rays of FIGURE Z-1.

FIGURE Z-3 shows the high-pass filtered difference travel times for a small portion of the time series obtained during the time of more frequent transmissions during the MST experiment. The bottom panel shows the time series after the phase-locked tidal signals have been removed.

FIGURE Z-4 shows the high-pass filtered sum travel times for a small portion of the time series obtained during the time of more frequent transmissions during the MST experiment. The bottom panel shows the time series after the phase-locked tidal signals have been removed. This tidal variability is caused by the internal tide.

After the travel time time series have been edited for outliers, high-pass filtered, and detided, the high-frequency variances are calculated (TABLE Z-1). Note that this table sometimes contains statistics for more rays than are indicated in TABLE B-1; some of the ray arrivals in TABLE Z-1 have not been identified with predicted arrivals. Also, sometimes there is initial ambiguity about the pairing of reciprocal arrivals, in which case sum and difference travel times are calculated for all reasonable cases; later it becomes obvious which arrivals have been improperly paired. The correlation $<T^+ T^->$ and variance $<T^2>$ are calculated from the sum and difference travel time variances in this table. The variance of the travel times is mainly due to internal wave variability, and this value determines the uncertainties assigned to the travel times in an inversion. The correlation coefficient is a measure of the reciprocity of reciprocal raypaths. This measure is conservative, because correlation is not a necessary condition for the determination of current from the difference of reciprocal travel times. Values of correlation that are 0.5 or greater assure that the reciprocal raypaths are indeed effectively identical, since good correlation implies that the reciprocal raypaths have not separated by more than an internal wave correlation length. Histograms of the detided, high-frequency travel times are shown in FIGURES Z-5 and Z-6; the variances from TABLE Z-1 are measures of the width of these histograms.

TABLES Z-2 and Z-3 show the results of tidal analysis of the time series of difference (current) and sum (sound speed) travel times. For these tables, the tidal analysis is performed on each travel time time series separately and then the average and rms of the harmonic constants are calculated. Current or sound speed amplitude is determined from travel time by a simple scaling factor; the harmonic constants are more accurately determined by inverting the data for current or sound speed (this is not done here).

TABLE Z-1. Travel Time Statistics 5b←→6.

Ray #	Number of data	$\langle (T^+ + T^-)^2 \rangle$ (ms^2)	$\langle (T^+ - T^-)^2 \rangle$ (ms^2)	$\langle T^+ T^- \rangle$ (ms^2)	$\langle T^2 \rangle$ (ms^2)	$\frac{\langle T^+ T^- \rangle}{\langle T^2 \rangle}$
1	425	21	13	18	24	0.74
2	456	19	12	16	22	0.73
3	527	18	10	16	21	0.75
4	524	19	10	17	22	0.78
5	539	20	8	18	22	0.82
6	572	16	4	15	17	0.87
7	618	14	2	14	15	0.93
8	590	15	6	13	16	0.81
9	612	19	6	17	20	0.86
10	613	17	3	16	18	0.91

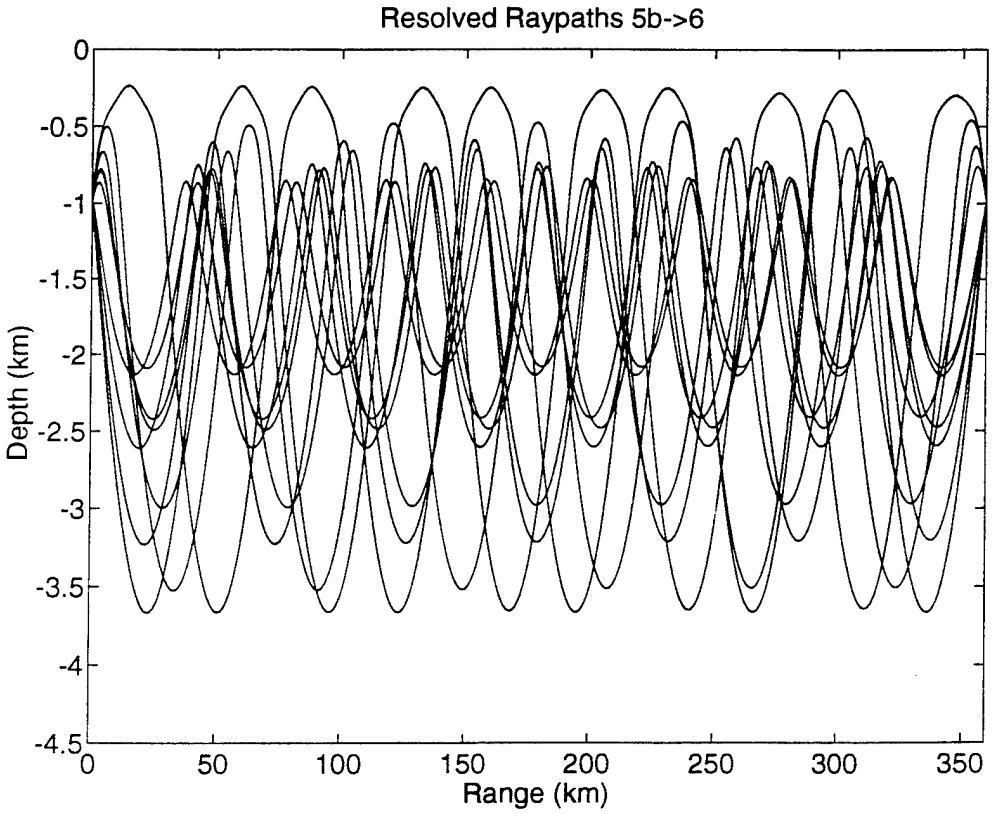

FIGURE Z-1

TABLE Z-2. Tidal Current Harmonic Constants 5b←→6.

Constituent	Amplitude (mm/s)	Uncertainty (mm/s)	Phase (°G)	Uncertainty (°)
M_2	12.29	0.79	105.2	3.6
S_2	3.17	0.67	129.5	24.6
N_2	3.26	0.85	76.8	14.6
K_2	1.23	0.66	142.4	61.2
O_1	0.90	0.49	313.7	71.1
K_1	1.61	0.65	251.9	24.5
P_1	0.72	0.37	192.5	119.1
Q_1	1.08	0.70	208.4	142.3

Values and their uncertainty are determined by the average and rms of harmonic constants from tidal analyses of the separate raypath travel time series. The amplitudes do not include the lunar node factors. 60 ± 16 % of the high-frequency variance is accounted for by the tides.

TABLE Z-3. Tidal Sound Speed Harmonic Constants 5b←→6.

Constituent	Amplitude (mm/s)	Uncertainty (mm/s)	Phase (°G)	Uncertainty (°)
M_2	6.65	1.82	72.6	18.0
S_2	1.67	0.70	218.1	36.7
N_2	1.90	0.69	37.8	32.6
K_2	1.47	0.77	193.8	87.2
O_1	2.77	0.79	157.7	15.3
K_1	2.68	0.79	261.7	29.1
P_1	1.95	0.61	341.0	43.6
Q_1	0.58	0.40	347.7	59.6

Values and their uncertainty are determined by the average and rms of harmonic constants from tidal analyses of the separate raypath travel time series. The amplitudes do not include the lunar node factors. 19 ± 6 % of the high-frequency variance is accounted for by the tides. Because sum travel times are used to derive these numbers, the amplitudes have been divided by a factor of two compared to the amplitudes for current.

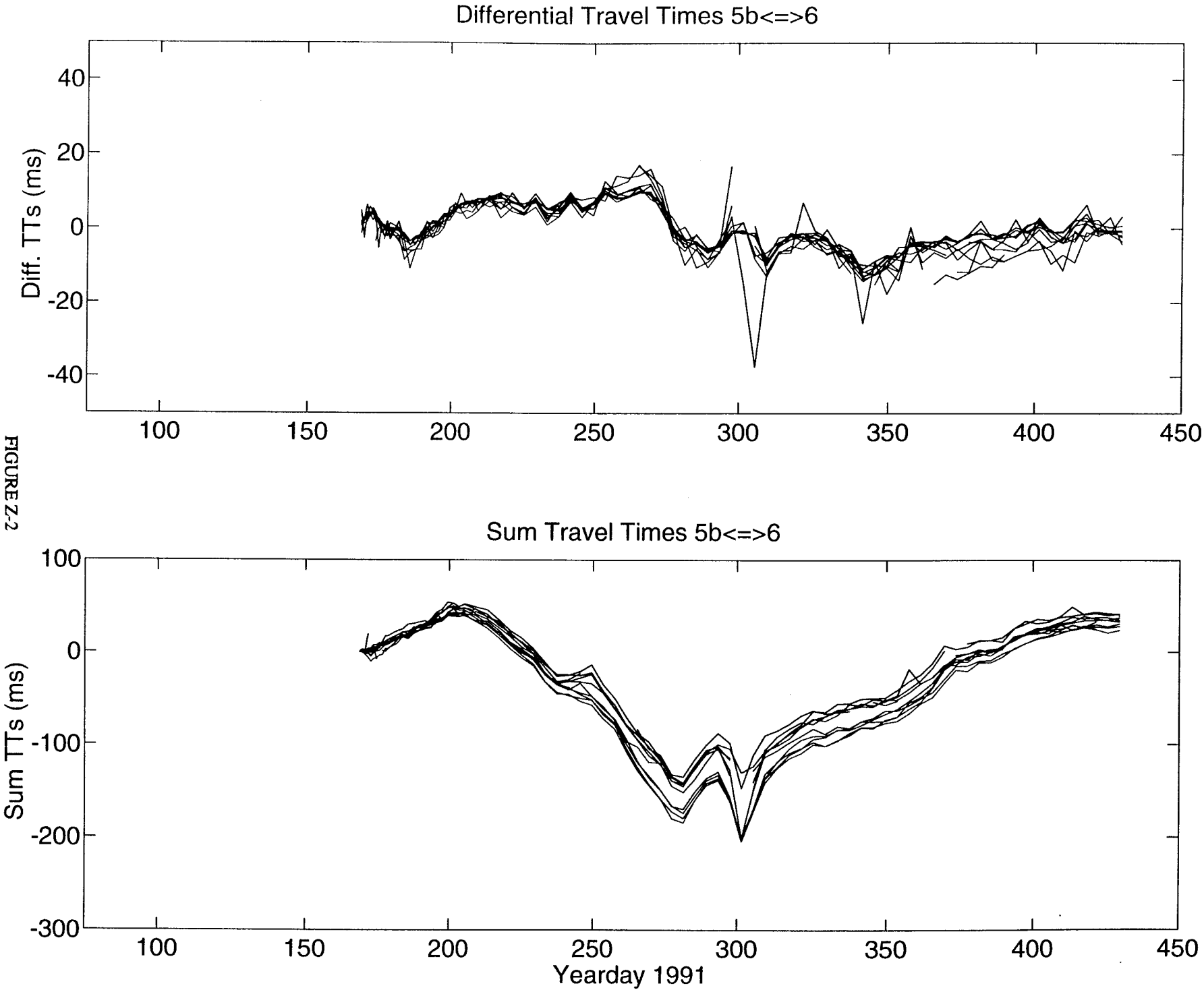
Differential Travel Times 5b<=>6
Diff. TTs (ms)
40
20
0
-20
-40
100
150
200
250
300
350
400
450
Sum Travel Times 5b<=>6
Sum TTs (ms)
100
0
-100
-200
-300
100
150
200
250
300
350
400
450
Yearday 1991

FIGURE Z-2

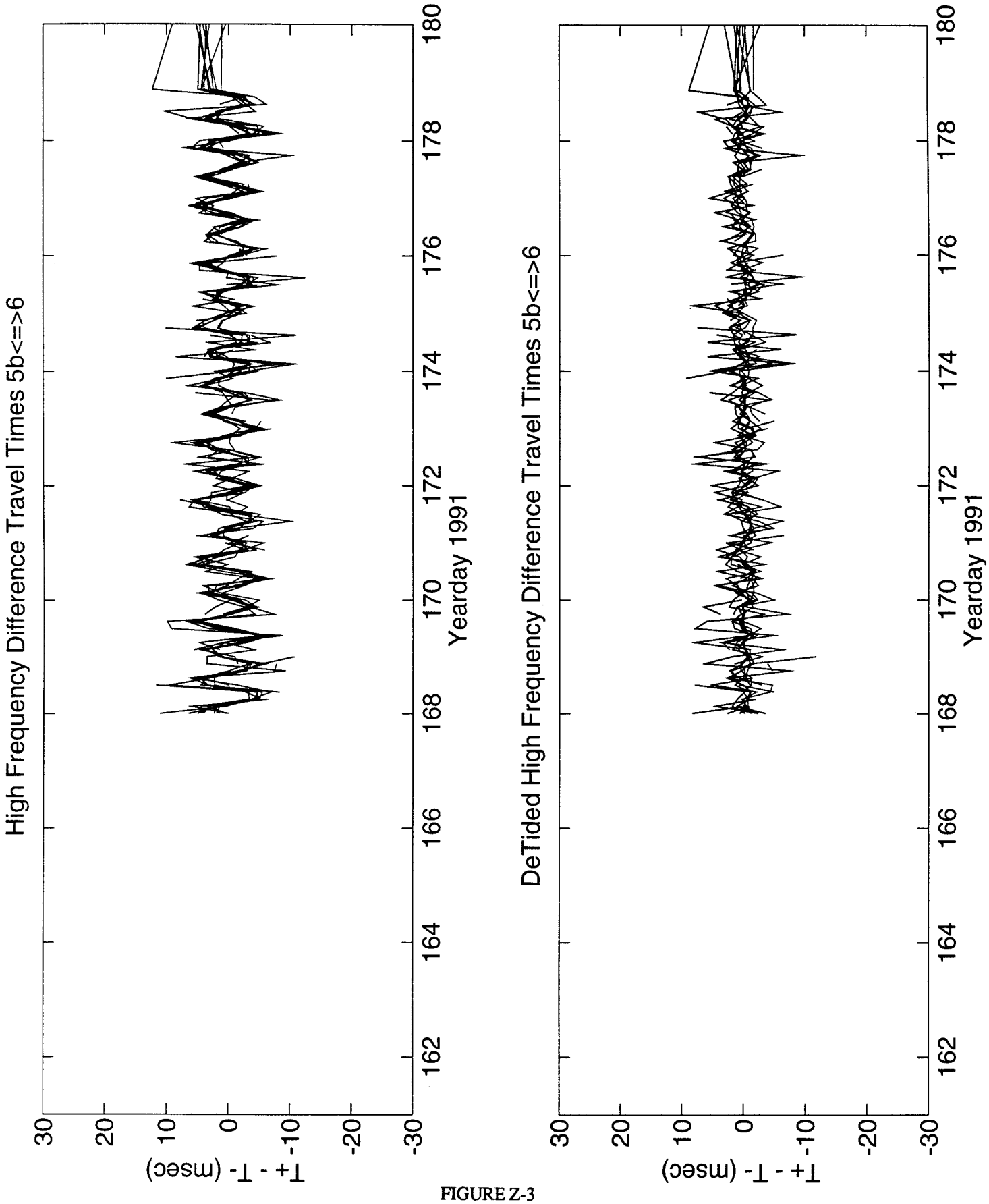
High Frequency Difference Travel Times 5b<=>6
T+ - T- (msec)
30
20
10
0
-10
-20
-30
162
164
166
168
170
172
174
176
178
180
Yearday 1991
DeTided High Frequency Difference Travel Times 5b<=>6
T+ - T- (msec)
30
20
10
0
-10
-20
-30
162
164
166
168
170
172
174
176
178
180
Yearday 1991

FIGURE Z-3

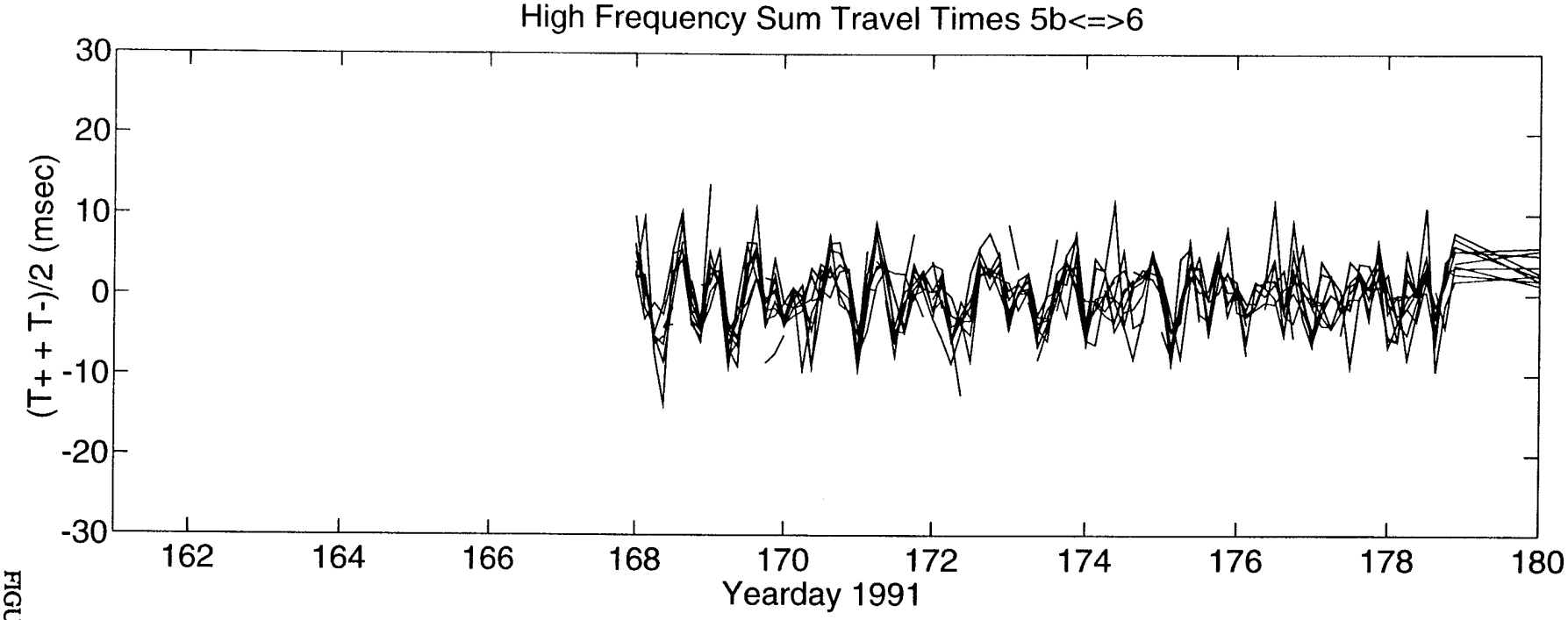
High Frequency Sum Travel Times 5b<=>6
(T+ + T-)/2 (msec)
30
20
10
0
-10
-20
-30
162
164
166
168
170
172
174
176
178
180
Yearday 1991

FIGURE Z-4

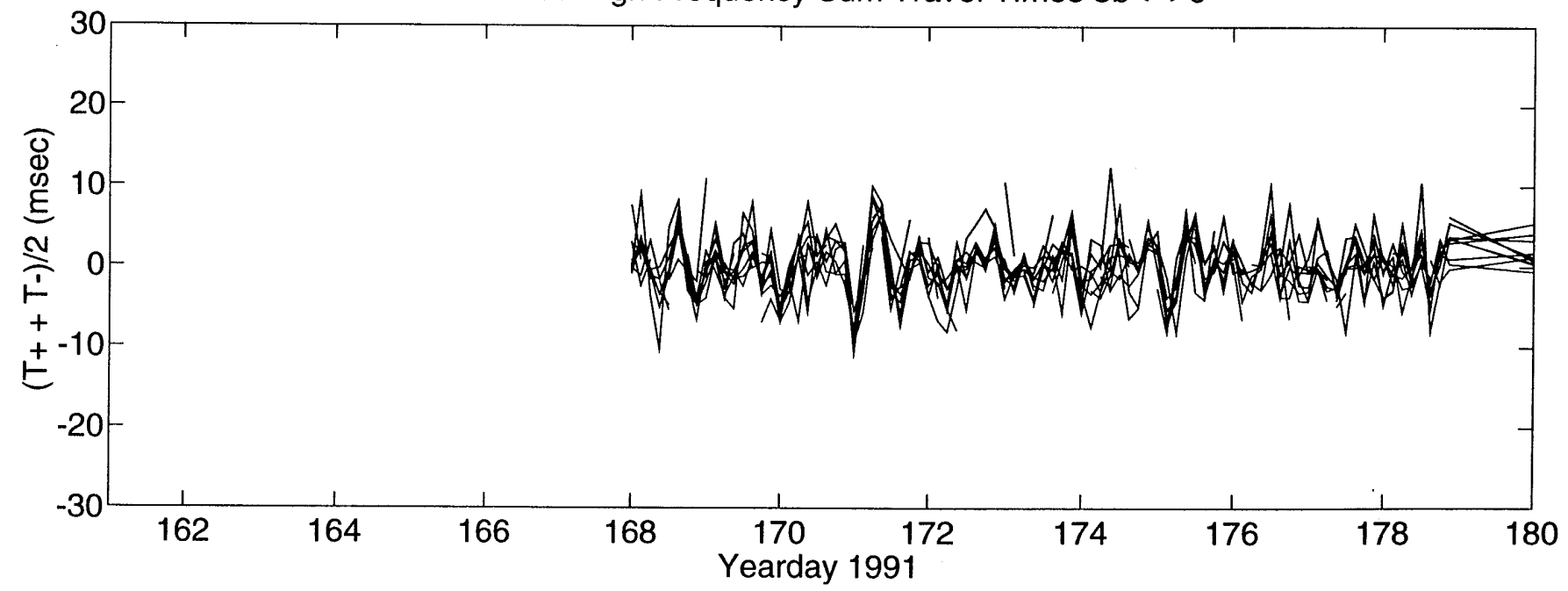
DeTided High Frequency Sum Travel Times 5b<=>6
(T+ + T-)/2 (msec)
30
20
10
0
-10
-20
-30
162
164
166
168
170
172
174
176
178
180
Yearday 1991

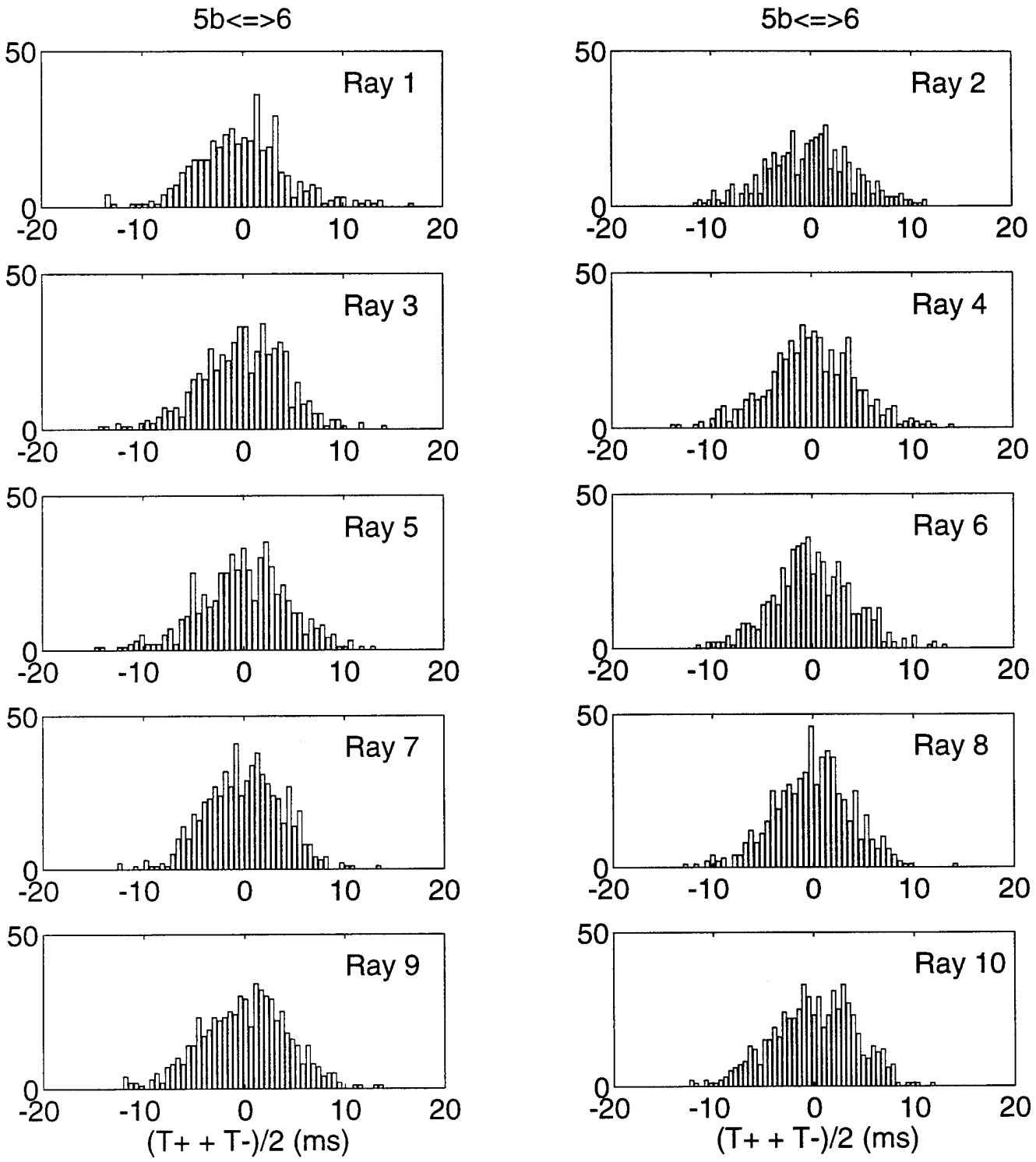
5b<=>6
Ray 1
Ray 2
Ray 3
Ray 4
Ray 5
Ray 6
Ray 7
Ray 8
Ray 9
Ray 10
50
0
-20
-10
0
10
20
(T+ + T-)/2 (ms)

FIGURE Z-5

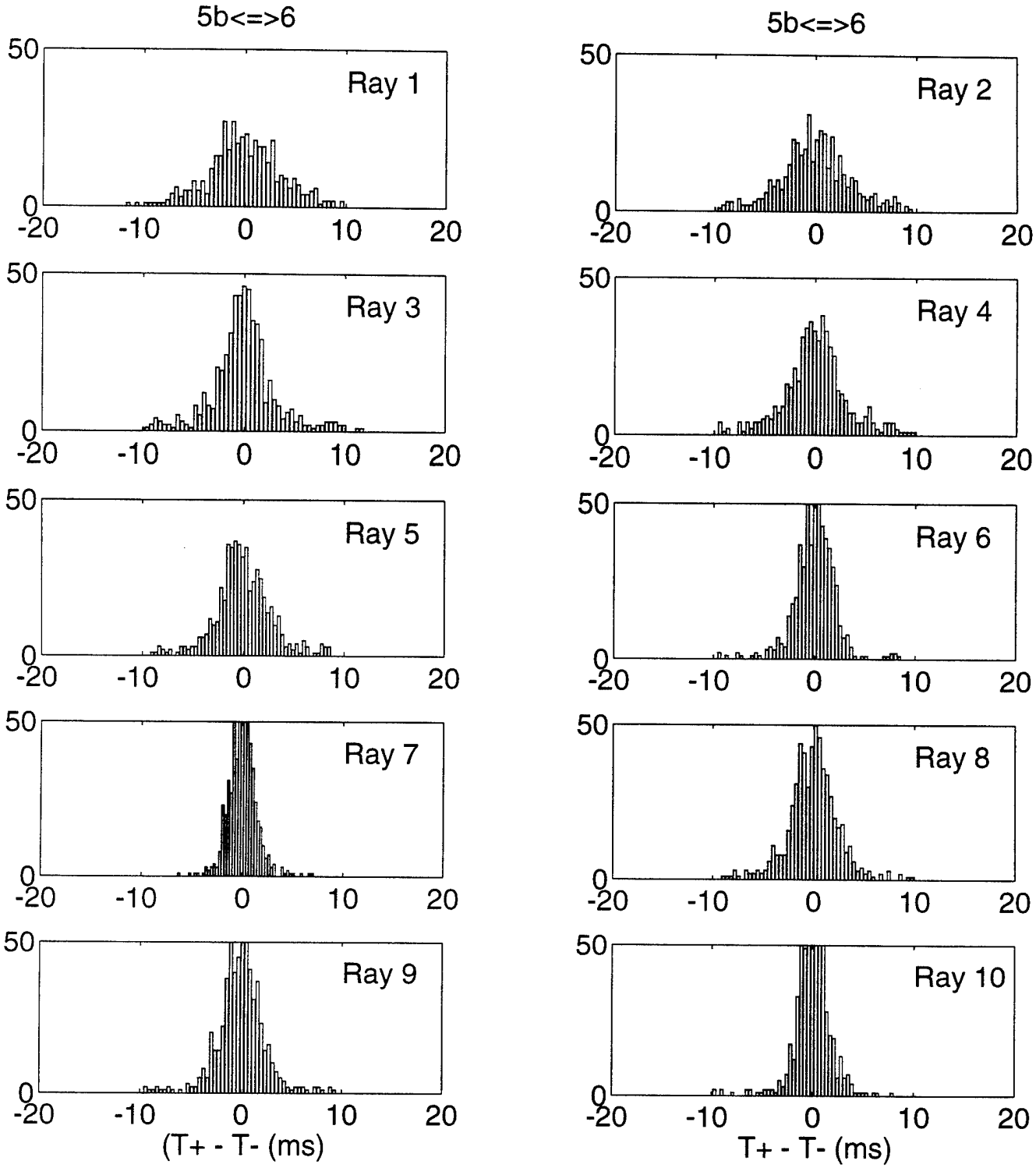
5b<=>6
Ray 1
Ray 2
Ray 3
Ray 4
Ray 5
Ray 6
Ray 7
Ray 8
Ray 9
Ray 10
50
0
-20
-10
0
10
20
(T+ - T- (ms)
T+ - T- (ms)

FIGURE Z-6

AA. DATA IN NODC FORMAT

The AMODE reciprocal travel time data have been put into a form suitable for submission to NODC, when it is appropriate to do so. In this section, this NODC format is described. This format was devised by Brian Dushaw, and the format is subject to modification.

FILE DESCRIPTION OF 1991–1992 AMODE TOMOGRAPHY DATA

This is a description of a file format for tomography travel time data applied to data obtained during the AMODE tomography experiment. These files are intended to have a prototype file structure for tomography data that are submitted to the National Oceanographic Data Center. Comments on and suggestions for improvement to this file organization are welcome. The format was modeled from (Dushaw's interpretation of) the NODC Users Guide.

File Structure

Each file contains all of the ray travel time data collected by a source/receiver pair during the experiment. For the AMODE experiment, six transceivers were deployed, and one was replaced midway through the experiment; hence there are 40 (= 15*2 + 5*2) source/receiver pairs (and 40 data files). The data are the end product of considerable data reduction and polishing. The raw data are NOT YET available from the principal investigator, Peter Worcester.

The file is broken into three sections:

1) The first section is a one line text record describing the parameters of the experiment.

2) The second section is six lines describing the properties of the resolved raypaths. Each column of this section describes the properties of a raypath that corresponds to the same column of travel times of the third section.

3) The third section contains the time of transmission (in yeardays) and the ray travel times. Each line is a yearday and a set of travel times of ray arrivals. Each column is a time series of ray travel times for the raypath which was described in the corresponding column of the second section.

File Format - First Section

PARAMETER	DESCRIPTION	SC	FL
Experiment Name	Name of Experiment	1	6
Principal Investigator	Principal Investigator	8	12
Institution	Institution of Principal Investigator	21	6
Start Date	Start Month of Experiment	28	2
Start Date	Start Year of Experiment	31	4
End Date	End Month of Experiment	36	2
End Date	End Year of Experiment	39	4
Source Latitude	Latitude of Acoustic Source (degrees)	44	3
Source Latitude	Latitude of Acoustic Source (minutes)	48	6
Source Longitude	Longitude of Acoustic Source (degrees)	55	3
Source Longitude	Longitude of Acoustic Source (minutes)	59	6
Source Depth	Depth of Acoustic Source (m)	66	5
Receiver Latitude	Latitude of Acoustic Receiver (degrees)	72	3
Receiver Latitude	Latitude of Acoustic Receiver (minutes)	76	6
Receiver Longitude	Longitude of Acoustic Receiver (degrees)	83	3
Receiver Longitude	Longitude of Acoustic Receiver (minutes)	87	6
Receiver Depth	Depth of Acoustic Receiver (m)	94	5
Number of Rays	Number of Resolved Ray Travel Time Arrivals	100	3
Number of Transmissions	Number of Recorded Acoustic Transmissions	104	4
Mooring Motion Correction	Travel Times Corrected for Mooring Motion (Y,N)	109	1
Mooring Corr. Available	Time Series of Mooring Positions Available (Y,N)	111	1
Clock Correction	Travel Times Corrected for Instrument Clock Drift (Y,N)	113	1
Clock Corr. Available	Time Series of Clock Correction Available (Y,N)	115	1
Source Type	Type of Acoustic Source Used for Transmissions	117	6
Center Frequency	Frequency of Acoustic Source (Hz)	123	5

File Format - Second Section

The second section of the file consists of six lines. The lines give the raypath information about the tracked travel times. If no ray identification was found (e.g., for nongeometric arrivals), the six numbers are all zero (this does not mean that ray trace predictions with some other reference ocean will not give ray predictions to match these travel times – ray identification is a black art.).

line 1:

PARAMETER	DESCRIPTION	SC	FL
Zero	Always Zero	1	8
Travel Time*	Predicted Travel Time of First Raypath (sec)	10	8

*Travel Times repeated (8 characters plus one space) for as many times as indicated by the Number of Rays field.

line 2:

PARAMETER	DESCRIPTION	SC	FL
Zero	Always Zero	1	8
Source Angle*	Predicted Launch Angle of First Raypath (deg)	10	8

*Angles repeated (8 characters plus one space) for as many times as indicated by the Number of Rays field.

line 3:

PARAMETER	DESCRIPTION	SC	FL
Zero	Always Zero	1	8
Receiver Angle*	Predicted Arrival Angle of First Raypath (deg)	10	8

*Angles repeated (8 characters plus one space) for as many times as indicated by the Number of Rays field.

line 4:

PARAMETER	DESCRIPTION	SC	FL
Zero	Always Zero	1	8
Lower Turning Depth*	Predicted Lower Turning Depth of First Raypath (km)	10	8

*Depths repeated (8 characters plus one space) for as many times as indicated by the Number of Rays field.

line 5:

PARAMETER	DESCRIPTION	SC	FL
Zero	Always Zero	1	8
Upper Turning Depth*	Predicted Upper Turning Depth of First Raypath (km)	10	8

*Depths repeated (8 characters plus one space) for as many times as indicated by the Number of Rays field.

line 6:

PARAMETER	DESCRIPTION	SC	FL
Zero	Always Zero	1	8
Number of Turning Points*	Predicted Number of turning depths of First Raypath	10	8

*Number of turning points repeated (8 characters plus one space) for as many times as indicated by the Number of Rays field.

File Format - Third Section

The third section of the file consists of trios of lines, with the number of line trios given by the Number of Transmissions field.

first line of trio:

PARAMETER	DESCRIPTION	SC	FL
Yearday	Time of Acoustic Transmission	1	8
Ray Travel Time*	Measured Travel Time of First Raypath (sec)	10	8

*Number of travel times repeated (8 characters plus one space) for as many times as indicated by the Number of Rays field.

second line of trio:

PARAMETER	DESCRIPTION	SC	FL
Yearday	Time of Acoustic Transmission	1	8
Signal-to-Noise Ratio*	Ratio of Ray Arrival Intensity to Background Noise (dB)	10	8

*Number of signal-to-noise ratios repeated (8 characters plus one space) for as many times as indicated by the Number of Rays field. A value of zero indicates no travel time, and a value of 999 is used to indicate unknown signal-to-noise ratio (e.g., the final cutoff travel times).

third line of trio:

PARAMETER	DESCRIPTION	SC	FL
Yearday	Time of Acoustic Transmission	1	8
Travel Time Error*	Error Due to Mooring Positioning and Clocks (sec)	10	8

*Number of errors repeated (8 characters plus one space) for as many times as indicated by the Number of Rays field. A value of zero indicates no travel time.

The line trios are repeated as many times as indicated by the Number of Transmissions field.

AB. SOSUS ARRAY RECEPTIONS: Dot Plots

In addition to the transmissions between the AMODE transceivers, the transmissions were also recorded at four Naval Facility hydrophone arrays (FIGURE AB-1). The locations and other information about these receivers are classified; hence FIGURE AB-1 shows fictive locations while still giving an accurate description of the spatial coverage of the acoustic paths. An additional acoustic source was located just south of Bermuda. Transmissions from this source were not recorded by the AMODE instruments, however. The area sampled by transmissions between these instruments spans about 1400 km X 1700 km. Though some initial inversions of the travel times to these Navy arrays were calculated, little work has been done on these data.

Here only the "dot plots" and tracked data are shown. The data were beamformed using a single azimuthal arrival angle; hence no allowance was made for any variation in vertical arrival angle (i.e., beamforming did not take into account the conical arrival angle.) Only peak picked data are available, and a 14 dB SNR threshold for saving peaks was used. Owing to disk storage limitations, the raw acoustic data have been lost. The receptions from the AMODE moorings have been corrected for the motion and clock error of those moorings. A large travel time offset has been added to the travel times in order to declassify them.

The "dot plots" generally show clearly resolved ray arrivals over a time period of 250–400 days. A gap unfortunately occurs in the record for some of the time series because of technical problems at the Navy facilities. Some of the "ray" arrivals are in the shadow zone of the predicted time front for the source/receiver geometry using the Levitus sound speed fields. The arrivals can be identified with the caustics, however. It is unlikely that realistic sound speed perturbations would be significant enough to enable these "shadow zone" arrivals to be identified with direct eigenray arrivals.

The "Amplitude" panel is the amplitude predicted using the ray propagation code "rdryt"; hence this panel may be ignored.

Including transmissions from both AMODE moorings 5a and 5b, there are 40 time series of data recorded by the SOSUS stations. The source/receiver pairs are indicated by the first/last two digits noted on each figure. Thus, "1007" refers to transmissions from the Bermuda source to SOSUS array 7, while "2413" refers to transmissions from AMODE source 4 to SOSUS array 13 (see FIGURE AB-1). AMODE source 5a is denoted by "27."

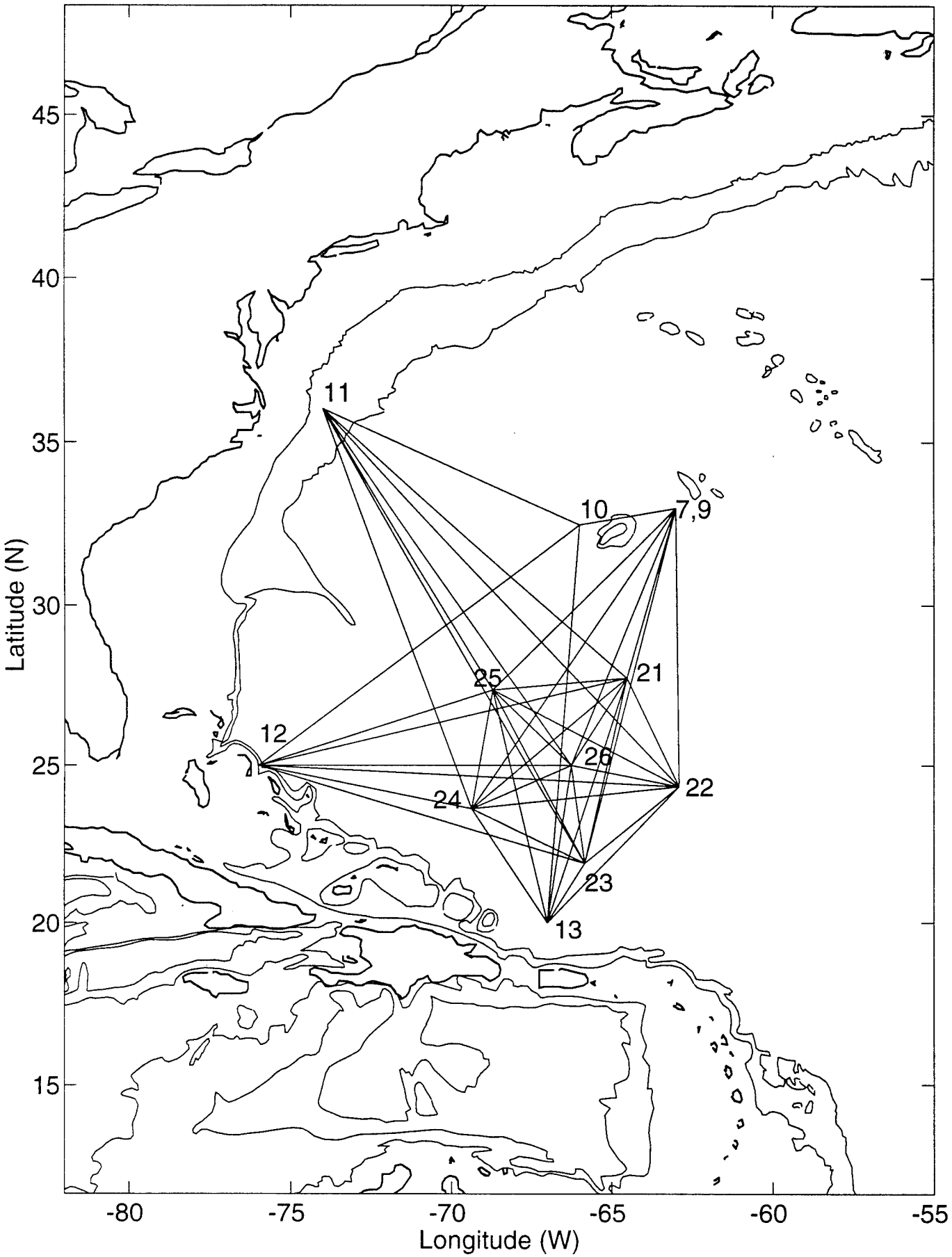

The locations of SOSUS arrays 7, 9, 11, 12, 13 shown on this figure are fictive.

FIGURE AB-1

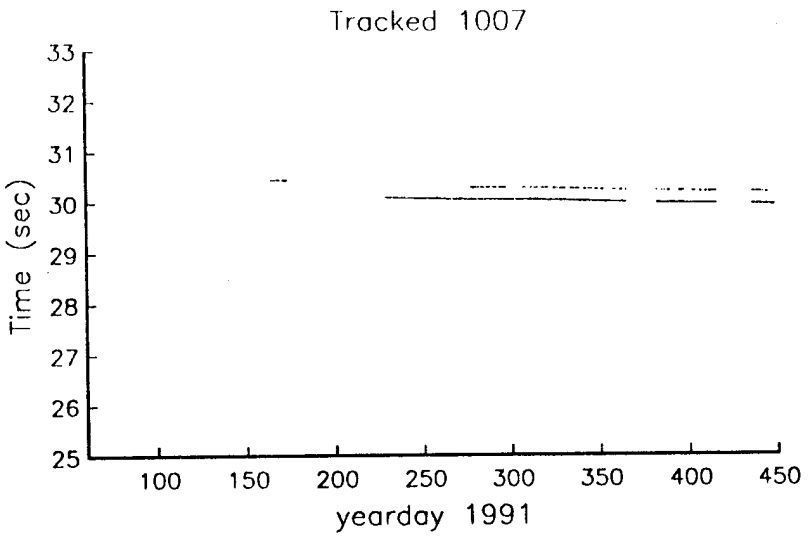
Tracked 1007
Time (sec)
33
32
31
30
29
28
27
26
25
100
150
200
250
300
350
400
450
yearday 1991

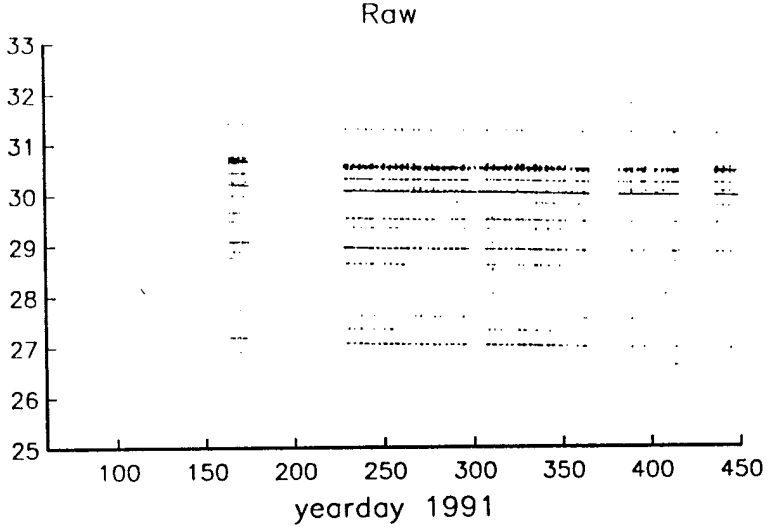
Raw
33
32
31
30
29
28
27
26
25
100
150
200
250
300
350
400
450
yearday 1991

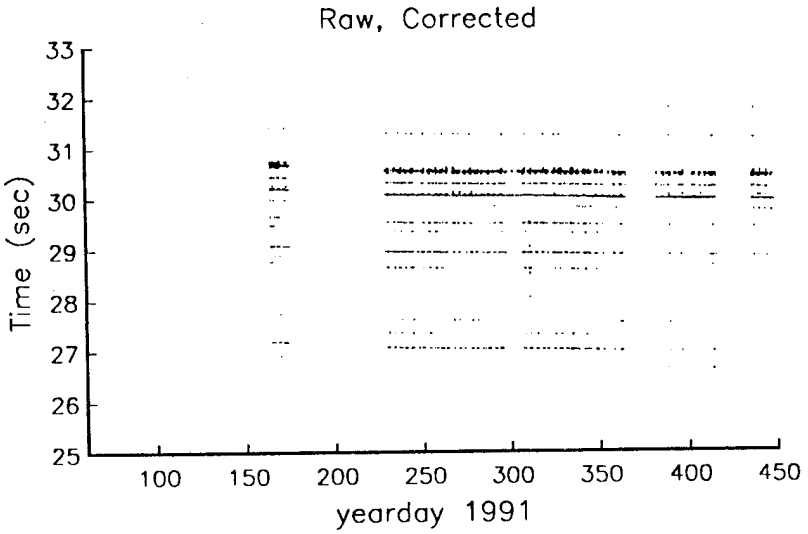
Raw, Corrected
Time (sec)
33
32
31
30
29
28
27
26
25
100
150
200
250
300
350
400
450
yearday 1991

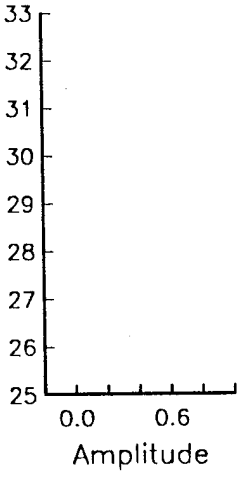
33
32
31
30
29
28
27
26
25
0.0
0.6
Amplitude

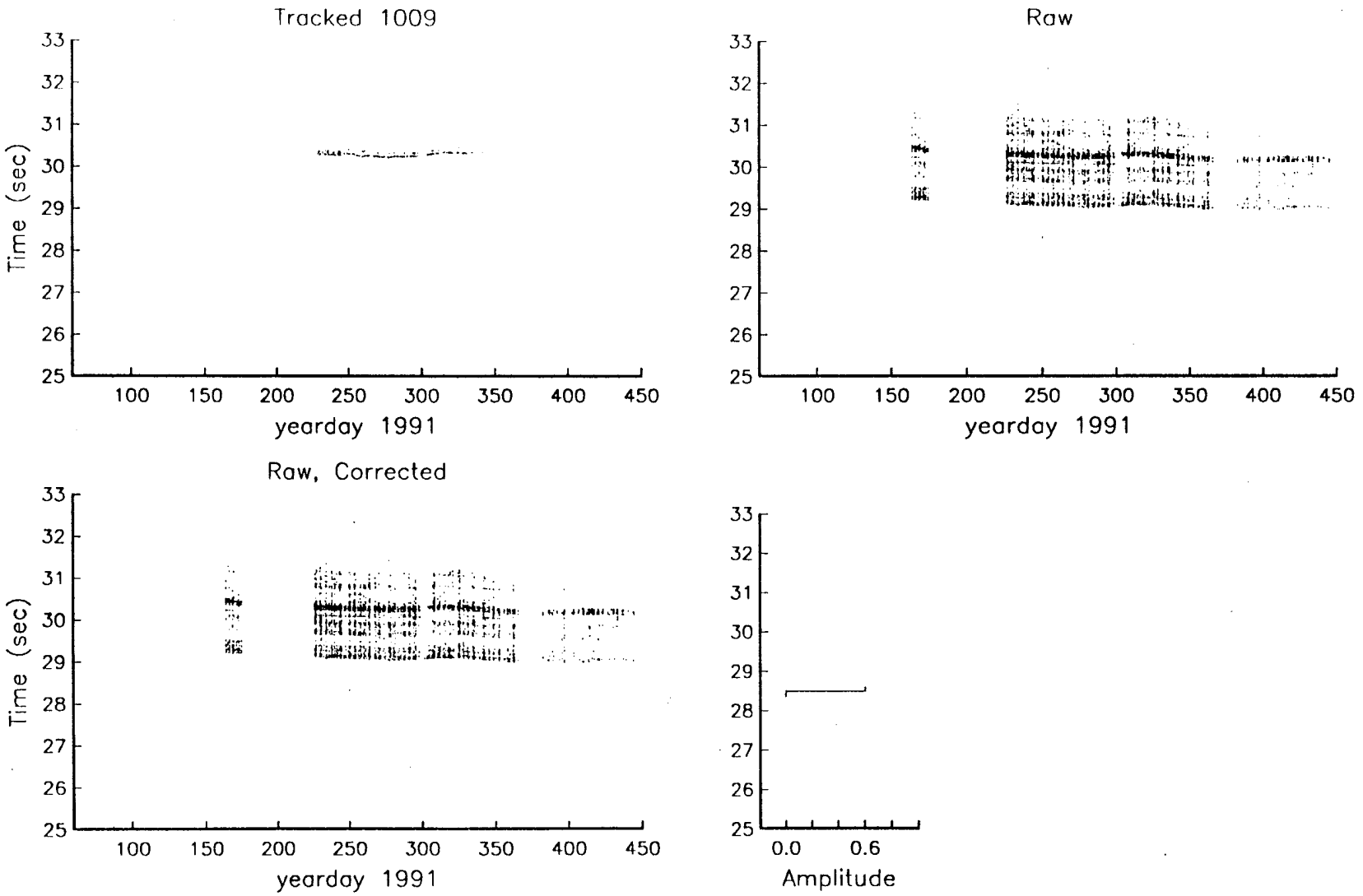
Tracked 1009
Time (sec)
yearday 1991
Raw
Time (sec)
yearday 1991
Raw, Corrected
Time (sec)
yearday 1991
Amplitude

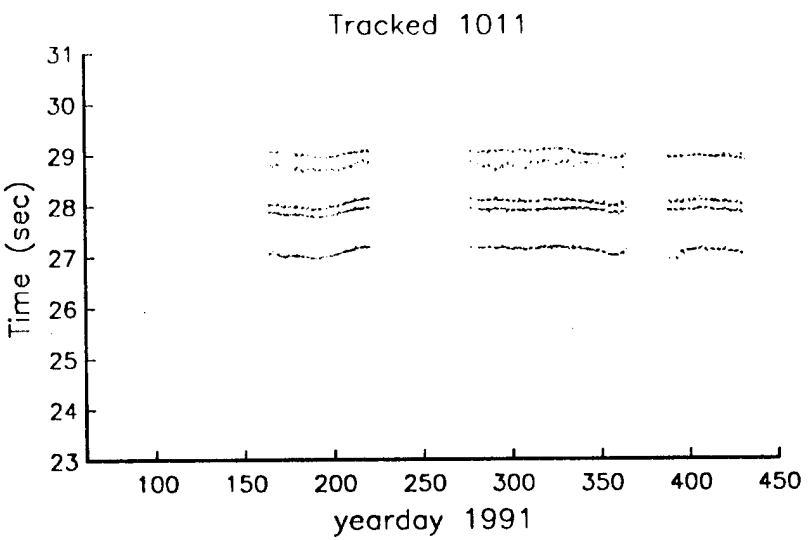
Tracked 1011
Time (sec)
31
30
29
28
27
26
25
24
23
100
150
200
250
300
350
400
450
yearday 1991

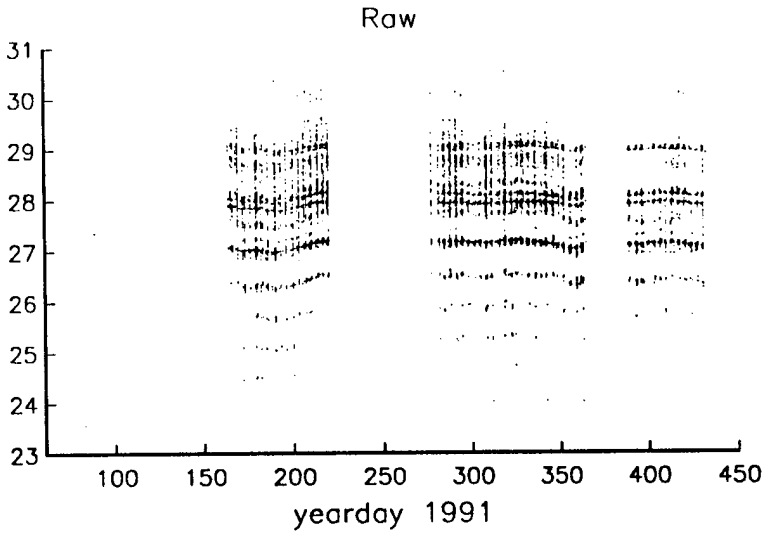
Raw
31
30
29
28
27
26
25
24
23
100
150
200
250
300
350
400
450
yearday 1991

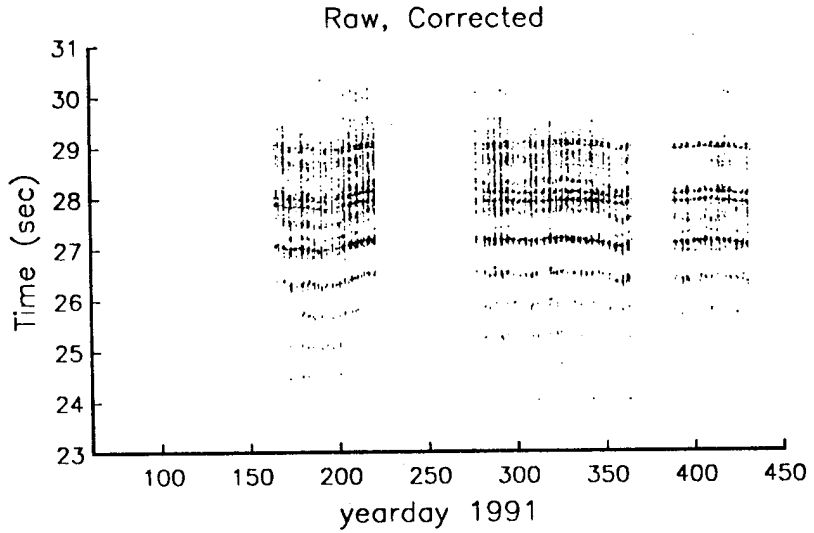
Raw, Corrected
Time (sec)
31
30
29
28
27
26
25
24
23
100
150
200
250
300
350
400
450
yearday 1991

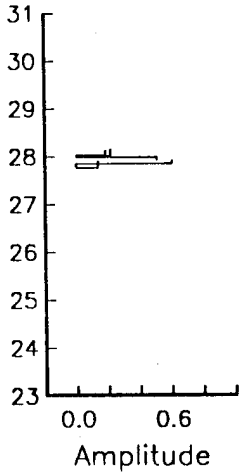
31
30
29
28
27
26
25
24
23
0.0
0.6
Amplitude

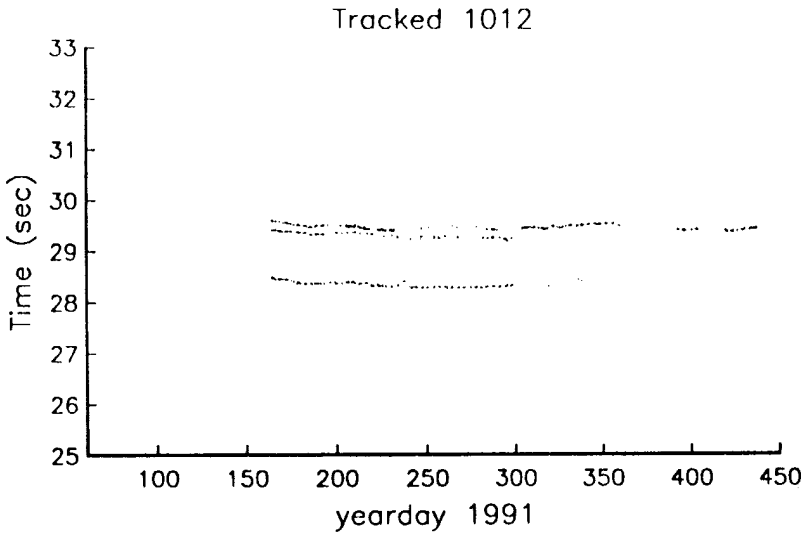
Tracked 1012
Time (sec)
33
32
31
30
29
28
27
26
25
100
150
200
250
300
350
400
450
yearday 1991

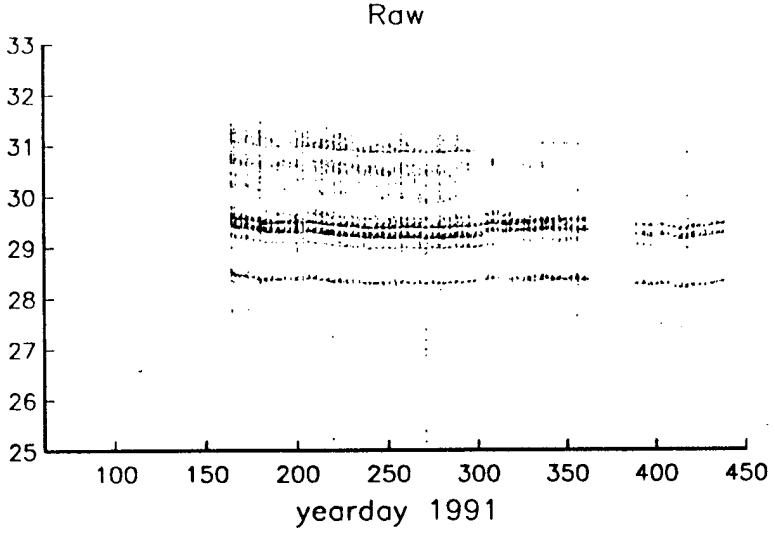
Raw
33
32
31
30
29
28
27
26
25
100
150
200
250
300
350
400
450
yearday 1991

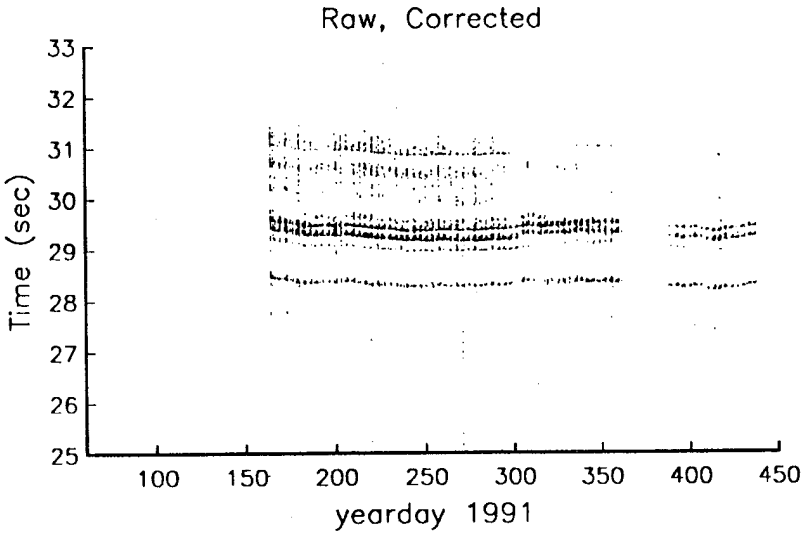
Raw, Corrected
Time (sec)
33
32
31
30
29
28
27
26
25
100
150
200
250
300
350
400
450
yearday 1991

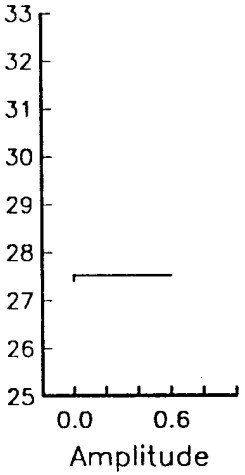
33
32
31
30
29
28
27
26
25
0.0
0.6
Amplitude

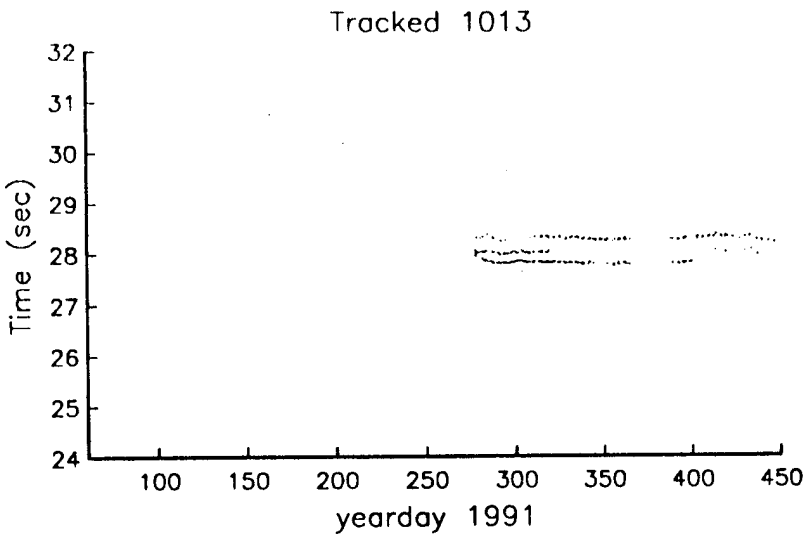
Tracked 1013
Time (sec)
32
31
30
29
28
27
26
25
24
100
150
200
250
300
350
400
450
yearday 1991

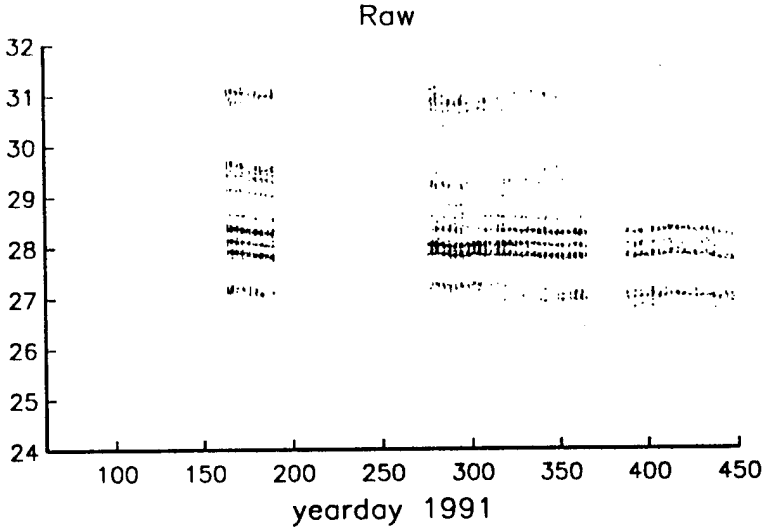
Raw
32
31
30
29
28
27
26
25
24
100
150
200
250
300
350
400
450
yearday 1991

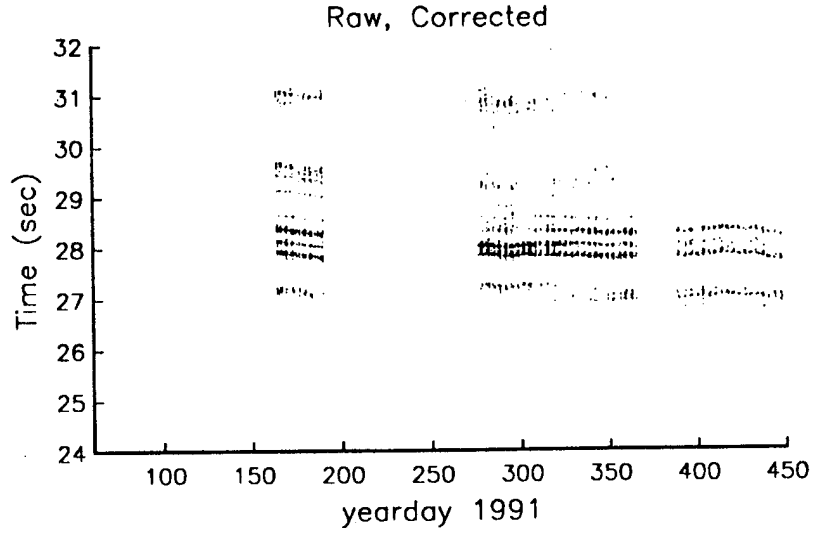
Raw, Corrected
Time (sec)
32
31
30
29
28
27
26
25
24
100
150
200
250
300
350
400
450
yearday 1991

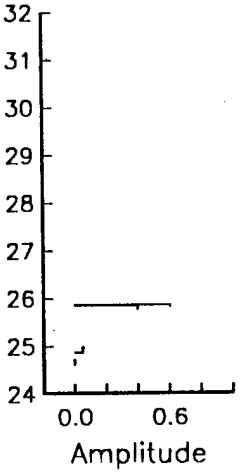
32
31
30
29
28
27
26
25
24
0.0
0.6
Amplitude

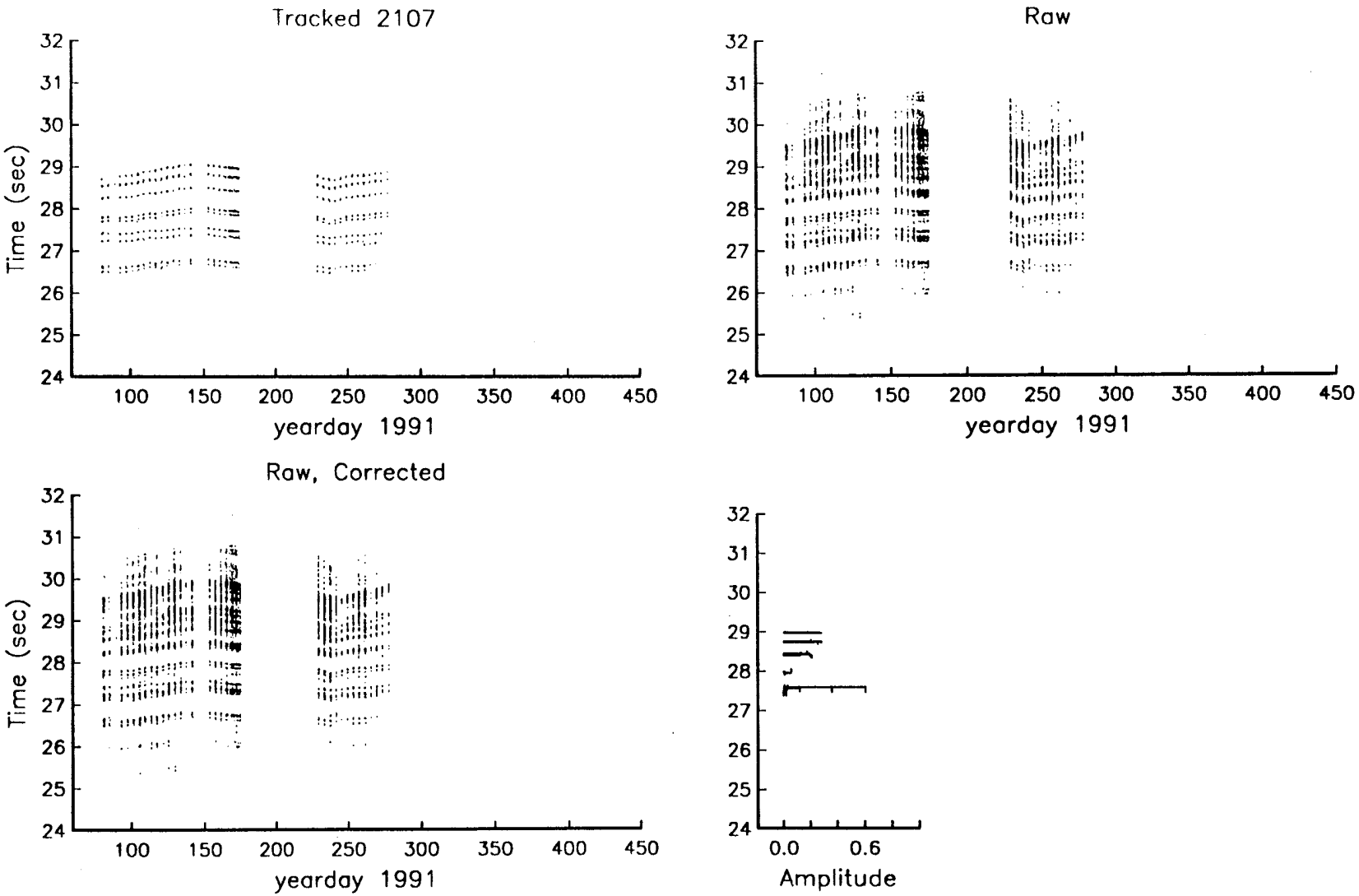
Tracked 2107
Raw
Raw, Corrected
Time (sec)
yearday 1991
Amplitude
32
31
30
29
28
27
26
25
24
100
150
200
250
300
350
400
450
0.0
0.6

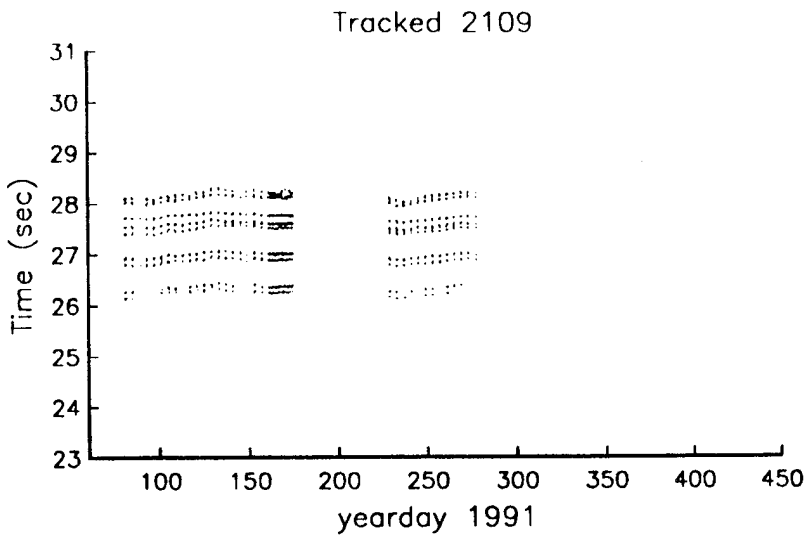
Tracked 2109
Time (sec)
31
30
29
28
27
26
25
24
23
100
150
200
250
300
350
400
450
yearday 1991

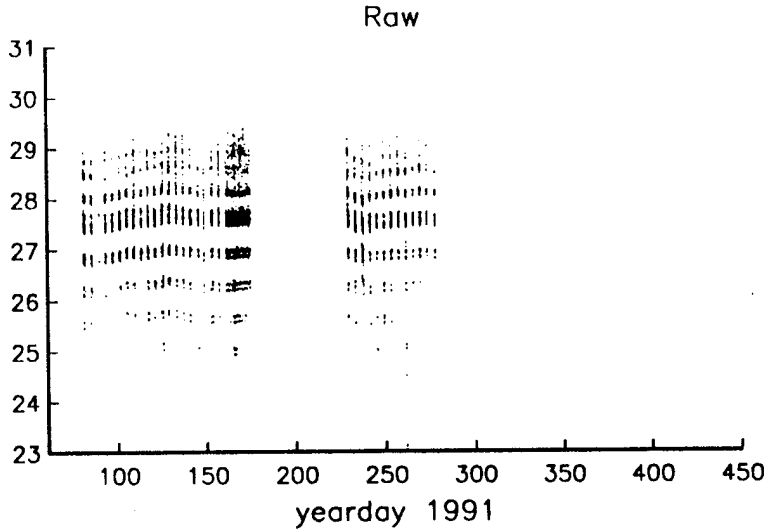
Raw
31
30
29
28
27
26
25
24
23
100
150
200
250
300
350
400
450
yearday 1991

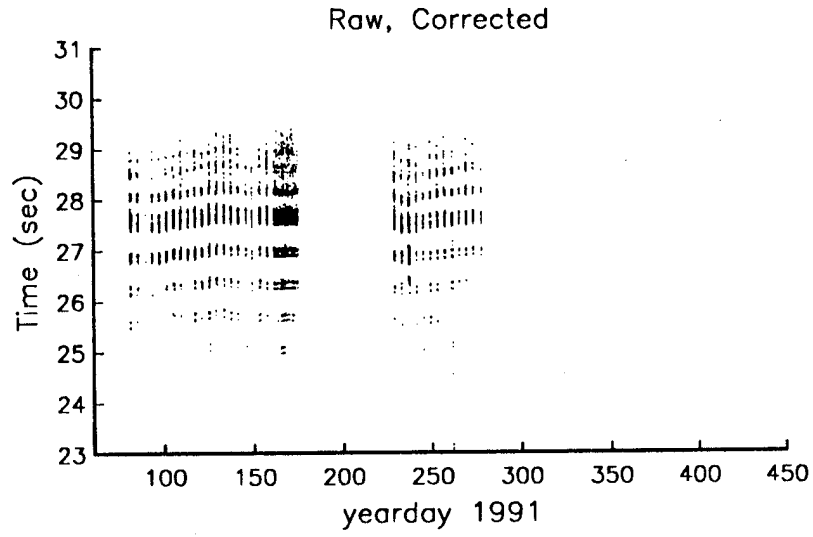
Raw, Corrected
Time (sec)
31
30
29
28
27
26
25
24
23
100
150
200
250
300
350
400
450
yearday 1991

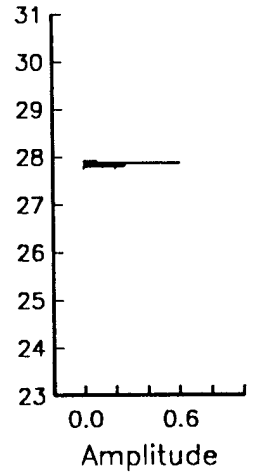
31
30
29
28
27
26
25
24
23
0.0
0.6
Amplitude

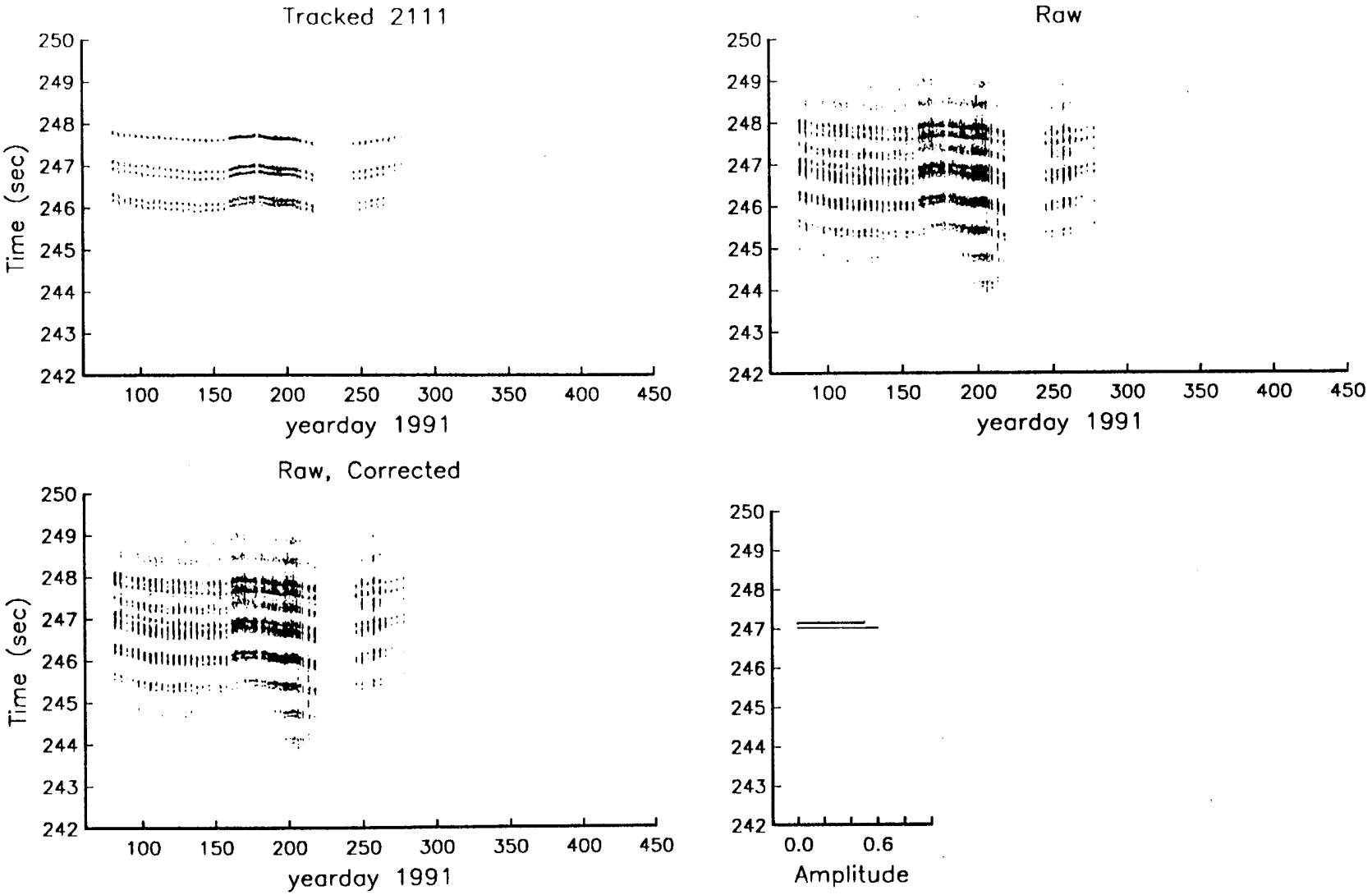
Tracked 2111
Raw
Raw, Corrected
Time (sec)
yearday 1991
Amplitude
250
249
248
247
246
245
244
243
242
100
150
200
250
300
350
400
450
0.0
0.6

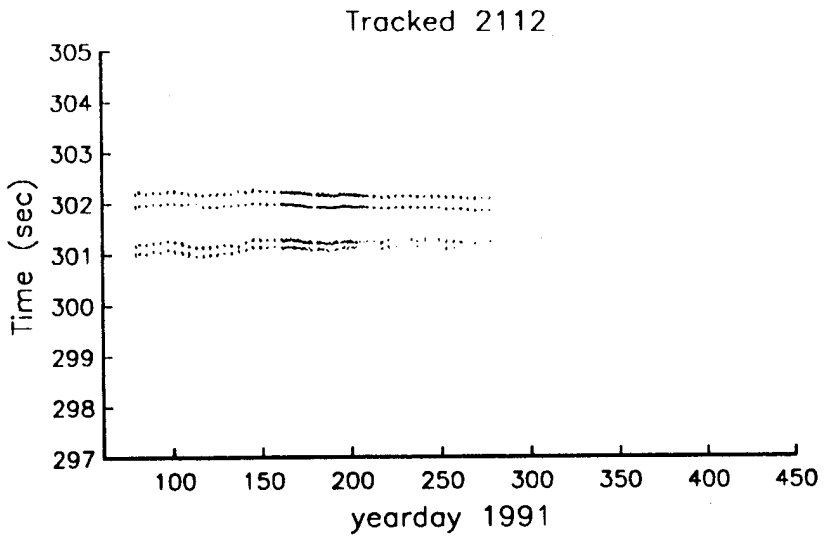
Tracked 2112
Time (sec)
305
304
303
302
301
300
299
298
297
100
150
200
250
300
350
400
450
yearday 1991

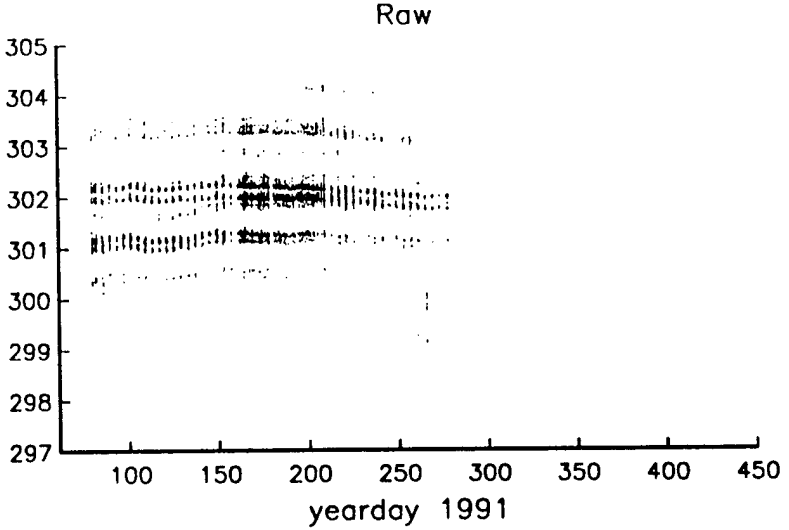
Raw
305
304
303
302
301
300
299
298
297
100
150
200
250
300
350
400
450
yearday 1991

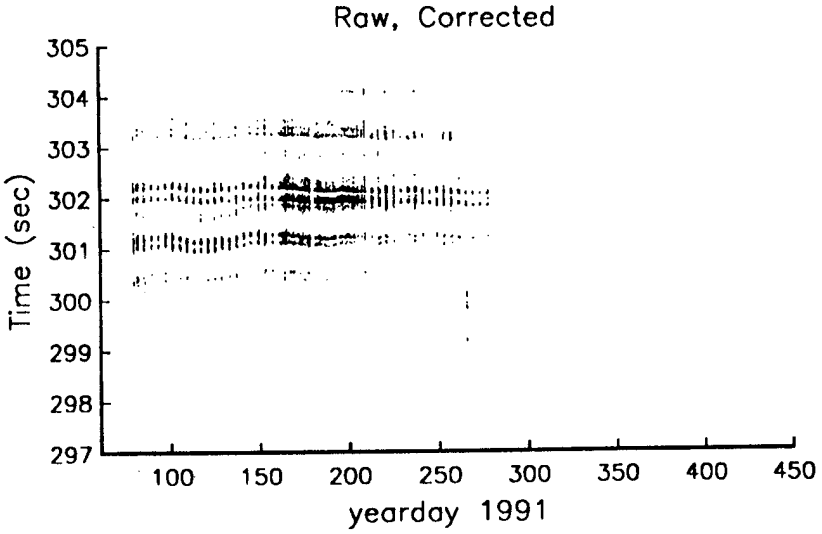
Raw, Corrected
Time (sec)
305
304
303
302
301
300
299
298
297
100
150
200
250
300
350
400
450
yearday 1991

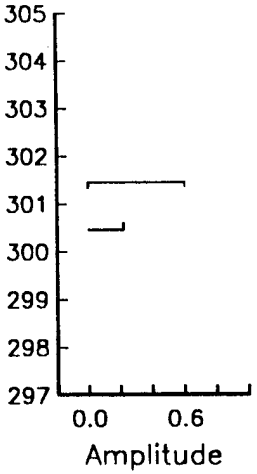
305
304
303
302
301
300
299
298
297
0.0
0.6
Amplitude

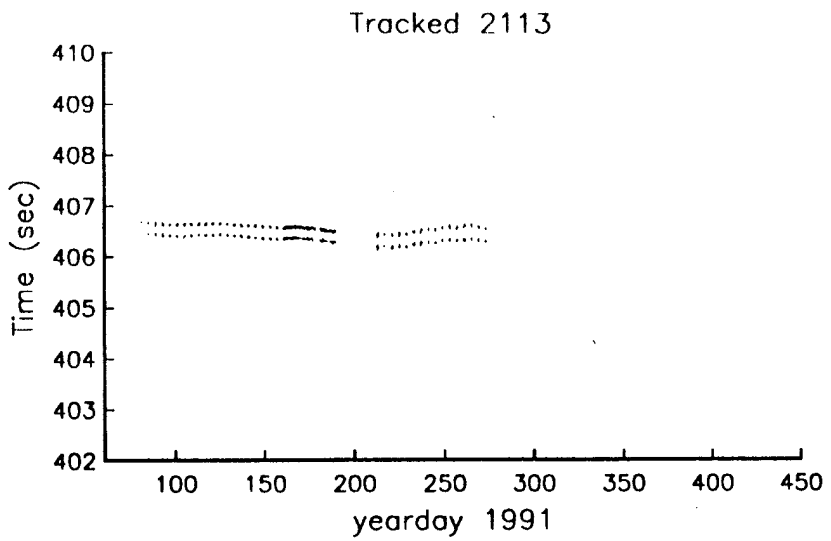
Tracked 2113
Time (sec)
410
409
408
407
406
405
404
403
402
100
150
200
250
300
350
400
450
yearday 1991

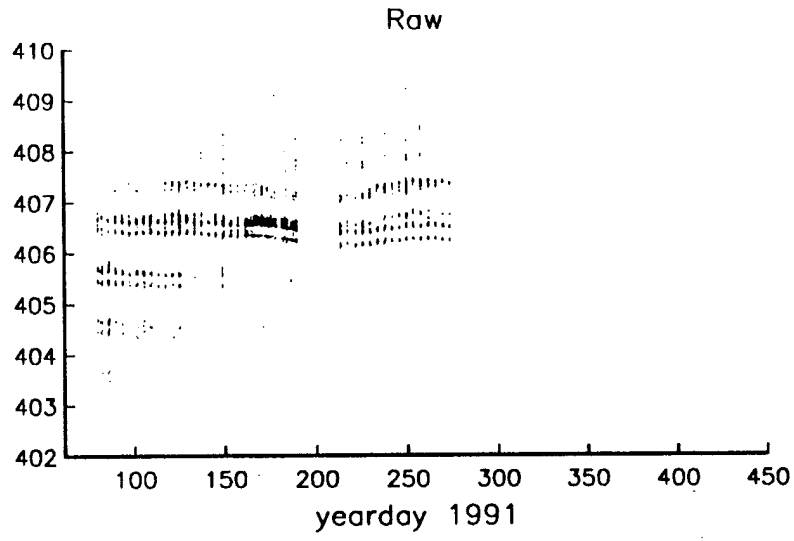
Raw
410
409
408
407
406
405
404
403
402
100
150
200
250
300
350
400
450
yearday 1991

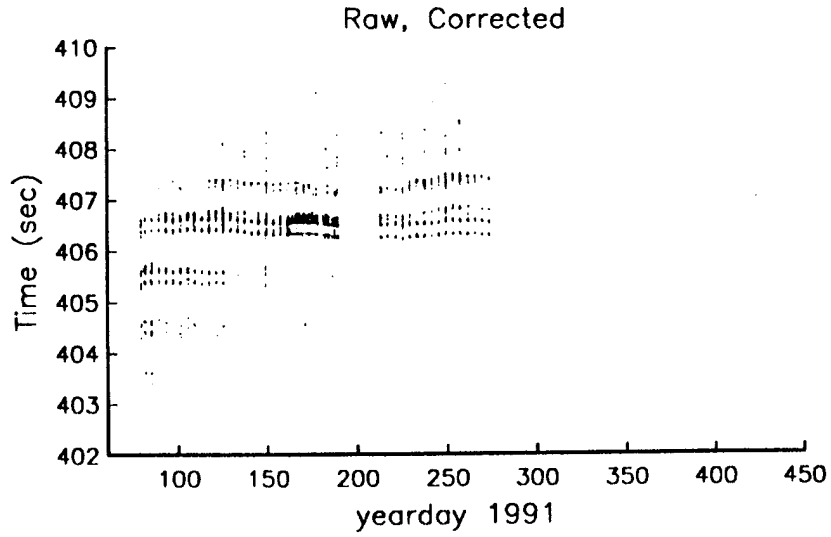
Raw, Corrected
Time (sec)
410
409
408
407
406
405
404
403
402
100
150
200
250
300
350
400
450
yearday 1991

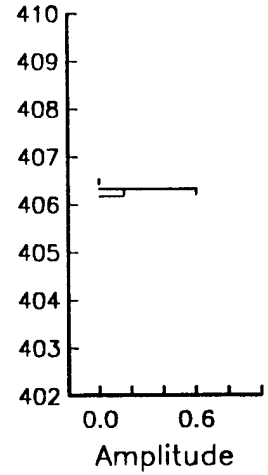
410
409
408
407
406
405
404
403
402
0.0
0.6
Amplitude

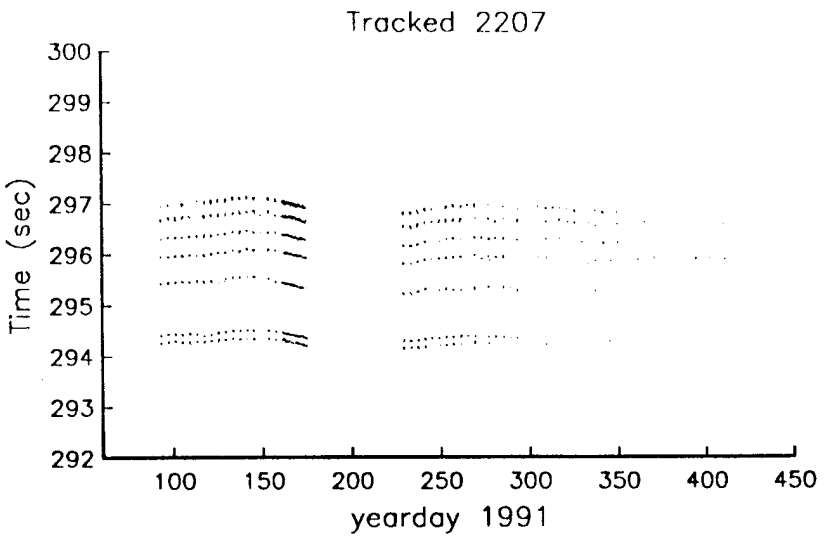
Tracked 2207
Time (sec)
300
299
298
297
296
295
294
293
292
100
150
200
250
300
350
400
450
yearday 1991

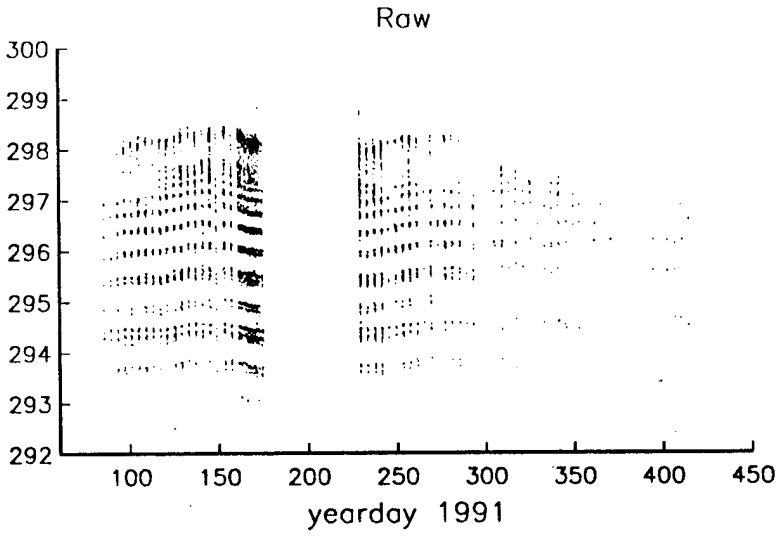
Raw
300
299
298
297
296
295
294
293
292
100
150
200
250
300
350
400
450
yearday 1991

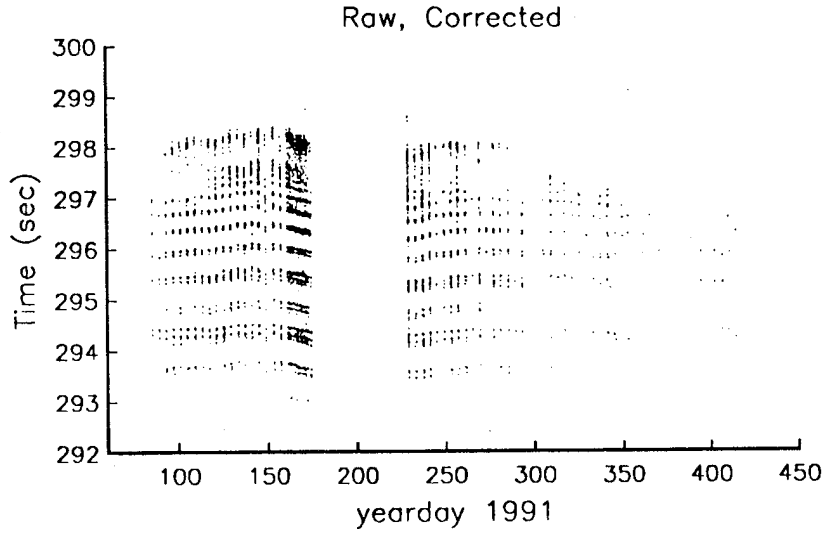
Raw, Corrected
Time (sec)
300
299
298
297
296
295
294
293
292
100
150
200
250
300
350
400
450
yearday 1991

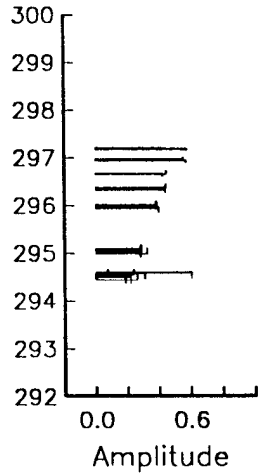
300
299
298
297
296
295
294
293
292
0.0
0.6
Amplitude

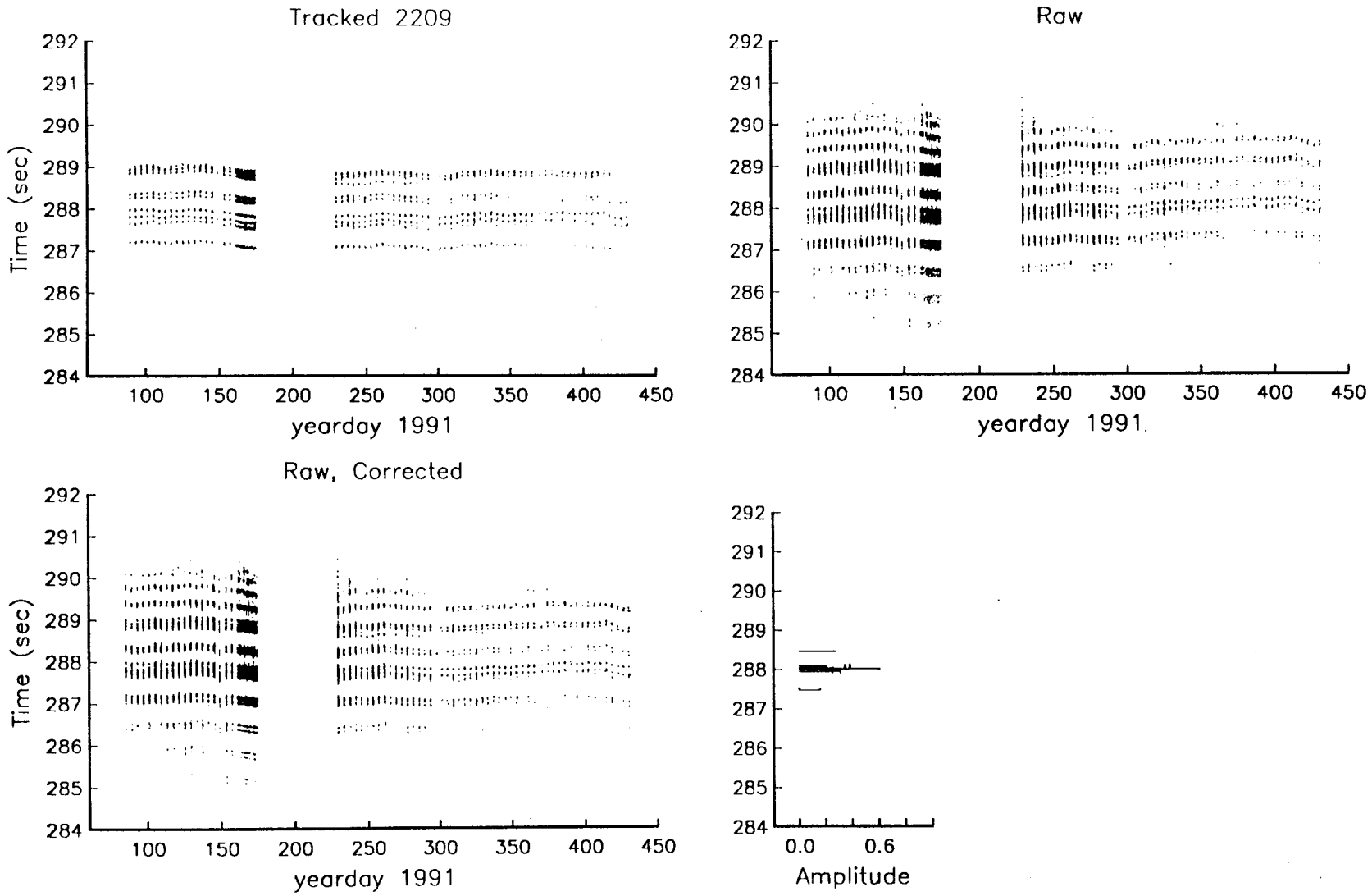
Tracked 2209
Raw
Raw, Corrected
Time (sec)
yearday 1991
Amplitude
292
291
290
289
288
287
286
285
284
100
150
200
250
300
350
400
450
0.0
0.6

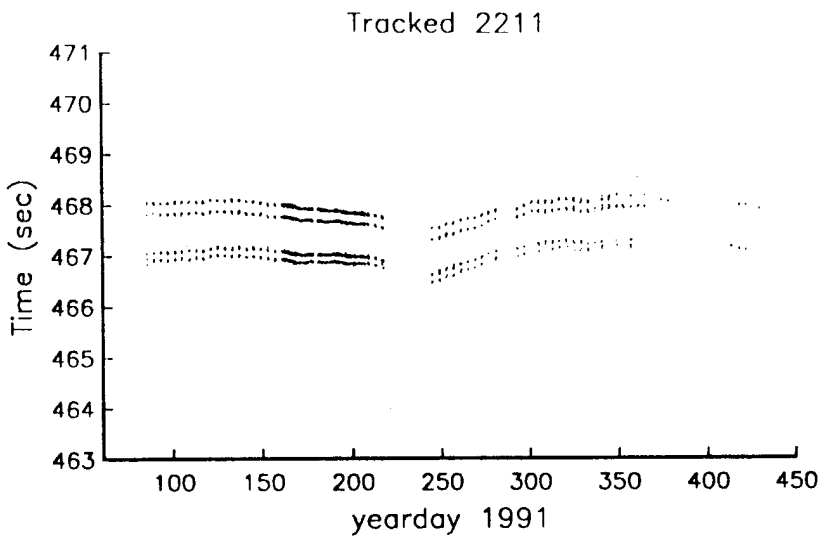
Tracked 2211
Time (sec)
471
470
469
468
467
466
465
464
463
100
150
200
250
300
350
400
450
yearday 1991

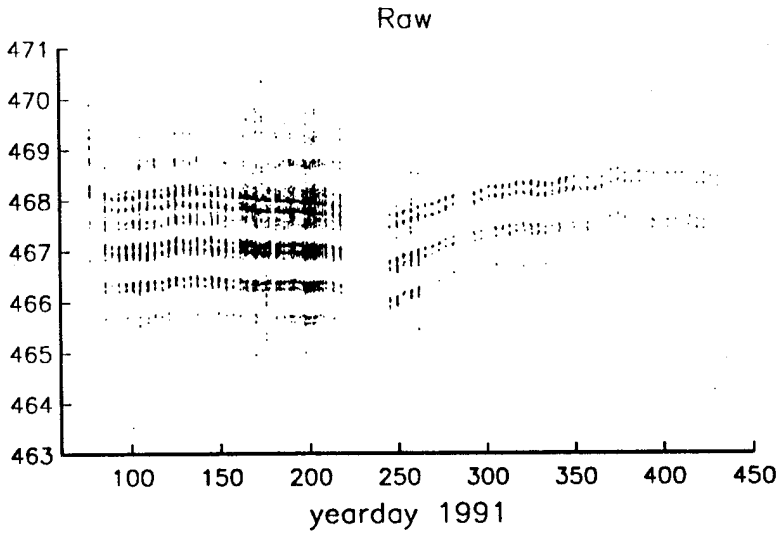
Raw
471
470
469
468
467
466
465
464
463
100
150
200
250
300
350
400
450
yearday 1991

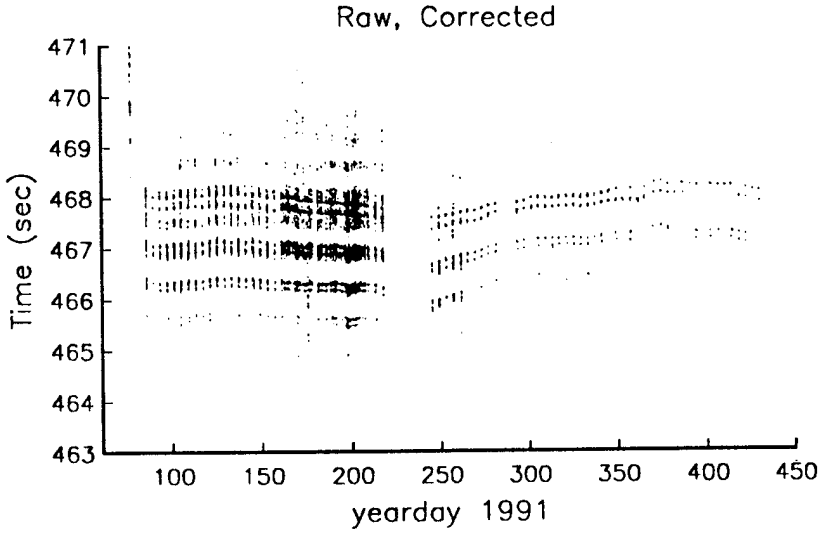
Raw, Corrected
Time (sec)
471
470
469
468
467
466
465
464
463
100
150
200
250
300
350
400
450
yearday 1991

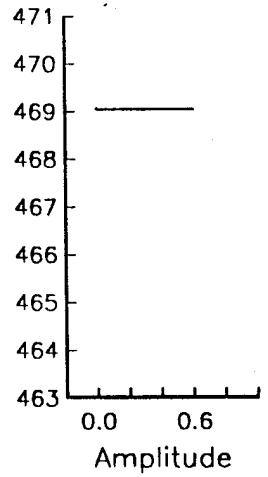
471
470
469
468
467
466
465
464
463
0.0
0.6
Amplitude

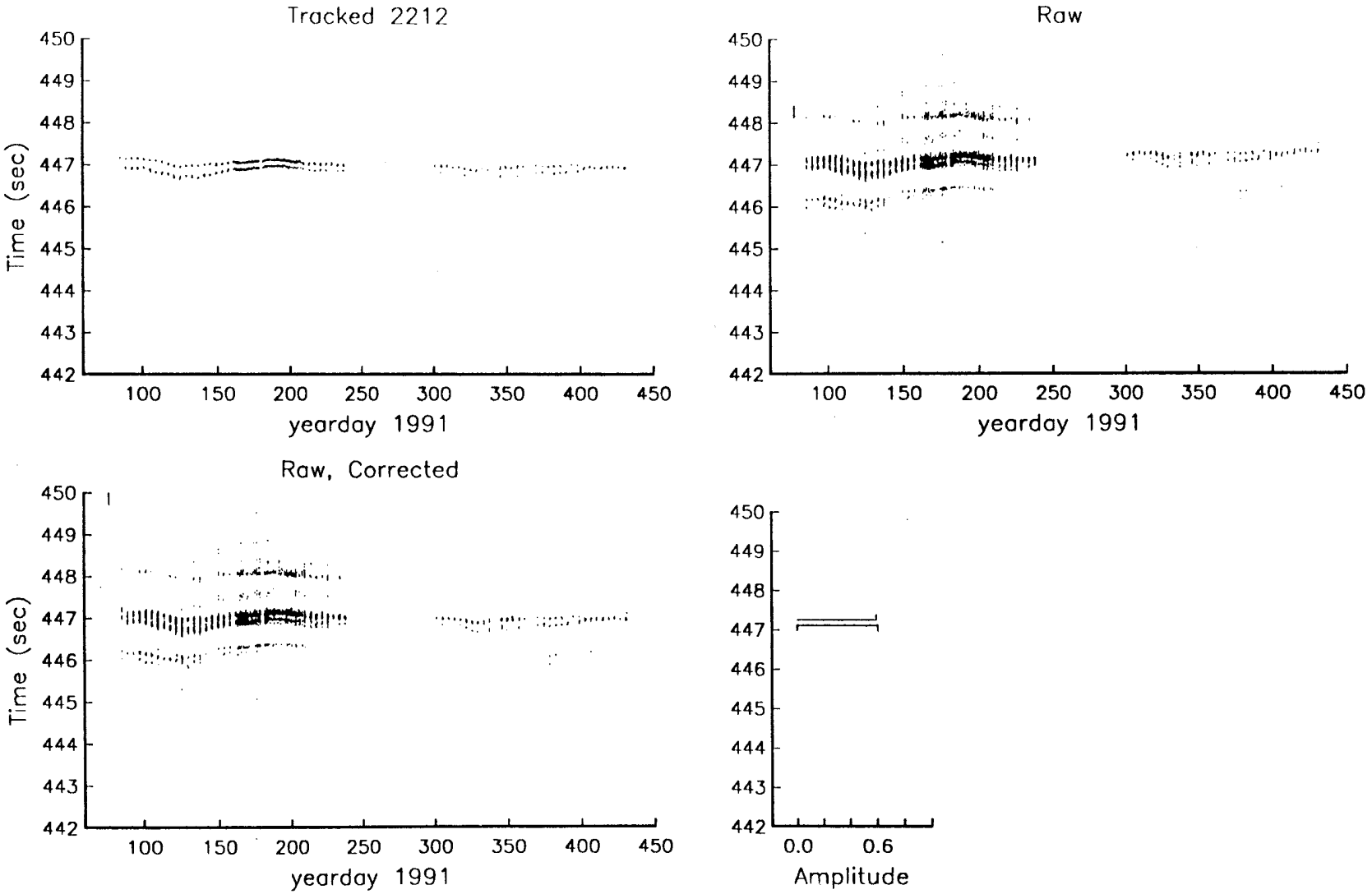
Tracked 2212
Raw
Raw, Corrected
Time (sec)
yearday 1991
Amplitude
450
449
448
447
446
445
444
443
442
100
150
200
250
300
350
400
450
0.0
0.6

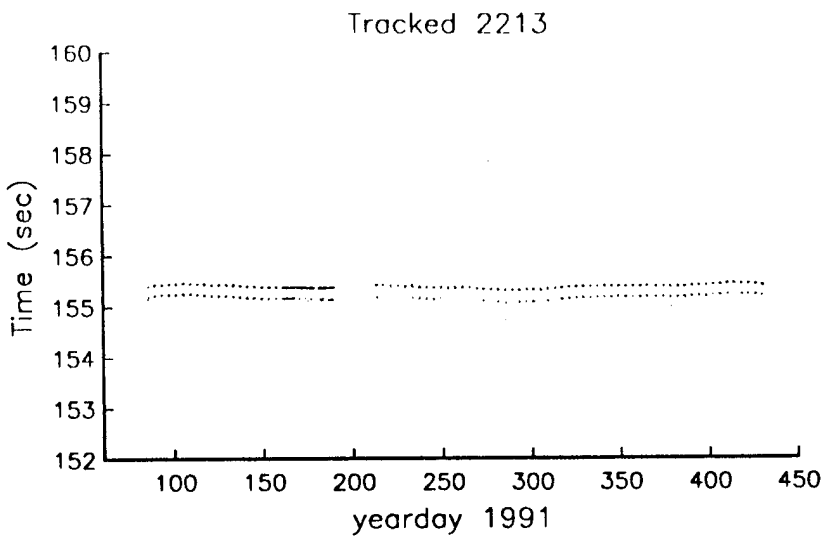
Tracked 2213
Time (sec)
160
159
158
157
156
155
154
153
152
100
150
200
250
300
350
400
450
yearday 1991

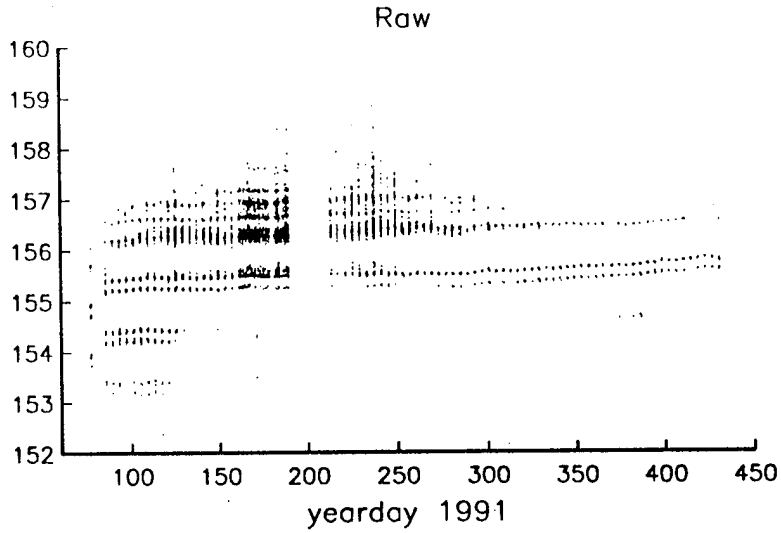
Raw
160
159
158
157
156
155
154
153
152
100
150
200
250
300
350
400
450
yearday 1991

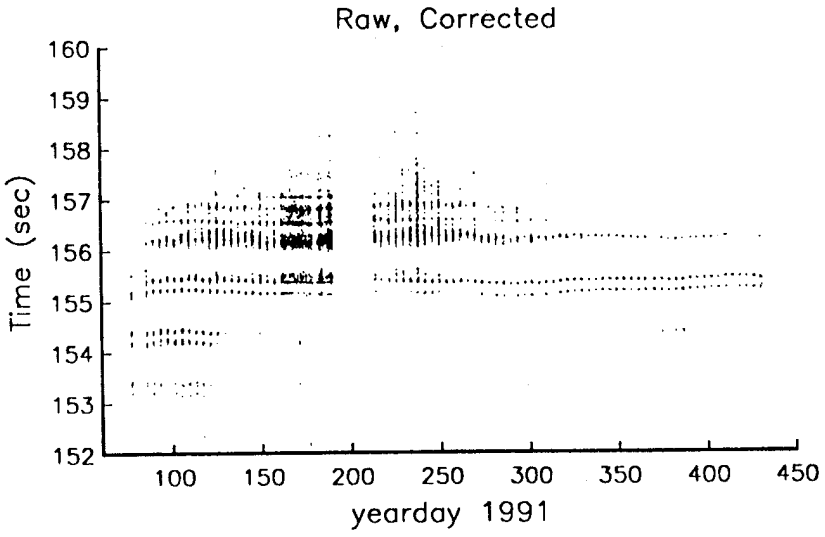
Raw, Corrected
Time (sec)
160
159
158
157
156
155
154
153
152
100
150
200
250
300
350
400
450
yearday 1991

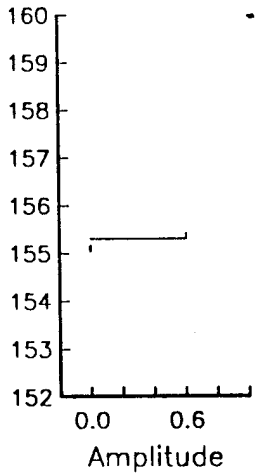
160
159
158
157
156
155
154
153
152
0.0
0.6
Amplitude

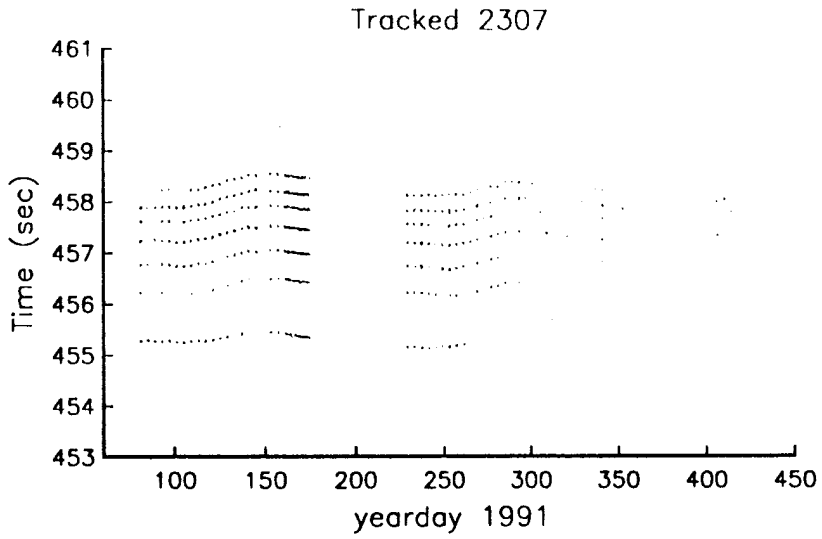
Tracked 2307
Time (sec)
461
460
459
458
457
456
455
454
453
100
150
200
250
300
350
400
450
yearday 1991

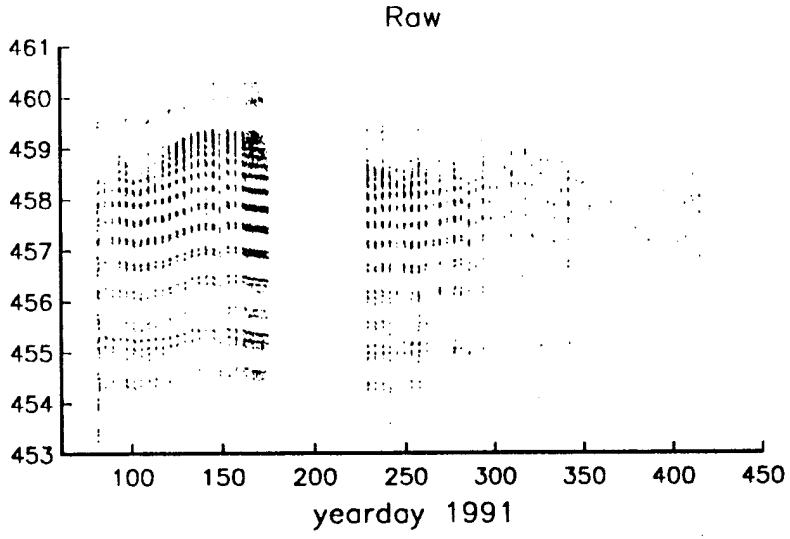
Raw
461
460
459
458
457
456
455
454
453
100
150
200
250
300
350
400
450
yearday 1991

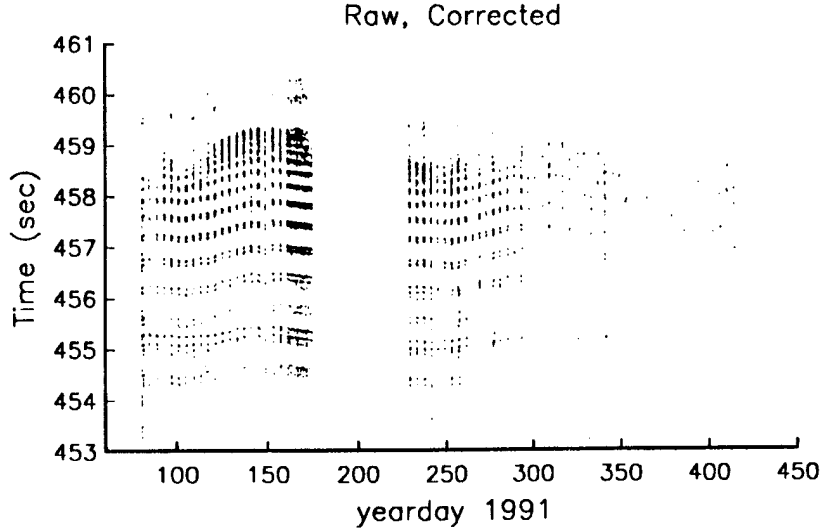
Raw, Corrected
Time (sec)
461
460
459
458
457
456
455
454
453
100
150
200
250
300
350
400
450
yearday 1991

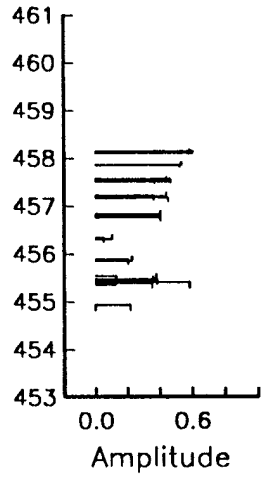
461
460
459
458
457
456
455
454
453
0.0
0.6
Amplitude

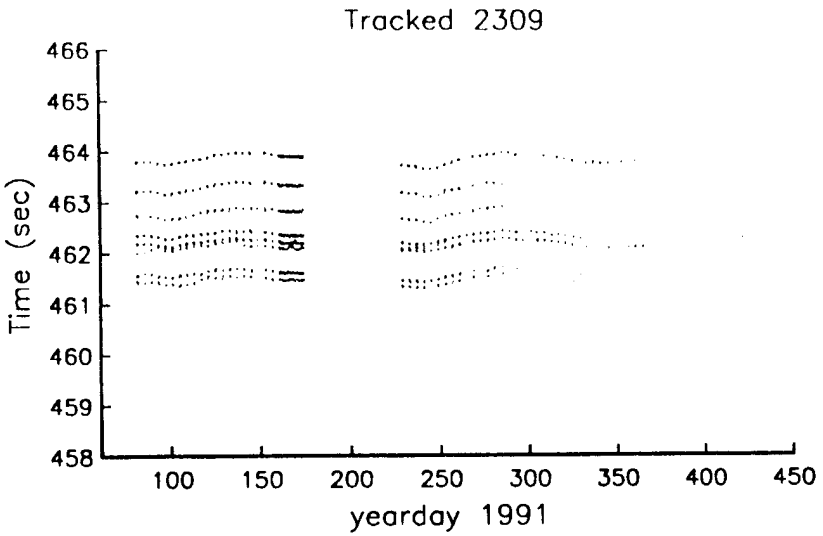
Tracked 2309
Time (sec)
466
465
464
463
462
461
460
459
458
100
150
200
250
300
350
400
450
yearday 1991

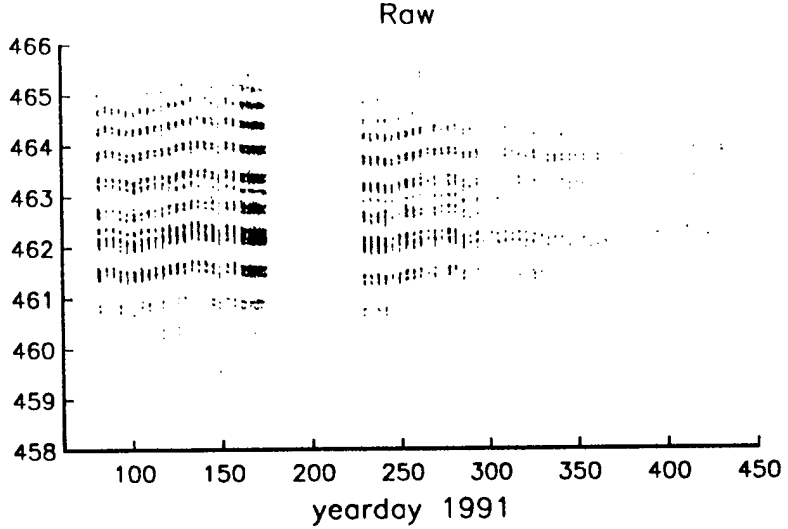
Raw
466
465
464
463
462
461
460
459
458
100
150
200
250
300
350
400
450
yearday 1991

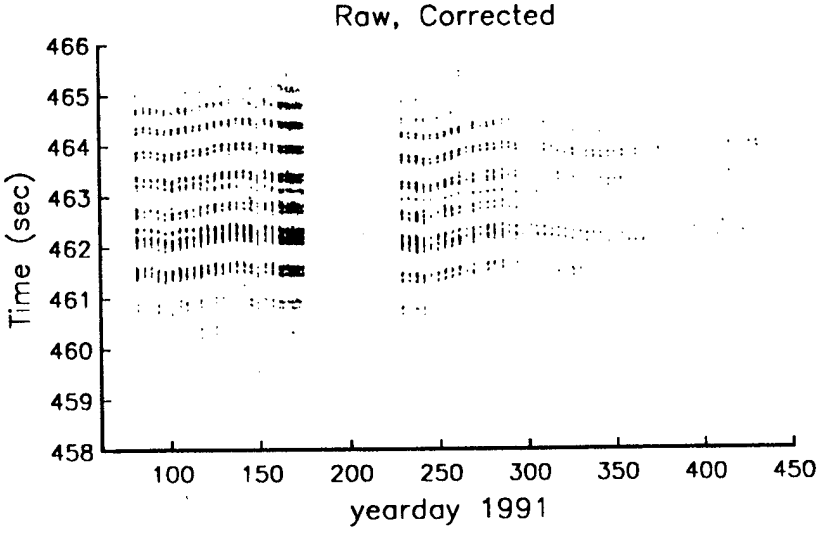
Raw, Corrected
Time (sec)
466
465
464
463
462
461
460
459
458
100
150
200
250
300
350
400
450
yearday 1991

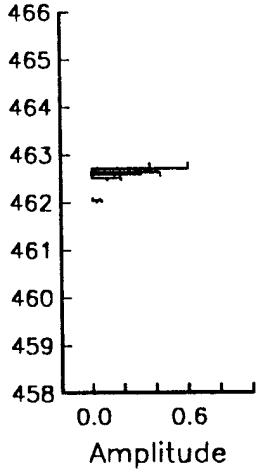
466
465
464
463
462
461
460
459
458
0.0
0.6
Amplitude

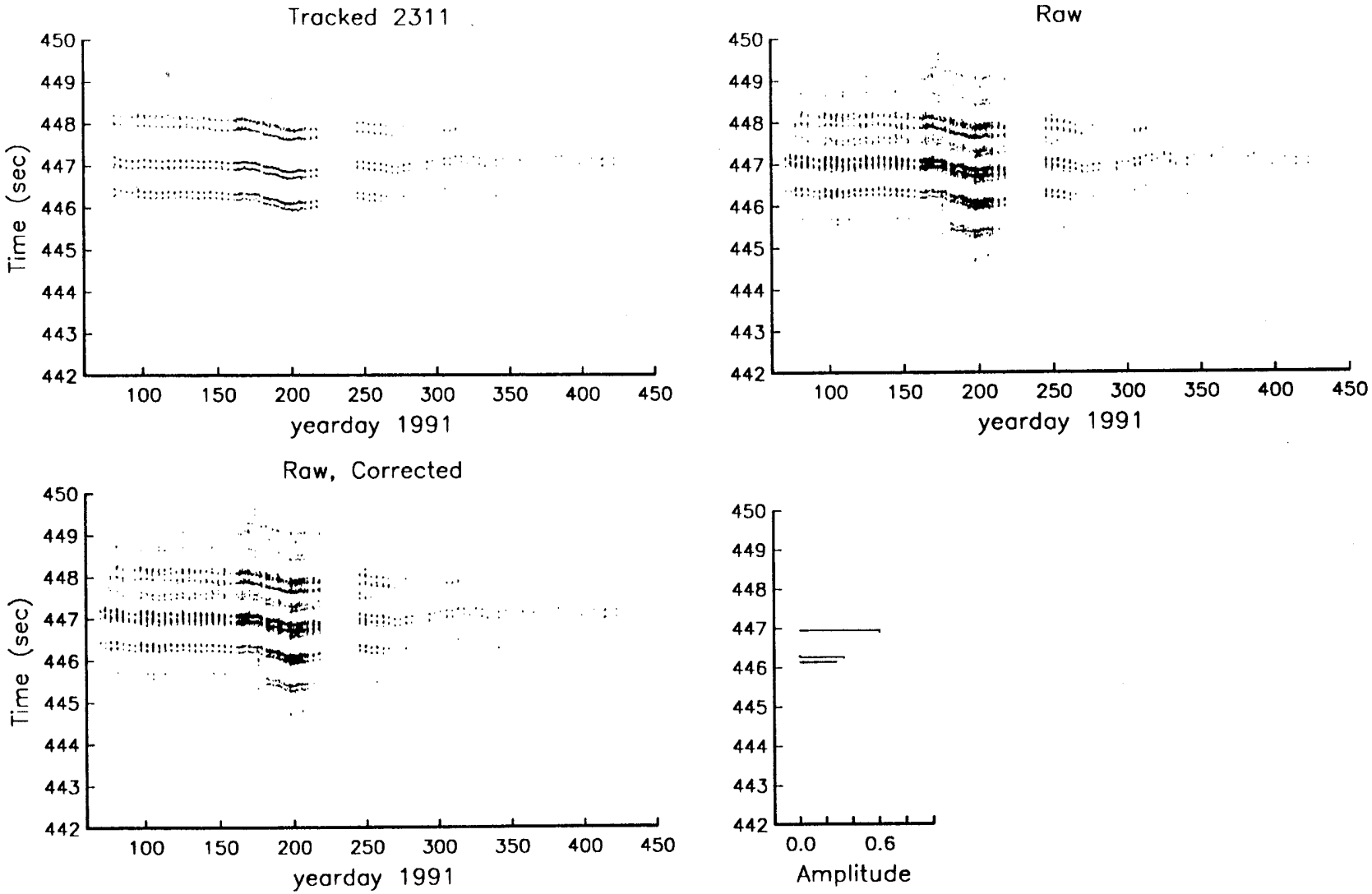
Tracked 2311
Raw
Raw, Corrected
Time (sec)
yearday 1991
Amplitude
450
449
448
447
446
445
444
443
442
100
150
200
250
300
350
400
450
0.0
0.6

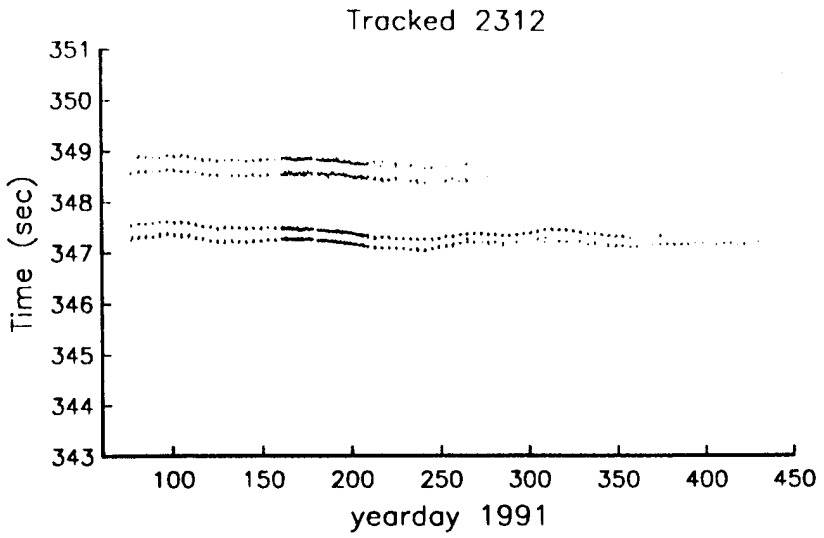
Tracked 2312
Time (sec)
351
350
349
348
347
346
345
344
343
100
150
200
250
300
350
400
450
yearday 1991

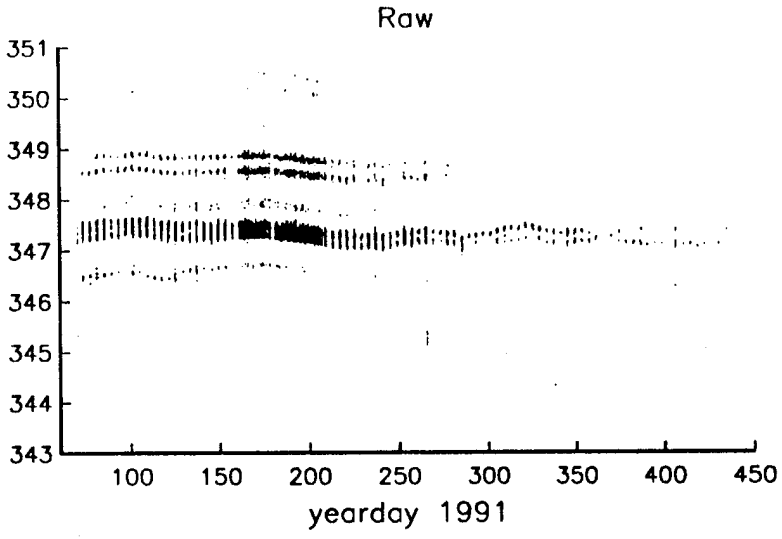
Raw
351
350
349
348
347
346
345
344
343
100
150
200
250
300
350
400
450
yearday 1991

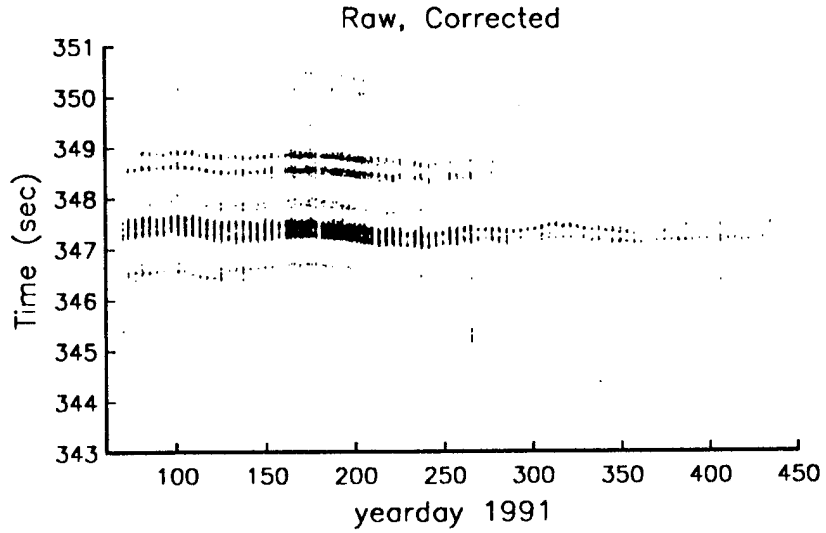
Raw, Corrected
Time (sec)
351
350
349
348
347
346
345
344
343
100
150
200
250
300
350
400
450
yearday 1991

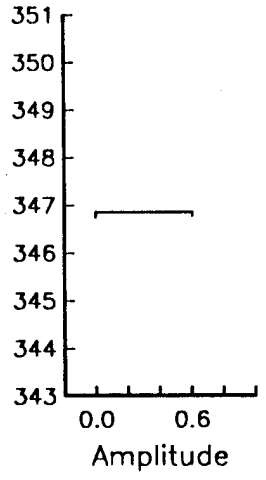
351
350
349
348
347
346
345
344
343
0.0
0.6
Amplitude

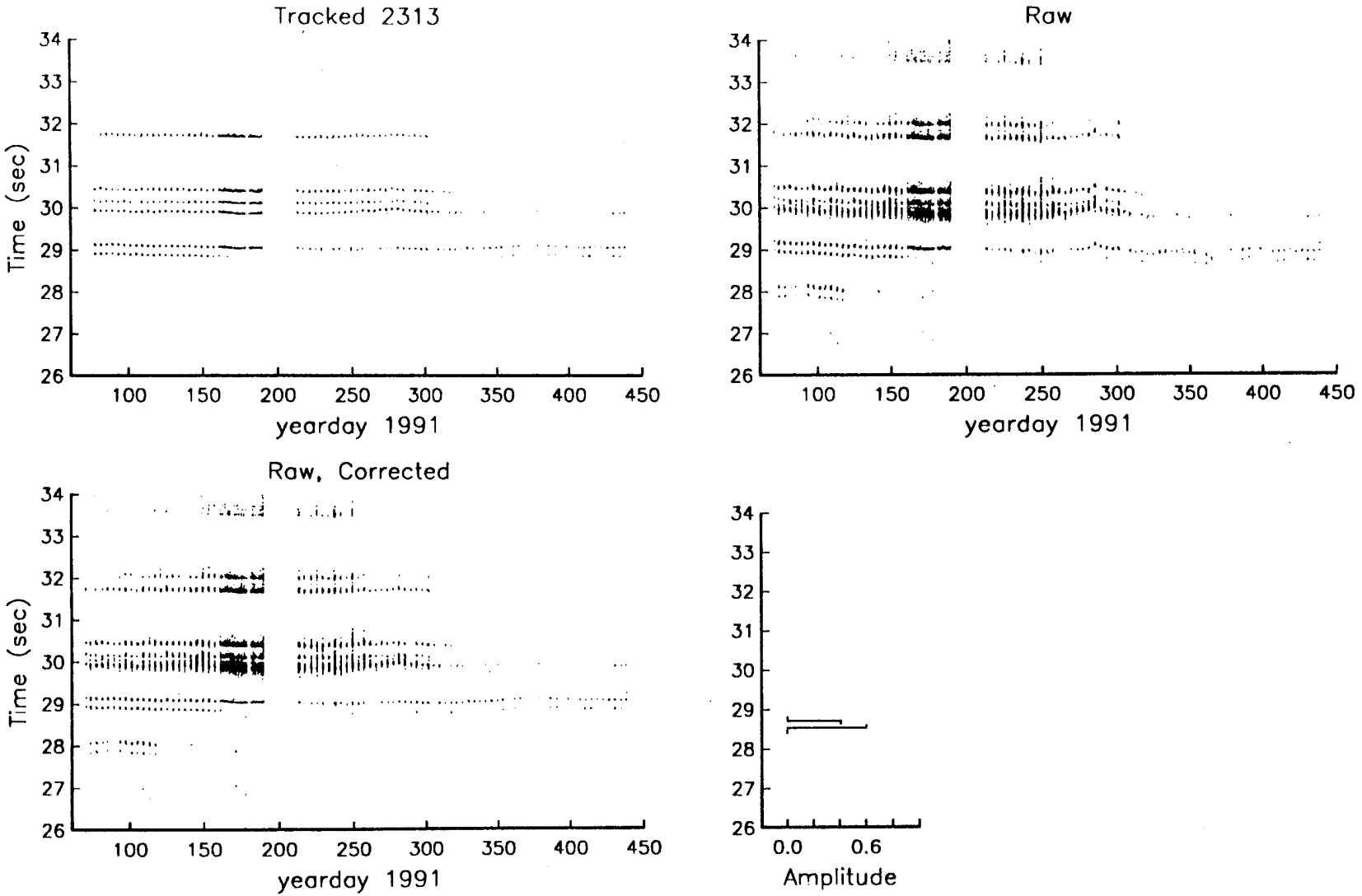
Tracked 2313
Raw
Raw, Corrected
Time (sec)
yearday 1991
Amplitude
34
33
32
31
30
29
28
27
26
100
150
200
250
300
350
400
450
0.0
0.6

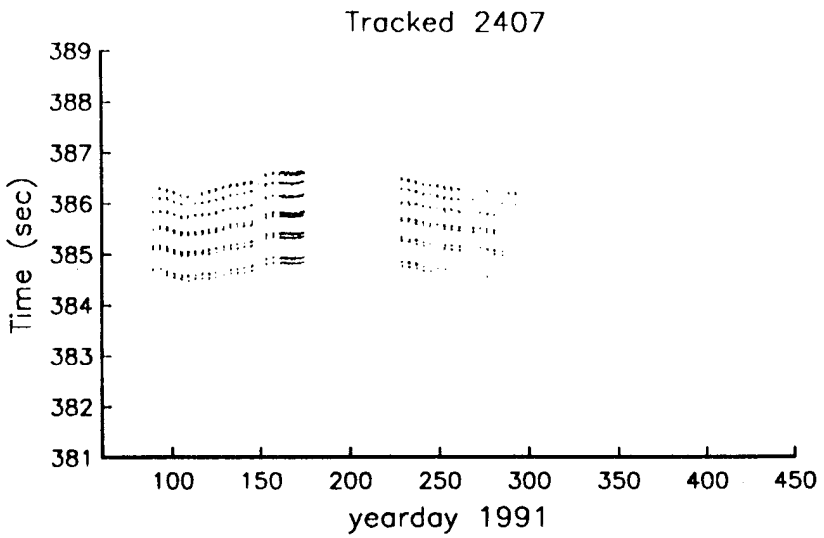
Tracked 2407
Time (sec)
389
388
387
386
385
384
383
382
381
100
150
200
250
300
350
400
450
yearday 1991

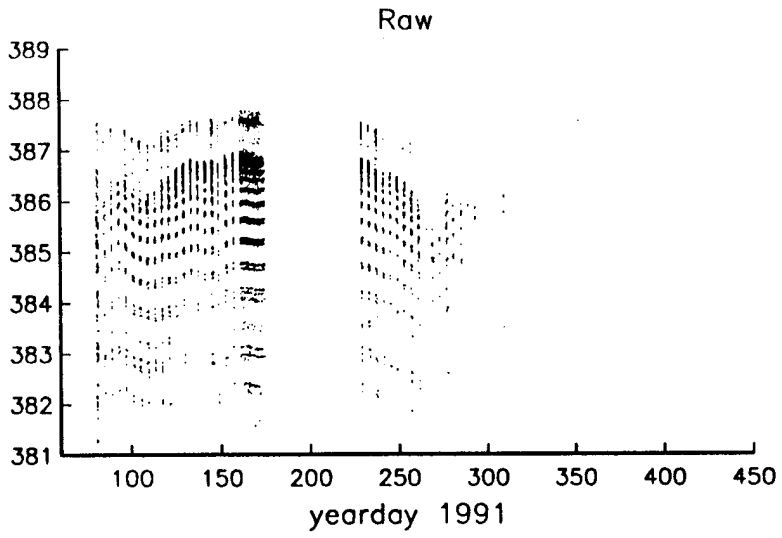
Raw
389
388
387
386
385
384
383
382
381
100
150
200
250
300
350
400
450
yearday 1991

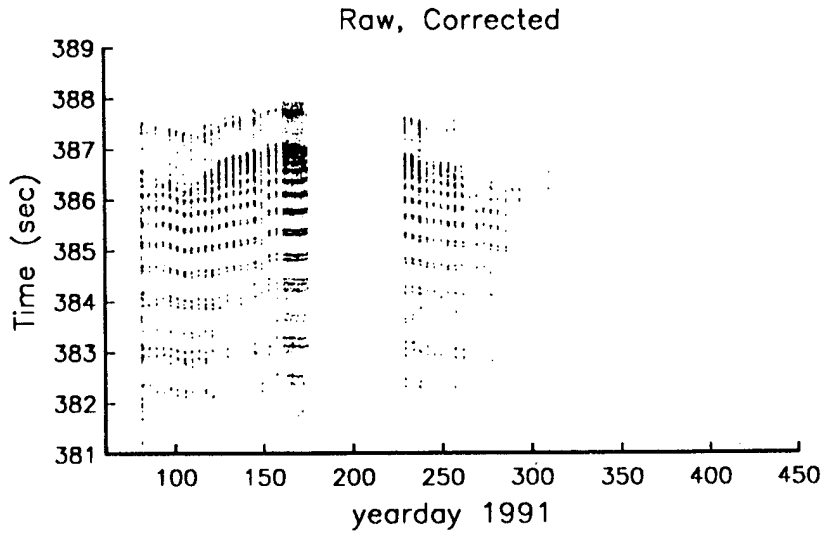
Raw, Corrected
Time (sec)
389
388
387
386
385
384
383
382
381
100
150
200
250
300
350
400
450
yearday 1991

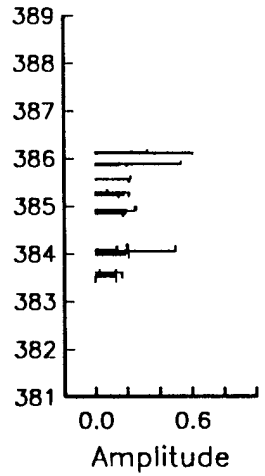
389
388
387
386
385
384
383
382
381
0.0
0.6
Amplitude

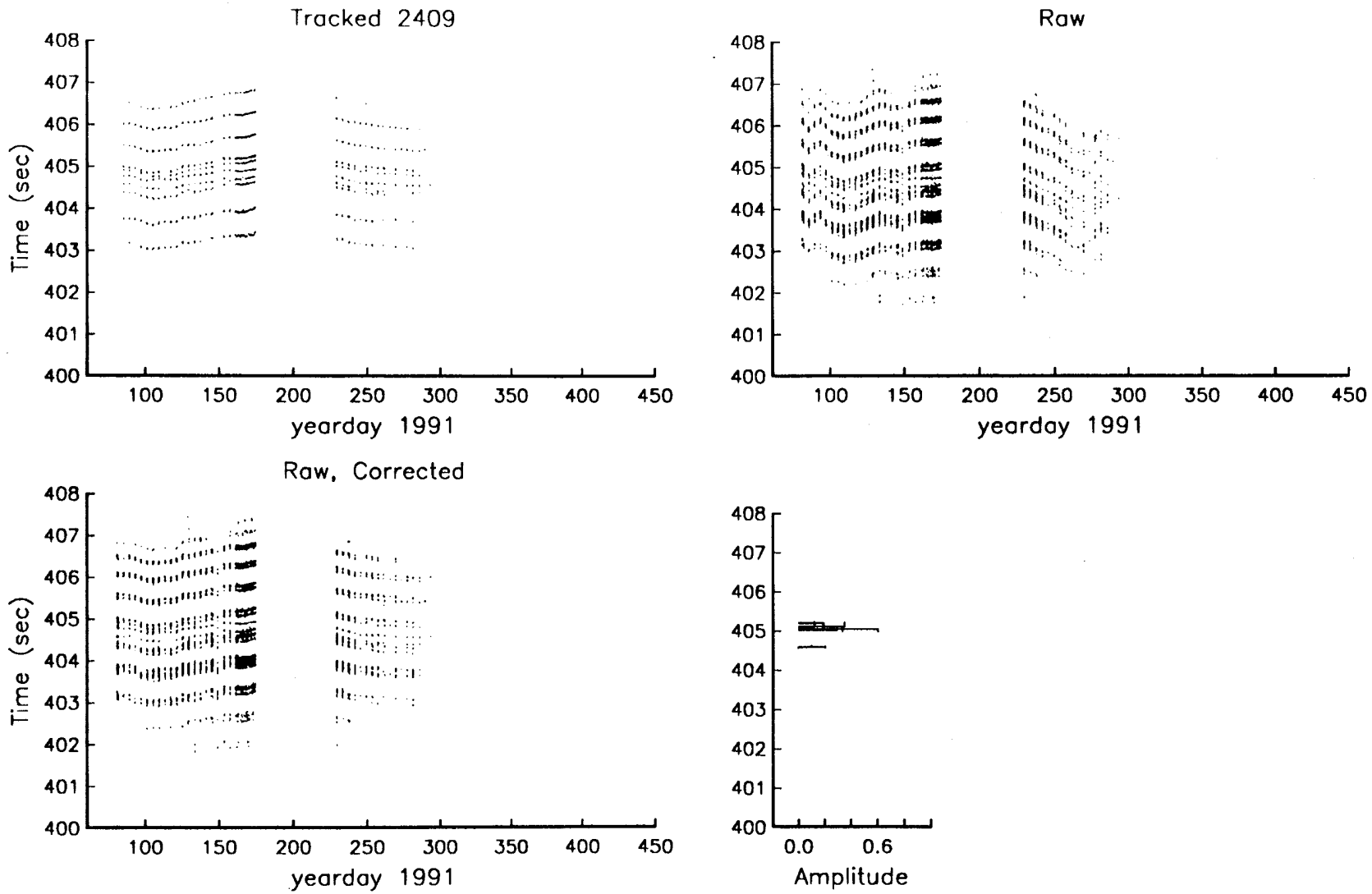
Tracked 2409
Raw
Raw, Corrected
Time (sec)
yearday 1991
Amplitude
408
407
406
405
404
403
402
401
400
100
150
200
250
300
350
400
450
0.0
0.6

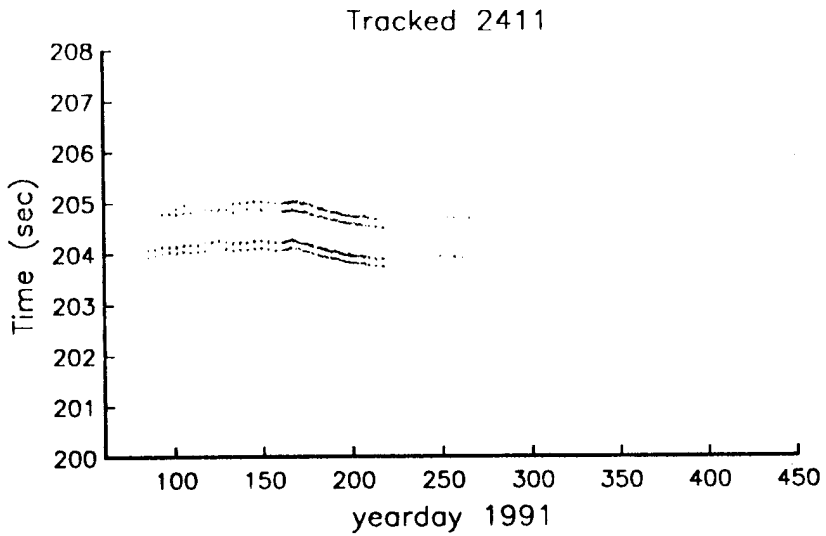
Tracked 2411
Time (sec)
208
207
206
205
204
203
202
201
200
100
150
200
250
300
350
400
450
yearday 1991

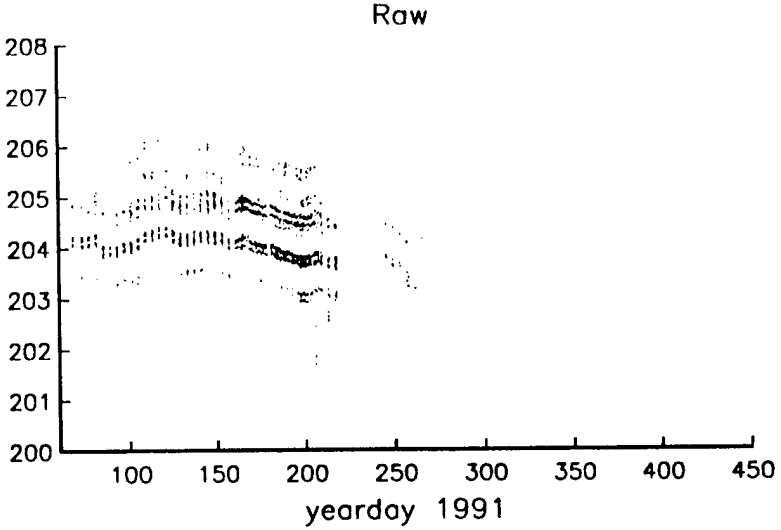
Raw
208
207
206
205
204
203
202
201
200
100
150
200
250
300
350
400
450
yearday 1991

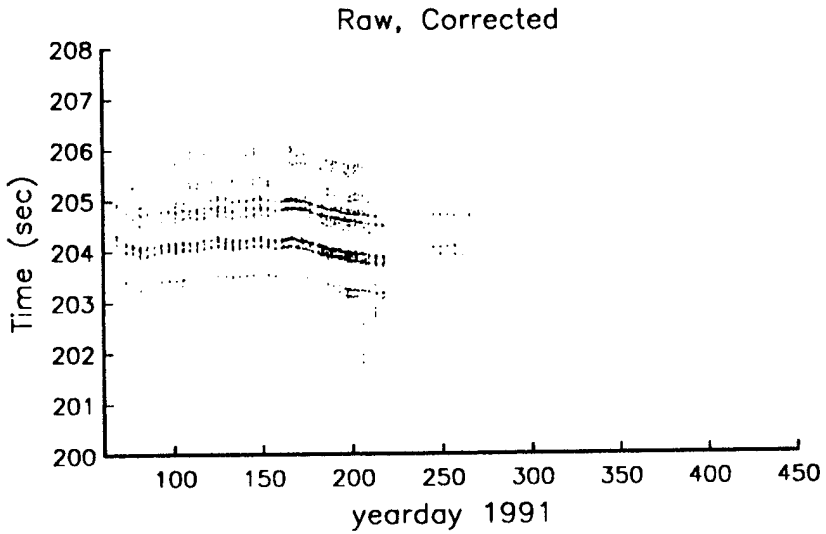
Raw, Corrected
Time (sec)
208
207
206
205
204
203
202
201
200
100
150
200
250
300
350
400
450
yearday 1991

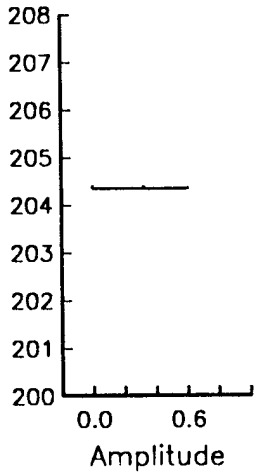
208
207
206
205
204
203
202
201
200
0.0
0.6
Amplitude

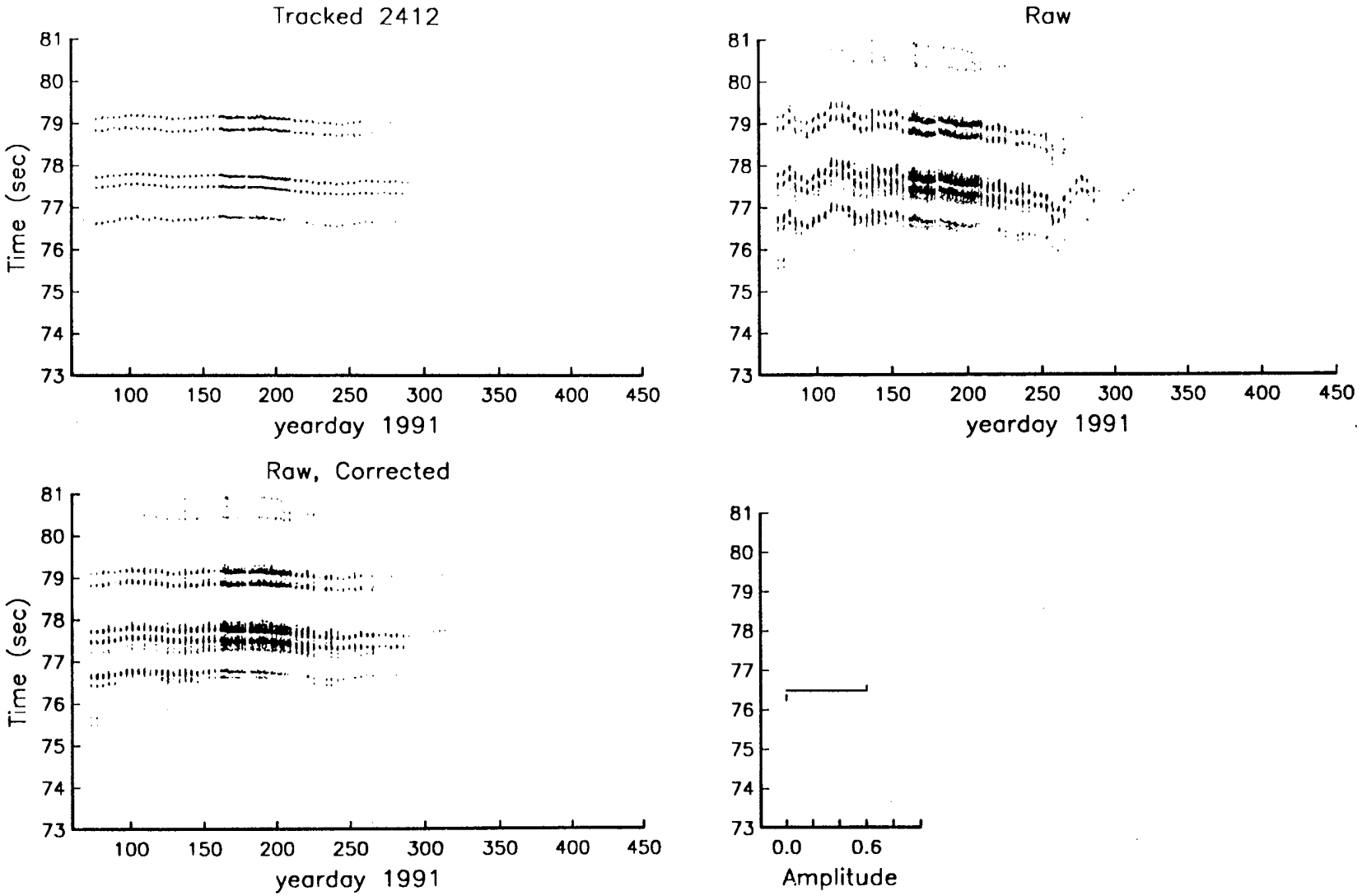
Tracked 2412
Time (sec)
81
80
79
78
77
76
75
74
73
100
150
200
250
300
350
400
450
yearday 1991
Raw
Raw, Corrected
0.0
0.6
Amplitude

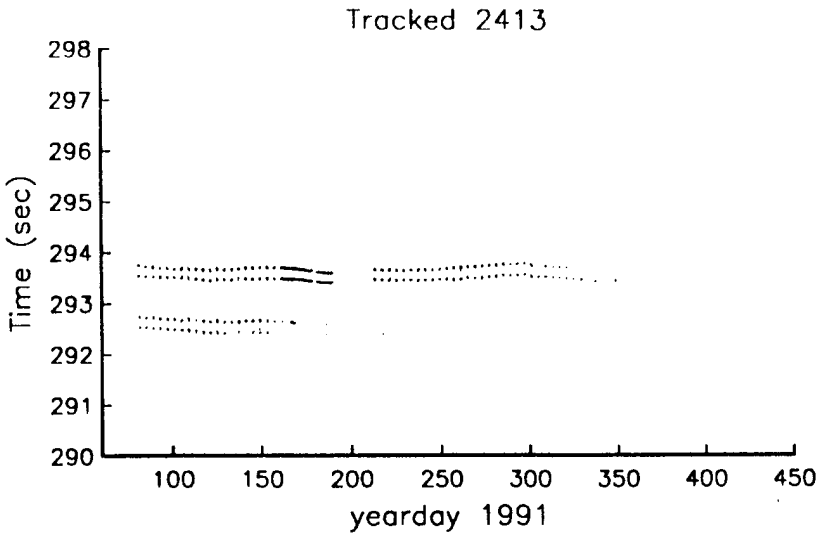
Tracked 2413
Time (sec)
298
297
296
295
294
293
292
291
290
100
150
200
250
300
350
400
450
yearday 1991

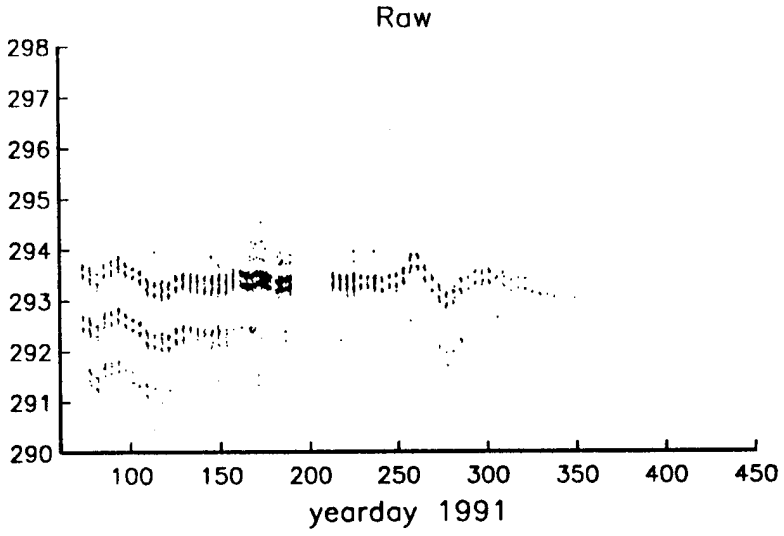
Raw
298
297
296
295
294
293
292
291
290
100
150
200
250
300
350
400
450
yearday 1991

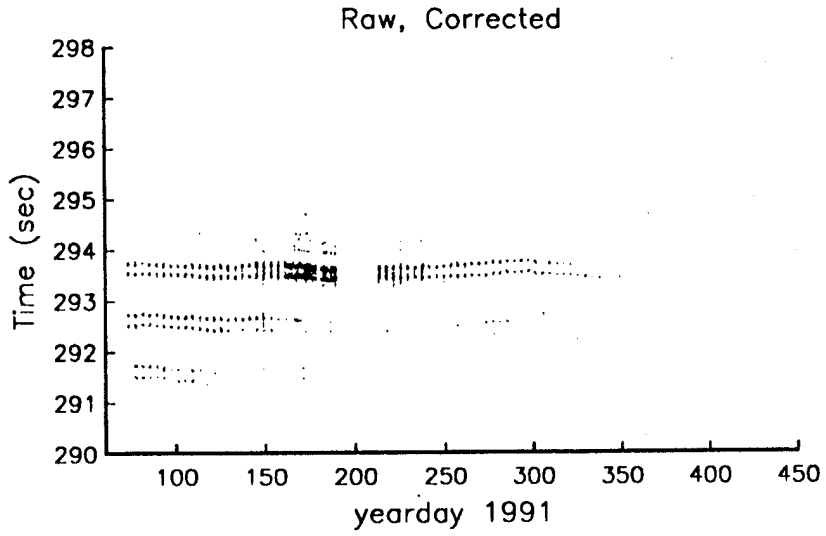
Raw, Corrected
Time (sec)
298
297
296
295
294
293
292
291
290
100
150
200
250
300
350
400
450
yearday 1991

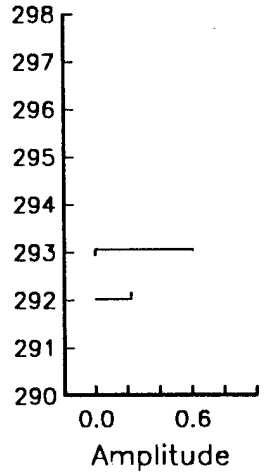
298
297
296
295
294
293
292
291
290
0.0
0.6
Amplitude

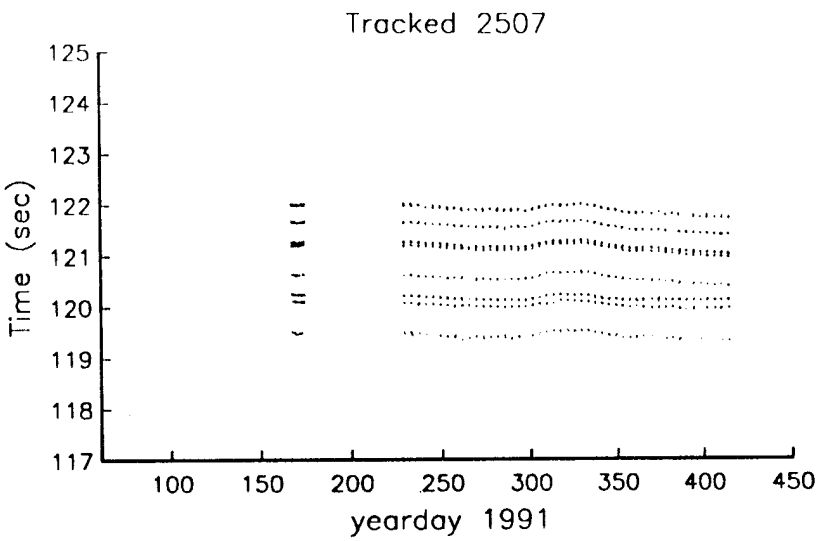
Tracked 2507
Time (sec)
125
124
123
122
121
120
119
118
117
100
150
200
250
300
350
400
450
yearday 1991

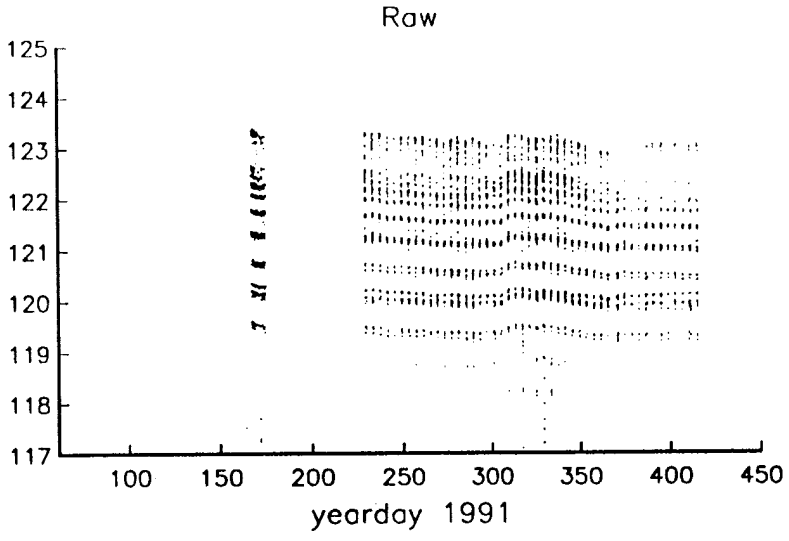
Raw
125
124
123
122
121
120
119
118
117
100
150
200
250
300
350
400
450
yearday 1991

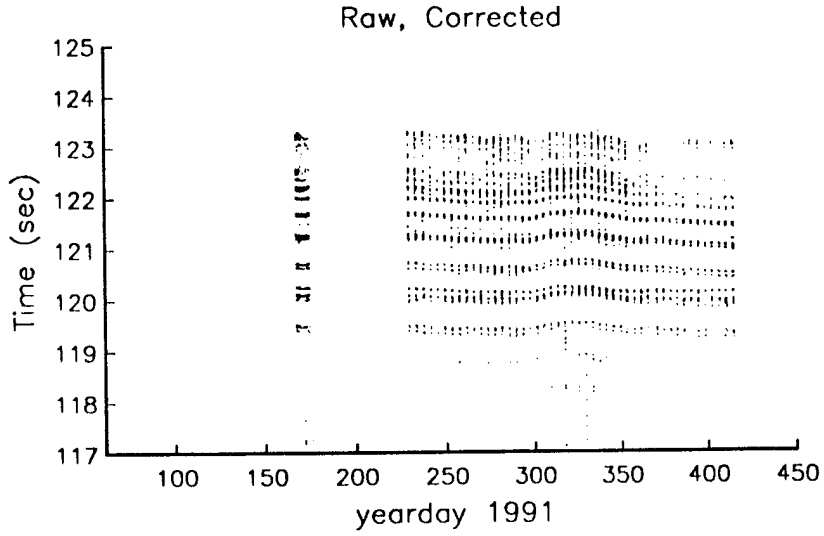
Raw, Corrected
Time (sec)
125
124
123
122
121
120
119
118
117
100
150
200
250
300
350
400
450
yearday 1991


125
124
123
122
121
120
119
118
117
0.0
0.6
Amplitude

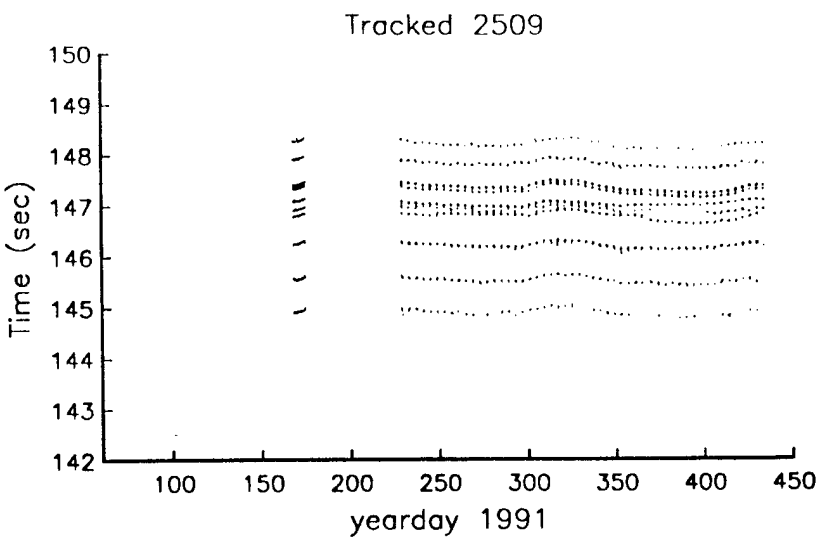
Tracked 2509
Time (sec)
150
149
148
147
146
145
144
143
142
100
150
200
250
300
350
400
450
yearday 1991

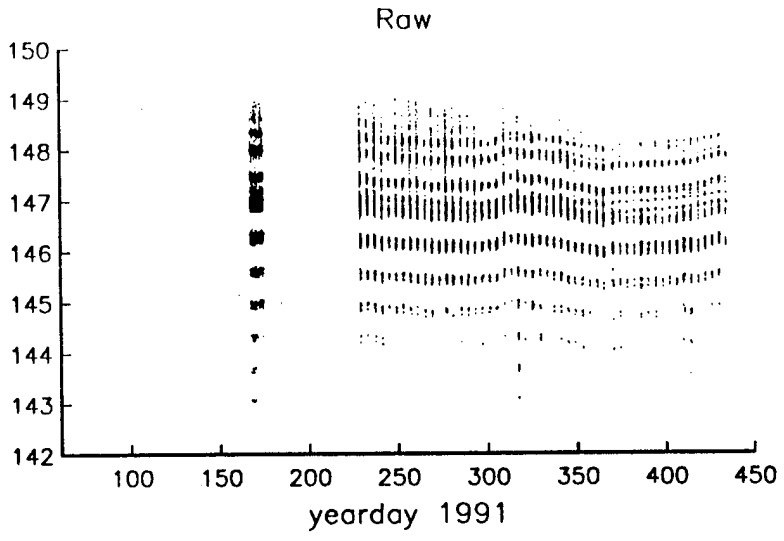
Raw
150
149
148
147
146
145
144
143
142
100
150
200
250
300
350
400
450
yearday 1991

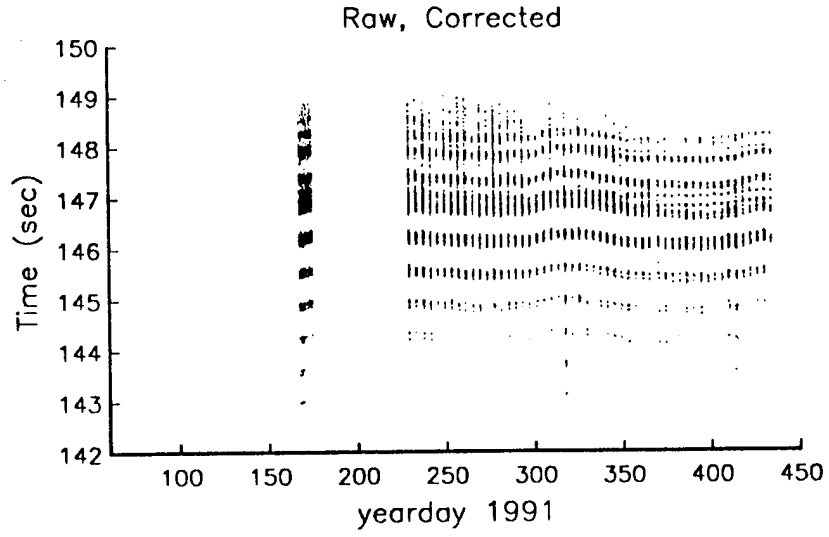
Raw, Corrected
Time (sec)
150
149
148
147
146
145
144
143
142
100
150
200
250
300
350
400
450
yearday 1991

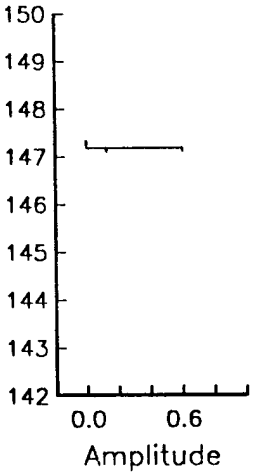
150
149
148
147
146
145
144
143
142
0.0
0.6
Amplitude

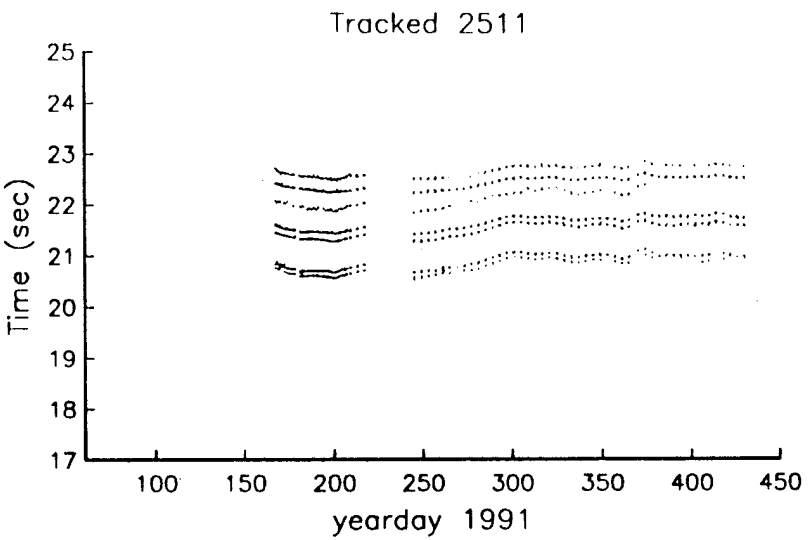
Tracked 2511
Time (sec)
25
24
23
22
21
20
19
18
17
100
150
200
250
300
350
400
450
yearday 1991

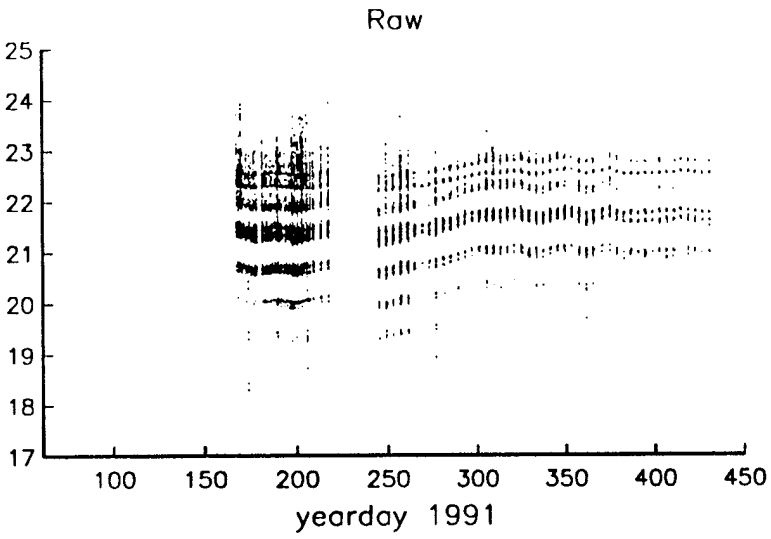
Raw
25
24
23
22
21
20
19
18
17
100
150
200
250
300
350
400
450
yearday 1991

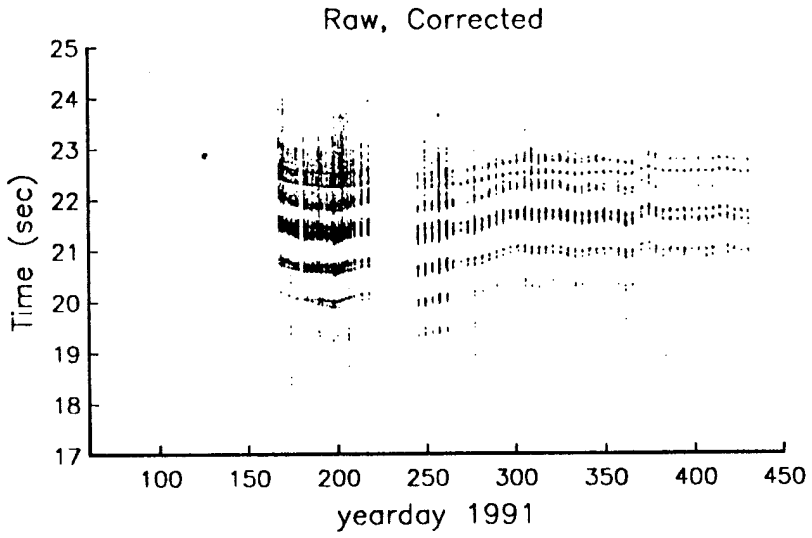
Raw, Corrected
Time (sec)
25
24
23
22
21
20
19
18
17
100
150
200
250
300
350
400
450
yearday 1991

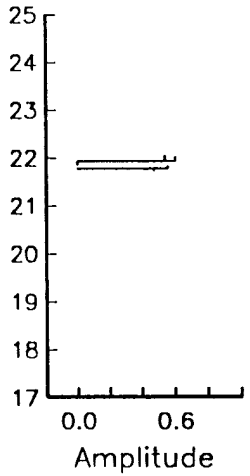
25
24
23
22
21
20
19
18
17
0.0
0.6
Amplitude

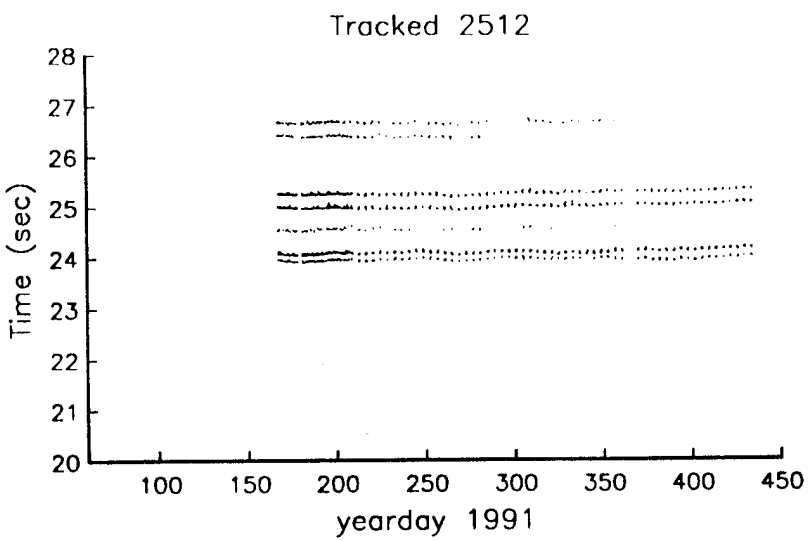
Tracked 2512
Time (sec)
28
27
26
25
24
23
22
21
20
100
150
200
250
300
350
400
450
yearday 1991

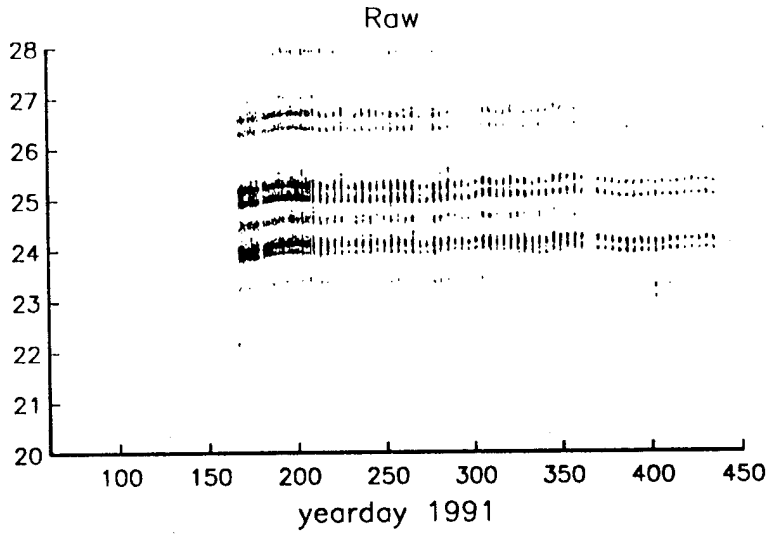
Raw
28
27
26
25
24
23
22
21
20
100
150
200
250
300
350
400
450
yearday 1991

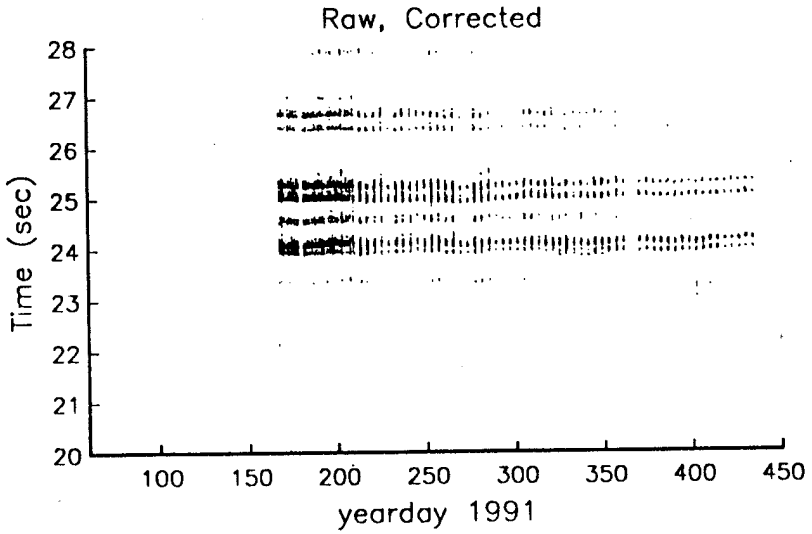
Raw, Corrected
Time (sec)
28
27
26
25
24
23
22
21
20
100
150
200
250
300
350
400
450
yearday 1991

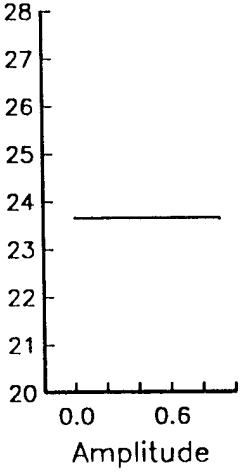
28
27
26
25
24
23
22
21
20
0.0
0.6
Amplitude

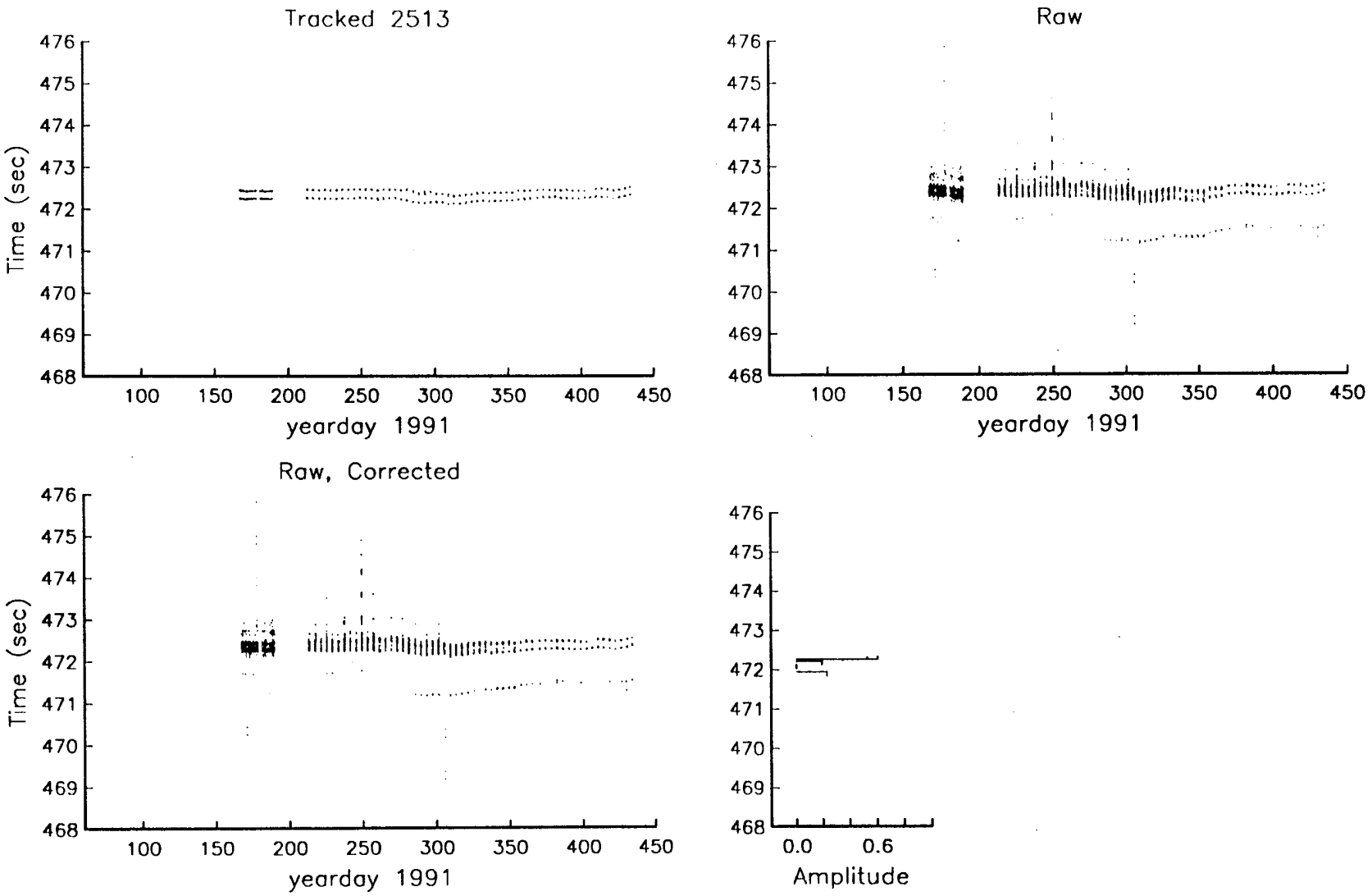
Tracked 2513
Raw
Raw, Corrected
Time (sec)
yearday 1991
Amplitude
476
475
474
473
472
471
470
469
468
100
150
200
250
300
350
400
450
0.0
0.6

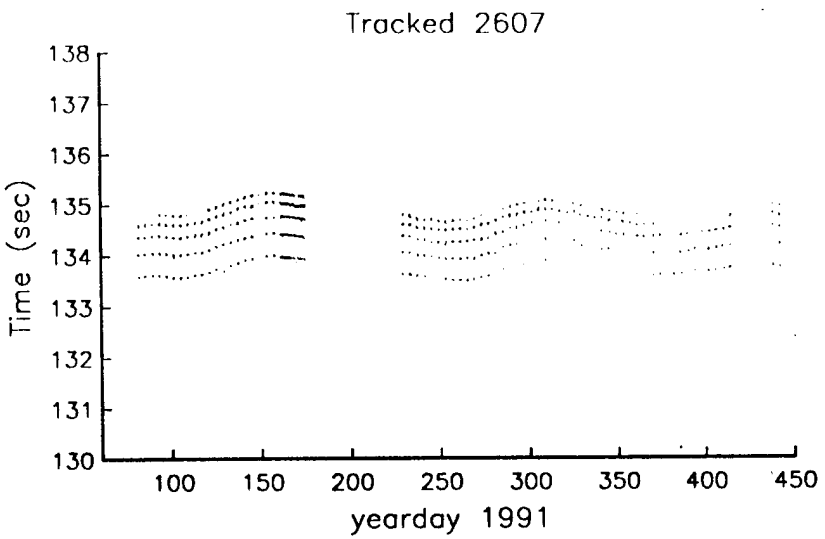
Tracked 2607
Time (sec)
138
137
136
135
134
133
132
131
130
100
150
200
250
300
350
400
450
yearday 1991

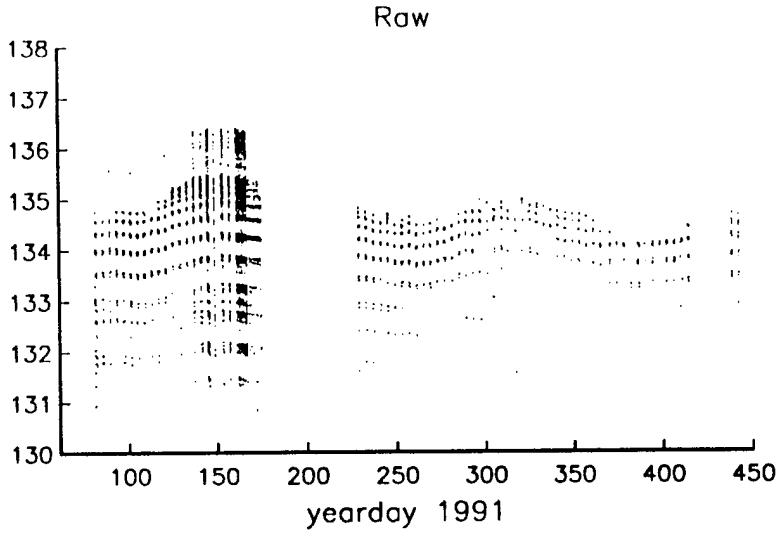
Raw
138
137
136
135
134
133
132
131
130
100
150
200
250
300
350
400
450
yearday 1991

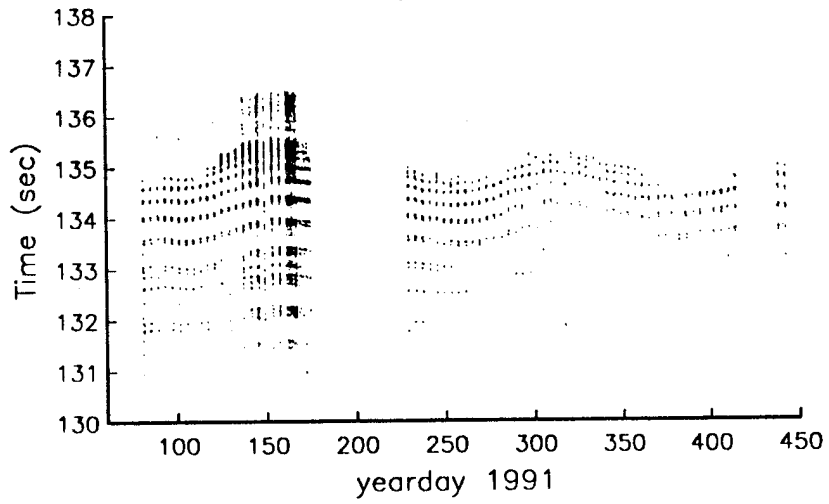
Raw, Corrected
Time (sec)
138
137
136
135
134
133
132
131
130
100
150
200
250
300
350
400
450
yearday 1991

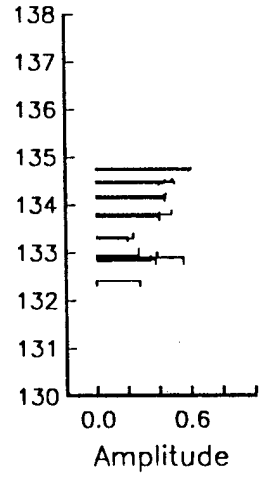
138
137
136
135
134
133
132
131
130
0.0
0.6
Amplitude

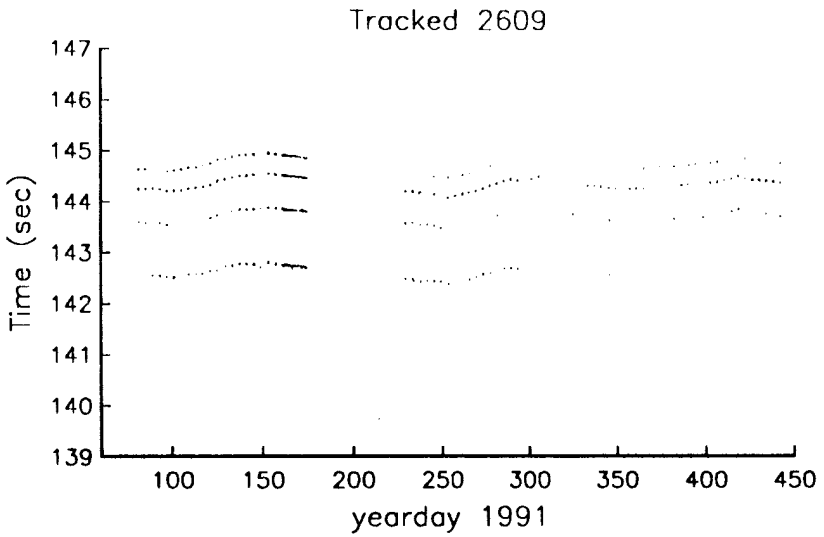
Tracked 2609
Time (sec)
147
146
145
144
143
142
141
140
139
100
150
200
250
300
350
400
450
yearday 1991

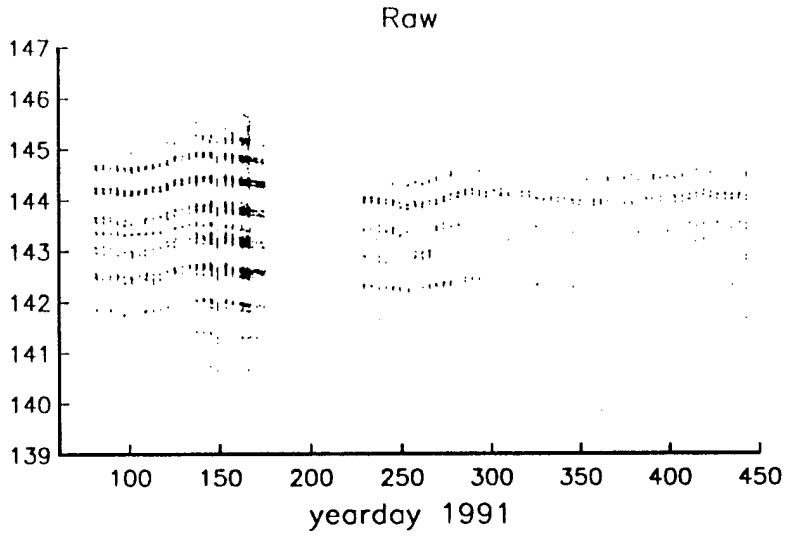
Raw
147
146
145
144
143
142
141
140
139
100
150
200
250
300
350
400
450
yearday 1991

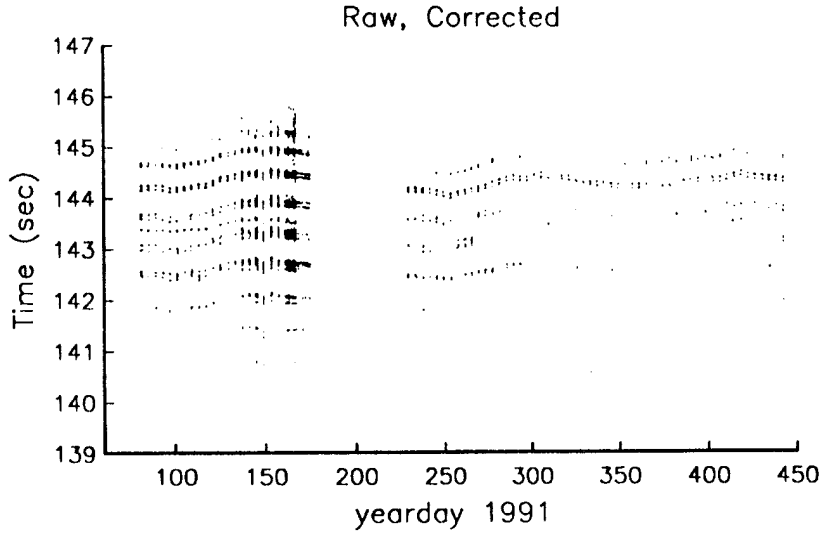
Raw, Corrected
Time (sec)
147
146
145
144
143
142
141
140
139
100
150
200
250
300
350
400
450
yearday 1991

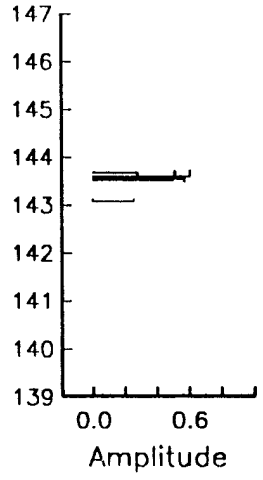
147
146
145
144
143
142
141
140
139
0.0
0.6
Amplitude

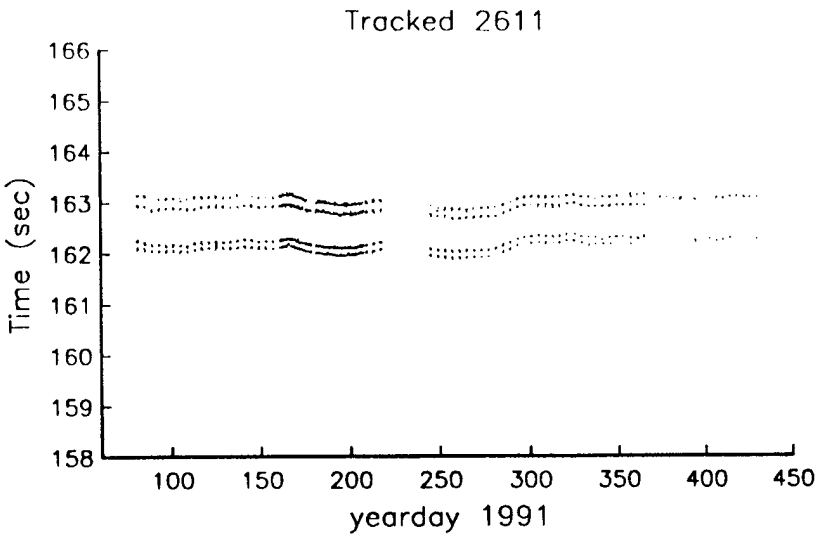
Tracked 2611
Time (sec)
166
165
164
163
162
161
160
159
158
100
150
200
250
300
350
400
450
yearday 1991

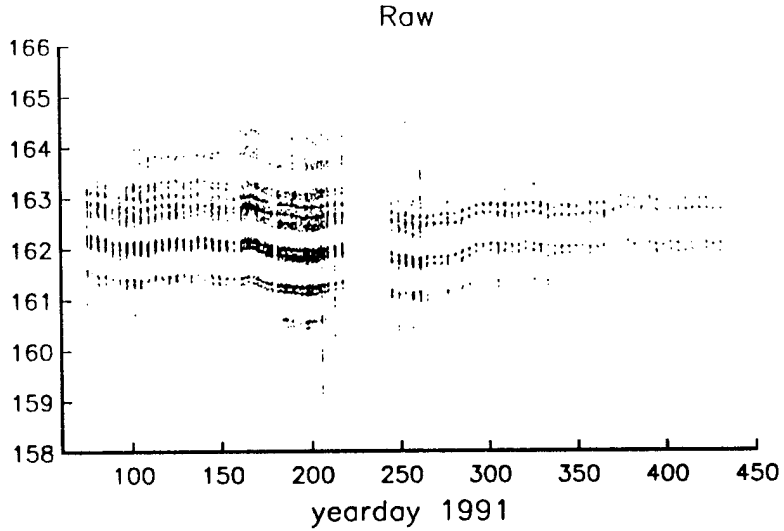
Raw
166
165
164
163
162
161
160
159
158
100
150
200
250
300
350
400
450
yearday 1991

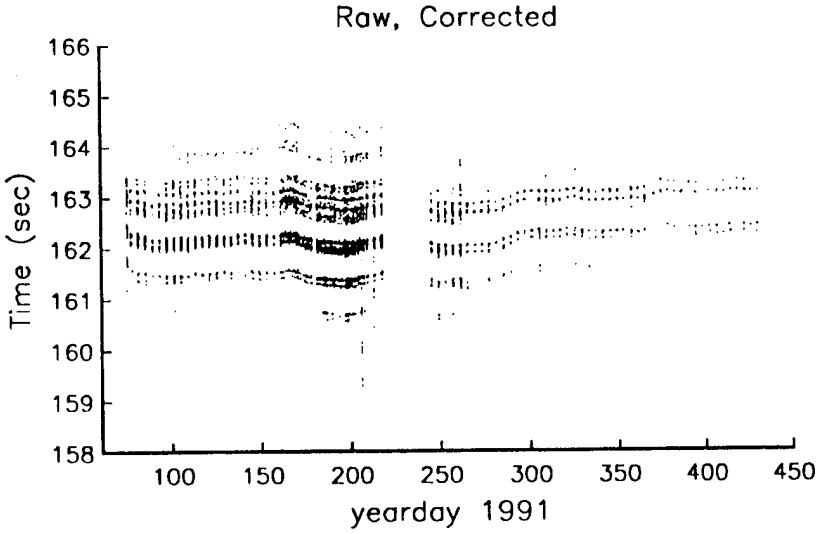
Raw, Corrected
Time (sec)
166
165
164
163
162
161
160
159
158
100
150
200
250
300
350
400
450
yearday 1991

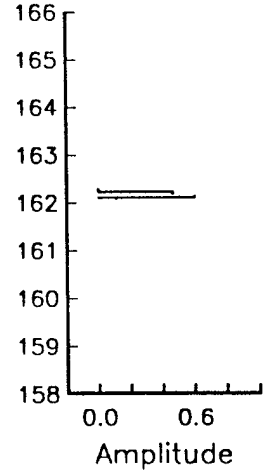
166
165
164
163
162
161
160
159
158
0.0
0.6
Amplitude

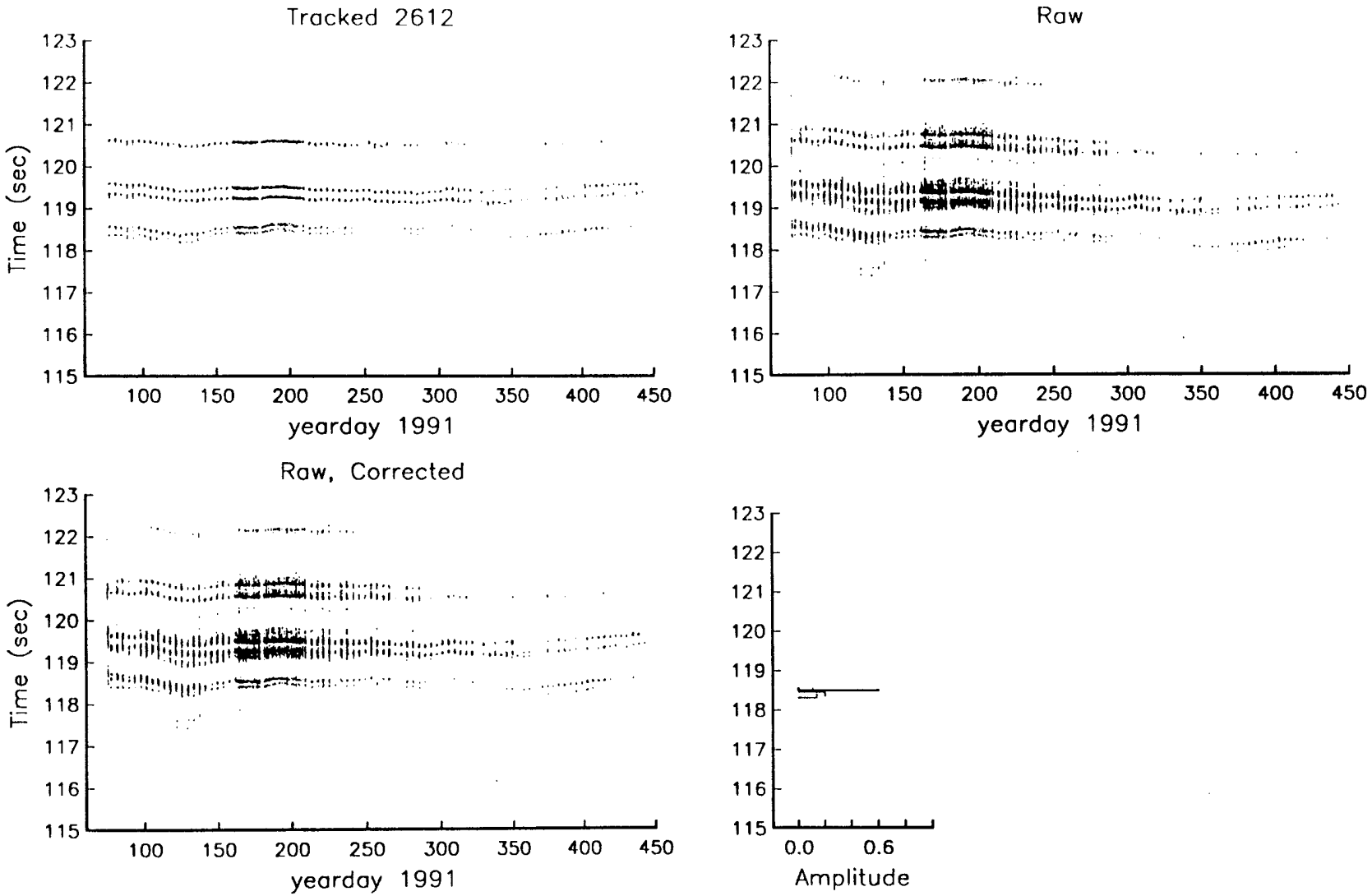
Tracked 2612
Raw
Raw, Corrected
Time (sec)
yearday 1991
Amplitude
123
122
121
120
119
118
117
116
115
100
150
200
250
300
350
400
450
0.0
0.6

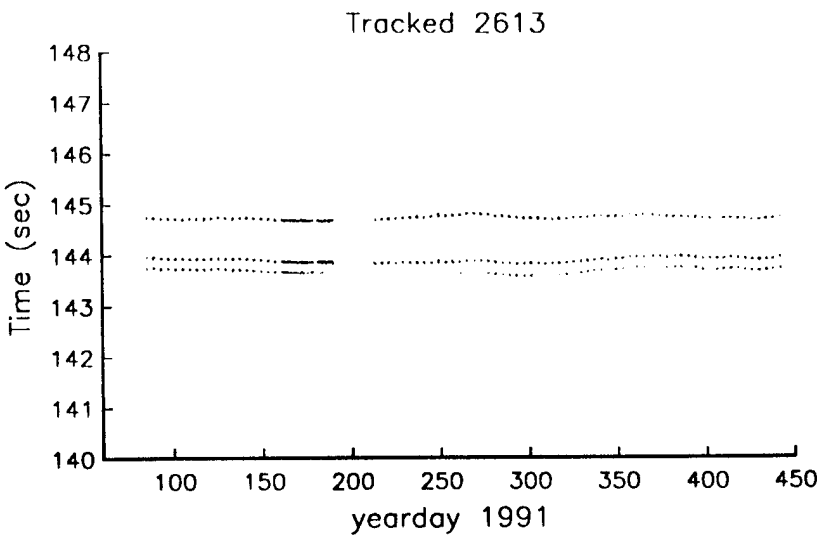
Tracked 2613
Time (sec)
148
147
146
145
144
143
142
141
140
100
150
200
250
300
350
400
450
yearday 1991

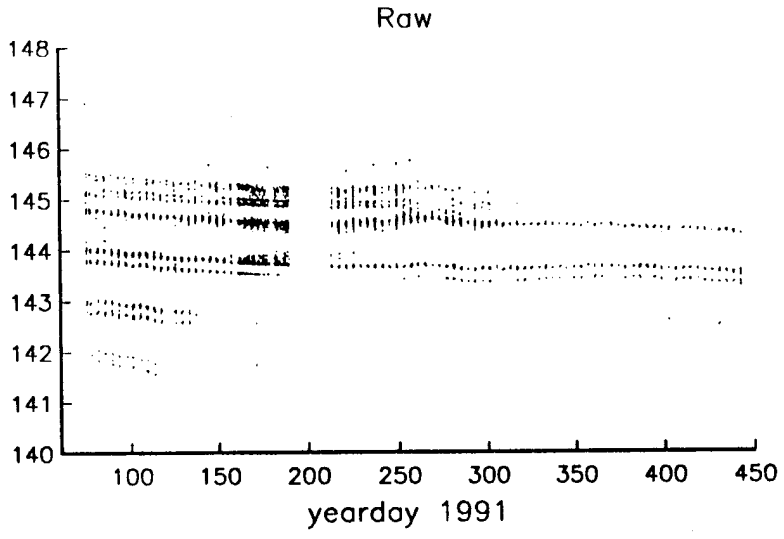
Raw
148
147
146
145
144
143
142
141
140
100
150
200
250
300
350
400
450
yearday 1991

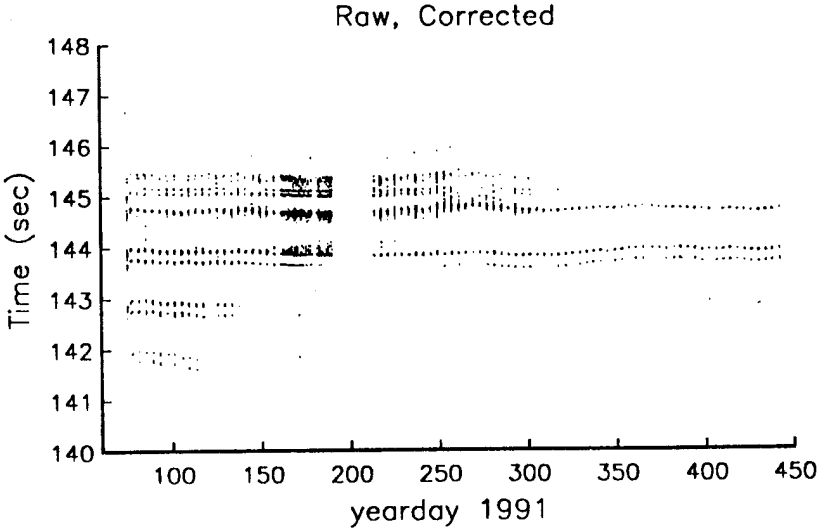
Raw, Corrected
Time (sec)
148
147
146
145
144
143
142
141
140
100
150
200
250
300
350
400
450
yearday 1991

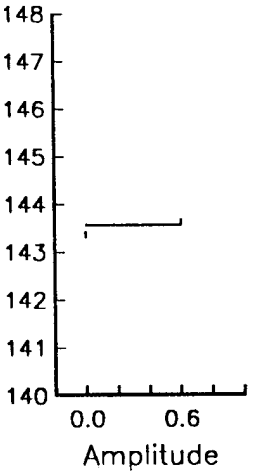
148
147
146
145
144
143
142
141
140
0.0
0.6
Amplitude

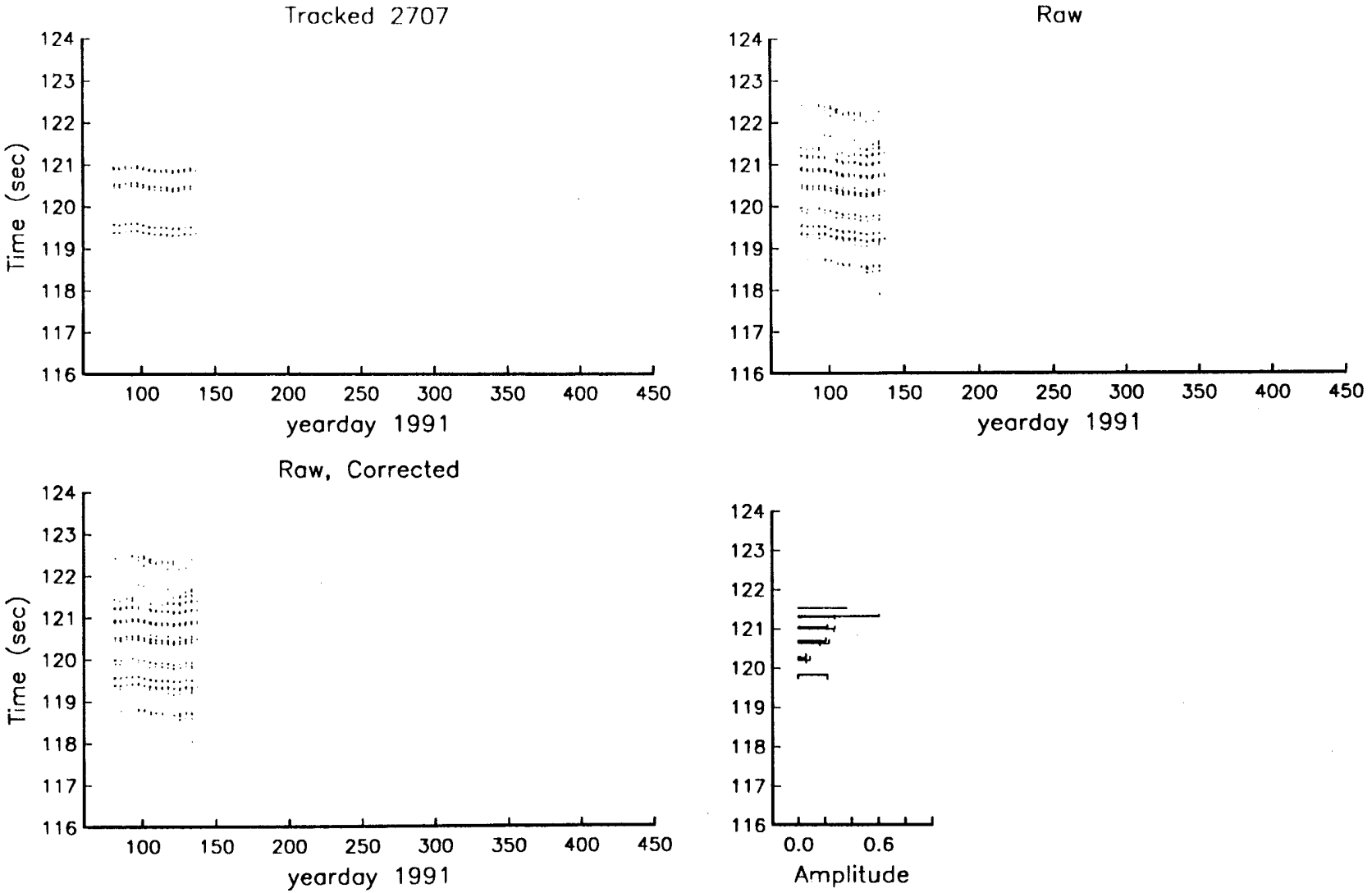
Tracked 2707
Raw
Raw, Corrected
Time (sec)
yearday 1991
Amplitude
124
123
122
121
120
119
118
117
116
100
150
200
250
300
350
400
450
0.0
0.6

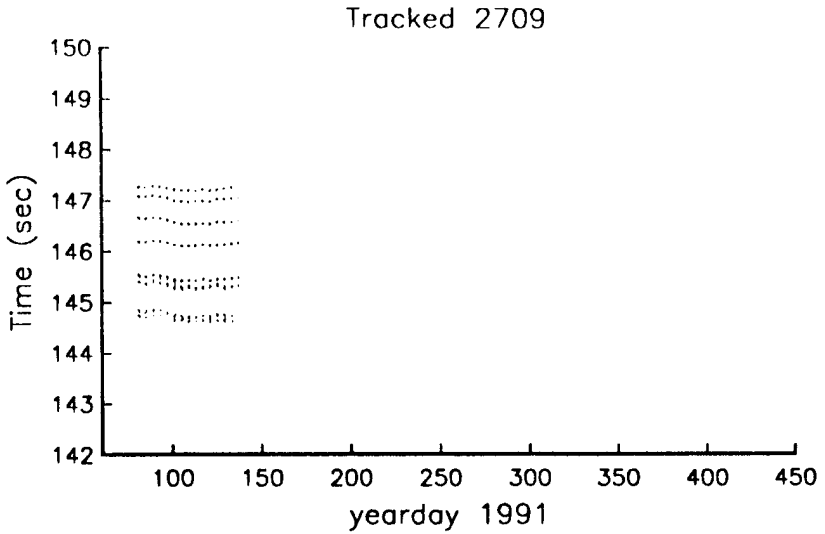
Tracked 2709
Time (sec)
150
149
148
147
146
145
144
143
142
100
150
200
250
300
350
400
450
yearday 1991

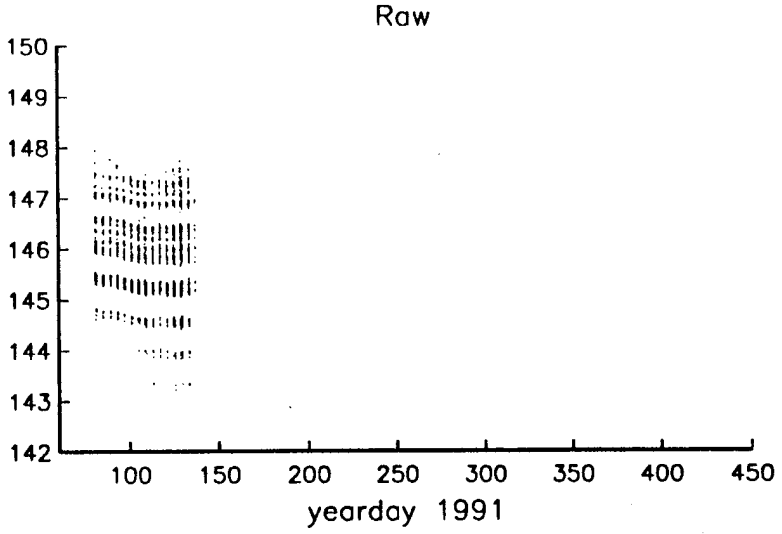
Raw
150
149
148
147
146
145
144
143
142
100
150
200
250
300
350
400
450
yearday 1991

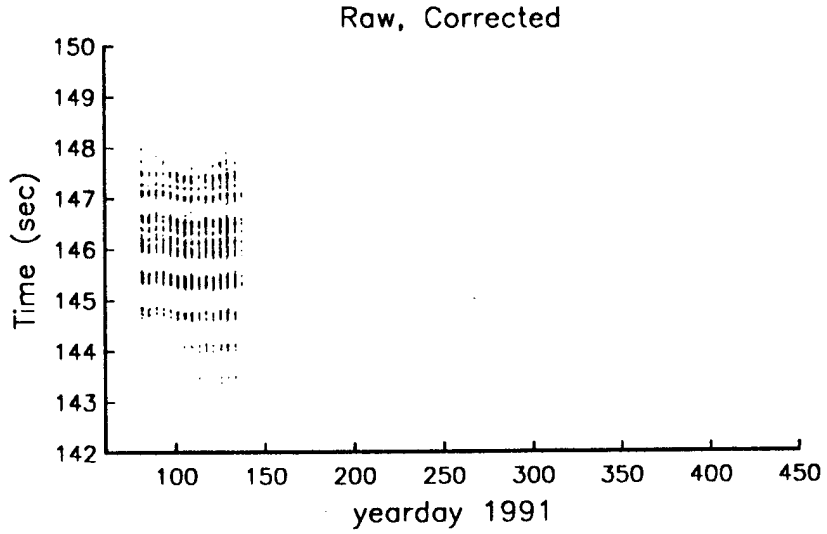
Raw, Corrected
Time (sec)
150
149
148
147
146
145
144
143
142
100
150
200
250
300
350
400
450
yearday 1991

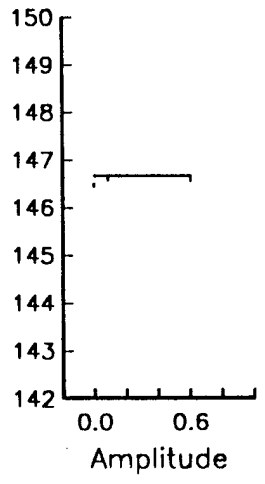
150
149
148
147
146
145
144
143
142
0.0
0.6
Amplitude

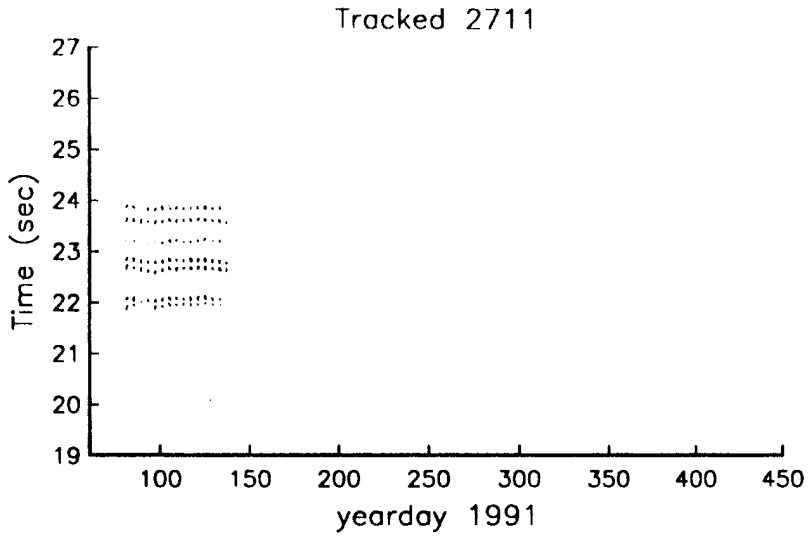
Tracked 2711
Time (sec)
27
26
25
24
23
22
21
20
19
100
150
200
250
300
350
400
450
yearday 1991

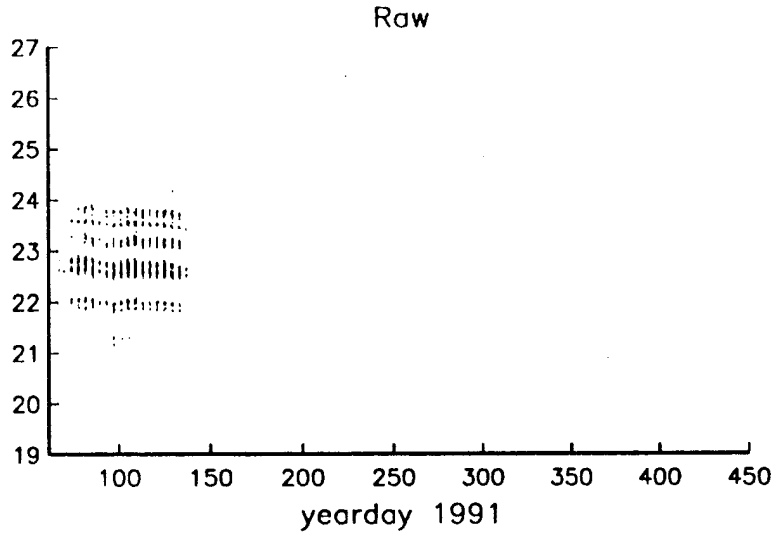
Raw
27
26
25
24
23
22
21
20
19
100
150
200
250
300
350
400
450
yearday 1991

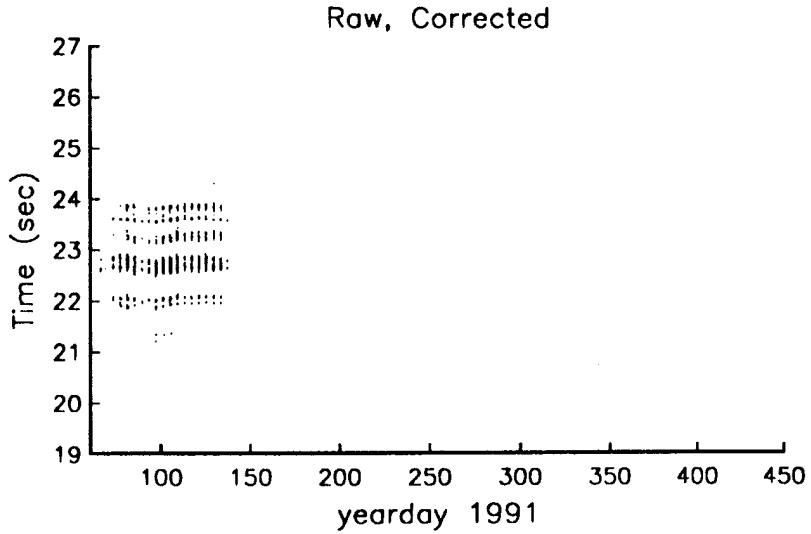
Raw, Corrected
Time (sec)
27
26
25
24
23
22
21
20
19
100
150
200
250
300
350
400
450
yearday 1991

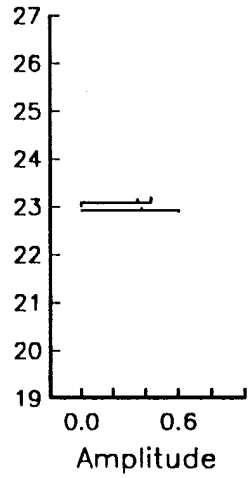
27
26
25
24
23
22
21
20
19
0.0
0.6
Amplitude

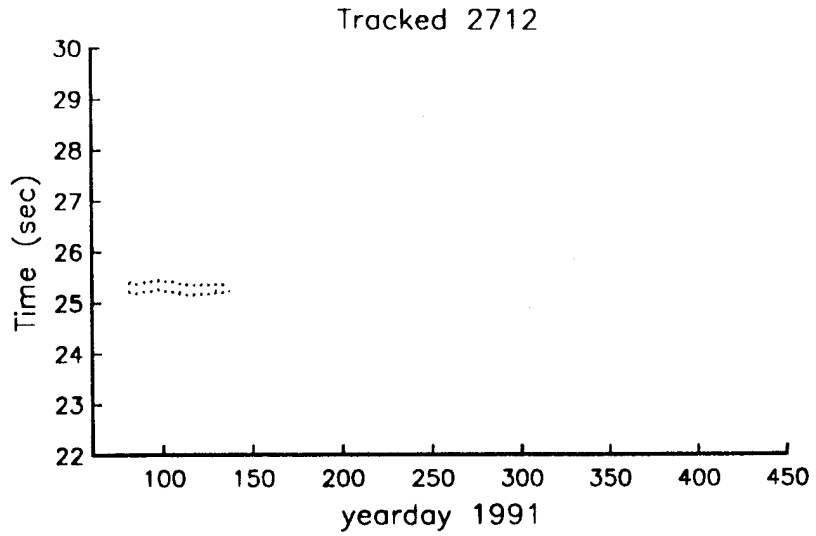
Tracked 2712
Time (sec)
30
29
28
27
26
25
24
23
22
100
150
200
250
300
350
400
450
yearday 1991

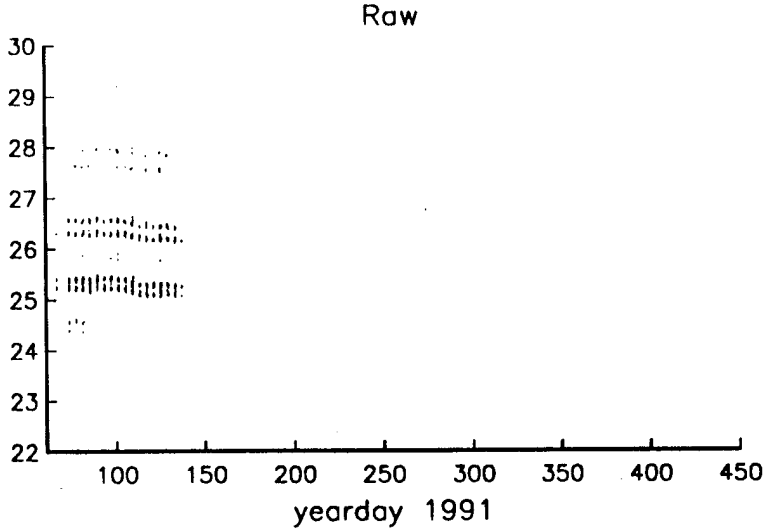
Raw
30
29
28
27
26
25
24
23
22
100
150
200
250
300
350
400
450
yearday 1991

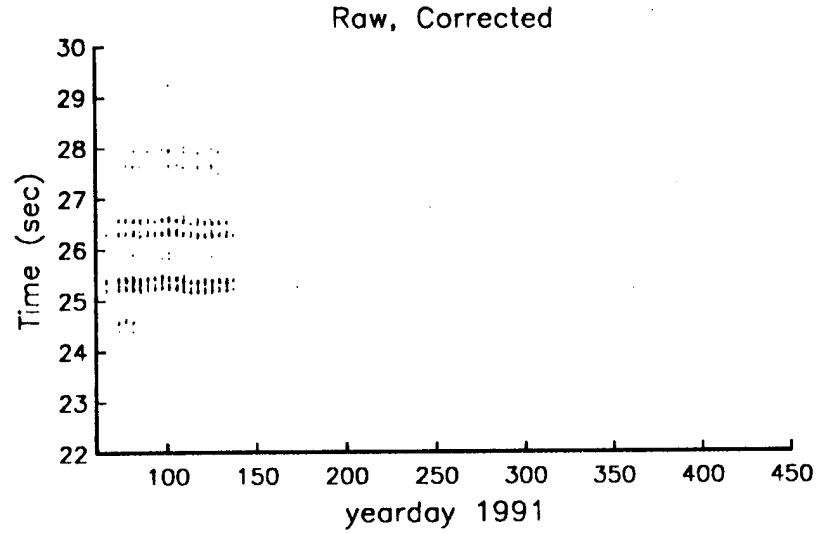
Raw, Corrected
Time (sec)
30
29
28
27
26
25
24
23
22
100
150
200
250
300
350
400
450
yearday 1991

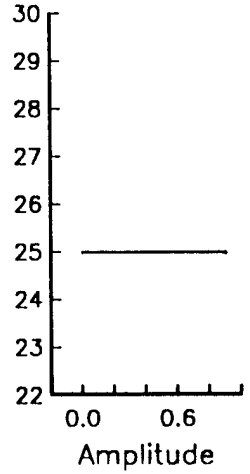
30
29
28
27
26
25
24
23
22
0.0
0.6
Amplitude

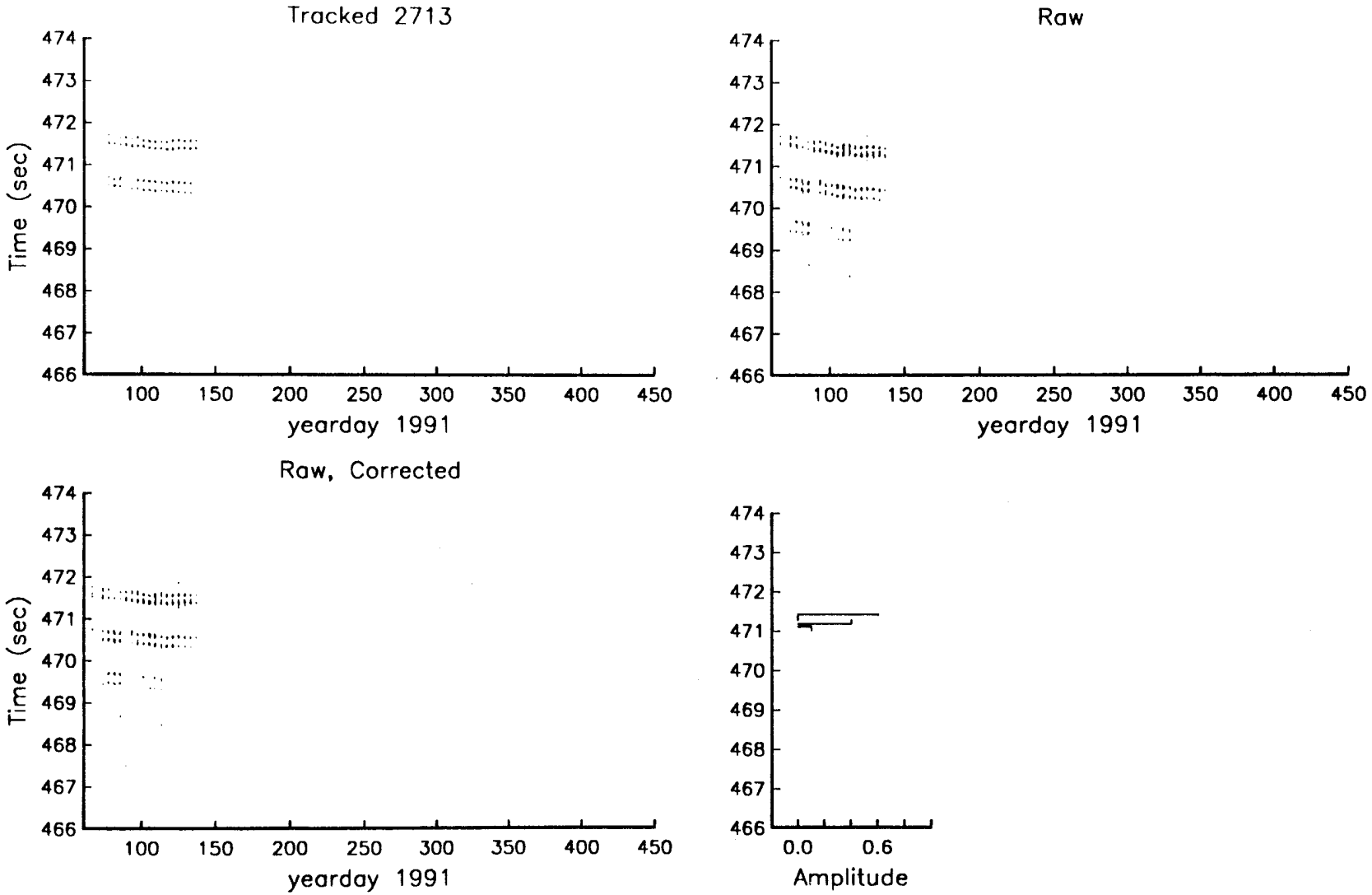
Tracked 2713
Raw
Raw, Corrected
Time (sec)
yearday 1991
Amplitude
474
473
472
471
470
469
468
467
466
100
150
200
250
300
350
400
450
0.0
0.6

REFERENCES

Acoustic Mid-Ocean Dynamics Experiment (AMODE) Group, 1994: Moving Ship Tomography in the North Atlantic. *EOS*, 75, pp. 17,21,23.

Boyd, J. D., D. M. Lavoie, R. K. Myrick, and R. S. Linzell, 1992: Environmental Data Catalog: MDA-91, June-July 1991, Technical Note 225, Naval Oceanographic and Atmospheric Research Laboratory, Stennis Space Center, Mississippi.

Boyd, J. D., B. D. Cornuelle, P. F. Worcester, R. A. Knox, B. M. Howe, J. A. Mercer, R. C. Spindel, T. G. Birdsall, K. Metzger, 1994: Comparison between in situ and Tomographic Measurements in the Western North Atlantic Subtropical Frontal Zone. *EOS, Suppl.*, 75, AGU 1994 Ocean Sciences Meeting, San Diego, CA, 132.

Chester, D. B., P. F. Worcester, B. D. Dushaw, and B. D. Cornuelle, 1994: Large-scale circulation and variability in the Northwest Atlantic between Bermuda and Puerto Rico. AGU Fall Meeting, San Francisco, California, *EOS, Transactions, American Geophysical Union*, 75, Supplement, 379.

Chester, D., P. Worcester, B. Cornuelle, and B. Dushaw, 1995a: Large-scale circulation and variability in the Northwest Atlantic as determined by long-range reciprocal acoustic transmissions. ASA Spring Meeting, Washington, D. C., *J. Acoust. Soc. Am.*, 97, 3249.

Chester, D. B., P.F. Worcester, B. D. Cornuelle, and B. D. Dushaw, 1995b: Circulation and variability in the western North Atlantic between Bermuda and Puerto Rico. IAPSO XXI General Assembly, Honolulu, HI, 5–12 August 1995.

Cornuelle, B., 1983: Inverse methods and results from the 1981 ocean acoustic tomography experiment, Ph.D. thesis, Woods Hole Oceangr. Inst./Mass. Inst. of Technol., Cambridge, Mass.

Cornuelle, B., P. Worcester, D. Chester, B. Dushaw, and B. Howe, 1995a: Testing a regional ocean model using acoustic travel time observations. ASA Spring Meeting, Washington, D. C., *J. Acoust. Soc. Am.*, 97, 3248.

Cornuelle, B., P. Worcester, D. Chester, B. Dushaw, and B. Howe, 1995b: Testing a regional ocean model using acoustic travel time observations. IAPSO XXI General Assembly, Honolulu, Hawaii, 5–12 August 1995.

Cornuelle, B., P. Worcester, D. Chester, 1996: Mesoscale Predictability in a Regional Ocean Model. *EOS, Suppl.*, AGU Ocean Sciences Meeting, San Diego, CA, February 1996.

Dushaw, B. D., 1992: Appendix: AMODE Recovery XBT, CTD, and Bathymetry Report. Unpublished, Scripps Institution of Oceanography, University of California,

San Diego.

Dushaw, B. D., P. F. Worcester, B. D. Cornuelle, and B. M. Howe, 1994a: High-frequency (>1 cpd) travel time variability of long-range reciprocal acoustic transmissions in the western North Atlantic. ASA Fall Meeting, Austin, Texas, *J. Acoust. Soc. Am.*, 96, 3236.

Dushaw, B. D., P. F. Worcester, B. D. Cornuelle, and B. M. Howe, 1994b: Barotropic and baroclinic tides of the western North Atlantic. AGU Fall Meeting, San Francisco, California, *EOS, Transactions, American Geophysical Union*, 75, Supplement, 307.

Dushaw, B. D., P. Worcester, B. Cornuelle, and B. Howe, 1995a: The Internal Tide of the Western North Atlantic Observed Using Long-Range Reciprocal Acoustic Transmissions. ASA Spring Meeting, Washington, D. C., *J. Acoust. Soc. Am.*, 97, 3263.

Dushaw, B. D., G. D. Egbert, P. F. Worcester, B. D. Cornuelle, B. M. Howe, and K. Metzger, 1995b: Validation of a TOPEX/POSEIDON global tidal model (TPXO.2) by comparison of model barotropic tidal currents with estimates from long-range reciprocal acoustic transmissions. *J. Geophys. Res.*, in preparation.

Dushaw, B. D., P. F. Worcester, B. D. Cornuelle, B. M. Howe, 1996: Tomographic Arrays and the Internal Tide. *J. Phys. Oceanogr.*, in preparation.

Ganse, A., and B. Howe, 1993a: Bathymetry Data for AMODE: Follow-up Report. Unpublished, Applied Physics Laboratory, University of Washington.

Ganse, A., and B. Howe, 1993b: Pressure and Temperature Data for AMODE. Unpublished, Applied Physics Laboratory, University of Washington.

Howe, B. M., B. D. Cornuelle, J. A. Mercer, K. Metzger, and P. F. Worcester, 1991: Acoustic Mid-Ocean Dynamics Experiment: 1991 Moving Ship Tomography Cruise, APL-UW TM 18-91, Applied Physics Laboratory, University of Washington.

Howe, B. M., and P. F. Worcester, 1994: Ocean Acoustic Tomography: Single Slice and Moving Ship Experiments. APL-UW TR 9308, Applied Physics Laboratory, University of Washington.

Howe, B. M., J. A. Mercer, R. C. Spindel, P. F. Worcester, B. D. Cornuelle, R. A. Knox, T. G. Birdsall, K. Metzger, and J. Boyd, 1994: Moving Ship Tomography in the Western North Atlantic. *EOS, Suppl.*, 75, AGU 1994 Ocean Sciences Meeting, San Diego, CA, 132.

Worcester, P. F., and B. D. Dushaw, 1993: The Acoustic Mid-Ocean Dynamics Experiment (AMODE): Recovery Cruise Report. Reference Series 93-8, Scripps Institution of Oceanography, University of California, San Diego.

Worcester, P. F., and B. M. Howe, 1991: The Acoustic Mid-Ocean Dynamics Experiment: Cruise Report of AMODE Deployment. Unpublished, Applied Physics Laboratory, University of Washington.

REPORT DOCUMENTATION PAGE

Form Approved
OPM No. 0704-0188

1. AGENCY USE ONLY *(Leave blank)*	2. REPORT DATE	3. REPORT TYPE AND DATES COVERED
	March 1996	Technical

4. TITLE AND SUBTITLE

Data Report: Acoustic Mid-Ocean Dynamics Experiment (AMODE)

5. FUNDING NUMBERS

NSF OCE-9415650
ONR N00014-87-K-0760
ONR N00014-91-J-4055

6. AUTHOR(S)

Brian D. Dushaw, Peter F. Worcester, Bruce D. Cornuelle, Anne R. Marshall, Bruce M. Howe, Shaun Leach, James A. Mercer and Robert C. Spindel

7. PERFORMING ORGANIZATION NAME(S) AND ADDRESS(ES)

Applied Physics Laboratory
University of Washington
1013 NE 40th Street
Seattle, WA 98105-6698

8. PERFORMING ORGANIZATION REPORT NUMBER

APL-UW TM2-96

9. SPONSORING / MONITORING AGENCY NAME(S) AND ADDRESS(ES)

National Science Foundation
4201 Wilson Boulevard
Arlington, VA 22230

10. SPONSORING / MONITORING AGENCY REPORT NUMBER

11. SUPPLEMENTARY NOTES

12a. DISTRIBUTION / AVAILABILITY STATEMENT

Public release; distribution is unlimited

12b. DISTRIBUTION CODE

13. ABSTRACT *(Maximum 200 words)*

This data report summarizes acoustic data collected during the 1991–1992 Acoustic Mid-Ocean Dynamics Experiment (AMODE). The data are reciprocal ray travel times from 300–700 km range acoustic transmissions. Data obtained at Navy SOSUS arrays during AMODE are also described.

14. SUBJECT TERMS

Long-Range Ocean Acoustic Transmissions
Ocean Acoustic Tomography

15. NUMBER OF PAGES

275

16. PRICE CODE

17. SECURITY CLASSIFICATION OF REPORT	18. SECURITY CLASSIFICATION OF THIS PAGE	19. SECURITY CLASSIFICATION OF ABSTRACT	20. LIMITATION OF ABSTRACT
Unclassified	Unclassified	Unclassified	SAR